H24/3172

MONASH UNIVERSITY
THESIS ACCEPTED IN SATISFACTION OF THE
REQUIREMENTS FOR THE DEGREE OF
DOCTOR OF PHILOSOPHY
ON 3 May 2002
[redacted]
Sec, Research Graduate School Committee

EXPERIMENTAL AND ANALYTICAL INVESTIGATION INTO THE SHEAR BEHAVIOUR OF ROCK JOINTS

BY

HELEN A. PEARCE, B.E., B.Ec

A THESIS SUBMITTED FOR THE DEGREE OF DOCTOR OF PHILOSOPHY IN THE DEPARTMENT OF CIVIL ENGINEERING, MONASH UNIVERSITY

DECEMBER, 2001

SYNOPSIS

Considerable research has been conducted over the past three decades to determine the behaviour of discontinuities under the application of a shear load. Empiricism has dominated most of this work due to the complex nature of the shear behaviour and in particular the scale dependency of the joint roughness. A reliable method to quantify the joint roughness has been investigated by many researchers with varying success. Most methods model the 3-dimensional roughness as a single 2-dimensional profile without experimental or theoretical justification for the simplification.

The Geotechnical Group at Monash University has investigated the performance of piles socketed into rock since the mid 1970's. This work has aimed to achieve a fundamental understanding of the mechanisms involved in the shear behaviour of the pile shaft. A theoretical model was developed and a computer program 'Rocket' produced to predict shaft performance.

Initial investigation has highlighted the similarity between the modelling of the concrete / rock interface and a rock joint. This project has provided the opportunity to further assess the applicability of these models to predict rock joint behaviour. An extensive experimental testing program based on constant normal stiffness direct shear tests on a range of 2-dimensional and 3-dimensional surfaces, has led to refinement of the existing analytical models. By testing a range of materials of varying strength – sandstone, siltstone, basalt and granite – the effect of strength on the models was assessed and necessary modifications made. This experimental work has also closely examined the accuracy of representing a 3-dimensional surface by a statistically similar 2-dimensional profile.

The modifications to the existing shear behaviour model to incorporate rock joints of varying strength, together with a method to quantify the 3-dimensional roughness of a rock joint, were incorporated into the computer program 'Rocket'. It is hoped that the resulting computer program can be used to provide reliable estimates of clean rock joint shear behaviour in a variety of materials and with all scales of roughness.

TABLE OF CONTENTS

STATEMENT

This thesis contains no material that has been previously submitted for any other degree or diploma in any university. To the best of my knowledge, the thesis contains no material published or written by others, except where due reference has been made in the text.

Helen A. Pearce

ACKNOWLEDGMENTS

I would like to extend my heartfelt gratitude to the people who have contributed to this project.

Firstly I would like to thank my supervisor, Associate Professor Chris Haberfield for his continual support, ideas and encouragement throughout the course of my candidature. Also his understanding of my family commitments, provided encouragement to continue when at time things were difficult. I would also like to thank my associate supervisor, Dr. Julian Seidel, for his support.

The experimental component of this project was assisted by the technical expertise of the staff in the Civil Engineering Laboratories. I would like to thank all the staff in the laboratories for their friendship and assistance. In particular I would like to thank Roger Doulis (testing equipment), Mike Leach (soil laboratory) and Tony Nixon (electronics).

I would also like to thank my fellow postgraduate students for their friendship and support. In particular I would like to thank Sarah Richards for her valued assistance and for always "listening to any problems".

I am grateful for financial support by the Australian Postgraduate Award Council and for funding of this work by the Australian Research Council.

Finally I would like to thank my family for their support and in particular my parents for providing an excellent baby sitting service.

NOTATION

All notation and symbols are defined where they first appear in the text. For convenience, they are also listed with their definitions below:

a	asperity height
a_n, a_o, A_k	fourier coefficient
a_s	shear area ratio
a^c	selected contact area on the contact plane c (Dong and Pan)
A	joint contact area
A	total projected joint area
A_o	global cross sectional area of joint
ACF	autocorrelation function
A_n	nominal area of fracture surface
A_s	area where asperities shear
A_t	actual area of fracture surface
b_n, b_o, B_k	fourier coefficient
B	width of loaded area
c	cohesion
c	constant
c_j	joint cohesion
c_p	peak cohesion
C	constant (chpt. 2)
CLA	centre line average
CCNS	cyclic constant normal shear
CNL	constant normal load
CNS	constant normal stiffness
C_x, C_y	constants in Line Scaling Method
C_o	compressive strength of intact rock
$[C_{eff}]$	effective compliance matrix
$\bar{d}$	normalised degradation rate
de	increment of elastic compression
dr_j^c	local relaxation tensor that accounts for sliding and dilation (Dong and Pan)
dR_i	global relaxation tensor (Dong and Pan)
du_m^g	global relative displacement (Dong and Pan)
dU	increment of internal strain energy

dx	increment of shear displacement
$dx, \Delta x$	distance between 2 measurements in x direction
$dy, \Delta y$	distance between 2 measurements in y direction
dy	increment of dilation
dw	increment of wear
D	depth of elastic medium
D	fractal dimension
Dx	constant distance lag
D_T	total depth of composite material
D_1	depth of interface half 1
D_2	depth of interface half 2
E	Young's modulus
E_{eff}	effective modulus of a composite material
E_1	elastic modulus of interface half 1
E_2	elastic modulus of interface half 2
$f(x)$	amplitude of asperity height at a distance x along the profile
F_1	settlement factor (Steinbrenner)
F_2	settlement factor (Steinbrenner)
$Gauss$	Gaussian random number
h	depth of rock sample
h	asperity height
h	distance between 2 adjacent roughness points (variogram method)
h	shear displacement
h_{tp}	horizontal displacement corresponding to peak shear strength
H	Hurst exponent
H_{lm}^{c}	heterogeneous tensor for change in local relative displacement (Dong & Pan)
i	effective dilation parameter
i	asperity inclination
$i(h)$	gradient of the dilatancy curve at shear displacement h
i_c	critical asperity angle
i_{tp}	dilation angle corresponding to peak shear strength
I_{effji}	effective influence factor
I_{1ji}	settlement influence factor for interface half 1
I_{2ji}	settlement influence factor for interface half 2
JCS	joint wall compressive strength
JMC	joint matching coefficient
JRC	joint roughness coefficient

k	frequency
k	bisection number (midpoint displacement method)
k_a	degree of apparent anisotropy
k_{ij}^c	contact stiffness tensor on the contact plane c (Dong and Pan)
K	constant
K	global normal stiffness
K	imposed constant normal stiffness in direct shear test
K_{ij}	global stiffness tensor (Dong and Pan)
K_{max}	maximum global normal stiffness
K_o	constant
K_s	asperity failure correction factor (Sokolovsky)
$[K]$	stiffness matrix
$[K_{eff}]$	effective stiffness matrix
L	asperity length
L	length of loaded area
L	length of rectangular jointed block
L	length of profile for determination of roughness
LVDT	linear variable differential transformer
L_l	asperity segment length (Ladanyi and Archambault)
L_x, L_y	number of points along x and y axis respectively
L_{proj}	length of a roughness profiles projection onto a reference line
m	parabolic failure envelope factor of Fairhurst
m_i	number of points (RMS method)
M	damage coefficient
M	number of measurements of roughness amplitude from a centre line
MSV	mean square value
n	parabolic failure envelope of Fairhurst
n	number of harmonics
n_w	number of windows (RMS method)
N	normal force
N	number of steps, segments or observations (N_x in x-direction, N_y in y-direction)
P	total load
P_s	sinuosity index
q	applied stress
q	inclined failure stress (Sokolovsky)
q_u	unconfined compressive strength

r	Schmidt hammer rebound on a wet joint wall
r	segment length
R	Schmidt hammer rebound on unweathered joint wall
R_L	linear roughness
R_s	3-Dimensional linear roughness
$Rand$	random number
RMS	root mean square (measurement of the average deviation of roughness from a centre line)
s	slope length (Sokolovsky)
s_h	standard deviation of chord heights
s_x	standard deviation of x co-ordinates
s_y	standard deviation of y co-ordinates
s_θ	standard deviation of chord angles
$s_{\theta,k}$	standard deviation of chord angles @ k^{th} bisection (midpoint displacement method)
s_o	distance from crest of slope to point of intersection of failure plane with the slope (Sokolovsky)
S	total shear force
SF	structure function to measure joint roughness
S_F	shear force required for sliding
S_1	shear component due to external work done in dilating against external force
S_2	shear component due to additional internal work due to dilatancy
S_3	shear component due to work done in internal friction of sample does not change volume
S_4	shear component due to shearing through asperities
t_F	infill thickness
T	period
T_{ij}^{c}	transforms local to global co-ords on the contact plane c
T_o	tensile strength of intact rock
T_s	surface tortuosity
UCS	unconfined compressive strength
w	wear angle
w	width of loaded area
x	shear displacement
$\bar{x}$	sample mean of x data
y	amplitude of asperity roughness from a centre line
$\bar{y}$	sample mean of y data

z_j	residuals on a linear trend (RMS method)
$\bar{z}$	mean residual on a linear trend (RMS method)
Z_2	root mean square of the 1st derivative of a roughness profile
Z_{2s}	root mean square of the 1st derivative of a 3-D rough surface
Z_3	root mean square of the 2nd derivative of a roughness profile
Z_4	roughness measurement of positive asperity slopes versus negative asperity slopes
$Z(x_i)$	height of roughness profile at location x_i
α	asperity angle
α, β	hyperbolic constants (Wollongong Shear Prediction Approach)
α_k	angle between the normal to the regression mean plane and the vertical
α_{eff}	effective dilation angle
β	spectral exponent
β	slope of spectral density plot
β	post-peak failure plane inclination
δ	load inclination (Sokolovsky)
δ	dilation (Wollongong)
ε	relative movement factor
ε	elastic deformation
ϕ	friction angle
ϕ	angle between the normal to a plane and the normal to the mean plane of the joint surface (roughness measurement)
ϕ_b	basic friction angle
ϕ_i	intact friction angle
ϕ_p	peak friction angle
ϕ_r	residual friction angle
ϕ_s	shearing angle (Dong and Pan)
ϕ_u	sliding friction angle
γ	specific weight of rock
γ	slope angle (Sokolovsky)
$\gamma(h)$	variogram function
η	degree of interlocking
λ	asperity segment length
μ	coefficient of friction
μ	angle subtended by failure plane and crest (Sokolovsky)
ν	Poisson's ratio

$\dot{\nu}$	rate of dilation
θ	chord angle
θ_p	2-dimensional mean angle
θ_s	3-dimensional mean angle
ρ	direction of major principal stress (Sokolovsky)
ρ	correlation coefficient
ρ_i	settlement of chord i
ρ_{Ti}	total settlement of chord i
ρ_{ji}	settlement of j^{th} chord due to stress at chord i
ρ_{1ji}	settlement of j^{th} chord due to stress at chord i on interface half 1
ρ_{2ji}	settlement of j^{th} chord due to stress at chord i on interface half 2
ρ_{Tji}	total settlement of j^{th} chord due to stress at chord i
σ	applied surface pressure
$d\sigma_i^g$	incremental global stress
σ_h	effective horizontal pressure
σ_n	normal stress (global)
σ_{no}	initial normal stress
σ_T	transition stress
σ_v	effective vertical pressure
$\sigma_n(h)$	normal stress at shear displacement h
τ	shear stress (global)
τ_p	peak shear stress
τ_{pp}	post peak shear stress
τ_s	shearing shear stress (Dong and Pan)
$\tau(h)$	shear stress at shear displacement h
ψ	slope angle (Sokolovsky)
ψ	dilation

Units: Metric units according to the S.I. system have been used unless otherwise stated

1.0 INTRODUCTION

1.1 Background

Unexpected shear failure of rock masses can be costly in terms of maintenance and rectification of infrastructure and in loss of life. On October 9th, 1963, the Vajont Dam located on the Vajont River in Northern Italy failed through a massive rock slide that moved more than 270 x 10^6 m^3 of rock. This double arched 276 m high dam was constructed during 1957 to 1960. The flood which followed it's catastrophic failure destroyed 5 villages and killed 1925 people. This example demonstrates the tragic outcome that may occur if civil works are constructed without a complete understanding of the rock mechanics involved.

Unlike man-made materials, rock is non-homogeneous and non-uniform. It contains variations on the micro and macro scales. Variations on the micro scale can be in the form of pores between the grains in sedimentary rocks, the presence of vesicles or vugs in volcanic or soluble carbonate rock or the presence of microfissures caused by internal deformation. These pores and fissures can reduce the rock strength, create stress dependency in material properties, produce variability and scatter in test results and introduce a scale effect into predictions of behaviour (Goodman 1980). On the macro scale, the rock mass is intersected by discontinuities that can take the form of either joints or faults. These discontinuities are typically the weakest part of the rock mass and hence govern its strength. This thesis deals only with rock joints as distinct from the rock mass.

The understanding of the nature of the discontinuities and their behaviour under load is vital to the development of engineering and mining structures founded on or within rock. These defects have been known to cause failure in dams, rock slopes and tunnels. However, to understand the mechanisms of failure within the rock mass it is first necessary to understand the behaviour of a single discontinuity.

Considerable research has been undertaken during the last three decades to determine the behaviour of discontinuities under the application of a shear load. This research has been based principally on empirical models that may lack universal application or on theoretical models that are typically derived from empirical results. The majority of these models do not explicitly model the kinematics of the shear development of the

interface. In most cases man-made rock and artificial joints have been used in laboratory testing to eliminate micro scale variations. This work has also typically tested small samples that may not be representative of large-scale discontinuities.

The Geotechnical Group at Monash University has been investigating the complex behaviour of concrete / rock interfaces as encountered in piles socketed into rock for the past 25 years. This work has involved the development of a micro-mechanical based model that can be used to predict shaft resistance. The concrete / rock interface is modelled by irregular deviations from the horizontal plane called asperities. During the shear process the rock surface may slide on these asperities, wear the asperities down or may completely shear them off. These basic processes together with several other elements comprise the basis of a theoretical model. A direct shear testing apparatus was designed to test the model by testing larger samples under more representative conditions.

There are obviously many similarities between concrete / rock interfaces and natural rock joints. Therefore during the last couple of years, the work on concrete / rock interfaces has been extended into the modelling of natural rock joints. Some testing of artificial joints in man-made rock and natural sandstone (Fleuter, 1997) has indicated that although there are differences, the model shows promise to be extended into natural rock joint applications.

1.2 Current Research

This dissertation investigates through laboratory experiments, the behaviour of two-dimensional and more realistic three-dimensional rock joints in several natural materials and one artificial material. The materials were selected to cover a range of strengths and compositions. Two of the natural materials form the main type of rock formations underlying the Melbourne central business district. These are the Melbourne mudstone, a Silurian Age interbedded siltstone, mudstone and sandstone, and the Newer Volcanics, a Tertiary Age basalt. The other natural materials tested were Sydney Hawkesbury sandstone, a Triassic Age sandstone which extensively underlays Sydney and Mt Bundey Granite, a Precambrian Age granite that is found in the Northern Territory near Darwin. All rock types are of considerable economic significance in their respective areas. An

artificial soft rock called Johnstone that has similar properties to weathered Melbourne mudstone was also tested.

The ultimate aim of the research at Monash University is to develop a theoretical model that can be used to predict the shear response of the rock mass under varying conditions. This is obviously a very complex task and one that must be developed step by step. Therefore the aims of this specific project were to:

1. Investigate whether the existing concrete / rock joint model was suitable for natural rock joints. Limited testing on soft rock joints had already been completed (Fleuter 1997). However, there was a need to extend the testing to harder rocks and to make changes to the model to incorporate any observed changes in behaviour.

2. The existing model has only been tested with two-dimensionally rough profiles. Testing needs to be extended to include more realistic three-dimensional surfaces that better replicate natural rock joint surfaces.

3. Due to the difficulties in accurately quantifying the roughness of a joint surface, an investigation into current methods of quantifying joint roughness was considered necessary. The aim of this investigation was to determine a reliable method of quantifying three-dimensional roughness and present it in a suitable form for input into a theoretical shear model. This investigation is based on a statistical analysis of natural rock joint surfaces and tensile split surfaces that are shown to approximate natural joints. The artificial rock Johnstone is also used to reproduce two-dimensionally statistically similar profiles of three-dimensional joint surfaces. Both two-dimensional and three-dimensional surfaces are tested in direct shear to ascertain if their behaviour is similar. Similar behaviour would provide significant support that three-dimensional roughness could be adequately represented in two dimensions.

1.3 Outline of Thesis

The advancement of the research into the development of a theoretically based shear model is presented in this dissertation in the following manner:

Chapter 2 Characterisation of Rock Joints

This chapter defines and describes rock joints and introduces the major factors that affect their behaviour under the application of a shear load. This dissertation will only concentrate on a few of these influential factors and these are listed in this chapter.

Chapter 3 Quantification of Joint Roughness

This chapter gives an outline of various techniques used to measure surface roughness of a rock joint. Several approaches used to quantify the surface roughness are then presented. Due to their current popularity, significant emphasis is placed on the description and analysis of the many fractal approaches that have been proposed. Using a laser profilometer, surface roughness data is collected and used to test the various approaches so that a representative method of roughness quantification can be adopted.

Chapter 4 Historical Review of Rock Joint Models

An outline of the historical development of various approaches to the determination of rock joint shear strength is presented. A detailed description of the theoretical approach under development at Monash University is given.

Chapter 5 Experimental Shear Testing

The choice of experimental conditions is outlined together with details on the experimental apparatus used in the direct shear tests. The materials to be tested are discussed together with their properties. The profiles tested are described and illustrated.

Chapter 6 Shear Test Results

A summary of the shear tests performed on the rock samples is provided. Complete results are presented in Appendix D. A discussion on the main observations made during the direct shear tests is presented.

Chapter 7 Representation of a three-dimensional Surface

This chapter looks at the statistical similarity of profiles taken across joint surfaces. Although this work assumes that the shear direction is known, a brief investigation into surface anisotropy has been included. The laboratory investigation into representing a surface by a single profile or a statistically equivalent profile is presented.

Chapter 8 Modelling of Shear Behaviour

Areas of the existing shear behaviour model highlighted during the laboratory work as requiring modification are discussed. The method proposed to quantify the surface roughness is presented.

Chapter 9 Predictions of Rock Joint Behaviour

The existing computer shear model including the modifications made during this current investigation, is used to predict the shear response of the rock joint shear tests. A complete set of predictions is presented in Appendix F.

Chapter 10 Summary and Conclusions

The results of the research program are summarized. Limitations of the work are acknowledged and future areas of study recommended.

2.0 CHARACTERISATION OF ROCK JOINTS

This project concentrates on the shear behaviour of rock joints. However, rock joints represent only one form of rock mass defect that can be collectively described under the term discontinuity. Before a detailed analysis of the shear behaviour of rock joints can be commenced, it is beneficial to define and describe what is meant by the term rock joint, how they may be formed and what will affect their behaviour under load. These aspects are discussed in this chapter.

2.1 What is a Discontinuity and How is it Formed?

ISRM (1978) describes a discontinuity as a mechanical break in the rock mass having zero or low tensile strength. There are two main types of rock mass defects or discontinuities - joints and faults. These will be discussed separately.

Joint - A break of geological origin in the continuity of a body of rock along which there has been no visible displacement (ISRM 1978). Joints result from fracturing due to stresses within the rock mass. This can be due to shrinkage (ie. slow drying and lateral shrinkage of sedimentary beds after deposition occurs, or cooling of igneous rocks results in contraction causing the creation of internal stresses that create tensile joints), weathering and erosion (stresses develop due to unloading or expansion of near surface rock causing tension joints) or stresses developed through igneous intrusions or tectonic movements (caused by residual stresses after tectonic movement has finished) (Read and Watson 1987).

Fault - A fracture or fracture zone along which there has been recognizable displacement (ISRM 1978). Faults are caused by tectonic movements. They can be classified according to their movements: normal faults (commonly called tension faults), reverse faults (commonly called compression faults), transcurrent faults and pivotal faults (Read and Watson 1987).

Displacement along a surface may cause damage to the surface. This damage would need to be measured and incorporated into any discontinuity model together with the displacement of the upper surface relative to the lower surface. As the damaged material is in a changed form, it would effectively act as rubble and would require modelling with different properties. This, together with the mismatching of the surface, is not an impossible task, but one that adds further complications to any model. In the initial development of a basic discontinuity shear model, these further complications are not desirable. So although the principles can be extended to include faults with some surface damage already present, this study concentrates purely on rock joints. These can either be bedding joints, cleavage or foliation joints, shear joints or tension joints. Unlike faults, there will have been no previous displacement along the joint surface. This implies that the joint surfaces are not damaged with the upper and lower surface still matching.

2.2 Factors that affect the behaviour of rock joints under load

As rock joints have low or negligible tensile strength and their compressive strength is primarily a function of infill properties and rock strength, these strength parameters are relatively simple to evaluate. However, to accurately predict the shear response of rock joints under the application of load, there are many factors that influence the joint behaviour that need to be considered. These factors are often very difficult to quantify and are often inter-related. A brief outline will be given in this section on some of the factors that affect shear behaviour. This current work investigates the behaviour of clean, unaltered rock joints in a variety of rocks.

2.2.1 Stresses acting on the Joint

There are many stresses that act on rock joints. These can be in-situ stresses or induced stresses from processes such as mining, drilling or pumping. In-situ stresses can be due to gravitational stresses, tectonic stresses that can be either active or remnant, residual stresses from such processes as magma cooling, or terrestrial stresses such as seasonal variation (Amadei and Stephansson 1997).

As can be appreciated, these stresses are difficult to measure. The following field measurement techniques have been suggested (Amadei and Stephansson 1997):

- Hydraulic Methods – hydraulic fracturing, sleeve fracturing, hydraulic tests on pre-existing fractures
- Relief Methods – surface relief methods, undercoring, borehole relief methods (overcoring, borehole slotting, etc), relief of large rock volumes
- Jacking Methods
- Strain Recovery Methods
- Borehole Breakout Methods

There is general consensus however, that in-situ stress measurements are not guaranteed to be accurate and that confidence intervals should be used. This uncertainty is predominantly related to the fact that it is difficult to corroborate field measurements.

Unless more accurate estimates are available, it is usually assumed that for a:

Horizontal Joint – the normal stress is equal to the weight of the overlying material

Vertical Joint – the normal stress is estimated from the lateral pressure coefficient such that:

$$\sigma_h = K\sigma_v \tag{2.1}$$

where σ_h=effective horizontal pressure

σ_v=effective vertical pressure

K=constant

Assuming the rock mass is:

1. Linear isotropic, ideal and homogeneous
2. rock is under gravity alone with no loading history
3. has no stresses of tectonic origin

then $K = K_0 = \frac{\nu}{1-\nu}$ (where ν = poisson ratio)

(Amadei and Stephansson 1997).

Although common to adopt this expression for K_o it must be used with great cation as it can lead to errors in prediction of rock behaviour. For example if tectonic forces are present they can cause K_o to be considerably greater than 1 or to become very small.

2.2.2 Boundary Conditions

The boundary conditions for rock joints vary according to the deformability of the surrounding rock. If the surrounding rock is deformable enough to allow dilation of the joint without reaction forces, then shearing will take place under zero normal stiffness. An example of this would be a rock slope where sliding along a joint occurs under the constant normal load resulting from the sliding block's self weight. This condition is known as Constant Normal Load (CNL) and can be is illustrated in Figure 2.1.

In most underground rock situations, rock blocks cannot slide freely due to constraint provided by the surrounding rock blocks. Dilation of the joint causes a reaction from the surrounding rock mass, which applies additional stress to the rock joint. This condition is known as Constant Normal Stiffness (CNS) and is also illustrated in Figure 2.1. This condition is applicable for a rock slope where the joints are constrained or rock bolts or cables have been installed or for underground situations. The CNL condition is a special case of the CNS condition in which stiffness equals zero.

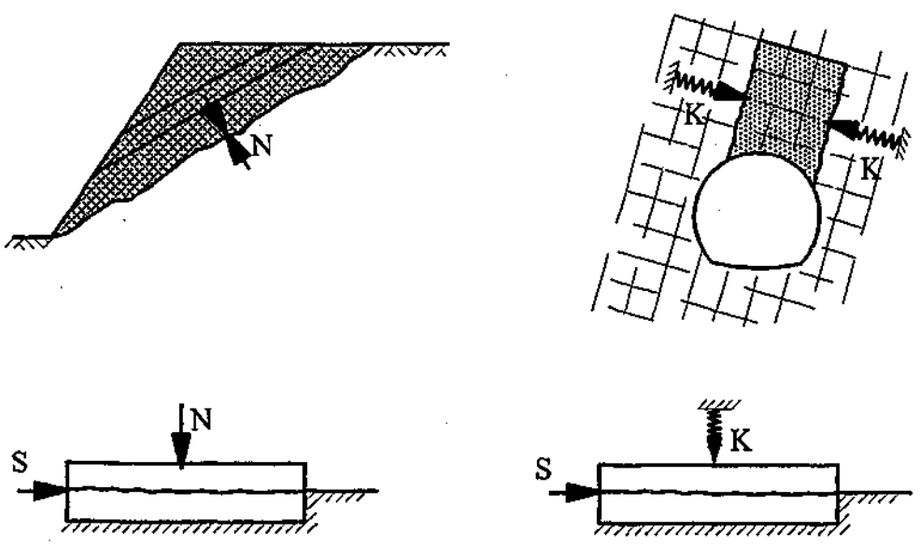

Figure 2.1: Examples of Boundary Conditions (after Leichnitz, 1985)

It is also possible to have variable normal stiffness conditions, where the increase in normal stress due to dilation is not linear but may be either increasing or decreasing. Seismic laboratory tests by Kocharyan et al. (1997) on artificial granite joints indicated that the normal stiffness was non-linearly related to the applied normal stress. This may be due to the presence of infill in the joints or where joint movements result in local plasticity effects.

Boundary stiffness may therefore vary linearly or non-linearly from zero to a maximum value corresponding to the stiffness of the solid rock. Skinas et al., 1990 suggested the following approximation of maximum stiffness:

$$K_{max} = \frac{E.L}{2c(1-\nu^2)} \qquad (2.2)$$

where K_{max} =maximum stiffness

E = Young's Modulus of rock mass

L = length of a rectangular jointed block

c = constant (no defined methods to estimate c are given)

ν = Poisson's Ratio

Insitu boundary stiffness can be estimated using seismic methods. Kocharyan et al. (1997) estimated the normal and shear stiffness of granite discontinuities by measuring the amplitude and time characteristics of seismic waves in front of the discontinuity and behind it. These insitu tests indicated that the normal stiffness was approximately inversely proportional to the distance between discontinuities whilst the shear stiffness was essentially dependent on the structure of the discontinuity (ie. amount of fracture zone, type of infill etc.).

In earlier investigations into the shear strength of rock joints, laboratory testing was predominantly conducted under CNL conditions, due mainly to the availability of suitable shear apparatus. In recent years however, the more widely applicable CNS testing has become popular by using specially designed shear boxes (eg. Leichnitz 1985; Johnston and Lam 1989; Archambault et al. 1990; Benjelloun et al. 1990; Ohnishi and Dharmaratne 1990; Skinas et al. 1990; Van Sint Jan 1990; Saeb and Amadei 1992; Seidel and Haberfield 1995; Wibowo et al. 1995; Indraratna and Haque 1997)

Comparisons of test results from CNS and CNL testing have concluded that:

- Increasing the normal stiffness increases the maximum shear strength
- Increasing the normal stiffness increases the shear displacement necessary to develop maximum shear strength
- The rate of strength reduction after peak shear strength reduces more quickly the higher the normal stiffness

Several authors have developed models to use laboratory results produced under CNL conditions combined with the stiffness of the surrounding rock normal to the joint, to more accurately represent in-situ conditions.

Fortin et al. (1988) produced an algorithm using the simple graphical procedure developed by Goodman (1980). This graphical procedure uses direct shear test data, obtained under CNL boundary conditions and predicts the shear stress – shear displacement relationship for a joint. The algorithm uses a polynomial interpolation procedure to adjust the data available from the experimental curves. A multi-linear approximation of the rock mass' normal stress-dilation curve is used to take into account the non-linear stiffness of the rock mass. Archambault et al. (1990) conducted a series of experiments that showed reasonable agreement with the model.

Saeb (1990) and Saeb and Amadei (1992) also formed a model that could be used to predict the shear response of a dilatant rock joint under a variety of boundary conditions using the results of normal compression and shear tests under CNL conditions. This approach can be represented in both graphical and mathematical forms.

The graphical form uses the normal load-displacement, shear load-displacement and dilatancy response curves for different levels of constant normal stress to construct the normal stress versus normal displacement curves at different levels of shear displacement. The shear strength of the joint can be predicted from these curves at various applied stiffnesses (Saeb 1990). This method was investigated experimentally by Wibowo et al. (1995) with satisfactory agreement being found.

Although the results have been compared favourably to laboratory test results, a major difficulty in using CNL test results to predict the response of the joint under CNS conditions is that several CNL tests need to be performed on an identical rock joint.

There appears to be no research undertaken to date where the results obtained using CNS conditions have been used to predict the response of a joint under CNL conditions. This approach would eliminate the difficulties of obtaining identical rock joint samples.

2.2.3 Joint Roughness

Joint surfaces possess many irregular departures from the plane both on the large scale (waviness) and on the small scale (unevenness) that are of varying angle and length. These departures have been called asperities and are one of the main geometrical properties that affect the mechanical behaviour of the joint. The degree and type of joint roughness depends on the rock's mineralogy and the rock joint's mode of formation and extent of weathering.

One of the most difficult aspects in attempting to quantify joint roughness is that it is scale dependent. As mentioned above, joint surfaces possess small scale unevenness and large scale waviness and a range of roughness in between. Different shear responses may be obtained depending on what scale of roughness is mobilized.

The presence of scale effects in using laboratory results to predict the shear strength of rock joints has been recognized for many years. Barton (1973) recognized that the asperities would be larger on the natural scale than the asperities in the small-scale laboratory sample. Later experimental work by Bandis et al. (1981) indicated that an increase in joint length caused the following:

- a lower peak shear strength
- an increase in the peak shear displacement
- a larger relative shear displacement was required to reach the peak shear strength
- there were insignificant scale effects if the joint was planar and smooth
- a reduction in the peak dilation angle
- a transition from a 'brittle' to 'plastic' mode of shear failure

A joint subjected to small shear displacements will be primarily influenced by small scale roughness. Small steep asperities control the peak shearing path of short joints, whilst larger but flatter asperities affect the shearing response of longer joints. Kabeya and Legge (1996) investigated the micro-roughness of several samples. Their laboratory tilt

tests indicated that when the stress level was very small, the size of the grains affected the peak friction angle with a finer grain size tending to have a lower peak friction angle. Similarly when the samples were very small the grain size affected the peak friction angle. It is therefore essential to know what scale of roughness is important in design and select the sample sizes to reflect this scale or modify the laboratory test results to predict behaviour at the correct scale. As this is not always possible, a preferable method would be to present the shear results at different scales.

Typically in most of the early approaches that describe the shear behaviour of rock joints, attempts were made to quantify the joint roughness as an effective dilation parameter, i. Each rock type can be assumed to possess a typical basic friction angle, ϕ_b. This friction angle can be measured from a shear test on a flat rock surface. Patton (1966) demonstrated on regular triangular asperities that the effect of an asperity is to increase the "apparent" friction angle from ϕ_b to (ϕ_b+i) where i is the inclination angle of the asperity. However, joint roughness is much more complex due to the random and irregular shapes of the asperities, the scale dependency of the roughness and the fact that it may alter during shear displacement. Typically any 'dilation parameter' will decrease as the shear displacement increases as the steeper asperities are sheared.

Therefore, due to the complexity of joint roughness, much research has been conducted on suitable quantification methods. Several approaches are listed:

- Comparison with standard roughness charts (Barton and Choubey 1977). This approach is quite subjective. As the standard profiles are 100mm length samples, scale effects are also of concern.
- Measurement with linear profiling, compass and disc-clinometer or photographgrammetric methods (ISRM 1978). These approaches are also subject to scale effects.
- Statistical Analysis. Reeves (1985) divided these methods into 2 approaches:
    1. Describing the magnitude of the roughness eg. Centre-line roughness, root mean square roughness
    2. Describing the texture of the rough surfaces eg. root mean squares of the derivatives of the surface profile, autocorrelation function, spectral density function, mean square value, structure function

However, the assumptions used in these statistical methods may not be correct for all rock joint situations and often include scaling problems.

- Fractal Analysis. Some of the more recent methods attempt to characterise the roughness profile with a fractal dimension. This approach attempts to take into account the scale effects of roughness. Although it has received significant interest from many researchers, it is has been shown to be difficult to use in a consistent manner.

Due to the importance of accurately quantifying joint roughness, each of these approaches will be discussed in further detail in Chapter 3.

Most of the available approaches analyse the joint surface as a two-dimensional profile. This assumes that the selected surface is not anisotropic and that the selected profile represents the full joint surface. These aspects are also discussed in further detail in Chapter 3. A laboratory and statistical investigation is presented in Chapter 7 to assess whether a three-dimensional joint surface can be adequately represented by a two-dimensional profile.

2.2.4 Rock Strength

During shear displacement, shear of the asperities may occur. This will be dependent on the strength of the asperities at the joint wall, asperity size and inclination, and the stresses applied. The asperity strength may be different to that of the intact rock strength if weathering has occurred. Weathering will typically weaken the joint wall strength, although the occurrence of iron penetration can make some joint walls stronger. The depth of penetration of weathering into joint walls depends largely on the rock type and in particular on its permeability.

Joint wall strength may be difficult to determine if the depth of weathering is too small to sample for laboratory testing. For weathered joints, ISRM (1978) have recommended the use of the Schmidt hammer. This field estimate is based on the ratio between the Schmidt hammer rebound (r) obtained from the wet joint wall and the rebound (R) on an unweathered rock surface. An average of several tests is required to decrease the potential errors due to operator error and variations such as sample movement or crushing of loose grains. Variation of rock density with depth and the presence of voids can also potentially alter the rebound number and therefore, unless calibrated extensively,

the results should only be used as an index. Joint roughness has also been shown to influence the scatter in Schmidt values (Bobji et al. 1999).

The work described in this dissertation is restricted to the shear behaviour of fresh unaltered joint surfaces. Therefore the strength of the asperities is assumed to be the same as the intact rock.

2.2.5 Joint Aperture

The joint aperture is the perpendicular distance separating the adjacent rock walls. It can be filled by either water or air. A completely open joint where none of the asperities touch will therefore possess zero shear strength. Shearing of a partially open joint may involve only some of the higher asperities with shallow asperities not becoming involved in the shearing process. This will obviously affect the magnitude of the peak shear strength.

Under the application of a normal stress, closing of the aperture may occur. This has been shown to reduce the amount of measured dilation of the asperities and alter the load applied to each asperity (Fleuter 1997). The presence of joint aperture will also effect the stiffness of the rock mass. Work by Hopkins et al. (1990) has indicated that joints with small contacts are stiffer than those with large and clustered contacts for a given percentage of contact area. Knowledge of the aperture is therefore required in predicting the peak shear strength of the joint. This is often difficult to measure as standard drilling techniques disturb the interface making aperture and contact area measurements unreliable.

The work described in this dissertation is restricted to the shear behaviour of tight joints.

2.2.6 Joint Infill

Many joint walls are separated by material that will typically reduce the shear strength of the joint. This infill can be carbonaceous, clay, silt, breccia or minerals. The effect on the shear strength will be dependent on the infill's thickness, composition, water content, degree of over consolidation, previous shear history and on the strength and roughness of the joint walls.

De Toledo and de Freitas (1995) conducted a series of laboratory tests on sandstone regular triangular asperity joints with clay or clayey sand infill in a rotary shear machine. Over-consolidated clay filled joints, where the strength of the rock was significantly stronger than the infill material, produced two peak shear strengths - initially the soil infill failed followed by the rock asperities. The soil infill peak shear strength decreased with increasing infill thickness until the thickness equalled the asperity height at which time it became constant. The soil infill peak shear strength was dependent on the degree of over-consolidation - the greater the over-consolidation the greater the peak shear strength. However, normally consolidated clay filled joints and clayey sand filled joints showed only early stages of a soil peak shear strength. Laboratory studies by Indraratna et al. (1999) indicated only one peak shear strength when a soft material such as gypsum plaster (similar strength properties to the infill material) was tested as the rock material.

Laboratory results by de Toledo and de Freitas (1995) indicated that the rock peak shear stress reduced with increasing infill thickness; first at a slow rate and then more rapidly as the infill thickness approached the asperity height. They found that the presence of even a small amount of clay infill reduced the rock peak shear strength from that of an unfilled joint. They believed that this was due to the change in frictional properties of the shear surface. This was confirmed by Indraratna and Haque (1997) with tests on triangular asperity profiles with bentonite infill. Indraratna et al. (1999) also observed that the effect of the asperities on shear strength was significant up to a critical infill thickness to asperity height ratio of 1.4-1.8 (ie. where damage was noted on the asperity surface) but beyond this critical value the shear behaviour was controlled by the infill properties. Laboratory tests by Cheng (1997) using regular triangular and irregular triangular synthetic siltstone (soft rock) / concrete interfaces separated by a bentonite clay layer (used to model the filter cake often present in pile sockets constructed with bentonite) or a silt layer (used to model rock smear), also indicated that the peak shear strength decreases as the thickness of the infill increases.

During his work of wear of rock surfaces, Gu (2001) developed an effective asperity angle, α_{eff}, which accounted for the effects of infill on the shear behaviour of rock joints. This effective angle can be used to model a joint interface when infill is present. This effective asperity angle increases with shear displacement. The calculation of this angle is shown in Equation 2.3.

$$\alpha_{effi} = \tan^{-1}\left[\frac{(L - x_i)\tan\alpha - t_{Fi}}{L - x_i}\right] \qquad (2.3)$$

where L = asperity chord length

x_i = shear displacement

α = asperity angle

t_{Fi} = infill thickness at displacement x_i

Knowledge of the type, strength and thickness of any infill is therefore necessary to predict the peak shear strength.

The work described in this dissertation is restricted to the shear behaviour of clean joints.

2.2.7 Shear Displacement Velocity

In early work by Hoek and Bray (1981) it was suggested that the shear strengths of rock joints were "generally not sensitive to the loading rate". They suggested a rate of less than 2mm/min. Typically most researchers appear to be using shear rates in the order of 0.1mm/min - 0.5mm/min.

However, other laboratory testing has indicated that the shear displacement velocity affects the magnitude of the shear resistance at stress levels applicable to engineering structures. Crawford and Curran (1981) conducted a series of CNL direct shear tests on air dried rock samples under a range of normal loads. Their research suggested that the magnitude of the rate effect depends on the rock type and the level of the normal stress. Laboratory results indicated a weak relationship between rock strength and shear rate although this was not quantified. They could find no obvious correlation between the rate effect and the mechanical or mineralogical properties of the rock. For harder rocks such as sandstone, the shear resistance was observed to decrease as shear displacement rates were increased above a critical velocity. The critical velocity was found to be dependent on the magnitude of the normal stress. The frictional resistance of soft rocks, such as syenite, was observed to also be dependent on the normal stress. Results indicated an initial increase in shear resistance as the shear velocity increased for normal stresses up to 1250kPa followed by a period of constant shear resistance. After a second critical velocity was reached, the shear resistance decreased as the shear velocity increased.

Indraratna and Haque (2000) performed a series of CNS direct shear tests on 18.5° triangular asperity profiles of soft rock where the rate of shear displacement was varied. Their work confirmed that the rate of shear displacement has a significant effect on the peak shear strength of rock joints.

This suggests that for each rock type to be tested, a critical shear velocity should be measured through laboratory testing under conditions similar to that expected insitu (ie. saturated or dry rock conditions). The shear velocity to be expected within the rock mass would also be required. Further work is required in this area on a range of rock types, roughnesses and conditions.

The work described in this dissertation is confined to one "quasi-static" rate of shearing.

2.2.8 Water

Many rock types are known to be strength dependent on saturation levels. Melbourne mudstone is known to increase in strength as it dries. A saturated rough mudstone joint will therefore have lower shear strength than a dry sample. It is therefore important to duplicate natural ground water content conditions when storing samples prior to testing.

The presence of water in the joint has also been found to reduce, increase or have no effect on the shear strength of the rock joint (Barton 1973). It is likely that the water may reduce the effective stress and reduce the surface energy. The extent of any alteration on shear strength though, appears to be dependent on the mineralogy and the smoothness of the joint and the development of pore pressures. It is therefore important for a rock joint model to take into account the effects of water.

The tests described in this dissertation have been conducted on moist rock samples with no free water present at the joint interface.

2.3 Summary

To be able to predict the behaviour of the rock mass it is first necessary to understand the behaviour of a single discontinuity. Although this discontinuity can take the form of either a fault or a joint, this work will be limited to the behaviour of clean, tight, unweathered rock joints, tested close to full saturation.

The determination of the tensile or compressive strength of rock joints is a relatively simple task compared to the estimation of its shear strength. This is due to the many factors that can affect the shear strength of an individual joint. These factors have been discussed in detail in this chapter.

The objective of the overall research project that this project forms part of, is to develop a theoretical shear behaviour model that is capable of incorporating all of these factors. However, due to the complexity of such a model, time limitations in this current work has meant that only the affects of stresses acting on the joint, boundary conditions, rock strength and joint roughness will be investigated.

3.0 QUANTIFICATION OF JOINT ROUGHNESS

As discussed in Chapter 2, rock joint surfaces are irregular and random causing researchers to struggle in their attempts to adequately classify the surface for their shear models. As joint roughness is a fundamental component of the joint shear behaviour, a method to adequately measure and quantify it is vital. There are currently various methods used by researchers to measure, reproduce and quantify joint roughness. The shortcomings of these methods will be discussed together with the approaches that have been adopted for this research.

To quantify joint roughness, measurement of the roughness either insitu or in the laboratory is required so that detailed analysis can be undertaken at various scales of interest in the office. Section 3.1 outlines various techniques to reproduce roughness including details on the laser profilometer used in this study.

Once data on the joint surface has been obtained, there are many popular techniques used for analysis. A critical review of these techniques is included in Section 3.2. The method chosen to analyse the joint surfaces in this current work will be discussed.

Joint surfaces have been shown to be strongly anisotropic for many rock joints. This highlights the need to either model the shear behaviour in the direction of potential shearing, or the need to develop a model that can be used to predict the shear behaviour in all directions. This is discussed in Section 3.3.

For modelling purposes it is often useful to be able to reproduce a joint surface that is similar to a natural joint surface. Several techniques have been developed to generate rock joint surfaces. These are discussed in Section 3.4 together with the method that has been adopted in this research.

3.1 Roughness Measurement

Whether faced with a rock slope or a series of rock cores, the geologist or field engineer must quantify joint characteristics for design. Field mapping has been traditionally achieved by recording dip and dip direction of the discontinuity asperities by linear profiling techniques, the compass and disc clinometer method or photographgrammetry

methods (ISRM 1978). More detailed analysis can be achieved by digitising linear profiles parallel to the predicted direction of potential shearing at specified digitising intervals (eg. 1, 5, 10 mm). This allows large amounts of data to be taken and computer analysed using various methods. Profiles can be taken using a mechanical profilometer or laser profilometer.

3.1.1 Linear Profiling

This method measures linear profiles parallel to the predicted direction of potential shearing. It uses either a 2 m length folding straight edge (graduated in mm) for small scale roughness or a 10 m length of light wire (graduated in 100 mm intervals) to measure larger scale roughness. This measuring tool is placed in contact with the highest asperity and parallel to the mean direction of potential sliding. The perpendicular distance between the measuring tool and the discontinuity surface is measured at specified tangential distances together with the dip of the measuring direction. Typically the minimum, most common and maximum roughness profiles are recorded (ISRM 1978). This method has an accuracy of approximately 1 mm and is also very time consuming and sensitive to operator error.

3.1.2 Compass and Disk Clinometer

If the potential direction of sliding is not known, the compass and disclinometer method can be used to sample roughness in 3 dimensions. It uses a Clar geological compass and 4 circular plates. Each plate is placed against the surface of the discontinuity in at least 25 positions and the dip direction and dip measured at each position. The sets of data obtained for the 4 plates are plotted on a separate area net diagram and contours drawn for each set of poles. Again this method is very time consuming and is sensitive to operator error.

3.1.3 Photographgrammetric Method

This method involves taking overlapping photographgraphs of the rock face so that a stereopair can be used to orient different planes. It is quite a costly procedure and is typically only cost effective if mapping of a large number of discontinuities is required. Although it orientates large planes quite precisely, it decreases in accuracy as the planes

become smaller. Problems also arise on sites where locating the tripods to obtain the required overlapping is difficult. The films should be developed on site so that if any problems have occurred the photographs can be taken again before the tripods are moved.

3.1.4 Profilometer Methods

These methods are used to digitise the discontinuity so that it can be analysed by the use of a computer. Traditionally mechanical profilometers were used although laser profilometers are becoming more popular. Mechanical profilometers use a contact sensor to trace the rock surface. These types of profilometers are restricted in the detail they can measure by the width of the contact sensor. They also have problems with the contact sensor leaving the surface or even damaging the surface. The beam of a laser profilometer, unlike a mechanical profilometer, does not leave the surface or damage it. They can be operated at high frequency allowing rapid surface scanning. Three-dimensional laser scanning equipment is also possible (Lanaro 2000). Laser profilometers are limited in their accuracy by the width of the laser beam.

Monash University has developed a laser profilometer to measure pile socket roughness (Collingwood, et al. 1999). The Monash Socket-Pro has a 1m traverse and can sample at a rate of up to 1000Hz. The laser distance sensor emits a laser beam that is reflected from the rock surface and collected by an optical receiver. This determines the angle of reflection and using geometry calculates the distance to the surface. A magneto-strictive linear displacement transducer is used to measure traverse position. The laser distance sensor has an accuracy of approximately ±0.05mm whilst the traverse position is recorded at an accuracy of approximately ±0.1mm. The spot diameter of the laser beam is approximately 3mm. This device can be seen in Figure 3.1.

The Monash Socket-Pro was used to measure the joint profiles for this current work. The rock joints were placed in an approximately vertical position on a timber frame approximately 60 mm from the front of the laser. Each joint was scanned at a 1000Hz frequency such that readings were taken at approximately 0.1 mm intervals. Several profiles were taken at 5 mm or 10 mm intervals across each block. The distance to the timber frame was used as a baseline to zero all the profiles in the Z direction. As the samples were difficult to place perfectly vertical, linear regression was used on the raw

data to remove any overlying angle on the profile (ie. non-stationarity). The resolution error (approx ± 0.1mm) in the vertical translation was removed by taking a moving average over approximately 1.4mm length. As the laser had been shown to move at relatively constant velocity (Collingwood 2000), this moving average was not considered to alter the accuracy of the data.

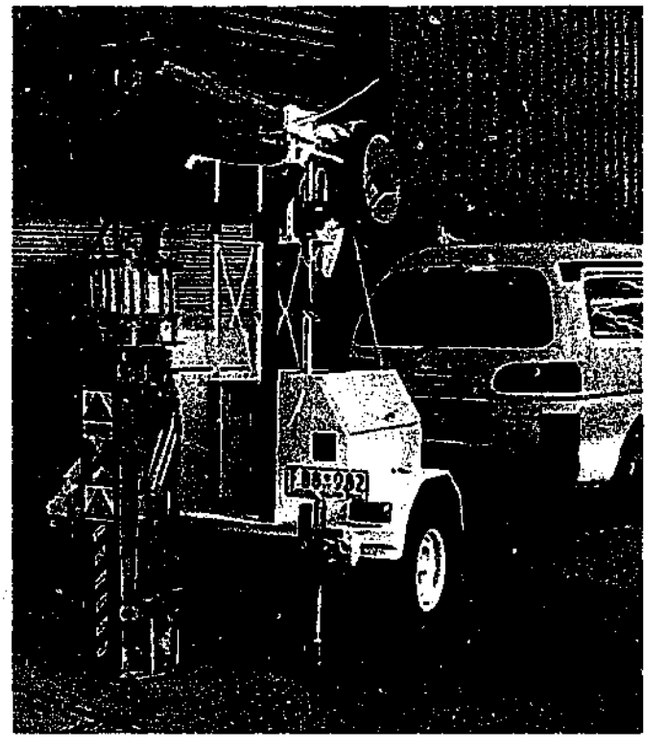

Figure 3.1: Monash Socket-Pro

3.2 Methods to Estimate Roughness

3.2.1 Statistical Methods

Many statistical parameters have been used to characterise joint roughness. These either describe the magnitude of the roughness or the texture of the rough surface (typically derivatives of the magnitude of the roughness) on a single scan line or traverse. In the following, the parameters that have been suggested by other researchers as being in popular use for the characterisation of rock joint roughness (Lam 1983; Reeves 1985; Lamas 1996) are described.

1. If a line is placed parallel to the general direction of the profile such that the area between the line and the profile is the same both above and below the line, then

measurement of the average deviation away from this line gives one measurement of roughness. This average deviation can be measured by the root mean square (*RMS*) defined in Equation 3.1(Assoc. 1955).

$$RMS = \left[\frac{1}{M}\int_{x=0}^{x=M} y^2 dx\right]^{1/2} \qquad (3.1)$$

where M = number of discrete measurements of the amplitude

y = amplitude of the roughness about the centre line

dx = small constant distance between 2 adjacent amplitude readings

2. A centre line average (*CLA*) can also be taken to measure the roughness as given by Equation 3.2 with units of length (Assoc. 1955).

$$CLA = \frac{1}{L}\int_{x=0}^{x=L} |y| dx \qquad (3.2)$$

where L = distance over which the average is taken

3. The linear roughness (R_L) is a relation between the total length of the profile L and the length of its projection on a reference line L_{proj} as defined by Equation 3.3.

$$R_L = L/L_{proj} \qquad (3.3)$$

4. Myers (1962) used the basic *RMS* method to propose three other parameters to describe particular components of surface roughness. The *RMS* of the first derivative of the profile (ie RMS gradient), Z_2; the *RMS* of the second derivative, Z_3; and the difference in length between where the slope of the surface is positive compared to negative divided by the total length, Z_4. These parameters are defined in Equations 3.4 – 3.6 and are all very sensitive to the sampling interval (Yu and Vayssade 1991). Reeves (1985) attempted to overcome the dependence of Z_2 on the sampling interval by using the average asperity gradient ie. *RMS/(xD)* where *xD*=correlation distance. This value was shown to be predominantly independent of the sampling interval for many rock surfaces.

$$Z_2 = \frac{1}{L}\int_{x=0}^{x=L}\left(\frac{dy}{dx}\right)^2 \qquad (3.4)$$

$$Z_2 = \frac{1}{L}\int_{x=0}^{x=L}\left(\frac{d^2y}{dx^2}\right)^2 \qquad (3.5)$$

$$Z_4 = \frac{\sum(xi)_{positive} - \sum(xi)_{negative}}{L} \qquad (3.6)$$

where xi = the ith segment of L

$L = \Sigma(xi)_{positive} + \Sigma(xi)_{negative}$

5. Bendat and Piersol (1986) suggested 2 statistical parameters that deal with the distribution of the asperity heights. These are the mean square value, *MSV* and the autocorrelation function, *ACF* as defined by Equations 3.7 and 3.8.

$$MSV = \frac{1}{L}\int_{x=0}^{x=L} y^2 dx \qquad (3.7)$$

$$ACF = \frac{1}{L}\int_{x=0}^{x=l} f(x)f(x+Dx)dx \qquad (3.8)$$

where $f(x)$ = amplitude of asperity height at the distance x along the length L

Dx = constant distance lag (method therefore limited to data at equally spaced intervals)

6. Sayles and Thomas (1977) modified the *ACF* to produce the structure function, *SF* (see Equation 3.9) that could be used over a proportion of the profile without a decrease in accuracy.

$$SF = \int_{x=0}^{x=L}\left(f(x) - f(x+Dx)\right)^2 \qquad (3.9)$$

7. Belem et al. (2000) extended several of these two-dimensional statistical approaches into parameters that attempted to capture the three-dimensional characteristics of roughness. They divided the roughness into 2 categories – primary roughness that attempts to capture the anisotropy of the joint; and secondary roughness that attempts to capture the distribution of asperity heights. They extended the existing linear parameters Z_2, R_L and sinuosity index P_s (Pikens and Gurland 1976) with their three-dimensional equivalents Z_{2s}, R_s and surface tortuosity T_s (measure of the degree of deviation of the fracture surface with respect to a mean plane) using a linear angularity parameter, θp, and its

three-dimensional equivalent, θs (refer to Figure 3.2). The surface anisotropy was quantified by a term they defined as the degree of apparent anisotropy k_a (calculated in 2 directions), and the surface relative roughness coefficient, R_s. The surface roughness was captured by its three-dimensional mean angle, θ_s, and the parameter Z_{2s}. Definitions of these terms are given below.

$$\theta_p = \tan^{-1}\left(\frac{1}{N_x - 1}\sum_{i=1}^{N_x-1}\left|\frac{z_{i+1} - z_i}{\Delta x}\right|\right) \tag{3.10}$$

$$\theta_s = \frac{1}{m}\sum_{i=1}^{m}(\alpha_k)_i \tag{3.11}$$

$$Z_{2s} = \left[\frac{1}{(N_x - 1)(N_y - 1)}\left[\begin{array}{l}\dfrac{1}{\Delta x^2}\displaystyle\sum_{i=1}^{N_x-1}\sum_{j=1}^{N_y-1}\frac{(z_{i+1} - z_{i,j+1})^2 + (z_{i+1,j} - z_{i,j})^2}{2} + \\ \dfrac{1}{\Delta y^2}\displaystyle\sum_{j=1}^{N_y-1}\sum_{i=1}^{N_x-1}\frac{(z_{i+1,j+1} - z_{i+1,j})^2 + (z_{i,j+1} - z_{i,j})^2}{2}\end{array}\right]\right]^{\frac{1}{2}} \tag{3.12}$$

$$R_S = A_t / A_n \tag{3.13}$$

$$T_s = A_t / A_n \cos\phi \tag{3.14}$$

k_a = geometric linear parameter along x-axis/geometric parameter along y-axis

where z_i = asperity height

N_x = number of intervals in x-direction

N_y = number of intervals in y-direction

Δx = sampling interval along the x-axis

Δy = sampling interval along the y-axis

α_k = angle between the normal to the regression mean plane and the vertical or z-axis (refer to Figure 3.2)

m = number of normal vectors from the mean plane (refer to Figure 3.2)

L_x = number of points along the x-axis

L_y = number of points along the y-axis

A_n = nominal area of the fracture surface (projection of the fracture surface on its mean plane)

A_t = actual area of the fracture surface

$$\approx (\Delta x \Delta y) \sum_{i=1}^{N_x-1} \sum_{j=1}^{N_y-1} \sqrt{1 + \left(\frac{z_{i+1,j} - z_{i,j}}{\Delta x} \right)^2 + \left(\frac{z_{i,j+1} - z_{i,j}}{\Delta y} \right)^2}$$

ϕ = angle between the normal to a plane (defined as the plane created by joining the 4 corners of the surface) and the normal to the mean plane of the joint surface

Analysis of a three-dimensional surface requires the use of sophisticated digitising equipment to be able to obtain the relevant three-dimensional data. The processing techniques would then require computer assistance.

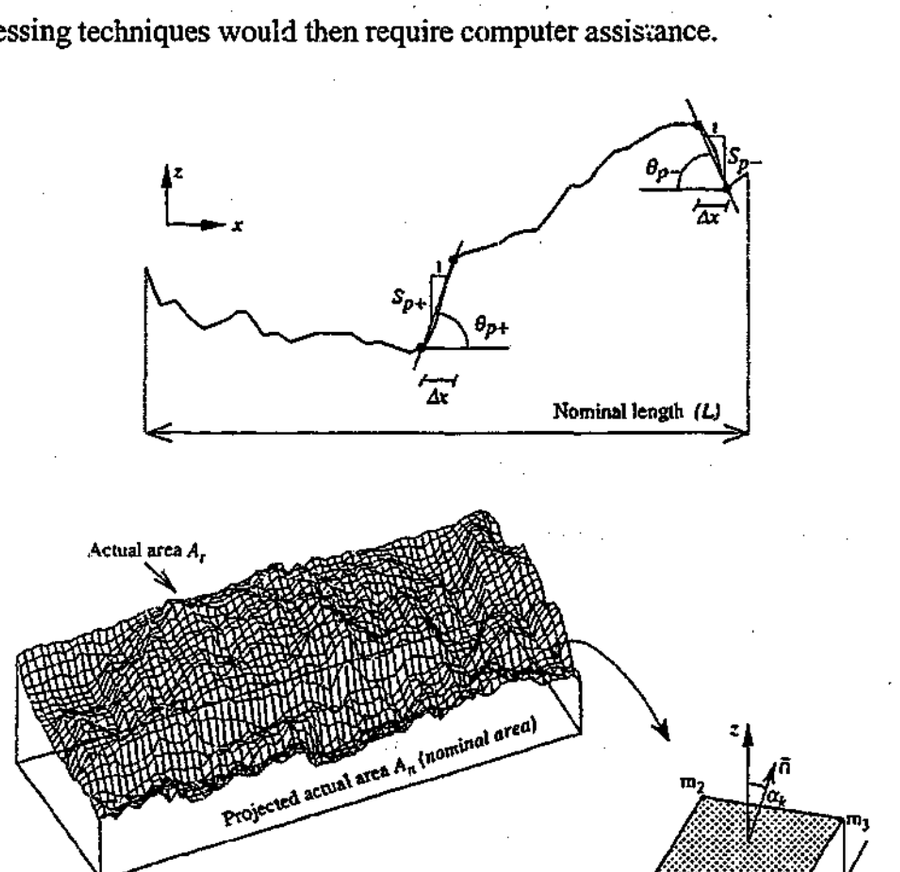

Figure 3.2: i) Slopes and angles of a topographic profile along the x-axis

ii) Illustration of inclination angle of the elementary surfaces (after Belem et al., 2000)

Many of the above parameters attempt to describe the same property and doubts exist about which are more appropriate. An investigation by Lamas (1996) showed that a significant difference existed between the amplitude indices *CLA* and *RMS*. Comparisons performed to compare these statistics with measurements of JRC (refer to next section) also indicate poor comparisons (Lamas 1996). Many of the above methods are also sensitive to changes in sampling interval with varying values of roughness index calculated with minor changes in sampling interval. However the main problem with these statistical approaches is their inability to capture the complex scale dependence of roughness with a single statistic or small set of statistics.

Other analytical techniques such as using Fourier transforms are discussed in Section 4.5.

3.2.2 Joint Roughness Coefficient

Barton (1973) suggested a joint roughness coefficient JRC, should be used to describe joint roughness. The JRC of a joint can be estimated by comparing it to standard roughness profiles or more preferably through simple classification tests. He suggested a sliding scale of roughness that varied from approximately 0 to 20. A standard roughness chart was developed by Barton and Choubey (1977) by profiling 136 joints and grouping their roughness profiles in the ranges 0-2, 2-4, etc. up to 18-20 and then selecting the most typical. These profiles are shown in Figure 3.3. These standard profiles have been accepted by the International Society for Rock Mechanics as a useful field measurement tool of joint roughness in their Commission on Standardization of Laboratory and Field Tests (ISRM 1978).

As visual comparison involves a considerable amount of subjectivity, several researchers have developed less subjective means to estimate JRC. Tse and Cruden (1979) proposed two statistical relationships shown in Equation 3.15 and 3.16 to relate the statistical parameters Z_2 and SF to JRC (details on the determination of Z_2 and SF are given in Section 3.2.1). The relationship with Z_2 was later modified to include different sampling intervals by Yu and Vayssade (1991). However, these relationships lead to negative JRC values at very small values of Z_2 and are developed using the 100mm long standard profiles and hence may not be representative at larger scales.

$$JRC=32.2+32.47Z_2 \quad (3.15)$$

$$JRC=37.28+16.58\log SF \quad (3.16)$$

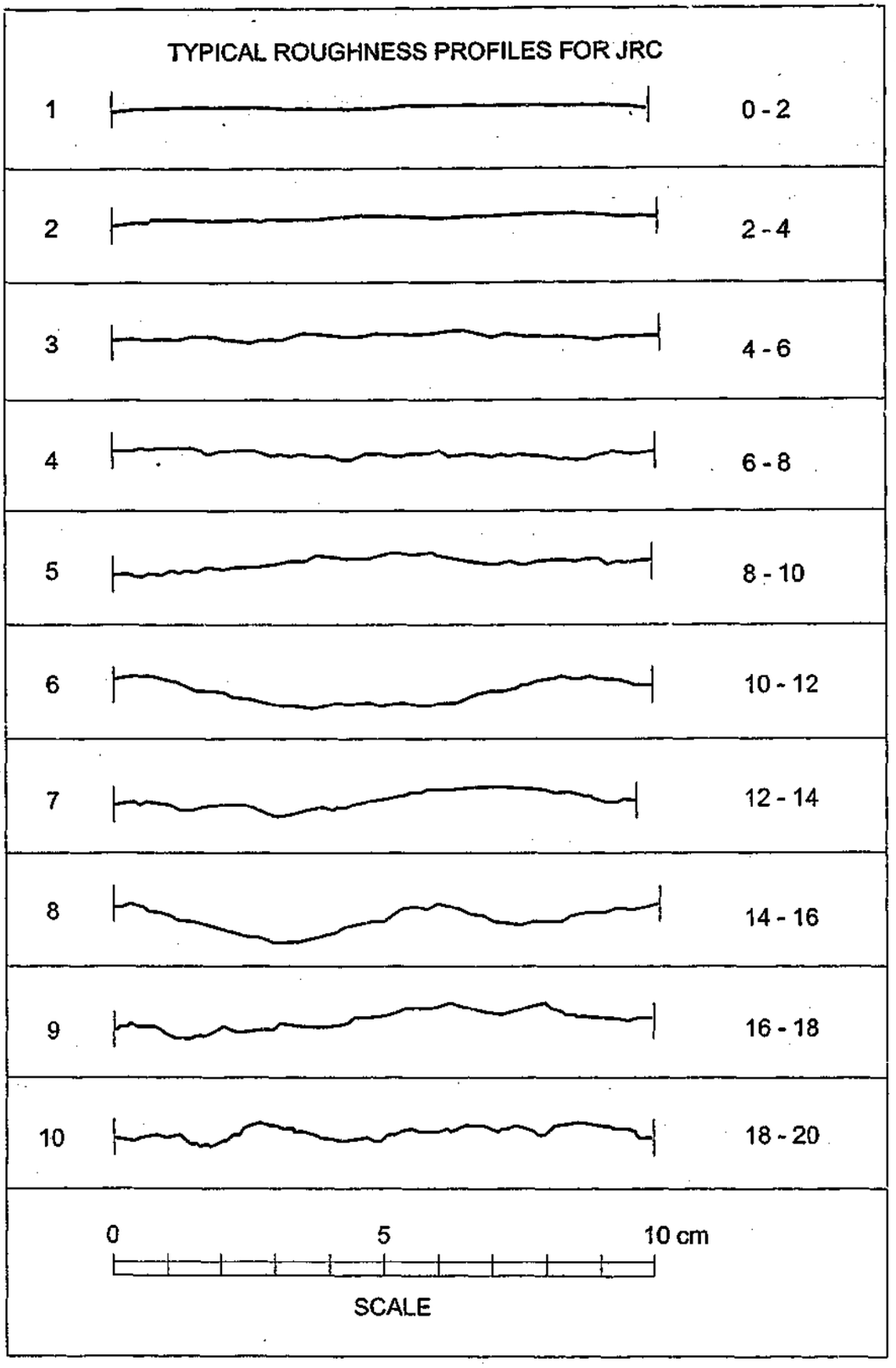

Figure 3.3: JRC Roughness Profiles (digitised from Barton and Choubey, 1977)

Lessard and Hadjigeorgiou (1998) have used artificial neural networks to estimate values of JRC. Artificial neural networks consist of simple, highly interconnected, parallel processing elements called nodes. An initial back-propagation neural network that classified roughness according to 3 categories: smooth, medium and rough, was enhanced to be able to classify according to the JRC categories. However, the quality of the neural network is highly dependent on the database. Predictions of joint roughness are only applicable if the roughness is similar to the profiles used in the database. As the standard roughness charts are only 100mm in length, concerns also arise that significant roughness at larger scales may be ignored.

3.2.3 Fractal Method

To be able to quantify the variation in roughness with changes in scale of the measuring interval, the use of fractals has been investigated. Fractals have been used to represent many observations in nature such as Brownian motion, topography, flow and transport through heterogeneous systems. Many researchers also view the fractal model as the most appropriate way to adequately represent the scale effects of rock joint profiles.

The fractal model is based on fractal geometry, which is the geometry of "chaos theory". This theory attempts to capture the random and chaotic characteristics of Nature. Mandelbrot (1983) introduced the concept of fractal dimension. He recognized that Euclidean geometrical forms such as straight lines, squares and triangles could not represent Nature. He used the example of the coastline of Britain to demonstrate his point. When measuring the length of the coastline, as the measuring scale is decreased, the length is seen to increase without limit as smaller and smaller details such as small bays, rock outcrops or even sand grains are considered. The features on the coastline are therefore much more complex than an Euclidean line but are not so complex as to completely fill a plane. Its fractal dimension therefore lies between that of a line, 1, and that of a plane, 2.

In Euclidean geometry if a line of unit length is divided into N segments of length r, the number of segments is then $N=1/r^1$. In a similar manner, a unit square can be divided into N squares of side length r so that $N=1/r^2$. If a cube is considered then, $N=1/r^3$. If the parameter D is defined as the dimension, then:

$$N = \frac{1}{r^D} \tag{3.17}$$

In the case of the coastline, the dimension D is fractional and greater than the topological dimension 1. Equation 3.17 can therefore be rearranged to obtain an expression for the fractal dimension:

$$D = -\frac{\log(N)}{\log(r)} \tag{3.18}$$

It can be recognized that although maps of a country drawn at different scales will differ in their specific details, they have the same generic features. Mandelbrot (1983) called this similarity in a statistical rather than geometrical sense, "statistical self similarity". This can be compared to the exact geometrical similarity of several mathematical constructions such as Koch's triadic island (Mandelbrot 1983).

Mandelbrot (1983) also introduced the concept of "self-affinity". A self-affine surface must be scaled differently in the perpendicular direction to maintain statistical self similarity.

The roughness of rock joints can be compared with the roughness analogy of the coastline. As the scale decreases, smaller and smaller asperities on the rock joint surface will become visible with ultimately variations due to grain size and shape having an effect. Mandelbrot (1985) recognized this similarity. He suggested that rock joint surfaces were self-affine.

Various techniques have been suggested to relate the fractal dimension value to common roughness statistics. Some of these relate the fractal dimension to the JRC (Carr and Warriner 1987; Lee et al. 1990) whilst others relate the fractal dimension to roughness statistics (Turk et al. 1987; Seidel 1993; Xie and Pariseau 1995).

Turk et al. (1987) estimated the relationship between the roughness angle and the fractal dimension by assuming that the overall profile traces of asperities could be represented by an equilateral triangle. Such that $\cos i = (XL)^{1-D}$ where L = direct length, i = average asperity angle, X = constant. However, the value of the constant X is estimated empirically.

Xie and Pariseau (1995) used the generator of the generalized Koch curve to simulate the roughness of a rock joint such that $D = \log 4 / \log\left[2\left(1+\cos\tan^{-1} 2h/L\right)\right]$ where h and L are the average height and base length of the higher order asperities.

Seidel and Haberfield (1995a) developed approximate theoretical relationships between the fractal dimension and the standard deviation of angle of the asperities, s_θ, and the standard deviation of heights, s_h, for self similar profiles. They used a similar approach to Mandelbrot's randomization of the Peano curve. The relationships are only applicable for self similar profiles or self-affine profiles below the cross-over length. They are as follows:

$$s_\theta \approx \cos^{-1}\left(N^{\frac{(1-D)}{D}}\right) \tag{3.19}$$

$$s_h \approx L\sqrt{N^{-2/D} - N^{-2}} \tag{3.20}$$

where D = fractal dimension

L = profile length

N = number of segments of constant length used to traverse the profile using the compass walking method (refer to Section 3.2.3.1)

These relationships rely on the distribution of chord angles being normally distributed. This assumption of normal distribution of chord angles is investigated in Section 3.5.

3.2.3.1 Methods of Estimating Fractal Dimension

Several methods for estimating fractal dimension are available. A brief description of these follows. Unfortunately each method provides a different estimate and as a result has sparked considerable discussion as to the correct approach to the quantification of roughness (eg. Brown 1987; Carr 1989; Huang et al. 1992; Lea Cox and Wang 1993; Hsiung et al. 1995).

Spectral Method

This approach represents the height of the profile at discrete intervals as a finite fourier series. The coefficient of each term in the series is known as its power and a plot of power versus frequency is the power spectrum. The raw power spectrum fluctuates significantly. Using a rectangular analysis window, the fourier transform data with

frequency plot, indicates a leakage of power at frequencies well separated from the main lobe of the spectral window (Bendat and Piersol 1986). To suppress this leakage problem, the data is tapered using various tapering or smoothing techniques. There are many types of smoothing techniques available – eg. cosine taper, Tukey, Daniall, Parzen, Bartlett and Hanning windows. Shirono and Kulatilake (1997) have recommended the use of the Parzen window or Hanning window. They rejected the other methods as they found that they produced negative powers for some frequencies or distorted the roughness profile when incorrect data windows were selected.

The first step in the spectral analysis method is to remove any non-stationarity. This can be done by least squares regression. The next step is to use a tapering method. A fast Fourier transform algorithm is then applied to the profile data to describe it as a sum of sine and cosine waves. Squaring of the amplitude at each frequency and normalizing it with respect to the profile length determines the power spectral density. Averaging of the overlapping profile segments is then conducted to determine an optimal solution. If very little averaging is conducted then the spectral density functions appear erratic whilst excessive averaging will distort the function and lead to an erroneous fractal dimension (Piggott and Elsworth 1995). The final spectral density function is then plotted against the spatial frequency on a log-log plot. The slope, β, can be used to calculate the fractal dimension, D, such that $\beta=2D-5$ (Brown and Scholz 1985). A log.(Amplitude) vs. log.(Frequency) plot can also be used. However, various formulas have been estimated to calculate the fractal dimension from the slope (Power and Tullis, 1991; Berry and Lewis, 1980). The slope, β, of a surface (as distinct from a line) can be estimated by $\beta=2D-8$ (Shirono and Kulatilake 1997).

This method has been recognized as suitable to analyse self-affine surfaces (Brown 1987) although it is not a trivial exercise due to the inaccurate estimates that can be obtained with incorrect inputs. Several problems with this method have been highlighted:

- The smoothing techniques vary among researchers and can be used to produce different answers depending on the window increment used. The non-stationarity of the profiles must be removed to obtain accurate estimates. (Shirono and Kulatilake 1997)
- There are numerous fast fourier transformation algorithms that can be used that produce different answers (Lea Cox and Wang 1993).

- Curve fitting errors can be large due to the non-linearity of the curves (Lea Cox and Wang 1993).
- The erratic nature of the results of the analyses requires careful interpretation (Piggott and Elsworth 1995).
- Variations in the determination of the fractal dimension from the slope of an amplitude plot.
- The high values often obtained for the fractal dimension using this approach compared to others.
- Work by Huang et al. (1992) has suggested that the spectral analysis cannot accurately calculate the fractal dimension when the dimension is close to 1 (line) or 2 (surface).

The large range of fractal dimensions that have been calculated for similar joint profiles has highlighted these problems. For example, Hsiung et al. (1995) calculated the fractal dimension using spectral analysis for the JRC standard profiles and found their values to be less than one (obviously not possible), whilst similar profiles were shown to have fractal dimensions between 0.9 and 1.4 by Carr and Warriner (1987).

Wavelets

In more recent years the use of wavelet analysis has become popular in areas of signal processing and geophysics. This analysis technique has advantages over standard fast fourier transform techniques typically used, as it easily accepts non-stationary data and can preserve the time information that fast fourier transforms lose. The frequency bands of fast fourier transforms are of equal length so that there is the same frequency resolution over every bin in the spectral plot. A wavelet transform however, breaks the original signal into a set of logarithmic rather than equal bands. Therefore it is capable of obtaining detailed high and low frequency information (ie. is able to handle scale effects better). To produce a wavelet transform, an initial waveform must be selected. This wavelet is called the mother wavelet and can be contracted or expanded to 'filter' the data to obtain the scale of interest. The output is therefore highly dependent on the selection of a suitable mother wavelet. Similar problems to those encountered when using fast fourier transforms, such as the correct selection of the mother wavelet and the amount of filtering required, can be envisaged. Although this procedure does address

several weaknesses of the fast fourier transform approach, considerable detailed investigation would be required for its application to rock joint roughness analysis. This is beyond the scope of this current work.

Compass Walking Method

The compass walking method, also known as ruler or divider method, is the oldest method and perhaps the simplest method of determining fractal dimension. The method can be viewed as walking a compass opened a distance r along the profile to estimate its total length. If the profile is self similar, the log of the curve length versus the log of the chord length, r, produces a straight line. The fractal dimension D equals one minus the slope (Mandelbrot 1983).

Mandelbrot (1985) indicated that if the profile was self-affine, the method would only give the correct answer if the chord length was less than the crossover length. Caution must therefore be taken in applying this method.

There have been a considerable number of researchers who have used this approach to estimate the fractal dimension of natural rock joints (eg. Carr 1989; Lee et al. 1990; Wakabayashi and Fukushige 1995). Their results suggest that the fractal dimensions of most natural joint profiles are close to unity using this method.

Several authors have also used the compass method to correlate the fractal dimension with the standard joint roughness profiles (Carr and Warriner 1987, Muralha and Charrua-Graca 1990, Turk et al. 1987, Seidel and Haberfield 1995a). A comparison by Seidel & Haberfield (1995a) of these results indicated some differences. Possible causes of these differences and concerns with the method are highlighted below:

- Errors due to the manual digitisation of the standard curves.
- Many different choices of step length are possible.
- Problems with the remainder section if the step length does not evenly divide into the profile length.
- The approach is not valid for step lengths greater than the crossover length therefore the crossover length must be determined.
- The approach is for a line rather than a surface. The measurement of the fractal dimension of a surface requires the averaging of many profiles and then adding 1 to

the dimension so that its range is between 2 and 3. This approach requires verification.

Similar methods such as the Box method, where various sized squares or circles are used to measure the length of the curve, have the same limitations as the compass method.

The compass method has been extended to include three-dimensional surfaces. This method, called the triangular prism surface area method, is described by Clarke (1986). It involves using equal length line segments or triangles in a grid formation. The height of the asperities on the points of an equally spaced grid, are determined and the elevation from 4 surrounding points so that a triangle is defined. The total approximate area can be calculated for this grid size and successively smaller grid sizes. The fractal dimension can be estimated from the slope of the log-log plot of the areas versus the grid size. The relationship between the area and the perimeter of the lines can also be used to estimate the fractal dimension (known as the area-perimeter relation). These methods were tested by Muralha and Charrua-Graca (1990) on sedimentary rock joints. They highlighted the necessity for some manual operations in the area perimeter method whereas the triangular prism method was quicker as it could be fully computerized. The size of the grid in both methods greatly affected the answer with a finer grid obviously being preferential.

A Fortran program has been used by the author to analyse two-dimensional data using the compass walking method. This program removes non-stationarity by using the least squares line of best fit. It also includes the remainder in the number of chord length calculations as a fraction. It will be used to analyse various joint profiles to obtain both fractal dimension numbers and the standard deviation of chord angle statistics.

Modified Divider Method

This method is similar to the compass walking method in that it divides the profile into equal segment lengths. Unlike the compass walking method however, the segment lengths are determined along the horizontal direction rather than along the actual profile. This alleviates the remainder problem as chord lengths that completely divide into the horizontal length are selected. If the profile is self-similar, the log of the curve length versus the log of the chord length, r, produces a straight line. The fractal dimension D equals one minus the slope (Mandelbrot 1983). This method is only applicable for self

similar profiles or self-affine profiles where the chord length is below the cross-over length.

The modified divider method has been used by several researchers (Brown 1987; Scavia 1996) to analyse natural joint profiles and to generate profiles. Their results indicate that it produces similar results to the compass walking method.

In this current work, a program was written in Visual Basic to analyse two-dimensional rock joint profiles using the divider method.

Brown Method

To analyse the profile as a self-affine curve, Brown (1987) suggested magnifying the vertical axis by a function of the cross over length to produce a new profile that could be analysed using the modified divider method. If the cross over length was not known, as would often be the case, he suggested magnifying the profile height by a factor 10^n until a stable fractal dimension was reached. The modified fractal dimension (d_m) can be obtained from the slope of the log.(chord) versus log.(length) plot. The true fractal dimension is then calculated from Equation 3.21.

$$D = 2-(1/d_m) \tag{3.21}$$

$$= 2-H \tag{3.22}$$

where H = Hurst exponent

The Brown method has been used by Miller et al. (1990), Brown (1995) and Scavia (1996) in their comparison of various methods. Their results indicate that the Brown method produces a higher fractal dimension compared to the modified divider method, with again considerable variation with results from other methods. Vertical magnification of profiles has also been carried out in conjunction with the compass walking method (Miller et al. 1990; Hsiung et al. 1995). Although the fractal dimensions produced using the compass walking method are in a similar range to those produced using the modified divider method, they are not identical.

The Box method can also be modified for use on self-affine curves by using rectangles or ovals to scale differently in the vertical direction.

Although this method addresses the self-affine nature of rock joints, a further source of error is added due to the estimation of a correct vertical scaling parameter.

In this current work, a program was written in Visual Basic to analyse two-dimensional rock joint profiles using the Brown method. This method is based on the divider method.

Slit-Island Method

This method involves slicing the surface horizontally to create surface contours. If the slice is viewed at the water level, then the shapes above the water level are viewed as islands whilst below the water level they are lakes. The perimeter and area of each island is measured and plotted on a log.-log. plot of perimeter versus area. The fractal dimension is calculated as 2/slope (Lea Cox and Wang 1993).

This approach has the advantage that it analyses surfaces rather than profiles. However, it does have a problem when there are "lakes within islands" or "islands within lakes" as shown in Figure 3.4.

Figure 3.4: Slit-Island method showing "island within lakes"

Variogram Method

This method involves using a variogram or semi-variogram to characterise the variability of the asperity heights over the surface. The variogram function can be defined as the average of the sum of the squares of the profile height differences as defined by Equation 3.23.

$$\gamma(h) = \frac{1}{2N}\sum_{i-1}^{N}\left[Z(x_i) - Z(x_i + h)\right]^2 \qquad (3.23)$$

Where $Z(x_i)$ = the height of the profile at location x_i

$Z(x_i + h)$ = the height of the profile at location $x_i + h$

N = the number of observations

h = the distance between two adjacent points

The fractal dimension is determined as 2-(slope/2) of the log.(variogram function) versus log.(lag interval) plot (Hsiung et al. 1995).

This method is suitable for self-affine profiles but has two main difficulties:

- correct choice of sampling interval
- correct estimation of the slope

In this current work, a program was written in Visual Basic to analyse several two-dimensional rock joint profiles using the variogram method.

Roughness-Length (RMS) Method

This method was proposed by Malinverno (1990) to measure the fractal dimension of self-affine profiles. The profile roughness is measured as the Root Mean Square (*RMS*) value of the residuals on a linear trend fitted to the sample points in a window of length w. Detrending is required to remove the effects of large wavelengths on small samples. The *RMS* is therefore calculated using relationship (3.24):

$$RMS(w) = \frac{1}{n_w} \sum_{i=1}^{n_w} \sqrt{\frac{1}{m_i - 2} \sum_{j \in w_i} (z_j - \bar{z})^2} \qquad (3.24)$$

where n_w = total number of windows of length w

m_i = number of points

z_j = residuals on the trend

$\bar{z}$ = mean residual in the i^{th} window w_j

The Hurst exponent, H, is measured from the slope of the log.-log. plot of roughness of the input series measured on a window length w (ie. *RMS*) versus w. In the example shown in Figure 3.5, H=0.6. The fractal dimension is calculated from D=2-H. The

crossover length is given as the length where the window length equalling the RMS roughness intersects the RMS roughness as shown in Figure 3.5.

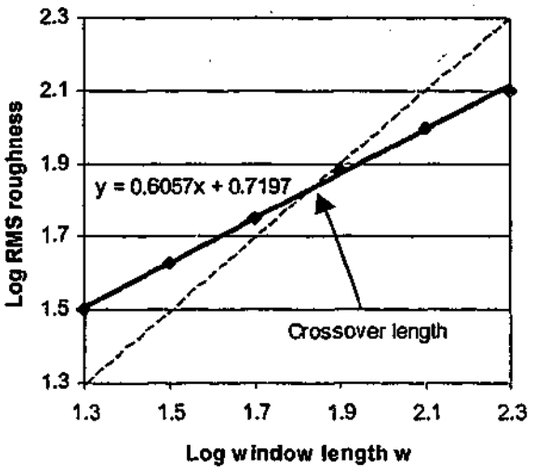

Figure 3.5: Example of roughness – length method

The main advantage of this method over the spectral method is that it may be applied to a series that is not uniformly spaced (Malinverno 1990). Results by Hsiung et al. (1995), Kulatilake and Um (1999) and Malinverno (1990) have indicated a large variation in results due to some of the problems listed below.

- Errors due to detrending.
- Inaccuracies in measuring the slope.
- Data densities of greater than or equal to 5.1 points per unit length are required.
- Window values between 2.5% and 10% of the profile length are required.

Line Scaling Method

This method introduced by Matsushita and Ouchi (1989) can be applied to self-affine profiles. It divides a segment of the joint profile into equal step sizes, a_o, (such that the segment length, L, equals a_o times the number of steps N) and using the Cartesian co-ordinates (x_i,y_i) of these points, computes the standard deviations of x and y (denoted by s_x and s_y) as shown in Equations 3.25 and 3.26 . The procedure is repeated for different random segments of the joint profile so that data is generated between the standard deviation and the segment length, L. These relationships are shown in Equations 3.27

and 3.28. By eliminating the length term the relationship between standard deviation of x and y as shown in Equation 3.29 is obtained.

$$s_x = \left\{ \frac{1}{n} \sum_{i=0}^{i=n} (x_i - \bar{x})^2 \right\}^{1/2} \tag{3.25}$$

$$s_y = \left\{ \frac{1}{n} \sum_{i=0}^{i=n} (y_i - \bar{y})^2 \right\}^{1/2} \tag{3.26}$$

$$s_x = C_y L^{v_x} \tag{3.27}$$

$$s_y = C_x L^{v_y} \tag{3.28}$$

$$s_y = C s_x^H \tag{3.29}$$

where $\bar{x}, \bar{y}$ = sample means for x_i and y_i.

C_x, C_y constants (can be estimated from log.-log. plots)

v_x, v_y are exponents (can be estimated from log.-log. plots)

H = Hurst exponent = v_y/v_x

C = constant = $C_y/(C_x)^H$

This method can be used to indicate whether a profile is self similar or self-affine.

Kulatilake et al. (1997) tested this method on several artificial and natural joint roughness profiles. They found that initial preprocessing to remove global trends was required and that the method was sensitive to the step interval chosen.

3.2.3.2 Fractal Analysis

Several natural basalt rock joints were collected from the Deer Park Quarry, near Melbourne, Australia and several natural siltstone rock joints were collected from the Transfield Obayashi City Link Project Burnley site, Melbourne (for properties refer to chapter 5). The surface roughness profiles of four of these joints were measured using the Monash Socket-Pro and analysed using two self similar fractal analysis methods – the compass walking and divider methods; and two self-affine fractal analysis methods – the variogram and brown methods (using divider method). Figure 3.6 shows the profiles analysed. Visually the siltstone joint 5e is the smoothest followed by the siltstone

bedding joint 1h followed by the basalt joint 4e with the basalt joint 1j appearing visually the roughest.

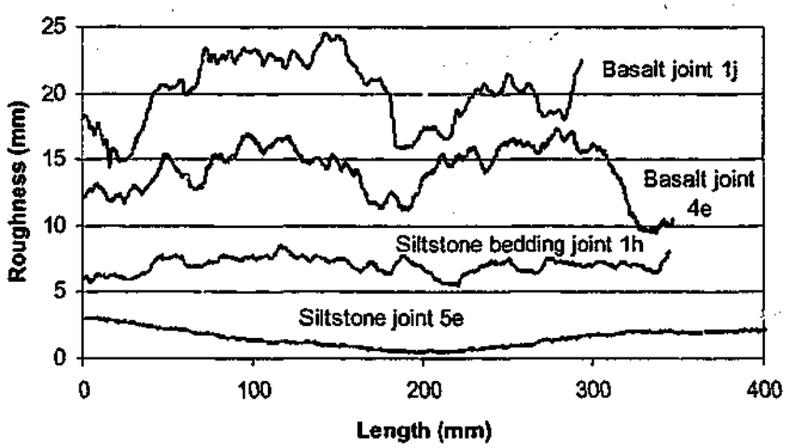

Figure 3.6: Diagram of analysed profiles

Table 3.1 shows the results of the analysis using the four methods. The profiles have been listed from roughest to smoothest as assessed visually. As can be seen, the two self similar approaches (Compass Walking and Divider methods) although not producing identical answers, are similar. They also consistently rank the profiles in order of increasing roughness as visually assessed. The self-affine fractal analysis methods produce considerably larger fractal dimensions given that the possible range must be between 1 and 2. Of most concern however, is that the self-affine methods do not rank the profiles in a consistent order of roughness. Their ranking also does not agree with the ranking assessed visually.

Table 3.1: Fractal Dimension calculated using various techniques

Joint Surface	Profile	Compass Walking Method	Divider Method	Variogram Method	Brown Method
Basalt joint 1a	j	1.0079	1.017	1.325	1.223
Basalt joint 4	e	1.0078	1.017	1.312	1.363
Siltstone bedding joint 1	h	1.0027	1.0059	1.369	1.391
Siltstone joint 5	e	1.0014	1.0038	1.292	1.12

The use of fractal methods to analyse data contains many problems due to variations in preprocessing and filtering techniques, interpretation of graphical outputs and concerns over stationary and non-stationary data. The inconsistency in results obtained by other researchers and the inability of various methods to even consistently rank joint profiles in increasing roughness, has led to the author's belief that fractal methods contain too many pitfalls for everyday use.

3.2.4 Statistical Representation

Due to the difficulties in obtaining accurate and consistent representations of joint roughness using either the JRC, fractal theory or any of the other statistical methods, the author has chosen to represent the joint surface roughness by a simple statistical relationship between standard deviation of chord angle and chord length (e.g. Haberfield and Seidel, 1999). This simple relationship can be easily determined by using the compass walking method over a range of chord lengths. Any non-stationarity is removed from the profile by a mathematical process such as least squares regression. This effectively makes the overall profile horizontal. A compass is used to step across the profile and the points of intersection are joined with a straight line. The profile is therefore approximated by a profile of equal chord lengths. The chord length is varied to accommodate different wavelengths of roughness. Small chord lengths accommodate small wavelengths of roughness whilst large chord lengths accommodate long wavelengths of roughness. For each chord length selected, the angle of inclination of each chord is measured and the standard deviation of the chord angles calculated. As the profile is horizontal the positive and negative chord angles have a mean of zero. The relationship between the standard deviation of chord angle and the chord length is then used to represent the profile roughness.

This method is shown diagrammatically in Figure 3.7. Digitisation of the profile has been done at several different chord lengths. The smaller the digitising length, the smaller the asperities that are captured. The graphical output shown indicates that when smaller asperities are included a higher standard deviation of angle is calculated. This is to be expected, as larger digitising intervals bridge many small asperities with a single chord. The many positive and negative angles of the bridged asperities are replaced by a single asperity angle. This decreases the standard deviation of chord angle at the larger digitising lengths.

1. **Digitising at different chord lengths**

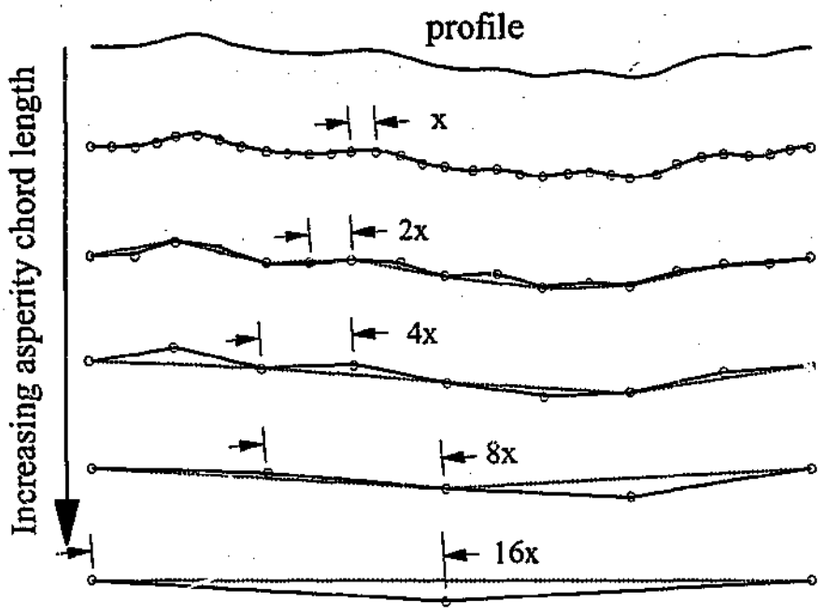

2. **The asperity chord angles are measured for each digitised chord length**

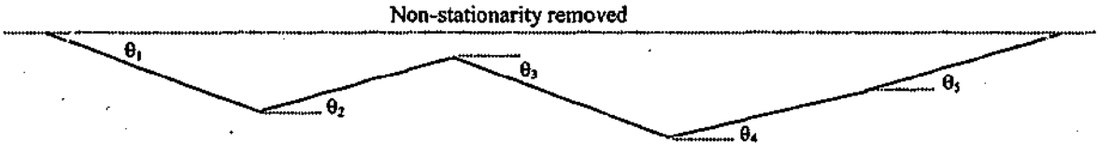

3. **The mean chord angle and then the standard deviation of chord angle is calculated for each digitised chord length**

4. **The standard deviation of chord angle calculated for each digitised chord length can be represented graphically**

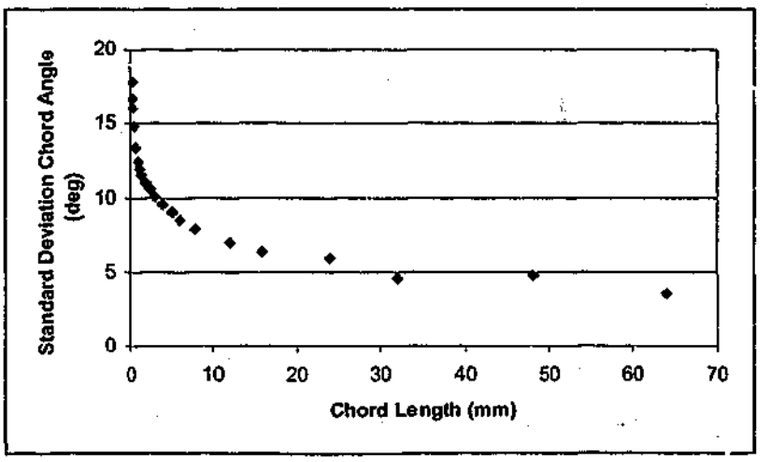

Figure 3.7: Development of standard deviation of chord angle statistics for a profile

The relationship between the standard deviation of chord angle and the chord length can be represented by a power function or exponential function (refer to section 3.4.4).

A downfall of this method, along with most of the described methods, is that it will only capture the statistics of the joint profile to a portion of the sample available. For example, a joint profile 500mm long with a global wavelength of roughness of 250mm will not be captured in this method as the sample size of statistics generated for the longer chord lengths is insufficient to statistically use to represent the profile. This can be overcome if longer samples are used.

3.3 Anisotropic Surface Roughness

An anisotropic surface has some physical property that varies with direction. If surface roughness is anisotropic, then the shear behaviour of the joint in one direction will not necessarily match the shear behaviour in another direction. This obviously has significant repercussions on developing a shear joint model capable of predicting shear response.

Seidel (1993) through laboratory testing of concrete / rock joints containing simple two-dimensional irregular triangular profiles showed that statistically similar profiles produced similar shear responses even if not geometrically identical. This would suggest that at least for simple two-dimensional triangular profiles, the profile could be tested in either direction providing the statistics were the same in both directions.

Kulatilake et al. (1995) and Kulatilake et al. (1998) conducted statistical and laboratory tests on 100-153cm diameter replicas of natural slate, sandstone and tuff joints made from plaster of Paris, sand and water. These tests indicated differences in the peak shear values between the forward and backward shearing direction. This was due to the non-stationarity trend (inclination / declination) angle on the samples. They also found in the three rock samples tested, that they were anisotropic in the six directions tested. Gentier et al. (2000), also performed tests in four directions on granite sample replicas and found that the shear results were dependent on the shear direction.

Xie et al. (1999) investigated fractal anisotropy on sandstone and mudstone 20 x 20 mm^2 samples using the divider method (refer to section 3.2.3.1). They found that under a

chord length of 1.0mm the samples were anisotropic but above this chord length the scans in four directions were similar.

The very small scale of the samples used for these previous investigations and the chord lengths investigated, mean that differences in the crystal structure of the sample in different planes may be being measured rather than the larger scale roughness of the surface. The scales of interest being tested for this current work are considerably larger.

3.3.1 Anisotropy of joint samples

A visual comparison and statistical test for anisotropy was conducted on several rock samples used in the current work. The statistical and visual comparisons were conducted in two perpendicular directions on siltstone and basalt joint samples. The siltstone natural joint samples were obtained from the Burnley tunnel site of the Melbourne City Link project, Victoria. The Slightly Weathered to Fresh samples of bedding joints and joints near perpendicular to bedding, had varying amounts of pyrite and carbonaceous coating (refer to Section 5.2.3 for siltstone rock properties). The basalt natural joint samples were obtained from the Boral quarry in Deer Park, Victoria. The Highly to Moderately Weathered and Moderately Weathered samples had some limonite or carbonaceous coating (refer to Section 5.2.4 for basalt rock properties).

Using the Monash Socket-Pro, two-dimensional profiles were taken of the longest length on the selected surfaces at 10mm or 20mm intervals across the samples. These measurements were then repeated in the direction perpendicular to the original scans. These profiles were compared visually. Using the compass walking method, the standard deviation of chord angle statistics for different chord lengths were produced. Example siltstone and basalt surfaces are shown in Figures 3.8 and 3.9 respectively. The correlation coefficients, between the mean statistics for the two directions have been calculated and are listed in Table 3.2. The two-dimensional profiles together with their three-dimensional surfaces and statistics are included in Appendix A.

Visual comparison of the 2 dimensional profiles in the 2 directions on the siltstone samples did not indicate significant anisotropy at the scale investigated. The basalt samples showed some visual signs of differences in roughness particularly in sample 1a. The statistical plots indicated small variations between the two directions in the siltstone samples with typically up to 1^{o} variation in the standard deviation of chord angle between

chord lengths of 15 and 30mm. The difference was greater with the basalt samples with one sample showing up to 5° difference in the standard deviation of chord angle plots above a 2mm chord length and the other sample up to 2° difference. These results indicate that on the samples to be tested for this current work at the scale of interest, the effects of anisotropy, although present, are not significant with the siltstone samples (sedimentary) but may be significant with the basalt samples (igneous).

Table 3.2: Correlation Coefficient for Mean Standard Deviation of Chord Angle Statistics in Perpendicular Directions.

BLOCK	Correlation Coefficient of Mean Statistics in Perpendicular Directions
Siltstone 1 – bedding joint	0.939
Siltstone 1 – joint	0.995
Siltstone 2 – bedding joint	0.996
Basalt 1a –joint	0.996
Basalt 4 – joint	0.996

3.4 Generation of Roughness Profiles

It is useful when investigating and testing methods of quantifying joint roughness, to be able to generate profiles of known statistics. Several methods have been suggested in the literature. These methods are based on either using spectral synthesis techniques or various modifications of the midpoint displacement method.

3.4.1 Spectral Synthesis

This method described by Saupe (1988) uses spectral synthesis to produce roughness profiles using the inverse Fourier transformation. A series of real random variables A_k and B_k are generated under the constraint shown in Equation 3.30.

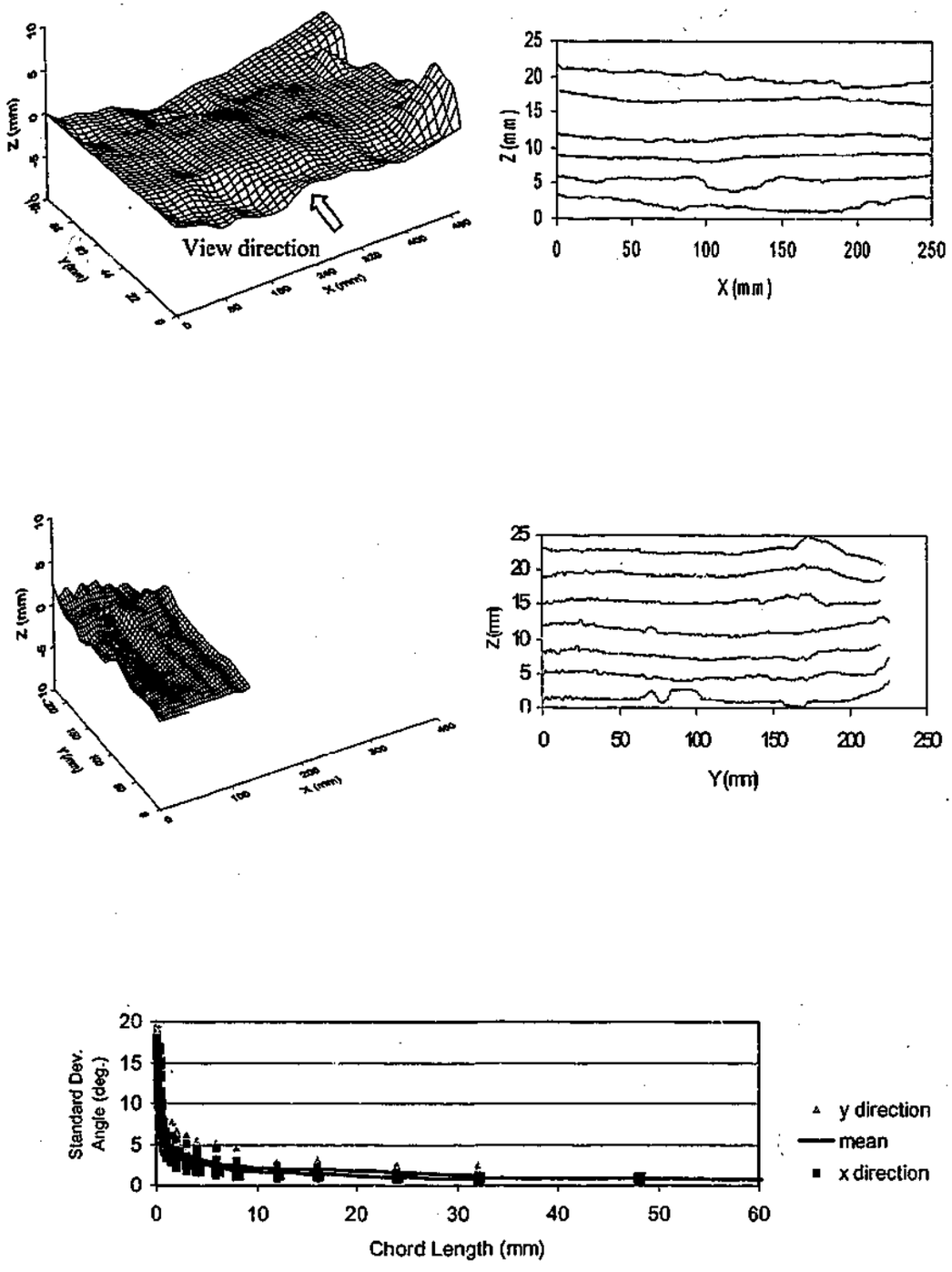

Figure 3.8: Comparison between siltstone profiles in perpendicular directions

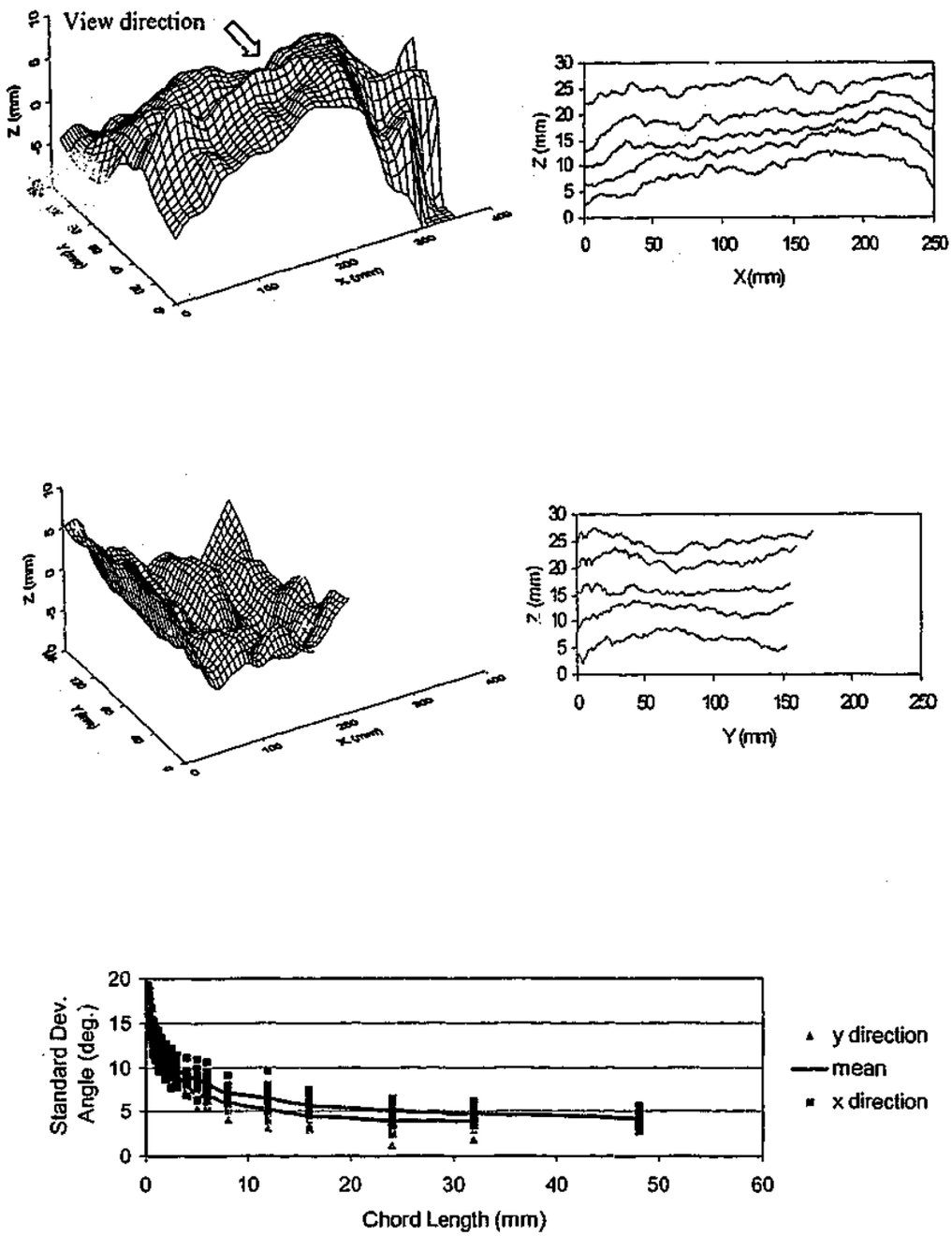

Figure 3.9: Comparison between basalt profiles in perpendicular directions

$$E\left(A_k^2 + B_k^2\right) \propto \frac{1}{k^{\beta}} \tag{3.30}$$

where k = frequency

β = spectral exponent = 2*Hurst exponent+1

$A_k = k^{-\frac{\beta}{2}}(Gauss)\cos\left(2\pi(Rand)\right)$ = real part

$B_k = k^{-\frac{\beta}{2}}x(Gauss)\sin\left(2\pi(Rand)\right)$ = imaginary part

Gauss = Gaussian random variable with mean zero

Rand = uniform random variable in interval [0,1]

The inverse Fourier transform can then be computed to obtain X by using Equation 3.31.

$$\overline{X}(x) = \sum_{k=1}^{N/2}\left(A_k \cos kx + B_k \sin kx\right) \tag{3.31}$$

This method can be used to generate two-dimensional profiles or three-dimensional surfaces (Saupe 1988). In this current work, a program was written in HPVee (Helfel 1988) to generate two-dimensional profiles using this method.

Fox (1987) also suggests an algorithm to generate profiles using spectral synthesis. This method differs from Saupes's method in that the random numbers are normalized to vary between π and $-\pi$ compared to 0 and 2π. The frequency, k, is also normalized to the profile length in the Fox method and not in the Saupe method. This last variation produces a large scaling difference in the resulting profile. Fox's program, written in Pascal, was run to generate two-dimensional profiles using this method. As could be expected there were large scaling differences between the profiles produced using Fox's program and that written using Saupe's method.

The spectral method has one main problem in that Fourier transforms generate periodic samples. This means that it is necessary to generate very large data files but only use a portion of the data points (Saupe 1988).

3.4.2 Random Midpoint Displacement

Mandelbrot (1983) described the technique of midpoint displacement. The method involves dividing a chord of any length into a number of segments, N, and displacing them perpendicularly at randomly chosen heights or angles. This process is then repeated a number of times until the desired fractal profile is achieved.

Seidel (1993) suggested a midpoint displacement according to a Gaussian distribution. He showed that a Gaussian distribution of roughness heights was dependent on the fractal dimension and number of segments (as discussed in Section 3.2.3). This could be related to the standard deviation of chord angles. Therefore a profile of a predetermined fractal dimension could be generated by input of the standard deviation of chord angle and the number of segments. This would generate a self similar profile.

To lessen the effect of the initial displacement on the overall profile, Seidel modified this method by initially deflecting a series of equal length chords by normally distributed angles generated randomly from a normal distribution with a specified standard deviation of angle. The generated profile is then rotated so that it starts and finishes at zero to remove the non-stationarity. As the profile is long in relation to the chosen chord length, this rotation only has a very small influence on the large scale roughness angles of the profile. The midpoint displacement method is then used on each of these chords. This method is shown diagrammatically in Figure 3.10. The initial chord length is viewed as the crossover length. This method can also be used to generate overlying wavelengths in the profile.

For this current work, a Visual Basic program was written to generate fractal profiles using Seidel's modified midpoint displacement method.

Saupe (1988) and Fournier et al. (1982) have suggested a midpoint displacement method that takes into account the self-affine nature of a rock joint profile. They require the input of the Hurst exponent and the initial standard deviation of asperity height. These methods calculate the fractal dimension using Equation (3.22). For this current work, a Visual Basic program was written to generate profiles using the method suggested by Saupe (1988). Based on work by Seidel and Haberfield (1995a), the fractal dimension is influenced by the standard deviation of chord angle. The profiles produced by this method therefore appear dependent on the initial chosen standard deviation of asperity height.

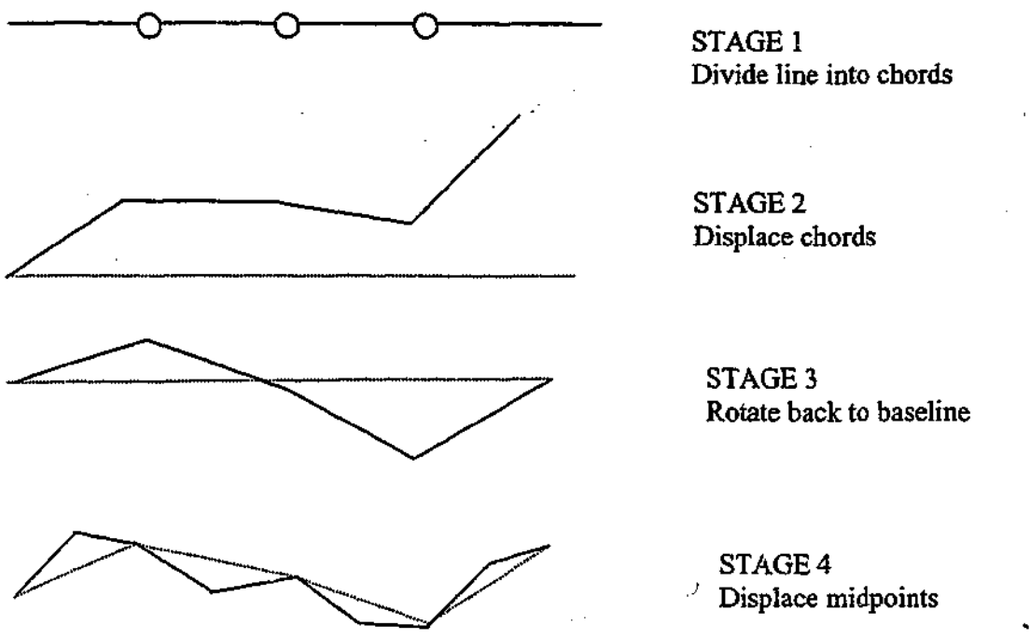

Figure 3.10: Modified Midpoint Displacement Method

3.4.3 Successive Random Additions

This method is very similar to the Midpoint Displacement Method. A standard deviation of asperity height is selected to generate a series of lengths that are used to displace each midpoint. However, to remove non-stationarity problems, all of the intersecting chords along the profile are displaced by a height taken from the series and not just the midpoint (Voss 1985; Saupe 1988).

3.4.4 Modified Midpoint Displacement Method using a Power or Logarithmic function

Whilst attempting to generate roughness profiles using the various methods described previously, several problems with the methods were encountered. The spectral method required the use of complicated fast fourier algorithms, generating large volumes of data that were not used and did not consistently capture the longer and shorter wavelengths. The midpoint displacement method as suggested by Saupe (1988) failed to generate the desired statistics as the dependence on the initial standard deviation of chord angle selected was not considered. The modified midpoint displacement method as suggested

by Seidel (1993) did not consistently capture both the longer wavelength roughness and the shorter wavelength roughness.

As a result a new method of generating profiles was developed. This method uses statistics from real rock joint surfaces to generate profiles. This allows an existing surface to be regenerated. Details of the method are as follows:

- To obtain the statistics of the joint surface, several profiles of the surface are taken. At several chord lengths the standard deviation of chord angle are calculated for each profile using the Compass Walking Method to divide the profile into different chord lengths. By averaging the standard deviation of angle at each chord length of all the profiles, a mean standard deviation of chord angle for each chord length is calculated.
- By profiling several natural siltstone and basalt joints obtained in Melbourne (details discussed in Chapter 5) using the Monash Socket-Pro, it was found that most of the natural joint surfaces were well described by a power function. However, several were better described by a natural logarithmic function. A complete set of graphs showing either a power or logarithmic description of the mean statistics, are shown in Appendix E. The mean statistics of a basalt joint and 2 siltstone joints are shown in Figure 3.11 together with a power function approximation of each.
- These graphs (and the graphs included in Appendix E) indicate that for the samples tested at longer wavelengths (typically around 20-30mm) the standard deviation of chord angle becomes relatively constant. This enables the surface to be regenerated via the Modified Midpoint Displacement method (refer to section 3.4.2). The chord length at which the standard deviation of angle becomes relatively constant is selected and input as the initial deflected chord length in the Modified Midpoint Displacement method with the corresponding standard deviation of chord angle used to determine the chord angles.
- After non-stationarity is removed, the Equation describing the mean standard deviation of chord angle statistics is used to determine the standard deviation of chord angle to be used with each new chord length as the Midpoint Displacement Method is implemented.

This method captures all the roughness wavelengths up to approximately 25% of the sample length. This length corresponds to the maximum chord length analysed to determine the standard deviation of chord angle statistics.

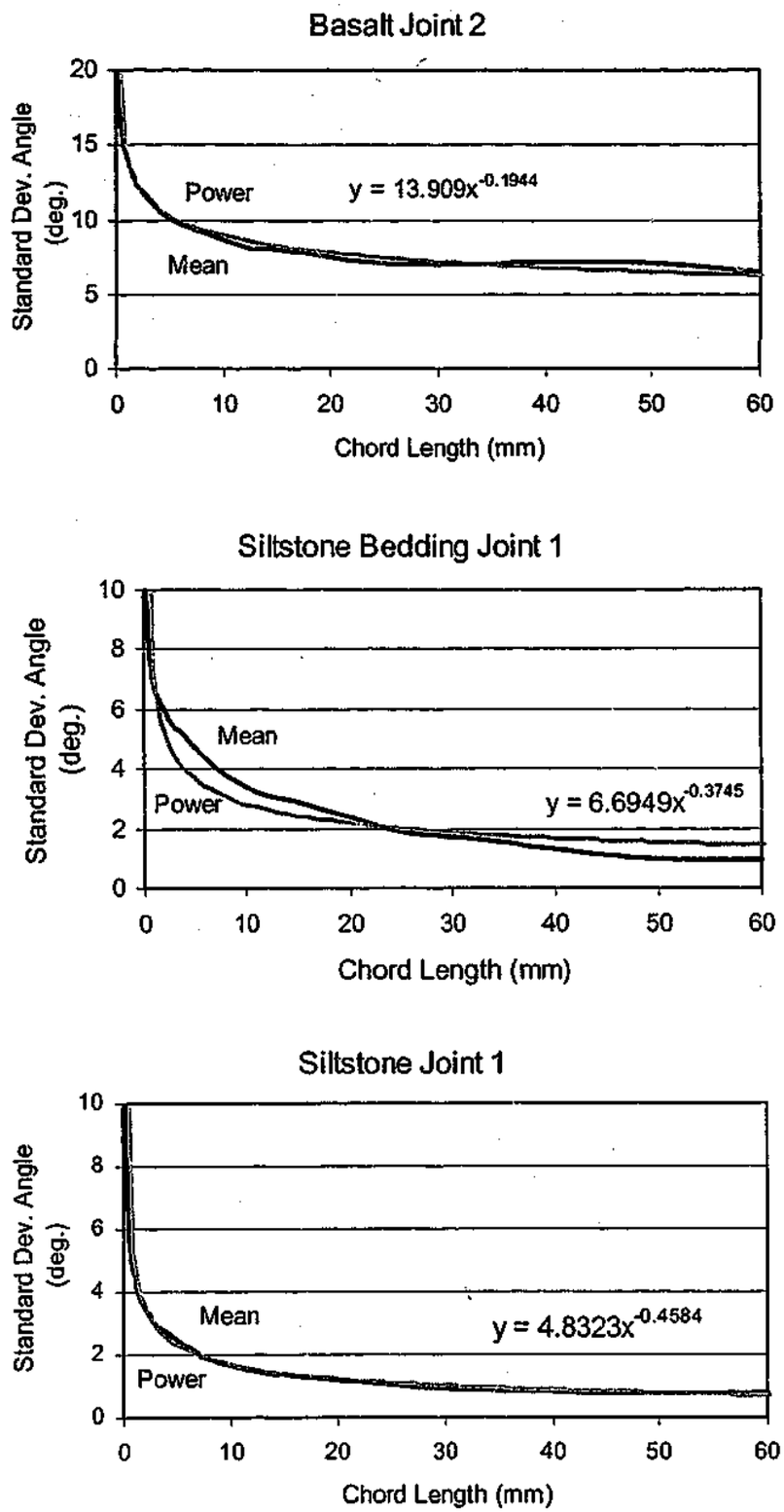

Figure 3.11: Mathematical representation of the mean curve of standard deviation of chord angles of the natural joint surfaces

This process is illustrated by regenerating siltstone joint 1 (shown in Figure 3.11). Below a chord length of 20mm the mean standard deviation of chord angle statistics of this surface are approximately 1°. To generate a profile 460mm in length, twenty-three 20mm chords are deflected by angles that are selected according to a Gaussian distribution with a standard deviation of 1° and mean of 0°. After this generated profile has been adjusted to remove non-stationarity, the power Equation, *Standard Dev. Angle* = 4.8323 x $(chord\ length)^{-0.4584}$, is used to select the standard deviation of chord angle to be used at each midpoint generation. For example, at the first midpoint generation, the 20mm chords are halved to a new chord length of 10mm. The midpoint will therefore be rotated anticlockwise by an angle determined using a Gaussian distribution with a standard deviation of angle = 1.68° and a mean = 0°. This midpoint procedure is repeated until the desired final chord length is achieved.

Several example reproductions at final chord lengths of approximately 3-4mm are compared with a centre profile from the original split surface in Figure 3.12. The surface's standard deviation of chord angle statistical plots are also shown. Several plots of natural siltstone and basalt joint standard deviation of chord angle statistics and the statistics of a reproduced surface are included in Appendix E.

This method appears to successfully regenerate a statistically similar profile that falls generally within the statistics of the surface. However, as discussed in Section 3.2.4 this may not represent roughness wavelengths greater than that statistically analysed, in this case 60mm.

This statistical regeneration method will be further verified in Chapter 7 on artificial rock joints and with some laboratory testing.

3.5 Distribution of Asperity Chord Angles

If a rough joint profile is to be described by a series of chord angles (or the standard deviation of these chord angles), then it is of interest to know the distribution of these chord angles. Likewise in all of the generation methods it is necessary to determine an appropriate distribution to generate asperity angles or heights. As the modified midpoint displacement method using a power or logarithmic function was used to generate profiles in this current work, an appropriate distribution to select asperity chord angles is required.

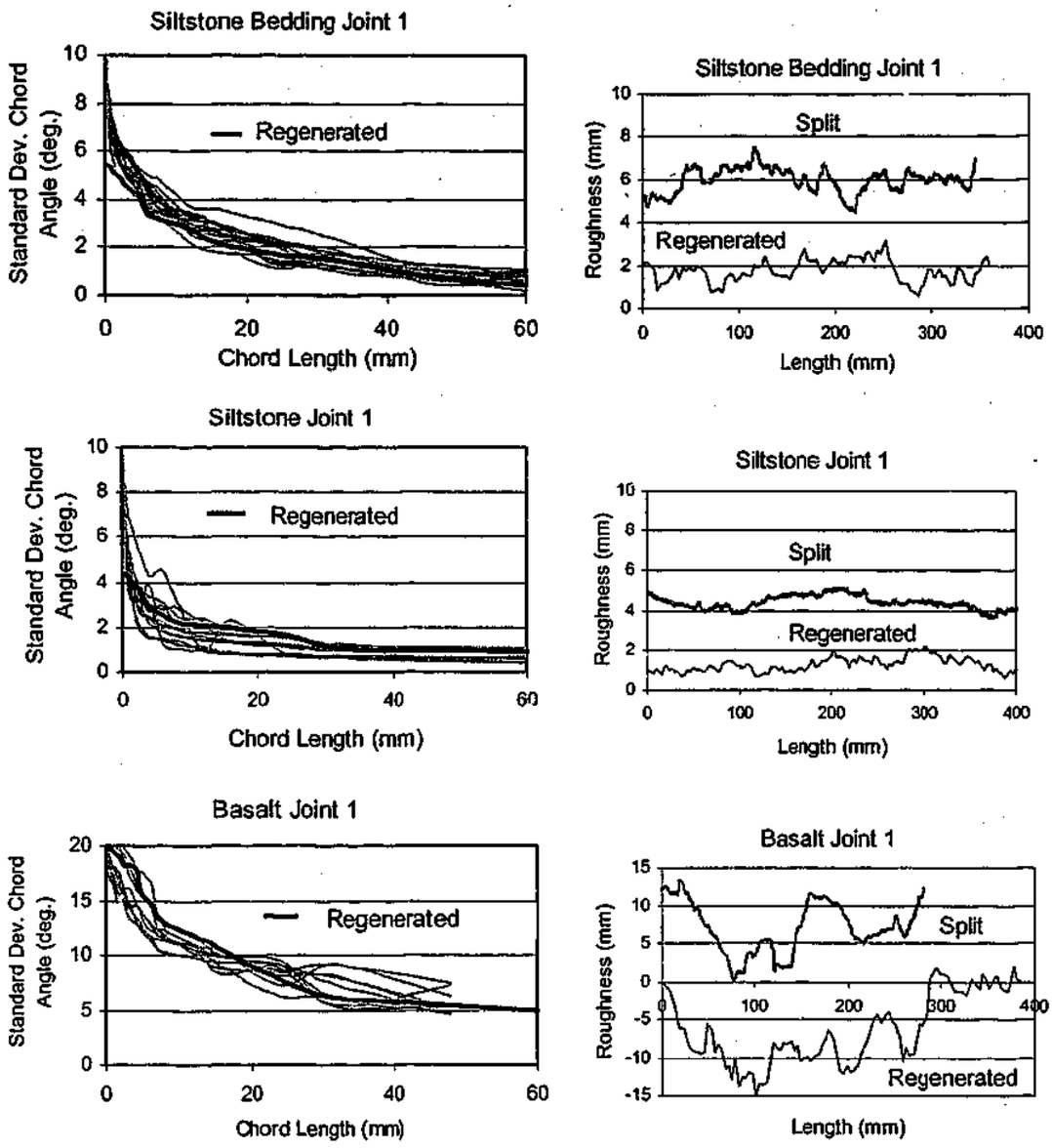

Figure 3.12: Comparison of Regenerated profiles and the original joint surfaces

Reeves (1985) in his quantification of rock surface roughness, assumed a Gaussian distribution function for surface asperity heights. He believed that this was a reasonable assumption for natural rock surfaces, although manufactured surfaces may have a skewed distribution. Similarly Seidel (1993) based his relationships between standard deviation of asperity height and fractal dimension on a Gaussian distribution of chord angles. Lanaro (2000) demonstrated that the standard deviation of the asperity heights for his samples had a Gaussian distribution.

Fournier et al. (1982) used a Gaussian distribution to generate profiles using the midpoint displacement method. Several other researchers have used Fournier's method to generate profiles (Brown 1987; Kulatilake and Um 1997; Shirono and Kulatilake 1997).

Digitised joint profiles from natural siltstone and basalt joints (refer to properties in Chapter 5) were analysed to verify whether a Gaussian distribution was appropriate. The results of this analysis are presented in Appendix E. Initially tests were conducted with distributions grouped in 5° intervals at several chord lengths. These distributions showed excellent bell shaped distributions that centre on a zero mean to chord lengths of approximately 2mm. For longer chord lengths, the distribution was not as well defined due predominantly to the small sample size. An example distribution taken from a siltstone bedding joint is shown in Figure 3.13 at 0.14mm, 0.5mm, 2.0mm chords and 8.0mm chord lengths. For greater accuracy, several distributions were grouped in intervals of 0.1°.. With this interval, Gaussian distribution checks could typically be done to a chord length of approximately 6-8.0mm. Beyond this chord length, due to the size of the samples, the number of values in each frequency interval was again too small to use accurately. The distributions again appeared to be normally distributed especially at the smaller chord lengths. The distributions were less well defined as the sample size became smaller. An example distribution taken from a siltstone bedding joint is shown in Figure 3.14.

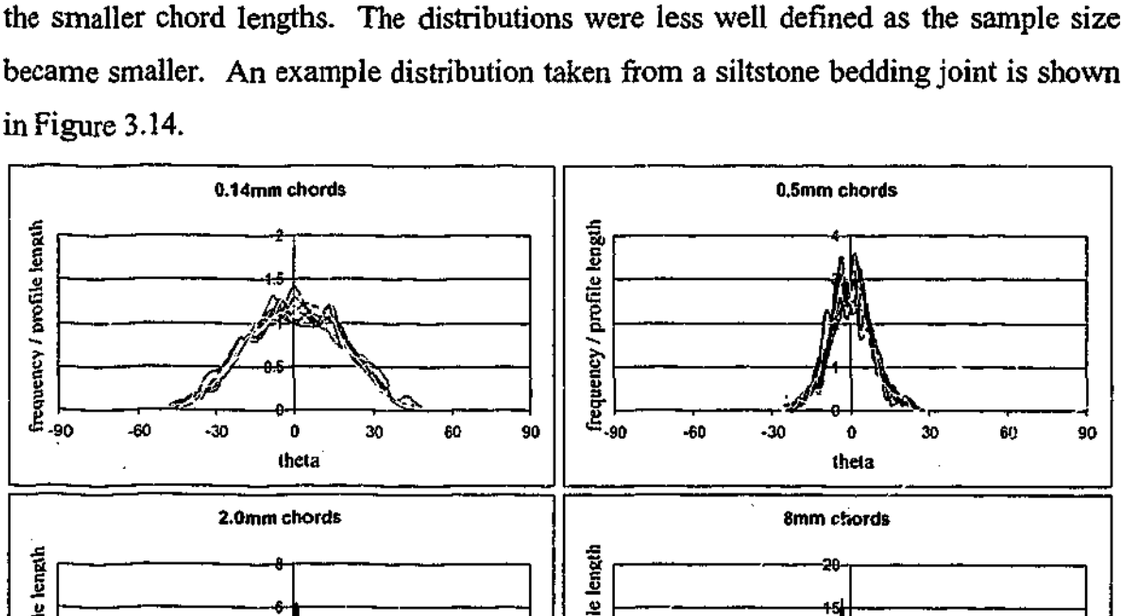

Figure 3.13: Siltstone Bedding Joint – all profiles at 5° bins

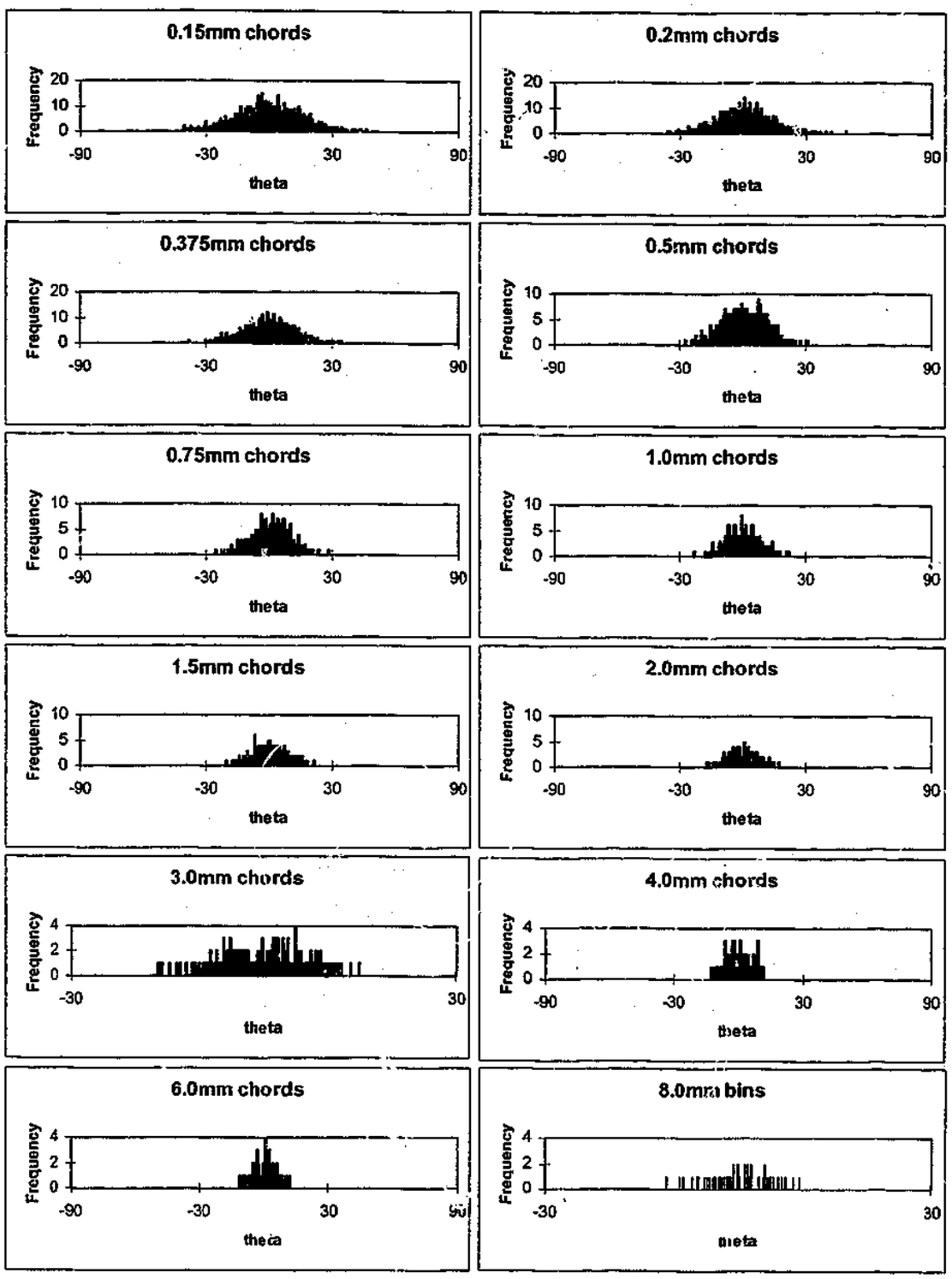

Figure 3.14: Siltstone Bedding Joint – all profiles at 0.1° bins

Based on these results it appears likely that the assumption of a Gaussian distribution is valid. Very large samples would be required to further validate this assumption at longer chord lengths.

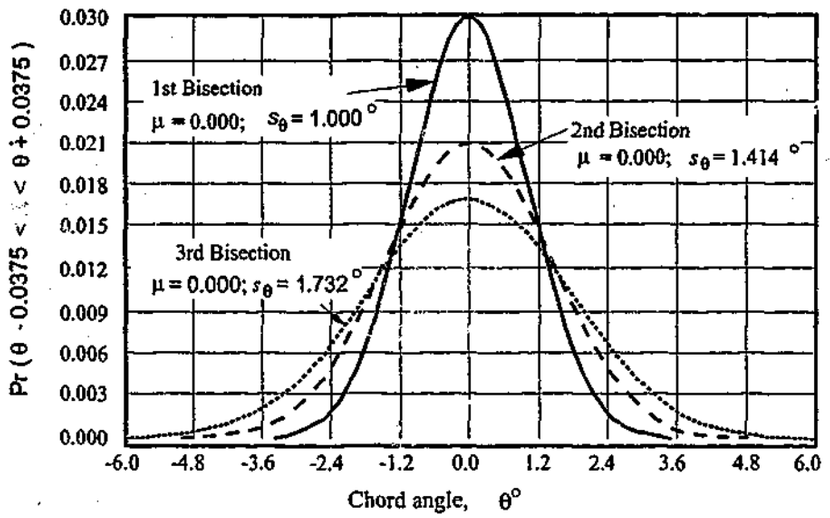

Figure 3.15: Chord angle distribution for successive chord bisections (after Seidel and Haberfield 1995a)

In the midpoint generation technique, each new bisection superimposes a new Gaussian distribution on the previous Gaussian distribution. Seidel and Haberfield (1995a) showed that the superposition of several bisections produced a net Gaussian distribution. However the standard deviation of chord angle increases with each successive bisection. This is shown in Figure 3.15 and can be described by the Equation 3.32.

$$s_{\theta,k} = \sqrt{k} s_{\theta,1} \tag{3.32}$$

where: k = bisection number

$s_{\theta,k}$ = standard deviation of chord angle for the k^{th} bisection

3.6 Summary

To analyse the shear response of a rock joint, it is first necessary to quantify the joint roughness.

There are several roughness measurement techniques that can be used to reproduce information about the surface. Recently the use of laser profilometry has become the most popular due to the high level of detail that can be obtained in only a few minutes of work. The current project uses a laser profilometer that was designed to measure pile socket roughness. Considering that the spot diameter is 3mm, the precision of this device can be considered to be approximately 3mm. However, calibration tests conducted using the laser profilometer on a machined stepped profile indicated a greater accuracy of approximately ±0.75mm. Laser readings were taken at approximately 0.1mm intervals for this current research to increase the confidence in the profile.

Once a digitised profile is obtained there are many techniques available to describe the roughness in quantifiable terms. These techniques have been shown in this research and by others to produce varying and inconsistent results. Therefore, for this project, joint roughness is quantified using the standard deviation of chord angles for a range of chord lengths. The standard deviation of chord angles is calculated using the compass walking method. The relationship between the standard deviation of chord angles and chord length can be presented graphically or via a power or logarithmic function. This approach is able to fully quantify the roughness over a range of scales, is independent on the fractal nature of the profile (self similar or self-affine) and can be used to mathematically regenerate the profile using the Modified Midpoint Displacement Method.

As a tool for analysis it is often useful to be able to generate profiles of known statistics. Several approaches have been proposed by various authors all of which have been shown to have significant problems. A new approach combining the Modified Midpoint Displacement method with a mathematical Equation of the standard deviation of chord angles for various chord lengths has been adopted in this research. This approach has been shown to adequately represent all wavelengths of joint roughness. In the statistical replication of an existing joint profile, the method is only limited by the length of the digitised profile.

In this current work, several generated profiles were cut into rock samples. Both the random midpoint displacement method (refer to section 3.4.3) and the modified midpoint displacement method using a power or logarithmic function (refer to section 3.4.4) were used. The joints formed were then tested in direct shear to provide data on the validity of representing three-dimensional roughness with two-dimensional profiles. The results of this testing are presented in Chapter 7.

4.0 HISTORICAL REVIEW OF ROCK JOINT MODELS

It is widely accepted that to determine the strength of a rock mass an understanding of the complex behaviour of the individual rock joints is required. During the past 3 decades, extensive research has been conducted on the behaviour of rock joints under the application of a shear load. Much of this work has centred on empirical approaches. A summary of the more significant aspects of this research are given in the following sections.

A detailed outline of the theoretical approach being developed at Monash University is discussed in Section 4.5. This approach was initially developed for concrete / rock joints on pile rock sockets. Most of this work therefore concentrated on the joint response under constant normal stiffness conditions. Initial investigations (Fleuter 1997; Haberfield and Seidel 1999) have highlighted the similarity between this approach and the behaviour of natural rock joints. The aim of this current work is to develop a theoretically based model to predict the performance of three-dimensional rock joints in direct shear. Through adopting a theoretical basis, the model should be applicable for a range of joint roughness, rock types and boundary conditions.

4.1 Patton's Bilinear Model

According to the classical law of Amonton, the shear resistance, τ, is related to the normal stress, σ_n, and the coefficient of friction, μ, by the following relationship:

$$\tau = \mu\sigma_n \qquad (4.1)$$

and $\mu = \tan\phi$ where ϕ=friction angle of the material

Patton (1966) investigated the mechanism of shear failure of rock joints by inspecting over 300 slopes in the Rocky Mountains, performing laboratory sliding friction tests and conducting direct shear tests on synthetic rock profiles. This work is significant in that it highlights the importance of asperities in the shearing resistance of the rock joint and adds to the classical law by Amonton.

His laboratory shear tests were performed on synthetic rock made from Plaster of Paris and either quartz sand or kaolinite. Various moulds with inclined saw teeth (asperities) at 25°, 35°, 45° and 55° were used, with the final sample produced being 2.95 inches (74.93mm) long, 1.75 inches (44.45mm) wide and 2.0 inches (50.8mm) high. The samples were then tested under constant normal load conditions.

In the laboratory shear tests, two modes of failure were observed –

- failure by sliding
- failure by shearing through the asperities.

The relative amounts of each type of failure were shown to be dependent on the asperity angle and the normal stress. For a normal stress (σ_n) less than the transition stress (σ_T), the shear stress (τ) is determined by sliding at the basic friction angle (ϕ_b) and the asperity inclination (i). Above this transition stress, shearing through the asperities occurs. This is represented graphically in Figure 4.1.

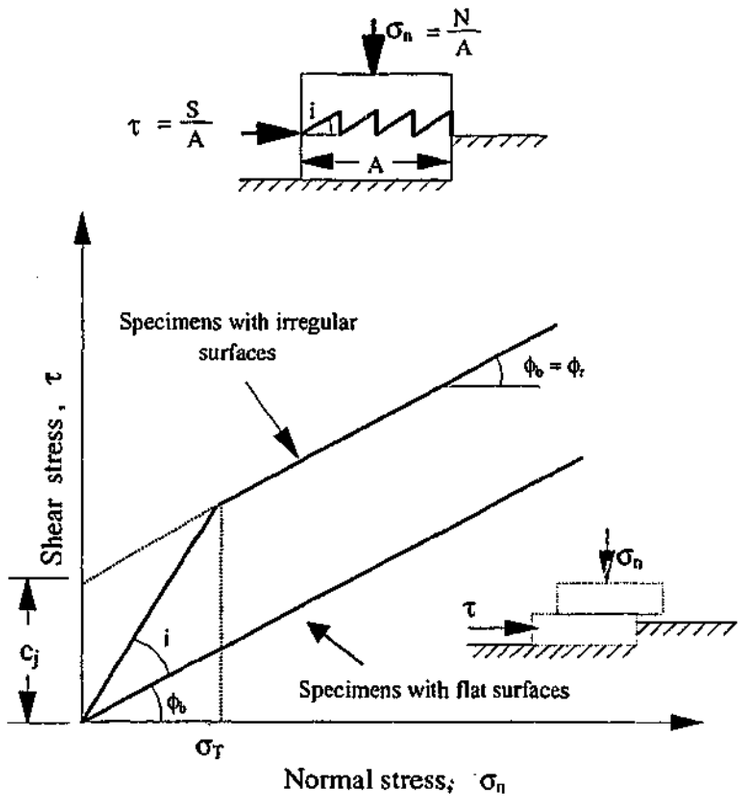

Figure 4.1: Patton's Bilinear failure Model (after Patton, 1966)

Patton demonstrated with his laboratory work that the joint cohesion value, c_j is dependent on asperity geometry and strength. It would therefore be difficult to predict for real joints.

Although this model highlights two basic mechanisms of rock joint behaviour, it is simplistic in that real rock joint surfaces are irregular, comprising many different asperity angles. Patton recognized that with various angles, sliding and shearing could occur simultaneously producing curved failure envelopes rather than linear responses. However, his approach treats sliding and shearing as two distinct mechanisms.

4.2 JRC-JCS Model

Given the non-linear failure envelopes of natural rock joints, Barton (1973) believed empiricism was required to predict the shear strength of rock joints. He proposed the empirical relationship shown in Equation 4.2 based on direct shear tests on over 200 artificial tension fractures.

$$\tau = \sigma_n \tan\left(JRC \log_{10}\left(\frac{JCS}{\sigma_n}\right) + \phi_b \right) \tag{4.2}$$

where, τ = peak shear strength

σ_n= effective normal stress

JRC = joint roughness coefficient

JCS = joint wall compressive strength

ϕ_b = basic friction angle

The Equation is similar to the Patton sliding model with the dilation angle,

$$i = \text{JRC} \log_{10}(\text{JCS}/\sigma_n) \tag{4.3}$$

The JRC, as discussed in Section 3.2.2, represents a sliding scale of roughness that varies from approximately 0 to 20. The standard roughness chart developed by Barton and Choubey (1977) is shown in Figure 3.3. These standard profiles were later adopted by the International Society for Rock Mechanics and together with the empirical relationship, suggested as a useful method to estimate the peak shear strength in their Commission on Standardization of Laboratory and Field Tests (ISRM 1978).

The JRC can be estimated by comparison with the standard profiles. This is obviously quite subjective. A number of other methods have been suggested in an attempt to decrease the subjectivity:

- Perform a Tilt Test, Pull Test or Push Test (Barton and Choubey 1977). A tilt test is conducted by tilting a matched joint until sliding just occurs. It corresponds to a shear test under very low normal stress. It can only be conducted on joints that are not excessively rough (JRC<8). A Push test is conducted by using a calibrated spring or hydraulic jack to push the top joint surface parallel to the joint face to measure the shear stress. As with the tilt test, the normal load is generated by the weight of the block and JCS and ϕ_b are estimated for the rock surface. It can be conducted on joints with an estimated roughness JRC<12. A Pull Test is required for rougher joints and is conducted by using a calibrated spring or hydraulic jack to pull the top joint surface parallel to the joint face. To obtain an accurate result, the average of a large number of tests is required. Large samples are also required for rough surfaces (Barton and Choubey 1977).

- Estimation of a statistical correlation between JRC and two roughness parameters - root mean square and the mean square of the first derivative of the profile - were estimated from digitised profiles by Tse and Cruden (1979). Further roughness parameters have been correlated with JRC by several authors since this time (Dight and Chiu 1981; Reeves 1985; Maerz et al. 1990; Yu and Vayssade 1991). Although several parameters describe the same property, the differences in the calculated values of JRC reflect the uncertainty in correctly choosing the correct parameter together with variations due to correct choice of a sampling interval.

- Determination of a fractal dimension and correlation of this with the JRC. There have been several correlations by various authors (eg. Carr and Warriner 1987; Lee et al. 1990). However, a uniform method of measurement has yet to be adopted with variations in the fractal dimension recorded for each fractal approach. Seidel and Haberfield (1995a) have indicated that when using the mid-point displacement procedure a direct correlation exists between the standard deviation of angle and the JRC.

During laboratory testing, joint surfaces can become mismatched. Mismatching will affect the normal closure of a joint, the measured stiffness of the rock mass, the shear

strength of the joint and its hydraulic conductivity. Further work by Zhao (1997) has included a joint matching coefficient (JMC) to be used with the JRC to take into account mismatching of the surface. The JMC is based on the percentage of joint surfaces in contact through primarily visual inspection.

The JCS is equal to the unconfined compressive strength (UCS) of the intact rock if the joint is unweathered. Weathering of the joint may reduce the UCS by up to 75%, (Barton 1973). The JCS value can be calculated in the laboratory or estimated in the field using a Schmidt hammer. This approach is detailed in Section 2.2.4 together with concerns regarding its accuracy. Empirical reduction factors for JCS are suggested by Barton and Choubey (1977) to take into account scale effects and difficulties associated with its measurement.

Laboratory testing by Pratt et al. (1972) on the scale dependency of rock joints, indicated approximately 40% drop in the peak shear strength with an increase of surface area from $60cm^2$ to $5000cm^2$. This occurred with an apparent four-fold reduction in JCS. With these results and a series of their own laboratory tests, Bandis, Lumsden and Barton (1981) recognized that an increase in sample size reduced the effective roughness and increased the contact area of the asperities. This was most noticeable with rough joints. To take this into account, scale correction formulas were empirically estimated for JRC and JCS to be used with the JRC-JCS model (Barton and Bandis 1982).

The peak shear stiffness and dilation angles can be empirically predicted (Barton and Choubey 1977). However, shear test results have indicated that during shear displacement, asperity failure can occur altering the asperity angles. For this reason, a further empirical damage coefficient has been estimated to model the "mobilized dilation" (Barton and Bandis 1990).

The JRC-JCS model, designed initially for CNL conditions, has been adapted and used by Skinas, Bandis and Demiris (1990) to model CNS conditions by utilizing the "mobilized dilation" component of the model.

The widespread use of JRC-JCS model by the geotechnical community and the acceptance of the approach by the ISRM, is an endorsement of the ease of use of the method. Its empirical nature however does generate several problems:

- Determination of JRC is either subjective if visual comparisons are used, or due to its scale dependency, potentially inaccurate.

- The failure mechanisms are not identified or accurately modelled.
- The heavy reliance on correction factors introduces uncertainty in the model that may lead to the imposition of higher factors of safety than necessary.
- Concerns on the applicability of the method to all rock joints.

4.3 Ladanyi & Archambraut's Model

Ladanyi and Archambault (1970) attempted to extend Patton's bilinear model to account for simultaneous sliding and shearing of rock joint asperities. They used energy principles similar to work conducted by Rowe (1962) for sand, to derive their Equations.

They considered that the total shearing force comprised four components:

S_1 = component due to external force done in dilating against the external normal force, N

= $N\dot{v}$, where $\dot{v}$ is the rate of dilation at failure, defined as the ratio between the increments of the normal displacement (dy) and the shear displacement (dx) at failure.

S_2 = component due to additional internal work done in friction due to dilatancy

= $S\dot{v}\tan\phi_u$, where ϕ_u is the sliding friction angle, S is the shear force

S_3 = component due to work done in internal friction if the sample does not change volume during shearing.

= $N\tan\phi_u$

S_4 = component due to shearing through the base of the asperities

= $As_o+N\tan\phi_o$, where s_o and ϕ_o denote the Coulomb shear parameters related to the strength of the rock substance and A is the total projected area of shearing.

To include simultaneous sliding and shearing, Ladanyi and Archambraut defined the area over which asperities sheared as area A_s with sliding occurring over the remaining portion (A- A_s). The total shear force could then be written as:

$$S = (S_1 + S_2 + S_3)(1-a_s) + S_4 a_s \qquad (4.4)$$

Where a_s = shear area ratio = A_s/A

Due to the difficulty in determining the Coulomb shear parameters s_o and ϕ_o, the intact rock shear strength was estimated using a parabolic failure criterion proposed initially by Fairhurst (1964):

$$S_4 = C_0 \frac{m-1}{n} \sqrt{1 + n\frac{\sigma}{C_0}} \tag{4.5}$$

Where: n = ratio of uniaxial and tensile strength of solid rock = $C_0/(-T_0)$

$m = (n+1)^{1/2}$

The proposed shear strength envelope can then be written as:

$$\tau = \frac{\sigma(1-a_s)(\dot{v} + \tan\phi_u) + a_s C_0 \frac{m-1}{n}(\sqrt{1+n\sigma/C_0})}{1-(1-a_s)\dot{v}\tan\phi_r} \tag{4.6}$$

The rate of dilation, $\dot{v}$, was initially determined empirically using the results of Ripley and Lee (1961), but was later modified to include further empirical data from Barton (1971), Rengers (1970) and Archambault (1972) (referenced in Ladanyi and Archambault (1980)) and reported in Ladanyi and Archambault (1980) as the following power laws:

$$a_s = \left(\frac{\sigma_n}{\eta\sigma_T}\right)^{0.75} \tag{4.7}$$

$$\dot{v} = \left[1 - \left(\frac{\sigma_n}{\eta\sigma_T}\right)^{0.25}\right]^{1.75} \tag{4.8}$$

where, σ_T = transition pressure

η = degree of interlocking

Saeb (1990) attempted to modify the Ladanyi and Archambault model by comparing it to the stress dilatancy theory of sand. He proposed replacing the total force, S, in the force component due to the additional work in friction due to dilatancy, with a shear force required for sliding S_F. Although this simplifies the Equation, it does not improve the overall effectiveness of the model.

Although introducing combined concepts of shear failure of asperities and dilation, the Ladanyi and Archambault model contains several shortcomings:

- Several authors have estimated the transition pressure of the rock material, σ_T, (e.g. Byerlee 1968; Mogi 1964; Goodman 1980). The results of this work have indicated a range of possible σ_T values. Celestino and Goodman (1979) have also suggested that this pressure may not be a fundamental property of the rock but may depend on the asperity geometry.
- The parameters $\dot{v}$ and a_s are empirically determined. Their accuracy therefore depends on the quality of the data used for their prediction.
- The interlocking factor η is difficult to predict and adequately represent the statistical nature of roughness.
- Celestino and Goodman (1979) demonstrated that the model is kinematically incorrect using a simple irregular triangular profile with two asperity angles. The Ladanyi and Archambault model assumes a dilation rate equal to the average angle of the asperities. Celestino and Goodman showed that the rate of dilation of the joint should be equal to the tangent of angle of the shallower angle whilst the steeper angle undergoes shear. In this case the stresses on all the asperities will not be constant.
- The model is based on an assumption of rigid asperities. Seidel and Haberfield (1995) have indicated that the assumption of rigidity underestimates the available sliding friction strength. Like Celestino and Goodman (1979), Seidel and Haberfield believed that the assumption of the equality of the joint dilation rate and the effective joint asperity angle was incorrect. They demonstrated that the shear strength of elastic rocks were dependent on individual asperity angles and the distribution of normal stresses on these asperities.
- The model does not accurately predict the shear strength of degrading materials. These materials have an elastic and an inelastic component that cannot be represented by the Ladanyi and Archambault joint dilation rate (Seidel and Haberfield 1995).
- The model is also limited to constant normal stress boundary conditions.

4.4 Seidel – Haberfield's Model

The Geotechnical Group at Monash University have been researching the performance of rock socketed piles for over 25 years. This work has concentrated on developing a theoretical approach to the behaviour of the concrete / rock interface during shear. This model uses the energy principles adopted by Ladanyi and Archambault (1970) but is based on a more fundamental approach without the use of empiricism. Initial testing was conducted under CNS conditions on regular triangular asperities (Johnston and Lam 1989). This was later extended into irregular triangular profiles (Haberfield 1987; Kodikara 1989) and then fractal profiles (Seidel 1993).

It was considered that the model developed for concrete / rock interfaces could be extended into rock joints. Initial testing on triangular and fractal profiles on a synthetic siltstone, Johnstone, and Hawkesbury Sandstone has suggested that the main mechanisms of shear behaviour are consistent across the two joint types (Fleuter 1997). Details of the model are given in the following sections.

4.4.1 Sliding Mechanism

If rock joint asperities are rigid, shear displacement would cause dilation on the steepest asperity and the other shallower asperities would be lifted out of contact. However, if the asperities are elastic, the sample can deform allowing some shallower asperities to remain in contact.

As discussed in Section 4.3, the Ladanyi and Archambault model for regular triangular asperities contains 3 components that relate to the sliding process ie. S_1, S_2, S_3. If the asperities are not rigid, but are elastic and hence undergo an elastic deformation, then the amount of dilation against the normal force is reduced from *dy* to (*dy-de*) as shown in Figure 4.2 (Seidel and Haberfield 1995).

As the relative movements between opposing surfaces remain unchanged, S_2 and S_3 are the same as for the rigid asperity case. The component S_1 however, is reduced by the amount of reduced dilation ie. from *dy* to (*dy-de*). This decrease in work in dilating against the normal force (N) is balanced by the additional work required to increase the internal strain energy (*dU*) (i.e. *dU*=N*de*) such that:

$$\tau = \sigma_n \tan(\phi_u + i) \tag{4.9}$$

Laboratory shear tests by Seidel (1993), Fleuter (1997) and Gu (2001) on regular triangular asperities have confirmed this elastic model.

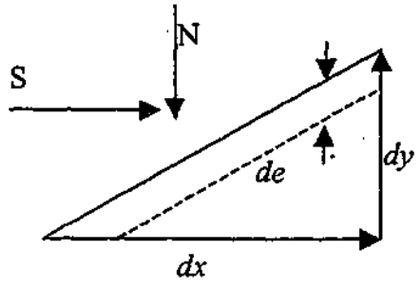

$$S_1 = \frac{N(dy - de)}{dx} + \frac{Nde}{dx} = N \tan i \tag{4.10}$$

$$S_2 = \tan i \tan \phi_u \tag{4.11}$$

$$S_3 = N \tan \phi_u \tag{4.12}$$

$$S = S_1 + S_2 + S_3 \tag{4.13}$$

Figure 4.2: Deformations due to elasticity (after Seidel, 1993)

For elastic surfaces with multiple asperities of varying angle, sliding can occur on not only the critical asperity but also on sub-critical asperities. Seidel (1993) and Seidel and Haberfield (1995) illustrated that S_1, the component due to external force done in dilating against the normal force N, remains unchanged. The component S_3, representing the work done in internal friction if the sample does not change volume in shear, also remains unaffected. However the component S_2, which is the additional work done in friction due to dilatancy, is reduced due to the decrease in the relative amount of dilation. This is illustrated in Figure 4.3. For an elastic rock joint profile with n asperities with a critical asperity slope of i_c and a dilation rate of $v < \tan i_c$ then :

$$\tau = \frac{1}{A} \sum_{j=1}^{j=n} a_j \sigma_{n,j} \tan(\phi_u + i_j) \tag{4.14}$$

where A is the total joint contact area and the n individual asperities of slope i_j have contact areas a_j and local contact stresses σ_{nj}.

With degradable rock types such as sandstone and calcarenite (the latter's structure may also collapse), sliding can also cause degradation of the joint surface. This degradation is inelastic with energy being lost. Seidel (1993) showed that this reduces the amount of relative dilation movement. If the current dilation rate is written as $\dot{v}$ then S_2 can be rewritten as:

$$S_2 = S\dot{v} \tan \phi_u \tag{4.15}$$

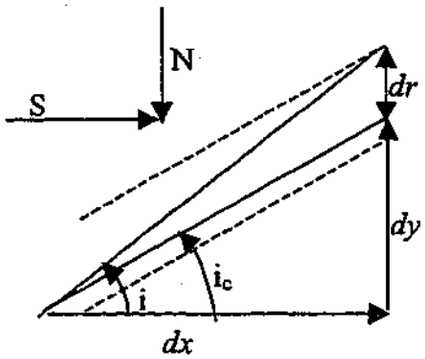

$$S_1 = \frac{N(dy+dr)}{dx} - \frac{Ndr}{dx} = N\tan i \qquad (4.16)$$

$$S_2 = S\tan i\tan\phi_u \qquad (4.17)$$

$$S_3 = N\tan\phi_u \qquad (4.18)$$

$$S = S_1 + S_2 + S_3 \qquad (4.19)$$

Figure 4.3: Sliding on subcritical asperity slopes (after Seidel, 1993)

Therefore the total shear stress due to sliding can be represented by the following Equation:

$$\tau = \frac{\sigma_n(\tan i + \tan\phi_u)}{(1-\dot{v}\tan\phi_u)} \qquad (4.20)$$

In practice deformations will comprise both elastic and inelastic components. Therefore in order to predict the response of degradable materials the elastic and inelastic components must be computed individually. Details on suitable methods to calculate these deformations are given in the following sections.

4.4.1.1 Elastic Deformations

It was recognized by Haberfield (1987), Kodikara (1989) and Seidel (1993) that to accurately model the deformation of each asperity, it would be necessary to not only acknowledge the distribution of stresses for the asperity being modelled but also the distribution of stresses on the surrounding asperities. To model a finite loaded area on an elastic medium of finite depth, would require complex numerical techniques such as finite element models. Therefore, an analogy of a footing at the surface of a finite elastic medium underlain by a rigid base was adopted (Haberfield 1987).

In analysing concrete / soft rock interfaces Seidel (1993) suggested modelling the elastic deformation of each asperity using the Steinbrenner (1934) solution for approximating the settlement of footings under the application of a load. This approach has been widely used to estimate settlements under the corner of a uniformly loaded rectangular area. Settlement of points within the uniformly loaded area and outside the area can be determined by algebraic summation. The Steinbrenner solution enables the deflection of

any asperity due to the load on any other asperity to be estimated by the construction of a compliance matrix. As the individual loads on each asperity are not known, the loads are calculated by the inversion of the compliance matrix to give a stiffness matrix which relates the load on any asperity to the displacement of the other asperities. Rather than performing an inversion, the process of LU-Decomposition (converts the compliance matrix into equivalent Lower and Upper triangular matrices (Press et al. 1990)) is used to more simply determine the stresses. The use of the Steinbrenner method is explained in detail in Seidel (1993).

In the analysis of rock joints, the material on each side of the interface is elastic and has the same elastic properties. This means that the net elastic sample depth, D, cannot be simply determined by the summation of the upper and lower halves using the Steinbrenner approach, due to the non-linearity of the influence factors with depth. Instead it is necessary to consider separately the material on each side of the interface. This is complicated by the interaction between the upper and lower face superimposing additional compatibility and equilibrium requirements.

Fleuter (1997) suggested a combined interface approach where the deformations of the interface halves are combined as a composite material. Figure 4.4 illustrates the displacement profiles due to the stress on the i^{th} chord for two compressible interface halves.

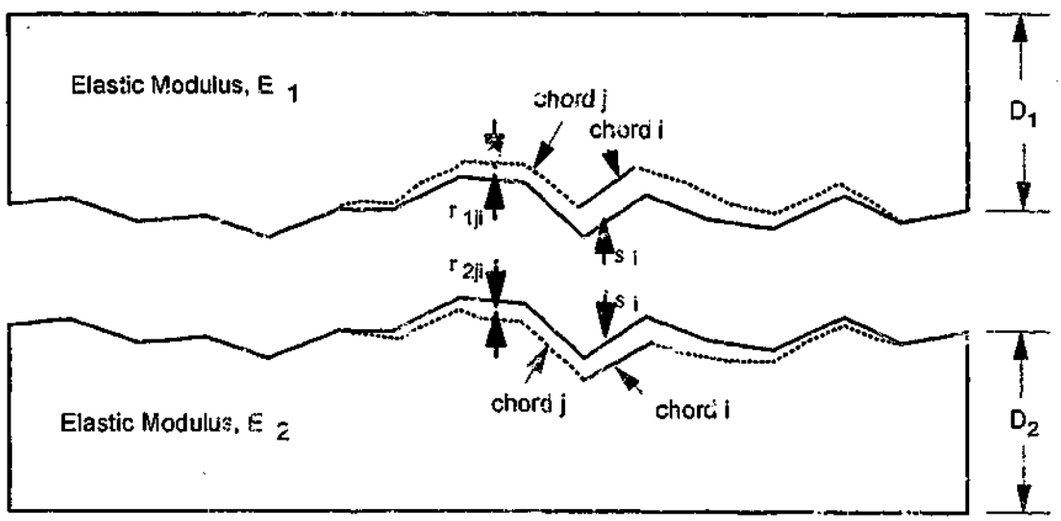

Figure 4.4: Displacement profiles due to stress on the i^{th} chord for two compressible interface halves (after Fleuter, 1997)

An effective modulus, E_{eff}, effective influence factors, I_{eff}, and a total depth of compressible material, D_T can be determined using the following Equations:

$$D_T = D_1 + D_2 \tag{4.21}$$

$$E_{eff} = \frac{D_T E_1 E_2}{D_1 E_2 + D_2 E_1} \tag{4.22}$$

$$I_{effji} = \frac{E_{eff}}{D_T}\left(I_{1ji}\frac{D_1}{E_1} + I_{2ji}\frac{D_2}{E_2}\right) \tag{4.23}$$

The effective compliance matrix, $[C_{eff}]$, is obtained from the multiplication of the effective influence factors by (D_T / E_{eff}). This represents the relative influence of stress on any asperity face on the displacement of any other asperity face as shown in Equation 4.24. The effective stiffness matrix, $[K_{eff}]$, is obtained by the inversion of the effective compliance matrix in order to obtain the stresses as a function of the chord displacements (ie. Equation 4.25).

$$[\rho] = [C_{eff}]\,[\sigma] \tag{4.24}$$

$$[\sigma] = [K_{eff}]\,[\rho] \tag{4.25}$$

The settlement on the i^{th} chord can be calculated by the summation of the individual settlements of chords i-k to i+k for both sides of the interface. This is shown in Equation 4.26 and 4.27. Individual chord displacements can be determined using Equation 4.28.

$$\rho_{Ti} = \sum_{j=i-k}^{i+k}(\rho_{1ji} + \rho_{2ji}) \tag{4.26}$$

$$\rho_{Ti} = \sum_{j=i-k}^{i+k} I_{effji}\frac{\sigma_i D_T}{E_{eff}} \tag{4.27}$$

$$\rho_i = x\tan\alpha_i - \psi \tag{4.28}$$

where x = shear displacement

α_i = angle of the i^{th} chord

ψ = dilation

In a rock joint shear test conducted in this project, the depth of each interface half is approximately the same. The modulus of the material on each side of the interface will also be equal and as the material properties are the same the influence factors will also be identical. This means that $D_1 = D_2$, $E_1 = E_2$. and $I_{1ji} = I_{2ji}$. Equation 4.27 can therefore be simplified to produce Equation 4.29.

$$\rho_{Ti} = \sum_{j=i-k}^{i+k} 2.I_{ji} \frac{\sigma_i D}{E} \tag{4.29}$$

4.4.1.2 Inelastic Deformations

Laboratory work by Seidel (1993) on Gambier Limestone (a calcarenite composed of angular bioclastic cemented grains) and concrete interfaces, demonstrated the inelastic component of shear strength during sliding. Under constant normal stiffness conditions, the normal stress on the interface is dependent on the cumulative degradation of the interface as this reduces the net dilation. To estimate the extent of the energy loss it is necessary to determine the instantaneous degradation rate and integrate this with respect to shear displacement to determine the cumulative degradation. The degradation rate was also found to be dependent on the asperity angle during laboratory testing on Hawkesbury sandstone artificial joints by Fleuter (1997). The following normalized degradation rate has been proposed:

$$\bar{d}_{n,i} = \frac{dy}{dx.\sigma_n.\tan i} \tag{4.30}$$

where dy = incremental degradation

dx = incremental shear

i = asperity angle

σ_n = normal stress

Further work by Gu (2001) has investigated the wear rate of sandstone / concrete interfaces. Gu (2001) through laboratory testing determined a wear angle, w, which is dependent on asperity angle (α), constant normal stiffness (K) and initial normal stress (σ_{no}) as shown in Equation 4.31.

$$w = \alpha[(7\text{x}10^{-12}K^2 - 1\text{x}10^{-7}K + 0.0004)K + (0.0002 - 6\text{x}10^{-8}\sigma_{no})\sigma_{no} - 0.02 \tag{4.31}$$

Although this is an empirical relationship, it is based on a more rigorous and physical treatment of the wear process than previous approaches. Gu (2001) tested this model on sandstone / concrete interfaces and limestone / concrete interfaces and obtained reasonable agreement with laboratory results.

The additional deformation due to wear, *dw*, can then be incorporated into the shear behaviour model as shown schematically in Figure 4.5. Shear component S_1 is reduced by a non-recoverable amount as shown in Equation 4.32. Shear component S_2 is also reduced as the relative dilation is reduced as shown in Equation 4.33.

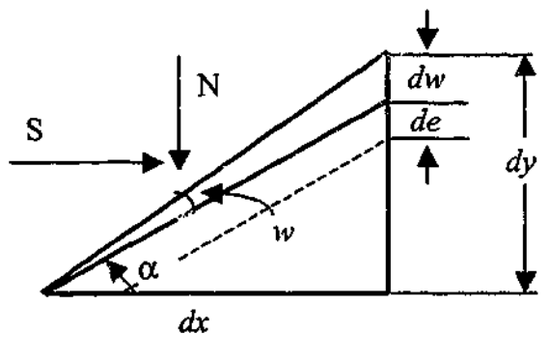

Figure 4.5: Deformations due to wear (after Gu, 2001)

$$S_1 = \frac{N(dy - de \cdots dw)}{dx} + \frac{Nde}{dx} = \frac{N(dy - dw)}{dx} = N\tan(\alpha - w) \qquad (4.32)$$

$$S_2 = S\tan(\alpha\text{-}w)\tan\phi_u \qquad (4.33)$$

4.4.2 Asperity Failure Mechanism

Observation of time-lapse videos of the shearing process of regular triangular soft rock / concrete interfaces, suggested that failure of the soft rock asperities occurred on a curved surface. This was also confirmed by Seidel (1993) with finite difference modelling using the program FLAC (Fast Lagrangian Analysis of Continua, Itasca (1993)). For this reason a slope stability analogy was used to model a loaded asperity. This is shown diagrammatically in Figure 4.6.

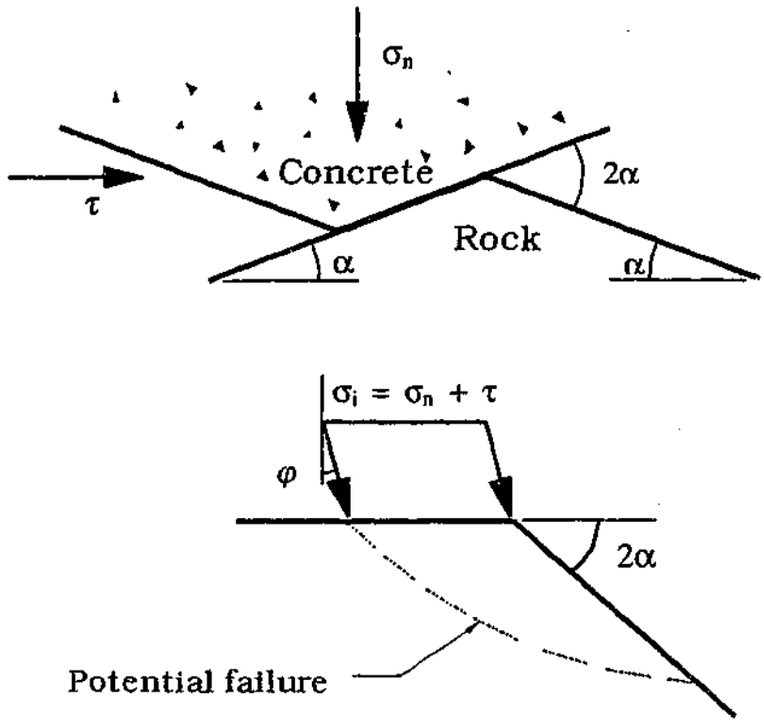

Figure 4.6: Slope stabilty anology of loaded asperity (after Fleuter, 1997)

For computational simplicity the Sokolovsky (1960) solution that produces an exact solution was used. This solution is derived for an inclined load on a slope of angle γ^o in a weightless $c-\phi$ soil. The weightless assumption was considered acceptable due to the negligible influence of self-weight on the strength of the asperity. Figure 4.7 illustrates the main features of this model.

The solution is obtained through the simultaneous solution of the following three Equations:

$$q\cos\delta = \sigma(1+\sin\phi\cos 2\rho) - H \qquad (4.34)$$

$$-q\sin\delta = \sigma\sin\phi\sin 2\rho \qquad (4.35)$$

$$q = \frac{H}{\cos\delta}\left\{\frac{1+\sin\phi\cos 2\rho}{1-\sin\phi}\exp[(\pi-2\gamma+2\rho)\tan\phi]-1\right\} = \text{stress} \qquad (4.36)$$

where $\sigma = \dfrac{(\sigma_1+\sigma_3)}{2}$

$H = c.\cot\phi$

δ = Inclination of load from normal

ρ = Direction of major principle axis

ϕ = Friction angle of soil

c = Cohesion of soil

γ = Angle of slope

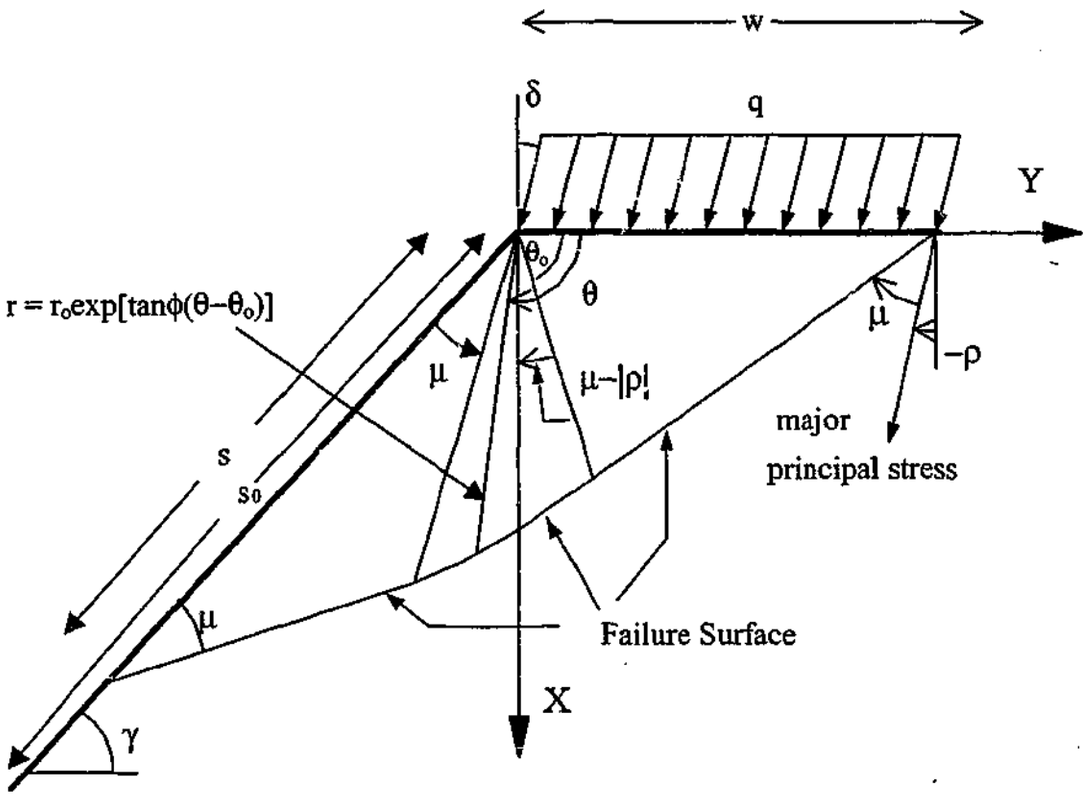

Figure 4.7: Solution for weightless c-ϕ soil (after Sokolovsky)

Seidel (1993) obtained the solution numerically by the application of the Newton-Raphson method (Kreyszig 1972) for which there is rapid convergence. He compared the solutions from the Sokolovsky's method and a slope stability program (EMU-92, Chen and Donald, 1992) and found the results to be within 3% of predicted values.

As the Sokolovsky method is only applicable to infinite slope lengths, an empirical constrained failure correction factor was estimated. This correction factor should be applied when the actual slope length (s), to loaded width (w), ratio exceeds the ratio of the length of the crest of the slope to the point of intersection of the failure plane (s_o), with the loaded width ie. when $s / w > s_o / w$. These lengths are shown on Figure 4.7 and

the relationship for s_o / w given in Equation 4.37. The correction factor is given in Equation 4.38.

$$\frac{s_o}{w} = \frac{2\cos\mu.\tan(\pi/2-\mu-|\rho|)(1+\tan^2(\pi/2-\mu+|\rho|))^{1/2}\exp(\tan\phi.(\pi/2-\gamma-|\rho|))}{|\tan(\pi/2-\mu-|\rho|)-\tan(\pi/2-\mu+|\rho|)|} \tag{4.37}$$

$$K_s = 0.85\exp\left[0.16\frac{s_o}{w}\right] \tag{4.38}$$

where · μ = Angle subtended by failure plane and crest

The above approach was adopted for a concrete / soft rock joints where the relative strength and rigidity of the concrete caused simultaneous failure along the entire length of the contacting soft rock asperity. However, Fleuter's (1997) video evidence of the failure of rock joints indicated that initial failure occurs with fretting of the contacting asperities outer edges. As the upper surface (analogously the "footing" applying the load) is the same material and hence has a similar stiffness as the founding material, the rigidity assumption is not correct. Nor is it correct to assume a flexible footing analogy. The correct assumption is most likely as a semi-rigid footing analogy.

Finite difference modelling by Fleuter (1997) using the program FLAC (Itasca, 1993), indicated reasonable correlation between the Sokolovsky failure stress and the average stress over 20% of the interface length closest to the asperity edge. Fleuter (1997) suggested an asperity multiplication factor of approximately 2 to the concrete / rock model to take into account the reduced failure area.

4.4.3 Joint Closure Effects

One of the factors that can affect the rock joint shear behaviour is the joint aperture (discussed in section 2.2.5). In natural rock joints the aperture is related to the stress history of the rock mass. In the laboratory situation, the cutting techniques such as band-saw cutting or water jet cutting that are used to produce the joint profiles, leave a slightly rippled surface. These ripples can prevent exact interface matching when the interface halves are re-mated. Upon the application of a load, the interface may close. A similar mismatching problem can arise with tensile split surfaces (used to represent three-dimensional joint surfaces). Joint closure under the application of a normal load or shear force would reduce the net amount of measured dilation. Under CNS conditions a

reduction in the amount of dilation will affect the level of the normal stress. This reduction in dilation can therefore affect the accuracy of the prediction of shear stress and normal stress and may also alter the distribution of stresses between asperities.

Fleuter (1997) conducted several load deflection tests on samples of water-jet cut samples of Johnstone and sandstone to determine the amount of joint closure present. Non-linear joint responses were found for both the Johnstone and sandstone samples. Adopting a simple bi-linear model, a maximum joint closure of 0.55 mm at a normal stress of approximately 2250 kPa was indicated for the Johnstone samples and a maximum joint closure of 0.58 mm at 4000 kPa normal stress for the sandstone samples. Fleuter's work concluded that the amount of joint closure was a function of the water-jet cutting procedure and independent of rock type whilst the normal stress at maximum joint closure was a function of the rock strength.

Test results by Fleuter (1997) on sandstone, where there is an appreciable wear rate, have indicated that the effects of joint closure are insignificant on materials that have wear damage to the contacting surfaces. In terms of the total dilation, joint closure is also less significant for high angle asperities or asperities with long segment lengths.

4.4.4 Post Peak Behaviour

Video records of concrete / rock interface testing have indicated that shear displacement after failure occurs through a chord linking the intersection points of the initial failure surface with the leading and trailing asperity faces. This is illustrated on Figure 4.8.

The inclination of this slope is defined in the Sokolovsky's method by the angle of the slope and the relative lengths of the slope distance and load width and given in Equation 4.37. The estimation of the post peak shear stress, (τ_{pp}), can be made using the relationship shown in Equation 4.39 developed by Seidel (1993).

$$\tau_{pp} = \frac{\sigma_n \{\tan(\phi+\alpha).[\tan\phi+\tan\beta]+\tan(\phi+\beta)[\tan\phi+\tan\alpha]\}}{[1+\tan\phi\tan\beta][\tan(\phi+\alpha)+\tan(\phi+\beta)]} \qquad (4.39)$$

where : α = concrete asperity angle

β = post peak failure plane inclination (determined by s_o/w ratio Equation 4.37)

ϕ = residual friction angle

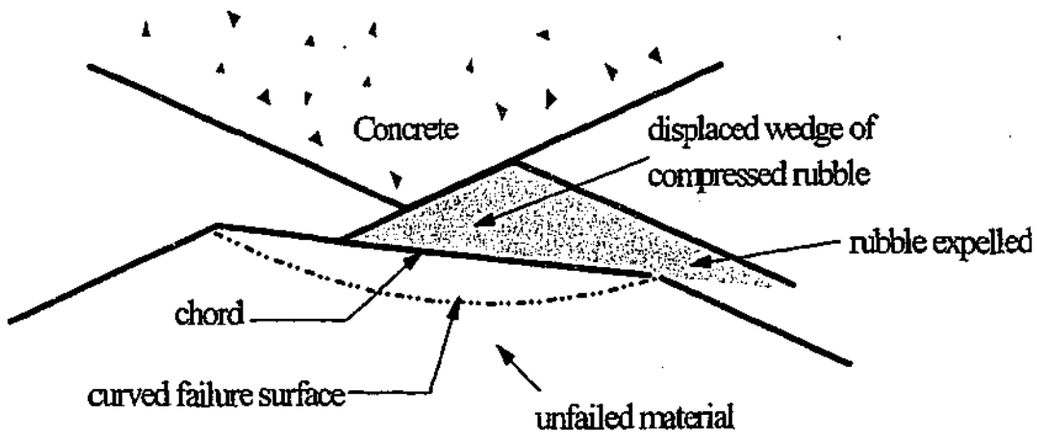

Figure 4.8: Schematic representation of post-peak shear displacement (after Seidel, 1993)

This model has not been modified for rock joint behaviour.

4.4.5 Overview of the Seidel – Haberfield Model

In this model, the joint roughness is represented by a series of asperities with varying chord angle but constant chord length. The chord lengths are varied to represent the profile at different scales. For example, a small chord length would be used to represent small scale roughness and the roughness that would be mobilised at small displacements.

A shear displacement loop is used to calculate the stresses at each increment of shear displacement. Due to the iterative nature of the procedures a computer programme, Rocket, was written to perform the calculations.

For each shear increment the contact length between the two sides of the interface is calculated (initially entire length of joint). For non-degrading materials this length is calculated for each asperity using the initial asperity length less the shear displacement and taking into consideration the additional length caused by load spreading due to elastic compression. For degrading materials an allowance is made for an additional contact length due to the degradation. Using Steinbrenner's method, the individual settlement effects of all the asperity faces are calculated for each loaded asperity and assembled into a compliance matrix. LU-Decomposition (a mathematical technique to manipulate linear Equations) is used to manipulate the compliance matrix to determine

the global stiffness matrix. Due to the difficulty in predicting the sample dilation with the varying local normal stresses, an iterative process is used to estimate the sample dilation. A matrix is used to record whether each asperity is in or out of contact with the opposite interface. A compression term is calculated for asperities in contact, taking into consideration joint closure and local elastic compression of the asperity. Dilation is calculated for each asperity based on sliding along the asperity face less the compliance components. These values are assembled into a matrix. Local stresses on each asperity are calculated from the global stiffness and dilation matrices and averaged over the contact length to estimate a global normal stress. Iteration is used until the dilation expected with the applied constant normal stiffness and global normal stress matches the calculated dilation and global normal stress terms. By multiplying the local normal stress by the tangent of the effective friction angle (ie. $i + \phi_r$) the local shear stress on the contacting asperities can be calculated. In the case of degrading materials, a revision is made to the effective friction angle. The global shear stress is calculated by dividing the summation of the local shear stresses by the total length of the profile. If asperities have come out of contact due to the dilation, the local and global stresses are recalculated with an adjusted contact area.

For each asperity a failure stress is calculated using the Sokolovsky failure model and the Newton-Raphson method to iterate to the solution. If the local normal stress exceeds the Sokolovsky failure stress for each asperity, failure of the asperity occurs. Failed asperities are assigned a new asperity angle.

This process is repeated for each increment of shear displacement.

The main advantage with the Seidel – Haberfield model is that it relies only on rock properties that are obtained through normal site investigation and laboratory testing (ie. Young's Modulus, Poison's ratio, peak cohesion and friction angle and residual friction angle) and on the joint roughness (represented by the standard deviation of chord angle at different chord lengths).

4.4.6 Problems with the Seidel – Haberfield Model

Most of the laboratory testing conducted to verify this model, has been performed on concrete-soft rock interfaces. Some limited testing has been conducted on Johnstone and sandstone interfaces but both of these rock types are of low strength. Therefore the

model has not been verified for strong rock joint interfaces or on a variety of material compositions.

Also the rock joints tested have all been manufactured two-dimensional joints with quite unrealistic surface roughness (minimum asperity chord lengths of 16mm have been tested on rock samples). A method to analyse the three-dimensional rough rock joint surfaces that would be encountered insitu has not been determined.

4.5 Other Recent Models

In recent years the development of a useable shear model has continued to attract interest. However much of this interest has concentrated on extending the empirical JRC-JCS approach. Two new models developed will be briefly discussed.

4.5.1 Dong and Pan Approach

A micro-mechanical approach has also been suggested by Dong and Pan (1996). Their model uses a homogenisation process to represent real asperities (seen as two contact rock surfaces) as a smooth basic contact plane on which Amonton's friction law applies. They assume that the basic contact plane is elastic before yielding and that after yielding the sliding and separation components can be considered through a relaxation stress. They select different contact planes to model the rock joint based on the level of shear and normal stress and on the joint scale. The following expressions were derived to estimate the incremental global stress, $d\sigma_i^g$, on each asperity:

$$d\sigma_i^g = \frac{1}{A_o}\sum_{c=1}^{N} a^c T_{ij}^c k_{jk}^c T_{ki}^{c-1} H_{lm}^c du_m^g - \frac{1}{A_o}\sum_{c-1}^{N} a^c T_{ij}^c dr_j^c = K_{ij} du_j^g - dR_i \quad (4.40)$$

where: A_o = global cross sectional area of joint

T_{ij}^c = coordinate transformation tensor (from local to global co-ordinate System) on the contact plane c

k_{ij}^c = contact stiffness tensor on the contact plane c

du_m^g = global relative displacement

H_{lm}^c = heterogeneous tensor to account for the variation of the local relative displacement.

a^c = selected contact area of the basic contact plane

dr_j^c = local relaxation stress tensor that accounts for the sliding and dilation on the contact plane.

K_{ij} = global stiffness tensor.

dR_i = global relaxation stress tensor.

The scale dependent properties of joint roughness are accounted for in a multi level asperity model.

The shearing aspect of joint failure is modelled by the low level asperities disappearing when the average shear stress in that level exceeds a shear stress, τ_s.

$$\tau_s = \sigma_n \tan\phi_s \tag{4.41}$$

where σ_n = normal stress

ϕ_s = shearing off angle

A hypothetical degradation model was also suggested to illustrate how the model could incorporate degradation by decreasing the contact inclined angle.

The limited comparison of the simulated data with direct shear tests, indicate that the approach tends to underpredict the peak shear stress by approximately 15%. This model relies on parameters that are not normally measured during site investigations and others that can be difficult to estimate (eg. Contact stiffness tensor, global stiffness tensor).

4.5.2 University of Wollongong Approach

A CNS direct shear rig has also been developed at the University of Wollongong to investigate the shear behaviour of rock joints. The modelling approach adopted by Indraratna et al. (1995) uses Fourier transform techniques to characterise the joint roughness. The dilation is fitted to a fourier series using Equation 4.42. The fourier coefficients (a_n and b_n) are estimated from experimental data. The normal stress can then be calculated at any shear displacement using Equation 4.45. The shear stress response with shear displacement can be calculated using Equation 4.46. This allows a variation in the asperity angle with shear displacement. By differentiating the shear stress

response with respect to shear displacement the peak shear stress can be estimated (Equation 4.47).

$$\delta(h)=\frac{a_o}{2}+\sum_{n=1}^{\infty}[a_n\cos(2\pi nh/T)+b_n\sin(2\pi nh/T)] \tag{4.42}$$

$$a_n=\frac{2}{T}\int_a^b f(x)\cos\frac{2\pi nx}{T}dx \tag{4.43}$$

$$b_n=\frac{2}{T}\int_a^b f(x)\sin\frac{2\pi nx}{T}dx \tag{4.44}$$

$$\sigma_n(h)=\sigma_{no}+\frac{K\delta(h)}{A} \tag{4.45}$$

$$\tau(h)=\sigma_n(h)\tan(\phi_b+i(h)) \tag{4.46}$$

$$\tau_p=\left[\sigma_{no}+\frac{K}{A}\left(\frac{a_o}{2}+a_1\cos\frac{2\pi h_{\tau_p}}{T}\right)\right]\left(\frac{\tan\phi_b+\tan i}{1-\tan\phi_b\tan i_{\tau_p}}\right) \tag{4.47}$$

where: δ = dilation

h = shear displacement

a_o, a_1, a_n, b_n = Fourier coefficients

n = number of harmonics

T = period = b-a

$\sigma_n(h)$ = normal stress at defined shear displacement

σ_{no} = initial normal stress

K = normal stiffness

A = joint surface area

$\tau(h)$ = shear stress at defined shear displacement

ϕ_b = basic friction angle

$i(h)$ = gradient of the dilatancy curve at defined shear displacement

$h_{\tau p}$ = horizontal displacement corresponding to peak shear stress

i_{tp} = dilation angle corresponding to peak shear stress

This model has been developed and verified on regular saw toothed, triangular and tensile split joints made from gypsum plaster that simulate a soft rock. Natural Hawkesbury sandstone joints have also been tested (Indraratna and Haque 2000). Further modelling would be necessary to verify the model with a range of rock strengths. The model has been developed to incorporate the effects of infill on the joint shear response. This is calculated as the shear response of an unfilled joint less the normalised strength drop due to the infill. This is defined in Equation 4.48.

$$(\tau_p)_{infilled} = (\tau_p)_{unfilled} - \sigma_{no}\left(\frac{t_F/a}{\alpha(t_F/a)+\beta}\right) \qquad (4.48)$$

where t_F/a = infill thickness to asperity height ratio

α, β = hyperbolic constants

The empirical estimation of the fourier coefficients and the hyperbolic constants relies on the analysis of field and laboratory test results. This makes this method site dependent and may limit its applicability when extrapolated to other sites.

4.6 Conclusions

This chapter has reviewed previous work conducted on rock joints by various researchers in their attempt to produce a realistic and widely applicable model of rock joints under the application of a shear load. Most of the earlier approaches were relatively simple models that only addressed some of the relevant failure mechanisms. Perhaps the most widely used approach today is the empirical JRC-JCS model. However, this model, although simple to use, does not model the mechanisms involved in the shear response of a rock joint and hence must be viewed conservatively.

It was these limitation of previous methods that led to the development of a micro–mechanical approach at Monash University that incorporates the various components of shear failure such as sliding, shearing and post peak behaviour. This model was originally developed for pile rock socket performance under axial loading. The model has only been tested for a limited number of rock types and profile configurations. Although initial tests indicate the model will be adaptable to the analysis of rock joints,

further work is required in this area. This chapter therefore presents the background for the continuation of the research into a micro-mechanical approach to rock joint behaviour.

5.0 EXPERIMENTAL SHEAR TESTING

To develop a widely applicable model capable of predicting the shear behaviour of rock joints, it is necessary to obtain data from direct shear tests on natural rock under conditions that closely simulate insitu conditions. Some of the relevant factors that affect the shear strength of rock joints have been highlighted in Chapter 2. The experimental work described in this chapter had the following aims:

- investigate the shear behaviour of rock joints in several rocks across a range of strengths
- investigate the suitability of the existing slightly modified rock / concrete shear model
- investigate the effects of changing the boundary conditions, joint roughness and scale
- investigate the shear behaviour of three-dimensional surfaces
- determine whether a three-dimensional surface can be modelled by a two-dimensional profile

This chapter describes the shear testing rig, the rock types that were tested and the rock joint roughness profiles used in the tests.

The shear testing rig used is a specially designed direct shear device developed at Monash University to test soft rock / concrete interfaces. This rig is capable of testing samples up to 600 mm long under different boundary conditions thus minimizing scale effects whilst providing representative boundary conditions. Details of this shear device are given in Section 5.1.

Initially a synthetic soft rock called Johnstone was tested. Details of this synthetic rock and its properties are given in Section 5.2.1. This rock is easily reproducible and relatively homogeneous and the data from these samples were used to establish whether a three-dimensional surface could be modelled by a two-dimensional profile and to confirm basic mechanisms of shear behaviour. Once the basic mechanisms had been established, the testing program was extended to include natural rocks of varying strength

and origin. Siltstone, sandstone, basalt and granite were selected. A description of the rocks used in the testing program and their basic properties are outlined in Section 5.2.

The testing performed in this research was conducted initially on samples with simple triangular asperity profiles, then samples with fractal two-dimensional profiles and finally samples with three-dimensional irregular profiles. The tests covered a range of interface roughnesses and boundary conditions. Details of the profiles tested are provided in Section 5.3. The testing of simple two-dimensional joint roughness profiles allowed the basic sliding and shearing mechanisms to be observed and modelled. The tests on the more complex fractal two-dimensional profiles provided data that allowed the interaction between shearing, sliding and deformation and post peak behaviour to be observed. The full three-dimensional joint profiles provided data on more realistic joint surfaces.

5.1 Cyclic Constant Normal Stiffness Shear Rig

The cyclic constant normal shear rig (CCNS) used in this research was developed at Monash University over a number of years. Figure 5.1 shows the shear rig and shear box. Design details are given in Seidel (1993) and are summarized here:

- SHEAR BOX. Standard shear boxes are typically 60mm by 60mm in dimension. To decrease scale effects, a much larger split shear box capable of testing samples up to 600 mm long, 200 mm wide and 135 mm in depth was developed. To prevent rotation the upper shear box was restrained from horizontal movement and the lower box from vertical movement. Vertical movement on the upper box and horizontal movement on the lower box are permitted by needle rollers. Frictional losses under maximum load of less than 10 kPa were measured by Seidel (1993) for a typical sample size of 500 mm x 80 mm.

- LOADS. The shear and normal loads are applied by servo-controlled Instron hydraulic actuators that have load capacities of ± 250 kN static and ± 500 kN dynamic. Displacement or load control can be used for the application of shear loading with automatic area correction for shear displacement. The rig is capable of monotonic or cyclic loading with the facility to vary waveforms and periods for realistic loading patterns. Only monotonic single ramp waveforms were used during the present work. As discussed in Section 2.2.2 the boundary conditions vary

according to the deformability of the surrounding rock. The constant normal stiffness condition is perhaps the most representative of in-situ rock conditions and was achieved in the Monash direct shear rig by placing the vertical actuator under load control and through a feed-back system simulating a spring of stiffness K. All tests for the present work were conducted under constant normal stiffness.

- DISPLACEMENTS. Two Schaevitz linear variable displacement transducers (LVDT's) (range ± 125 mm, accuracy ± 0.06 mm) are mounted internally to the vertical and horizontal actuators to measure the actuators displacement. Three LVDT's of reduced range but increased accuracy are mounted externally to measure the displacement of the shear box. One is mounted in the horizontal or shear direction (range ± 25 mm, accuracy ± 0.01 mm) and the remaining two are mounted on each side of the upper split shear box (range ± 5 mm, accuracy ± 0.002 mm). These measure displacements relative to a reference plate attached to the lower split shear box. Tests can be conducted under varying shear displacement velocities. The tests conducted for this dissertation were performed at a constant shear displacement velocity of 0.5mm/min. As discussed in Section 2.2.7, the shear displacement velocity can affect the peak shear resistance as undrained and drained parameters typically vary. The rate of 0.5mm/min was shown to be sufficiently slow to allow full drainage of Johnstone samples (Seidel 1993) and was used for the siltstone, basalt and granite samples.
- MEASUREMENTS. Automatic computer logging of the displacement and load in both shear and normal directions is achieved using a 16-bit acquisition card. Real time display is provided with PC-based digital control using the program HP-Vee (Helfel 1988). The shearing process can also be monitored with video cameras.

5.2 Rock Types Tested

A range of rock types of different strength, origin, grainsize and mineral composition were selected for direct shear testing. The initial tests were conducted on a synthetic rock, Johnstone. Some two-dimensional profiles had previously been tested on this rock (Fleuter 1997) and this work was to be extended into more realistic three-dimensional profiles. Testing was also conducted on several natural rocks - sandstone (two-

dimensional roughness profiles had been previously tested by Fleuter (1997)), siltstone, basalt and granite.

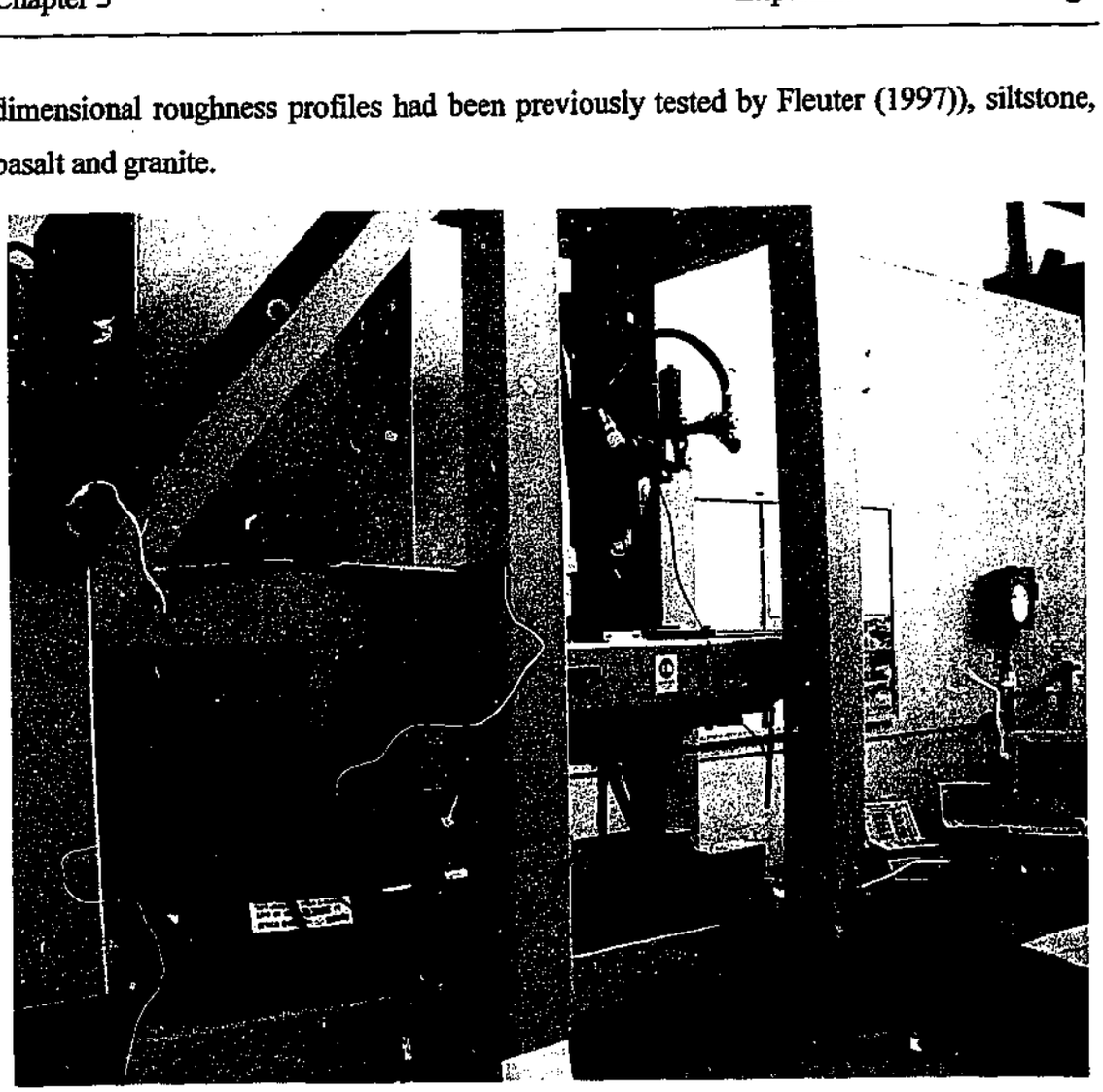

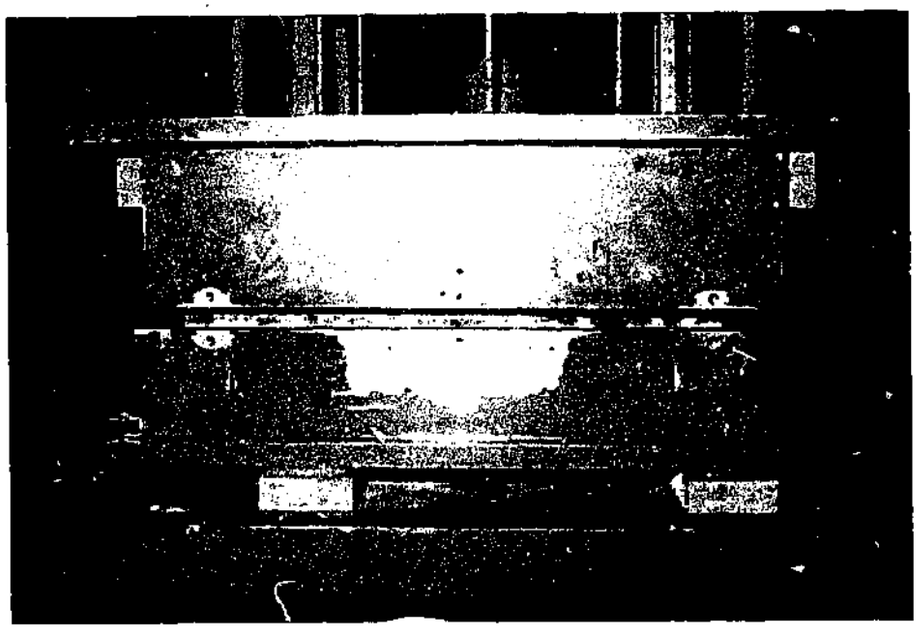

Figure 5.1: Constant normal stress shear rig and shear box

5.2.1 Johnstone

To obtain a realistic modelling material for laboratory testing without the inherent variability of natural rock, Johnston and Choi (1986) developed a synthetic soft rock with properties similar to the naturally occurring Melbourne Mudstone / Siltstone. Unlike natural siltstone, this material is relatively homogeneous and isotropic and easily reproducible in large volumes.

Natural mudstone / siltstone is formed over many millions of years from the consolidation and cementation of fine-grained marine sediments. Johnston and Choi's approach to the formation of the synthetic siltstone, later called "Johnstone" (Johnston and Choi 1986), models at a greatly accelerated rate the naturally occurring geological processes resulting in the formation of mudstone / siltstone.

A finely ground siltstone powder is used as the basic material and Ordinary Portland Cement is added to model the natural cementation process. These powders are mixed dry and combined with water and a 10% calcium chloride solution. Calcium chloride is used as an accelerating agent to reduce the curing time. After mixing of the powder and liquid for approximately 90 seconds, the mixture is manually compacted into a mould and then compressed under a pressure of approximately 5.8 MPa for 4 to 6 hours to reconsolidate the powder and induce particle bonding. The sample is then cured for 28 days in a fog room (100% humidity and 23°C ± 2°C).

Table 5.1: Mix proportions of Johnstone

Ingredient	Proportion	Quantity
Mudstone Powder	97.5% of dry mix by weight	28.8 kg
Cement	2.5% of dry mix by weight	0.720 kg
Water	12% of weight of mudstone powder	3.456 kg
10% Calcium Chloride	288 ml	0.370 kg

The mudstone powder used in this research project for the manufacture of the Johnstone, was obtained from the Nubrick brick quarry in Scoresby, Victoria. Compaction testing conducted by Cheng (1997) on this powder, indicated an optimum moisture content of approximately 12%. The mix proportions indicated in Table 5.1 were therefore used to produce samples approximately 560mm x 160mm x 160mm in size.

Chiu (1981) demonstrated that the saturated water content of the Melbourne Mudstone could be used as an indicator of rock properties. Laboratory test results by Lam (1983); Choi (1984); Haberfield (1987); Kodikara (1989) and Cheng (1997), have indicated that the Johnstone rock properties can also be estimated from the saturated moisture content.

atches were made for the present study, the first in August 1998 and the second in mid February 1999. The results of the classification tests conducted on these Johnstone samples are summarised in Appendix B. The first batch of samples had a moisture content of approximately 14.2% and an average unconfined compressive strength of 8.3 MPa. The second batch of samples had an average saturated moisture content of approximately 14% and an average unconfined compressive strength of 4.3MPa. These results are combined with results by Choi (1984) and shown graphically in Figure 5.2. This graph indicates that the unconfined compressive strength of batch 1 is approximately 60% higher than that of Johnstone of the same water content produced by Choi. It is believed that this higher strength is due to higher strength cement used in this first batch, resulting in a higher peak cohesion.

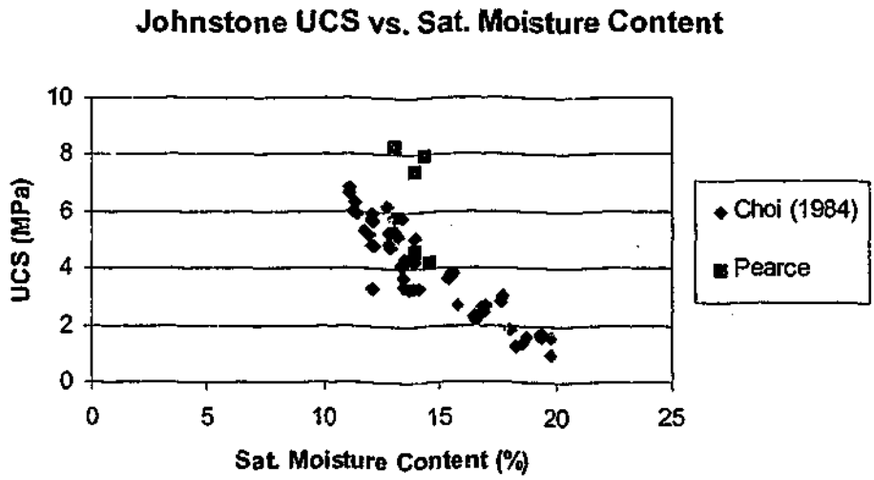

Figure 5.2: Comparison of Johnstone Unconfined Compressive Strength with moisture content

Using this data combined with previous test results (Johnston and Choi 1986) and correlations with moisture content, the parameters indicated in Table 5.2 were adopted.

Table 5.2: Adopted Johnstone parameters

Parameter	Adopted value (batch 1)	Adopted value (batch 2)
Saturated Moisture Content	14.2%	14.0%
Uniaxial Compressive Strength	8.3 MPa	4.3 MPa
Young's Modulus	900 MPa	900 MPa
Poisson's Ratio	0.25	0.25
Intact Friction Angle	35°	34°
Residual Friction Angle	24.5°	24.5°
Cohesion	1500 kPa	1050 kPa

Table 5.3: Adopted Sandstone parameters

Parameter	Adopted Value
Saturated Moisture Content	5.0%
Uniaxial Compressive Strength	21.7MPa
Young's Modulus	3.2 GPa
Poisson's Ratio	0.1
Intact Friction Angle	50.0°
Residual Friction Angle	32°
Cohesion	2200kPa

5.2.2 Sandstone

The sandstone used in this current research was obtained from the Gosford Quarries in New South Wales and is a sedimentary rock of Triassic Age. This material, known as Sydney Hawkesbury Sandstone, underlies much of the Sydney area and is relatively uniform and blocky. The Slightly Weathered sandstone samples are orange brown and interbedded yellow brown in colour and comprised predominantly subangular fine to medium quartz grains within an argillaceous matrix and some siderite cement.

At the same time as the current project was being undertaken, Gu (2001) was completing related work on concrete-sandstone interfaces for rock socketed pile research. He had

completed a series of uniaxial compressive tests, triaxial tests and intact direct shear tests on the Hawkesbury Sandstone. These results have been used to establish strength and deformation parameters of this material under saturated conditions. The adopted parameters are given in Table 5.3.

5.2.3 Siltstone

The siltstone was collected from the Burnley Tunnel Section of the Melbourne City Link Project, Victoria. Samples were recovered from approximately 40 m below ground surface (Approx. RL –30m). The rock is commonly and incorrectly referred to as Melbourne Mudstone and is a sedimentary rock of Silurian Age consisting of interbedded mudstones, siltstones and sandstones with siltstone predominating. The colour of the rock is dependent on the degree and type of weathering. The samples obtained were Slightly Weathered to Fresh, very thinly bedded and dark grey with pale grey. Jointing was predominantly parallel and perpendicular to the bedding.

Chiu (1981) demonstrated that the saturated water content of the Melbourne Mudstone could be used to estimate the rock properties. He conducted a large range of tests on mudstone weathered in both oxidising and reducing environments with saturated water contents in the range of 4% to 20%.

The rock used in this project had a saturated moisture content of approximately 1.5%. As this was considerably lower than rock previously tested, a series of tests were conducted to verify the established relationships with moisture content. As the Melbourne Mudstone possessed joints parallel and near perpendicular to bedding, it was decided to test the samples in these directions. This meant that several intact direct shear tests were conducted on samples in the bedding direction to obtain bedding strength parameters and perpendicular to the bedding to obtain intact strength values. The results from these tests indicated that there was no appreciable difference between the bedding strength and intact strength values. However, it must be recognised that the strength of the bedding may be quite variable. A peak friction angle of 66° and cohesion of 1700kPa was obtained from these direct shear tests. As these are relatively high values and given the potential variability of the bedding strength, more conservative values as calculated by the Hoek - Brown failure criteria (Hoek and Brown 1988) were selected for test analysis. Further details are given in Chapter 9.

The following tests were conducted to determine the strength and deformation parameters:

- 3 uniaxial compressive strength tests (in accordance with the suggested ISRM Test method (ISRM 1981))
- 5 uniaxial tensile strength tests (in accordance with the suggested ISRM Test method (ISRM 1981))
- 5 intact direct shear tests
- 3 shear tests on flat planar interfaces

The results of these tests have been combined with Chiu's (1981) results and are presented in Figure 5.3. They are also tabulated in Appendix B. Table 5.4 indicates the adopted parameters of the tested siltstone.

Table 5.4: Adopted Siltstone parameters

Parameter	Adopted Value
Saturated Moisture Content	1.5%
Uniaxial Compressive Strength	55MPa
Uniaxial Tensile strength	7.7MPa
Young's Modulus	25.4 GPa
Residual Friction Angle	28.5°

5.2.4 Basalt

The basalt quarried in Melbourne, known as the Newer Volcanics, is typically of Tertiary Age and can be in the form of lava (basalt) or pyroclastics (scoria, tuff and ash). The basalts are usually dark bluish grey to black or brown and can be vesicular with their mineralogy typically consisting of olivine, plagioclase, feldspar, clinopyroxene and opaque oxides (Dahlhaus and O'Rourke 1992). Basalt flows are typically highly vesicular near the surface where they have cooled quickly, becoming less vesicular with depth. Jointing is typically caused by shrinking due to cooling and hence joint characteristics may vary from flow to flow.

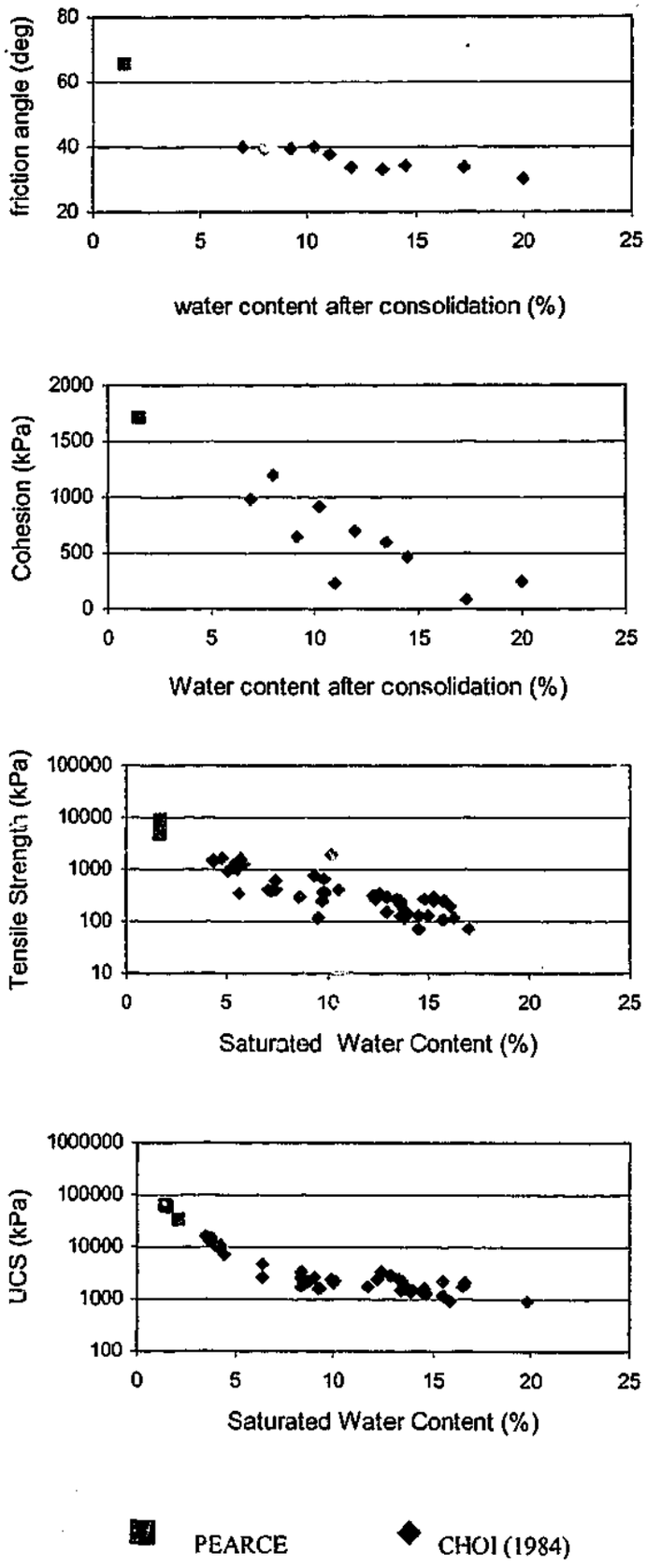

Figure 5.3: Comparisons of siltstones properties with water content.

The basalt used in this current research was obtained from two sources:

- Source 1. Samples from the Boral Quarry in Deer Park, Victoria were used to form the triangular and irregular two-dimensional profiles;
- Source 2. The split samples were formed from basalt blocks purchased from a garden centre in Clayton (original origin unknown).

The samples were visually similar. All samples obtained were typically Moderately Weathered, slightly vesicular and black grey and blue grey in colour. Natural joints were often coated with thin layers of carbonaceous material.

To assess strength and deformation parameters the following tests were conducted:

- 4 uniaxial compressive strength tests on source 1 samples and 5 uniaxial compressive strength tests on source 2 samples (in accordance with the suggested ISRM Test method (ISRM 1981))
- 2 uniaxial tensile tests on source 1 samples (in accordance with the suggested ISRM Test method (ISRM 1981))
- 3 direct shear tests on flat planar interfaces on source 1 samples

The results of these tests are summarised in Appendix B. The uniaxial tests conducted on the two different sources produced nearly identical strength parameters (ie. E_1=62GPa, UCS_1=120MPa; E_2=63GPa, UCS_2=123MPa). Due to this similarity one set of parameters will be used. The adopted properties are summarized in Table 5.5.

Table 5.5: Adopted Basalt Parameters

Parameter	Adopted Value
Saturated Moisture Content	2.5%
Uniaxial Compressive Strength	120MPa
Uniaxial Tensile Strength	11MPa
Young's Modulus	62GPa
Residual Friction Angle	34°

5.2.5 Granite

The granite used in this current research came from Mt Bundey in the Northern Territory. The rock is known as Mt. Bundey Granite and is an intrusive igneous rock of Precambrian Age and is a hornblende biotite granite. The samples obtained were Slightly Weathered, medium to coarse grained and pinkish brown in colour.

To estimate strength and deformation parameters the following tests were conducted:

- 3 uniaxial compressive strength tests (in accordance with the suggested ISRM Test method (ISRM 1981))
- 4 uniaxial tensile tests (in accordance with the suggested ISRM Test method (ISRM 1981))
- 4 direct shear tests on flat planar interfaces

The results of these tests are given in Appendix B. The adopted parameters are summarized in Table 5.6.

Table 5.6: Adopted Granite Parameters

Parameter	Adopted Value
Saturated Moisture Content	0.4%
Uniaxial Compressive Strength	180MPa
Uniaxial Tensile Strength	10MPa
Young's Modulus	61GPa
Residual Friction Angle	36.5°

5.3 Sample And Profile Preparation

Direct shear testing was conducted on joint samples containing two-dimensional regular triangular surfaces, two-dimensional fractal triangular surfaces and irregular three-dimensional surfaces. Details of the profiles selected and preparation methods adopted for each rock type are summarised in this section.

Due to the strength of the rock and the small chord length profiles required in the two-dimensional surfaces, bandsaw cutting or circular saw cutting techniques were not

appropriate. Cutting techniques that generated considerable heat were also considered to be inappropriate because of the possible effect on the properties of the rock. Therefore water-jet cutting techniques were selected to cut two-dimensional profiles into the rock surface. This procedure involves spraying water mixed with fine sand through a nozzle under high pressure. The resulting water-jet is approximately 1.2mm in diameter although some minor flaring can occur. An accurate surface can be cut although a slight "ripple" effect is left on the surface. This ripple is typically less than approximately 1mm in height although on harder rocks it can become more accentuated at the deepest edge of the cut. Figure 5.4 shows the typical ripple present along the surface of a siltstone sample.

Figure 5.4: Siltstone water-jet cut triangular asperity profile showing fine ripples along the asperities

Unfortunately during the course of the research project, inconsistent quality was obtained from the water-jet cutters. The first 2 water-jet cut samples made in 1997 as initial test samples of Johnstone, produced excellent replication of the desired surface as shown in Figure 5.5. However, later cuts using the same equipment and operator, were typically overcut producing a rougher surface than desired as shown in Figure 5.6. Discussions

with the water-jet cutters could not identify any possible reasons for the loss in accuracy. However, the spot diameter of the water jet was in the order of 1.2mm so the inaccuracies of up to ±2mm are in the realm of expected accuracy. This level of inaccuracy was not of concern for the triangular or irregular triangular profiles (providing the cut surface was measured) but it was of concern if reproduction of joint interface surfaces was being attempted. These problems are discussed in further detail in Section 7.1.

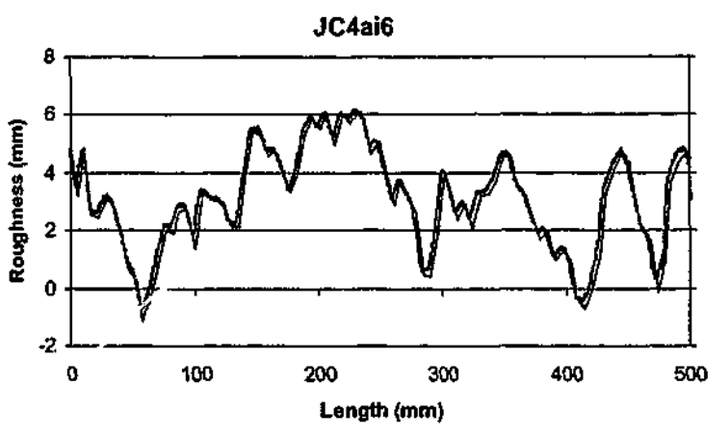

Figure 5.5: Excellent water-jet matching of Johnstone cut with desired profile

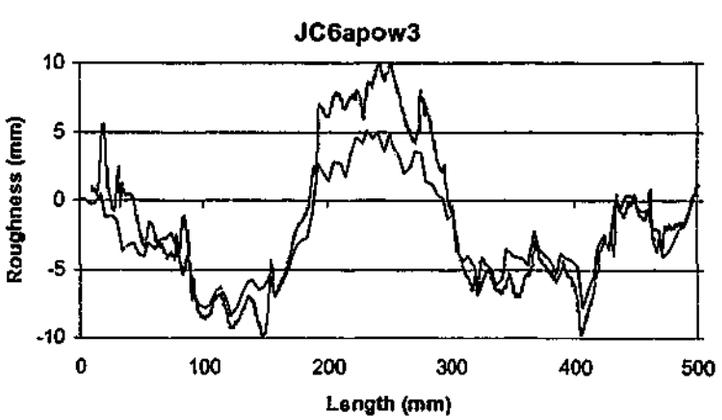

Figure 5.6: Johnstone profile overcut

Initially roughness profiles were cut at 6mm chord lengths as there was uncertainty about the accuracy that could be achieved using the water-jet cutting process. Due to the almost perfect water jet cuts that were obtained for the two samples, the next profiles were cut at 3mm chord lengths. Although this was still in the range of cutting size that should have been achievable by the equipment, some overcutting was measured in these samples. The next few profiles were cut at 12mm chord lengths and 4mm chord lengths in the hope that they would be more accurate. As the 12mm profile was still slightly overcut, it was considered to be a problem independent of the chord length and specific to the material and equipment. The two samples that were cut accurately at 6mm chord length were from batch 1 of Johnstone and had a UCS of 8.3MPa compared to 4.3MPa of batch 2. Therefore the decrease in accuracy may have been related to the decrease in strength of the material although this was not considered a plausible reason by the water-jet cutters.

5.3.1 Johnstone

Since 1980, considerable work has been conducted on Johnstone / concrete joints to investigate rock socketed pile performance under axial loading. Fleuter (1997) conducted a series of direct shear tests on planar profiles, regular two-dimensional triangular profiles and two-dimensional fractal profiles using Johnstone / Johnstone interfaces to extend this research into rock joints. He found that the Johnstone / concrete joint shear behaviour model had potential to model Johnstone / Johnstone interfaces. He modified this model by including the elastic deformations of both interfaces, including a joint closure component and applying an empirical correction factor to the asperity failure model (discussed in Section 4.4). In this current research several irregular triangular profiles were to be tested to verify Fleuter's results. This work was to then be extended into three-dimensional profiles. Johnstone, due to its relative uniformity and reproduction capabilities, was also to be used to evaluate hypothesis relating to the representation of joint roughness (refer to Chapter 7).

Nine Johnstone samples were produced in two batches from a mould 560mm x 160mm x 160mm. These samples were cut using a bandsaw and diamond tipped circular saw to block sizes of 560mm long x 130 mm high x 80 mm wide.

As the Johnstone is compacted in layers and then consolidated, the rock is slightly cross-anisotropic. To produce a three-dimensional surface, a 5 mm deep groove was cut around the centre-line of several blocks parallel to this layering. These blocks were split by placing a reinforced cutting blade in the grooves along the 560 mm long lengths and gradually applying pressure to both sides via a hydraulic press whilst supporting the outer edges of the block. Seven split surfaces were created in this manner. A typical split-surface can be seen in Figure 5.7.

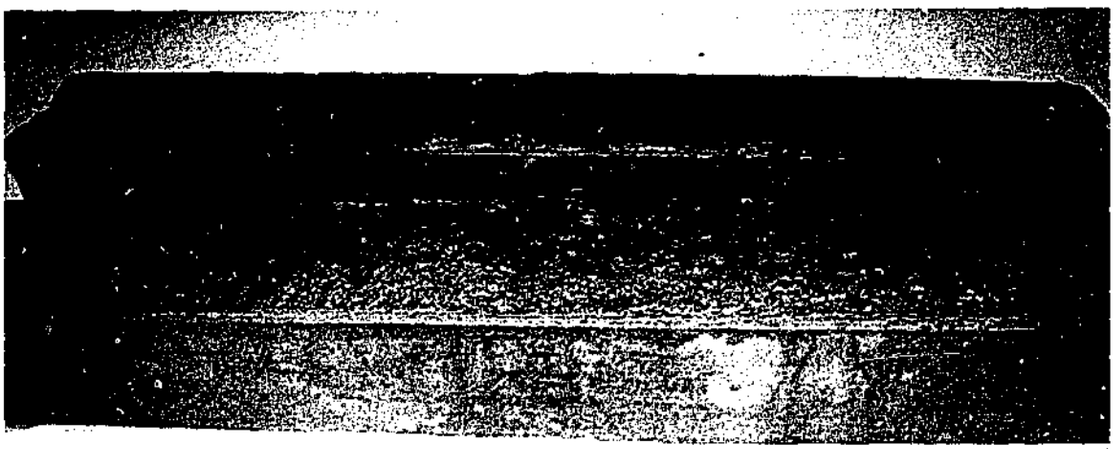

Figure 5.7: Photograph of typical Johnstone split surface

Profiles of the split surfaces parallel to the shearing direction were measured at 5mm spacings (across the width of the sample) using the Monash laser profilometer Socket-Pro (refer to Section 3.1.4). Roughness heights were taken at 0.07mm intervals in each profile. The two-dimensional profiles together with the three-dimensional surfaces are included in Appendix C. One such set of data is illustrated at an exaggerated vertical scale in Figure 5.8.

As discussed, several fractal profiles were tested to verify Fleuter's results. Several fractal profiles were produced using two-dimensional profiles taken of the Johnstone split surfaces. These split surfaces adequately replicate natural bedding joints (refer to Section 7.1.2.1). Therefore, these profiles are better replications of natural profiles than previously tested. They are also produced at smaller chord lengths than previously tested, increasing the range of roughness wavelengths investigated. The two-dimensional profiles were water-jet cut into the Johnstone samples. The following profiles were produced:

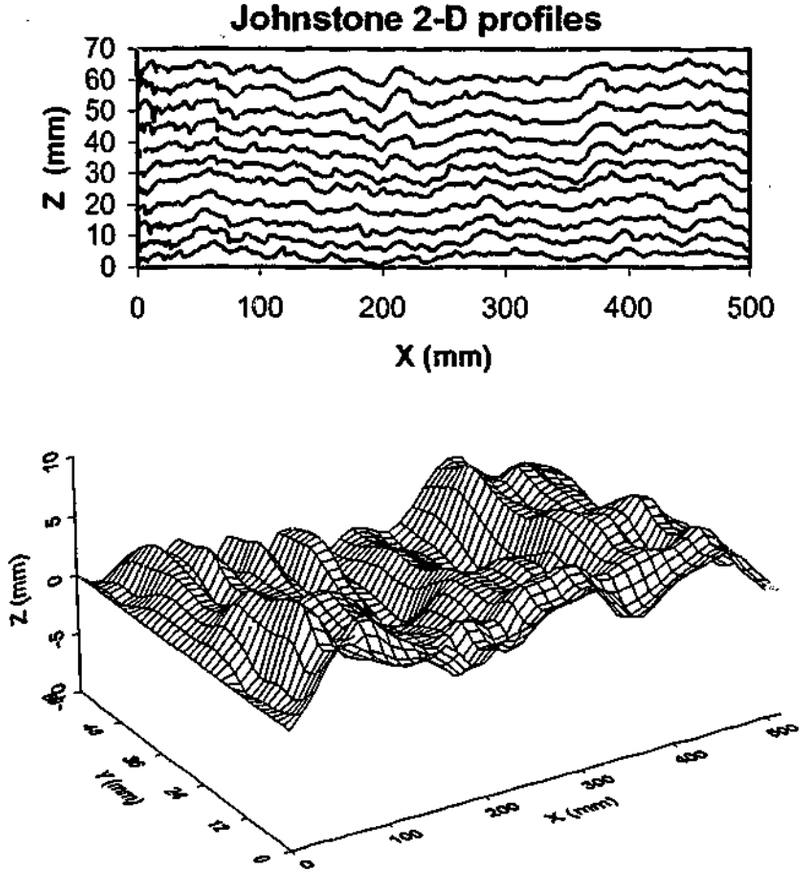

Figure 5.8: Johnstone Split surface 4a

- A compass, open a distance of 3mm, was walked along a centre profile of split surface JS3a. The locations where the compass intersected the profile were joined by chords (3mm long) to produce fractal profile JF12_3 (Figure 5.9). Chord lengths of 3mm were considered to be the smallest chord length accurately cut by the water-jet process. This two-dimensional profile was water-jet cut into a Johnstone sample from batch 2. It had a standard deviation of chord angle of 12^{o} at 3mm chord length when water-jet cut. The profile and its roughness statistics are shown in Figure 5.9.

- A compass, open a distance of 12mm, was walked along a centre profile of split surface JS4a. The locations where the compass intersected the profile were joined by chords (12mm long) to produce fractal profile JF8_12 (Figure 5.10). This two-dimensional profile was water-jet cut into a Johnstone sample from batch 2. It had a standard deviation of chord angle of 8^{o} at 12mm chord length when water-jet cut. The profile together with its roughness statistics are shown in Figure 5.10.

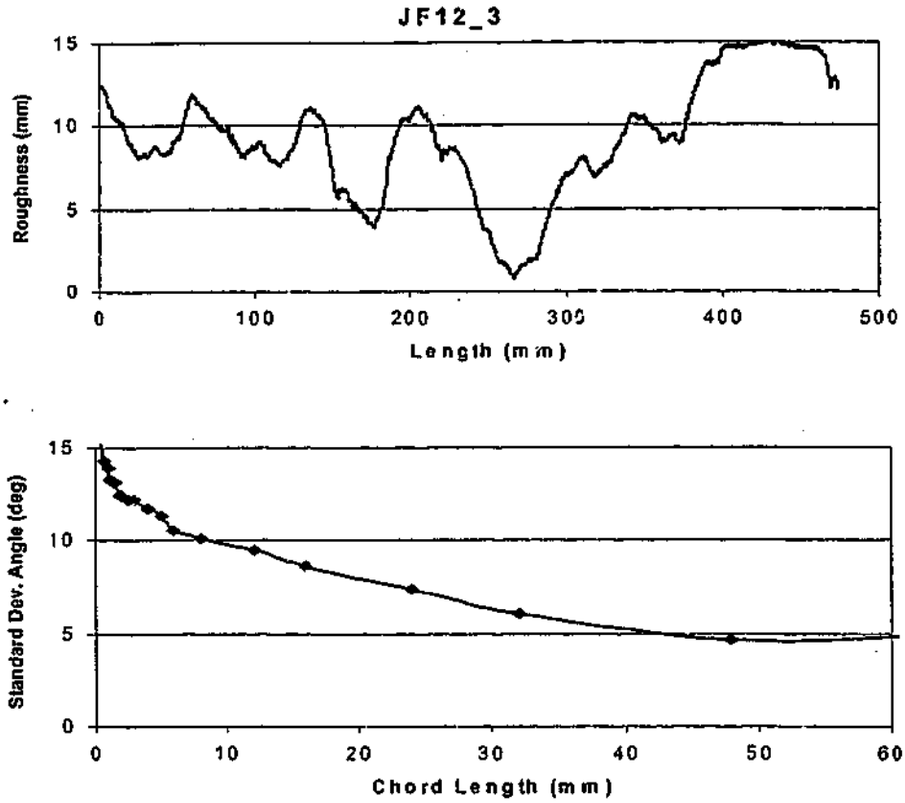

Figure 5.9: Profile JF12_3 and roughness statistics

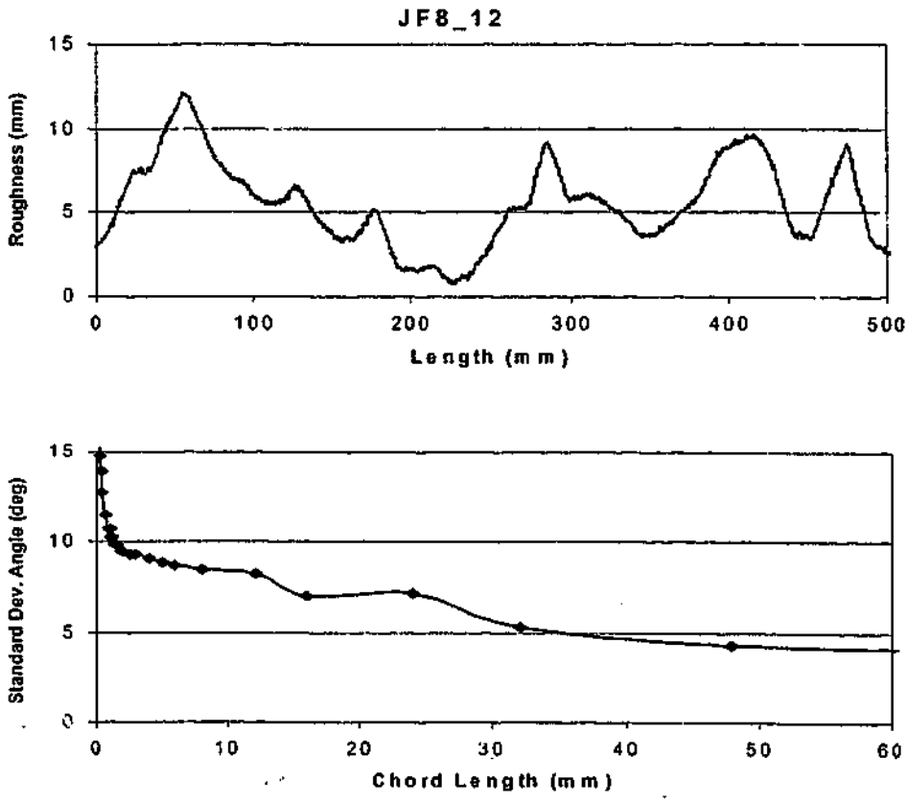

Figure 5.10: Profile JF8_12 and roughness statistics

- A compass, open a distance of 3mm, was walked along a centre profile of split surface JS4a. The locations where the compass intersected the profile were joined by chords (3mm long) to produce fractal profile JF15a_3 (Figure 5.11). This two-dimensional profile was water-jet cut into a Johnstone sample from batch 2. It had a standard deviation of chord angle of 15° at 3mm chord length when water-jet cut. The profile together with its roughness statistics are shown in Figure 5.11.

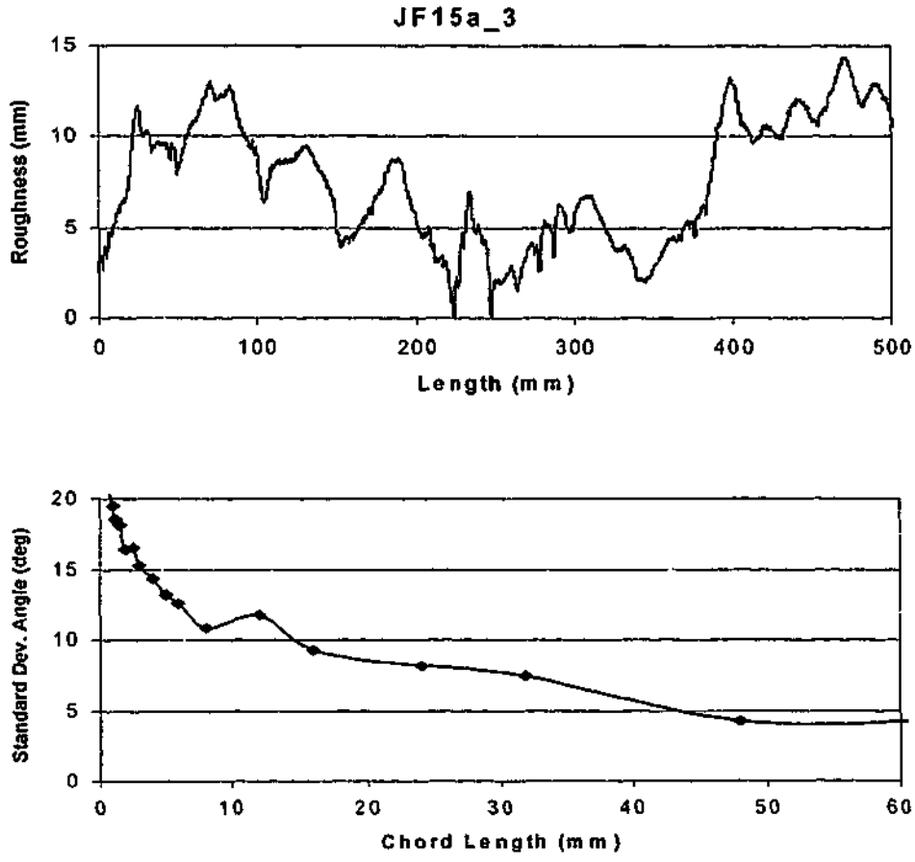

Figure 5.11: Profile JF15a_3 and roughness statistics

- Profile JF15_3 was generated at 3mm chord lengths using the modified midpoint displacement method and a power function of the split surface JS3a statistics (method discussed in Section 3.4.4). This two-dimensional profile was water-jet cut into a Johnstone sample from batch 2. It had a standard deviation of chord angle of 15° at 3mm chord length when water-jet cut. The profile together with its roughness statistics are shown in Figure 5.12.

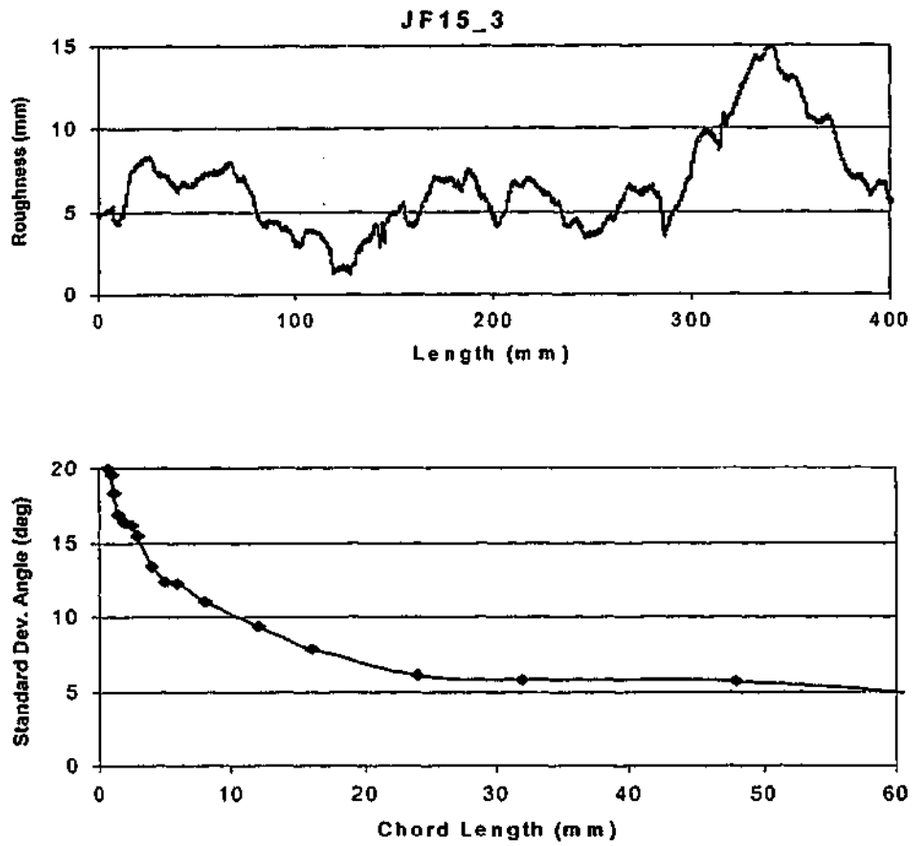

Figure 5.12: Profile JF15_3 and roughness statistics

- Fractal profile JF21_3 was generated at 3mm chord lengths using the modified midpoint displacement method and a logarithmic function of the split surface JS3b statistics (method discussed in Section 3.4.4). This two-dimensional profile was water-jet cut into a Johnstone sample from batch 2. It had a standard deviation of chord angle of 21° at 3mm chord length when water-jet cut. The profile together with its roughness statistics are shown in Figure 5.13.

The samples were placed into the centre of the direct shear box. To minimise compression of the material used to set the sample into the box, steel blocks were placed between the sample and the shear box at the ends where the shear force was being applied. Plaster of Paris was used to hold the sample into the box. Once the shear box was assembled, there was a 20mm gap between the top and bottom shear boxes (shown in Figure 5.1). This was to allow for potential compression of the sample, shearing of the sample along the joint without interference from the shear box, and also to allow easy viewing of the joint during the shearing process.

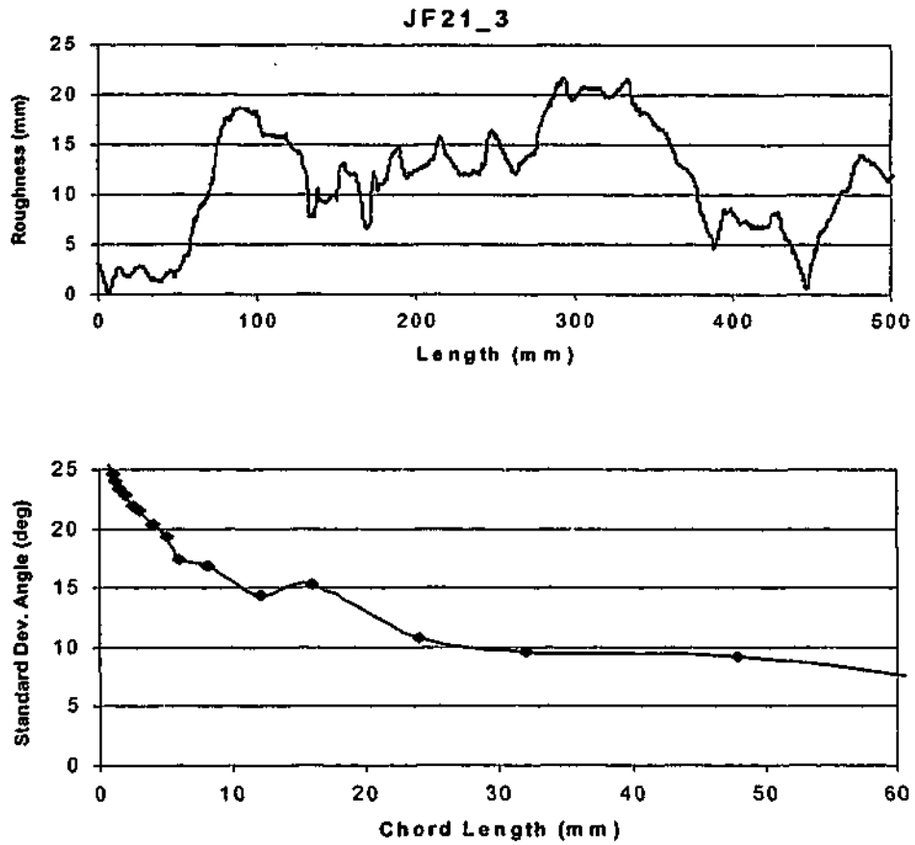

Figure 5.13: Profile JF21_3 and roughness statistics

In addition several Johnstone samples were prepared to test the hypothesis that three-dimensional surfaces could adequately be represented by a single two-dimensional profile. Details of the profiles selected and the direct shear tests performed are presented in Chapter 7.

5.3.2 Sandstone

In addition to tests on Johnstone, Fleuter (1997) conducted a series of shear tests on sandstone / sandstone interfaces containing planar, regular two-dimensional triangular and two-dimensional fractal roughness profiles. The current research extends this work to three-dimensional surfaces.

The three-dimensional surfaces were produced by splitting blocks in a similar manner to the Johnstone splits. Two split surfaces were created in this manner. Profiles of the split surfaces were measured at 5mm spacings using the Monash laser profilometer.

Roughness heights were taken at 0.07mm intervals in each profile. The two-dimensional profiles together with the three-dimensional surfaces are detailed in Appendix C. One surface is shown in Figure 5.14.

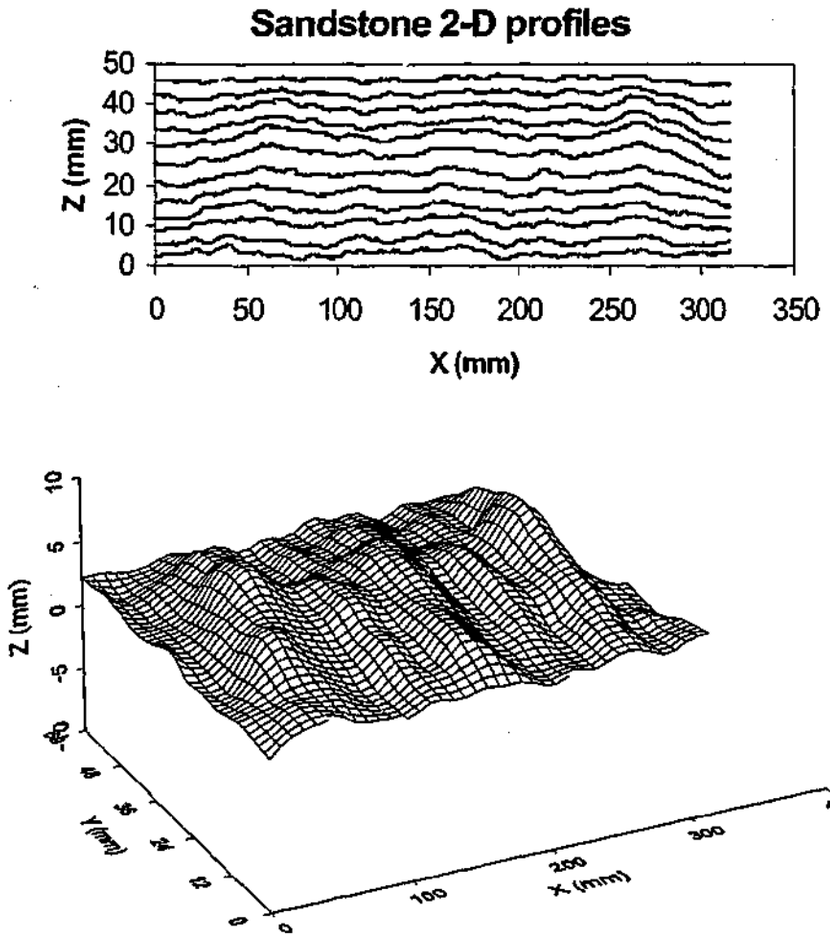

Figure 5.14: Sandstone Split Surface 1

The samples were placed and set into the direct shear box in the same manner as the Johnstone samples.

5.3.3 Siltstone

The blocks of siltstone obtained were irregular in shape and needed to be trimmed to fit into the shear box. Due to the large overall dimensions and weight of the blocks, 5 blocks were initially sent to a stonemasons where they were cut in half to become a more

manageable size. All blocks were then cut "in-house" into rectangular samples using a diamond tipped circular saw. Samples were cut to maximize their length with a width of approximately 80mm usually adopted and a height of 100 – 130 mm.

Despite completing many tests on Johnstone samples, it was considered necessary to repeat these tests on the siltstone samples due to the significantly higher strength and stiffness of this material. The profiles tested therefore included:

- regular triangular asperities at angles of 5°, 10° and 15° at a chord length of 16mm and 10° angles at chord lengths of 8mm and 48mm. All profiles were water-jet cut at mid height of the siltstone samples.
- two-dimensional fractal profiles. These profiles were generated using the modified midpoint displacement method (refer to Section 3.4.2) with target[1] standard deviation - chord angles of 5°, 10° and 15° at 5mm chord length. Four profiles were generated ese are shown in Figures 5.15 – 5.18 (as water-jet cut).
- three-dimensional surfaces. The siltstone samples were split along prominent bedding planes using the same technique as that used for the Johnstone. One split surface is shown in Figure 5.19. The split surfaces were digitised using the Monash laser profilometer. The produced profiles are shown in Appendix C together with the three-dimensional surface. One surface is shown in Figure 5.20.

The samples were placed into the centre of the direct shear box. Samples that were smaller than 130mm high (height of the shear box with a 20mm spacer at the interface) were placed on steel plates so that the joint was approximately at the mid point of the 2 boxes once assembled. As with the Johnstone and sandstone samples, steel blocks were placed between the sample and the shear box at the ends where the shear force was being applied. A high strength grout mixture (approximately 35MPa) was used to hold the top and bottom halves of the sample into the split shear box.

[1] Target- this was the desired value and not necessarily the actual value achieved when following water-jet cutting

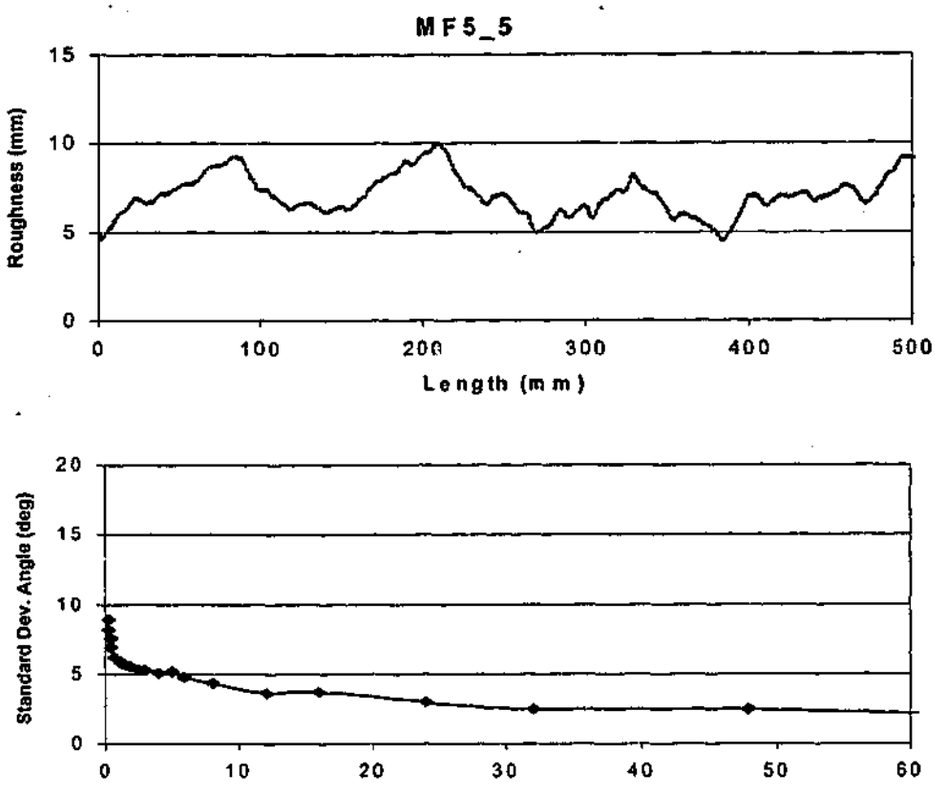

Figure 5.15: Fractal Profile MF5_5

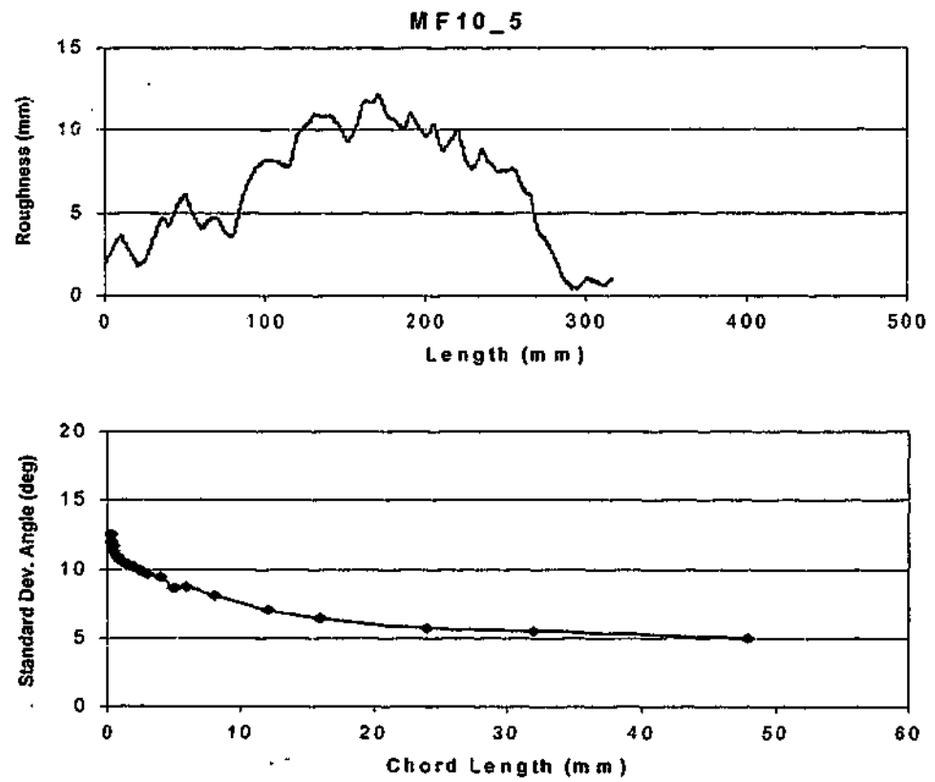

Figure 5.16: Fractal Profile MF10_5

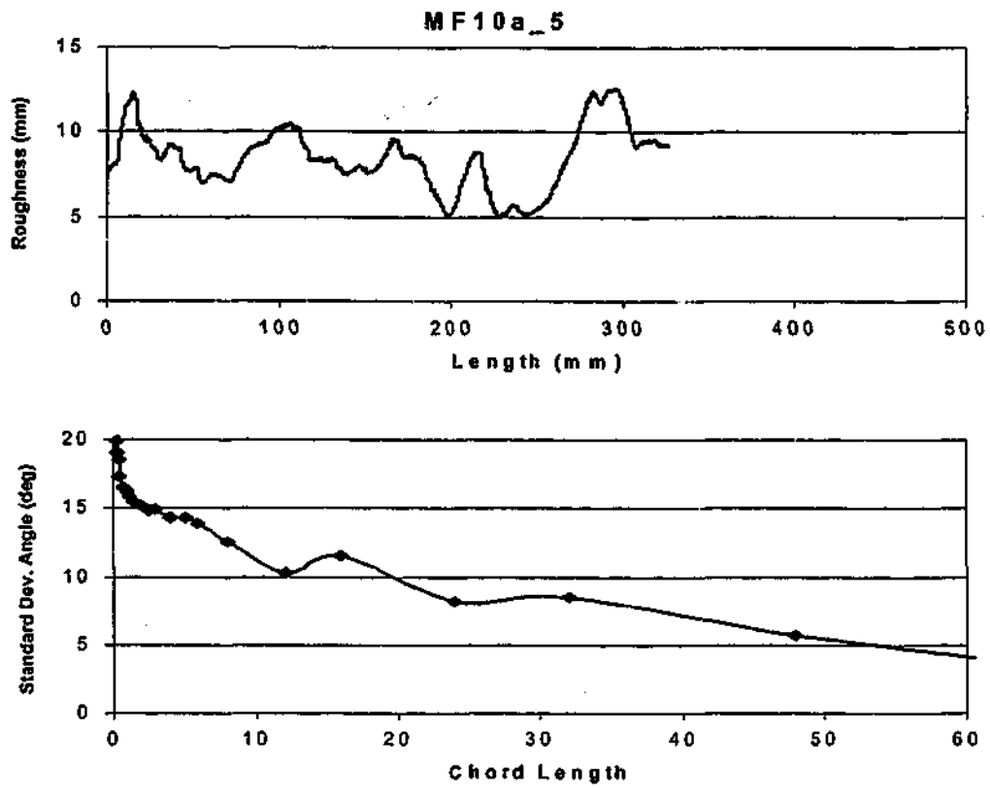

Figure 5.17: Fractal Profile MF10a_5

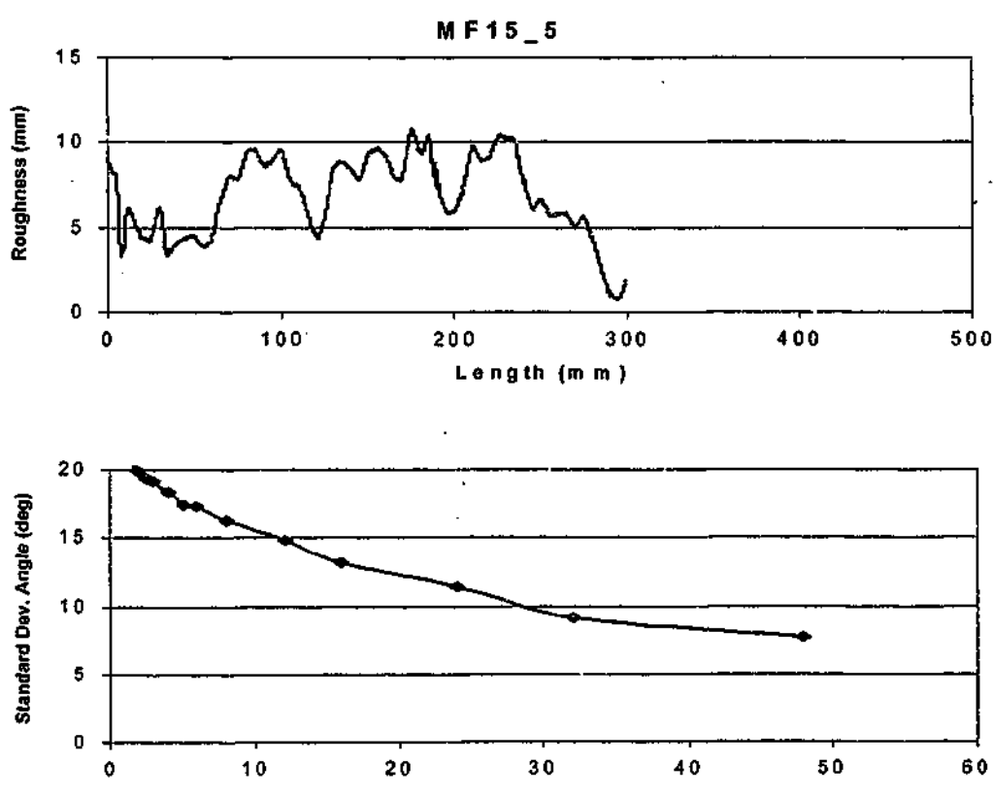

Figure 5.18: Fractal Profile MF15_5

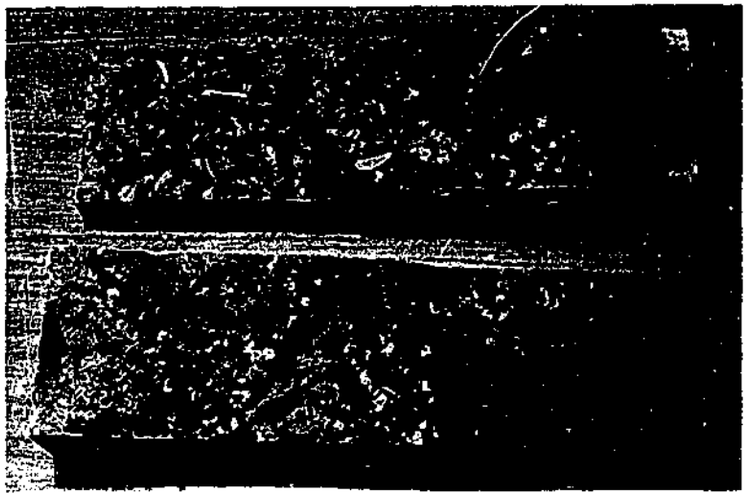

Figure 5.19: Photograph of split siltstone surface

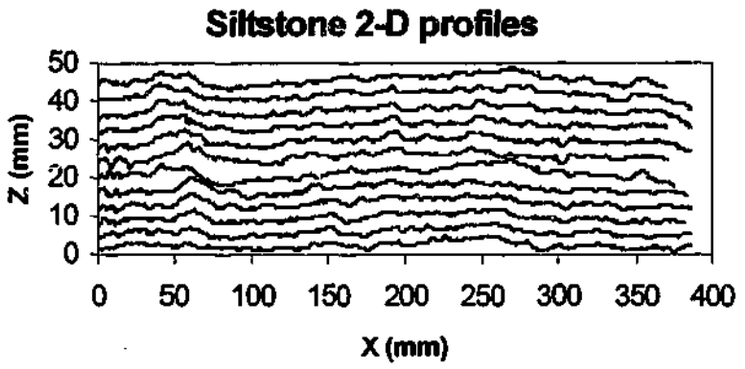

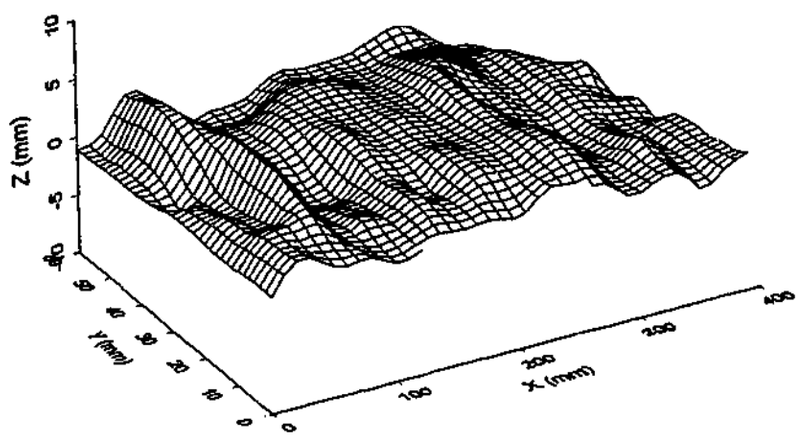

Figu 0: Siltstone Split surface 1

5.3.4 Basalt

The blocks of basalt obtained from the quarry were irregular in shape and required trimming to fit the shear box. The blocks were cut into rectangular samples at Monash University using a diamond tipped circular saw. Samples were cut to maximize their length with a width of approximately 80mm usually adopted and a height of 90 – 130 mm.

This igneous rock is considerably stronger than the rock types previously tested in the CCNS rig. There were concerns that the mechanisms of failure may have been significantly different than for the lower strength rocks. It was therefore necessary to perform a range of tests to develop the failure model. The profiles tested therefore included:

- regular triangular asperities at angles of 5°, 10° and 15° at 16mm chord lengths. These two-dimensional profiles were produced using water-jet cutting techniques. Due to the strength of the rock it was necessary to slow down the rate of advance of the cutting head. This meant that some distortion occurred on the outer edge of the sample. The samples were trimmed along this outer edge to remove this distortion. This produced narrower samples than typically tested (ie. 60mm instead of 80mm wide).

- two-dimensional fractal profiles. The profiles were generated using the modified midpoint displacement method with target standard deviation of chord angles of 10° and 15° at 5mm chord length. These were the same profiles as used for the siltstone. These profiles are shown in Figures 5.15-5.18. The two-dimensional profiles were cut by water-jet.

- three-dimensional split profiles. The basalt blocks were split by impacting each block with a 7 lb sledge hammer. One surface is shown in Figure 5.21. The surfaces were digitised using the laser profilometer. The produced profiles are shown in Appendix C together with the three-dimensional surface. One surface is shown in Figure 5.22.

Figure 5.21: Photograph of basalt split surface

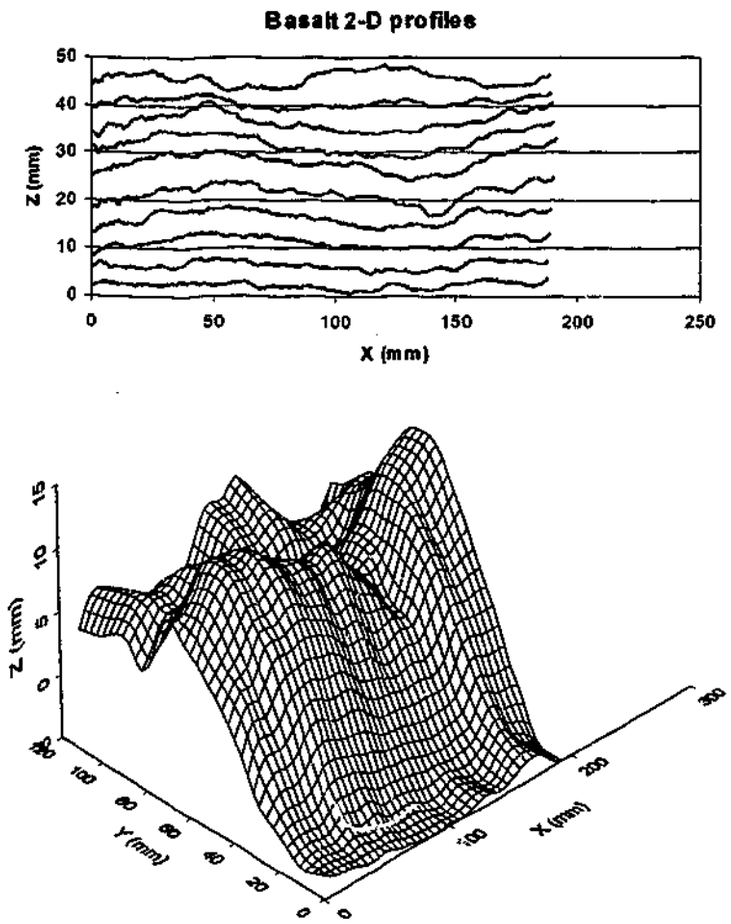

Figure 5.22: Basalt Split surface 1

The samples were placed and set into the direct shear box in a similar manner as the siltstone samples.

5.3.5 Granite

The high quartz content and strength of the rock meant that cutting the blocks on the Monash University circular saw was too difficult and hence all the blocks were cut to size by a stonemason.

The range of profiles tested were:

- regular triangular asperities at angles of 10° and 20° at 8mm chord lengths. These two-dimensional profiles were produced using water-jet cutting techniques.
- three-dimensional split profiles. The granite samples were hydraulically fractured at the laboratories of CSIRO Petroleum Resources Division, Syndal. Steel tubing was first grouted into predrilled 10mm diameter holes along the longest length of the sample and then water mixed with a small amount of oil pumped into the block via these tubes whilst the block was placed under axial loading. One split surface is shown in Figure 5.23. The split surfaces were digitised using the laser profilometer. The joint profiles are shown in Appendix C together with the three-dimensional surface plot. One of these surfaces is shown in Figure 5.24.

The samples were placed and set into the direct shear box in a similar manner as the siltstone and basalt samples.

Figure 5.23: Photograph of granite split surface

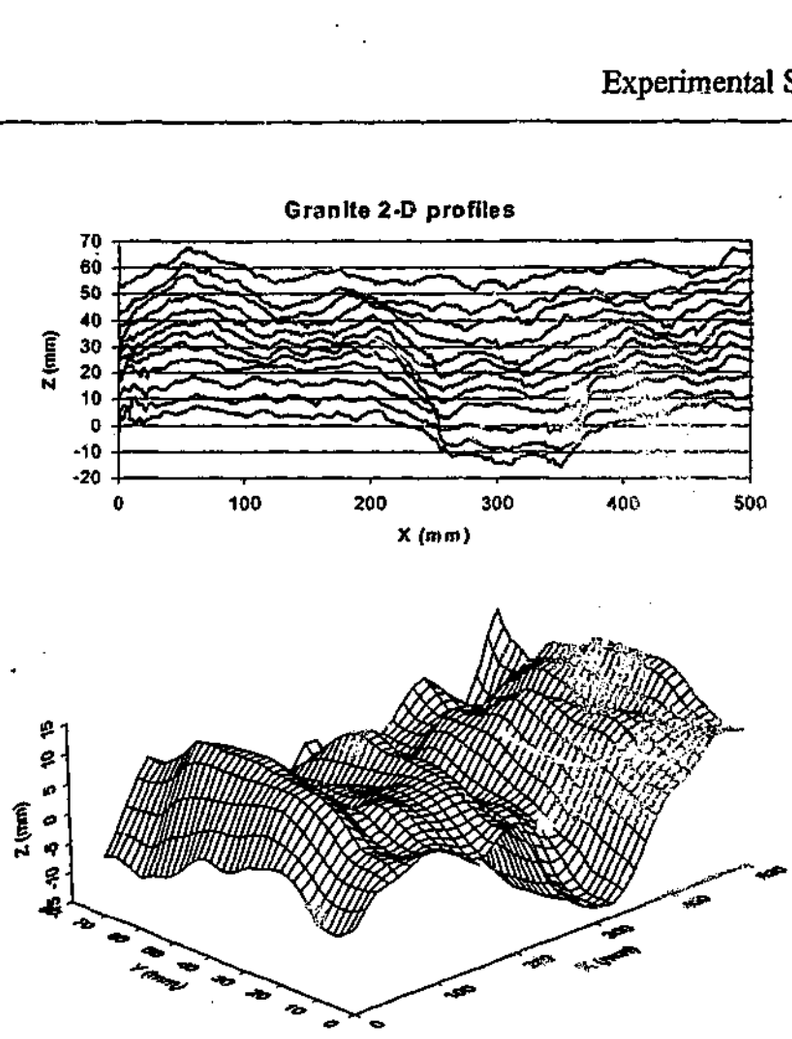

Figure 5.24: Granite Split surface 1

5.4 Summary

In this chapter the CCNS shear rig was briefly described. Details on the various rock types tested and the joint profiles analysed have been given.

The results of the direct shear tests will provide data to investigate the suitability of the soft rock / concrete interface shear model to represent rock joint behaviour. They will be used to develop the model and investigate methods to quantify three-dimensional joint roughness.

Chapter 6 will present the results of the direct shear tests.

6.0 SHEAR TEST RESULTS

A series of laboratory direct shear tests have been conducted to investigate the affects of boundary conditions, scale, roughness, rock strength and rock type and to provide data to verify and develop a rock joint shear behaviour model. This chapter summarizes the results of the direct shear tests performed on the joint samples.

The test program is initially outlined, giving details on the profiles and boundary conditions tested. The effects of varying the boundary conditions, roughness, scale, rock type and strength are discussed. The components of the shearing process (sliding, shearing, wear and post peak behaviour) that were highlighted during the shear tests are also discussed.

6.1 Test Program

A test program was developed that would:

- Confirm the factors influencing shear behaviour and the effects that each of these have on performance eg. varying joint roughness, applied stresses, boundary conditions and scale.
- Identify and analyse differences between concrete-rock behaviour and rock joint behaviour
- Determine the effects of varying rock types and strengths and include these into the model
- Investigate the validity of modelling three-dimensional roughness with two-dimensional profiles.

All shear tests were conducted in only one direction at a shear velocity of 0.5mm/min.

All triangular, fractal and split profiles were tested under constant normal stiffness conditions as this was considered to be more representative of the majority of rock joint situations.

As the split and fractal tests were being conducted for the purpose of model validation and development, testing a range of initial normal stress and normal stiffness values was considered appropriate.

Lower limits of the load transducers meant that normal and shear loads had to be greater than 5kN. This restricted the minimum initial normal stress values to 400 kPa for many of the smaller samples. Initial normal stress values of between 300 kPa and 1000 kPa were selected. This represents a vertical stress on a horizontal joint located at between approximately 14 m and 70 m below ground level.

At high stiffness, stick-slip behaviour was observed on the granite samples and to a lesser extent with the basalt samples. Stick-slip behaviour can occur when rough and high strength joint surfaces interlock and develop a high frictional resistance. Work by Dieterich (1978) has indicated that the transition from stable sliding to stick-slip is a function of normal stress, stiffness and roughness and a consequence of time-dependent friction. However, in these tests it was also partly due to compliance of the direct shear rig frame. As it was not possible to reduce the compliance of the direct shear rig, it meant that restrictions had to be placed on the magnitude of the constant normal stiffness adopted for testing.

The exact stiffness conditions applicable to rock joints depend on the orientation and deformability of the surrounding rock or man-made structures. This was discussed in Section 2.2. As stronger rock with high values of Young's Modulus will deform less, some higher values of stiffness were selected (within the limitations of the direct shear rig). Constant normal stiffness values between 400 kPa/mm and 1200 kPa/mm were selected for testing.

The initial normal stress and stiffness values for the regular triangular profiles were selected to maximize chances of shear failure of asperities occurring whilst remaining within the limitations of the direct shear rig.

Details of the direct shear tests are summarized in Table 6.1. The test nomenclature is as follows:

First letter: material type – **B**asalt, **G**ranite, **J**ohnstone, **M**udstone, **S**andstone

Second letter: profile type – **I**ntact, **P**lanar, **C**ut, **R**egular, **F**ractal, **S**plit

Number before underscore: applied normal stress for intact and planar samples, asperity angle for regular profiles, standard deviation of chord angle for fractal profiles, 3-D copied sample number for cut 2-D Johnstone samples

First number and letter after underscore: sample number for split Johnstone blocks, chord length for regular triangular and fractal profiles, sample number for split blocks, details of replication for 2-D cut Johnstone blocks

Table 6.1: Summary of direct shear tests

Sample	Profile Description	σ_{no} (kPa)	K (kPa/mm)
JF12_3	Johnstone fractal s_θ=12°, 3mm chord length	400	400
JF8_12	Johnstone fractal s_θ=8°, 12mm chord length	400	400
JF15a_3	Johnstone fractal s_θ=15°, 3mm chord length	400	400
JF15_3	Johnstone fractal s_θ=15°, 3mm chord length	400	400
JF21_3	Johnstone fractal s_θ=21°, 3mm chord length	560	600
JS_1a	Johnstone split block 1a, 264mm long	600	400
JS_1b	Johnstone split block 1b, 270mm long	600	400
JS_2a	Johnstone split block 2a, 474mm long	600	400
JS_2b	Johnstone split block 2b, 410mm long	700	800
JS_3a	Johnstone split block 3a, 445mm long	400	400
JS_3b	Johnstone split block 3b, 560mm long	560	600
JS_4a	Johnstone split block 4a, 560mm long	400	400
JS_6a	Johnstone split block 6a, 560mm long	400	400
JS_7a	Johnstone split block 7a, 500mm long	400	400
JC3a_stat6	2-D cut sample of block 3a generated using standard deviation of angle statistics at 6mm chords	400	400
JC4a_6	2-D cut sample at 6mm chords of centre profile from block 4a	400	400

Sample	Profile Description	σ_{no} (kPa)	K (kPa/mm)
JC6a_3	2-D cut sample at 3mm chords of centre profile from block 6a	400	400
JC6a_pow3	2-D cut sample of block 6a generated using power function at 3mm chords	400	400
JC7a_4	2-D cut sample at 4mm chords of centre profile from block 7a	400	400
JC7a_log4	2-D cut sample of block 7a generated using a logarithmic function at 4mm chords	400	400
SS_1	Sandstone split sample 315mm long	400	400
SS_2	Sandstone split sample 330mm long	400	800
MI400	Siltstone intact sample 320mm long	400	0
MI600	Siltstone intact sample 200mm long	600	0
MI800	Siltstone intact sample 272mm long	800	0
MI1200	Siltstone intact sample 244mm long	1200	0
MI1600	Siltstone intact sample 233mm long	1600	0
MP400	Siltstone planar sample 285mm long	400	0
MP800	Siltstone planar sample 206mm long	800	0
MP1600	Siltstone planar sample 233mm long	1600	0
MR5a_16	Siltstone 5° regular x 16mm long	800	800
MR5_16	Siltstone 5° regular x 16mm long	2000	800
MR10_8	Siltstone 10° regular x 8mm long	2000	3200
MR10_16	Siltstone 10° regular x 16mm long	2000	1600
MR10a_16	Siltstone 10° regular x 16mm long	2000	1600
MR10_48	Siltstone 10° regular x 48mm long	1200	600
MR10a_48	Siltstone 10° regular x 48mm long	2000	533

Sample	Profile Description	σ_{no} (kPa)	K (kPa/mm)
MR15_16	Siltstone 15° regular x 16mm long	1400	1600
MF5_5	Siltstone fractal s_θ=5°, 5mm chord length	800	800
MF10_5	Siltstone fractal s_θ=10°, 5mm chord length	1200	600
MF10a_5	Siltstone fractal s_θ=10°, 5mm chord length	600	600
MF15_5	Siltstone fractal s_θ=15°, 5mm chord length	600	600
MS_1	Siltstone split 395mm long	600	400
MS_2	Siltstone split 335mm long	400	400
MS_3	Siltstone split 175mm long	800	800
MS_4	Siltstone split 188mm long	800	400
MS_5	Siltstone split 214mm long	600	600
MS_6	Siltstone split 156mm long	1000	600
MS_7	Siltstone split 162mm long	800	600
BP400	Basalt planar 208mm long	400	0
BP800	Basalt planar 180mm long	800	0
BP1600	Basalt planar 170mm long	1600	0
BR5_16	Basalt 5° regular x 16mm long	1600	1600
BR10_16	Basalt 10° regular x 16mm long	1600	1600
BR15_16	Basalt 15° regular x 16mm long	1600	1600
BF10_5	Basalt fractal s_θ=10°, 5mm chord length	600	600
BF15_5	Basalt fractal s_θ=15°, 5mm chord length	600	600
BS_1	Basalt split 195mm long	400	1000
BS_2	Basalt split 212mm long	400	800

Sample	Profile Description	σ_{no} (kPa)	K (kPa/mm)
BS_3	Basalt split 192mm long	400	800
BS_4	Basalt split 215mm long	400	1000
GP300	Granite planar 450mm long	300	0
GP600	Granite planar 450mm long	600	0
GP1200	Granite planar 450mm long	1200	0
GP2000	Granite planar 450mm long	2000	0
GR10_8	Granite 10° regular x 8mm long	2000	2000
GR10a_8	Granite 10° regular x 8mm long	2000	4000
GR20_8	Granite 20° regular x 8mm long	2000	4000
GS1	Granite split 451mm long	400	1000
GS2	Granite split 449mm long	300	600
GS3	Granite split 210mm long	600	1200
GS4	Granite split 210mm long	600	600

Complete test results are presented in Appendix D. These results are illustrated using five graphs
- shear stress vs. shear displacement
- shear stress vs. normal stress
- dilation vs. shear displacement
- normal stress vs. shear displacement
- normal stress vs. dilation

Results of the shear testing which impact on the modelling of the shear behaviour will be discussed in this chapter. The ramifications of three-dimensional roughness modelling are dealt with in Chapter 7.

6.2 Rock Joint Behaviour

The observed behaviour of the rock samples under the application of a shear load can be divided into several phases:

- Initial closure of the joint under the application of the normal load and commencement of shearing. During this phase the contact area on the joint surface increases. Shear stress rises quickly with the application of shear load. The samples typically experienced initial negative dilation or compression of up to ~0.1mm. As shear displacement occurred, the two interfaces were able to reseat themselves typically into a more mated position. This has also been noted in work by others eg. Gentier et al. (2000). This reseating was most noticeable on the softer rock and on the water-jet cut surfaces. Overall the split surfaces experienced less initial closure. This indicates that it is a laboratory set-up condition rather than something that may be observed insitu.
- As the shearing process continues dilation commences as sliding along the steepest asperities occurs. This dilation is accompanied by a steep increase in shear stress up to the peak shear stress. If the test is conducted under constant normal stiffness conditions, dilation causes a corresponding increase in the normal stress that also increases the shear stress. The sample deforms due to the increase in normal load.
- At the point of peak shear stress, failure of asperities commences. This will occur at different times for different asperities.
- During the post peak phase samples will continue to degrade through shearing, wear and crushing. This increases the area in contact at the interface. Dilation usually continues to increase and if the test is conducted under constant normal stiffness conditions the normal stress also continues to rise. This continues until the sample reaches residual strength with no further dilation occurring.

Edge effects were often observed during testing. On most of the samples, the ends of the sample that were not constrained experienced tensile splitting through the matrix as shown in Figure 6.1. Although this breakage was only approximately 10mm long on the interface, it would reduce the contact area of the sample. Several samples also had minor edge effects along the side of the samples (in particular the softer Johnstone samples). This is also shown in Figure 6.1. Occasionally in the stronger rock a tensile break

occurred through the rock matrix rather than through an asperity. This was due to local stress concentrations from opposing asperities. This is also shown in Figure 6.1.

All these aspects could alter the shear behaviour of the sample. The first 2 situations reduce the contact area therefore causing higher stresses to be applied to the sample. With a constant normal stiffness test, this would be difficult to model as the change in area would need to be accounted for during the test. A tensile split through the sample matrix may not alter the shear behaviour providing there is no rotation or translation across the fracture. However translation or rotation did occur for several siltstone, basalt and granite samples. These test results were disregarded.

Several of the key areas of rock joint behaviour: sliding, shearing, wear and post peak behaviour are discussed in the next sections.

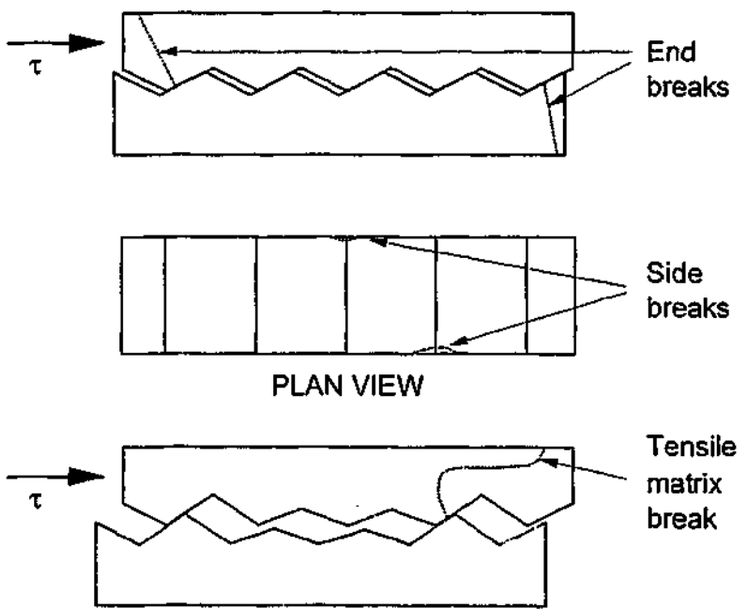

Figure 6.1: Locations on Samples where Tensile Break Occurred

6.2.1 Sliding

Pure sliding can be observed in the direct shear test results on the regular triangular interfaces. These two-dimensional profiles were water-jet cut into samples of siltstone, basalt and granite at constant asperity angles of 5°, 10°, 15° or 20°. The profiles were laser profiled to verify the angle cut by the water-jet cutting procedure. The average angles varied slightly due to slight inaccuracies in the water-jet cutting procedure as discussed in Section 5.3. The as cut average asperity angle was used to analyse the sliding behaviour. The normal stress versus shear stress plots for several tests are shown in Figure 6.2.

As expected, the shear tests indicate purely frictional sliding at an angle of $(i+\phi)$, where ϕ=28.5° for siltstone joints, 34° for basalt joints and 36.5° for granite joints. There was no cohesion present in the sliding response and the shear stress was seen to be adequately predicted using the theoretical expression for sliding proposed by Patton (1966) and given by Equation 6.1.

$$\tau = \sigma_n \tan(i+\phi_b) \qquad (6.1)$$

where τ = shear stress

σ_n = normal stress

i = angle of asperity

ϕ_b = basic friction

Several tests were continued to large deformations so that the frictional sliding down the rear face of the asperity could be measured. The frictional sliding at an angle of $(\phi - i)$ has been marked on some of the graphs shown in Figure 6.2. There is no cohesion present and all of the tested materials gradually indicate purely frictional sliding at the corresponding predicted angle of $(\phi - i)$. The delay in reaching this angle may be due to the slight shearing of the very tips of the asperities as they are overtopped.

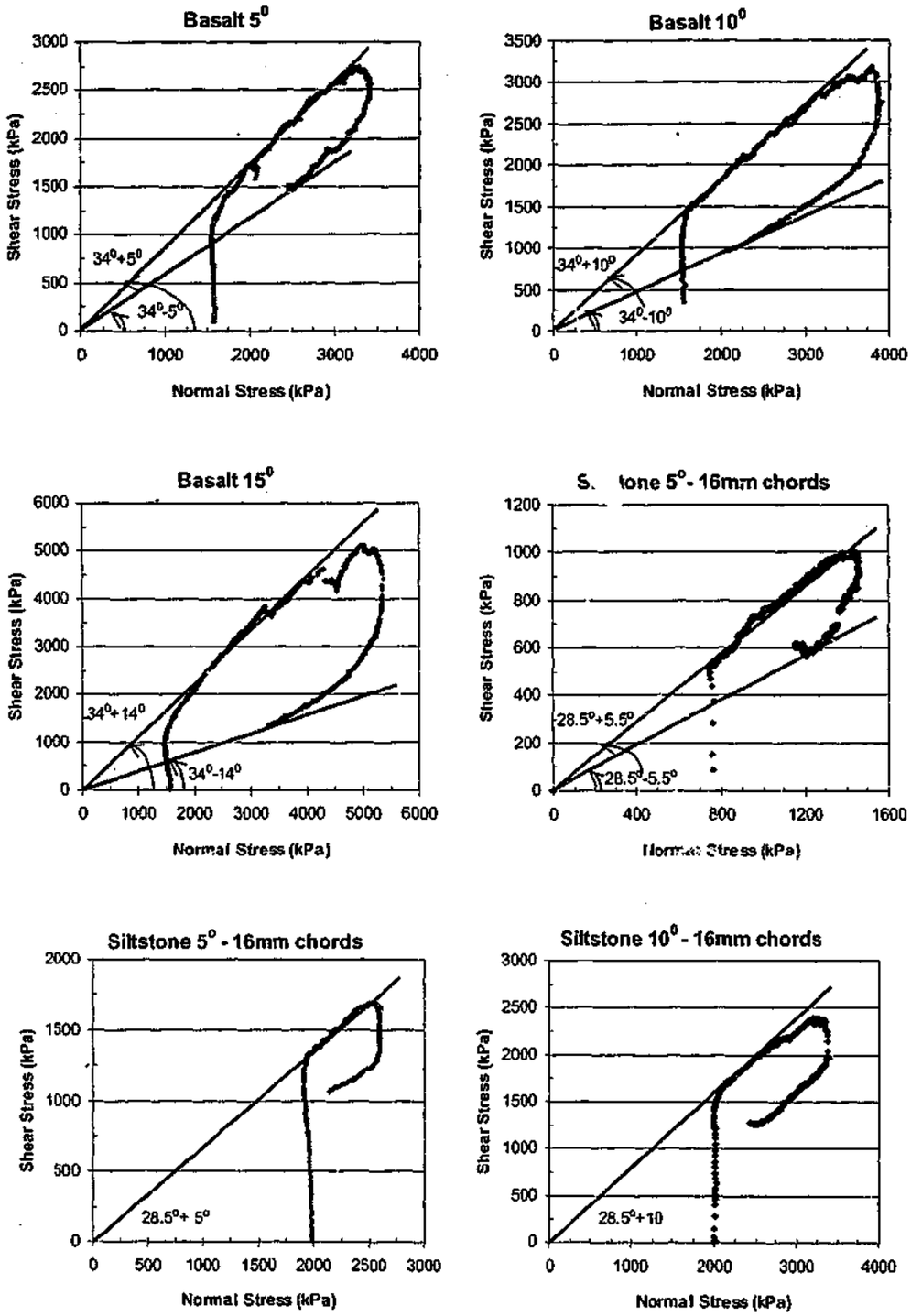

Figure 6.2: Sliding angles of tested materials

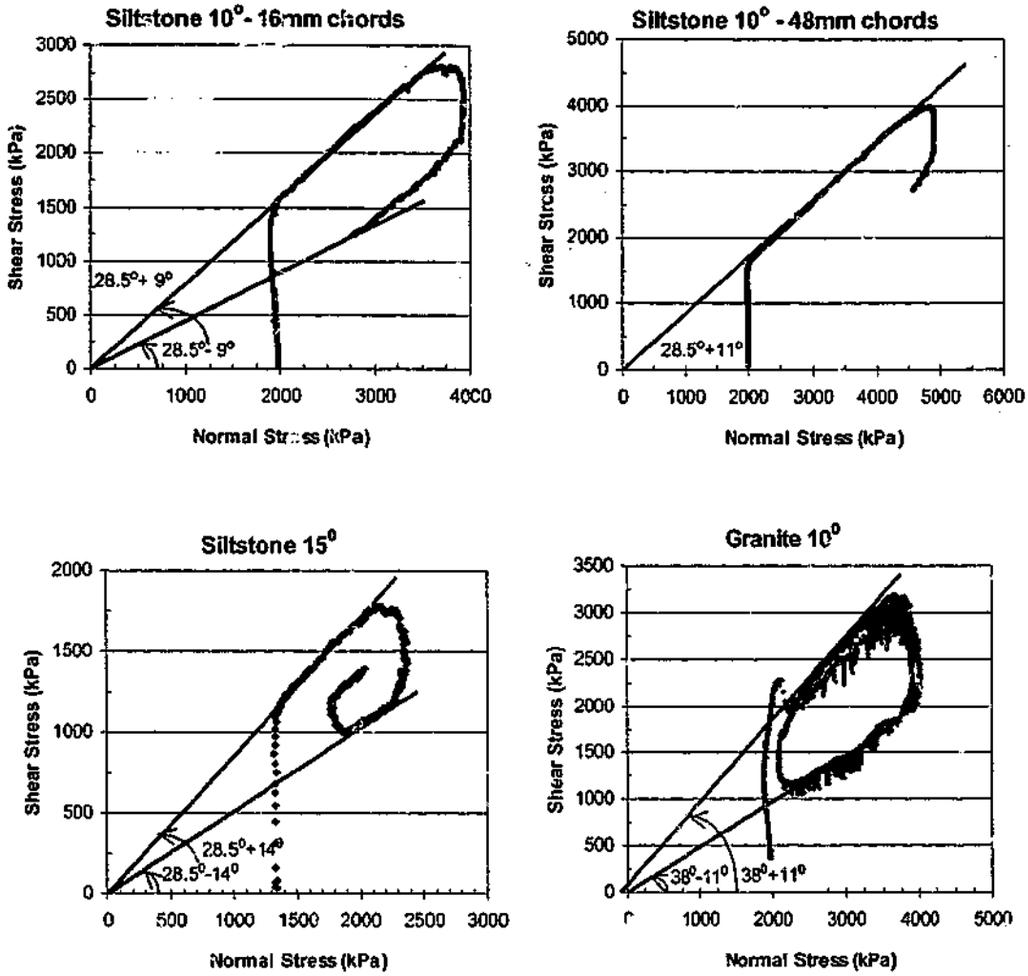

Figure 6.2 (cont'd): Sliding angles of tested materials

6.2.2 Shearing

Shear tests performed on siltstone regular triangular asperities parallel to the bedding plane indicated a small amount of asperity shearing along the bedding plane. This shearing occurred at the tips of both interfaces as the local stresses increased. This is shown diagrammatically in Figure 6.3. The tests conducted on the two-dimensional fractal siltstone profiles also indicated some shearing of the steeper and larger asperities. Sliding and dilation on the steeper asperities caused part of the interface to move out of contact causing the stresses to become highly localized in the area of the steep asperities. When this was greater than the strength of the intact rock, shearing of these asperities occurred.

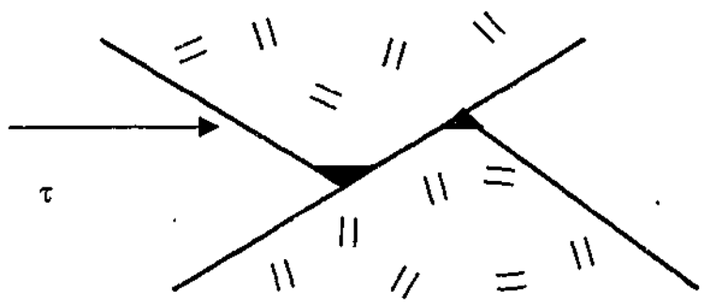

Figure 6.3: Shearing of the tips of asperities

Very little shearing occurred on the basalt or granite triangular asperities. Only minor tip shearing occurred as the asperities were overtopped. A basalt 10° 16mm triangular interface was retested as shown in Figure 6.4. This test was conducted at an initial normal stress of 1600kPa and constant normal stiffness of 1600kPa/mm. The test results indicate that only a small amount of damage was done to the surface during the initial 25mm of displacement.

The s_θ = 15° (chord length = 5mm) fractal basalt profile experienced some shearing during shear displacement. This shear occurred through the base of a long wavelength, high angle asperity and therefore included several smaller asperities as shown in Figure 6.5.

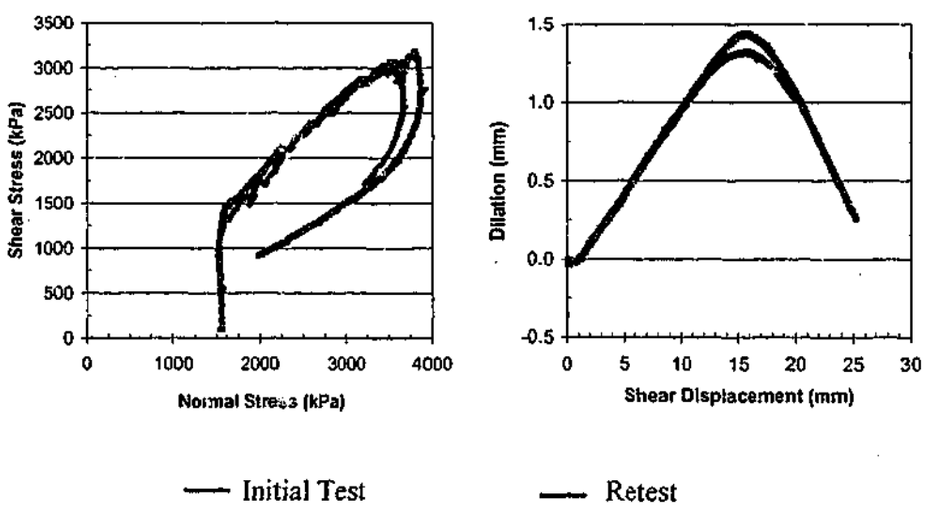

Figure 6.4: Basalt 10° shear tested twice to measure amount of damage to surface

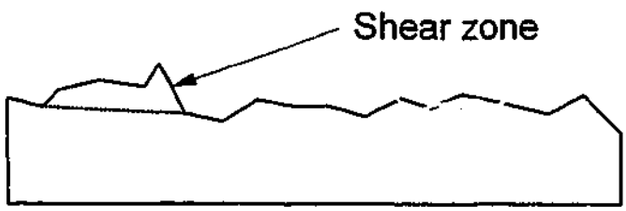

Figure 6.5: Shear through longer asperity

All of the split samples experienced shearing of some asperities.

Unfortunately shear failure mechanisms could not be clearly observed during the shear tests or in later analysis of video footage.

6.2.3 Wear

Wear on the contacting surfaces reduces the amount of dilation and hence under constant normal stiffness conditions will decrease the amount of applied normal stress. Very minor wear marks were visible on the surface of the siltstone, basalt and granite triangular samples after shear testing. The net friction angle ($\phi+i$) obtained from the shear test results performed on these regular triangular asperities remained relatively constant over the length of the asperity also indicating that very little wear occurred.

Previous work on sandstone regular triangular and fractal interfaces indicated that considerable wear had occurred (Fleuter 1997). In the sandstone split surface tests it was difficult to distinguish between wear of the surface and asperity shearing due to the very fine asperities present. Crushing of the granite asperities was also seen in the granite split interfaces. The crushed material formed whitish powder debris between the interfaces. It is believed that this crushed material would behave in a similar manner to worn material forming debris on the surface.

6.2.4 Post Peak Behaviour

After the peak shear stress is obtained, the samples were observed to be experiencing various forms of degradation. Shearing of the steeper asperities occurred with a corresponding (inferred) redistribution of load between asperities. This typically

increased the contact area between the two interfaces. The edge effects discussed previously typically became apparent during the post peak stage.

With several of the samples there was an overlying positive trend to the interface that caused a gradual increase in dilation and hence, as the tests were conducted under constant normal stiffness conditions, the normal stress also rose. This caused a gradual increase in the shear stress that masked some decline in shear stress once degradation commenced.

With the smoother surfaces and softer rock samples, further shear displacement ultimately reached the residual strength of the rock with dilation stopping and the shear stress and normal stress becoming relatively constant.

6.3 Factors Affecting Shear Behaviour

6.3.1 Applied Stresses

Previous laboratory direct shear tests conducted on Johnstone / concrete interfaces have indicated that an increase in initial normal stress causes an increase in the peak shear strength (Seidel 1993). A direct shear test was performed on a triangular rock joint profile to verify this behaviour in strong rock joints. Two regular 5° triangular siltstone interfaces were tested with a constant normal stiffness of 800kPa/mm with one sample subjected to an initial normal stress of 800 kPa and the other an initial normal stress of 2000 kPa. The results shown graphically in the shear stress - shear displacement plot and shear stress – normal stress plot in Figure 6.6, indicate that the increase in initial normal stress caused a significant increase in the shear stress. This is to be expected as shear stress is proportional to normal stress as shown by the Equation $\tau = \sigma \tan(\phi+i)$.

The shear stress versus normal stress plot indicates a frictional sliding angle ($\phi+i$) of approximately 33.5° for both samples (Figure 6.6). This corresponds to a basic friction angle of 28.5° and asperity angle of 5°. However, the actual dilation angle indicated on the dilation versus shear displacement plot is approximately 4.0° for sample MR5_16 (σ_{no}=800kPa) and 3.5° for sample MR5_16a (σ_{no}=2000kPa). Both are lower than the actual asperity angle with the change in dilation angle being greater the higher the initial normal stress. This decrease in dilation angle is due to compression of the sample,

compression of the casting material, closure of the interface and normal compliance in the shear rig. These components are all stress dependent.

The dilation versus shear displacement plot also indicates a considerable amount of initial compression of the samples as shear displacement commences. This is typical of most of the shear tests conducted and is due predominantly to closure of the interface upon commencement of shear displacement and shear compliance of the direct shear rig. This initial compression was higher with the higher initial stress indicating it is dependent on normal load.

(a)

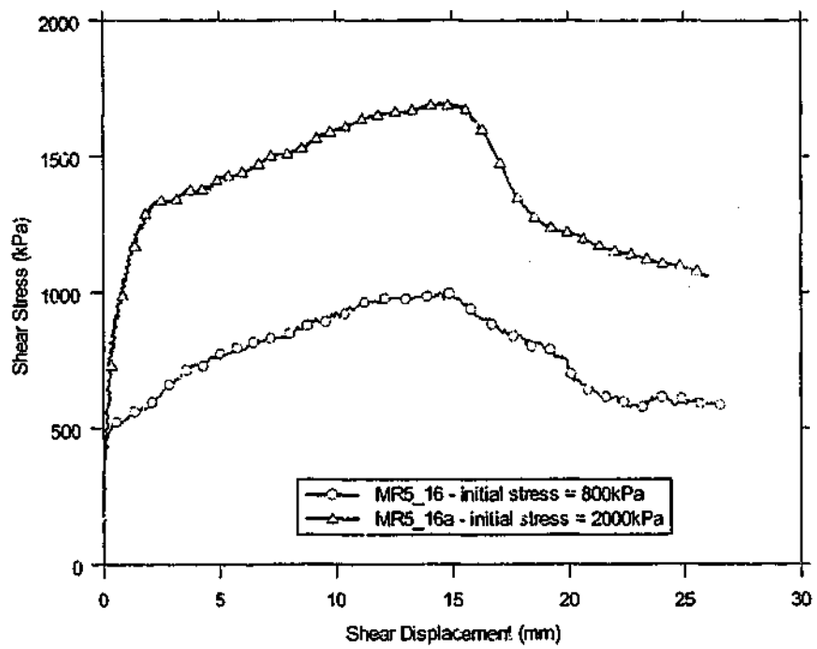

Figure 6.6: Initial normal stress comparison – 5° regular siltstone asperities

(b)

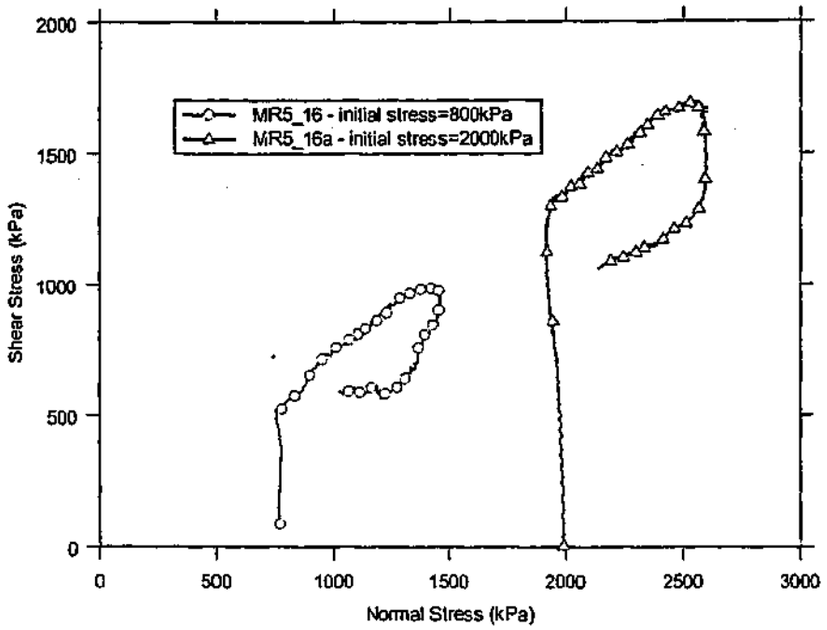

(c)

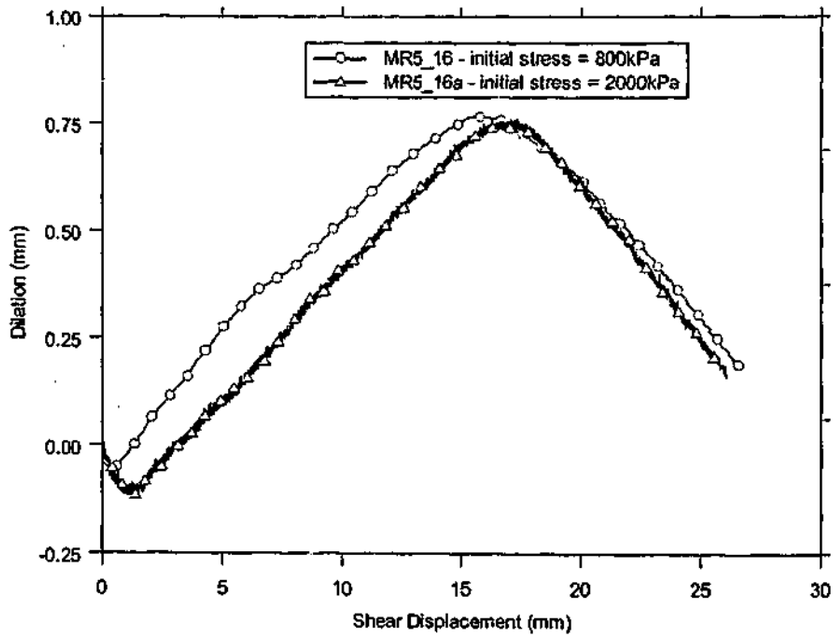

Figure 6.6 (cont'd): Initial normal stress comparison – 5° regular siltstone asperities

6.3.2 Boundary Conditions

Boundary conditions can be altered in the direct shear tests by applying different constant normal stiffness conditions. Previous tests on Johnstone and sandstone regular triangular asperities by Fleuter (1997) indicated that increasing stiffness causes an increase in the peak normal stress.

A test to verify the effects of varying the normal stiffness conditions was conducted on two granite regular triangular asperity samples. The two 10° regular triangular granite interfaces were subjected to an initial normal stress of 2000 kPa with a constant normal stiffness of 2000kPa/mm applied to one sample and a constant normal stiffness of 4000kPa/mm applied to the other. The results shown graphically in Figure 6.7 in the shear stress - shear displacement plot and shear stress – normal stress plot, indicate a higher peak shear stress for the sample with the higher constant normal stiffness. This would be expected as the higher constant normal stiffness causes a greater increase in normal stress as dilation occurs. As previously discussed a higher normal stress will increase the shear stress.

The shear stress versus normal stress plot indicates a frictional sliding angle ($\phi+i$) of approximately 48° for sample GR_10a. This corresponds to a basic friction angle of 38° and asperity angle of 10°. Sample GR_10 has a similar friction angle although there is an initial drop in shear stress that when observed during the shear test was thought to be stick-slip behaviour. Stick-slip can be seen through both test samples at intervals by sharp drops in the shear stress. The actual dilation angle indicated on the dilation versus shear displacement plot is approximately 8.4° for sample GR10 (K=2000kPa/mm) and 6.1° for sample GR10a (K=4000kPa/mm). Both are lower than the actual asperity angle with the reduction in dilation angle being greater the higher the constant normal stiffness. This decrease in dilation angle is due to compression of the sample, compression of the casting material, closure of the interface and normal compliance in the shear rig. These components are all stress dependent. When stick-slip behaviour occurred lower shear stresses were obtained. This is thought to be due to a dissipation of the stored energy in the direct shear rig frame. The higher the constant normal stiffness, the greater the stick-slip experienced by the sample.

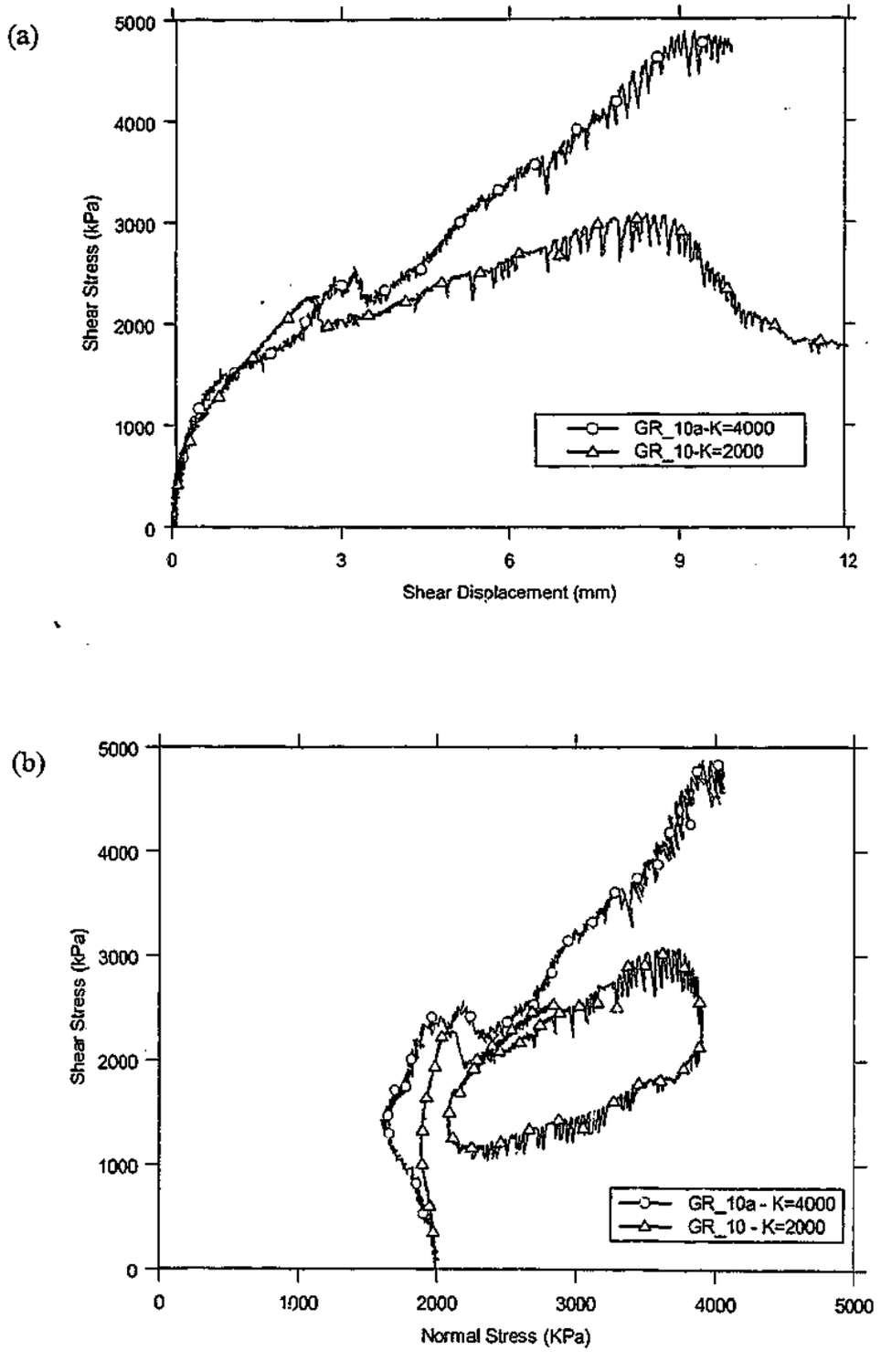

Figure 6.7: Constant normal stiffness comparison – 10° regular granite asperities

(c)

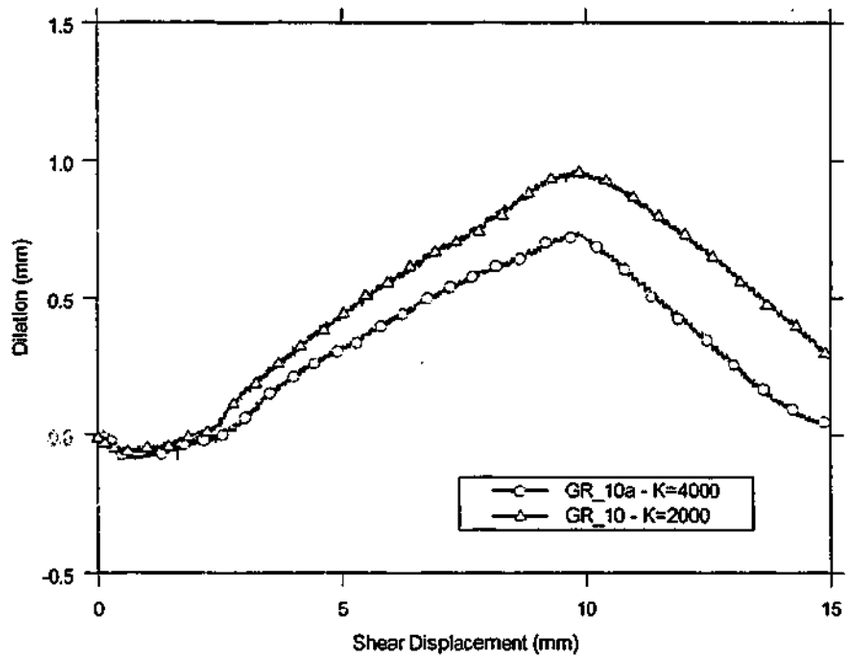

Figure 6.7 (cont'd): Constant normal stiffness comparison – 10° regular granite asperities

There is an initial compression of the sample as shear displacement commences. This compression is partly due to machine compliance and joint closure on the application of shear displacement. This reduces the measured peak dilation. The higher the constant normal stiffness the smaller the measured peak dilation as the compliance and elastic compression components are stress dependent.

These accumulative effects on the dilation of the sample mean that the peak shear stress is not proportionally higher as predicted using the Equation $\tau = \sigma\tan(\phi+i)$ and calculating directly the increase in the normal stress due to the higher constant normal stiffness.

6.3.3 Roughness

As the surface roughness increases, so does the peak shear strength as the greater roughness produces a larger total friction angle (ie. $(\phi+i)$) and hence shear strength (ie. $\tau=c+\sigma_n\tan(\phi+i)$). Under constant normal stiffness conditions, the rougher the surface the greater the dilation rate thus resulting in an increased rate of additional normal stress. An increase in normal stress will increase the shear stress.

A comparison of the effect of changing roughness in different rock types was conducted on siltstone and basalt rock samples. Fractal profiles with standard deviation of chord angle (s_θ) of 10° and 15° at 5mm chord lengths (these profiles can be seen in Section 5.3.3) were water jet cut into two siltstone and two basalt samples. The direct shear test results are shown in Figure 6.8 and Figure 6.9.

The rougher surfaces (ie. s_θ=15°) indicate a greater initial peak shear stress for both the siltstone and basalt profiles. The s_θ=15° shear results indicated a stiffer initial response than the s_θ=10° shear results due to the higher initial dilation caused by the steeper asperities. The later part of the siltstone s_θ=15° shear results continues increasing in shear stress due to an overlying trend of approximately 5° causing further dilation. The basalt s_θ=15° shear results indicate a decrease in shear stress after approximately 9mm due to shearing of several asperities.

6.3.4 Scale

As discussed in Section 2.2.3, roughness is scale dependent. To be able to compare laboratory test samples and natural scale joints it is important to be able to predict results at any scale. Fleuter (1997) conducted a series of scale tests on Johnstone and sandstone profiles containing regular triangular asperities. He showed that for scale equivalence between joints, the respective joint stiffnesses, K, are related by the inverse of the scaling factor. This means that if asperity segment lengths, λ, of 16mm and 48mm were selected, the normal stiffness adopted for the larger asperity sample should be scaled by 1/3. For exact scale equivalence, this relationship also requires the sample depths to be related by the inverse of the scaling factor. Due to limitations of the depth of the direct shear box and difficulties of obtaining samples of significantly larger depth, this was not possible in the direct shear tests conducted for Fleuter's work or this current project and as a result similar sample depths were used. This would lead to disproportional elastic deformations that could lead to higher normal and peak shear stresses for the longer chord length samples.

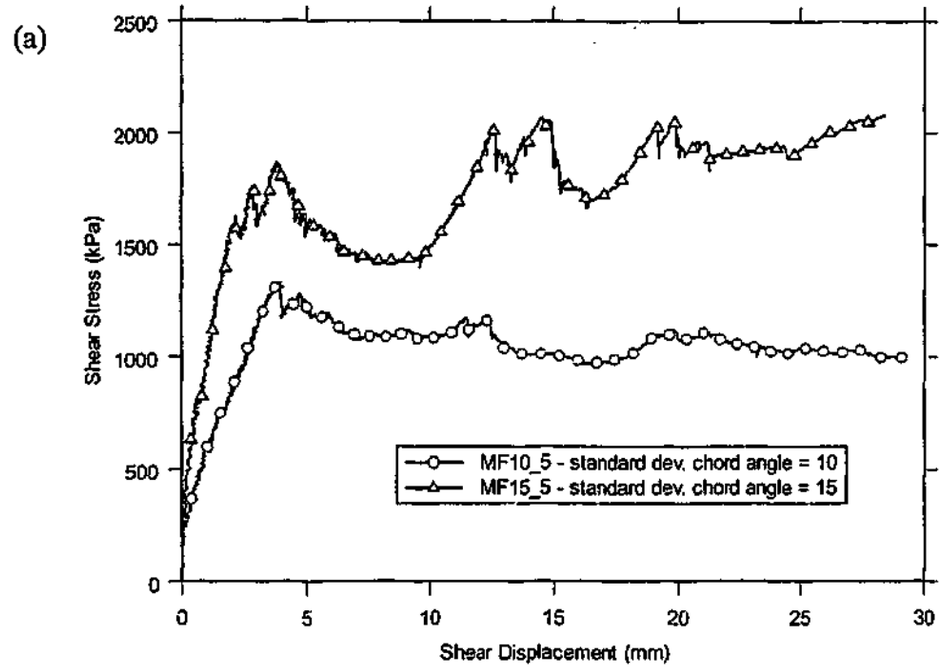

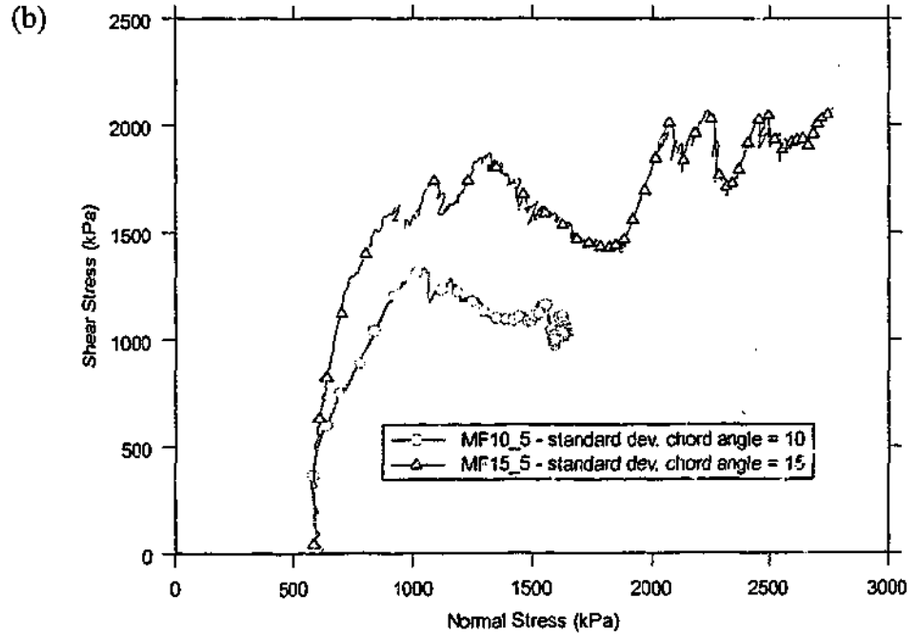

Figure 6.8: Roughness comparison – siltstone fractal profiles σ_{no}=600kPa, K=600kPa/mm

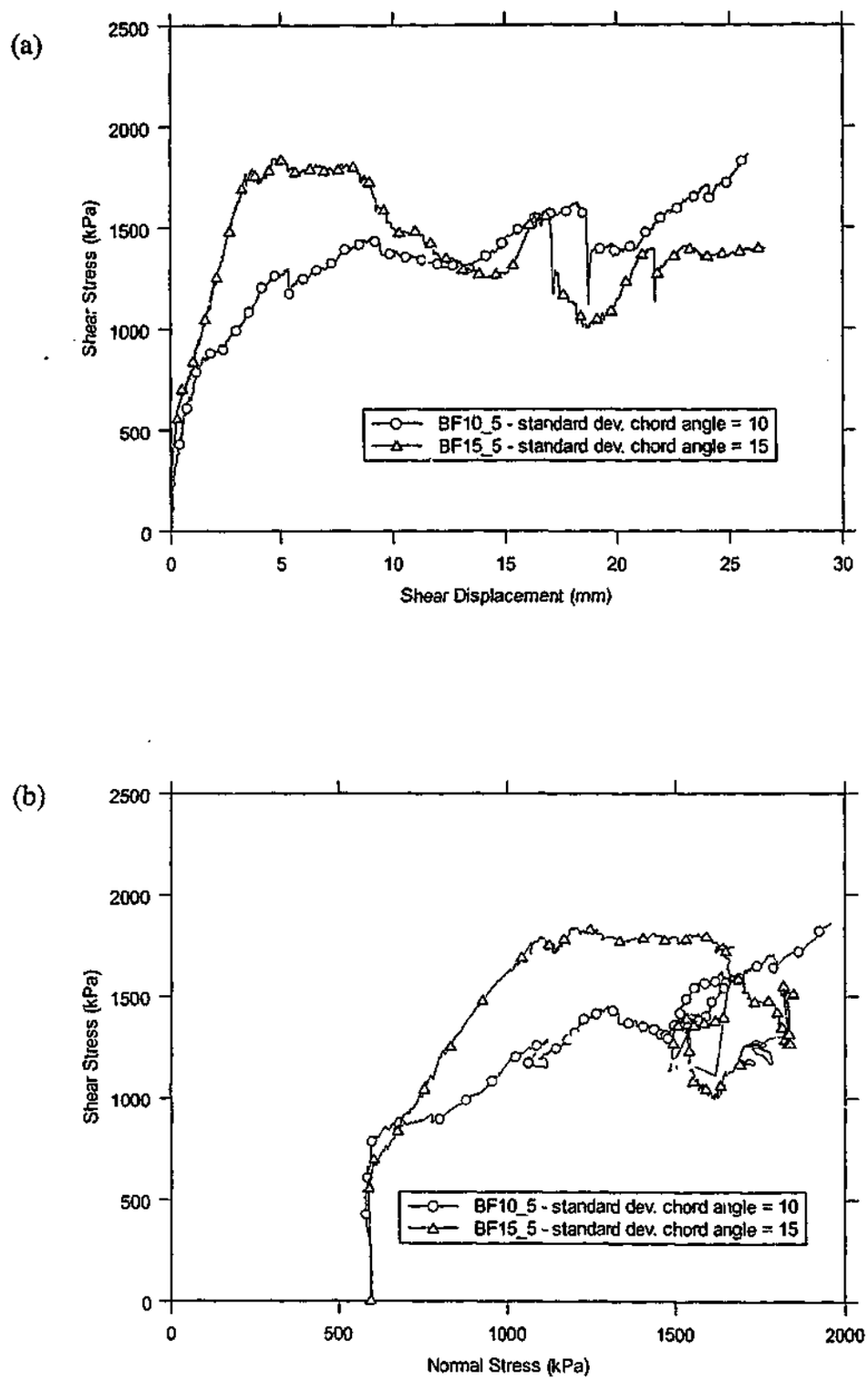

Figure 6.9: Roughness comparison – basalt fractal profiles σ_{n0}=600kPa, K=600kPa/mm

Tests conducted on Johnstone by Fleuter (1997) showed excellent agreement of both peak shear stress and peak dilation between the 16mm and 48mm chord length samples. However, tests conducted on sandstone samples consistently had larger dilation and higher peak shear stress for the 48mm chord length asperities. This variation was attributed to violation of sample depth scaling and an inability to take into consideration any wear components and joint closure effects.

A scale test was conducted by the author on a 10° regular asperity siltstone profile to investigate this overestimation of dilation. One siltstone sample was water-jet cut with asperity chord lengths of 16mm and another with asperity chord lengths of 48mm. Both samples were tested at an initial normal stress of 2000kPa. The constant normal stiffness applied to the 16mm chord length sample was 2000kPa/mm. The constant normal stiffness applied to the 48mm chord length sample was 533kPa/mm (ie. 1/3 of the normal stiffness applied to the 16mm chord length sample). The direct shear test results can be seen in Figure 6.10. The 48mm chord length asperity profile again overestimated the dilation compared to the 16mm chord length asperity profile. This has been attributed to the violation of sample depth scaling together with a greater initial compression of the smaller chord length sample. The 16mm chord length asperity result indicates a significantly less stiff initial response compared with the 48mm chord length asperity results. With no elasticity, joint closure or machine compliance effects the 16mm chord length asperity profile would be expected to dilate approximately 2.8mm. However, the test results indicate only 1.25mm dilation (45% of the expected dilation). This sample had approximately 0.25mm of negative dilation at the commencement of shear displacement. This is due to sample closure and shear compliance of the direct shear rig and sample. With no elasticity, joint closure or machine compliance effects the 48mm chord asperity profile would be expected to dilate approximately 8.3mm. However, the test results indicate 5.8mm dilation (70% of the expected dilation). This indicates that there has been disproportionate compression of the sample and the sample setting for the smaller chord length sample.

Two other scale tests were conducted on a 8mm chord length sample and another 16mm chord length sample in the siltstone rock. The results of these tests can be seen in Appendix B. These tests experienced a small amount of dilation followed by a negative dilation[2] of the sample. This may indicate that initial mismatching of the samples allowed further seating to occur once the surface was sufficiently displaced. It also may indicate

[2] joint compression or closure of interface

the presence of compliance of the shear rig in the shear direction. Due to these problems the results were difficult to compare to the 48mm chord length profile.

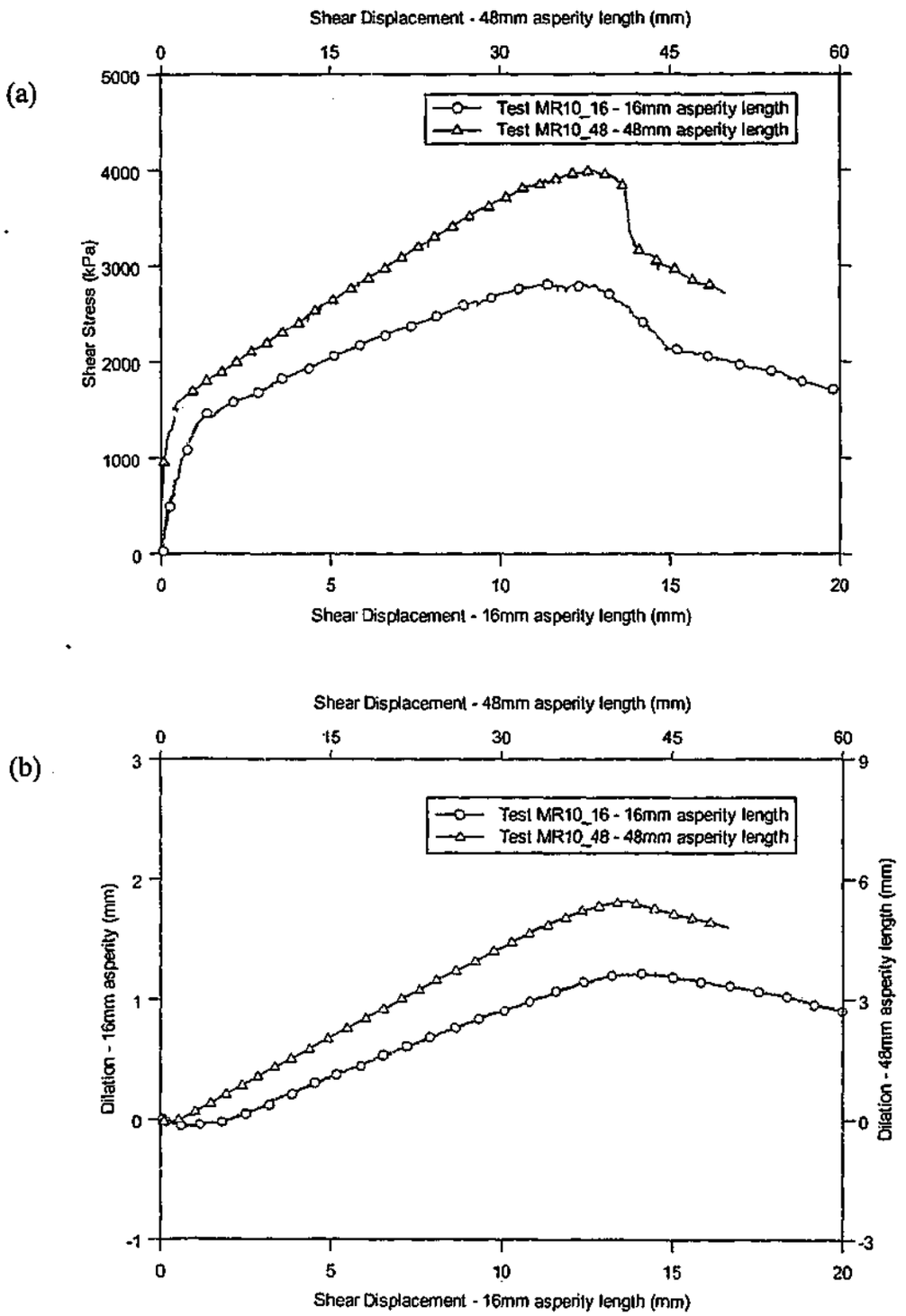

Figure 6.10: Scale comparison – siltstone 10° regular triangular asperities

Although the scale equivalence tests conducted for this work produced varied results due predominantly to sample variation, sample depth variation and set-up problems, these results combined with test results by Fleuter (1997) and Seidel (1993) suggest that scale equivalence between joints can be obtained if the respective joint stiffnesses, K, are related by the inverse of the scaling factor. Further work is required to confirm this.

6.3.5 Rock Strength and Type

Johnstone, a low strength artificial sedimentary rock; sandstone, a low to medium strength sedimentary rock; siltstone, a medium to high strength sedimentary rock; basalt, a high strength igneous rock with some vesicles; and granite, a high to very high strength igneous rock were tested as part of this work. The strength and type of rock were observed to influence the components of the shearing behaviour. All rock types were observed to undergo sliding (discussed in section 6.3.1). As the normal loads tested were kept within realistic near surface rock conditions, the stronger rock types did not experience significant shearing. The various rock types were also shown to produce different roughness profiles when split. A comparison of the typical standard deviation of chord angle with chord length statistics produced for each material can be seen in Figure 6.11. This chart has been produced using the average statistics of one typical surface. Each rock type is briefly discussed in turn below.

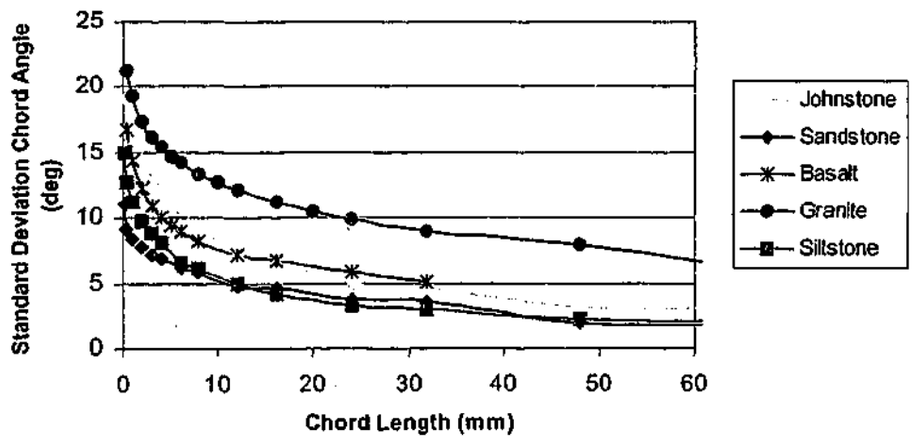

Figure 6.11: Comparison of Standard Deviation of Chord Angle Statistics for Different Rock Types

The Johnstone, being a softer rock, experienced significant shearing when the local stresses were greater than the strength of the intact material. The samples appeared to shear rather than undergo any wear. The Johnstone split profiles were typically relatively similar in the fine scale roughness with some variation in the longer wavelength roughness. Typically the longer roughness wavelengths (chord lengths greater than 30mm) possessed a standard deviation of chord angle of approximately 4° although several profiles had up to 10° standard deviation of chord angle (eg. JS3b and JS7a). The shear test results of the split surfaces typically showed an initial peak shear stress due to interlocking of asperities, followed by relatively constant shear stress associated with little change in dilation. An example shear test result is shown in Figure 6.12. Damage was sustained to a large proportion of the joint surface as the surfaces were relatively flat and considerable shearing of asperities took place.

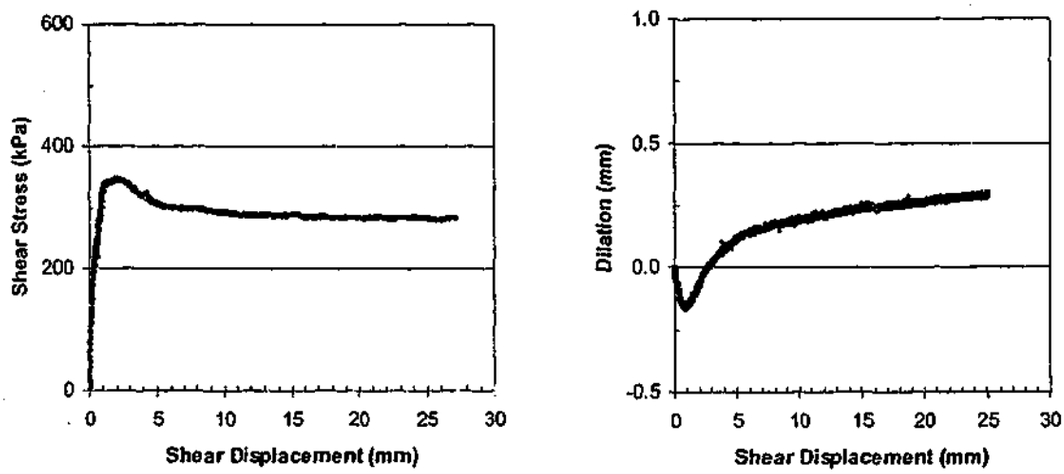

Figure 6.12: Johnstone Split Surface Direct Shear Test Results

The sandstone splits were typically smoother than the other rock types at chord lengths less than 10mm. They had minimal longer wavelength roughness with the standard deviation of chord angle above chord lengths of 40mm 2.5° or less. As the samples were unintentionally sheared with the profile on a slight angle, some dilation continued throughout the tests (as shown in Figure 6.13). Taking this overall angle into account however, the shear test results of the split surfaces typically showed a gradual increase in the shear stress to the peak value and then almost constant shear stress. Due to the fine roughness of the split samples, it was not possible to differentiate between wear on the

sample surface and shear failure of the asperities. Some debris remained on the joint surfaces where contact of the two interfaces was made during shear displacement.

In general the siltstone samples gave variable results. This was due to potential variation in the sample properties and the orientation and strength of the bedding. The Melbourne Mudstone used as the source rock, possessed joints parallel and near perpendicular to bedding. It was therefore decided to test the samples in similar orientations. Most of the triangular samples were sheared parallel to the bedding plane with only a couple of samples tested perpendicular to bedding. This meant that any shearing that occurred was along the bedding with the samples tested perpendicular to bedding overtopping. To estimate the bedding strength parameters, several intact shear tests were conducted parallel to the bedding direction. However, these parameters can only be considered as estimates as the strength of the bedding was found to vary significantly. The siltstone splits were created along bedding planes so that again any shearing was along the bedding plane. The fractal samples were cut across the bedding so that any shearing that occurred was through the rock matrix. The tests on the siltstone samples indicated very minor wear.

The manufactured siltstone split samples were typically relatively similar in roughness. They were also similar to the Johnstone splits although smoother at all scales (refer to Figure 6.11). The siltstone splits overlying longer roughness wavelengths typically possessed a standard deviation of chord angle of less than 5°. As with the Johnstone split shear tests, there was an initial peak shear stress due to an interlocking of the asperities followed by relatively constant shear stress (refer to Figure 6.14).

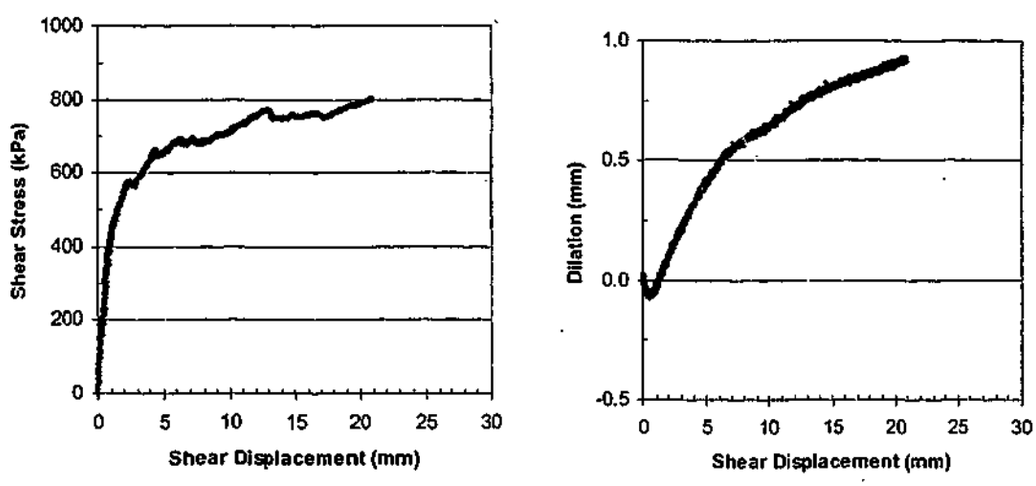

Figure 6.13: Sandstone Split Surface Direct Shear Test Result

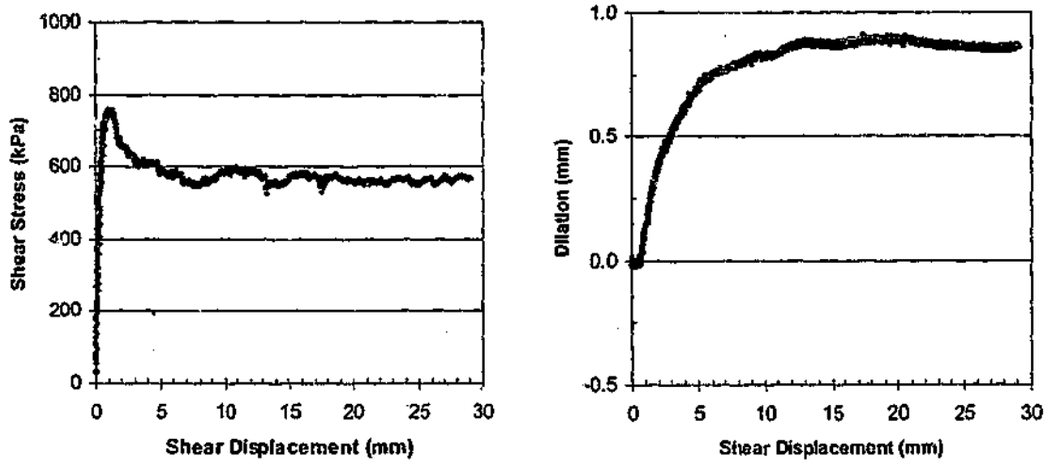

Figure 6.14: Siltstone Split Surface Direct Shear Test Result

The basalt samples typically underwent sliding with very little shearing of asperities. Wear was not observed. The basalt split samples were typically rougher than the siltstone and sandstone split samples at all wavelengths but less rough than the Johnstone splits at wavelengths less than 16mm. The basalt split samples longer roughness wavelengths typically possessed a standard deviation of chord angle of approximately 5° (refer to Figure 6.11). Due to the irregularity of the split surfaces, several of the basalt split samples were tested with an overlying sample angle causing the dilation to gradually increase. Several of the splits appeared to have an interlocking effect causing a higher initial peak shear stress (refer to Figure 6.15). This was followed by a gradual increase in shear stress due to the longer overlying wavelengths causing further dilation.

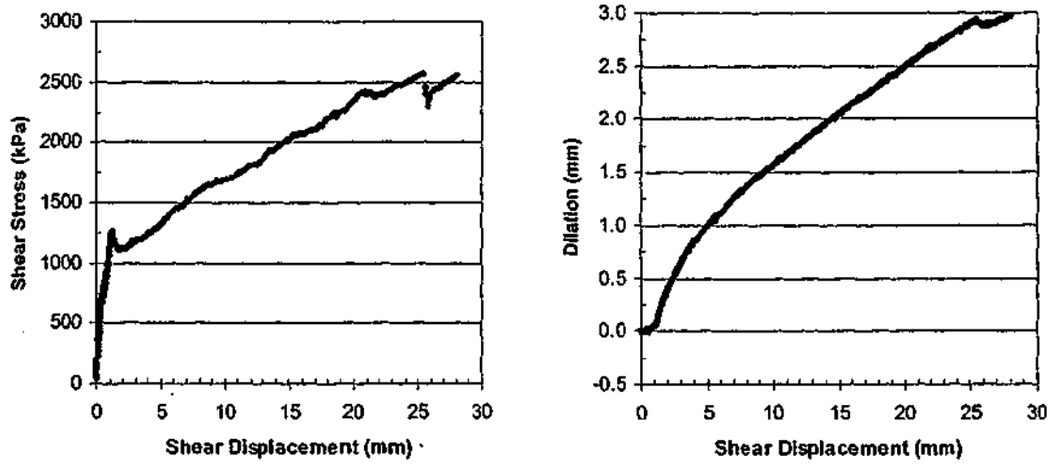

Figure 6.15: Basalt Split Surface Direct Shear Test Result

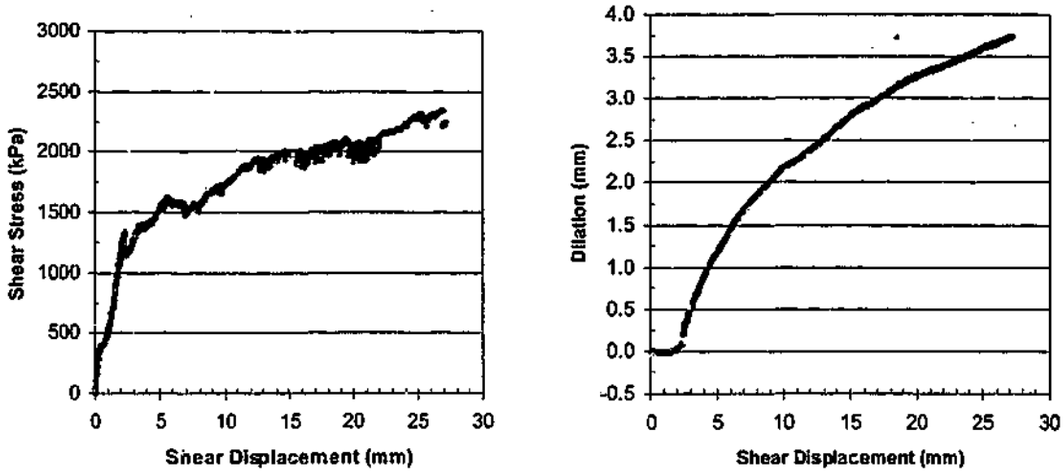

Figure 6.16: Basalt Split Surface Direct Shear Test Result

The strength of the granite samples and the corresponding high loads and stiffness applied caused significant stick-slip on these samples as previously discussed. The granite split samples were typically very rough due to the crystalline nature of the samples and are considerably rougher than the other samples tested. They experienced significant interlocking at the commencement of shear displacement that caused an initial peak in the shear stress. This was followed by sharp increases and decreases in the shear stress due to the stick-slip and often corresponding shear failure of an asperity (refer to Figure 6.16). Inspection of the split sample surfaces after shearing indicated several small zones of damage. These zones appeared to have undergone shearing and also crushing of some asperities.

To provide a visual comparison of the effects of rock strength and type, a comparison has been made between two similar s_θ=15° (at 5mm asperity chord length) fractal profiles for basalt and siltstone samples. The basalt had been shown to have higher compressive strength, tensile strength and residual friction angle than the siltstone. The samples were both tested at an initial normal stress of 600kPa and constant normal stiffness of 600kPa/mm. The direct shear test results are shown in Figure 6.17.

The peak shear stress results are similar for the two materials although the post peak behaviours are different. Until the peak shear stress is reached there is very little shearing of asperities. The dominant shear response is sliding along the steepest asperities at an angle of (ϕ+i). As there is very little difference in the basic friction angle (basalt ϕ_b=34°, siltstone ϕ_b=28.5°) the change in the total friction angle is quite small and

not obvious. In the post peak stage, significant shearing of the basalt asperities occurred whilst little shearing occurred in the siltstone sample. Although the basalt has higher compressive and tensile strengths than the siltstone, there was more asperity failure in the basalt sample than in the siltstone sample. This may be due to the inherent variability of natural rock and a weaker zone in the basalt sample.

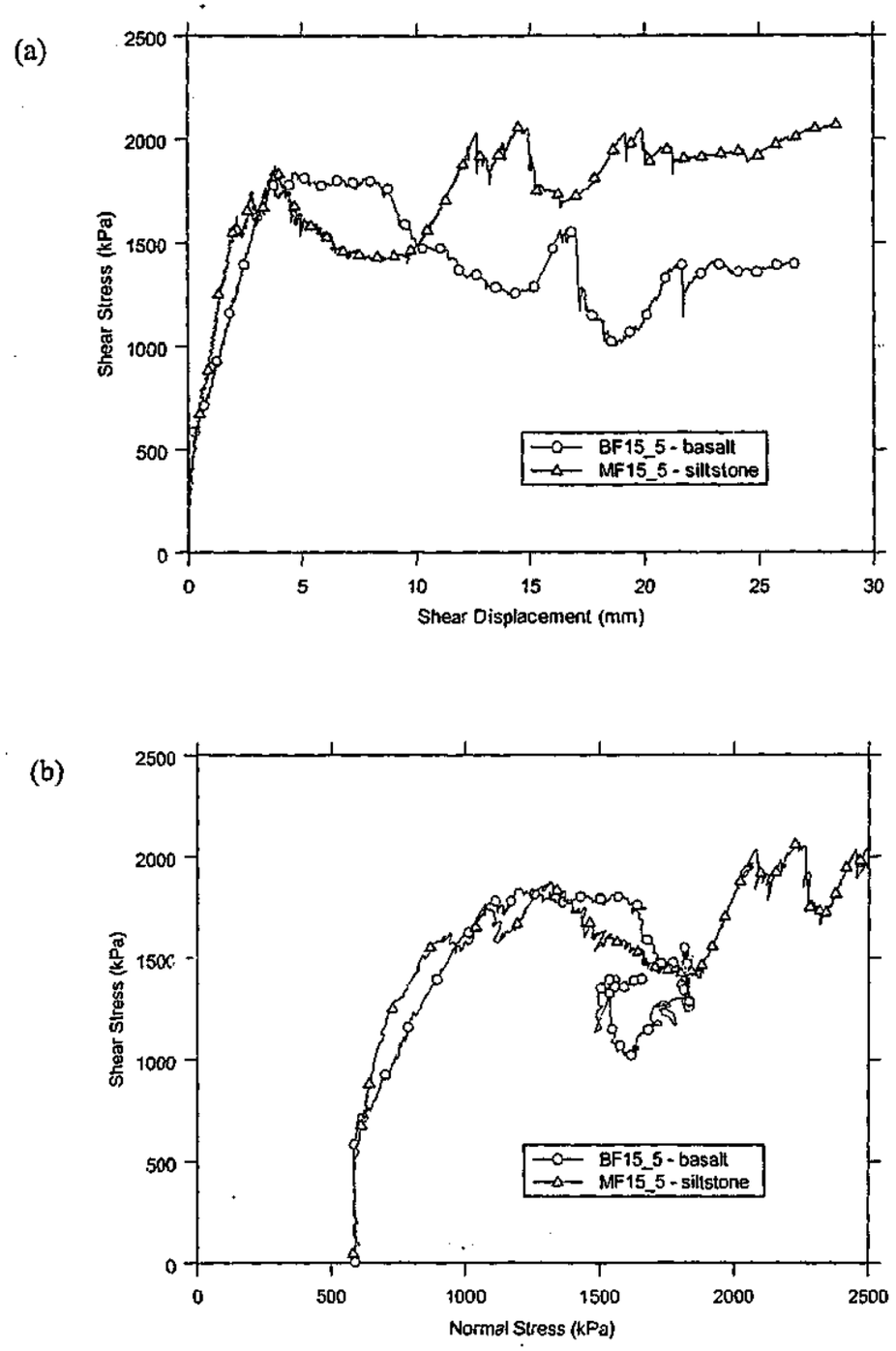

Figure 6.17: Strength comparison – siltstone and basalt fractal profile

(c)

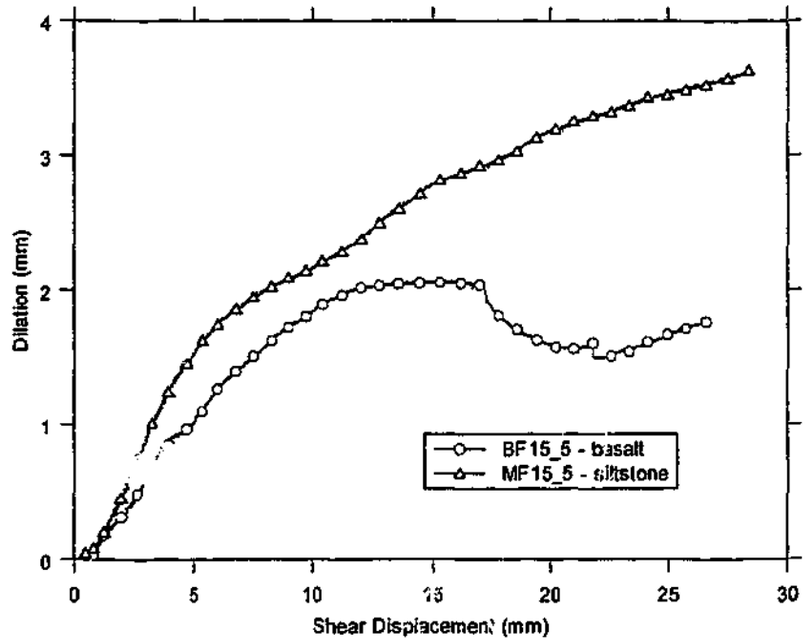

Figure 6.17: (cont'd): Strength comparison – siltstone and basalt fractal profile

6.4 Summary

The series of direct shear tests that were performed have highlighted a typical sequence of events –

1. Closure of the joint interface
2. Dilation of the interface with increase in shear stress
3. Peak shear stress
4. Post peak phase

During the initial dilation pnase before the peak shear stress is reached, sliding along asperities is the prime component of shear behaviour. Once the peak shear stress is reached some of the steeper asperities commence shearing. If shear displacement continues the dilation will ultimately stop and constant shear and normal stresses will be reached.

The peak shear stress obtained is dependent on normal stress levels. A higher normal stress level will cause a higher corresponding shear stress. Although this is predicted by

the relationship $\tau = c + \sigma \tan(\phi + i)$ it is not a proportional increase due to compressibility of the sample and compliance of the shear rig (further details given in Chapter 8).

The peak shear stress obtained is also dependent on the constant normal stiffness. As the sample dilates the constant normal stiffness causes an increase in the normal stress. This is not a proportional increase due to compressibility effects.

The peak shear stress is dependent on the sample roughness. A rougher sample causes higher dilation and under constant normal stiffness conditions this will increase the normal stress and shear strength.

Minimal shearing of asperities occurs prior to reaching peak shear stress. Therefore the stronger the rock sample the higher the peak shear stress that can be obtained as higher strength material requires more load to shear. As different materials have different basic friction angles, the initial shear response, which is predominantly sliding along the steepest asperity, will depend on the type of material.

The significance of the sample closure, compression of the rock and casting material and machine compliance has been highlighted in the laboratory direct shear tests. Chapter 8 discusses the changes required to the shear model developed by previous researchers at Monash University based on these further test results.

7.0 REPRESENTATION OF A 3-DIMENSIONAL SURFACE

Most conventional approaches of quantifying roughness, including the popular JRC method, seek to represent the joint surface roughness in two dimensions. Even the more recent fractal methods use the fractal dimension of a profile and add 1 to estimate the fractal dimension of the surface. This simplification of using a two-dimensional profile to represent a surface needs to be justified through laboratory testing and statistical analysis.

Section 7.1 investigates whether a two-dimensional profile taken parallel to the shearing direction of a three-dimensional surface can adequately, for modelling purposes, represent the surface. A series of statistical comparisons on two-dimensional profiles in natural rock joints and laboratory split surfaces are performed. Several laboratory tests on two-dimensional profile reproductions of the split surfaces are also conducted to test the proposition.

Every two-dimensional profile taken from a three-dimensional surface will be geometrically different. However, if they are statistically similar, it may be possible to use the statistics of the surface to represent the surface at all scales. This may allow a two-dimensional profile that possesses similar statistics to the surface to be used to represent the surface for modelling purposes. This hypothesis is tested in Section 7.2.

To reproduce a statistically representative two-dimensional profile, a method is required to mathematically regenerate the surface across all scales. Section 3.4.4 investigated a method to statistically regenerate a joint surface in two dimensions. Section 7.2 uses the results of shear tests on split surfaces to further investigate this statistical reproduction.

7.1 Representation of a 3-D Surface by a Single 2-D Profile Taken from the Surface

The statistical similarity of profiles taken across natural and laboratory manufactured joint surfaces is investigated. Laboratory direct shear tests are also used to investigate

the potential statistical similarity of the profiles. If the profiles are statistically similar then a single profile could be used to represent the surface.

7.1.1 Natural Rock Surfaces

The Monash laser profilometer, Socket-Pro, was used to measure linear profiles of several natural rock joints in the laboratory. The following rock samples were profiled:

- Siltstone samples (refer to Section 5.2.3 for siltstone rock properties) – joints typically had varying amounts of pyrite and carbonaceous coating.
- Basalt samples (refer to Section 5.2.4 for basalt properties) – joints typically had limonite or carbonaceous coating.

Plots of two-dimensional profiles taken from several joint surfaces are shown in Figure 7.1. Visual comparison indicates that the 2 dimensional profiles taken from the three-dimensional joint surfaces are all reasonably similar. All the two-dimensional profiles together with their three-dimensional surfaces are included in Appendix A.

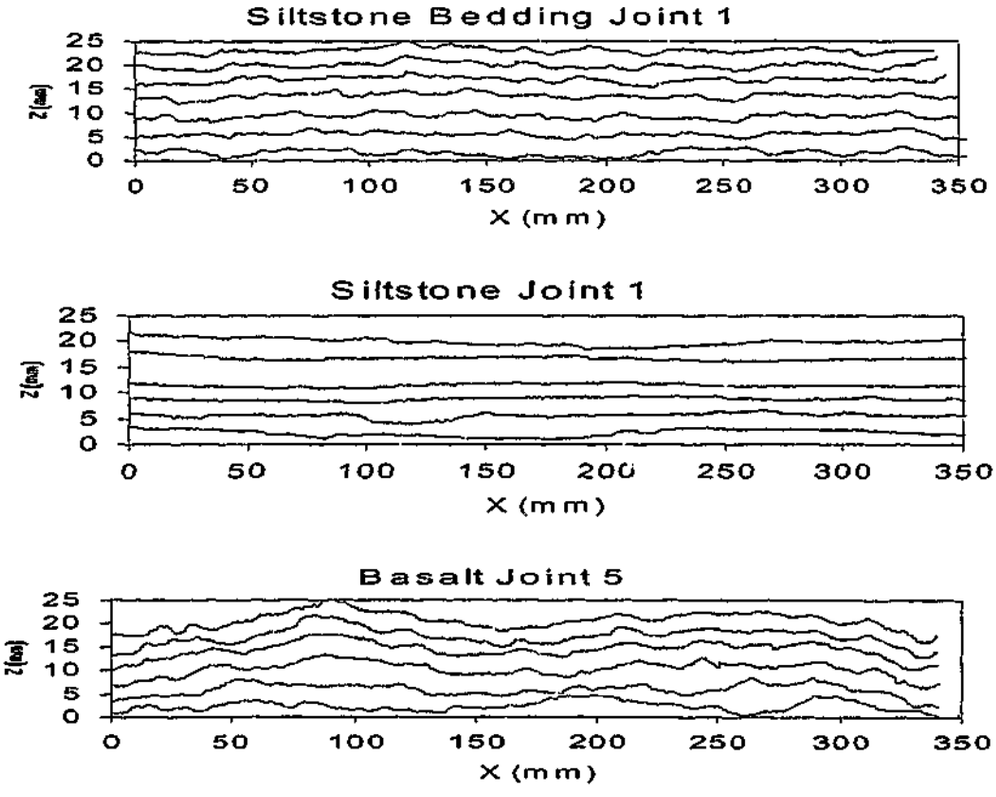

Figure 7.1: two-dimensional Profiles of Several Natural Joints

The two-dimensional profiles were analysed using the compass walking method (refer to section 3.2.3.1). As considerable debate still rages over the application of this method, amongst others, in the determination of a fractal dimension, analysis has been restricted to the determination of the variation of the standard deviation of chord angle with chord length (Seidel and Haberfield, 1995a). To ascertain whether the profiles were statistically similar for each joint, the standard deviation of angle, s_θ, at various chord lengths, r, were visually compared for each profile (eg. Figure 7.2). The envelope produced for each surface was relatively narrow suggesting that the surface could potentially be adequately represented by any of the profiles. Plots of standard deviation of chord angle versus chord length (statistical plots) for several surfaces are shown in Figure 7.2. A complete set of statistical plots on natural joint surfaces are shown in Appendix A.

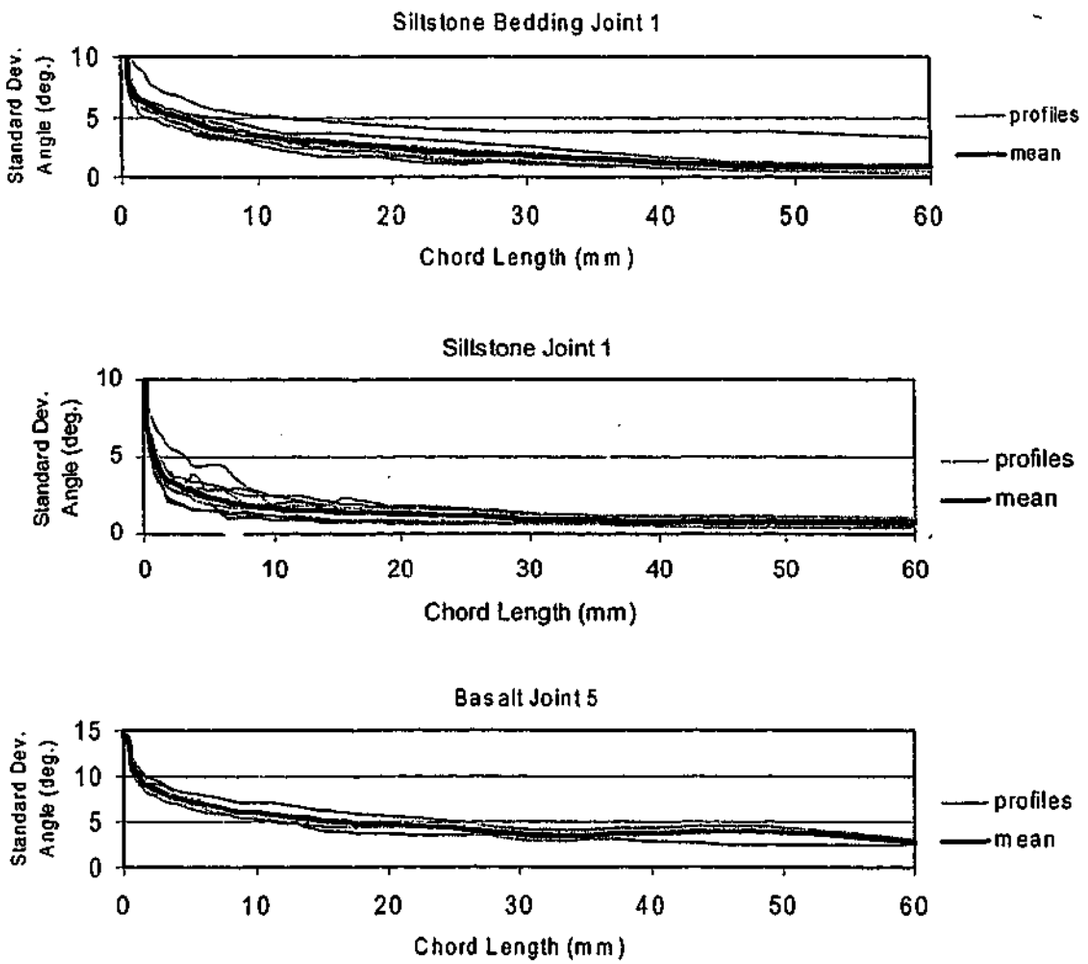

Figure 7.2: Statistical plots for Several Natural Joint Surfaces

Correlation coefficients can be used to measure the relationship between data sets. The correlation coefficient is defined in Equation 7.1. The correlation coefficient of the standard deviation of chord angle at various chord lengths was calculated for each pair of profiles. These correlation coefficients were then averaged for each surface. The average value has been presented in Table 7.1. The high correlation coefficients obtained imply that the profiles are statistically similar. The correlation coefficient between the standard deviation of chord angles at various chord lengths for each profile and the mean standard deviation of chord angles was also calculated and has been presented in Table 7.1. The high correlation coefficients obtained suggest that if a surface can be generated using mean statistics a better representation of the surface may be achieved.

$$\rho_{s_\theta,r} = \frac{\frac{1}{N}\sum_{i=1}^{N}(s_{\theta i} - \mu_{s_\theta})(r_i - \mu_r)}{\sigma_{s_\theta}\sigma_r} \qquad (7.1)$$

where $\rho_{s_\theta,r}$ = correlation between standard deviation of chord angle data (s_θ) and chord length (r)

N = number of values

μ_{s_θ} = mean of standard deviation of chord angle data

μ_r = mean of chord length data

σ_{s_θ} = standard deviation of standard deviation of chord angle data

σ_r = standard deviation of chord length data

7.1.2 Split Surfaces

To extend the number of two-dimensional profile statistical comparisons in various materials and strengths and to allow laboratory verification, several tensile split surfaces were also analysed. The samples tested in this manner were Johnstone, sandstone, siltstone, basalt and granite (refer to section 5.2 for properties). The split surfaces were created as outlined in Chapter 5 and then profiled using the Monash Socket-Pro.

Table 7.1: Average Correlation Coefficient of Standard Deviation of Chord Angle Statistics

Block	Average Correlation Coefficient	Average Correlation Coefficient to the Mean
Siltstone 1 – bedding joint	0.996	0.998
Siltstone 1 – joint	0.994	0.997
Siltstone 2 – bedding joint	0.994	0.997
Siltstone 3 – bedding joint	0.989	0.994
Siltstone 3 – joint	0.972	0.987
Siltstone 4 – joint	0.933	0.968
Siltstone 5 – bedding joint	0.990	0.995
Siltstone 5 – joint	0.997	0.999
Basalt 1	0.989	0.995
Basalt 1a	0.992	0.996
Basalt 2	0.988	0.994
Basalt 3	0.978	0.990
Basalt 4	0.991	0.996
Basalt 5	0.994	0.997

7.1.2.1 Comparison of Split Surfaces with Natural Joint Surfaces

Initially a comparison was undertaken between natural joints and tensile split surfaces in the same material to compare whether the split surfaces approximated natural fractures. Samples of siltstone bedding joints and basalt joints were used for this comparison. These surfaces are shown in Appendix A. A siltstone bedding joint and split and basalt joint and split are compared in Figure 7.3. A visual comparison of the split and natural surfaces and the two-dimensional profiles from the split and natural surfaces, suggested that the splitting procedure did produce reasonable approximations of natural joint surfaces. Standard deviation of chord angle statistics generated from the natural joints

and the split samples were also within a similar range for each material. The average statistics of several split and bedding joint surfaces are shown in Figure 7.4.

An analysis using spectral and statistical techniques to compare the statistical properties of man-made tensile and shear granite joints to natural granite joints by Power and Durham (1997) has also suggested that man-made fractures may be an acceptable substitute for natural granite fractures.

Therefore, tensile split samples will be used to represent natural joint surfaces. This eliminates the difficulty in obtaining large samples containing rock joints.

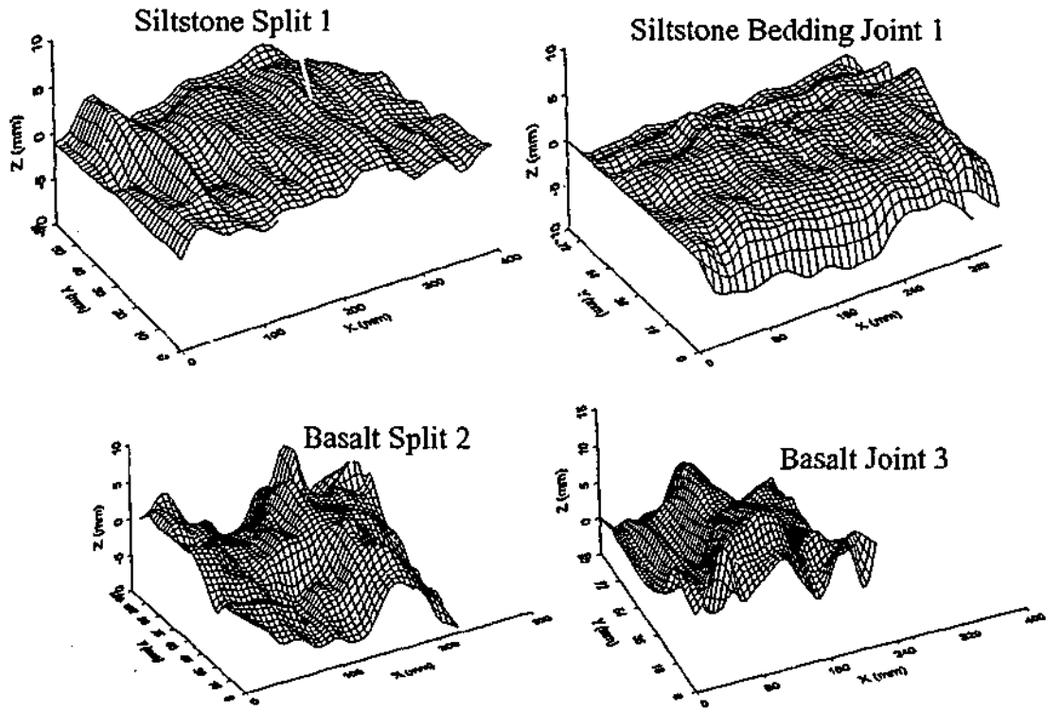

Figure 7.3: Comparison of Natural Joints with Split Surfaces

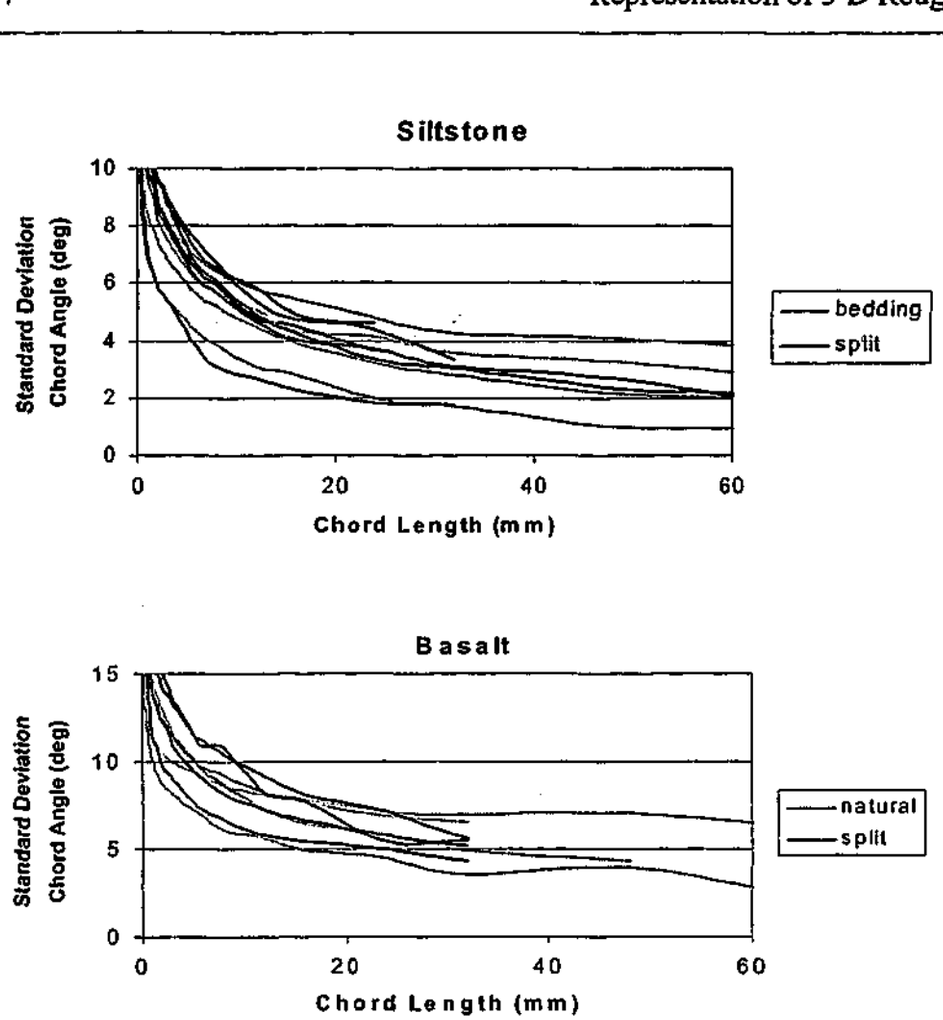

Figure 7.4: Comparison of Standard deviation of Chord Angle Statistics for Natural and Split Surfaces

7.1.2.2 Visual and Statistical Comparison of Split Profiles

A visual comparison was undertaken of the two-dimensional profiles obtained from each split surface. These profiles appeared to be visually similar. Several example profiles are shown in Figure 7.5. The complete set of two-dimensional profiles at a larger scale used for this comparison are included in Appendix C.

The variation of standard deviation of chord angles with chord length derived using the compass walking method were also compared from one profile to another. The graphical output indicates a reasonably narrow envelope of curves. Several example graphs are given in Figure 7.6. The complete set of graphical outputs produced to investigate the statistical consistency of the two-dimensional profiles are included in Appendix C.

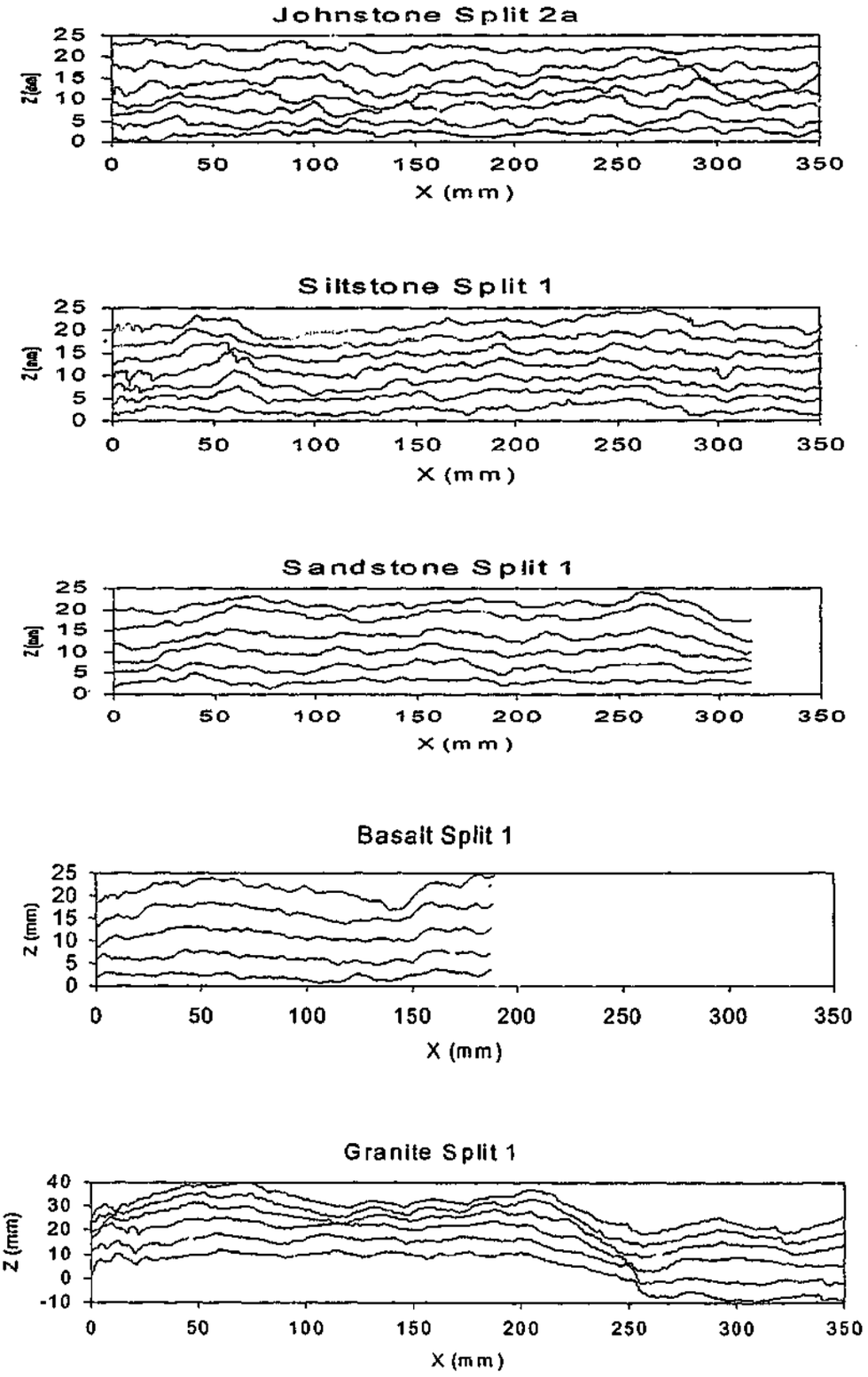

Figure 7.5: two-dimensional Profiles of Several Splits

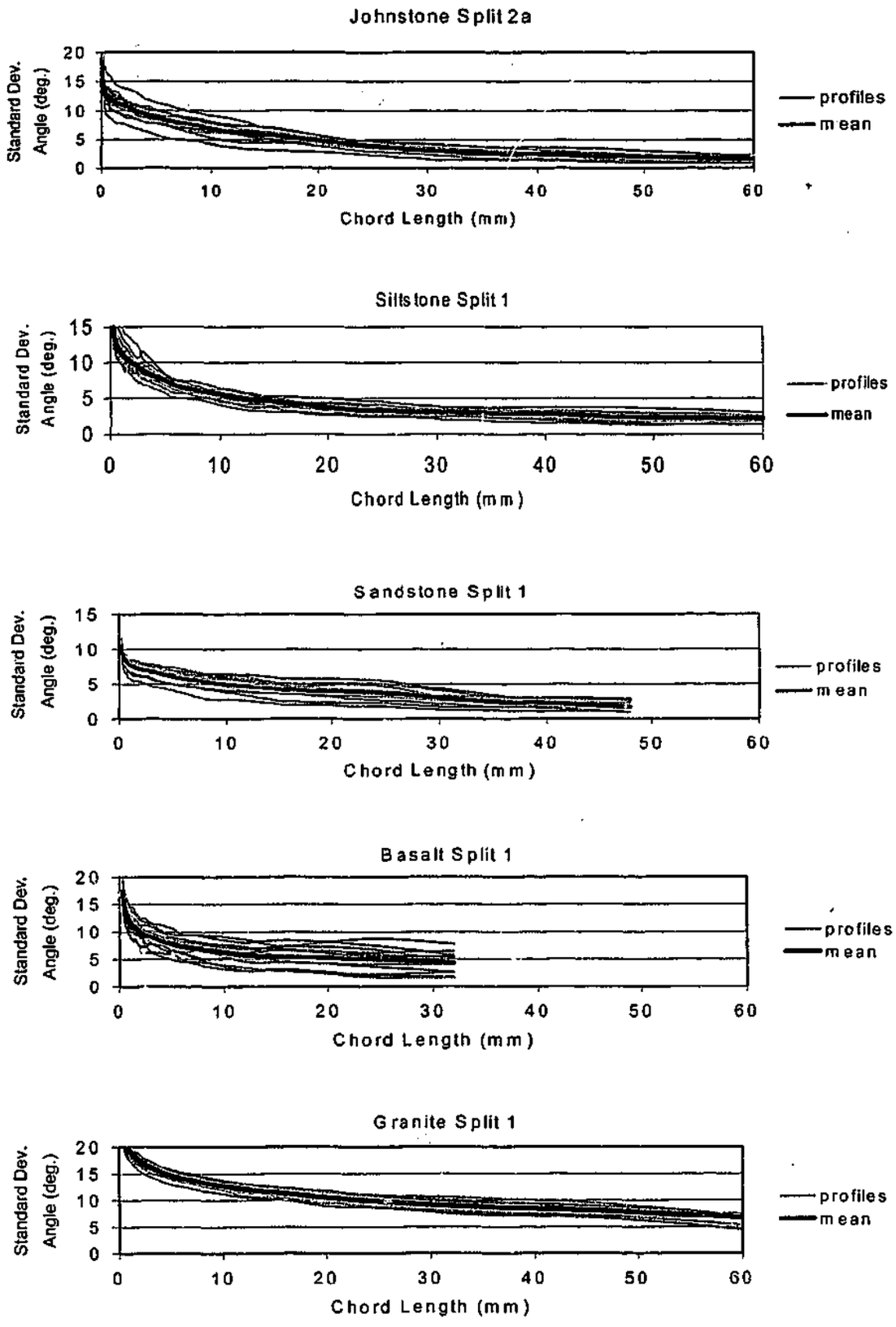

Figure 7.6: Statistical Analysis of Several Split Surfaces

Table 7.2: Correlation Coefficients between Standard Deviation of Chord Angles on the Split Surfaces

Block	Average Correlation Coefficient	Average Correlation Coefficient to the Mean
Johnstone 1a	0.984	0.992
Johnstone 1b	0.987	0.994
Johnstone 2a	0.993	0.997
Johnstone 2b	0.985	0.993
Johnstone 3a	0.996	0.998
Johnstone 3b	0.993	0.997
Johnstone 4a	0.996	0.998
Johnstone 6a	0.991	0.996
Johnstone 7a	0.991	0.996
Siltstone 1	0.994	0.997
Siltstone 2	0.995	0.997
Siltstone 3	0.982	0.992
Siltstone 4	0.983	0.992
Siltstone 5	0.983	0.992
Siltstone 6	0.981	0.991
Siltstone 7	0.976	0.989
Sandstone 1	0.984	0.993
Sandstone 2	0.991	0.996
Basalt 1	0.991	0.996
Basalt 2	0.947	0.975
Basalt 3	0.985	0.993
Basalt 4	0.986	0.994
Granite 1	0.992	0.996
Granite 2	0.991	0.996
Granite 3	0.989	0.995
Granite 4	0.992	0.996

Table 7.2 lists the average correlation coefficients, ρ, for the standard deviation of chord angle statistics of the joint profiles for each split surface. A very good correlation between the standard deviation of chord angle statistics of each profile exists. Also in Table 7.2 is a list of the average correlation coefficients to the mean standard deviation of angle statistics for each surface. These indicate that if a mean surface can be generated a slightly better correlation can be achieved.

7.1.2.3 Laboratory Comparison of profiles

Direct shear testing was carried out to determine whether a three-dimensional joint surface could be represented by a single profile taken in the potential shear direction. Each joint surface selected was laser scanned to produce several profiles of the surface. One of these profiles was selected and then water-jet cut into an identical rock sample to produce a two-dimensional joint interface. The joint surface and the two-dimensional profile were then tested in direct shear under identical conditions and the behaviour compared.

Due to the difficulty in cutting a profile at the same fine detail as the original surface, the two-dimensional profile was reproduced at a selected chord length (typically 3-4 mm). This unfortunately eliminated the effects of the roughness below this selected chord length. An example surface and a two-dimensional profile are shown in Figure 7.7. As the water-jet cutting process produced a fine ripple there were roughness wavelengths at very fine chord lengths (<2mm). This is shown in the statistical plot of standard deviation of chord angle versus chord length in Figure 7.8b by a sharp increase in the standard deviation of chord angle below approximately 2mm chord lengths.

Ideally these tests should be performed on natural rock samples. However, due to the natural variability of rock it would be extremely difficult to obtain a natural rock joint and identical sample to replicate a profile. Therefore a series of direct shear tests were performed on the man-made Johnstone samples that were relatively homogeneous (refer to Section 5.2.1).

However some difficulties were encountered during this testing program due to:

1. Batch 1 and Batch 2 of Johnstone, although their moisture contents were similar, the two batches had different UCS values of 8.3MPa and 4.3MPa respectively (this is discussed in Section 5.2.1).

2. The inconsistent quality obtained from the water-jet cutters (as discussed in Section 5.3) made it difficult to compare the performance of the two-dimensional joint interface with the three-dimensional surface.

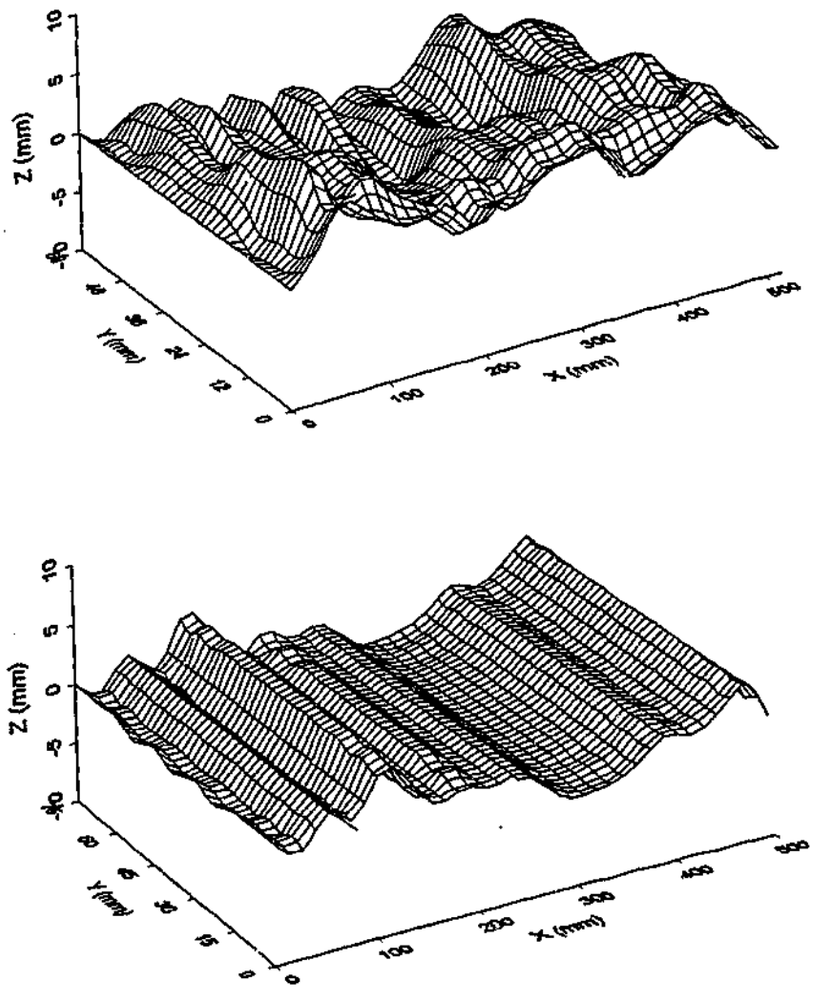

Figure 7.7: three-dimensional surface and cut two-dimensional profile

TEST 1 – split surface JS_4a

One of the laser digitised profiles from the middle of Johnstone split surface JS_4a was reproduced at 6mm chord lengths by mathematically walking a compass with a 6mm opening along the profile and drawing chords between each intersection point. The two-dimensional profile, JC4a_6, was water-jet cut into a Johnstone block from the same batch. The moisture content of the original and water-jet sample were 14.1% and 13.8% respectively. The water-jet cut surface was almost a perfect match with the selected profile. The water-jet profile JC4a_6 is shown in Figure 7.8a together with the original

central profile, JS4a. As can be seen, the small scale roughness has been omitted but the roughness of the original profile greater than a 6 mm chord length has been maintained. Figure 7.8b shows the comparison of the standard deviation of chord angle statistics (produced using the compass walking method) of the cut profile and the scanned profiles from surface JS_4a. This omission of the small scale roughness of the profile is clearly illustrated in Figure 7.8b: the standard deviation of chord angle of the water-jet cut sample for chord lengths less than about 6mm is significantly less than the original profile.

The cut profile is statistically similar at chord lengths greater than 6mm. Below 6mm chord lengths the water-jet profile is much smoother as it has had the small scale roughness omitted. As previously discussed, the water-jet cutting process has left a fine ripple on the cut surface. This can be seen by a sharp increase in the standard deviation of chord angle statistics below a chord length of approximately 2mm.

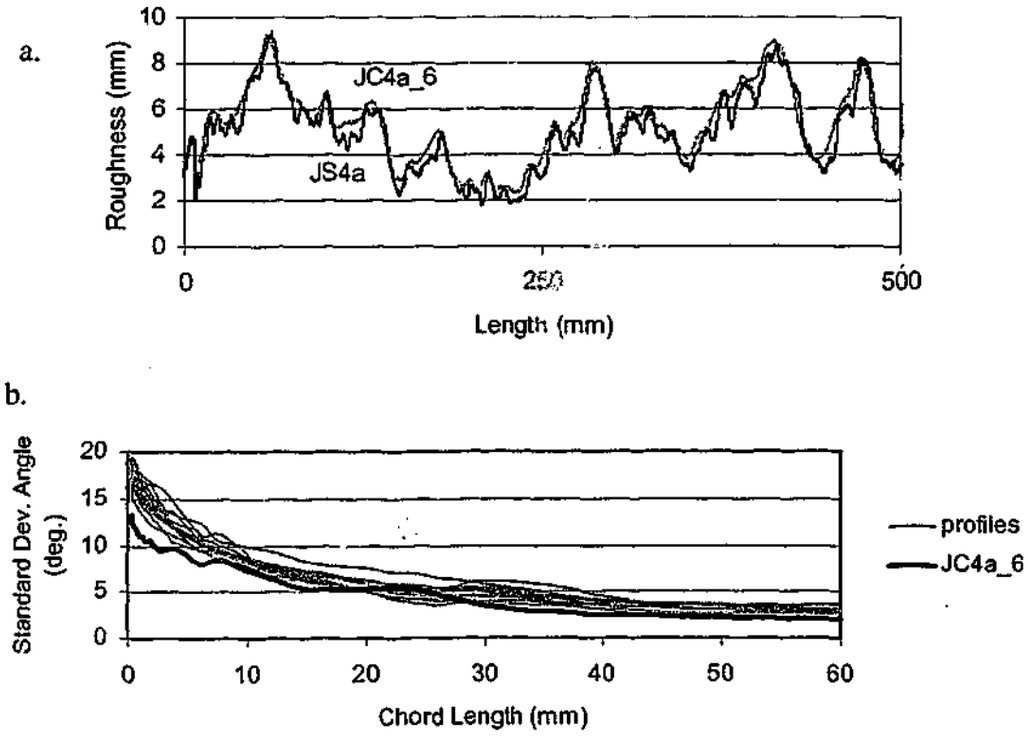

Figure 7.8: a. Centre profile from Johnstone split surface JS_4a, JS4a, and its regeneration at 6mm chords, JC4a_6

b. Statistics of cut profile and original surface

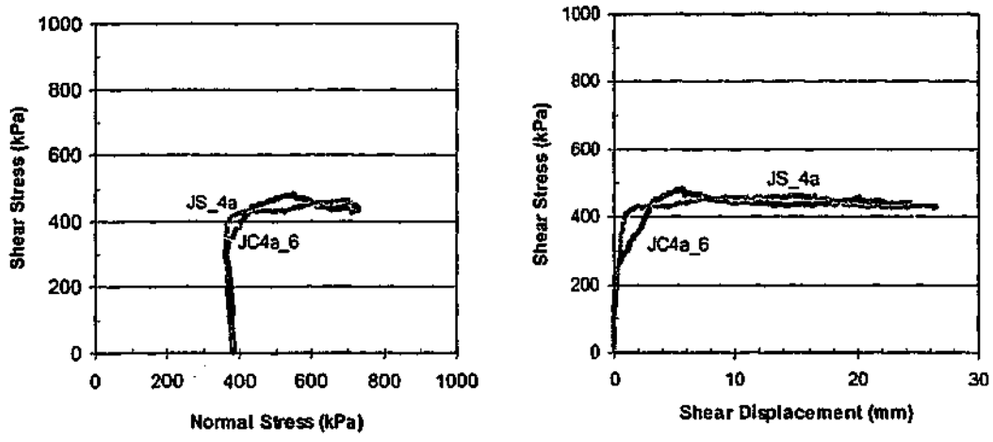

Figure 7.9: Shear test results of 3-D surface, JS_4a, and 2-D profile, JC4a_6

The sample was tested in direct shear at the same initial normal stress and constant normal stiffness as sample JS_4a (ie. K=400kPa/mm, σ_{no}=400kPa). Figure 7.9 compares the shear test results of the three-dimensional surface and the two-dimensional surface. The three-dimensional surface initially has a stiffer response at small displacements due to the smaller scale roughness (that is present in this surface, but not in the reproduced surface) but at larger displacements the shear stress versus shear displacement curves are very similar. This suggests that the shear response of the larger wavelengths has been captured.

Test 2 – Split surface 6a

A central laser digitised profile, JS6a, of Johnstone split surface JS_6a was reproduced at 3mm chord lengths by mathematically walking a compass with a 3mm opening along the profile and drawing chords between each intersection point. The two-dimensional profile, JC6a_3, was water jet cut into a Johnstone block from the same batch. The moisture content of the original and water-jet sample was 14.3% and 14.9% respectively. The water-jet cut surface was overcut by approximately 2mm as shown in Figure 7.10a. This has steepened the sharpest peaks and deepened the troughs. Figure 7.10b shows the comparison of the standard deviation of chord angle statistics (produced using the compass walking method) of the cut profile and the profiles taken from the surface. As would be expected, the cut profile is statistically rougher due to the overcutting.

The sample was then tested in direct shear at the same initial normal stress and constant normal stiffness as JS_6a (ie. K=400kPa/mm, σ_{no}=400kPa). Figure 7.11 compares the shear test results of the three-dimensional surface and the two-dimensional surface. It is usual in the shear response to experience some minor seating of the interface at the commencement of the shearing process (up to 0.05mm) as indicated by the cut surface JC6a_3 in the dilation shear displacement graph in Figure 7.11. However, the split surface experienced some initial compression of approximately 0.3mm as indicated by the extension of the dilation shear displacement graph in Figure 7.11. This may have been due to an initial mismatching of the surface. Under a constant normal stiffness of 400kPa/mm this compression has caused a reduction in normal stress of 120kPa and a subsequent decrease in the shear stress.

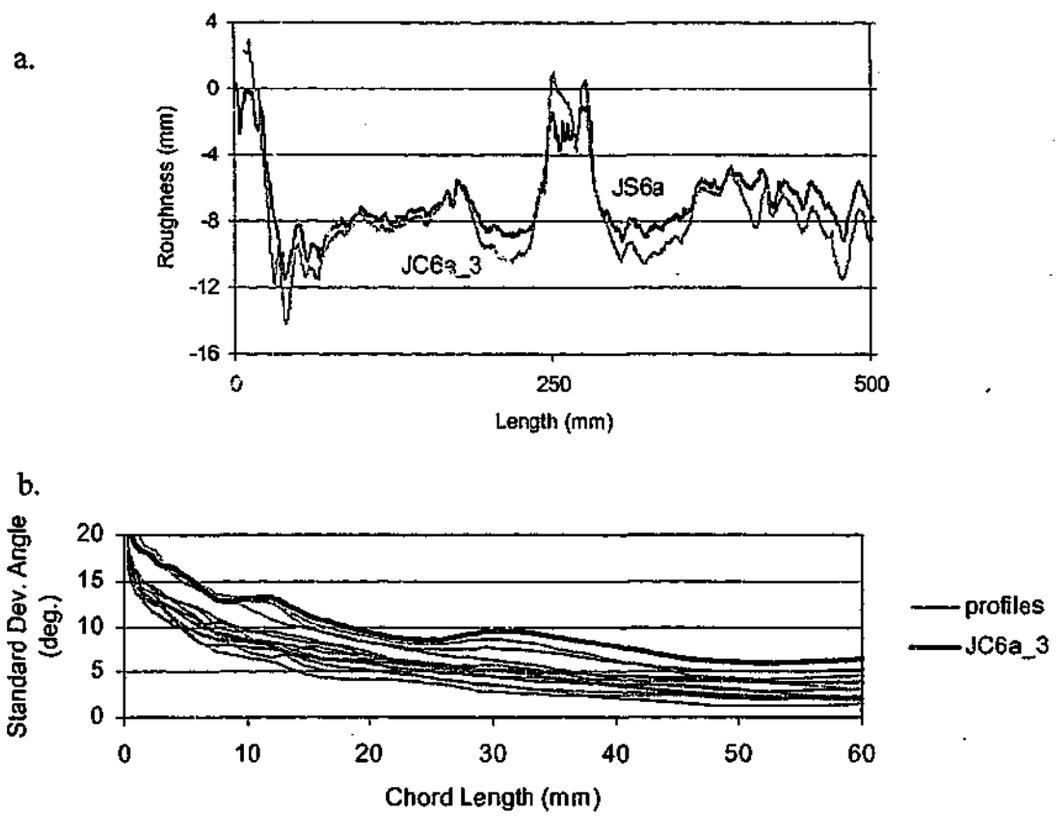

Figure 7.10: a. Centre profile from Johnstone split surface JS_6a, JS6a, and its regeneration at 3mm chords, JC6a_3

b. Statistics of cut profile and original surface

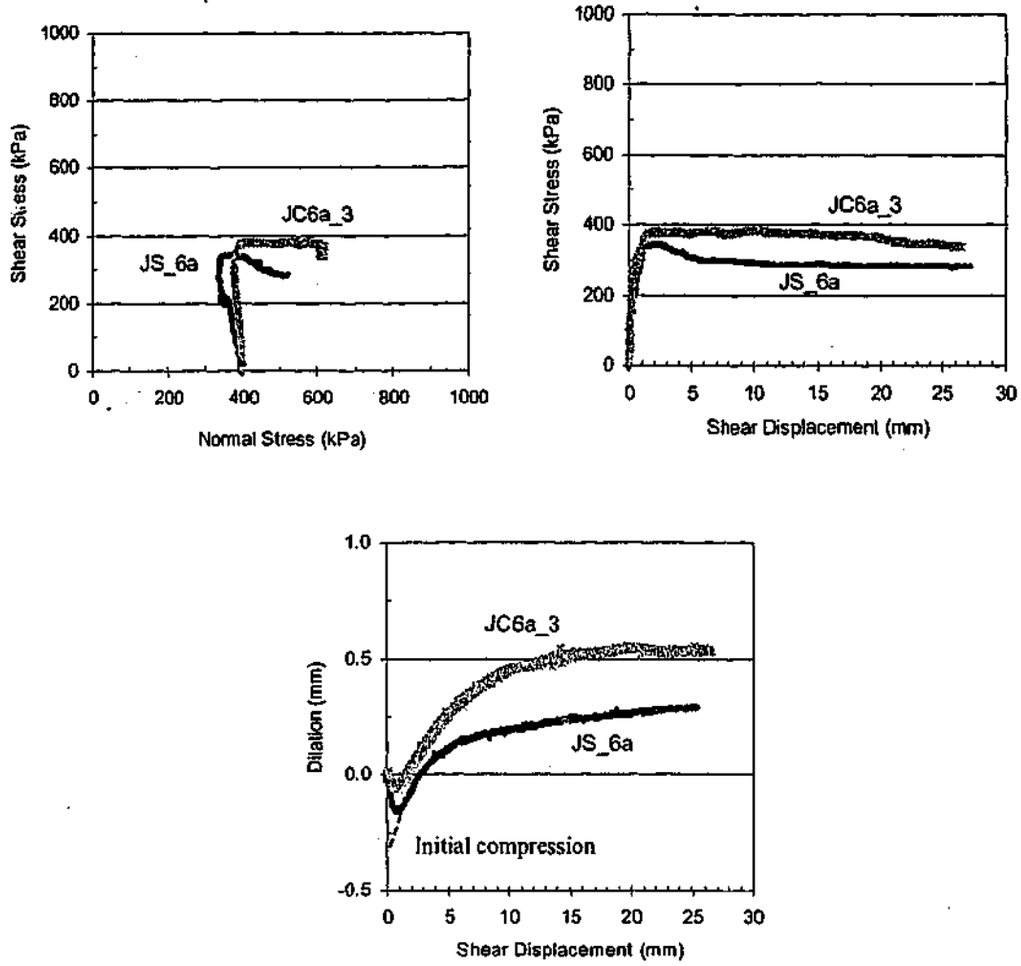

Figure 7.11: Shear test results of 3-D surface, JS_6a, and 2-D profile, JC6a_3

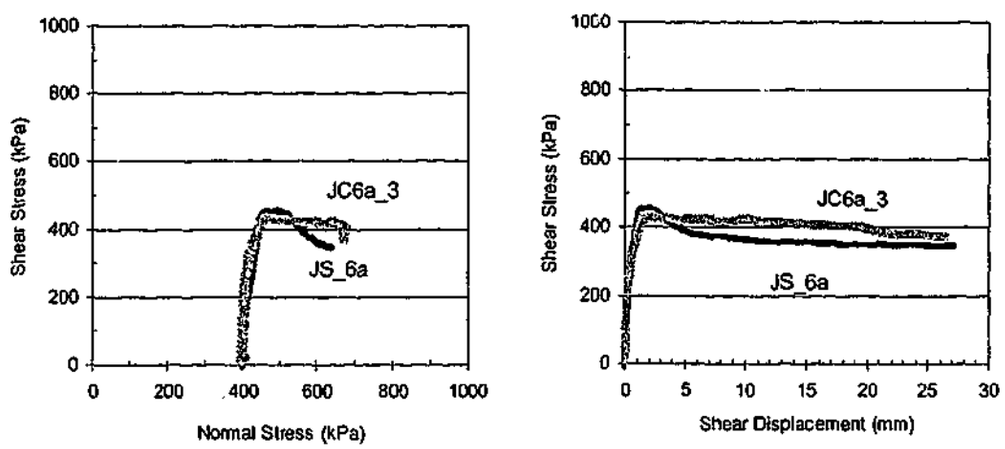

Figure 7.12: Adjusted shear test results of 3-D surface, JS_6a, and 2-D profile, JC6a_3

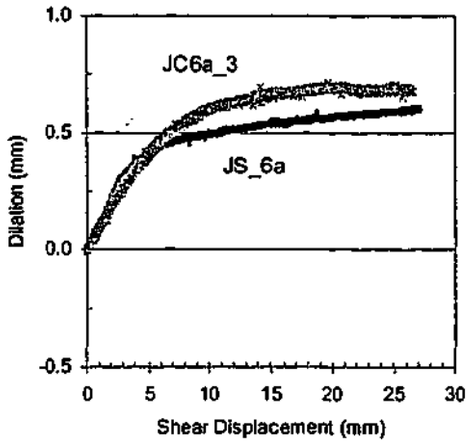

Figure 7.12 (cont'd): Adjusted shear test results of 3-D surface, JS_6a, and 2-D profile, JC6a_3

The shear response has been adjusted to remove the initial compression in the split sample and cut surface in Figure 7.12. A much closer prediction is then achieved. However, due to the overcutting of JC6a_3 producing larger asperities, there was greater dilation experienced by the cut sample at longer wavelengths. This allowed the shear stress to be maintained whilst the three-dimensional surface displayed post peak softening.

Test 3 – Johnstone Split surface JS_7a

A central laser digitised profile of Johnstone split surface JS_7a was reproduced at 4mm chord lengths by mathematically walking a compass with a 4mm opening along the profile and drawing chords between each intersection point. The two-dimensional profile so obtained, JC7a_4, was water-jet cut into a Johnstone block from the same batch. The water-jet cut surface was overcut as shown in Figure 7.13a. The saturated moisture content of the original and water-jet sample was 14.0% and 14.3% respectively. Figure 7.13b shows the comparison of the standard deviation of chord angle statistics produced using the compass walking method on the cut profile and the envelope of original scanned profile statistics. The cut profile statistics lie at the upper boundary of the original profile's statistical envelope due to the overcutting.

The sample was tested in direct shear at the same initial normal stress and constant normal stiffness as JS_7a (ie. K=400kPa/mm, σ_{no}=400kPa). Figure 7.14 compares the shear test results of the three-dimensional surface and the two-dimensional surface. As the cut sample was cut at 4mm chord lengths and did not possess the small scale roughness of the three-dimensional surface, it produced a less stiff initial shear stress versus shear displacement response. At longer wavelengths the two-dimensional sample captured the shear behaviour of the three-dimensional surface even though it was at the top of the roughness statistical envelope. This may indicate that it was the steeper asperity sections (captured by the uppermost profiles on the statistical plot) that dominated the overall response of the three-dimensional split surface.

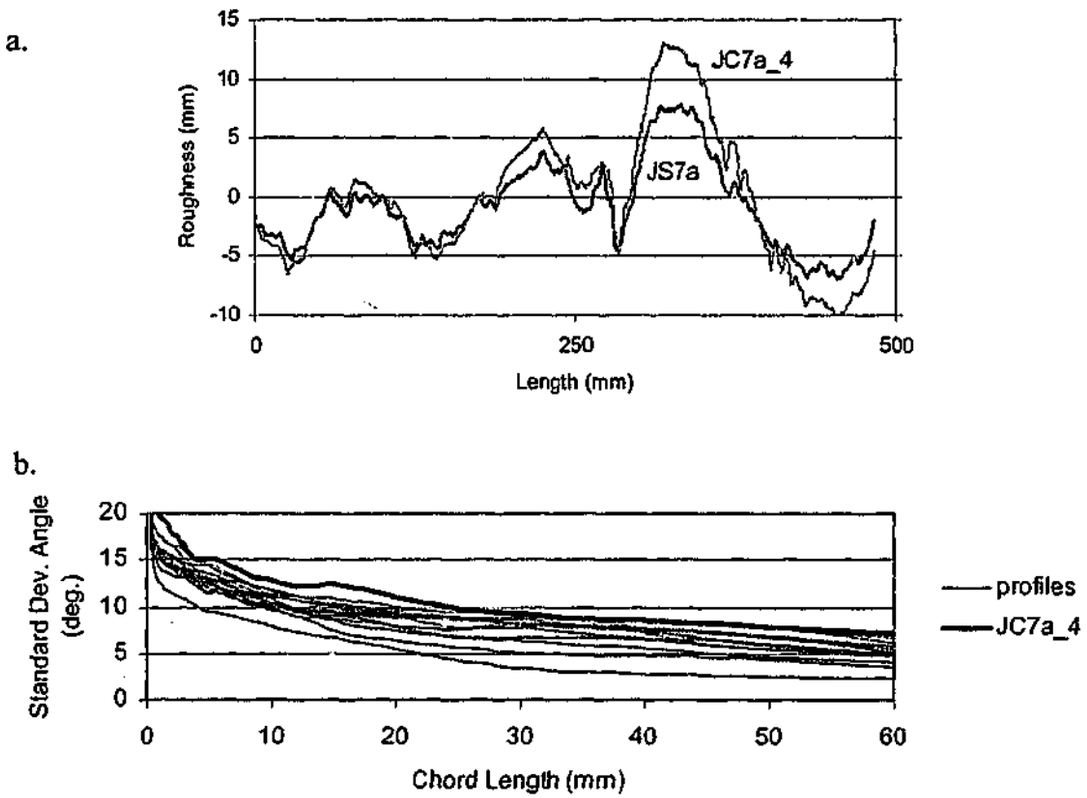

Figure 7.13: a. Centre profile from Johnstone split surface JS_7a, JS7a, and its regeneration at 4mm chords, JC7a_4

b. Statistics of cut profile and original surface

The previous three tests support the hypothesis that a three-dimensional surface can be approximated by a single two-dimensional profile taken from the surface.

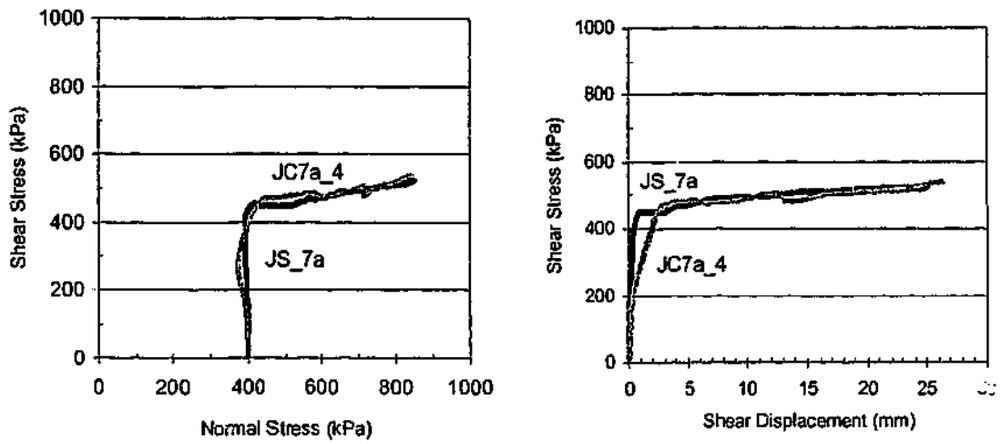

Figure 7.14: Shear test results of 3-D surface JS_7a, and 2-D profile JC7a_4

7.2 Statistical Reproduction of a Surface

The previous section indicated that the mean statistics of a surface provided a better representation of the surface than any individual profile. Therefore a series of direct shear tests were conducted to investigate whether a three-dimensional surface could adequately be represented by a two-dimensional surface created using the statistics of the surface. This involved the development of a method to create a two-dimensional profile using the three-dimensional surface statistics.

The two-dimensional profiles were again water-jet cut into Johnstone samples. This meant that similar problems of minimum chord lengths and water-jet cutting accuracy as discussed in Section 7.1.2.3 were encountered.

7.2.1 Statistical Reproduction Using Compass Walking Method

The compass walking method was used to generate a profile with a specified standard deviation of chord angle at a set chord length. Thirteen profiles had been taken of Johnstone split JS_3a. The compass walking method was used to digitise these profiles

into 6mm chord lengths (method described in section 3.2.3.1). At this chord length, the average standard deviation of chord angles was 8°. The random midpoint displacement method was then used to generate a profile with an 8° target standard deviation of chord angle at a final chord length of 6mm (method described in section 3.4.2). This profile was water-jet cut into a Johnstone sample from the same batch as JS_3a to form the two-dimensional profile, JC3a_stat6. The water-jet cut surface was almost an exact match of the desired profile requested with no evidence of overcutting. The saturated moisture contents of the original and water-jet cut samples were 14.0% and 16.1% respectively.

The generated profile, JC3a_stat6, is shown in Figure 7.15a together with a median profile from the original surface, JS3a. Figure 7.15b shows the comparison of the standard deviation of chord angle statistics produced using the compass walking method on the cut profile and the envelope of original scanned profile statistics. Below the chord length of 6mm, the statistics fall below the three-dimensional surface's statistical envelope as these smaller chord lengths were not cut into the profile. At 6mm chord length the cut profiles statistics are similar to the average of the surface as would be expected. However, this method does not attempt to replicate the longer statistics and hence at chord lengths greater than 6mm the cut profile tends to be on the lower side of the three-dimensional surface's statistical envelope.

The sample was then tested in direct shear at the same initial normal stress and constant normal stiffness as JS_3a (ie. K=400kPa/mm, σ_{no}=400kPa). Figure 7.16 compares the shear test results of the three-dimensional surface and the two-dimensional surface.

The shear test results for this statistical reproduction indicate that the cut profile has not successfully modelled the split surface. The profile was cut at 6mm chord lengths and therefore does not include the effects of smaller scale roughness (ignoring the minimal effects due to the surface ripple produced by the water-jet cutting process). This produced a lower shear stress at smaller displacements. This is indicated by the less stiff initial response of the cut surface. The method also only used the 6 mm chord length statistics for regeneration and did not attempt to include the specific effects of larger roughness wavelengths. The larger roughness wavelengths that are present have been randomly achieved by the midpoint generation method. In this case they were less steep than the three-dimensional surface and therefore produced a lower shear stress response at larger displacements. These effects may also be exacerbated as the water-jet cut sample had a higher moisture content which usually indicates a lower strength.

This test shows the importance of capturing all wavelengths of roughness.

a.

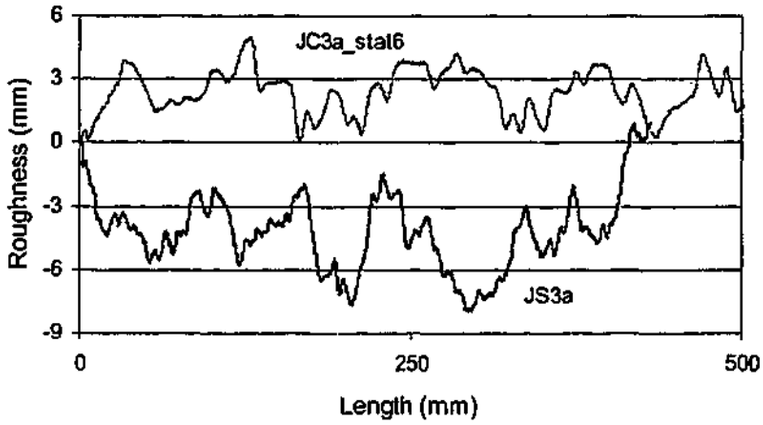

b.

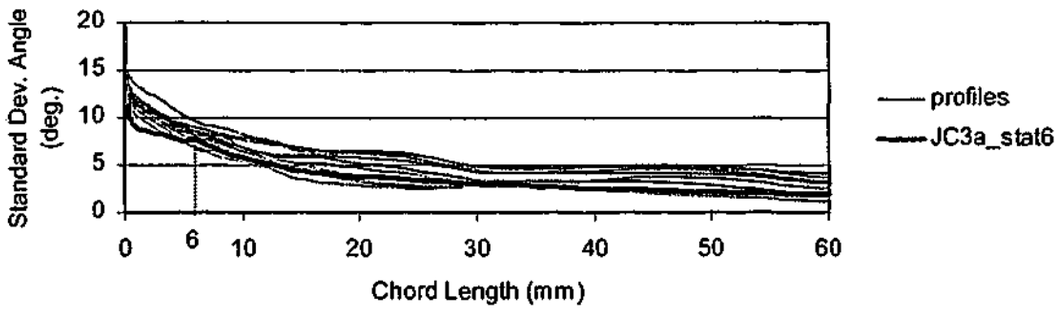

Figure 7.15: a. A central profile from Johnstone split JS_3a, JS3a, and a statistically regenerated profile at 6mm chords, JC3a_stat6

b. Statistics of cut profile and original surface

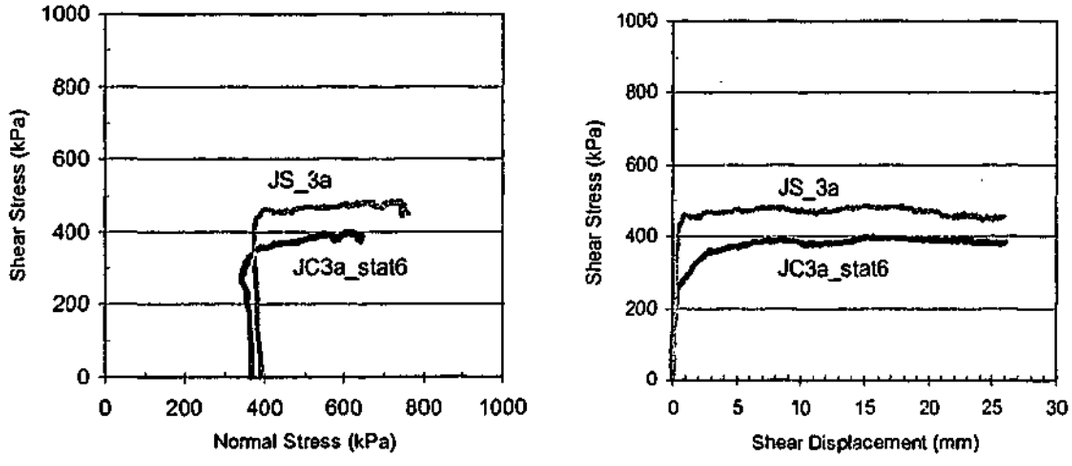

Figure 7.16: Shear test results of 3-D surface, JS_3a, and 2-D profile, JC3a_stat6

7.2.2 Statistical reproduction using Power or Logarithmic function combined with the Modified Midpoint Displacement Method

Chapter 3.4.4 described how the standard deviation of chord angle versus chord length plots of natural joint surfaces can be accurately represented by logarithmic or power functions. As the split surfaces provide similar surface roughness profiles to natural joints, it is no surprise that the standard deviation of chord angle statistics for the split surfaces can also typically be well described by a natural logarithmic function or a power function. Several examples are shown in Figure 7.17. Further split surface mathematical representations are included in Appendix E.

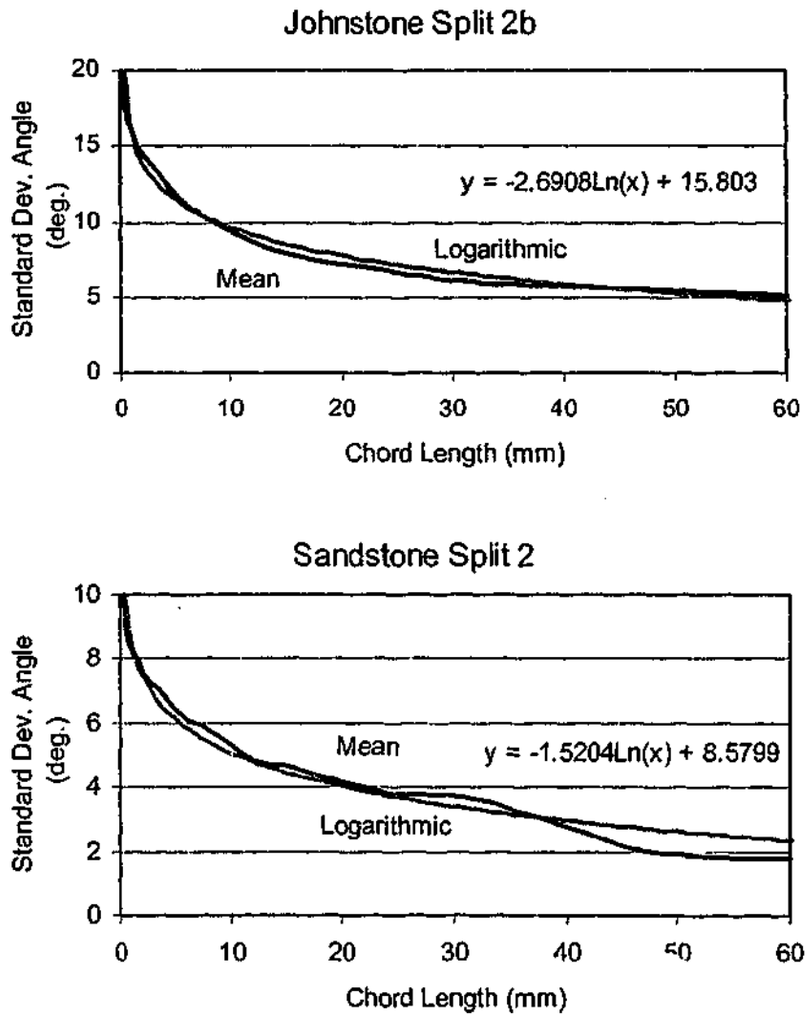

Figure 7.17: Mathematical representation of the mean curve of standard deviation of chord angles of the split surfaces

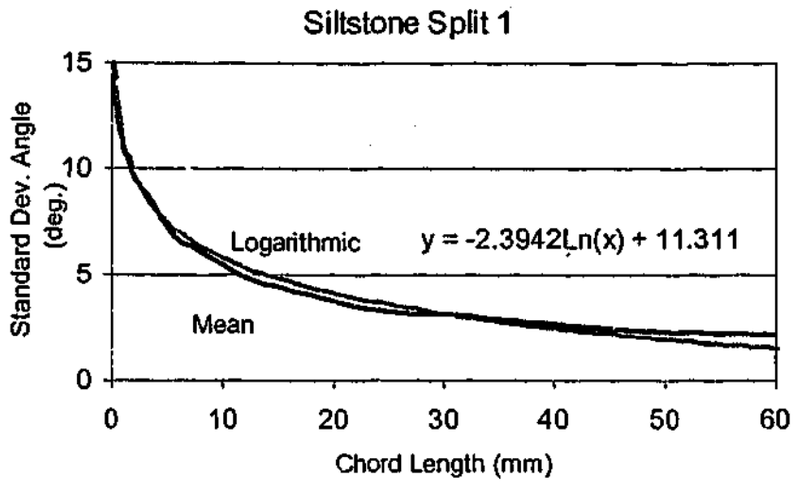

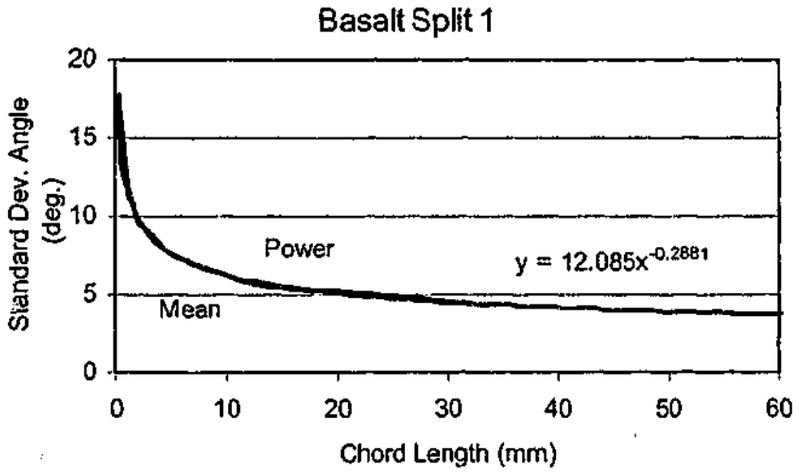

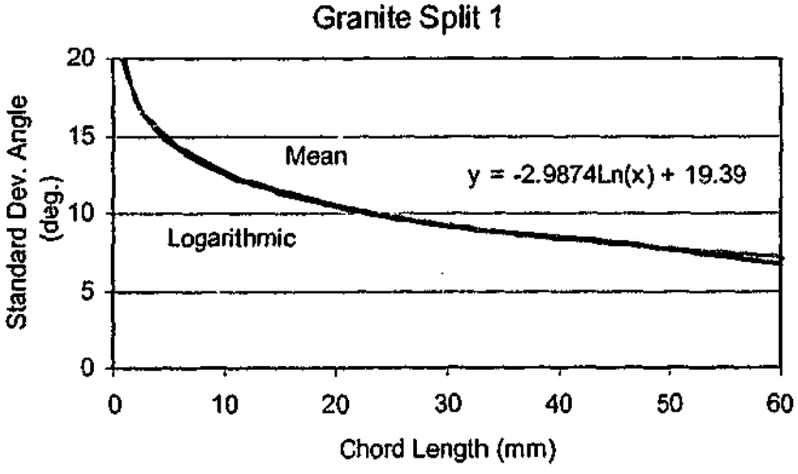

Figure 7.17 (cont'd): Mathematical representation of the mean curve of standard deviation of chord angles of the split surfaces

As with the natural joint profiles, these profiles could be reproduced using the Modified Midpoint Displacement method combined with either a power or logarithmic function as discussed in Section 3.4.4. Several example reproductions at approximately 3-4mm chord lengths and a centre profile from the original split surface are shown in Figure 7.18 together with their standard deviation of chord angle statistical plots. The reproduced statistics fall within the statistical envelope of the original split surface indicating a statistically similar two-dimensional profile has been generated. This must be qualified by the points noted in Section 3.4.4 that this statistical reproduction may not be capturing roughness wavelengths greater than 60mm.

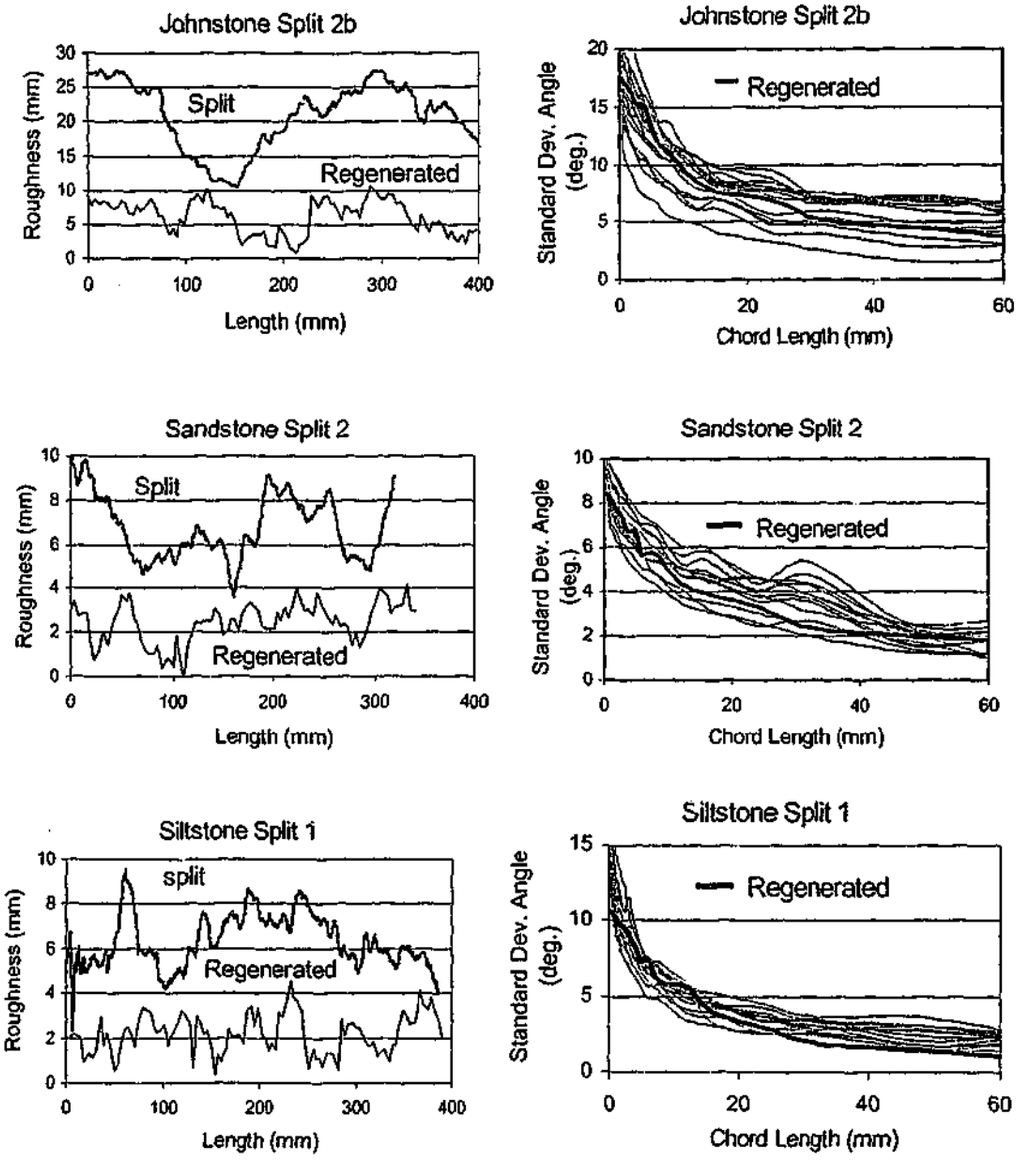

Figure 7.18: Comparison of regenerated profiles and the original split surfaces

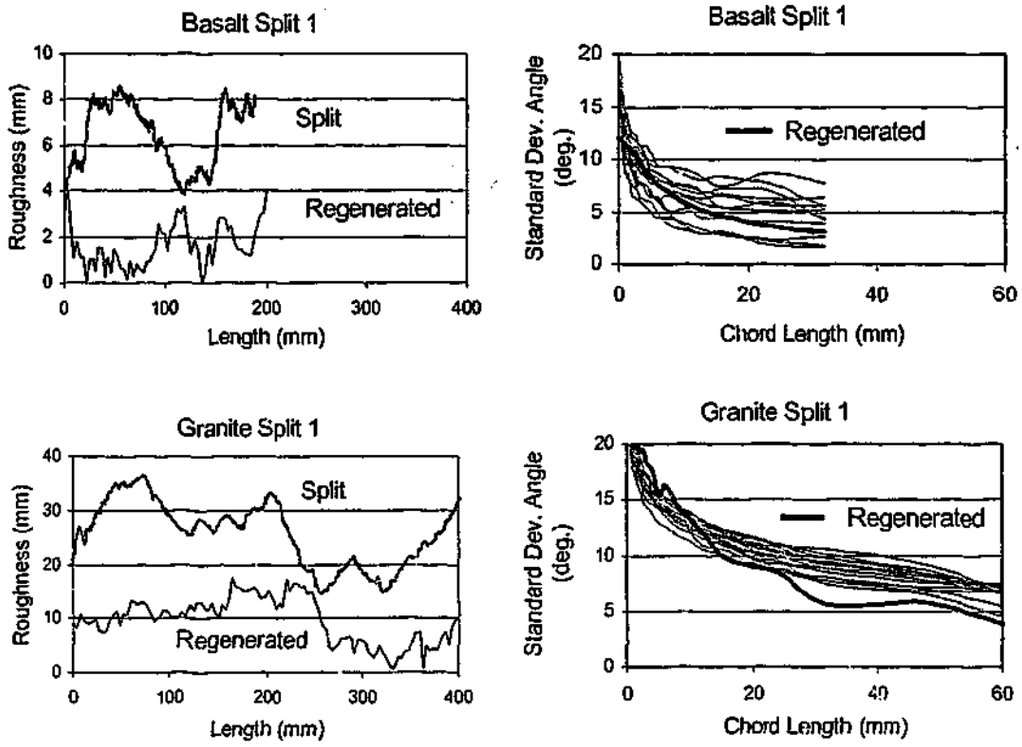

Figure 7.18 (cont'd): Comparison of regenerated profiles and the original split surfaces

Two split surfaces were regenerated using the modified midpoint generation method and either a power or logarithmic function to describe the statistics of the surface so that the regeneration method could be tested using laboratory testing.

Using the compass walking method, the average standard deviation of chord angle statistics for the thirteen two-dimensional profiles of Johnstone split sample JS_6a was determined. These statistics were approximated by a power function according to $s_\theta = 16.065 L_c^{-0.3227}$, where s_θ = standard deviation of chord angle (deg), L_c = chord length. A profile, JS6a_pow4, was then generated using the modified midpoint displacement method and this power function for chord lengths of less than 30mm. The generated profiles statistics fell within the standard deviation of chord angle envelope of the split surface. This can be seen in Figure 7.19.

The profile was water-jet cut into a Johnstone sample from the same batch as JS_6a to form the two-dimensional profile, JC6a_pow4. Unfortunately an overcut replication of the desired surface was obtained thus producing a rougher surface. The saturated moisture content of the original and water-jet cut samples were 14.3% and 13.4% respectively.

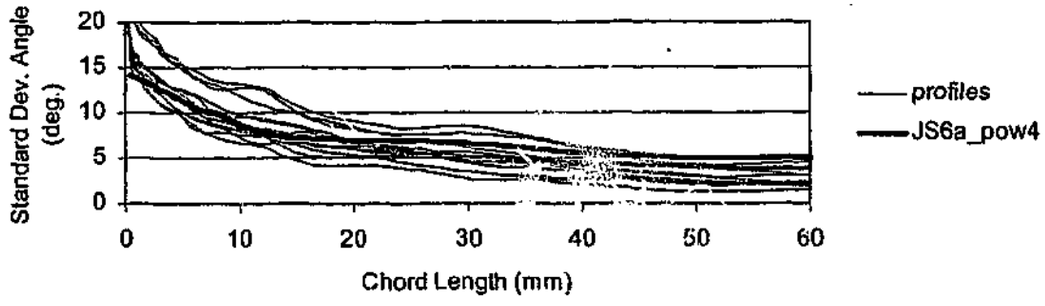

Figure 7.19: Standard deviation of chord angle statistics for generated profile and original surface

The as-cut generated profile is shown in Figure 7.20a together with a centre profile of the original surface, JS6a. Figure 7.20b shows the comparison of the standard deviation of chord angle statistics produced using the compass walking method of the cut profile and the envelope of original scanned profile statistics. The cut profile lies on the upper side of the envelope due to the overcutting by the water-jet process in particular below approximately 9mm chord length. This is unusual as the roughness below 4mm chord has actually been omitted from the cut surface (ignoring the ripple effect caused by the water-jet cutting process). This suggests that the overcutting of the profile has produced steep angled peaks that are comprised of 4mm chords but accumulate to a steep angle. This can be seen in Figure 7.20a with profile JC6a_pow4 having many very sharp asperities.

The sample was tested in direct shear at the same initial normal stress and constant normal stiffness as JS_6a (ie. K=400kPa/mm, σ_{no}=400kPa). Figure 7.21 compares the shear test results of the three-dimensional surface and the two-dimensional surface. The results indicate that the cut profile has not successfully modelled the split surface. Some initial seating of the split sample occurred causing approximately 0.15mm of initial contraction. However significant dilation occurred in the generated sample due to the larger longer wavelength roughness that was not present in the split sample. This may have been accentuated by the overcutting of the sample by the water-jet cutting process. The steeper angle asperities below approximately 9mm chord lengths would have caused the initial peak shear stress to be higher. Some shearing of these steeper asperities can be seen in the sudden decreases in shear stress in the shear stress versus normal stress plot at about 700kPa normal stress.

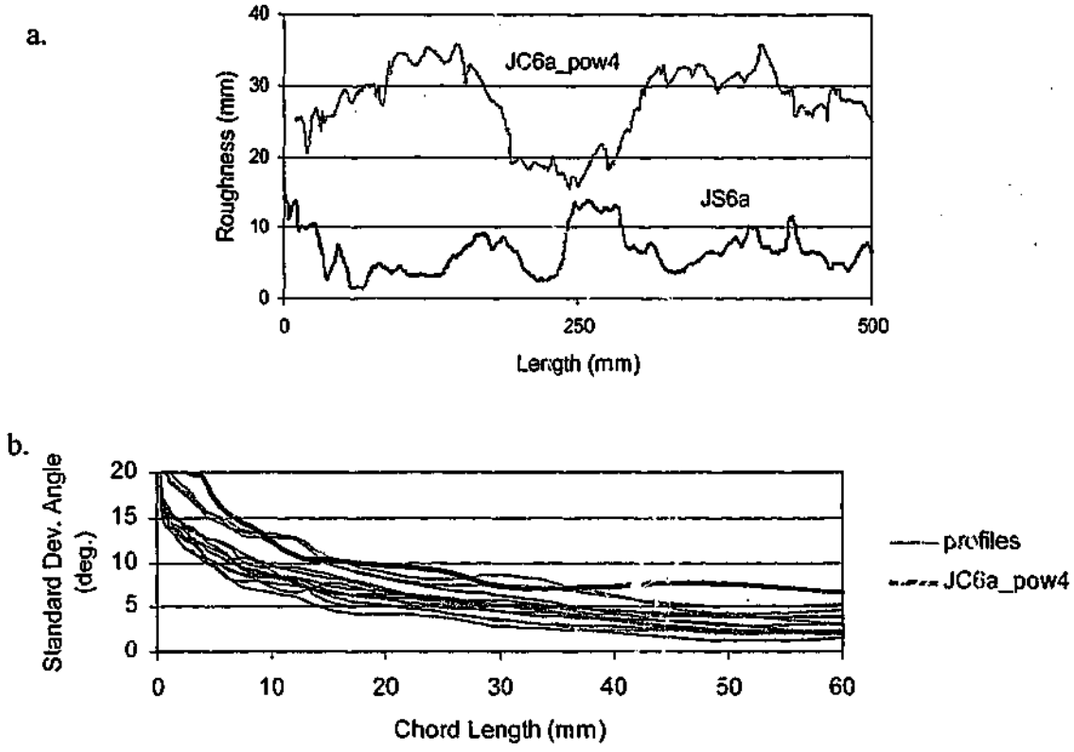

Figure 7.20: a. Centre profile from Johnstone split JS_6a, JS6a, and regenerated profile at 4mm chord lengths, JC6a_pow4

b. Statistics of cut profile and original surface

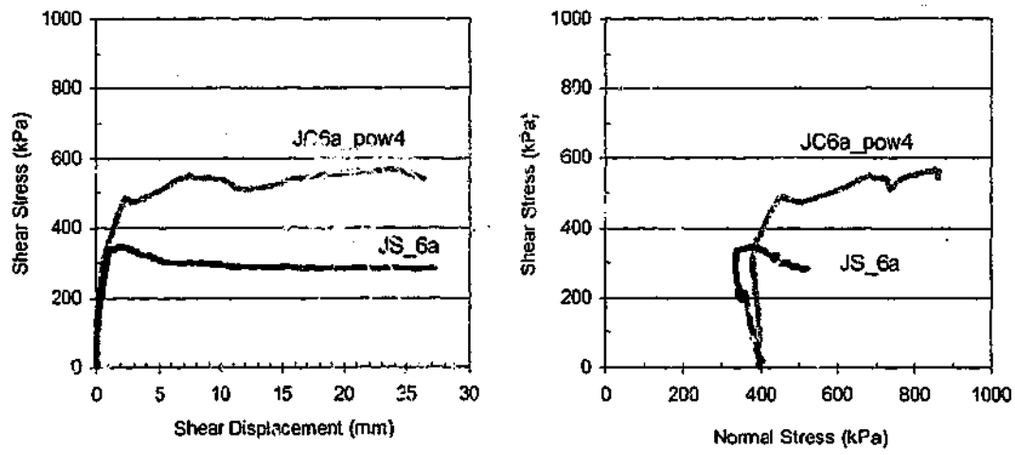

Figure 7.21: Shear test results of 3-D surface, JS_6a, and 2-D profile, JC6a_pow4

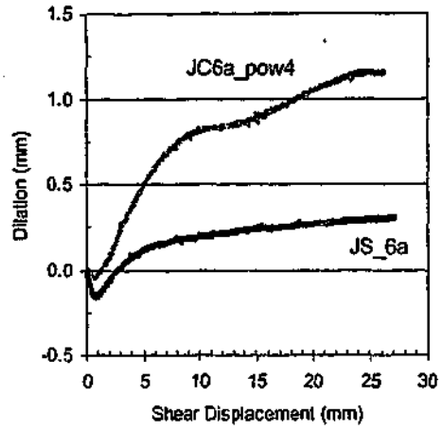

Figure 7.21 (cont'd): Shear test results of 3-D surface, JS_6a, and 2-D profile, JC6a_pow4

Using the compass walking method, the average standard deviation of chord angle statistics for the thirteen two-dimensional profiles of Johnstone split JS_7a were determined. These statistics were approximated by a natural logarithmic function according to s_θ=-2.5198Ln(L_c)+16.35, where s_θ=standard deviation of chord angle (deg), L_c=chord length. The modified midpoint displacement method with a standard deviation of chord angle of 7.5° was used to generate a profile with chord lengths of 32mm. Below a chord length of 32mm, the logarithmic function was used to estimate the standard deviation of chord angle to be used with the midpoint displacement method. The final generated profile had chord lengths of 4mm. The statistics of this generated profile fall within the standard deviation of angle envelope of the split surface as shown in Figure 7.22.

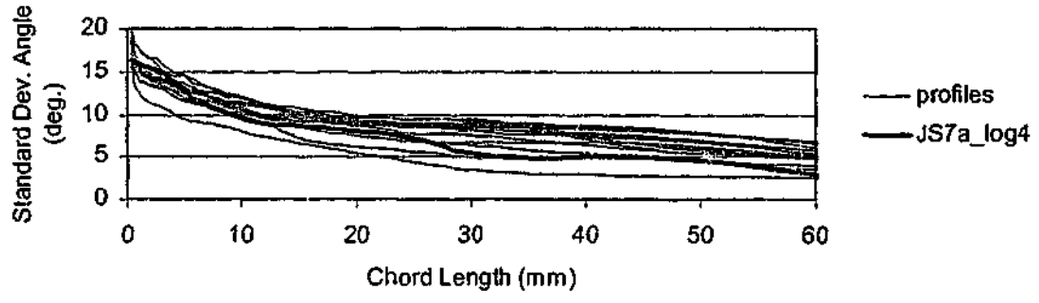

Figure 7.22: Standard deviation of chord angle statistics for generated profile and original surface

The profile was water-jet cut into a Johnstone sample from the same batch as JS_7a to form the two-dimensional profile, JC7a_log4. An overcut replication of the desired surface was obtained through water-jet cutting. The saturated moisture contents of the original and water-jet cut samples were 14.3% and 14.5% respectively. The as-cut generated profile is shown in Figure 7.23a together with a centre profile of the original surface. Figure 7.23b compares the standard deviation of chord angle statistics produced using the compass walking method of the cut profile and the envelope of original scanned profile statistics. The cut profile tends to be on the upper side of the envelope in particular below approximately 7mm chord length due to the overcutting by the water-jet process. This is unusual as the roughness below 4mm chord has actually been omitted from the cut surface (ignoring the ripple effect caused by the water-jet cutting process). This suggests that the overcutting of the profile has produced steep angled peaks that comprise of 4mm chords but accumulate to a steep angle.

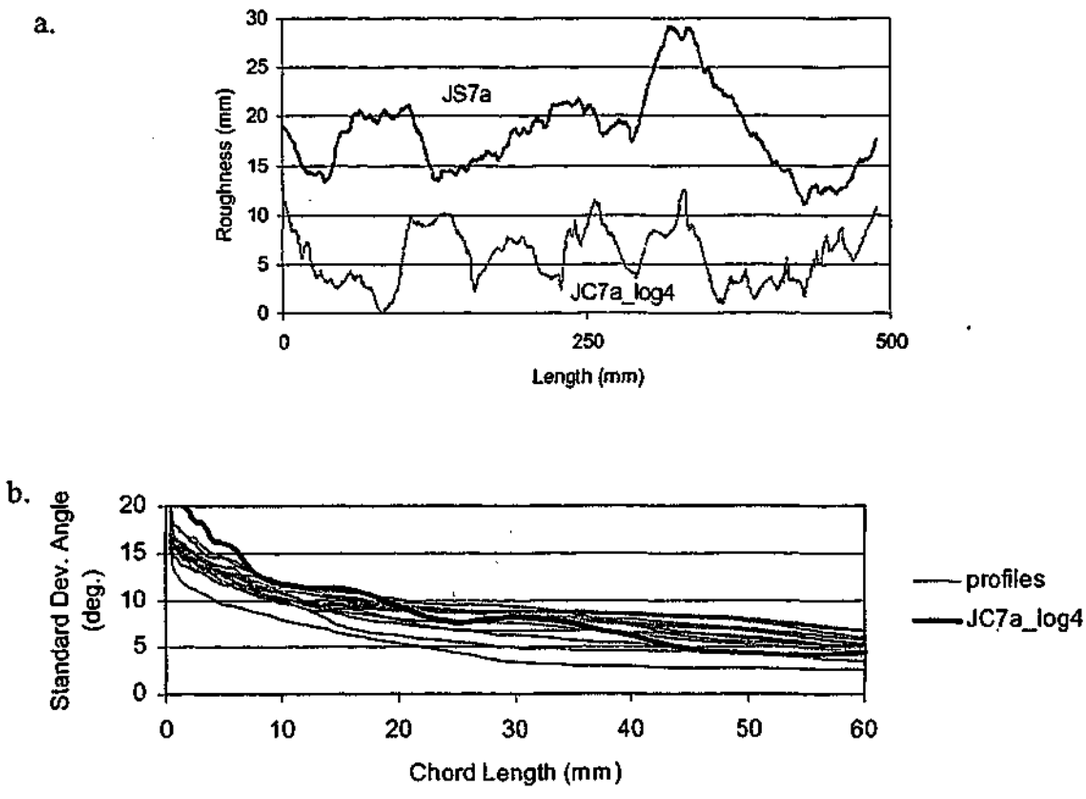

Figure 7.23: a. Centre profile from Johnstone split JS_7a, JS7a, and regenerated profile at 4mm chord lengths, JC7a_log4

b. Statistics of cut profile and original surface

The sample was tested in direct shear at the same initial normal stress and constant normal stiffness as JS_7a (ie. K=400kPa/mm, σ_{no}=400kPa). Figure 7.24 compares the shear test results of the three-dimensional surface, JS_7a, and the two-dimensional surface, JC7a_log4. These results indicate that the cut profile has overpredicted the shear response of the split surface. Due to the lack of fine roughness cut into sample JC7a_log4, the initial response is considerably less stiff than the split surface. However, the cut profile is rougher than the split surface below a chord length of approximately 7mm and its peak shear stress is approximately 20% higher than the split surface's peak shear stress. The shear stress continues to be higher until approximately 19mm shear displacement when an asperity is sheared and the shear stress drops to the same as the split surface. Until approximately 6mm shear displacement, the dilation of the two tests was similar. After this point the dilation measured during the cut surface shear test is slightly higher than that measured during the split surface shear test.

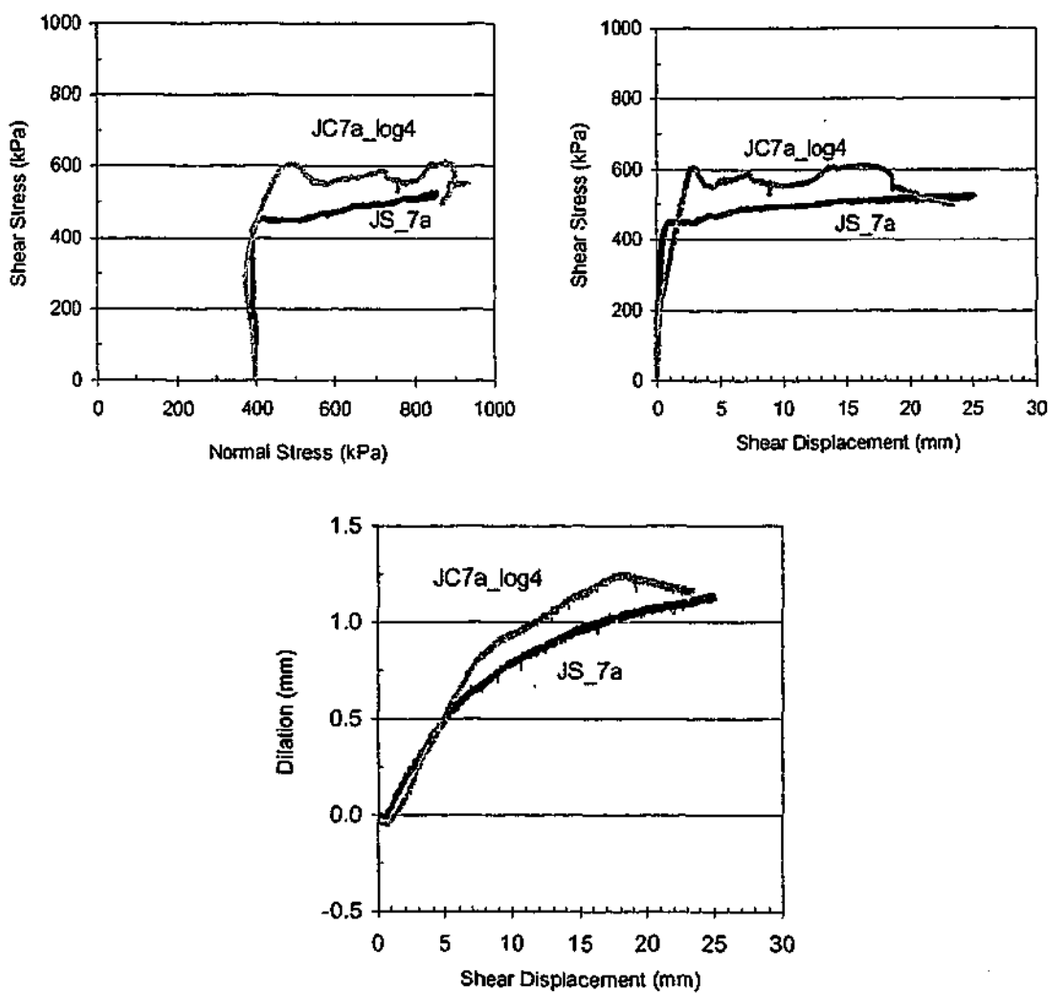

Figure 7.24: Shear test results of 3-D surface, JS_7a, and 2-D profile, JC7a_log4

7.2.3 Statistical Reproductions

To accurately represent a split surface, the standard deviation of chord angle statistics at various chord lengths (as generated using the compass walking method) of the two-dimensional cut samples need to be within, or close to, the envelope of standard deviation of chord angle statistics of the split surface. Due to the difficulties encountered in machining surfaces to a desired roughness profile, only a limited number of replications accurate enough to be used were obtained from the water-jet cutters. To provide further data, the statistics of several overcut samples were compared to split sample statistics from the same Johnstone batch. Three of these two-dimensional surface statistics fell within the standard deviation of chord angle envelope from split surface JS_6a. One two-dimensional surface statistic fell within the standard deviation of chord angle envelope for split surface JS_7a.

In each case, as the cut profile does not include roughness below a defined chord length (either 3mm, 4mm or 12mm), the initial shear response is less stiff than the split surface. However, below 1mm length chords, the ripple effect produced in the water-jet cutting process produces a sharp increase in roughness. At longer chord lengths, each of the cut profile's statistics being compared with split surface JS_6a, lay at the top of the split surface's statistical envelope. This indicates that the cut profiles had large overlying roughness that would cause larger dilation at larger displacements. As very few of the split surface profiles had this longer roughness, it is inferred that shearing occurred unevenly across the sample in these areas in preference to dilation.

Details of these surfaces and test results are given below.

Test 1 – Split Surface JS6a

The first two-dimensional cut surface that fell within the statistical envelope of split surface JS_6a, was taken from a centre profile of split surface JS4a. This profile designated JF8_12, was generated by using the compass walking method at a 12mm chord length along a centre profile. The profile following water-jet cutting of a Johnstone sample, had a standard deviation of chord angle of 8^{o} at 12mm chord length. As the smallest chord length included in the profile was 12mm, the profile would not be expected to replicate the shear behaviour at small displacements but should be reasonable for larger shear displacements. The as-cut profile is shown in Figure 7.25a together with

a centre profile of the split surface JS_6a. Figure 7.25b shows the standard deviation of chord angle statistics of the cut profile and the envelope of scanned profile statistics from surface JS_6a. The saturated moisture contents of the split and cut surfaces were 14.3% and 13.9% respectively.

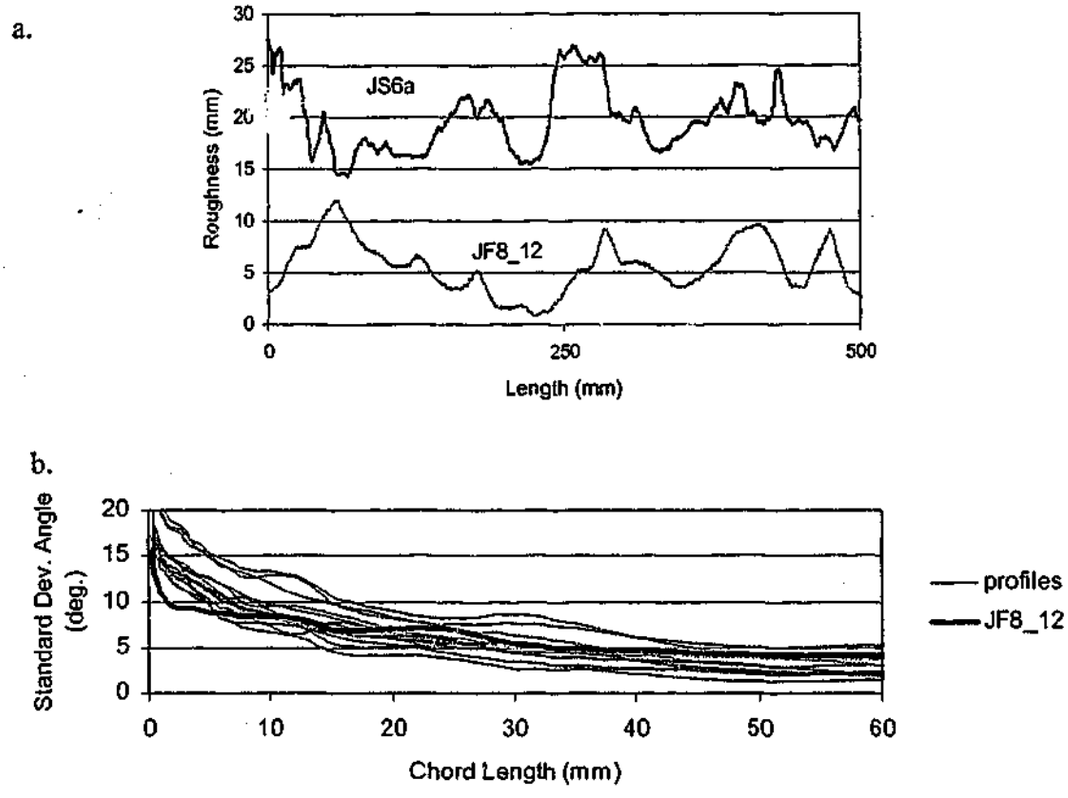

Figure 7.25: a. Centre profile from Johnstone split JS_6a, JS6a, and fractal profile, JF8_12

b. Statistics of cut profile and original surface

Sample JF8_12 was tested in direct shear at the same initial normal stress and constant normal stiffness as JS_6a (ie. K=400kPa/mm, σ_{no}=400kPa). Figure 7.26 compares the shear test results of the three-dimensional surface, JS_6a, and the two-dimensional surface, JF8_12.

The shear test results for this statistical reproduction indicate that the cut profile reasonably successfully modelled the split surface. The peak shear stress of the cut surface is approximately the same as the split surface although it occurs at a much higher shear displacement. After the peak shear stress, the cut surface continues to dilate as shown in Figure 7.25 and by the gradual increase in shear stress with shear displacement.

This may be due to the longer roughness wavelengths or an overlying slope in the sample set-up. The dilation of the split sample however, becomes relatively constant after approximately 5mm of displacement. This leads to the decline in shear stress observed after the peak.

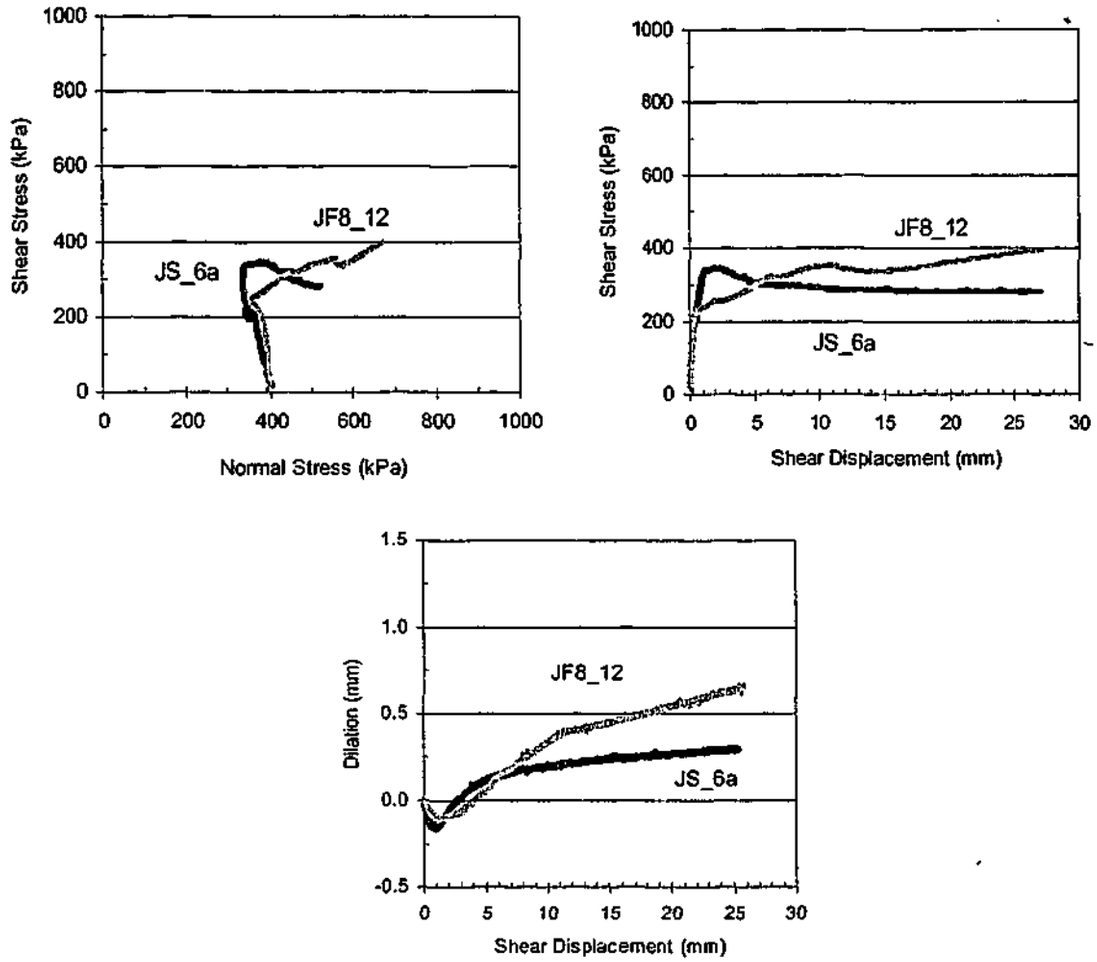

Figure 7.26: Shear test results of 3-D surface, JS_6a, and 2-D profile, JF8_12

The second two-dimensional cut surface that fell within the statistical envelope of split surface JS_6a, was taken from a centre profile of split surface JS3a. This profile designated JF12_3, was generated by using the compass walking method at a 3mm chord length along a centre profile. When water-jet cut into a Johnstone sample, the resulting profile had a standard deviation of chord angle of 12°. The as-cut generated profile is shown in Figure 7.27a together with a median profile of the split surface JS_6a. Figure 7.27b shows the standard deviation of chord angle statistics of the cut profile and the envelope of scanned profile statistics from surface JS_6a. The saturated moisture contents of the split and cut surfaces were 14.3% and 14.1% respectively.

Sample JF12_3 was tested in direct shear at the same initial normal stress and constant normal stiffness as JS_6a (ie. K=400kPa/mm, σ_{no}=400kPa). Figure 7.28 compares the shear test results of the three-dimensional and two-dimensional surfaces. The shear test results for this statistical reproduction indicate that the cut profile reasonably successfully modelled the split surface up until a shear displacement of about 3 to 5mm. However sample JF12_3 continued to dilate rapidly until approximately 15mm displacement after which time the dilation became minimal. Longer roughness wavelengths can be observed on the plot in Figure 7.27a and in the statistical plot of Figure 7.27b. The peak shear stress was approximately 20% higher in the cut sample. Peak shear stress was reached at approximately 2mm shear displacement in the split sample and 15mm shear displacement in the cut sample.

a.

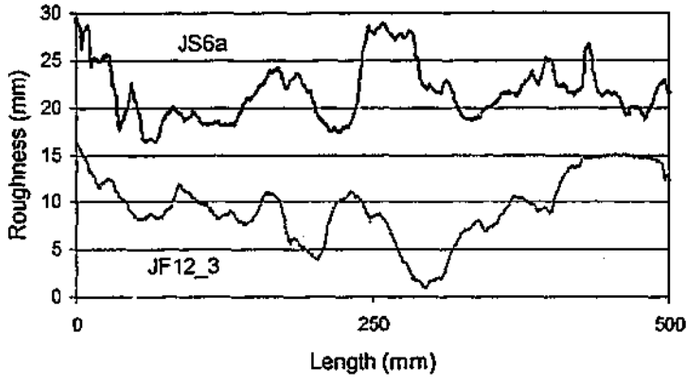

b.

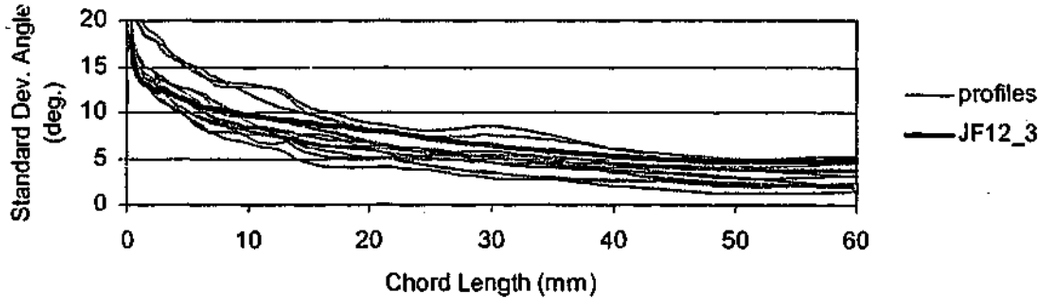

Figure 7.27: a. Centre profile from Johnstone split JS_6a, JS6a, and fractal profile, JF12_3

b. Statistics of cut profile and original surface

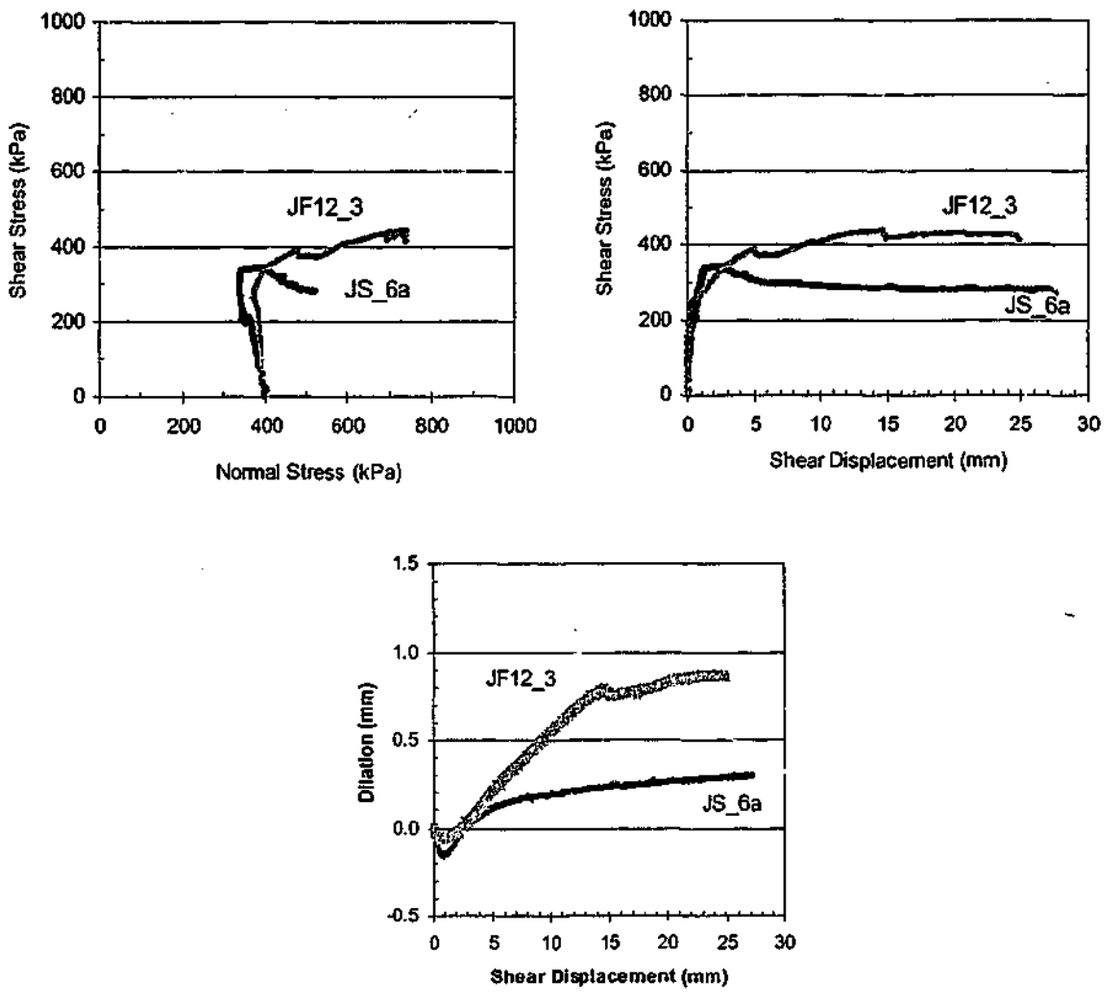

Figure 7.28: Shear test results of 3-D surface, JS_6a, and 2-D profile, JF12_3

The third two-dimensional cut surface that fell within the statistical envelope of split surface JS_6a, was taken from a centre profile of split surface JS_4a. This profile designated JF15a_3, was generated by using the compass walking method at a 3mm chord length along a centre profile. The resulting water-jet cut sample had a roughness profile with a standard deviation of chord angle of 15° (at 3mm chord length). The as-cut profile is shown in Figure 7.29a together with a centre profile of the split surface JS_6a. Figure 7.29b shows the comparison of the standard deviation of chord angle statistics of the cut profile and the envelope of scanned profile statistics from surface JS_6a. The saturated moisture content of the split and cut surfaces were 14.3% and 13.8% respectively.

Sample JF15a_3 was tested in direct shear at the same initial normal stress and constant normal stiffness as JS_6a (ie. K=400kPa/mm, σ_{no}=400kPa). Figure 7.30 compares the shear test results of the three-dimensional surface and the two-dimensional surface.

The shear test results for this statistical reproduction indicate that the cut profile reasonably successfully modelled the split surface. The initial peak shear stress of the cut surface is less than 10% higher than the split surface. However, after the peak shear stress, the shear stress of the cut surface remains relatively constant whilst the split sample displayed a decrease in shear stress following the peak and overall experiences less dilation than the cut sample.

a.

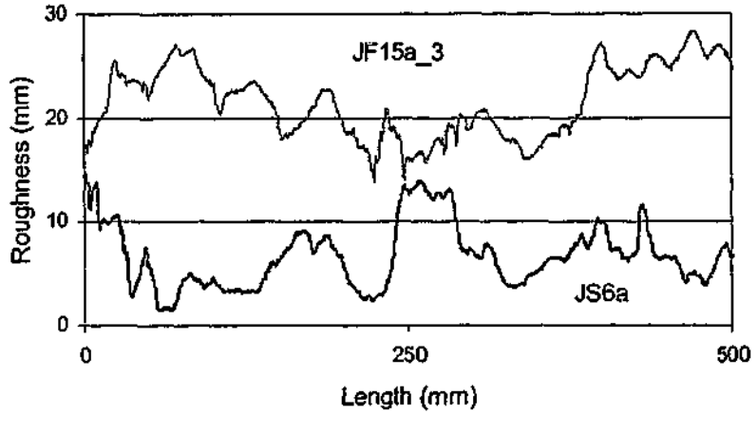

b.

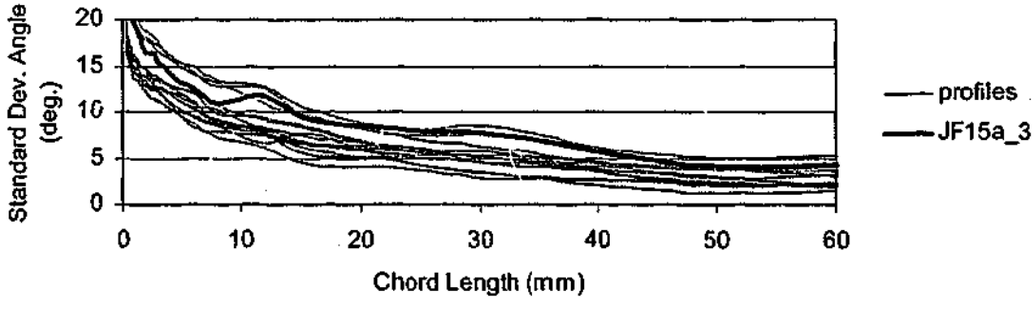

Figure 7.29: a. Centre profile from Johnstone split JS_6a, JS6a, and fractal profile, JF15a_3

b. Statistics of cut profile and original surface

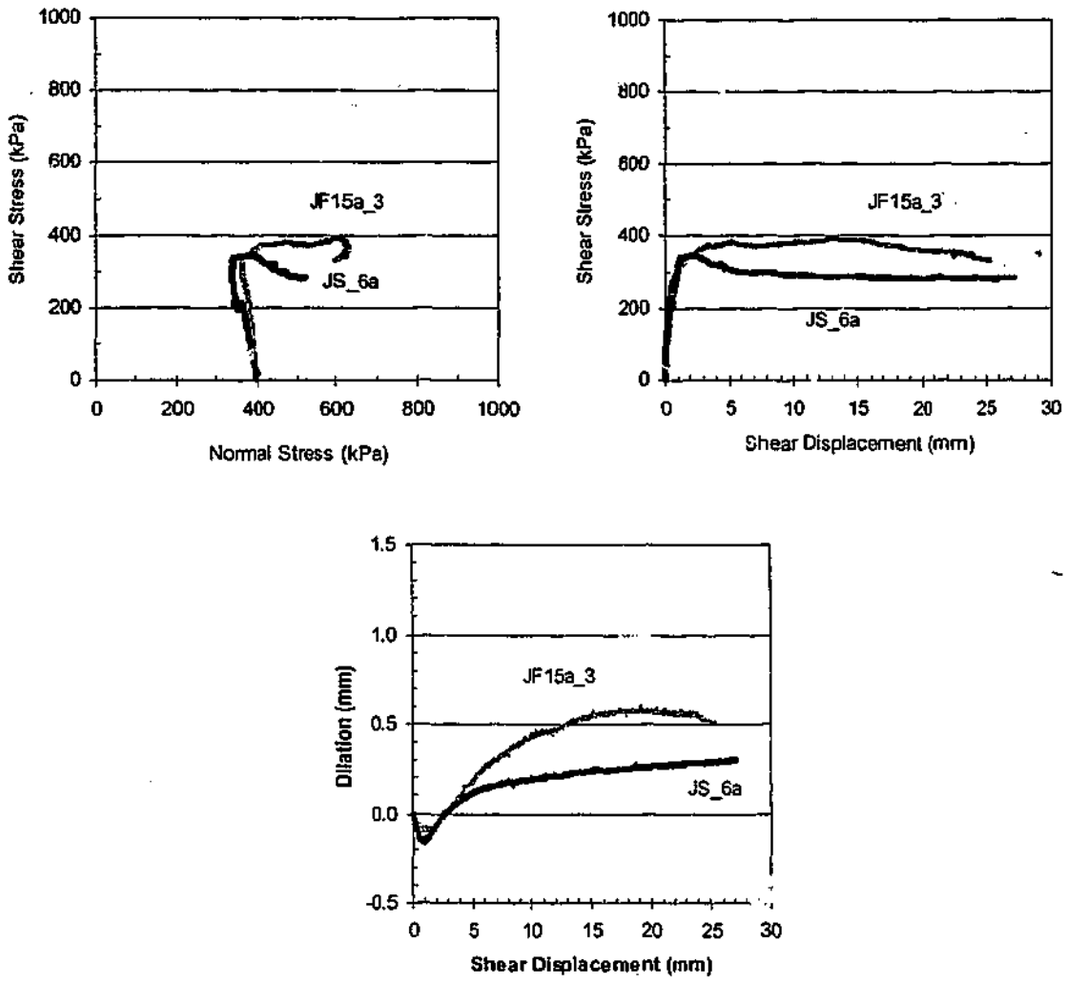

Figure 7.30: Shear test results of 3-D surface, JS_6a, and 2-D profile, JF15a_3

All of the cut samples continued to dilate, whilst the split sample's dilation became minimal after approximately 5mm shear displacement. Peak shear stress was only reached on the cut samples at considerably larger shear displacements than the split samples.

Test2 – Split Surface JS7a

The two-dimensional cut surface that fell within the statistical envelope of split surface JS_7a, was generated at 3mm chord lengths using the modified midpoint displacement method and a power function of the split surface JS_3a statistics. This profile, designated JF15_3, had a standard deviation of chord angle of 15° at 3mm chord length when water-jet cut into a Johnstone sample. The as-cut generated profile is shown in

Figure 7.31a together with a centre profile of the split surface JS_7a. Figure 7.31b compares the standard deviation of chord angle statistics of the cut profile and the envelope of profile statistics from surface JS_7a. This graph indicates that the roughness of the cut surface JF15_3 is higher than the split surface between 2 and 10mm chord lengths. The saturated moisture content of the split and cut surfaces were 14.3% and 13.6% respectively.

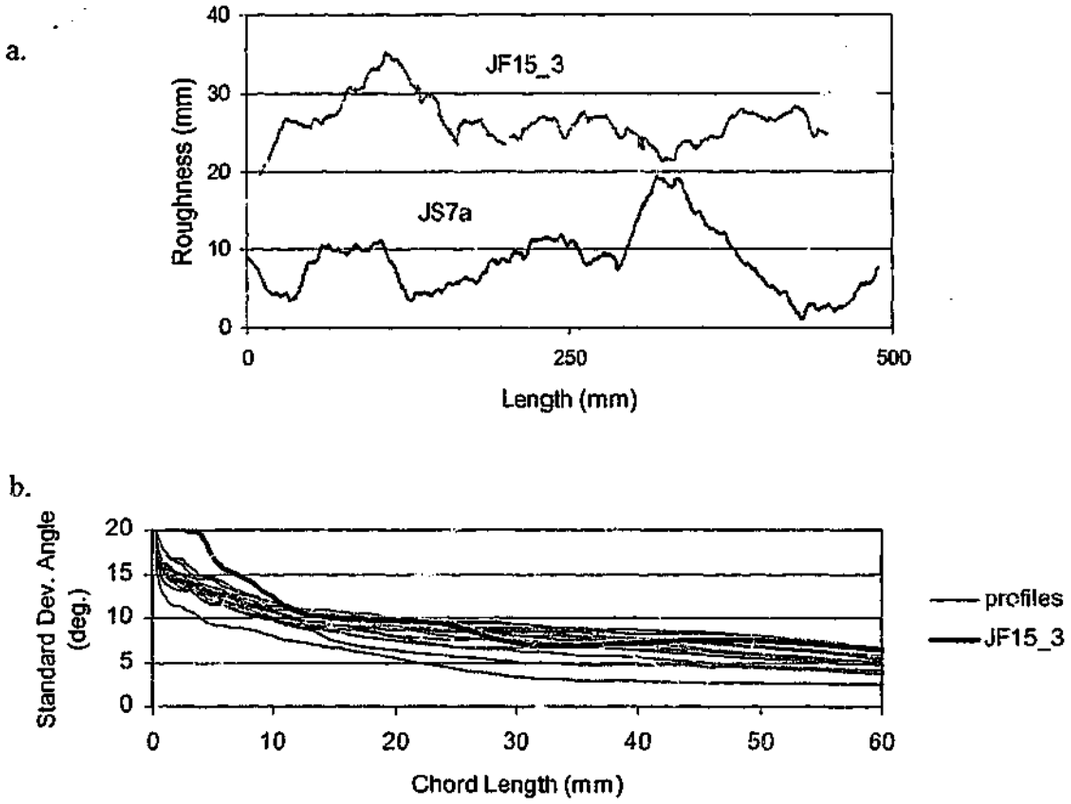

Figure 7.31: a. Centre profile from Johnstone split JS_7a, JS7a, and fractal profile, JF15_3

b. Statistics of cut profile and original surface

The sample was tested in direct shear at the same initial normal stress and constant normal stiffness as JS_7a (ie. K=400kPa/mm, σ_{no}=400kPa). Figure 7.32 compares the shear test results of the three-dimensional surface and the two-dimensional surface. The initial peak shear stress of the cut surface is approximately 10% higher than the initial peak shear strength of the split surface. The dilation of the cut sample is also

approximately 10% higher than the dilation response of the split surface. As the cut sample experienced more negative dilation at the commencement of shearing than the split sample, these differences would be slightly higher if the initial negative dilation was removed. The higher shear stresses and dilation obtained by the cut sample may be explained by the larger roughness of the cut sample between 2 and 10mm chords. Taking this into consideration, the shear test results for this statistical reproduction indicate that the cut profile successfully modelled the split surface.

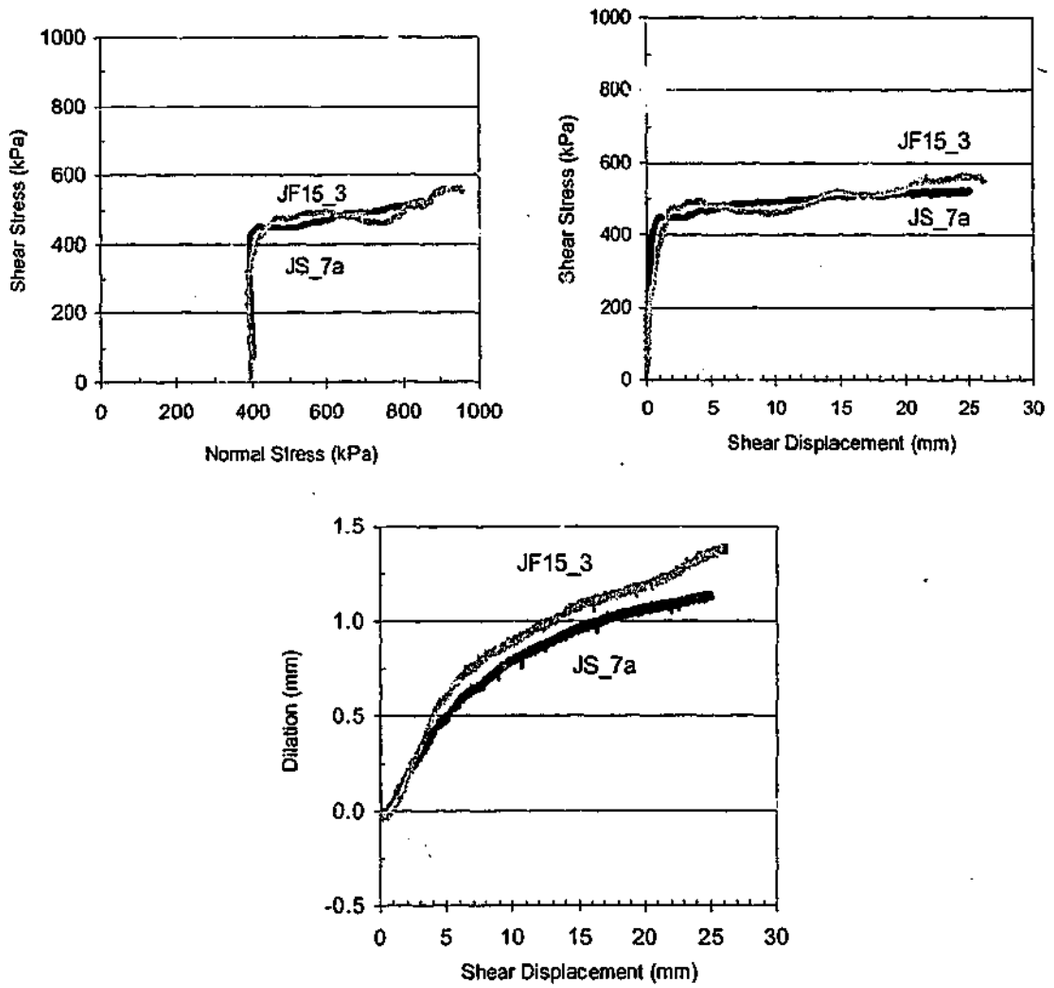

Figure 7.32: Shear test results of 3-D surface, JS_7a, and 2-D profile, JF15_3

7.3 Discussion

7.3.1 Representation of a 3-D Surface by a 2-D Profile taken from the Surface

Visual comparison of two-dimensional profiles in one direction along natural and artificial joint surfaces, has suggested that the profiles, although not geometrically identical, may be statistically similar. Statistical analysis of these profiles using the standard deviation of chord angle versus chord length statistics produced using the compass walking method, indicate a relatively narrow envelope of statistics and correspondingly good correlation coefficients. This correlation is improved if the correlation is calculated to the mean standard deviation of angle statistics for each surface. This suggests that if a mean surface is generated a slightly better correlation can be achieved.

This statistical analysis indicated that the surface statistics were relatively similar across the entire surface (in the same direction). Therefore statistically, the surface could be represented by any of its individual profiles.

To justify the statistical analysis, three laboratory direct shear tests were performed on split Johnstone samples (considered representative of natural siltstone bedding joints) and two-dimensional profiles that were water-jet cut into similar samples. The two-dimensional profiles were randomly selected from the profiles taken of each surface. The profiles were taken in the proposed shear direction of the split sample. Several points to note in these tests were as follows:

- These profiles were cut at chord lengths of 3mm, 4mm or 6mm. This meant that the fine roughness below these chord lengths was omitted. This was visible by a flattening of the statistical plots below this chord length and in the less stiff initial shear displacement response.
- The water-jet cutting process left fine ripples on the surface of the samples. These ripples were visible in the standard deviation of chord angle statistics with a sharp rise in the statistics below a chord length of approximately 1mm.
- The water-jet cutting process did not always produce the desired surface with some overcutting often present.

- Initial matching of the split surface was difficult to achieve with very minor mismatching changing the dilation and hence shear response of the surfaces.

Taking the above factors into account, the shear response of the two-dimensional profiles were typically within experimental variation of the respective surface responses. This again suggested that a single profile taken from the surface could adequately represent the three-dimensional surface. Most of the longer wavelength roughness present in the split surfaces tended to have a standard deviation of chord angle of about 5^0. This meant that following the initial peak shear value, the dilation was minimal and hence the shear stress became relatively constant. This was also observed for the cut samples. However, if longer chord length roughness were present, as in sample JS_7a, these longer wavelengths could be captured by representing the surface with a profile containing the longer wavelengths.

7.3.2 Statistical Reproduction of a Surface

The use of a power or logarithmic function to describe the standard deviation of chord angle statistics combined with the modified midpoint displacement method has been visually and statistically demonstrated to produce a two-dimensional profile with statistics that typically fall within the statistical envelope of natural and artificial joint surfaces.

As highlighted in the statistical comparison of various natural and artificial joint surfaces, if a mean surface is generated a slightly better correlation may be achieved between a two-dimensional profile and the three-dimensional surface. One laboratory direct shear test was conducted on a two-dimensional profile that had been generated using the modified midpoint displacement method and the 6mm chord length average standard deviation of chord angle statistics of a three-dimensional surface. The shear response of this profile did not capture the shear response of the three-dimensional surface as both the finer and coarser than 6mm roughness were not being modelled. This highlighted the need to model all wavelengths of roughness present in the three-dimensional surface.

Two laboratory direct shear tests were conducted on two-dimensional profiles generated using a power or logarithmic function describing the standard deviation of chord angle statistics of three-dimensional surfaces combined with the modified midpoint displacement method. Unfortunately both two-dimensional profiles produced were

considerably rougher than the three-dimensional surfaces at the smaller chord lengths. This was predominantly caused by overcutting of the test sample by the water-jet cutters. It meant however, that the shear response of the two-dimensional profiles were 20-40% higher than the three-dimensional surfaces.

As it appears difficult to have exact water-jet replication of desired surfaces, several two-dimensional profiles were created that were then matched with the statistics of the three-dimensional surfaces. Four two-dimensional profiles with statistics that fell within the statistical envelope of three-dimensional surfaces were selected. Taking into consideration the factors outlined in section 7.3.1, the shear response of these two-dimensional profiles were typically within experimental variation of the statistically equivalent three-dimensional surface. This suggested that providing the statistics of the three-dimensional surface were captured, the two-dimensional profiles were capable of adequately representing the surface.

7.4 Conclusions

These results support the contentions that:

- A three-dimensional surface can be adequately represented by a single two-dimensional profile of the surface provided the same shear direction is used.
- The modified midpoint displacement method combined with a power or logarithmic function of the surface's standard deviation of chord angle statistics can be used successfully to regenerate a surface.
- A three-dimensional surface can be successfully represented by a single two-dimensional profile, providing all wavelengths are captured and the potential shear direction is known. However, care must be taken with this process as longer wavelengths of roughness are not always captured in simple analysis. This large wavelength roughness can significantly increase the dilation and hence affect the normal stress and shear response under constant normal stiffness conditions.

8.0 MODELLING OF SHEAR BEHAVIOUR

Chapters 6 and 7 have outlined the basic mechanisms of the shear behaviour of rock joints and the quantification of joint roughness. As discussed in Chapter 4, some preliminary modifications were made to the existing concrete / rock shear behaviour model described by Fleuter (1997). These modifications involved inclusion of elasticity components of displacement of both sides of the joint; changes to the failure stress of asperities and the inclusion of a simple joint closure model. The current work has explored in further detail the shear response of rock joints including the behaviour of stronger rock and three-dimensional surfaces. This chapter discusses what changes were required to the model as a result of this more extensive testing.

The model developed for the shear behaviour of concrete-rock interfaces had previously been incorporated into a computer model by Seidel (1993). This computer program, Rocket, is discussed in this chapter together with the modifications made by Fleuter to include the behaviour of rock joints. Details of the further modifications required based on testing carried out for this project are presented.

8.1 Joint Closure and Machine Compliance

Bandis et al. (1983) investigated rock joint closure of several rock types under the application of applied stresses up to 55MPa. They concluded that the closure varied nonlinearly with normal stress until a state of maximum closure. This value depended upon the previous stress history of the joint. They also concluded that the joints when unloaded, experienced hysteresis and large permanent sets.

Some preliminary work was conducted by Fleuter (1997) into the effects of joint closure on the shear behaviour of rock joints in the Monash direct shear device. This work was conducted on soft rock samples with water-jet cut surfaces that appeared to have a maximum correction to dilation of approximately 0.55mm. Fleuter concluded that the effects of machine compliance were minimal and that a bilinear model could be used as an approximation of the joint closure. This bilinear model took into account elastic compression of the intact material and closure of the rock joint.

The current research has highlighted the importance of including the machine compliance components in measurements of joint closure and elastic compression of the intact rock. Joint closure has also been shown to depend predominantly on joint roughness and asperity strength.

8.1.1 Machine Compliance

All machinery has some compliance. In the case of the Monash University direct shear rig, compliance can be encountered between the sample interfaces and the shear box, in the metal interfaces of the shear box, between interfaces of the shear box and the direct shear rig, between the base of the vertical load cell and the top of the shear box and in the direct shear rig frame (refer to Figure 5.1 for diagram of shear rig and box).

To estimate the direct shear rig compliance, a block of steel 400mm x 80mm x 130mm was tested in the device under axial loading. The block was placed directly into the direct shear box without the use of plaster or grout. The block was strain gauged on the two longer edges. The strain gauge results indicate that almost negligible compression occurred within the steel block to the applied stresses of 6.5 MPa. This meant that the movements measured by the vertical LVDT's could be considered to be all compliance of the system. This enabled a polynomial relationship between applied normal stress (σ_n MPa) and compression (δ mm) to be estimated as shown graphically in Figure 8.1 and represented by Equation 8.1.

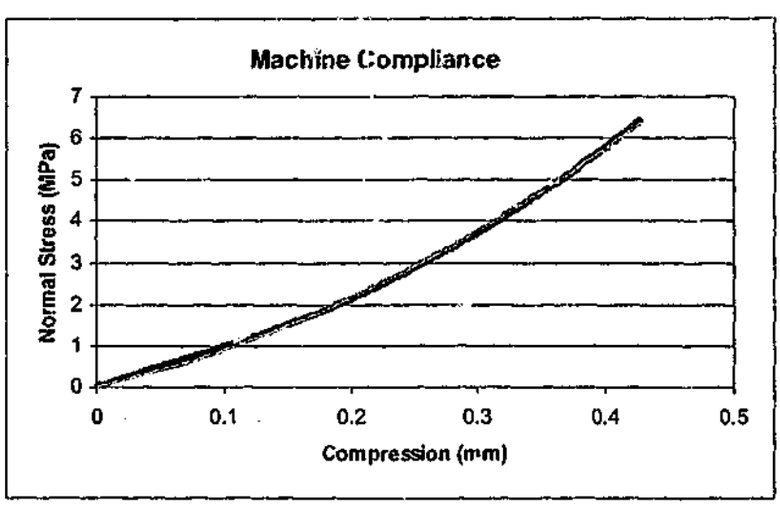

Figure 8.1: Machine Compliance relationship between normal stress and compression

$$\sigma_n=18.23(\delta)^2+7.11(\delta) \quad (8.1)$$

This estimation of machine compliance is based on axial loading and does not include potential compliance affects created during shear displacements. Due to the difficulty in measuring these compliance effects and the negligible rotation found in the bearing systems of the rig (Seidel 1993) the machine axial compression relationship will be used to estimate the machine compliance.

8.1.2 Elasticity of Intact rock

To estimate the elastic compression of the intact halves of the rock samples, a series of axial compression tests were conducted on intact test samples of sandstone, siltstone, basalt and granite in the direct shear rig. These samples were approximately 100-130mm high and were placed directly in the shear box without the use of plaster or grout. Previous tests had been conducted by Fleuter (1997) on intact Johnstone samples so these were not retested. After the machine compliance was subtracted from the compression results, an estimate of the sample stiffness was obtained. These stiffness values would naturally be dependent on the sample height. The values are listed in Table 8.1.

Unconfined compressive strength tests in a 500kN Baldwin compression test machine were also conducted on each rock type on 52mm diameter core samples approximately 130-140mm high. The ends of the samples were machined flat and parallel to the loading platen. An estimate of the Young's Modulus was made using a middle third rig. By dividing these results by the test sample length, an estimate of the stiffness for these samples was obtained. The values are also shown in Table 8.1.

As the heights between the two methods were comparable, a comparison of the stiffness calculated by the 2 methods can be made. The comparison consistently indicates higher sample stiffness measured in the Baldwin test machine (ie. there is considerably larger deformations measured in the direct shear rig). This large variation was considered to be due to sample compliance. The direct shear rig samples had been typically cut using a circular saw and it was likely that the surfaces of the direct shear test samples were not perfectly flat or parallel (as is the case with the UCS samples). Uneven surfaces may cause high local stresses on the sample. These high local stresses on the samples may have caused larger deformations. As the calculations of sample stiffness were carried out using the global normal stress and not local stresses, underestimation of the stiffness may

have occurred in the direct shear rig samples. The core samples in the uniaxial testing machine had been machined flat so that uniform loading was produced on these samples. Due to difficulties of machining the direct shear rig samples (eg. High strength and large size) it was deemed unfeasible for the limited number of samples to be tested. However, it should also be noted that the maximum difference obtained between the two test methods is only in the order of 0.06mm compression per 1MPa of applied stress for the worse case granite sample. These very small movements would be difficult to eliminate.

Table 8.1: Intact stiffness values of each rock type

Rock Type	Estimate of intact stiffness with compression test	Estimate of stiffness with UCS results
Johnstone	2.5 MPa/mm	6.9 MPa/mm
Sandstone	1.8 MPa/mm	24.6 MPa/mm
Siltstone	8.2 MPa/mm	195 MPa/mm
Basalt	24.2 MPa/mm	442 MPa/mm
Granite	16.6 MPa/mm	451 MPa/mm

In the determination of sample compression to be used in modelling, the Young's Modulus as estimated by testing samples in the Baldwin test machine will be used together with the sample thickness.

8.1.3 Joint Stiffness

In the current research the regular triangular and fractal profiles were cut using water-jet cutting techniques. This process leaves a slightly rippled profile on the surface. Under the application of a load this surface becomes more closely mated. Similarly, any gaps between the two interfaces of a split surface due to unmatching, diminishes under the application of a load. Previous work by Bandis et al. (1983) has suggested the need for a hyperbolic model to predict this joint closure behaviour. However, Bandis' model is designed to include high loads as potentially encountered in deep underground rock situations. This current research is restricted to relatively small loads. Over this range, a linear approximation of the joint closure is reasonable.

To obtain joint stiffness values, compression tests were conducted in the direct shear rig on water-jet and split samples of each rock type. As the samples were to be used for subsequent shear testing, the applied stresses were kept to within the range expected during the shear testing to eliminate permanent closure or damage to the joint surface. The sandstone and Johnstone samples were placed directly on the base of the shear box and then set in Plaster of Paris. This meant that there was approximately 10mm of plaster between the top of the sample and the top of the shear box. Gu (2001) had performed compression tests on a plaster block to estimate the compression of the plaster under loading. After adjustment to remove the machine compliance component, the results indicated that the plaster compressed by the bilinear relationship shown in Equations 8.2 and 8.2a (per mm thickness). The siltstone, basalt and granite samples were set in high strength concrete grout. Gu (2001) performed compression tests on a similar high strength concrete grout to estimate the compression of the concrete. These results were used and after adjustment to remove the machine compliance component, the results indicated that the concrete grout per mm thickness compressed by the linear relationship given in Equation 8.3 up to a normal stress of 2000kPa. Further application of load did not see further compression of the material.

$$\delta_c = 4E\text{-}7 * \sigma_n \qquad \sigma_n < 2000kPa \qquad (8.2)$$

$$\delta_c = 3E\text{-}7 * \sigma_n + 0.0006 \qquad \sigma_n \geq 2000kPa \qquad (8.2a)$$

$$\delta_c = 3.85E\text{-}7 * \sigma_n \qquad \sigma_n < 2000kPa \qquad (8.3)$$

where δ_c = casting material compression (mm)

σ_n = normal stress (kPa)

To calculate the average joint stiffness values of the water-jet cut and split surfaces, machine compliance, elastic compression of the intact material and compression of plaster or concrete at the top of sample was removed. This leaves a value of compression that includes closure of the joint under various applied stresses. An approximate linear relationship was developed between applied stress and amount of compression. This relationship is only applicable to normal stresses up to 6MPa. If higher applied stresses are to be expected a parabolic relationship may be required.

The joint stiffness values given in Table 8.2 are the average joint stiffness values that were used to model the direct shear tests performed in this current work. These values

include sample compliance due to potentially uneven surface as discussed in Section 8.1.2. When modelling natural insitu joints the joint stiffness value may be higher as it would not include these sample compliance components.

Table 8.2: Joint Stiffness values

Rock Type	Surface	Modelling Stiffness
Johnstone	Waterjet	6.0 MPa/mm
	Split	5.4 MPa/mm
Sandstone	Split	2.1 MPa/mm
Siltstone	Waterjet	6.2 MPa/mm
	Split	3.9 MPa/mm
Basalt	Waterjet	7.6 MPa/mm
	Split	7.5 MPa/mm
Granite	Waterjet	7.8 MPa/mm
	Split	7.5 MPa/mm

Table 8.2 indicates that stiffness appears to be dependent on the surface roughness and rock type. It is therefore necessary to obtain accurate joint stiffness data for each rock joint to be modelled. The amount of joint closure, δ_j, can then be calculated via a linear relationship between joint stiffness, K_j, and the local normal stress, σ_n, as shown in Equation 8.4. This relationship is only valid for low normal stresses up to approximately 6MPa. If normal stresses are considerably higher a hyperbolic model as suggested by Bandis may be required.

$$\delta_j = K_j \sigma_n \tag{8.4}$$

8.2 Shear Modelling

In concrete / soft rock interface modelling by Seidel (1993), the Sokolovsky solution for an infinite slope was used to assess the shear failure of the soft rock asperities (as discussed in Section 4.4). Fleuter (1997) performed a finite difference analysis on a rock joint model. This analysis indicated reasonable correlation between the Sokolovsky

failure stress and the average stress over 20% of the interface closest to the asperity edge. Fleuter suggested an asperity multiplication factor of approximately 2 to the concrete / rock model to take into account the reduced failure area.

Estimations of asperity failure using Fleuter's recommendations are shown in Figure 8.2 for 10° regular triangular asperity profiles of different rock types. These simulations take into account the full compliance effects as discussed in Section 8.1. The results indicate that reasonable agreement is found for the Johnstone material (8% difference between predicted peak shear stress and laboratory peak shear stress). The peak shear stress for the sandstone material is well predicted although the shear displacement to failure is overpredicted and the amount of dilation at peak is underpredicted by 14%. The failure stress does not appear to be correctly modelled for the stronger materials.

An analysis was therefore conducted to determine the actual failure stress for each of the test materials. Direct shear test results on regular triangular asperities where shear failure had occurred were used for this analysis. The local normal stress at failure could be calculated using the peak shear stress and contact area sheared as shown in Equation 8.5.

$$\sigma_f = (\tau_p L_T) / (N L_S \tan(\phi + i)) \qquad (8.5)$$

where σ_f = local failure stress

N = number of asperities

L_S = sheared length

ϕ = friction angle

i = asperity angle

τ_p = peak shear stress

L_T = total sample length

Regular triangular asperity direct shear tests on Johnstone and Sydney Hawkesbury sandstone samples were conducted by Fleuter (1997) and were not repeated during this current testing. Fleuter's test results were therefore used for these materials. Due to minimum and maximum load limitations of the direct shear rig, asperity failure was not observed in the granite samples tested in this current work and hence analysis of this material could not be conducted.

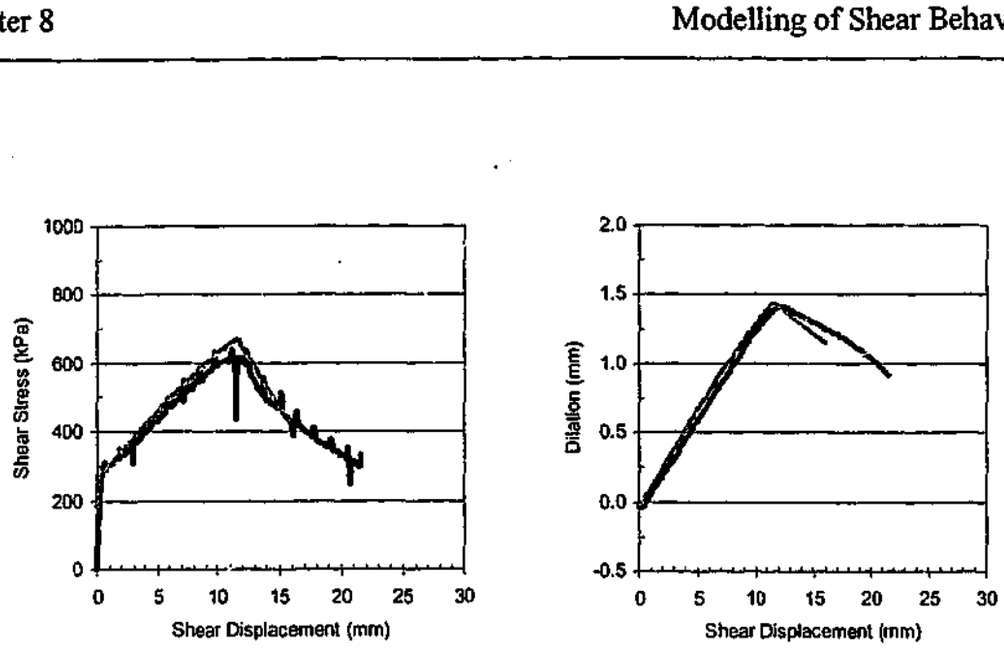

Fleuter (1997) Johnstone 10° Regular Triangular Profile

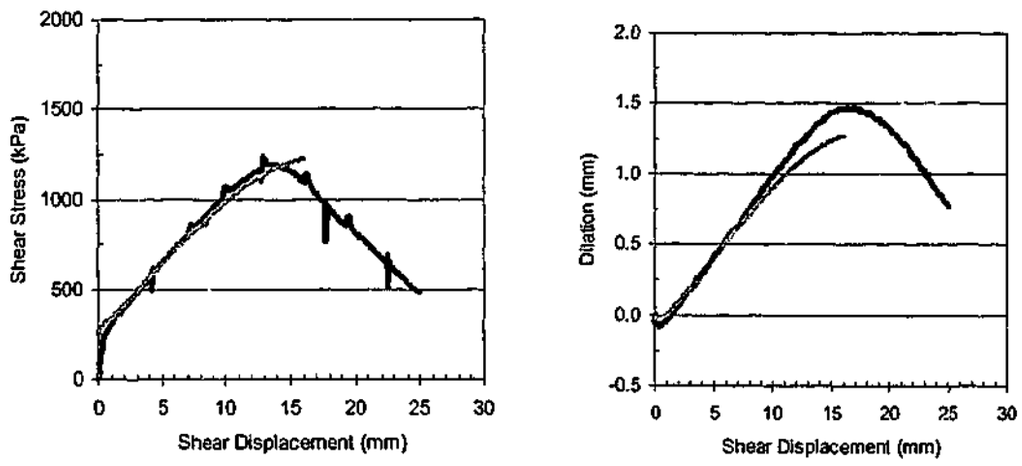

Fleuter (1997) Sandstone 10° Regular Triangular Profile

Test Result Prediction

Figure 8.2: Shear stress vs shear displacement predictions using stress concentration factor = 2

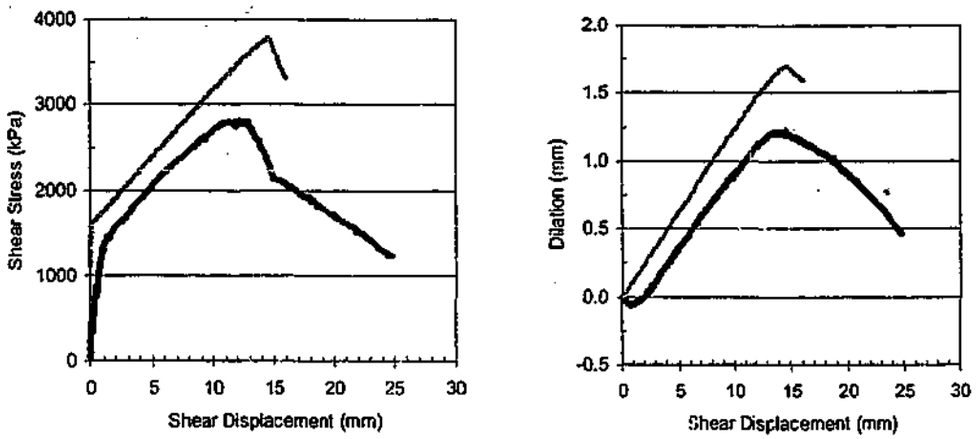

Siltstone 10° Regular Triangular Profile

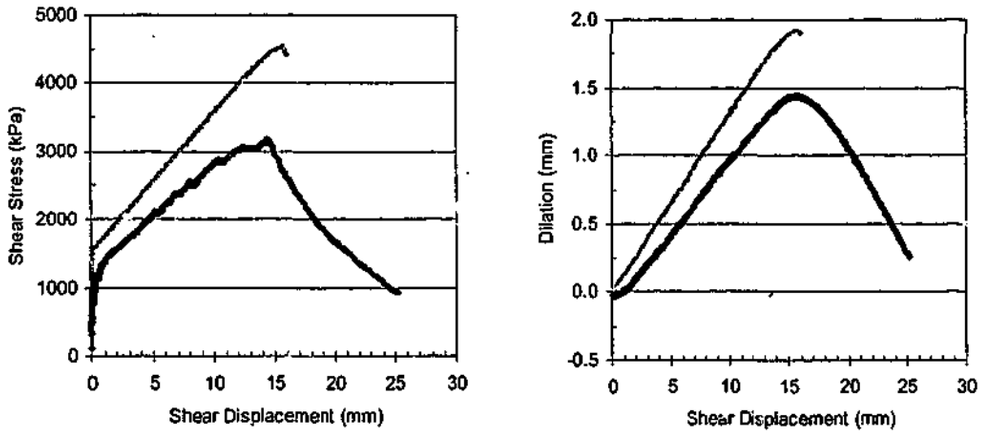

Basalt 10° Regular Triangular Profile

Test Result Prediction

Figure 8.2 (cont'd): Shear stress vs shear displacement predictions using stress concentration factor = 2

Using the direct shear test results of the regular triangular asperities where shearing of the asperities had occurred, a plot of failure stress versus asperity angle could be constructed for each material. The failure stresses assessed using the Sokolovsky solution has also been added to this plot together with the Unconfined Compressive Strength of the rock sample. These plots are shown in Figure 8.3. They indicate the following:

- Soft rock. The failure stress of the Johnstone (UCS = 4.0MPa) and Hawkesbury sandstone samples (UCS = 14MPa) appear to be consistently lower than that predicted by the Sokolovsky model. In the case of the Johnstone, the failure stress on average was 38% lower than the Sokolovsky failure stress. In the case of the sandstone the failure stress on average was 26% lower than the Sokolovsky failure stress.
- Medium to hard rock. The failure stress of the stronger rock appears to coincide with the unconfined compressive strength of the rock. The siltstone regular triangular samples were tested parallel to their bedding direction and hence the unconfined compressive strength of the sample along the bedding direction was used (30MPa). The basalt samples were shown to have an unconfined compressive strength of approximately 120MPa.

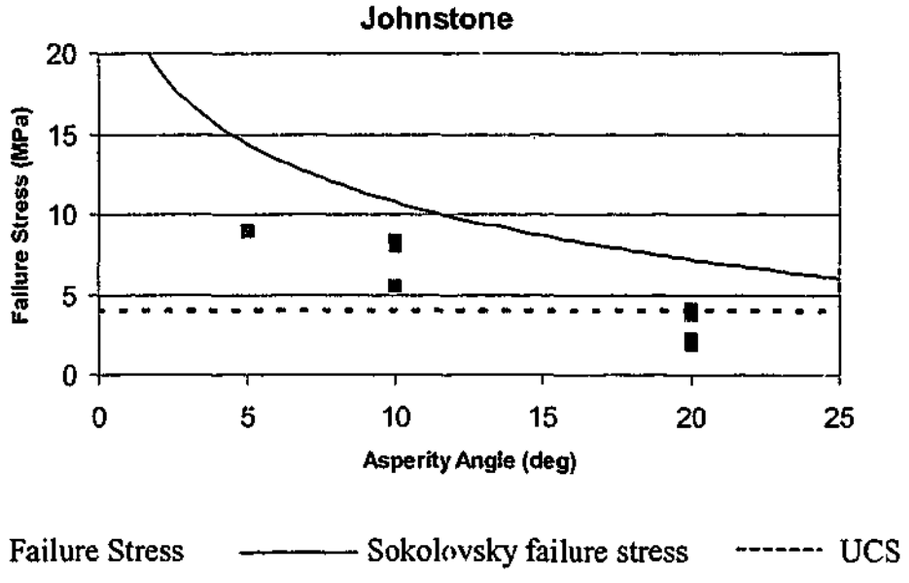

Figure 8.3: Failure Stress Plots

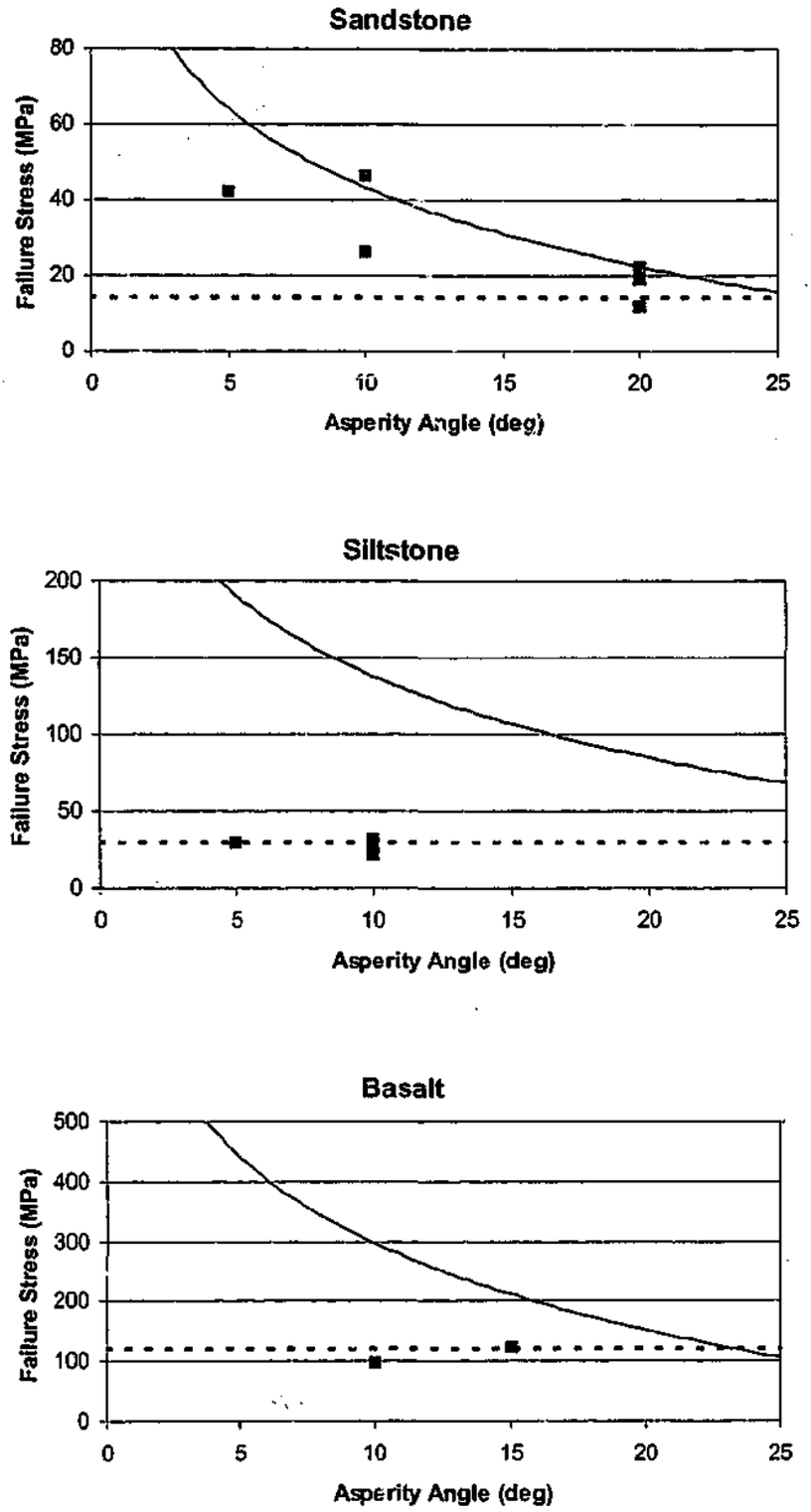

Figure 8.3 (cont'd): Failure Stress Plots

This analysis indicates that for softer rock samples the slope stability analysis can be used and modified to take into account the reduced failure (contact) area of rock joints compared to rock / concrete interfaces. However harder rock samples will fail when the local normal stress reaches the unconfined compressive strength of the rock.

8.3 Joint Roughness Representation

The analysis of three-dimensional natural joints and man-made surfaces described in Chapter 7, indicated that for modelling purposes, profiles taken in one direction could be treated as statistically similar. This suggested that if the roughness statistics of the surface were captured, the surface could be analysed more simply as a two-dimensional rough profile. Joint roughness can be quantified by calculating the standard deviation of chord angles for various chord lengths. By using different chord lengths the scale affects of the joint shear behaviour can be captured.

The analysis described in Chapter 7 indicated that an individual profile taken from the joint surface typically captured the shear behaviour of the surface at chord lengths greater than the minimum chord length reproduced. It would therefore be ideal if this profile could be used to represent the joint surface in the shear analysis. Unfortunately, due to the accumulation of either positive or negative chord angles in these profiles, computer modelling of these profiles are difficult to program. This instability is due to the use of slope stability analogies in modelling asperity failure mechanisms. This is shown diagrammatically in Figure 8.4. A similar situation was encountered when the statistics of the surface were used to regenerate a statistically similar profile. Although this regenerated profile included various scales to minimize scale effects, it was not suitable for computer analysis.

To overcome these modelling difficulties, irregular triangular asperities are used to simulate roughness. A series of chord angles with varying standard deviations are selected according to a Gaussian distribution (refer to Section 3.5) such that the angles are forced to alternate between positive and negative angles to produce triangular asperities. By selecting a chord length, a roughness profile with a known standard deviation of chord angle can be produced. This profile can be used to represent the joint surface at one defined chord length. If several chord lengths are analysed, superposition

can be used on the envelope of shear responses to predict the behaviour of the surface at different scales.

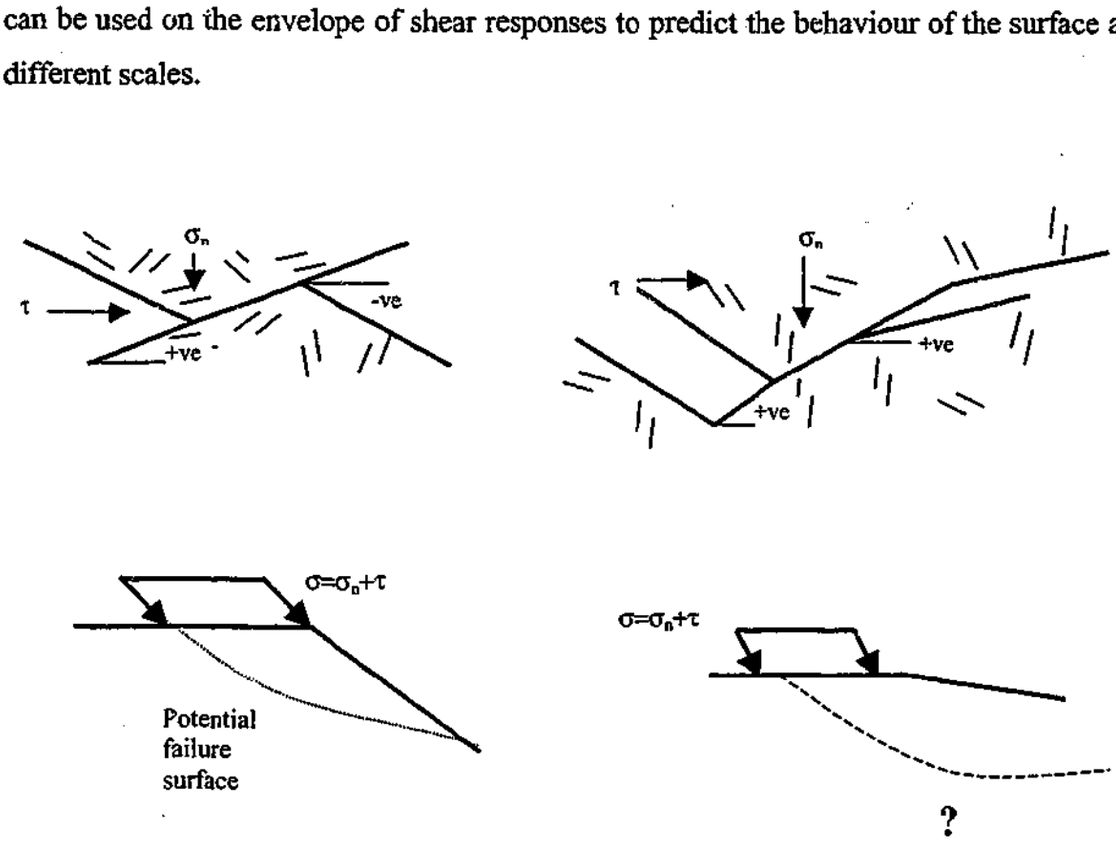

Figure 8.4: Diagrammatic representation of potential failure surfaces

8.4 Modifications to the program Rocket

The program ROCKET was written originally in 1993 in C language to model pile socket response under axial loading (Seidel 1993). This program was later interfaced with Windows and the code adjusted where required so that it could be understood by C++ processors. Later modifications were made by a computer programmer under contract to include rock joint behaviour so that predictions could be made for the Masters candidature of Fleuter (1997). Based on the more extensive testing of rock joint behaviour in this present work and the need to include the behaviour of strong rock and three-dimensional profiles, this program has been further modified by the author. The modifications are discussed in this section.

8.4.1 The Existing Algorithm

The computer program can be divided into two main parts with these being:

- the algorithm
- the windows interfacing

The algorithm is written in a series of modules that are called from the main module Rocket30. These modules are typically stand-alone and perform a specific part of the calculations of joint shear behaviour. Figure 8.5 shows a flow diagram that illustrates the basic sequence of modules. A summary of each module follows:

GEOM This is the geometric input module. To simulate plane strain conditions, the asperity width (ie. dimension perpendicular to the shear direction) is set to 10 times the asperity length (ie. dimension parallel to the shear direction). The profiles modelled by the program are regular triangular profiles (5°, 10° and 20°), 3 standard profiles used in Seidel's (1993) research work and 2 constant chord length two-dimensional fractal profiles (s_θ=10° and s_θ=15°). These profiles are stored as data files of chord angles (in degrees). They are scaled within the model by user input chord lengths and number of chords. These profiles could be up to 50 chords long with a minimum chord length of approximately 6mm.

POSN This module computes the current mid-point location of each asperity by calculating the original position plus half the shear displacement.

INCLUDE This module determines the included angles for an asperity and the previous and net asperity faces. These angles are used to calculate the slope failure stress and to calculate the additional interface contact length under high local stresses.

SOKOLOV This module determines the failure stress of an asperity based on the closed form solution after Sokolovsky (1960). The Newton-Raphson method is used to iterate to the solution. To take into account premature failure of the rock in localized regions of high stress, the effective Sokolovsky failure stress is reduced inversely in proportion to the computed increase in local stresses over the higher stress regions.

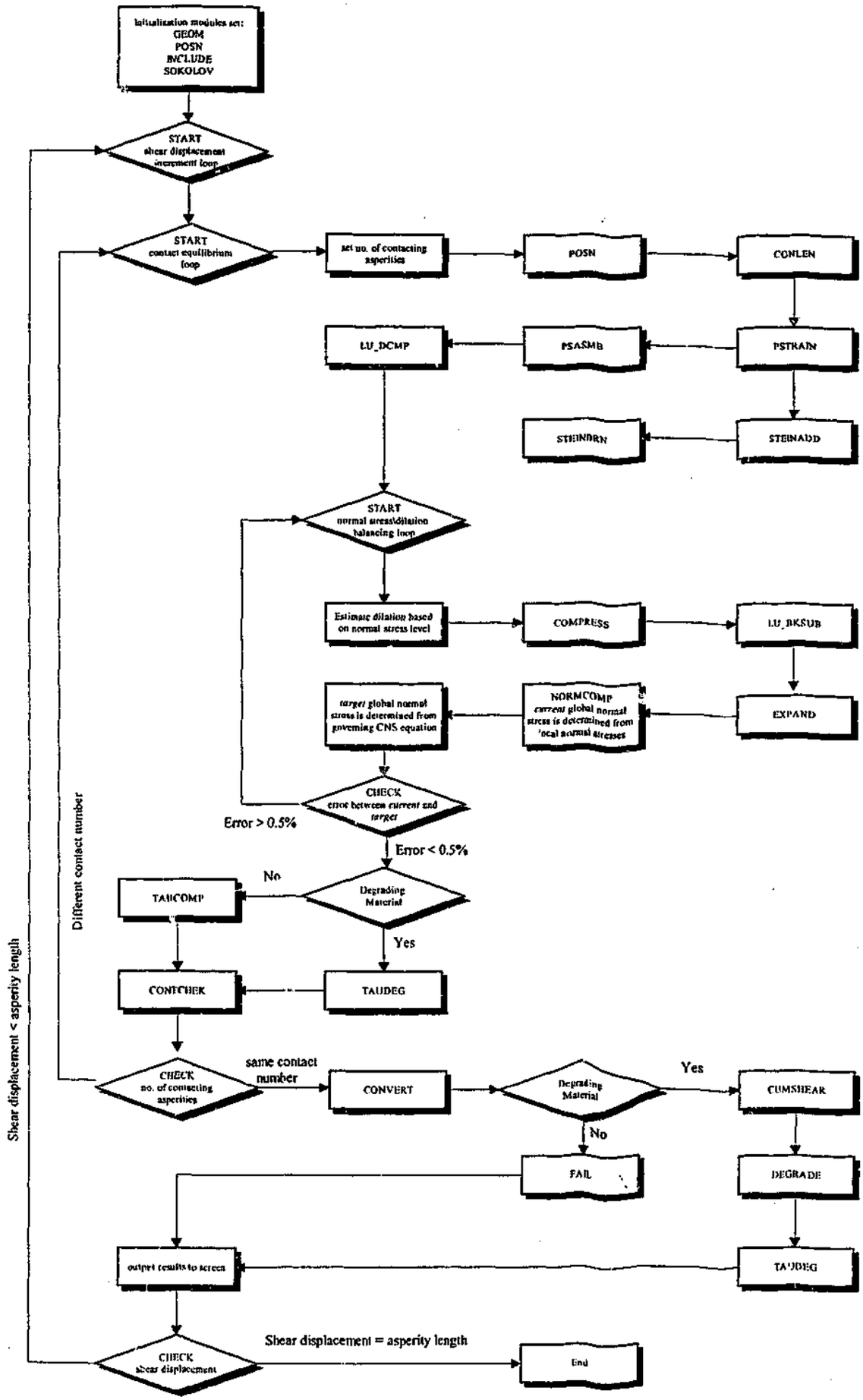

Figure 8.5: Sequence of Modules in Rocket

CONLEN This module computes the contact length between the two sides of the interface. For non-degrading materials, the contact length is determined by the asperity length less the global shear displacement. For degrading materials allowance is made for an increased contact length due to the effects of degradation and higher normal stresses. For asperities that have failed, the contact length is determined by the geometry and the relative movements along the failure plane and the original surface.

PSTRAIN This module computes the displacement at 16 asperity faces either side of the loaded asperity face being analysed. It also assembles the local compliance vector for each asperity.

STEINADD This module computes the individual influence factors relating to any loaded asperity using Steinbrenner's method.

PSASMB This module assembles the global compliance matrix from the local compliance vectors for each asperity excluding any non-contacting asperities.

LUDCMP2 This module performs the LU-Decomposition (L-lower U-upper triangular is a mathematical manipulation of linear Equations) of the global compliance matrix to determine the global stiffness matrix. This module is used in combination with module LUBKSUB to solve a set of simultaneous Equations.

INTRFACE This module takes into account the reduction in dilation due to joint closure of the sample.

COMPRESS This module computes the net elastic compression, ρ, of each asperity from the asperity geometry, current dilation, ψ, computed degradation and joint closure, δ_j. The current dilation is an estimate used to produce a more accurate estimate of the true dilation after several iterations.

LUBKSUB The stiffness matrix determined in module LUDCMP2 is multiplied by the net elastic compressions and via solving a set of simultaneous linear Equations the local stresses acting on each asperity are estimated.

EXPAND As the stiffness matrix is computed only for the asperities in contact, this module is required to take the values from LUBKSUB and assign the values to the original asperities.

NORMCOMP This module computes the global normal stress from the sum of the product of local stresses and asperity contact lengths and averaging over the full sample length.

TAUCOMP This module multiplies the normal stresses acting on each asperity by the effective friction angle $(\phi+i)$ to obtain the shear stresses acting on each asperity. The sum of the shear stresses is then computed to obtain the global shear stress.

TAUDEG This module computes the shear resistance of asperities experiencing degradation.

CONTCHEK This module checks each asperity for contact. The total number of contacts is checked against the initial number of contacts and if the number of contacting asperities is not equal then the contact equilibrium loop is re-entered.

CONVERT This module converts the local normal and shear stresses in global coordinates to local coordinates.

FAIL This module determines whether the current local stress on a given asperity exceeds the Sokolovsky failure stress. If they do then failure flags are set.

CUMSHEAR This module accumulates the shear displacement that has occurred on each asperity face.

DEGRADE This module computes an incremental degradation rate. Four wear rate models are supplied for user selection.

The windows interfacing framework is located in the main module Rocket. This in turn calls the Rocket2 module that handles user requests together with the resource file (*.rc) and dialog resource script files (*.dlg). Separate modules are written for such processes as printing, graphs, dongle access etc.

The current program requires selection that a rock joint is being analysed. Once this selection is made, the user is required to input the following properties or parameters:

- Young's Modulus for top and bottom joint surface (limited to soft rock values)
- Sliding and shearing friction angles
- Cohesion value
- Poisson's ratio for top and bottom joint surface
- Depth of top joint surface and bottom joint surface
- Stress Concentration Factor (refer to Fleuter (1997))
- Select a data file to load the geometry, choose the chord length and number of chords (currently limited to several profiles with chord lengths greater than approximately 6mm)
- Initial normal stress and constant normal stiffness
- Select whether to include interface compliance. If selected, input interface modulus, maximum joint closure and sample modulus. The joint closure can be calculated using either global normal stress or local stresses (although problems occur using the local stress for some profiles)
- Select whether the material degrades. If selected, choose a degradation model from 4 options.

For each execution of the program one chord length can be analysed. This means that the model analyses the joint at only one particular scale per execution. The scale is defined by the chord length selected with the corresponding geometry. By analysing several chord lengths, an envelope of shear response at a range of scales can be developed (Haberfield and Seidel, 1999). This enables the scale dependency of joint shear modelling to be captured.

This process is illustrated graphically in Figure 8.6.

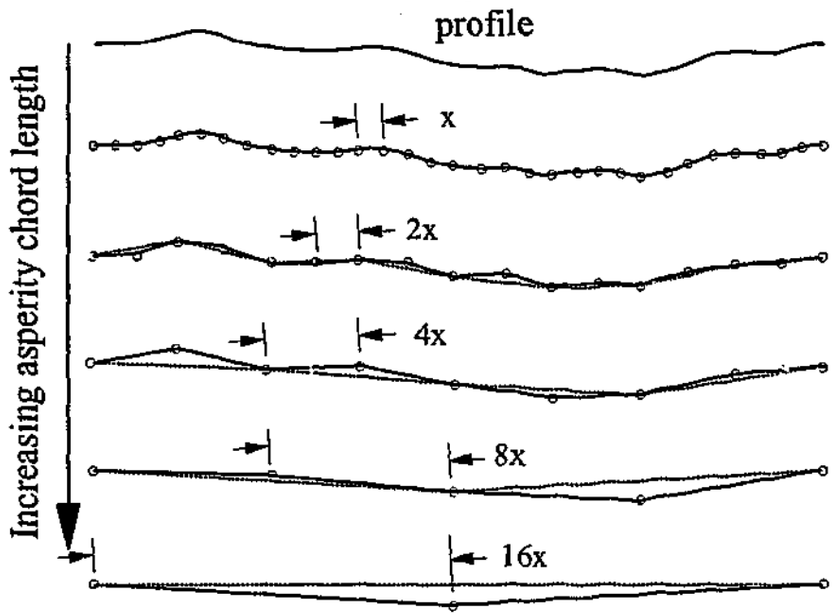

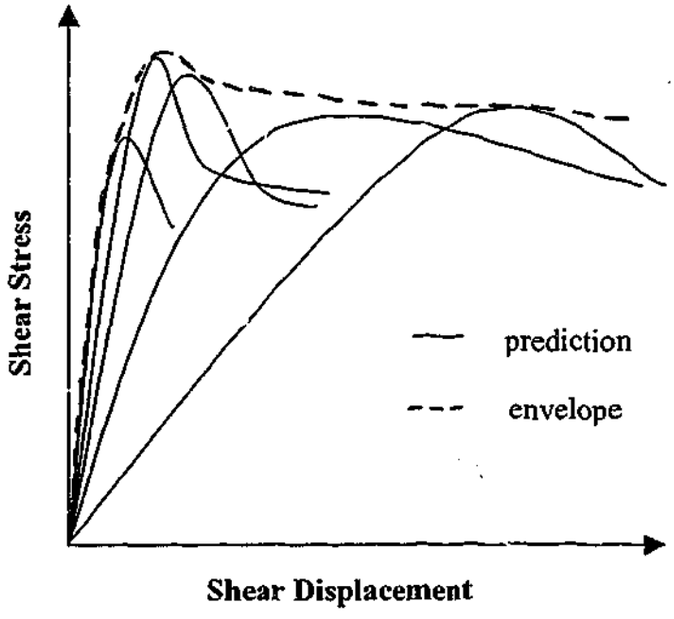

Shear response for several chord lengths with the shear envelope.

Figure 8.6: Procedure of capturing the shear behaviour of a rock joint at several scales

8.4.2 Modifications to stress – dilation balancing loop

The existing Rocket code was unstable at small chord lengths, for high Young's Modulus values and high combinations of normal stress and constant normal stiffness in particular at the commencement of shearing.

The existing stress – dilation balancing loop can be summarised as follows:

- estimate a global initial dilation
- calculate individual asperity's dilation taking into account the dilation on the asperity due to shear displacement less any effects due to compliance or wear, and subtracting the estimated dilation
- use these individual asperity dilations to calculate the local normal stress on each asperity
- if the local normal stress was negative, take the asperity out of contact and set the local normal stress to zero
- summate the local normal stresses and normalise to obtain a global normal stress
- compare this global normal stress to the global normal stress calculated by using the initial normal stress plus the stiffness times the global dilation.
- If the error is greater than 0.05% and the loop has not been repeated 25 times, the loop is repeated setting the new estimate of global dilation to be the existing estimate plus the difference in normal stress multiplied by the sample depth divided by sample modulus.
- Once this loop is finished the number of asperity contacts are checked against the original number of asperity contacts. If the number of contacts are different the entire process is repeated up to 4 times.

This process was improved by taking only one asperity out of contact during each loop. As shear displacement commenced the rear side of each asperity would typically move out of contact (taking into account any potential elastic effects). This sudden removal of contact areas caused typically half of the asperity sides to initially be taken out of contact and then recontacted through a programming error. This caused an initial instability (oscillation between extreme normal stress values were encountered) in the program that meant that the error was not reduced to less than 0.05% before 25 loops were performed.

By removing only one asperity at a time and reprogramming the incorrect coding, this problem was avoided and the error consistently reduced to below 0.05% within several loops. The number of iterations was repeated up to the number of asperities being modelled.

These adjustments, together with a few minor programming errors in the existing code, enabled very small chord lengths to be modelled together with any combination of Young's Modulus, initial normal stress and constant normal stiffness without instability.

8.4.3 Modifications for Joint Closure and Compliance

As a joint undergoes shear displacement, sliding commences on the steepest asperities causing dilation of the sample. In the absence of elastic compression and compliance this dilation can be calculated by the shear displacement multiplied by the tan of the steepest asperity angle (ie. $\psi = x\tan\theta$). However in rough joints, elastic effects with load sharing, closure of the interface and compression of the intact rock are present. In a laboratory situation there is also machine compliance and sample set-up compliance. In the Rocket code the module COMPRESS computes the amount of dilation, ψ, of each asperity. The joint closure, δ_j, elastic compression of the intact rock, machine compliance, C_m (in the case of laboratory testing) and compression of the casting material δ_c (in the case of laboratory testing), reduce the amount of expected dilation. These reductions are calculated in the module INTRFACE and are summarized by Equation 8.6.

$$\psi = x.tani - degradation - elastic\ compression\ of\ intact\ rock\ -C_m - \delta_j - \delta_c \quad (8.6)$$

For degrading materials the component of dilation attributed to degradation is removed via a selection of one of 4 options. For laboratory samples, the machine compliance is calculated via a polynomial relationship with the global normal stress as specified in Equation 8.1.

The amount of joint closure is calculated via a linear relationship between the joint stiffness and the local normal stress as expressed in Equation 8.4. The joint closure is calculated only for contacting asperities.

The amount of elastic compression of the asperity due to the local stress is calculated by dividing the local normal stress by the asperity height.

8.4.4 Modifications for shear failure

As discussed in section 8.2 the existing shear failure model using Sokolovsky's slope stability analogy only partially modelled the soft rock joints and did not capture the shear failure of hard rock joints. The rock joints consistently underwent premature failure in localized regions of high stress.

To take into account this premature, brittle failure, the soft rock joints were modelled using a modified Sokolovsky failure stress. Allowance was made in the user interface of the program Rocket to input a modification factor. The Sokolovsky failure stress was divided by this modification factor. In the case of Johnstone the modification factor is 1.38 and in the case of sandstone 1.26.

The harder rock samples fail at their unconfined compressive strength values. Therefore the UCS was used as the failure stress rather than using a Sokolovsky solution. This modification was made in the FAIL module of Rocket.

8.4.5 Modifications for data entry

The existing Rocket program was designed to read text files of chord angles. The existing text files represented triangular profiles of 5°, 10° and 20° chord angles, fractal profiles with a standard deviation of chord angle of 10° and 15° and 3 standard profiles used in Seidel's (1993) research work. As the program needed to be extended to analyse more realistic surfaces a more extensive database of profiles was required.

A set of chord angles were generated using a program written in Visual Basic so that each set had a predefined standard deviation of chord angle with angles that alternated between positive and negative values. A range of standard deviation of chord angles between 1° and 20° in 1° intervals was generated and saved as text files to be accessed from the computer shear model.

To quantify the roughness of the joint surface either the statistics of the surface must be known in terms of the variation of the standard deviation of chord angle with chord length, or several profiles from the surface taken and analysed to produce standard deviation of chord angle statistics. The average of these statistics can be used to determine an average standard deviation of chord angle at a specified chord interval. By selecting the standard deviation of chord angle at several chord lengths, an envelope of

shear response can be generated using the standard deviation of chord angle text files within the computer model. This process is shown diagrammatically in Figure 8.7.

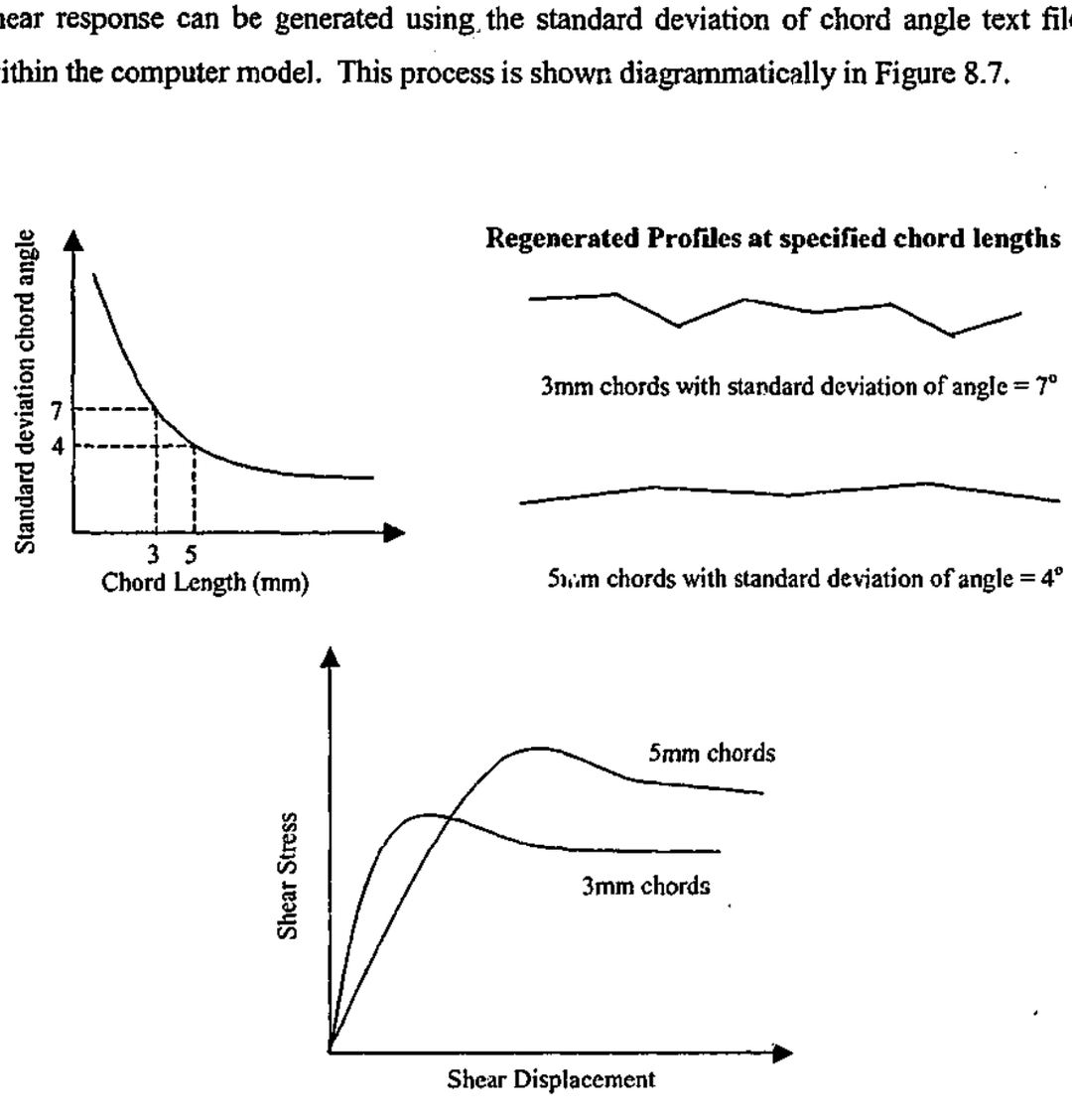

Figure 8.7: Roughness Input and analysis

The modified program has removed references to pile socket analysis. The user is required to input the following properties or parameters:

- Young's Modulus for top and bottom joint surface (no limiting value)
- Sliding and shearing friction angles
- Cohesion value
- Poisson's ratio for top and bottom joint surface
- Depth of top joint surface and bottom joint surface

- Sokolovsky Modification Factor
- Rock Unconfined Compressive Strength
- Select a data file to load the geometry, choose the chord length (no limiting chord length value) and number of chords.
- Initial normal stress and constant normal stiffness
- Joint compliance is always included in the model. A selection can be made to include machine compliance. If machine compliance is included, the user can select whether the sample is set in plaster or concrete and it's thickness so that the compression in this medium can be calculated. The user must input a joint stiffness value and a sample modulus.
- The user can select whether the material degrades. If selected the degradation model suggested by Fleuter (1997) or Gu (2001) can be used.

8.5 Conclusion

The series of laboratory direct shear tests conducted for this work has indicated that the basic shear model developed for concrete / rock interfaces can be used for the analysis of jock joints. Work by Fleuter (1997) had already included the elastic components of both interfaces. This further work has highlighted the need to more accurately model compliance effects, develop methods to analyse three-dimensional surfaces and that modifications to the shear failure model were required.

The following changes to the model have been made to address these issues:

- Joint closure is present both in the laboratory and insitu conditions. This is dependent on applied stress levels, rock strength and roughness and can be represented by a joint stiffness. The model has been changed to include a joint stiffness value that can be used to determine the joint closure under an application of a normal load. This value must be input by the user. Although a hyperbolic model may more closely replicate joint closure effects, as this work is limited to near surface rock situations and hence low stresses a linear model has been used. This model adequately represents the closure in these conditions and is naturally far simpler to implement for a range of rock types.

- Machine compliance is present in laboratory test situations. The machine compliance of the Monash direct shear rig used for the test program varies according to a polynomial relationship with axial loading. The compliance effects due to shear loading have not been included. This is not considered of significant concern for near surface rock situations with low stress levels as being modelled in this current work. However, for higher loads and stronger rock (such as the granite tested) it may need to be included.

- In laboratory testing, compression in the casting materials used to fix the joint into the shear box also plays a minor component in the overall measured dilation. Bilinear relationships were developed for the compression in the casting plaster and concrete grout used during this work.

- Due to the complexity of analysing a three-dimensional surface, it is desirable to convert the surface into a two-dimensional equivalent. Three-dimensional surfaces were shown in Chapter 7 to be adequately captured by statistically representative two-dimensional profiles. To capture the scale effects of an irregular two-dimensional profile, the statistics over a range of chord lengths can be used. By using several chord lengths, an envelope of shear behaviour at a range of chord lengths can be developed. This approach of representing firstly the three-dimensional surface statistically by the average of several profiles, and then analysing the resulting profile at various chord lengths, will be used to approximate the shear behaviour of a surface.

- Using the existing multiplication factor on the Sokolovsky predicted failure stress of 2 to predict the local normal stress level where shear failure will occur, underpredicts the peak shear strength for soft rock and overpredicts the peak shear strength for harder rock. Analysis of actual failure stresses indicate that lower modification factors (than 2) to the Sokolovsky failure stress are required for soft rock situations. In hard rock situations the failure stress can be approximated by the rocks unconfined compressive strength. For modelling purposes, it has been suggested that for rock with an unconfined compressive strength of greater than 20MPa the failure stress be set equal to the unconfined compressive strength. Further testing is required to confirm this.

9.0 PREDICTIONS OF ROCK JOINT BEHAVIOUR

This chapter compares prediction from the theoretical joint model with results from the direct shear tests. The predictions are made using the modified computer program Rocket.

Due to the high strength of some of the materials tested, it was necessary to empirically estimate several of the shear strength parameters. The parameters selected and the methodology used in their estimation is discussed in Section 9.1.

This chapter discusses each rock type and category of roughness profile separately, providing example predictions of each. A complete compilation of predictions is provided in Appendix E. The predictions shown in Appendix E are represented by 4 graphs:

- shear stress vs. shear displacement
- shear stress vs. normal stress
- dilation vs. shear displacement
- normal stress vs. shear displacement

The shear and normal stresses are average values based on the total plan area of the interface less an allowance for shear displacement. Each graph shows the laboratory test results together with one prediction if the profile has a single chord length, or three predictions at different chord lengths for irregular profiles. As shown in Figure 9.1, when three predictions at different chord lengths are used, an envelope of shear response can be drawn onto the graph.

9.1 Estimation of Shear strength parameters

Due to the high strength of several of the rock types tested in this current work, it was not possible to obtain shear strength parameters through intact sample direct shear testing or triaxial testing using the available equipment. For this reason the shear strength parameters were estimated for the siltstone, basalt and granite using the Hoek - Brown

failure criterion (Hoek and Brown 1980; Hoek and Brown 1988) expressed in Equation 9.1.

$$\sigma_{1f}^{'} = \sigma_3^{'} + \sqrt{R_m m_i \sigma_c \sigma_3^{'} + s(\sigma_c)^2} \qquad (9.1)$$

where $\sigma_1^{'}$ and $\sigma_3^{'}$ = principal stresses

σ_c = critical stress at failure

R_m, m_i and s = empirical constants that relate to rock type and degree of fracturing

For intact rock: σ_c = Unconfined Compressive Strength

$R_m = s = 1$

m_i siltstone = 10

m_i basalt = 17

m_i medium grained granite = 22

These values were combined with the Unconfined Compressive Strength values and cohesion and peak friction angle values estimated by constructing Mohr circles. A range of stresses up to 300 kPa was used to construct the Mohr circles. The estimated values are given in Table 9.1.

Table 9.1: Estimated Cohesion and Peak Friction Values

Material	Cohesion (MPa)	Peak Friction Angle (^{0})
Siltstone	12	40
Basalt	20	48
Granite	35	50

The values for the Johnstone and sandstone were taken from intact direct shear tests and triaxial testing and are discussed in Section 5.2.

9.2 Johnstone Predictions

As discussed previously, the direct shear tests conducted on this artificial material were limited to fractal profiles and split surfaces as previous tests had been conducted on regular triangular profiles by Fleuter (1997). A range of fractal profile roughnesses were

tested to verify the model at varying roughness. Similarly, a range of split surface roughnesses were tested under a range of boundary conditions.

Predictions were based on the parameters listed in Table 9.2. Compliance due to compression of the setting plaster, machine compliance and joint closure was included in the calculations. A modification factor of 1.38 to the Sokolovsky failure stress was used to predict the point of shear failure of the asperities (discussed in Chapter 8).

Table 9.2: Johnstone Parameters

Parameter	Adopted value
Young's Modulus	900MPa
Poisson's Ratio	0.25
Intact Friction Angle Batch 1	35°
Intact Friction Angle Batch 2	34°
Residual Friction Angle	24.5°
Cohesion Batch 1	1500kPa
Cohesion Batch 2	1050kPa
Joint Normal Stiffness – water-jet surface	6.0MPa/mm
Joint Normal Stiffness – split surface	5.4MPa/mm
Failure Stress	1.38 * Sokolovsky failure stress

9.2.1 Fractal profiles

The modified Rocket program was used to assess the shear response of five fractal joints. These are compared to the laboratory test results in Appendix E. Diagrams of these profiles together with their roughness statistics are shown in Section 5.3.1.

The results of the comparison between laboratory and Rocket estimates are summarised in Table 9.3. This table indicates the average percentage difference of the shear stress prediction compared to the laboratory shear stress test result at smaller displacements (<5mm) and larger displacements (5-15mm). It also indicates where initial negative dilation was encountered and the amount measured. A calculation of the change in normal stress that this negative dilation would induce (ignoring compliance effects) is also included.

Table 9.3: Summary of Johnstone Fractal Predictions

Sample	Difference between Laboratory Result & Prediction <5mm	Difference between Laboratory Result & Prediction 5mm-15mm	Initial Negative Dilation	Induced Change in Normal Stress
JF8_12	-40%	-50%	0.35mm	140kPa
JF12_3	-35%	-20%	0.3mm	120kPa
JF15a_3	-35%	-30%	0.25mm	100kPa
JF15_3	0%	0%	0.05mm	20kPa
JF21_3	-50%	-20%	0.4mm	240kPa

Four of the five laboratory tests experienced considerable initial negative dilation at the commencement of shear displacement. As discussed in Section 6.2, this initial closure of the joint under the application of a shear force in a constant normal stiffness test, decreases the normal stress leading to a decrease in the shear stress. For these samples, the dilation, shear stress and normal stress has been overpredicted by various amounts of up to 50%. However, the overall shape of the predicted responses are consistent with the laboratory test results.

Example shear stress - shear displacement and dilation - shear displacement plots are shown in Figure 9.1 for the fractal profile JF8_12. The profile and roughness statistics are also shown. This profile was cut at 12mm chord lengths and 2 chord lengths of 12mm and 16mm were used to obtain the shear response at 2 different scales. The smaller chord length prediction captures the effects of finer roughness and hence produces a stiffer initial response than the longer chord length prediction. The envelope of these predictions can be used to predict the shear response over a range of scales. This envelope has been drawn onto the plot. If the dilation - shear displacement plot is extended back towards zero shear displacement, approximately 0.35mm of initial compression was experienced for this test. If this compression is added back to the test results such that the entire curve is shifted upwards, then almost exact matching is obtained for the dilation prediction. Based on a normal stiffness of 400kPa/mm, the addition of 0.35mm dilation increases the normal stiffness by 140kPa. Therefore the lower shear stress and normal stress of the test, can be explained by this initial negative dilation. A higher normal stress would lead to the development of more compliance

effects in the form of joint closure, elastic compression, machine compliance and casting material compression. However for an increase of 140kPa these effects are small.

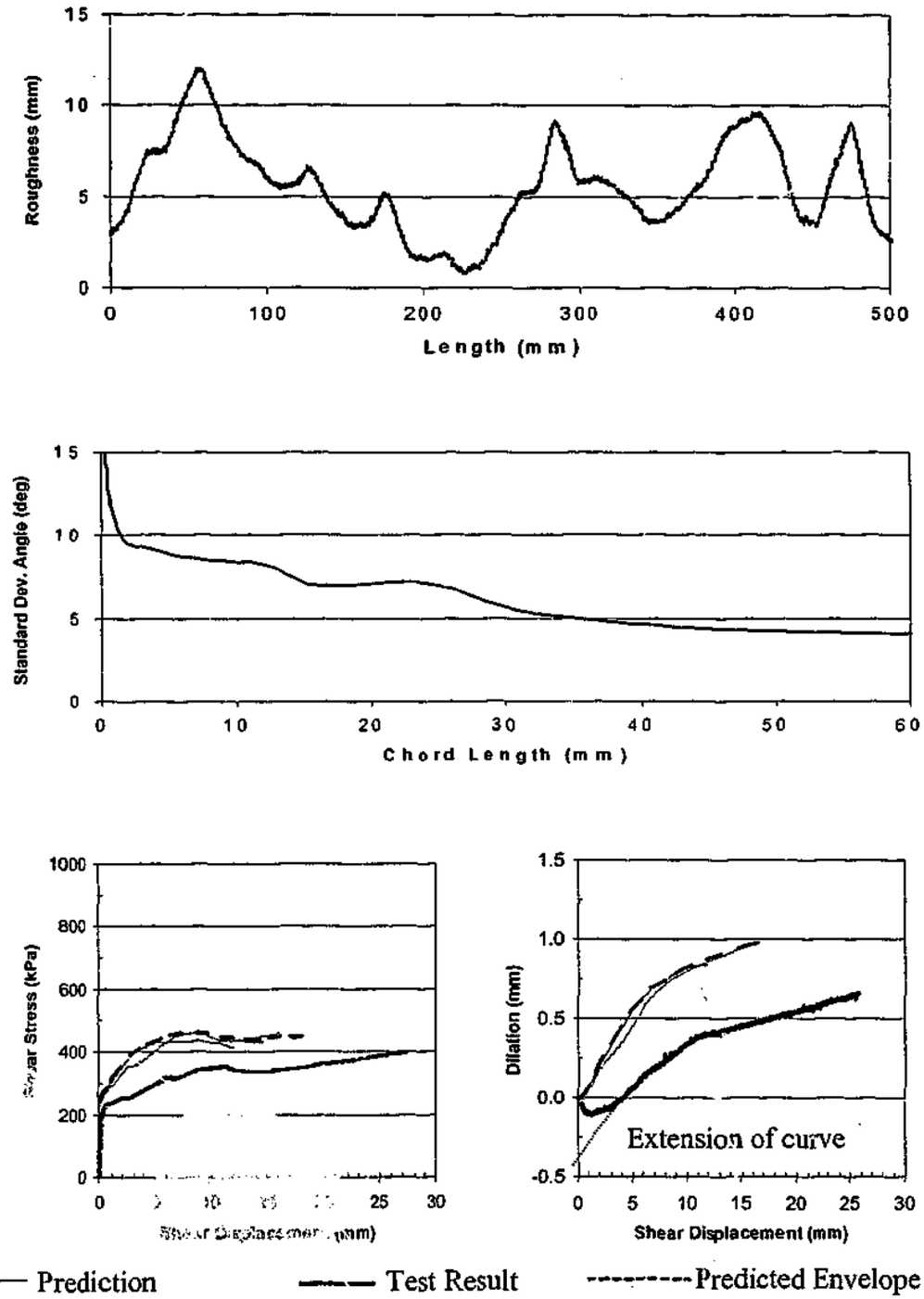

Figure 9.1: Prediction of shear response for profile JF8_12

The adjusted shear stress - shear displacement and dilation - shear displacement plots for sample JF8_12 are shown in Figure 9.2. These graphs indicate that if there had not been initial compression of the sample, the shear stress and normal stress prediction would be very similar to the laboratory results. This would also be the case with the other laboratory test predictions included in Appendix E.

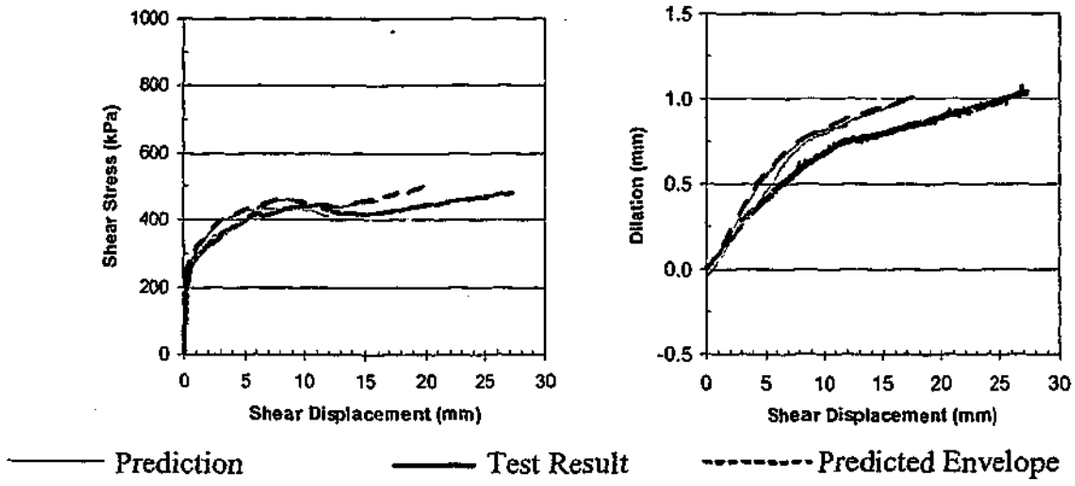

Figure 9.2: Adjusted prediction of shear response for profile JF8_12

The initial compression component is inconsistent between samples and is believed to be not only dependent on sample strength and roughness conditions but also a compliance component of the general set-up of the sample in the laboratory. Due to the variability of the magnitude of this initial compression and that it is due to laboratory conditions and would not be present in insitu conditions, it has not been included in the computer model. However, by estimating the change in overall dilation experienced by the sample due to the initial compression, modified shear stresses and normal stresses can be estimated. This allows comparison of the test results with the predictions to allow verification of the model.

The test sample that experienced almost negligible initial compression at the commencement of shear displacement, JF15_3, produced an excellent prediction of the laboratory test result. Shear stress - shear displacement and dilation - shear displacement plots for this sample are shown in Figure 9.3 together with a diagram of the profile and its roughness statistics. Chord lengths of 3mm, 8mm and 24mm were used to obtain the shear response at 3 different scales. The envelope of these curves has been included.

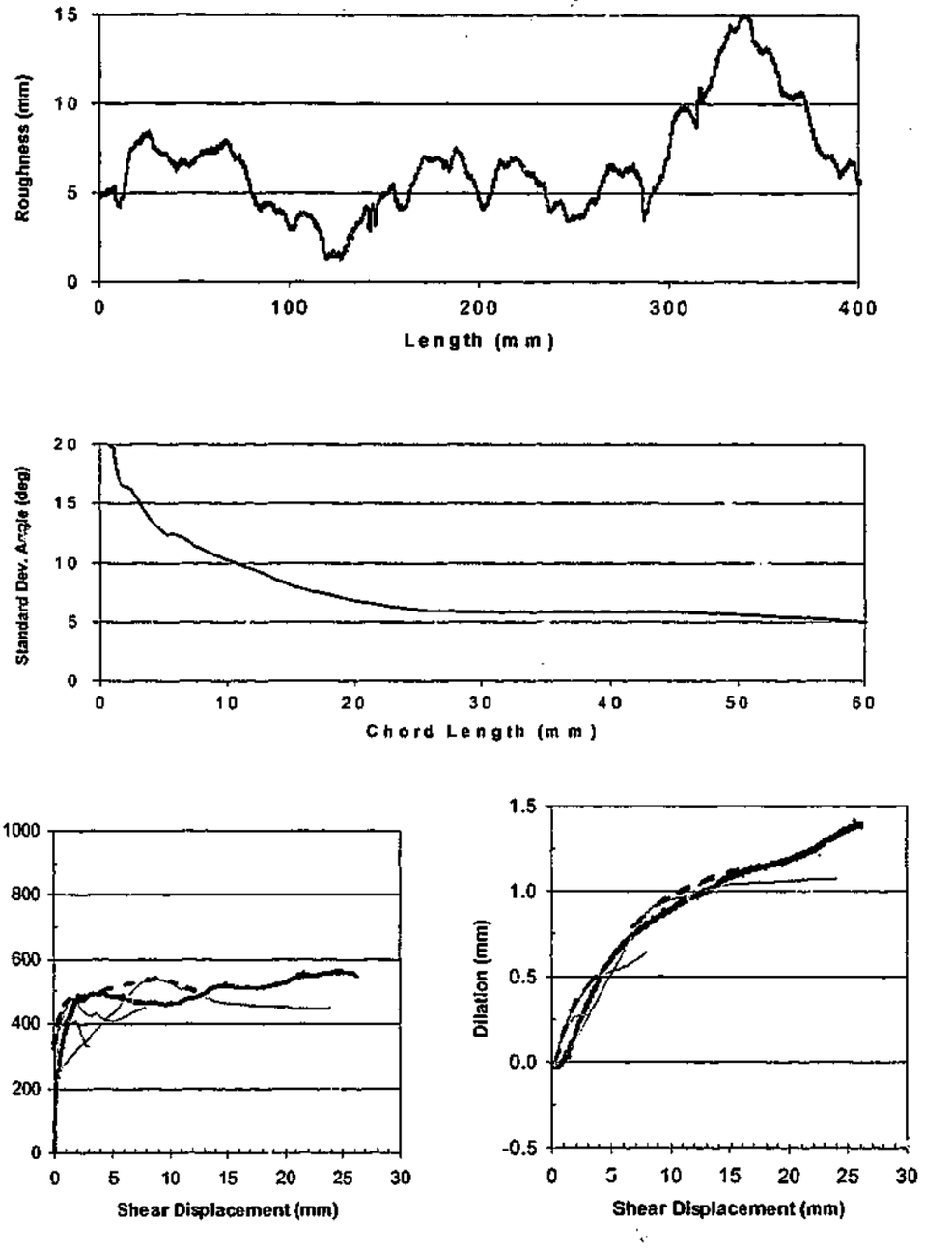

Figure 9.3: Prediction of Shear response for profile JF15_3

Based on these test results and taking into account the presence of initial compression on some samples, it is considered that the shear model adequately predicts the shear response of the Johnstone fractal tests at different scales.

9.2.2 Split profiles

Nine Johnstone split samples were tested. Movement in the sample plaster was noted during the testing of sample JS_2b. This result has therefore been ignored. Shear response predictions have been conducted for each of the other tests and are included in Appendix E. Diagrams of these surfaces together with their profiles and roughness statistics are shown in Appendix C.

The results of the predictions have been summarised in Table 9.4.

Table 9.4: Summary of Johnstone Split Predictions

Sample	Difference between Laboratory Result & Prediction <5mm	Difference between Laboratory Result & Prediction 5mm-15mm	Initial Negative Dilation	Induced Change in Normal Stress
JS_1a	0%	0%	0mm	-
JS_1b	+15%	+20%	0.2mm	80kPa
JS_2a	0%	0%	0.2mm	80kPa
JS_3a	0%	-5%	0.15mm	60kPa
JS_3b	+10%	-15%	0.20mm	120kPa
JS_4a	0%	-5%	0.1mm	40kPa
JS_6a	-15%	-50%	0.3mm	120kPa
JS_7a	-5%	-5%	0mm	-

This table indicates that for most of the samples the initial negative dilation is quite small. Once the compliance effects are included due to the increase in normal stress, the overall increase would be minimal and would not have a significant effect on the test results. Sample JS_6a is the exception. This sample experienced the most initial negative dilation of approximately 0.3mm. In this case the effect on the shear results is noticeable. By removing this initial compression a closer prediction is achieved. This is demonstrated in Figure 9.4. Although the prediction of the peak shear stress is quite accurate, dilation at the longer chord lengths is still overpredicted. This may suggest that longer profiles are required to obtain quality statistics at the longer chord lengths.

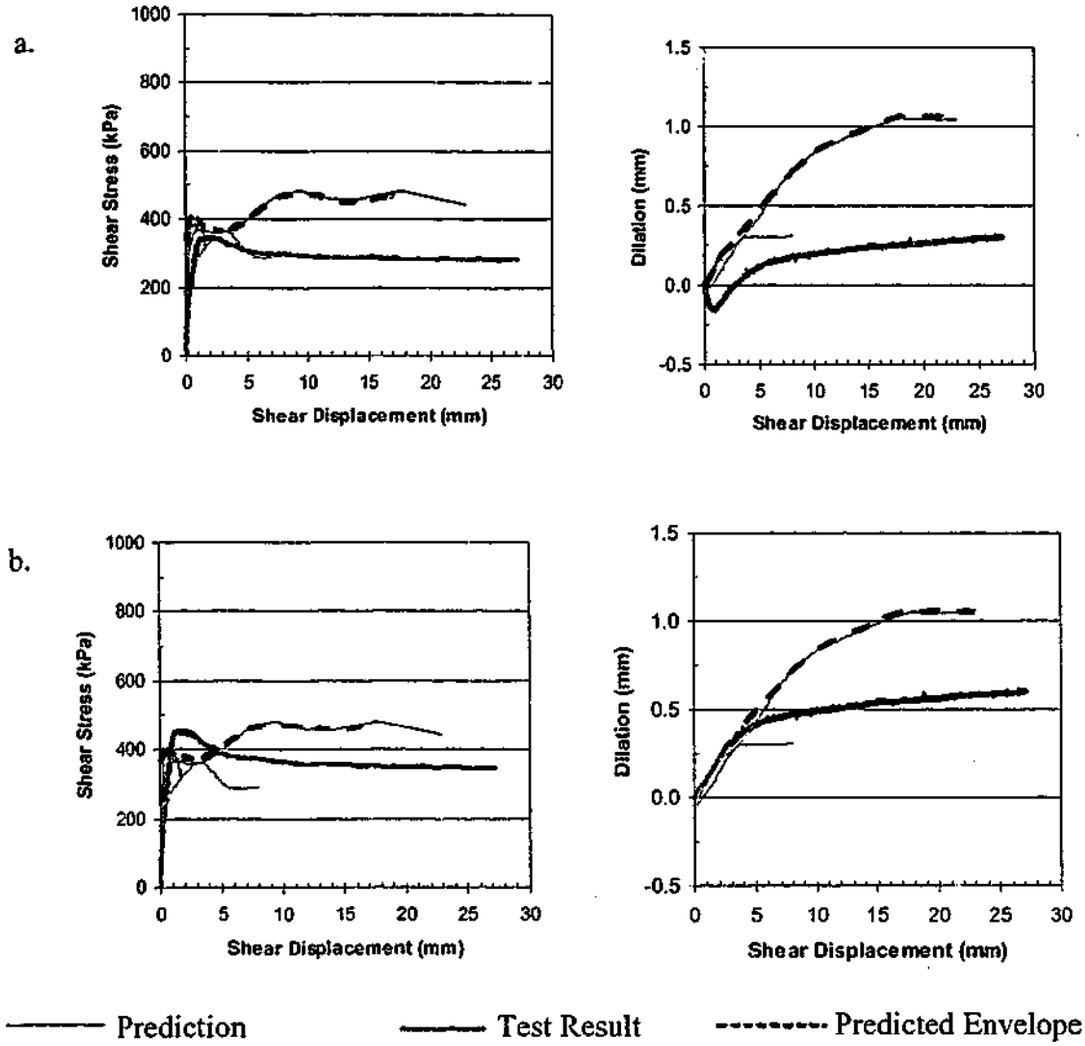

Figure 9.4: a. Prediction of split surface JS_6a

b. Adjusted prediction of split surface JS_6a

Sample JS_7a did not experience initial negative dilation. The shear test result is shown in Figure 9.5 together with a diagram of the surface and a statistical analysis of its roughness. This test was conducted at an initial normal stress of 400kPa and constant normal stiffness of 400kPa/mm. The average standard deviation of chord angle for various chord lengths from several profiles was used to represent the surface. Three chord lengths of 1.5mm, 9mm and 23mm were used to capture the shear response at different scales.

These results indicate that if the initial negative dilation is small or can be removed an excellent match of the prediction to the laboratory test results is achieved.

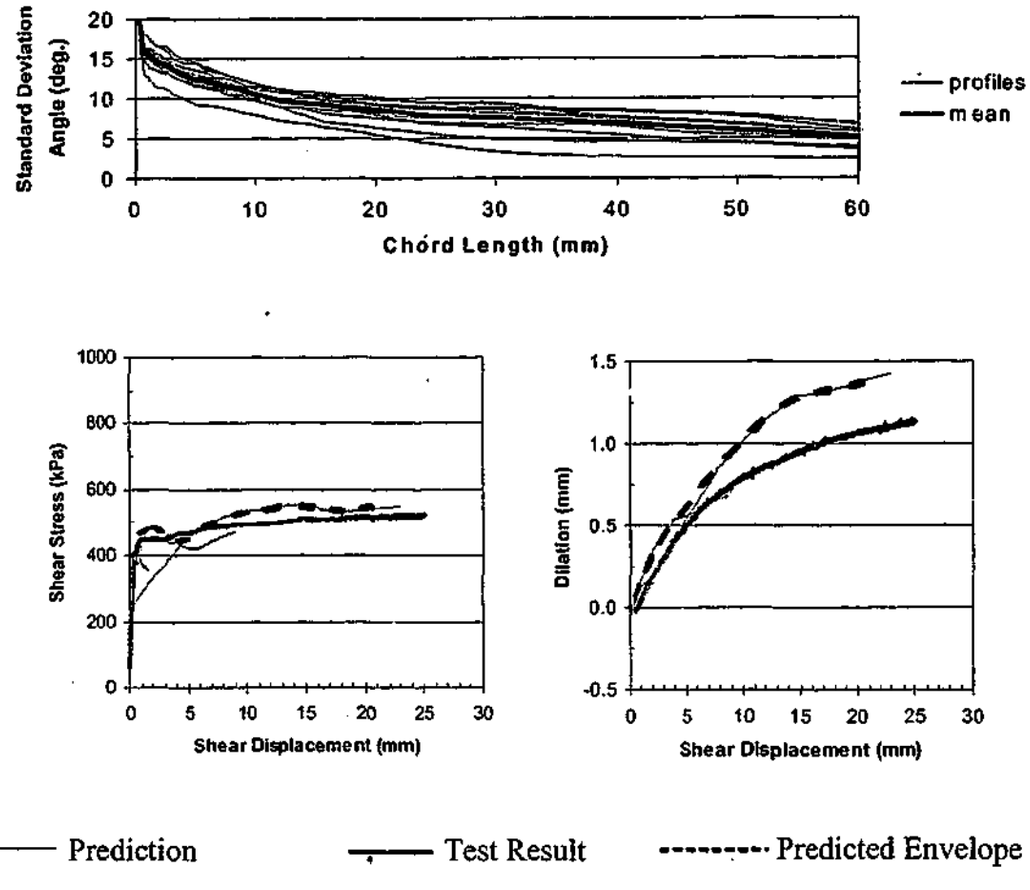

Figure 9.5: Prediction of Shear response for profile JS_7a

Sample JS_1b produced the worst prediction of shear response. As can be seen by its graphical representation and statistical analysis shown in Figure 9.6, this surface had long roughness wavelengths towards the centre of the sample. These longer wavelengths have dominated the shear response and have not been captured by the prediction (see Appendix F9).

Using the average statistical profile to represent the surface may not include roughness wavelengths that dominate the shear response. Therefore, in general, the samples that are consistent across their surface produce more accurate estimates of the shear response.

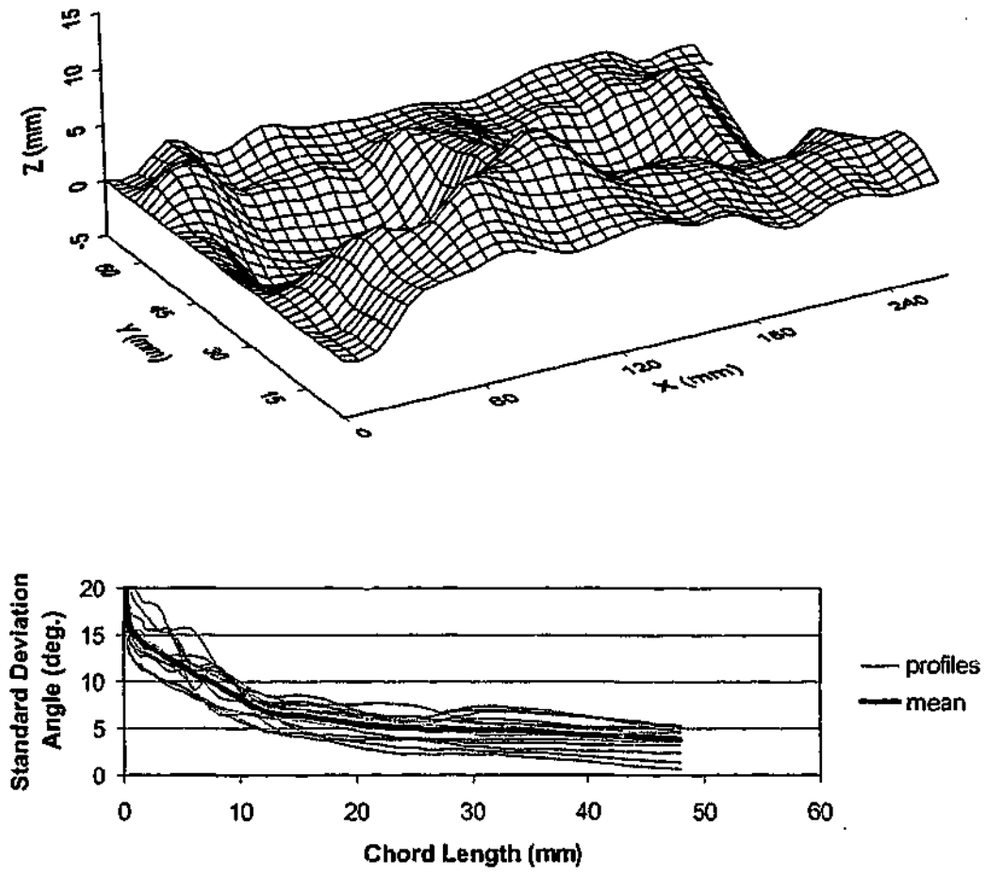

Figure 9.6: Surface JS_1b and its statistical analysis

9.3 Sandstone Predictions

As discussed previously, the direct shear tests conducted on this material were limited to split surfaces as previous tests conducted by Fleuter (1997) included regular triangular and fractal profiles.

Predictions were obtained using the parameters listed in Table 9.5. Compliance due to compression of the setting plaster, machine compliance and joint closure was included in the calculations. A modification factor of 1.26 to the Sokolovsky failure stress was used to predict the point of shear failure of the asperities (discussed in Chapter 8).

Table 9.5: Sandstone Parameters

Parameter	Adopted value
Young's Modulus	3200MPa
Poisson's Ratio	0.1
Intact Friction Angle	50°
Residual Friction Angle	32°
Cohesion	2200kPa
Joint Normal Stiffness – split surface	2.1MPa/mm
Failure Stress	1.26 * Sokolovsky failure stress

9.3.1 Split profiles

Two sandstone split samples were tested and shear response predictions on each conducted. These predictions are shown in Appendix E.

An analysis of the split surface shear results with the wear models developed by Seidel (1993), Fleuter (1997) and Gu (2001) consistently underpredict the peak shear stress and dilation. The models developed by Seidel (1993) and Gu (2001) were developed for concrete / soft rock interfaces where it could be inferred that wear of the softer material by the much harder material would occur. The profiles tested for this work are three-dimensional surfaces and more closely replicate a natural joint surface than profiles tested by Fleuter (1997). These current tests indicate that wear is not a significant component of the shear behaviour. An example of the shear stress produced on sample SS_2 if the normalized degradation rate with respect to asperity angle as recommended by Fleuter (1997) is incorporated into the model, is shown in Figure 9.7. Two chord lengths of 6.5mm and 21mm were used to produce the estimate. As can be seen the predicted shear stress is considerably lower than the test results. For this reason wear has not been incorporated into the predictions conducted for this work.

The shear behaviour prediction of split surface SS_1 is shown in Figure 9.8 together with a diagram of the surface and a statistical analysis of its roughness. This sample experienced quite significant initial negative dilation (approximately 0.5mm) leading to a considerable decrease in the normal stress. Ignoring compliance effects the normal stress would increase by 200kPa based on a constant normal stiffness of 400kPa/mm if this

initial negative dilation had not occurred. This would correspondingly increase the shear stress. By removing the initial negative dilation an excellent prediction of the split surface shear response is produced as shown in Figure 9.8.

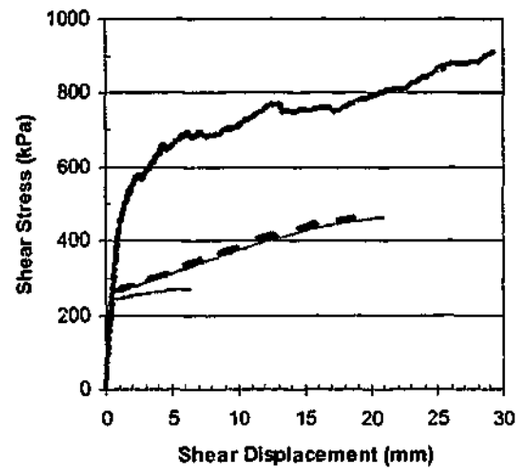

Figure 9.7: Prediction of Shear response for profile SS_2 incorporating wear

Split surface SS_2 experienced much less initial negative dilation (approximately 0.2mm). The shear behaviour prediction of this sample is shown in Figure 9.9 together with a diagram of the surface and a statistical analysis of its roughness. This test was conducted at an initial normal stress of 400kPa and constant normal stiffness of 800kPa/mm. The average standard deviation of chord angle for various chord lengths from several profiles was used to represent the surface. Three chord lengths of 1.5mm, 6.5mm and 21mm were used to capture the shear response at different scales. These plots indicate an excellent prediction of the dilation has been made. The initial shear stress prediction below approximately 3mm chord lengths is also very good. Above this chord length the prediction is approximately 20% larger than the laboratory test results. As it is a natural material with natural variability, this may be explained by a variation in the material properties.

Based on these two results it is considered that the model, not incorporating a wear component, captures the shear behaviour of the sandstone joint.

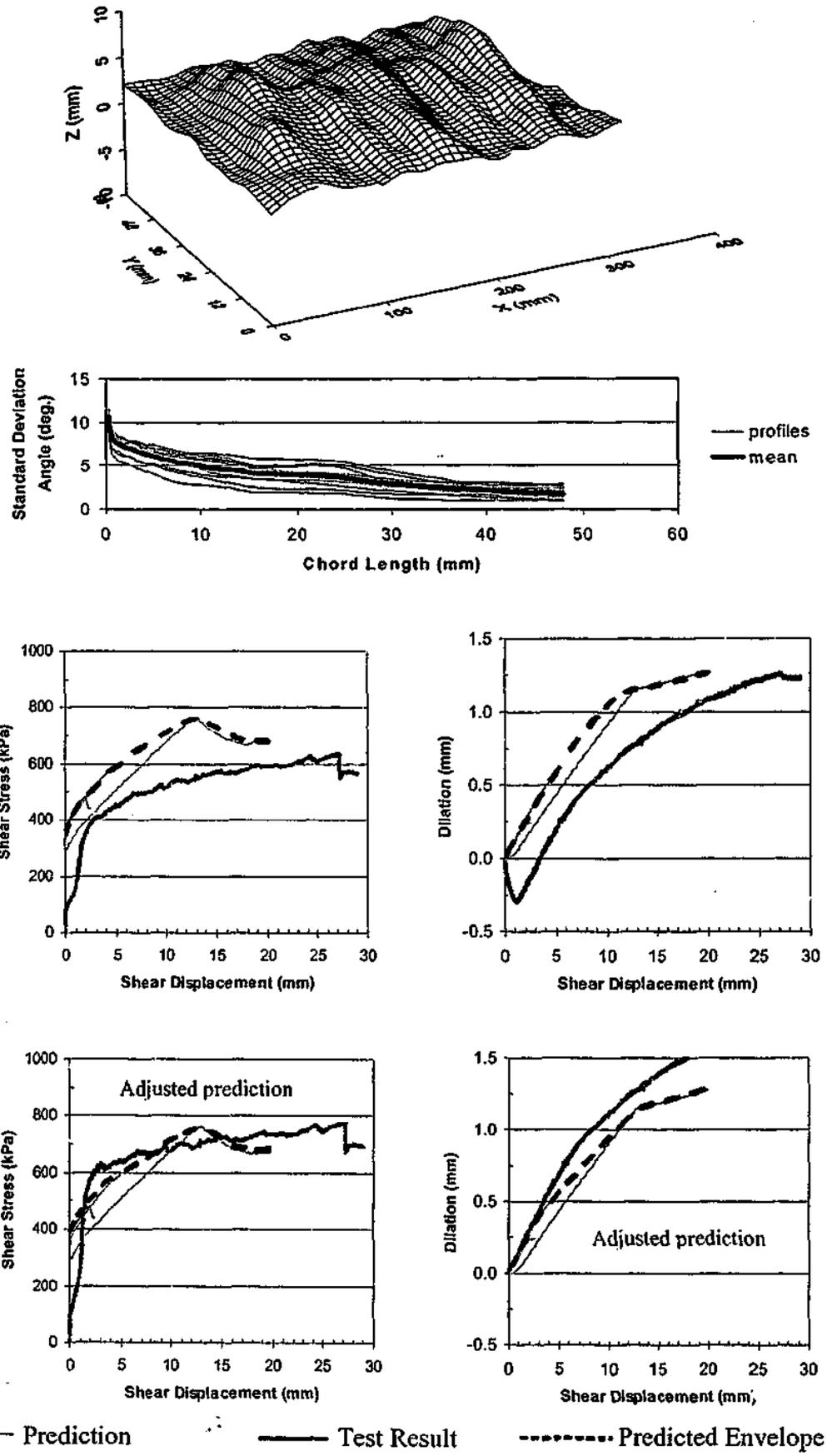

Figure 9.8: Prediction of Shear response for profile SS_1

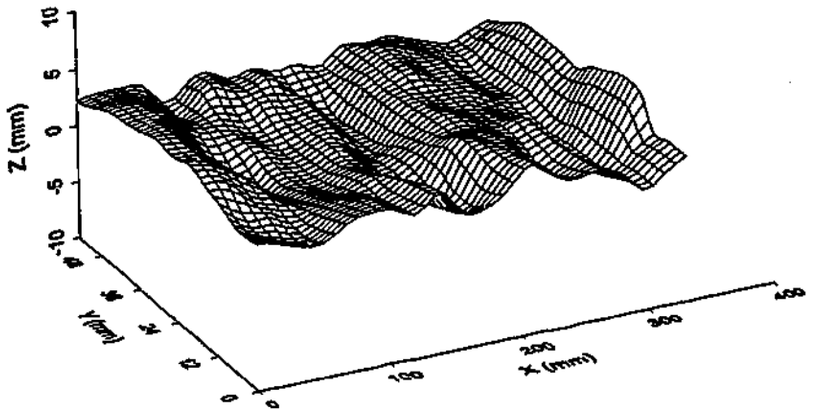

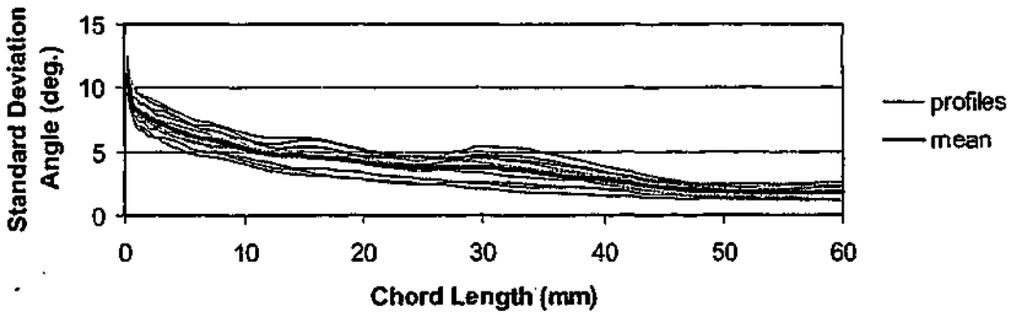

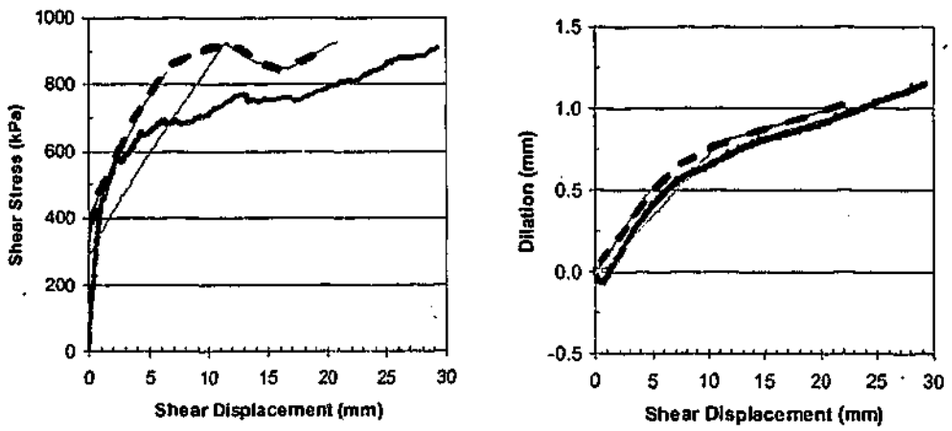

Prediction — Test Result ---- Predicted Envelope

Figure 9.9: Prediction of Shear response for profile SS_2

9.4 Siltstone Predictions

Direct shear tests were conducted on regular triangular profiles, fractal profiles and split surfaces.

Predictions were based on the parameters listed in Table 9.6. Compliance due to compression of the concrete, machine compliance and joint closure was included in the calculations. A shear failure stress equal to the unconfined compressive strength in the bedding direction was used for tests where shearing occurred along the bedding (regular triangular and split surfaces) and a failure stress equal to the unconfined compressive strength through the matrix where shearing occurred through the rock matrix (fractal surfaces) (discussed in Chapter 8).

Table 9.6: Siltstone Parameters

Parameter	Adopted value
Young's Modulus	25.4GPa
Poisson's Ratio	0.15
Intact Friction Angle	40°
Residual Friction Angle	28.5°
Cohesion	12MPa
Joint Normal Stiffness – water-jet surface	6.2MPa/mm
Joint Normal Stiffness – split surface	3.9MPa/mm
Failure Stress – shear along bedding	30MPa
Failure Stress - shear through matrix	55MPa

9.4.1 Regular triangular profiles

Direct shear tests were conducted on regular triangular asperities of 5°, 10° and 15° inclination at chord lengths of predominantly 16mm with one test on a 10° asperity profile with 48mm chords. Movement of the sample within the shear box was suspected during the testing of sample MR15_16 due to the unrealistically small dilations produced. This result has therefore been ignored. Shear response predictions have been

conducted for each of the other tests and are included in Appendix E. Diagrams of these surfaces together with their profiles and roughness statistics are shown in Appendix C.

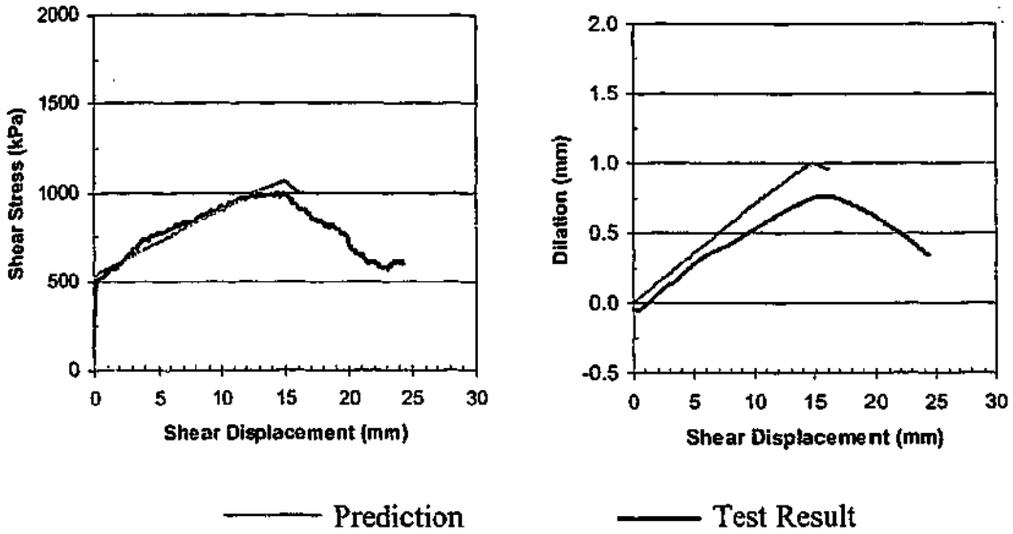

Figure 9.10: Prediction of Shear response for profile MR5_16

An example regular triangular asperity prediction of sample MR5_16 is shown in Figure 9.10. This test was conducted at an initial normal stress of 800kPa and constant normal stiffness of 800kPa/mm. A 5° regular triangular profile of 32 asperities was used to model the surface.

The results of the predictions have been summarised in Table 9.7. This table indicates the average percentage difference of the shear stress prediction compared to the laboratory shear stress test result. It also indicates where initial negative dilation was encountered and the amount measured. An estimate of the change in normal stress that this negative dilation could induce (ignoring compliance effects) is also included.

Table 9.7: Summary of Siltstone Regular Triangular Asperity Predictions

Sample	Difference between Laboratory Result & Prediction	Initial Negative Dilation	Induced Change in Normal Stress
MR5_16	0%	0.1mm	80kPa
MR5a_16	-5%	0.25mm	200kPa
MR10a_16	-30%	0.25mm	400kPa
MR10a_48	+5%	0.25mm	130kPa

Overall the predictions compare well with the laboratory test results for shear stress and dilation. However, shear failure was typically predicted at an earlier shear displacement than measured in the laboratory tests. This may be partly explained by the fact that most sample responses were overpredicted due predominantly to the initial negative dilation experienced by the samples. However, this is not the case for the 48mm chord length 10^0 sample where a lower peak shear stress was predicted at a smaller shear displacement. This may indicate weaker areas in the natural rock.

9.4.2 Fractal profiles

Four tests were performed on samples containing 5mm chord length fractal profiles that had been water-jet cut into blocks of siltstone. Shear response predictions were conducted on each. The predictions are shown in detail in Appendix E. Diagrams of the profiles together with their roughness statistics are shown in Section 5.3.3.

An example fractal surface prediction of sample MF15_5 is shown in Figure 9.11 together with a diagram of the surface and a statistical analysis of its roughness. The test was conducted at an initial normal stress of 600kPa and constant normal stiffness of 600kPa/mm. The average standard deviation of chord angle for various chord lengths from several profiles was used to represent the surface. Three chord lengths of 5.3mm, 10mm and 25mm were used to capture the shear response at different scales.

The results of the predictions have been summarised in Table 9.8.

Table 9.8: Summary of Siltstone Fractal Predictions

Sample	Difference between Laboratory Result & Prediction <5mm	Difference between Laboratory Result & Prediction 5mm-15mm	Initial Negative Dilation	Induced Change in Normal Stress
MF5_5	-15%	-10%	0.1mm	80kPa
MF10_5	+20%	+5%	0.2mm	120kPa
MF10a_5	0%	+25%	0.1mm	60kPa
MF15_5	+10%	+10%	0mm	-

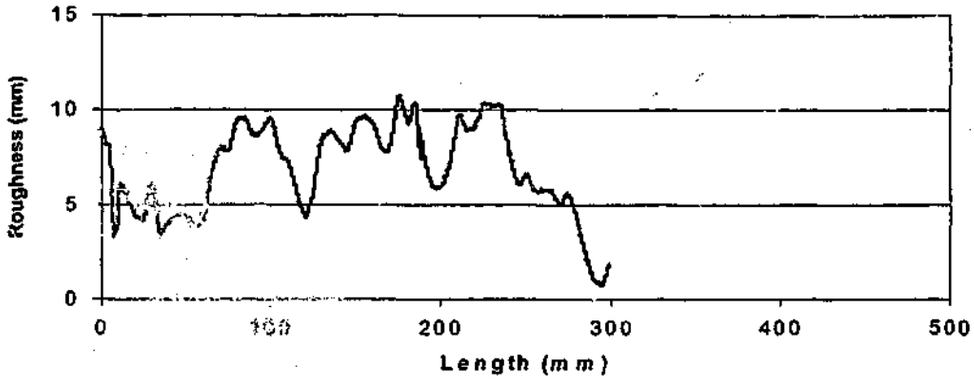

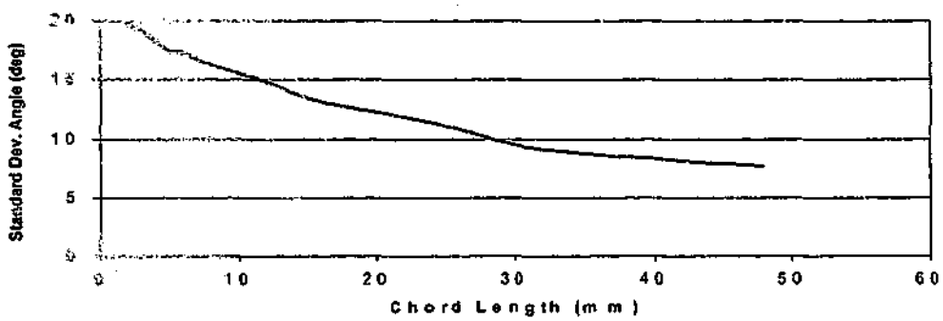

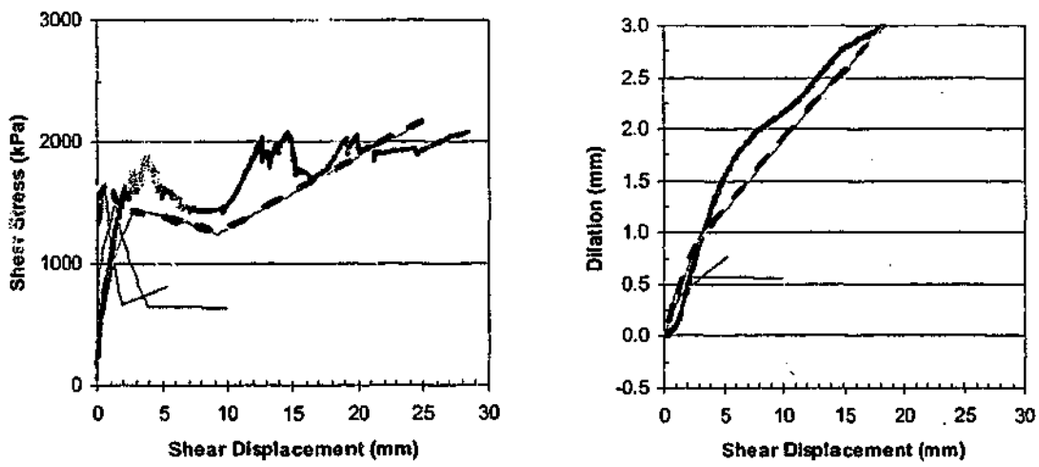

Figure 9.11: Prediction of Shear response for profile MF15_5

These fractal profiles were water-jet cut at approximately 5mm chord lengths. Their peak shear strength occurred at approximately 5mm chord length. The lowest chord length used for the predictions was also 5mm. However the predictions have produced a significantly stiffer response for this small chord length than the laboratory test results. This indicates that the shear failure of the prediction, although occurring at a comparable stress level to the test results, is occurring prematurely. This was also encountered with the triangular asperity profiles.

The prediction for Sample MF10a_5 compares well with the laboratory initial peak shear stress but has not captured the effects of the underlying longer roughness wavelengths. Alternatively the prediction for sample MF10_5 has captured the shear behaviour of the longer chord lengths but has underestimated the shear response at the shorter chord lengths. This profile, as seen in Figure 5.16, has considerable concavity that has immediately dominated the shear response at the commencement of shearing. This has not been modelled.

Overall the shear model captures the general behaviour of the fractal profiles and acceptable shear stress predictions are achieved (<20% difference). However, peak shear stress is consistently predicted at a lower shear displacement.

9.4.3 Split profiles

Predictions have been carried out for the direct shear tests of seven split surfaces. Many of the split samples (MS_3 to MS_7) were shorter in length (typically 180mm long) due to difficulties in obtaining longer profiles. This has constrained the statistical analysis to chord lengths below 32mm in length. This has meant that some of the longer roughness wavelengths may not be captured in the analysis and hence in the prediction.

The results of the predictions using the failure stress equal to the bedding unconfined compressive strength have been summarised in Table 9.9.

Figure 9.12 shows the standard deviation of chord angle at various chord lengths for the seven siltstone split surfaces. This graph indicates that the roughness of the samples are similar for all samples except sample MS_3 which is considerably rougher and sample MS_5 which is considerably smoother. However, sample MS_3 experienced less dilation and produced lower shear stress values than the other samples even though it was

statistically rougher. This suggests that the shear test result for sample MS_3 may be unreliable.

Table 9.9: Summary of Siltstone Split Predictions

Sample	Difference between Peak Shear Stress Laboratory Result & Prediction using failure stress = $UCS_{bedding}$	Difference between Residual Shear Stress Laboratory Result & Prediction using failure stress = $UCS_{bedding}$	Initial Negative Dilation	Induced Change in Normal Stress
MS_1	+5%	+10%	0.1mm	40kPa
MS_2	+20%	+15%	0.1mm	40kPa
MS_3	-45%	-25%	0.1mm	80kPa
MS_4	+30%	+30%	0.1mm	40kPa
MS_5	-20%	0%	0.25mm	150kPa
MS_6	+30%	0%	0.1mm	60kPa
MS_7	+20%	+10%	0.1mm	60kPa

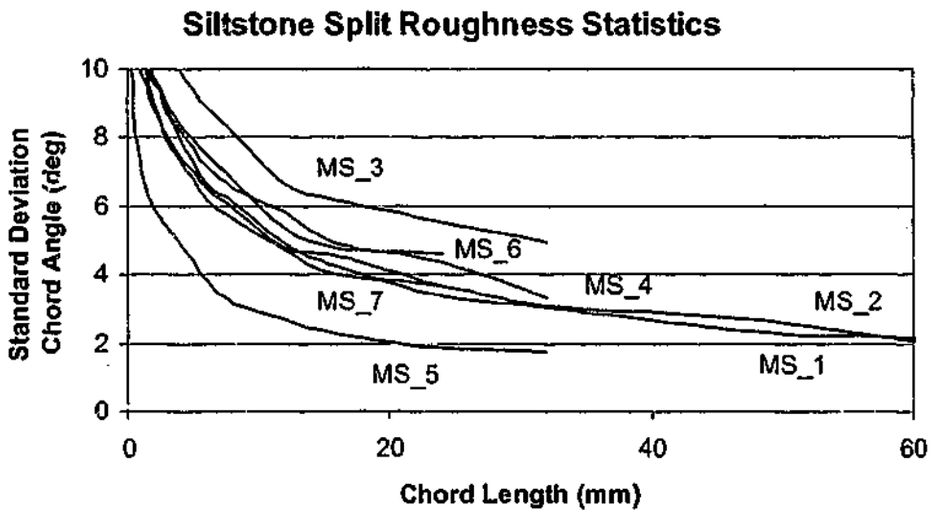

Figure 9.12: Comparison of siltstone split surface roughness

Taking into account the initial closure present in sample MS_5, the variation between peak shear stress prediction and test result is minimal (refer to Figure 9.13).

a.

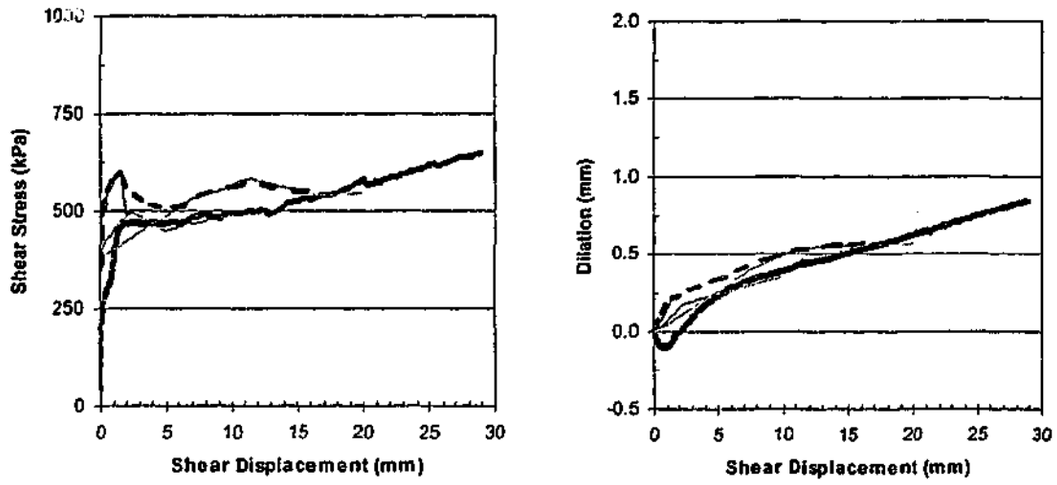

b.

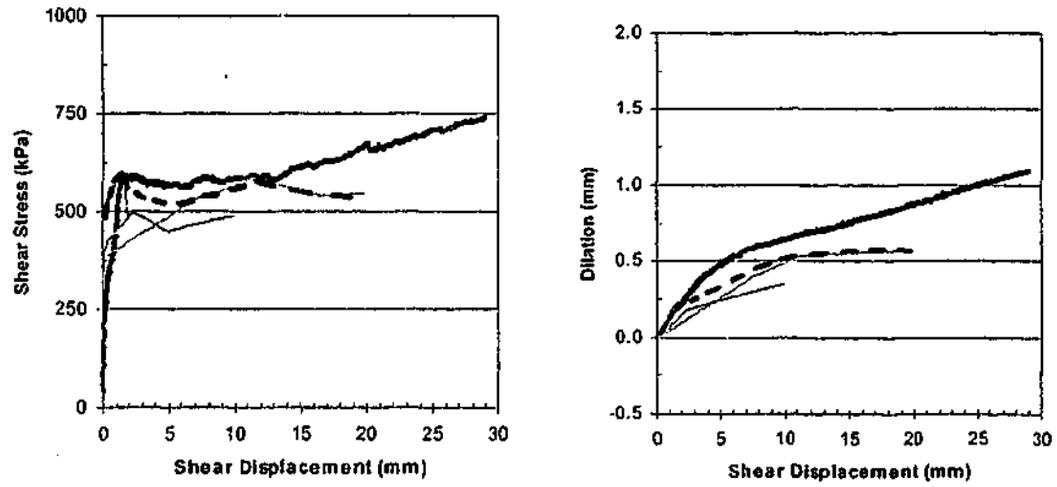

Prediction Test Result Predicted Envelope

Figure 9.13: a. Prediction of Shear response for surface MS_5

b. Adjusted shear test result for sample MS_5

The predictions for the other samples underpredict the initial peak shear stress. In fact the difference between the predicted shear stress values and that obtained by the direct shear tests, are notably larger for the siltstone split tests than for the previous tested

profiles. One possible explanation is the potential variability of the bedding unconfined compressive strength.

The majority of tests displayed a high initial peak shear stress followed by a rapid decline in the shear stress. The exception to this were tests MS_3 and MS_5. This may indicate that some interlocking is occurring. This interlocking may cause failure to occur initially through the rock matrix (ie. on an angle to the shear direction) followed by failure along the bedding. If this is the case, the failure stress adopted (the unconfined compressive strength of the siltstone in the bedding direction) may be an underestimate of the true failure stress of the material at the commencement of shearing. A reanalysis of surfaces MS_1, MS_2, MS_4, MS_6 and MS_7 using the failure stress equal to the matrix unconfined compressive strength at chord lengths less than 2mm produced a closer prediction at the smaller shear displacements. The results are summarized in Table 9.10.

Table 9.10: Summary of Siltstone Split Predictions

Sample	**Difference between Peak Shear Stress Laboratory Result & Prediction using failure stress = UCS_{matrix}**
MS_1	-5%
MS_2	+13%
MS_4	+25%
MS_6	+20%
MS_7	+10%

These predictions are shown in detail in Appendix E using the failure stress = UCS_{matrix} for chord lengths less than 2mm and failure stress = $UCS_{bedding}$ at chord lengths greater than 2mm. Diagrams of these surfaces together with their profiles and roughness statistics are shown in Appendix C.

An example split surface prediction of sample MS_1 is shown in Figure 9.14 together with a diagram of the surface and a statistical analysis of its roughness. This test was conducted at an initial normal stress of 600kPa and constant normal stiffness of 400kPa/mm. The average standard deviation of chord angle for various chord lengths from several profiles was used to represent the surface. Three chord lengths of 2mm, 8mm and 20mm were used to capture the shear response at different scales.

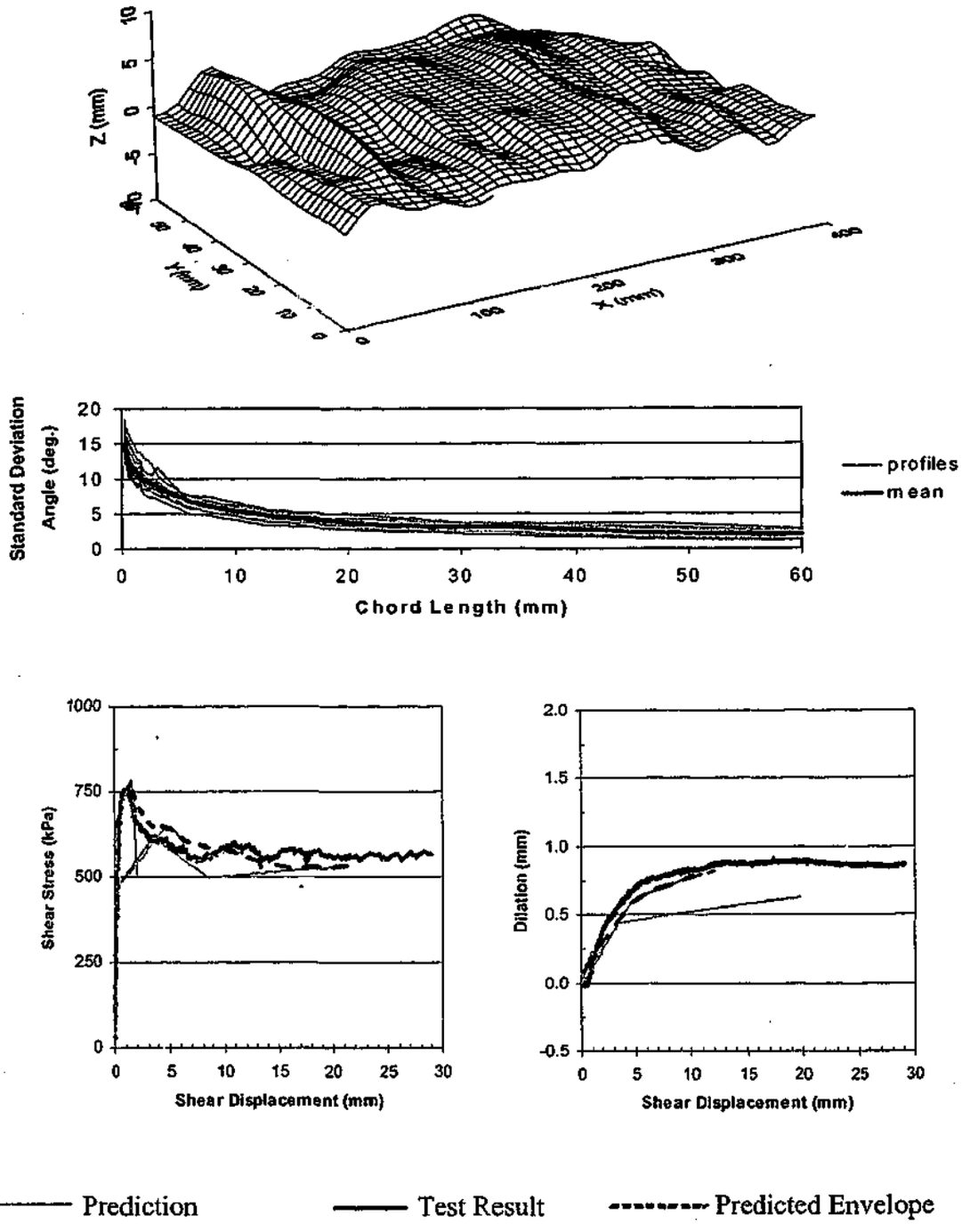

Figure 9.14: Prediction of Shear response for surface MS_1

Taking into consideration the adjustment due to the initial compression of sample MS_5 and using both the unconfined compressive strength of the bedding and the matrix to

estimate the shear failure stress, reasonable predictions of the shear behaviour are achieved. The predictions are typically within 20% variation of the laboratory results.

9.5 Basalt Predictions

Direct shear tests were conducted on regular triangular profiles, fractal profiles and split surfaces.

Predictions were based on the parameters listed in Table 9.11. Compliance due to compression of the concrete, machine compliance and joint closure was included in the calculations. A shear failure stress equal to the unconfined compressive strength of the material was used (discussed in Chapter 8).

Table 9.11: Basalt Parameters

Parameter	Adopted value
Young's Modulus	62GPa
Poisson's Ratio	0.15
Intact Friction Angle	48°
Residual Friction Angle	34°
Cohesion	20MPa
Joint Normal Stiffness – water-jet surface	7.6MPa/mm
Joint Normal Stiffness – split surface	7.5MPa/mm
Failure Stress	120MPa

9.5.1 Regular triangular profiles

Predictions were conducted on regular triangular asperity samples with 5°, 10° and 15° inclination and chord lengths of 16mm. These are shown in detail in Appendix E.

The results of the predictions have been summarised in Table 9.12.

The 5° asperity profile BR5_16 prediction produced a good match with the laboratory result. This prediction is shown in Figure 9.15. This test was conducted at an initial normal stress of 1600kPa and constant normal stiffness of 1600kPa/mm. A 5° regular triangular profile of 32 asperities was used to model the surface.

Table 9.12: Summary of Basalt Regular Triangular Asperity Predictions

Sample	Difference between Laboratory Result & Prediction	Initial Negative Dilation	Induced Change in Normal Stress
BR5_16	+7%	0	-
BR10_16	-40%	0.2	320kPa
BR15_16	-35%	0.2	320kPa

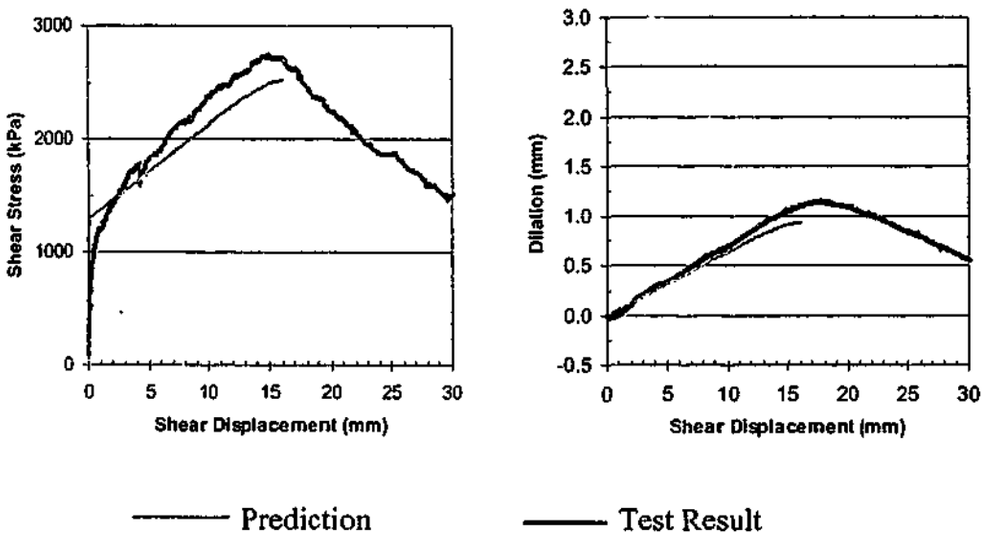

Figure 9.15: Prediction of Shear response for profile BR5_16

However, the steeper asperity profile predictions were not as accurate. The shear test result for sample BR10_5 is shown in Figure 9.16a. The accuracy of the prediction is improved if the initial negative dilation is removed from the shear test results. Figure 9.16b shows the adjusted shear test results for sample BR10_5. This graph shows a reasonable prediction of dilation and shear stress up to approximately 5mm of shear displacement. Beyond this however, a higher shear stress and dilation is predicted than observed in the laboratory results.

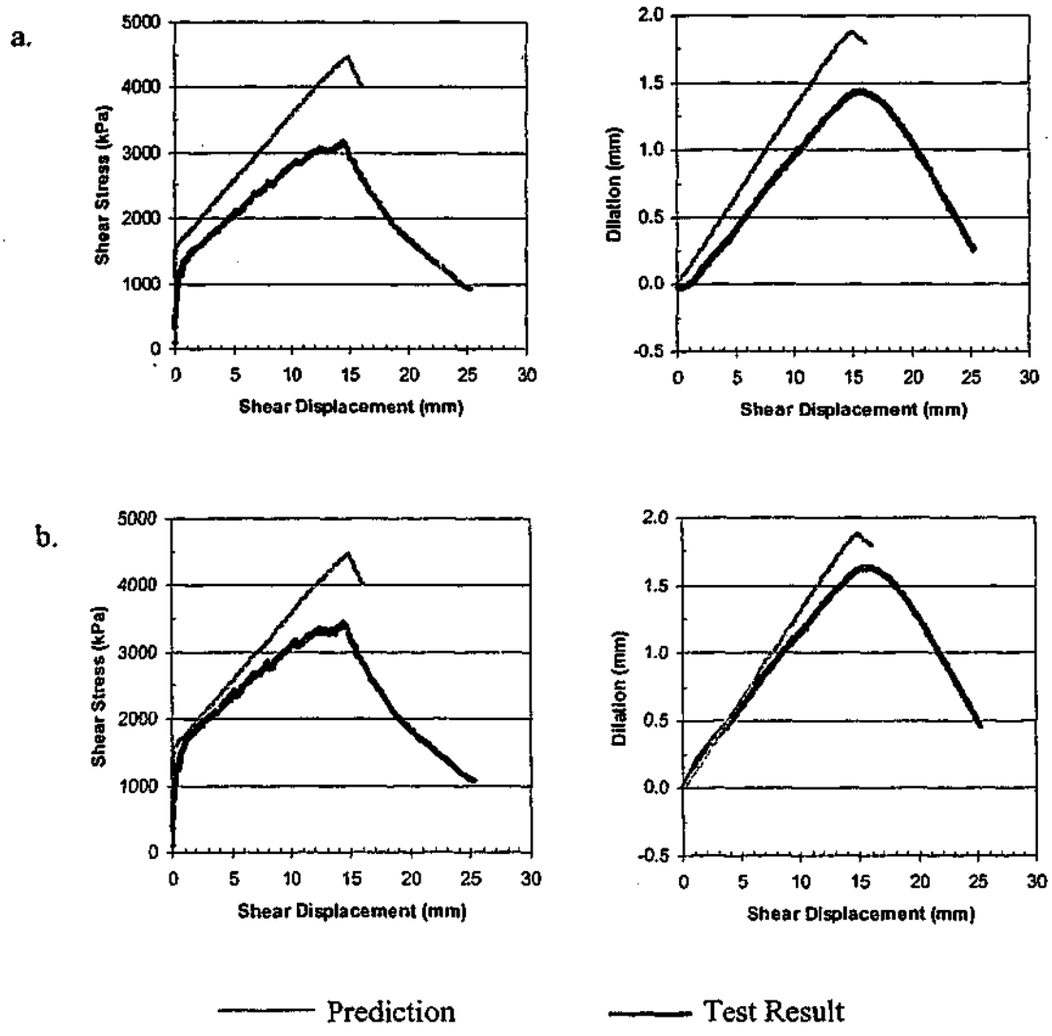

Figure 9.16: a. Prediction of Shear response for profile BR10_5

b. Adjusted shear test result for sample BR10_5

The laboratory shear stress – shear displacement plots indicate partial failures of the basalt samples from approximately 8mm displacement. This is shown in Figure 9.17a for sample BR15_5. Figure 9.17b shows the same plot with the shear stress adjusted to remove the initial negative dilation and an estimate of the shear stress without failures together with a prediction of shear response. As retesting of sample BR10_16 indicated approximately 0.1mm less dilation at peak shear stress, only minor shear failure of the asperity tips was occurring on the basalt samples (refer to section 6.2.2). This suggests that the fretting experienced at the sides of the samples and at the ends of the sample (as shown diagrammatically in Section 6.2) may be causing the slight drops in shear stress

shown in Figure 9.17a. These partial failures would act to decrease the contact area causing a slight increase in local normal stress on the remaining contact area. Higher local normal stresses would cause an increase in local compliance effects and premature failure. This fretting of the edges of the sample is a laboratory boundary condition that would not be present insitu. It can be minimised by using large samples.

a.

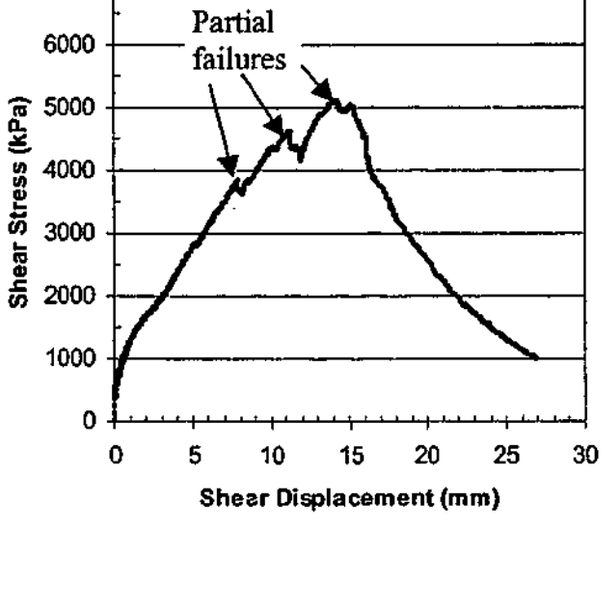

b.

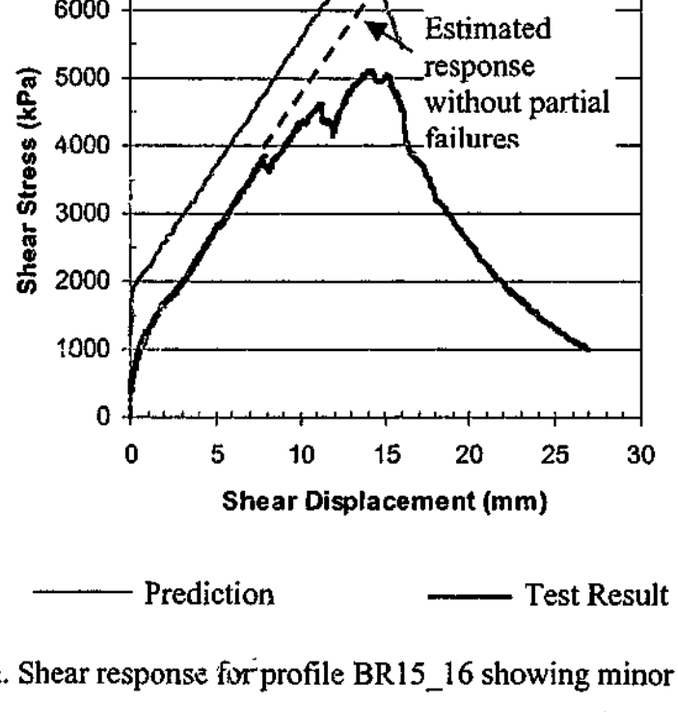

Figure 9.17: a. Shear response for profile BR15_16 showing minor failure areas

b. Prediction and adjusted shear response for profile BR15_16

Overall the shear model appears to capture the general behaviour of the triangular profiles. Once the initial negative dilation and edge effects are removed, acceptable stress and dilation predictions have been achieved.

9.5.2 Fractal profiles

The shear response of two fractal profiles have been conducted. These are shown in detail in Appendix E. Diagrams of these profiles together with their roughness statistics, are shown in Section 5.3.3.

The results of the predictions have been summarised in Table 9.13.

Table 9.13: Summary of Basalt Fractal Predictions

Sample	Difference between Laboratory Result & Prediction <5mm	Difference between Laboratory Result & Prediction 5mm-15mm	Initial Negative Dilation	Induced Change in Normal Stress
BF10_5	-85%	-60%	0.25	150kPa
BF15_5	-40%	-10%	0.15	90kPa

Both samples experienced initial negative dilation. This would have decreased the amount of dilation, reducing the amount of normal stress applied and hence shear stress developed.

An example fractal surface prediction of sample BF15_5 is shown in Figure 9.18 together with a diagram of the surface and a statistical analysis of its roughness. The profile was water-jet cut into a basalt sample at 5mm chord lengths. The test was conducted at an initial normal stress of 600kPa and constant normal stiffness of 600kPa/mm. The average standard deviation of chord angle for various chord lengths from several profiles was used to represent the surface. Three chord lengths of 6mm, 12mm and 28mm were used to capture the shear response at different scales.

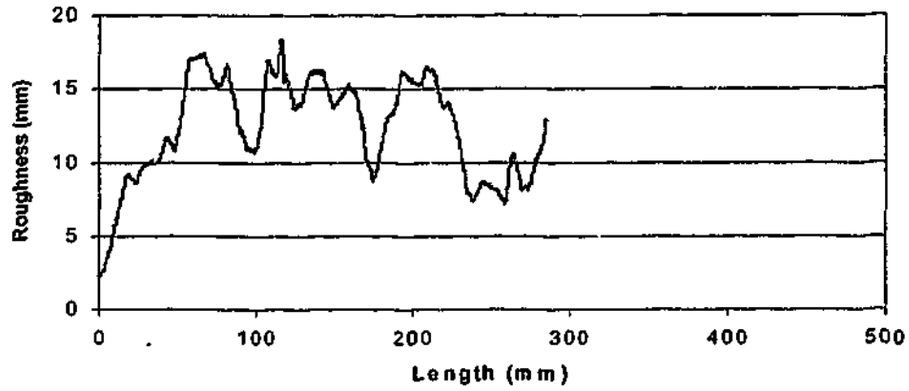

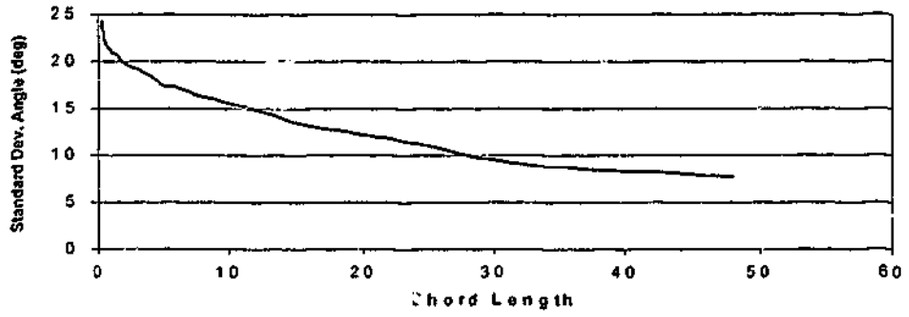

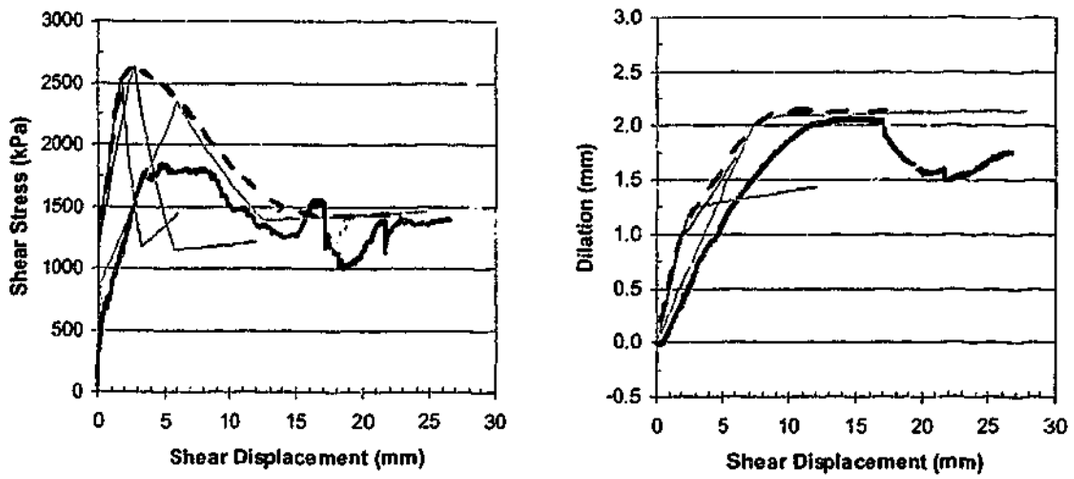

Figure 9.18: Prediction of Shear response for profile BF15_5

Both of the basalt fractal predictions overpredict the dilation of the sample. This means that the elasticity of the sample is not completely captured. Although this is not excessive it does cause the surface shear response to also be overpredicted. The profiles were water-jet cut into basalt blocks at chord lengths of approximately 5mm length. Due to the lack of roughness below this chord length, the peak shear strength is achieved at approximately 5mm shear displacement. The shear responses of the predictions are stiffer below 5mm chord length than the test results due to the overprediction of dilation. Shear failure is predicted at a smaller shear displacement than the test results indicate due to these higher initial shear stresses. This is similar behaviour to what was observed in siltstone fractal shear tests.

9.5.3 Split profiles

Direct shear tests were conducted on 4 split samples. Movement of the sample setup was suspected during the testing of sample BS_4 due to the unrealistically small dilations produced. As the statistical analysis of sample BS_4 indicated similar roughness to the other samples, especially at the longer chord lengths, its dilation would be expected to be similar to the other samples. This result has therefore been ignored. Predictions of the shear response predictions for the other split surfaces have been conducted. These are shown in detail in Appendix E. Diagrams of these surfaces together with their profiles and roughness statistics are shown in Appendix C.

The results of the predictions have been summarised in Table 9.14.

Table 9.14: Summary of Basalt Split Predictions

Sample	Difference between Peak Shear Stress Laboratory Result & Prediction	Difference between Residual Shear Stress Laboratory Result & Prediction	Initial Negative Dilation	Induced Change in Normal Stress
BS_1	-10%	-15%	0.15mm	150kPa
BS_2	-15%	-10%	0.25mm	200kPa
BS_3	-30%	-10%	0mm	-

The split surface predictions provide a reasonable estimate of the laboratory results. However, they all tend to overpredict the shear stress and dilation. This in part may be explained by the slow commencement of dilation at the start of shear displacement. This slow response would be due to the compliance of the shear rig in the shear direction. This compliance was shown to be present at higher stiffnesses and in particular with the granite test samples where significant stick-slip occurred.

An example split surface prediction of sample BS_1 is shown in Figure 9.19 together with a diagram of the surface and a statistical analysis of its roughness. This test was conducted at an initial normal stress of 400kPa and constant normal stiffness of 1000kPa/mm. The average standard deviation of chord angle for various chord lengths from several profiles was used to represent the surface. Three chord lengths of 2mm, 6.5mm and 20mm were used to capture the shear response at different scales.

9.6 Granite Predictions

Direct shear tests were conducted on regular triangular profiles and split surfaces. Stick-slip was encountered in all of the tests. This stick-slip caused a considerable reduction in the expected amount of dilation that in turn reduced the expected peak shear stress.

Predictions were based on the parameters listed in Table 9.15. Compliance due to compression of the setting concrete, machine compliance and joint closure was included in the calculations. A shear failure stress equal to the unconfined compressive strength of the material was used (discussed in Chapter 8).

Table 9.15: Granite Parameters

Parameter	Adopted value
Young's Modulus	61GPa
Poisson's Ratio	0.15
Intact Friction Angle	50°
Residual Friction Angle	36.5°
Cohesion	35MPa
Joint Normal Stiffness – water-jet surface	7.8MPa/mm
Joint Normal Stiffness – split surface	7.5MPa/mm
Failure Stress	180MPa

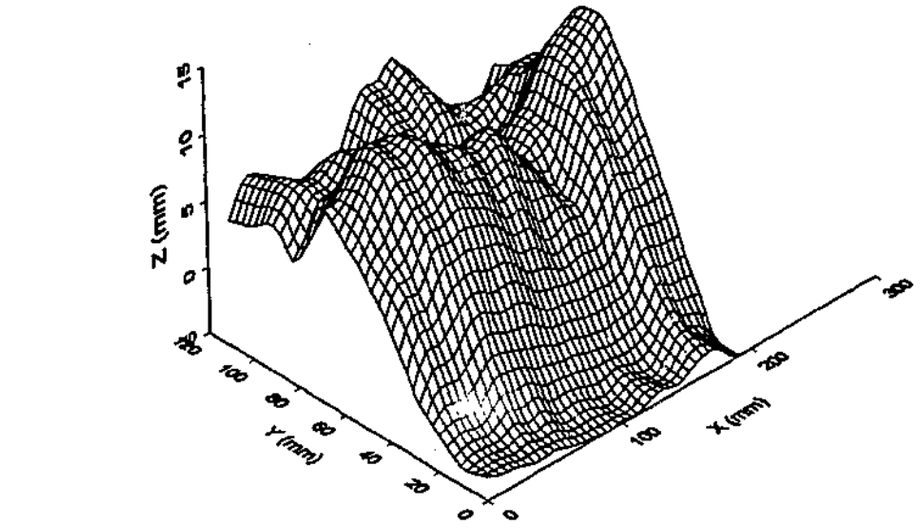

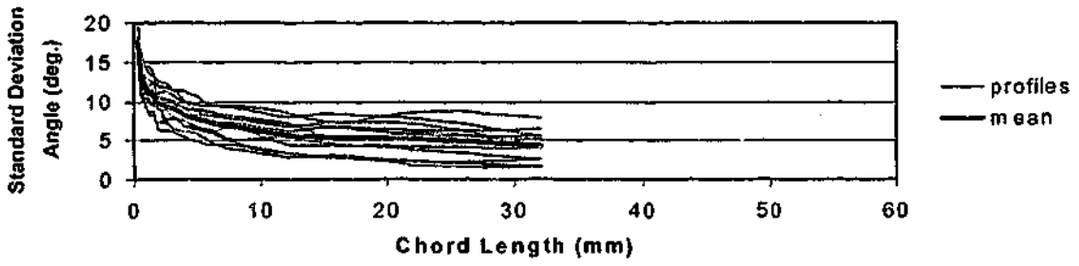

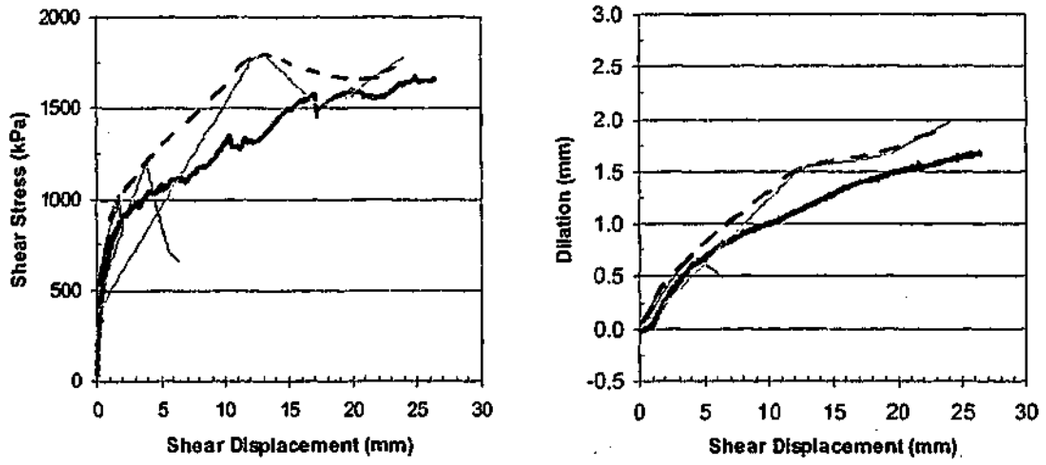

Prediction Test Result Predicted Envelope

Figure 9.19: Prediction of Shear response for profile BS_1

9.6.1 Regular triangular profiles

Predictions were conducted on regular triangular asperities of 10° and 20° inclination at chord lengths of 8mm. These are shown in detail in Appendix E.

An example regular triangular asperity prediction of sample GR10_8 is shown in Figure 9.20. This test was conducted at an initial normal stress of 2000kPa and constant normal stiffness of 2000kPa/mm. A 10° regular triangular profile of 32 asperities was used to model the surface.

The shear stress – shear displacement plot shows the presence of stick-slip as sudden decreases in shear stress. As shear displacement occurs due to the application of the shear force, movement of the shear rig in the horizontal direction occurs. The rig continues to deform storing energy until the shear resistance reaches a value that causes the sample to slide. This violent release of stored energy in the shear device frame, results in energy loss and a reduced peak shear stress. Significant stick-slip can be seen at the commencement of the shear test with negligible dilation occurring until almost 3mm shear displacement. It can be seen from these plots that if the stick-slip had not occurred the shear model may have produced a reasonable prediction of the shear response.

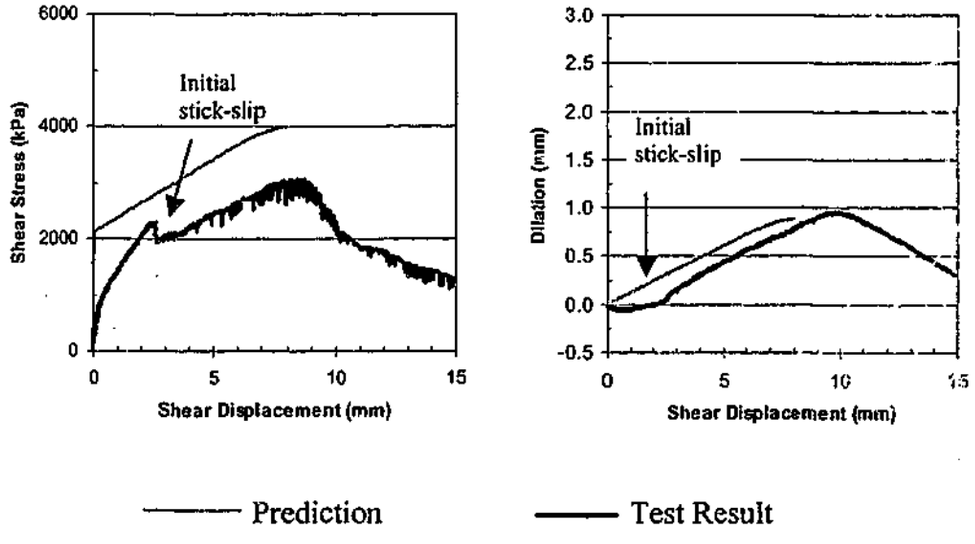

Figure 9.20: Prediction of Shear response for profile GR10_8

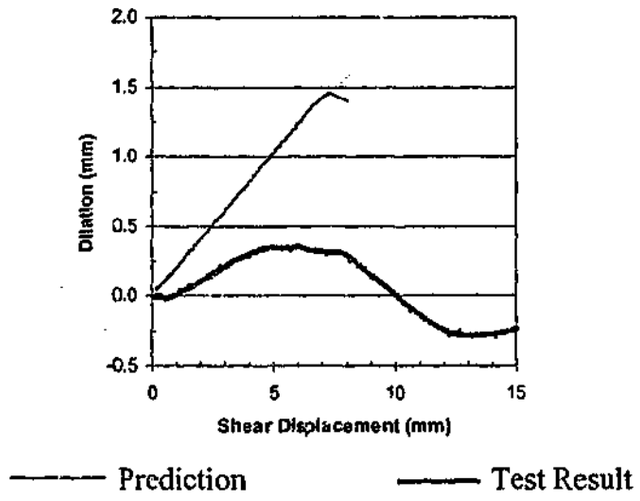

Figure 9.21: Dilation response and prediction for profile GR20_8

The tests conducted on the other 2 regular triangular asperity samples (10° and 20°) experienced less than 5mm of dilation followed by negative dilation as the asperity is overtopped (for >10mm shear displacement in Figure 9.21). This suggests that there may be movement of the sample within the concrete and rotation has occurred. These results must be disregarded due to this movement.

Therefore the laboratory results do not reflect the true peak shear stress due to the inadequate stiffness of the shear rig when testing these very hard rocks. Without considerable modifications to the shear rig (that were not possible in the time frame available) the produced laboratory results should be disregarded. Significant movement of the sample within the shear box has also occurred as highlighted by the unrealistically small dilations followed by negative dilations. These test results therefore have not reflected the true shear behaviour of the samples. However the general behaviour of the granite samples appears to be captured by the model indicating that if these problems can be overcome an acceptable prediction of granite joints may be achieved.

9.6.2 Split profiles

Predictions have been conducted for four shear tests on split samples. These are shown in detail in Appendix E. Diagrams of these surfaces together with their profiles and roughness statistics are shown in Appendix C.

An example split surface prediction of sample GS_2 is shown in Figure 9.22 together with a diagram of the surface and a statistical analysis of its roughness. This test was conducted at an initial normal stress of 300kPa and constant normal stiffness of 600kPa/mm. The average standard deviation of chord angle for various chord lengths from several profiles was used to represent the surface. Three chord lengths of 2.2mm, 6mm and 23mm were used to capture the shear response at different scales.

Again the experimental results indicate significant stick-slip at the commencement of shear displacement (2mm of shear displacement before dilation commenced) and during the test (sudden decreases in shear stress). This has meant that the shear prediction overpredicts the dilation and shear stress.

The results of the predictions are summarised in Table 9.16. This table includes the amount of shear displacement before the sample commenced sliding. A calculation of the change in normal stress that the initial stick-slip behaviour may induce (ignoring compliance effects) is also included.

Table 9.16: Summary of Granite Split Predictions

Sample	Difference between Laboratory Shear Stress Result & Prediction, <5mm	Difference between Laboratory Shear Stress Result & Prediction, 5-15mm	Initial Shear Displacement before sample starts sliding	Induced Change in Normal Stress
GS_1	-100%	-60%	2.7mm	1200kPa
GS_2	-50%	-50%	2.4mm	600kPa
GS_3	-150%	0%	0mm	-
GS_4	-60%	-80%	1.2mm	300kPa

Again due to the significant stick-slip experienced, the laboratory shear test results do not represent the conditions being modelled in the predictions. The results are therefore

difficult to compare. It is considered however that as the overall shape of the predictions is similar to the direct shear test results, that the model has potential in predicting the shear response of insitu rock conditions where compliance effects are not of concern.

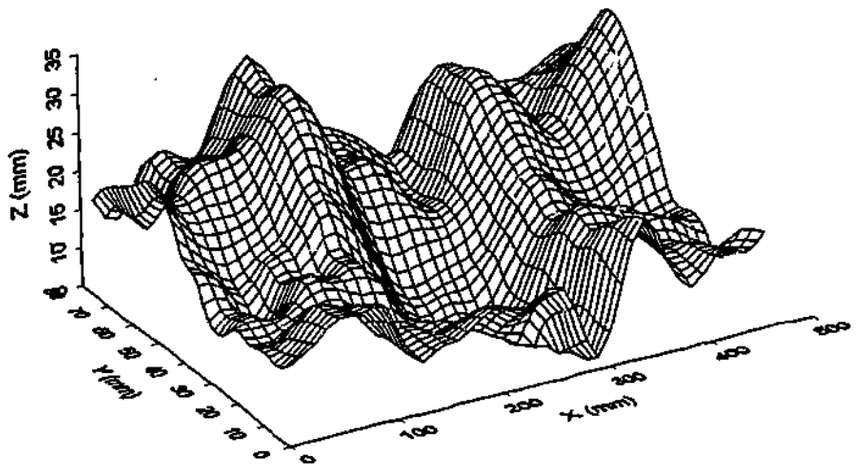

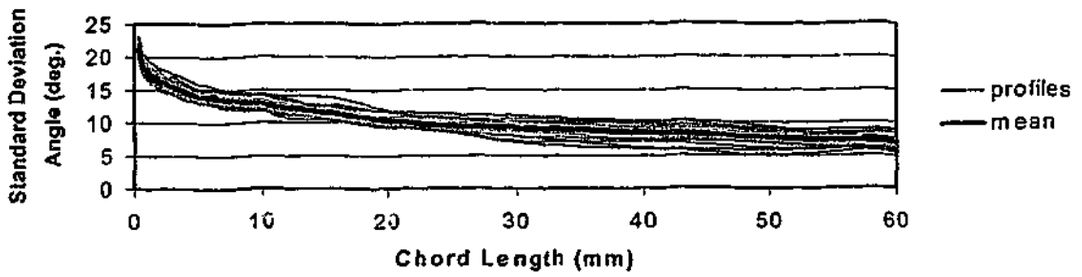

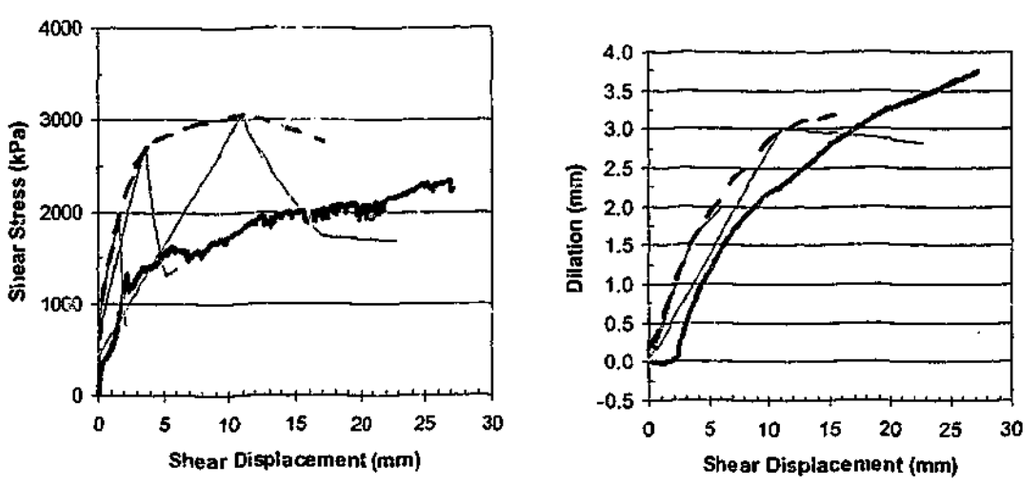

Prediction Test Result Predicted Envelope

Figure 9.22: Prediction of Shear response for profile GS_2

9.7 Field Applications

The model can be used to predict shear behaviour of insitu rock joints if the insitu rock parameters are known or can be estimated. The strength parameters such as Young's Modulus, Poisson's Ratio, intact friction angle, residual friction angle, cohesion and unconfined compressive strength can be obtained through laboratory testing. The applied load and normal stiffness can be estimated or measured insitu. The joint stiffness value (dependent on joint roughness, rock strength and infill) can be estimated through insitu testing or can be estimated from previous experience of the rock type and roughness.

At this stage in its development the model can only be used to analyse an individual joint and not the rock mass. The interaction of several rock joints will require further investigation.

Due to time restrictions in this current research, field data was not obtained to verify the model. A literature search failed to obtain suitable data to use with the model. Insitu direct shear tests are rarely conducted and typically do not obtain roughness information prior to shearing. A similar problem was found with data given in the literature on sites where rock failure had occurred. Typically several joints were involved and the roughness of the joint surfaces were not measured.

9.8 Summary

This chapter has presented the predictions of the laboratory direct shear tests conducted during this research. The predictions were made using the modified Rocket program.

Several problems with the laboratory results have been highlighted. One of the main problems encountered was an initial negative dilation of the laboratory shear samples at the commencement of shear displacement. This initial negative dilation was due to compliance of the sample and shear rig under shear loading. This problem is only likely to be observed during laboratory testing and is not something that would be encountered under insitu conditions. Due to its variability it has not been included in the shear model.

An even greater problem was highlighted during the testing of hard rock samples. This was the inability of the Monash direct shear rig to accurately test the stronger rock, in particular the granite samples, due to the development of significant stick-slip. This

stick-slip caused dissipation of energy in the shear rig frame leading to a dissimilarity between laboratory conditions and the conditions being modelled in the predictions.

Allowing for experimental variability and a dissimilarity in laboratory conditions and those used in the model, the model has produced predictions that are in reasonable agreement with the laboratory direct shear tests. This suggests that the shear model is capable of capturing the general behaviour of a rock joint.

The predictions also indicate the potential of using a single statistically similar profile to represent the three-dimensional surface. However, as could be expected, accuracy is improved if the sample roughness is consistent across the surface.

In general the predictions of the hard rock behaviour were poorer than those of the soft rock behaviour, in particular with the fractal and triangular asperity samples. This indicates that the failure model for this harder rock requires further investigation. These tests often displayed premature failure of the asperities compared to the laboratory test results. Unfortunately the shear failure mechanisms could not be clearly identified during the shear tests or in later analysis of the video footage. This has prevented a specific failure model and post peak failure model to be developed. In order to fail these stronger samples and view failure mechanisms, loads not realistic of near surface conditions would be required but more importantly, modifications to the Monash direct shear rig would be necessary.

Better predictions were also obtained for shallower asperities indicating that steeper asperities may also have a different failure mechanism. This has meant that the more realistic split surfaces often perform better than the more simplistic fractal and triangular profiles in the predictions. Further investigation is also required in this area.

10.0 SUMMARY AND CONCLUSIONS

As discussed in the introduction to this dissertation, the ultimate aim of the Geotechnical Group at Monash University is to produce a theoretical shear model capable of producing accurate predictions of rock mass behaviour under shear loading. This is obviously a very complex area and one that requires considerable investigation. The precursor of this investigation was the development of a theoretical model to analyse the response of a rock socketed pile under axial loading. The aims of this thesis were to extend this model into rock joint analysis. Specifically the aims were to investigate the models performance with significantly stronger rock than had been previously modelled and to determine a method to model more representative three-dimensional surfaces than previously investigated.

To investigate the applicability of the model to three-dimensional rock surfaces in a variety of rock types, an experimental program of direct shear tests performed under constant normal stiffness conditions was conducted. Rock materials tested were Johnstone, an artificial soft rock with similar properties to Melbourne Mudstone; Hawkesbury sandstone, low strength; Melbourne Mudstone, a medium to high strength interbedded siltstone, sandstone and mudstone; Newer Volcanics, a high strength basaltic rock; and Mt Bundey Granite, high to very high strength. A variety of roughness profiles were tested from regular triangular asperities in materials that had not been previously tested at Monash, to more realistic three-dimensional split surfaces that were shown to approximate natural joint surfaces. The samples were tested under a variety of boundary conditions.

A statistical and experimental program was conducted to evaluate suitable methods to quantify the joint surface roughness.

10.1 Modelling Joint Roughness

The following observations and conclusions can be drawn from the laboratory and statistical investigation into rock joint surface roughness:

- Joint surfaces may be anisotropic. When modelling the shear performance either the potential shear direction is required or an analysis is required in more than one direction.
- A statistical analysis including the determination of the standard deviation of asperity chord angle for various chord lengths, is a simple and repeatable method that is able to capture roughness at various scales.
- The joint surfaces that were measured appeared to be statistically similar across the surface in one direction. This enabled the surfaces to be represented mathematically by the average standard deviation of asperity chord angle at different chord lengths. This relationship has been shown to be adequately represented by a logarithmic or power function.
- A joint surface can be statistically reproduced in two dimensions using the logarithmic or power function statistical representation of the joint surface combined with a Modified Midpoint Displacement method.
- Predictions of the shear behaviour of a joint can be conducted using the standard deviation of chord angle statistics at several chord lengths. An envelope of these different chord length shear responses can be constructed to capture the shear response at various scales.

10.2 Shear Behaviour Modelling

The following observations and conclusions can be drawn from the laboratory investigation into rock joint shear behaviour:

- The basic shear model developed for concrete / rock interfaces and modified for rock / rock interfaces, captures the general behaviour of the stronger rock types and more realistic three-dimensional surfaces.
- As a sample commences shear displacement, some initial negative dilation is encountered. This shear compliance is dependent on sample strength, roughness and initial mating of interfaces. It is therefore considered a laboratory condition and one that would not be significant insitu. However, in particular under constant normal

stiffness conditions, it can have a significant effect on the peak shear stress as measured in the laboratory.

- To test strong rock samples, direct shear testing apparatus must be very stiff to avoid the creation of stick-slip. When stick-slip occurs energy is lost and lower peak shear stresses may be produced.
- Detailed joint closure modelling is required to accurately model joint shear behaviour. Joint closure exists in insitu conditions as well as in laboratory conditions. Joint closure can be modelled by a joint stiffness parameter that is specific to different rock strengths and roughnesses. For near surface conditions encountering low stress situations, a linear relationship is adequate to represent the joint stiffness. Joint stiffness estimates were evaluated for laboratory test samples. A different joint stiffness was calculated for water-jet cut surfaces and natural split surfaces. In the case of laboratory testing, compliance of the sample and equipment is also important. A polynomial relationship was developed so that the effect of machine compliance could be extracted from the laboratory results. Further linear relationships were estimated to remove compression in the material used to cast the sample into the shear box.
- The failure mechanisms for rock joints are different to concrete / rock interfaces. A modification factor can be used with a Sokolovsky failure mechanism to model soft rock situations (UCS<20MPa). Harder rock samples fail at considerably lower failure stresses than that predicted by the Sokolovsky failure mechanism. These harder samples were shown to fail when the local stress at the contacting asperity reached the materials unconfined compressive strength.
- Although previous work had indicated a significant wear component in concrete / sandstone interfaces and also in sandstone joints containing large "macro" asperities, wear did not appear to be a significant component of the shear behaviour of three-dimensional sandstone joints.

10.3 Limitations and Further research

As previously mentioned, this work is only another step in the direction of creating a theoretical model to analyse rock mass behaviour. There are still many areas that require considerable research. This work has also highlighted specific areas of rock joint behaviour that require further investigation.

10.3.1 Failure Mechanism

For concrete / soft rock asperities the failure stress is adequately predicted by the Sokolovsky closed form solution. Soft rock joints have been shown to fail at a modified Sokolovsky shear failure stress. Hard rock joint samples have been shown to fail at their unconfined compressive strength.

Model predictions using a modified Sokolovsky shear failure stress produce reasonable shear behaviour predictions on soft rock samples.

Model predictions on stronger rock using the unconfined compressive strength values produced reasonable predictions for split surfaces, taking into consideration sample and experimental variability. However, the peak shear strength of the steeper angled triangular and fractal profiles tend to be overpredicted. Shear displacement to the commencement of shear failure tends to be underpredicted.

Unfortunately shear failure mechanisms could not be clearly observed during the shear tests or in later analysis of video footage. This was due to the difficulty in applying a high enough load to cause overall shear failure of the asperities. This prevented specific failure models and post peak failure models to be developed. In order to fail these stronger samples, stick-slip behaviour must be eliminated. This requires modifications to the Monash direct shear rig. These modifications require significant stiffening of the shear device frame, which may require complete refabrication of the device.

10.3.2 Wear

Modelling of the shear test results on three-dimensional split surfaces has indicated that wear may not be a significant component of the shear behaviour. When the existing wear models were incorporated (based predominantly on concrete / sandstone interfaces that would easily cause wear on the softer surface of the interface), significant

underprediction of the dilation and peak shear stress was produced. Further tests would be required to verify the applicability of wear models in rock joint analysis.

10.3.3 Factors Affecting Rock Joint Shear Behaviour

As discussed in Chapter 2 there are many factors that influence the shear behaviour of a rock joint. This current work has been limited to the investigation of clean, tight joints. Further work would be required to incorporate the effects of infill, aperture, presence of water and change in shear displacement rate.

10.3.4 Field Predictions

To date the model has only been confirmed on laboratory test data. Comparison with field direct shear test results would be desirable.

10.3.5 Rock Mass Behaviour

This work has investigated the shear response of a single joint under the application of shear loading. This work will need to be extended to include multiple joint patterns as encountered in rock masses. To analyse an insitu rock joint the response of the surrounding joints must also be included.

REFERENCES

Amadei, B. and O. Stephansson (1997). Rock stresses and its measurement. UK, Chapman and Hall.

Archambault, G., M. Fortin, D. E. Gill, M. Aubertin and B. Ladanyi (1990). Experimental investigations for an algorithm simulating the effect of variable normal stiffness on discontinuities shear strength. Proc. on the Conf. on Fractured and Jointed rock masses - Rock Joints, Rotterdam, Balkema.141-148

Assoc., A. S. (1955). "Surface roughness, waviness and lay, ASA." **B46.1.**

Bandis, S., A. C. Lumsden and N. R. Barton (1981). "Experimental studies of scale effects on the shear behaviour of rock joints." Int. J. Rock Mech. Min. Sci. & Geomech. Abs. **18**: 1-21.

Bandis, S. C., A. C. Lumsden and N. R. Barton (1983). "Fundamentals of rock joint deformation." Int. J. Rock Mech. Min. Sci. and Geomech. Abs. **18**: 1-21.

Barton, N. (1971). A relationship between joint roughness and joint shear strength. Rock Fracture; Proc. Int. Symp. Rock Mech., Nancy.Paper I:8

Barton, N. (1973). "Review of a new shear - strength criterion for rock joints." Engineering Geology **7**: 287-332.

Barton, N. and S. Bandis (1982). Effects of block size on the shear behaviour of jointed rock. Symp. on Rock Mech., Berkeley.739-760

Barton, N. and S. Bandis (1990). Review of predictive capabilities of JRC-JCS model in engineering practice. Proc. on the Conf. on Fractured and Jointed Rock Masses - Rock Joints, Rotterdam.603-610

Barton, N. and V. Choubey (1977). The shear strength of rock joints in theory and practice. Rock Mechanics.1-54

Belem, T., F. Homand-Etienne and M.Souley (2000). "Quantitative parameters for rock joint surface roughness." Rock Mech. Rock Engng **33**(4): 217-242.

Bendat, J. S. and A. G. Piersol (1986). Random data analysis and measurement procedures, Wiley Interscience.

Benjelloun, Z. H., M. Boulon and D. Billaux (1990). Experimental and numerical investigation on rock joints. Proc. on the Conf. on Fractured and Jointed rock masses - Rock Joints, Rotterdam, Balkema.171-178

Berry, M. V. and Z. V. Lewis (1980). "On the Weierstrass-Mandelbrot fractal function." Proc. Roval Soc. London **370**(A): 459-484.

Bobji, M. S., K. Shivakumar, H. Alehossein, V. Venkateshwarlu and S. K. Biswas (1999). "Influence of surface roughness on the scatter in hardness measurements - a numerical study." Int. J. of Rock Mech. & Min. Sci. **36**: 399-404.

Brown, S. (1995). Measuring the dimension of self-affine fractals: Example of rough surfaces. Fractals in the earth sciences. P. L. P. CC Barton. New York, Plenum Press.

Brown, S. R. (1987). "A note on the description of surface roughness using fractal dimension." Geophysical Research Letters **14**(11): 1095-1098.

Brown, S. R. and C. H. Scholz (1985). "Broad bandwidth study of the topography of natural rock surfaces." J. of Geophysical Res. **90**(B14): 12,575-12,582.

Byerlee, J. D. (1968). "Brittle-ductile transition in rocks." J. of Geophysical Res. **73**(14): 4741-4750.

Carr, J. R. (1989). Stochastic versus deterministic fractals : The controversy over applications in the earth sciences. Eng. Geology and Geotech. Engng.297-302

Carr, J. R. and J. B. Warriner (1987). Rock mass classification using fractal dimension. 28th U.S. Symp. on Rock Mech., Tucson.73-80

Celestino, T. B. and R. E. Goodman (1979). Path dependency of rough joints in bi-directional shearing. Proc. 4th Cong. Int. Soc. of Rock Mech., Montreaux.91-98

Cheng, F. K. K. (1997). A laboratory study of the influence of wall smear and residual drilling fluids on rock socketed pile performance. Civil Eng. Melbourne, Monash University.

Chiu, H. K. (1981). Geotechnical properties and numerical analysis for rock socketed pile design in weak rock. Civil Eng. Melbourne, Monash University.

Choi, S. K. (1984). The bearing capacity of foundations in weak rock. Civil Eng. Melbourne, Monash University.

Clarke, K. (1986). "Computation of the fractal dimension of topographic surfaces using the triangular prism surface area method." Computers & Geosciences **12**(5): 713-722.

Collingwood, B. (2000). The effect of construction practices on the performance of rock socketed bored piles. Civil Engineering. Melbourne, Monash University: Chpt 5.

Collingwood, B., J. P. Seidel and C. M. Haberfield (1999). Laser based roughness measurement for design and verification of rock socketed piles. 8th ANZ Conf. on Geom., Hobart

Crawford, A. M. and J. H. Curran (1981). "The influence of shear velocity on the frictional resistance of rock discontinuities." Int. J. Rock mech. Min. Sci. & Geomech Abs. **18**: 505-518.

Dahlhaus, P. G. and M. O'Rourke (1992). The newer volcanics. Engineering Geology of Melbourne, Balkema.205-212

de Toledo, C. P. E. and M. H. de Freitas (1995). The peak shear strength of filled joints. Fractured and Jointed Rock Masses.385-392

Dieterich, J. (1978). "Time-dependent friction and the mechanics of stick-slip." Pure & App. Geophysics **116**: 790-806.

Dight, P. M. and H. K. Chiu (1981). "Prediction of shear behaviour of joints using profiles." Int. J. Rock Mech. Min. Sci. & Geomech. Abs. **18**: 376-386.

Dong, J. J. and Y. W. Pan (1996). "A hierarchical model of rough rock joints based on micromechanics." Int. J. Rock Mech. Min. Sci. & Geomech. Abs. 33(2): 111-123.

Fairhurst, C. (1964). "On the validity of the 'Brazilian' test for brittle materials." Int. J. Rock Mech. & Min. Sci. **1**: 535-546.

Fleuter, W. T. (1997). Analytical and experimental investigation into the shear performance of joints in soft sedimentary rocks. Civil Eng. Melbourne, Monash University.

Fortin, M., G. Archambault, M. Aubertin and D. Gill (1988). An algorithm for predicting the effects of a variable normal stiffness on shear strength of discontinuities. Proc. 15th Canadian Rock Mechanics Symposium.109-117

Fournier, A., D. Fussell and L. Carpenter (1982). "Computer rendering of stochastic models." Communications of the Association for Computing Machinery **25**(6): 371-384.

Fox, C. (1987). "An inverse fourier transform algorithm for generating random signals of a specified spectral form." Computers & Geosciences **13**(4): 369-374.

Gentier, S., J. Riss, G. Archambault, R. Flamand and D. Hopkins (2000). "Influence of fracture geometry on shear behaviour." Int. J. of Rock Mech. & Min. Sci. **37**: 161-174.

Goodman, R. E. (1980). Introduction to rock mechanics, John Wiley & Sons.

Gu, X. F. (2001). Shear behaviour of sandstone-concrete joints and pile shafts in sandstone. Civil eng. Melbourne, Monash University.

Haberfield, C. M. (1987). The performance of the pressuremeter and socketed piles in weak rock. Civil Eng. Melbourne, Monash University.

Haberfield, C. M. and J. P. Seidel (1999). "Some recent advances in the modelling of soft rock joints in direct shear." Geotech. & Geological Eng. **17**: 177-195.

Helfel, R. (1988). Visual programming with HPVee. New Jersey, Prentice Hall.

Hoek, E. and J. W. Bray (1981). Rock slope engineering. London, Institution of Mining and Metallurgy: p94.

Hoek, E. and E. T. Brown (1980). "Empirical strength criterion for rock masses." Journal of the Geotech. Eng. Division, Proc. of the American Society of Civil Eng **106**(No. GT9): 1013-1035.

Hoek, E. and E. T. Brown (1988). The hoek-brown failure criterion - a 1988 update. Proc. 15th Canadian Rock Mech. Symp., Rock Eng. for Underground Excavations, Toronto.31-38

Hopkins, D. L., N. G. W. Cook and L. R. Myer (1990). Normal joint stiffness as a function of spatial geometry and surface roughness. Proceedings of the International Symposium on Rock Joints, Loen, Norway, Balkema.203-210

Hsiung, S. M., A. Ghosh and A. H. Chowdhury (1995). On natural rock joint profile characterization using self-affine fractal approach. Rock Mechanics, Proc. of the 35th U.S. Symp., Rotterdam, Balkema.681-687

Huang, S. L., S. M. Oelfke and R. C. Speck (1992). "Applicability of fractal characterisation and modelling to rock joint profiles." Int. J. Rock Mech. Min. Sci. & Geomech. Abs. **29**(2): 89-98.

Indraratna, B. and A: Haque (1997). "Experimental study of shear behaviour of rock joints under constant normal stiffness conditions." Int. J. of Rock Mech. & Min. Sci. **34**(3-4): No. 141.

Indraratna, B. and A. Haque (2000). Shear behaviour of rock joints, Balkema.

Indraratna, B., A. Haque and N. Aziz (1999). "Shear behaviour of idealized infilled joints under constant normal stiffness." Geotechnique **49**(3): 331-355.

Indraratna, B., A. Herath and N. Aziz (1995). Characterisation of surface roughness and its implication on the shear behaviour of joints. Mechanics of Jointed and Faulted Rock, Vienna, Balkema.515-520

ISRM (1978). "Suggested methods for the quantitative description of discontinuities in rock masses." Int. J. Rock Mech. Min. Sci. **15**: 319-368.

ISRM (1981). Rock characterisation testing and monitoring, ISRM suggested methods, Pergamon Press.

Itasca (1993). FLAC users manual. Itasca Consulting Group. Minnesota, U.S.A.

Johnston, I. W. and S. K. Choi (1986). "A synthetic soft rock for laboratory model studies." Geotechnique **36**(2): 251-263.

Johnston, I. W. and T. S. K. Lam (1989). "Shear behaviour of regular triangular concrete/rock joints - analysis." J. of Geotech. Eng. ASCE **115**: 711-727.

Kabeya, K. K. and T. F. H. Legge (1996). Influence of particle size on the shear behaviour of rock joints. Eurock '96, Balkema.151-158

Kocharyan, G. G., V. N. Kostyuchenko and D. V. Pavlov (1997). "The structure of various scale natural rock discontinuities and their deformation properties. Preliminary results." Int. Journal Rock Mech. & Min. Sci. **34:3-4**(Paper No. 159).

Kodikara, J. K. (1989). Shear behaviour of rock-concrete joints and side resistance of piles in weak rock. Civil Eng. Melbourne, Monash University.

Kreyszig, E. (1972). Advanced engineering mathematics, John Wiley and Sons.

Kulatilake, P. and J. Um (1997). "Requirements for accurate quantification of self affine roughness using the roughness-length method." Int. J. Rock Mech. & Min. Sci. **34:3-4**(Paper No. 166).

Kulatilake, P. H. S. W. and J.Um (1999). "Requirements for accurate quantification of self-affine roughness using the roughness-length method." Int. J. of Rock Mech. & Min. Sci. **36**: 5-18.

Kulatilake, P. H. S. W., G. Shou, T.H.Huang and R. M. Morgan (1995). "New peak shear strength criteria for anisotropic rock joints." Int. J. of Rock Mech. & Min. Sci. **32**(7): 673-697.

Kulatilake, P. H. S. W., J. Um and G. Pan (1997). "Requirements for accurate estimation of fractal parameters for self-affine roughness profile using the line scaling method." Rock Mech. Rock Engng **30**(4): 181-206.

Kulatilake, P. H. S. W., J. Um, B. B. Panda and N.Nghiem (1998). "Development of a new peak shear strength criterion for anistropic rock joints." Int. J. of Rock Mech. & Min. Sci. **35**(3-4): Paper No. 040.

Ladanyi and Archambault (1980). "Direct and indirect determination of shear strength of rock mass." Preprint 80-25 AIME.

Ladanyi, B. and G. Archambault (1970). Simulation of shear behaviour of a jointed rock mass. Proc. 11th Symp. on Rock Mech., Rock Mechanics: Theory and Practice.105-125

Lam, T. S. K. (1983). Shear behaviour of concrete-rock joints. Civil Eng. Melbourne, Monash University.

Lamas, L. N. (1996). An experimental and analytical study of the roughness of granite joints. Eurock '96, Balkema.117-126

Lanaro, F. (2000). "A random field model for surface roughness and aperture of rock fractures." Int. J. of Rock Mech. & Min. Sci. **37**: 1195-1210.

Lea Cox, B. and J. S. Y. Wang (1993). "Fractal surfaces: Measurement and applications in the earth sciences." Fractals **1**(1): 87-115.

Lee, Y. H., J. R. Carr, D. J. Barr and C. J. Haas (1990). "The fractal dimension as a measure of the roughness of rock discontinuity profiles." Int. J. Rock Mech. Min. Sci. & Geomech. Abs. **27**(6): 453-464.

Leichnitz, W. (1985). "Mechanical properties of rock joints." Int. J. Rock Mech. Min. Sci. & Geomech. Abs. **22**: 313-321.

Lessard, J.-S. and J. Hadjigeorgiou (1998). "Quantifying joint roughness using artificial neural networks." Int. J. of Rock Mech. & Min. Sci. **35:4-5**(Paper No. 093).

Maerz, N. H., J. A. Franklin and C. P. Bennet (1990). "Joint roughness measurements using shadow profilometry." Int. J. Rock Mech. Min. Sci. & Geomech. Abs. **27**(5): 329-343.

Malinverno, A. (1990). "A simple method to estimate the fractal dimension of a self-affine series." Geophysical research Letters **17**(11): 1953-1956.

Mandelbrot, B. B. (1983). The fractal geometry of nature, W.H. Freeman and Company.

Mandelbrot, B. B. (1985). "Self-affine fractals and fractal dimension." Physica Scripta **32**: 257-260.

Matsushita, M. and S. Ouchi (1989). "On the self-affinity of various curves." Physica D **38**: 246-251.

Miller, S., P. McWilliams and J. Kerkering (1990). Ambiguities in estimating fractal dimensions of rock surfaces. Rock Mechanics Contributions and Challenges, Balkema.471-478

Mogi, K. (1964). "Pressure dependence of rock strength and transition form brittle fracture to ductile flow." Bulletin of the Earthquake Research Institute **44**: 215-232.

Muralha, J. and J. G. Charrua-Graca (1990). An experience on the application of fractal theory to basic shear strength studies. Proc. of the Conf. on Fractured and Jointed rock masses - Rock joints, Rotterdam, Balkema.667-671

Myers, N. O. (1962). "Characteristics of surface roughness." Wear **5**: 182-189.

Ohnishi, Y. and P. G. R. Dharmaratne (1990). Shear behaviour of physical models of rock joints under constant normal stiffness conditions. Proc. on the Conf. on Fractured and Jointed rock masses - Rock Joints, Rotterdam, Balkema.267-273

Patton, F. D. (1966). Multiple modes of shear failure in rock. Proc. 1st Cong. Int. Soc. Rock Mech., Lisbon.509-513

Piggott, A. R. and D. Elsworth (1995). A comparison of methods of characterizing fracture surface roughness. Fractured and jointed rock masses, Rotterdam, Balkema.471-477

Pikens, J. R. and J. Gurland (1976). Metallographic characterization of fracture surface profiles on sectioning planes. 4th Int. Congr. Stereol., Gaithersburg

Power, W. L. and W. B. Durham (1997). "Topography of natural and artificial fractures in granitic rocks: Implications for studies of rock friction and fluid migration." Int. J. of Rock Mech. & Min. Sci. **34**(6): 979-989.

Power, W. L. and T. E. Tullis (1991). "Euclidean and fractal models for the description of rock surface roughness." J. Geophysical Res. **96**(B1): 415-424.

Pratt, H. R., A. D. Black, W. S. Brown and W. F. Brace (1972). "The effect of specimen size on the mechanical properties of unjointed diorite." Int. J. Rock Mech. & Min. Sci. **9**: 513-529.

Read, H. H. and J. Watson (1987). Introduction to geology volume 1 - principles.

Reeves, M. J. (1985). "Rock surface roughness and frictional strength." Int. J. Rock Mech Min. Sci. & Geomech. Abs. **22**: 429-442.

Rengers, N. (1970). Influence of surface roughness on the friction properties of rock planes. Proc. 2nd Cong. Int. Soc. Rock Mech., Belgrade.1-31

Ripley, C. F. and K. L. Lee (1961). Sliding friction tests on sedimentary rock specimens. Proc. 7th Cong. on Large Dams, Rome.657-671

Rowe, P. W. (1962). "The stress-dilatancy relation for static equilibrium of an assembly of particles in contact." Proc. Royal Soc. London **269**(A): 500-527.

Saeb, S. (1990). A variance on the Ladanyi and Archambault's shear strength criterion. Proc. of the Conf. on Fractured and Jointed Rock Masses - Rock Joints, Rotterdam, Balkema.701-705

Saeb, S. and B. Amadei (1992). "Modelling rock joints under shear and normal loading." Int. J. Rock Mech. Min. Sci. & Geomech. Abs. **29**(3): 267-278.

Saupe, D. (1988). Algorithms for random fractals. The science of fractal images. H. O. Peitgen and D. Saupe, Springer-Verlag: 71-113.

Sayles, R. S. and R. R. Thomas (1977). "The spatial representation of surface roughness by means of the structure functions, a practical alternative to correlation." Wear **42**: 263-276.

Scavia, C. (1996). "The effect of scale on rock fracture toughness: A fractal approach." Geotechnique **46**(4): 683-693.

Seidel, J. P. (1993). The analysis and design of pile shafts in weak rock. Civil Eng. Melbourne, Monash University.

Seidel, J. P. and C. M. Haberfield (1995). The application of energy principles to the determination of the sliding resistance of rock joints. Rock Mechanics and rock engineering.211-226

Seidel, J. P. and C. M. Haberfield (1995a). "Towards an understanding of joint roughness." Rock Mech. Rock Engng **28**(2): 69-92.

Shirono, T. and P. h. S. w. Kulatilake (1997). "Accuracy of the spectral method in estimating fractal/spectral parameters for self-affine roughness profiles." Int. J. of Rock Mech. & Min. Sci. **34**(5): 789-804.

Skinas, C. A., S. C. Bandis and C. A. Demiris (1990). Experimental investigations and modelling of rock joint behaviour under constant stiffness. Proc. on the Conf. on Fractured and Jointed rock masses - Rock Joints, Rotterdam, Balkema.301-308

Sokolovsky, V. (1960). Statics in soil media. London, Butterworth Scientific Publications.

Steinbrenner, W. (1934). "Tafeln zur setzungsberechnung." Die Strasse **1**.

Tse, R. and D. M. Cruden (1979). "Estimating joint roughness coefficients." Int. J. Rock Mech. Min. Sci. & Geomech. Abs. **16**: 303-307.

Turk, N., M. J. Greig, W. R. Dearman and F. F. Amin (1987). Characterization of rock joint surfaces by fractal dimension. 28th U.S. Symp. on Rock Mech., Tucson.1223-1236

Van Sint Jan, M. L. (1990). Shear tests of model rock joints under stiff normal loading. Proc. on the Conf. on Fractured and Jointed rock masses - Rock Joints, Rotterdam, Balkema.323-327

Voss, R. (1985). Random fractal forgeries. Fundamental algorithms for computer graphics. R. Earnshaw. Berlin, Springer-Verlag: 805-835.

Wakabayashi, N. and I. Fukushige (1995). Experimental study on the relation between fractal dimension and shear strength. Fractured and Jointed Rock Masses, Rotterdam, Balkema.119-124

Wibowo, J. T., B. Amadei, S. Sture, A. B. Robertson and R. Price (1995). Shear response of a rock joint under different boundary conditions: An experimental study. Fractured and Jointed Rock Masses, Rotterdam, Balkema.425-430

Xie, H. and W. G. Pariseau (1995). Fractal estimation of joint roughness coefficients. Fractured and jointed rock masses, Rotterdam, Balkema.125-131

Xie, H., J.-A. Wang and M. A. Kwasniewski (1999). "Multifractal characterization of rock fracture surfaces." Int J. of Rock Mech. & Min. Sci. **36**: 19-27.

Yu, X. and B. Vayssade (1991). "Joint profiles and their roughness parameters." Int. J. Rock Mech. Min. Sci. & Geomech. Abs. **28**(4): 333-336.

Zhao, J. (1997). "Joint surface matching and shear strength. Part a: Joint matching coefficient." Int J. of Rock Mech. & Min. Sci. **34**(2): 173-178.

APPENDIX A

NATURAL JOINT SURFACES

COMPARISON OF JOINT ROUGHNESS IN 2 DIRECTIONS

Basalt Joint 1

Table of Contents – Appendix A

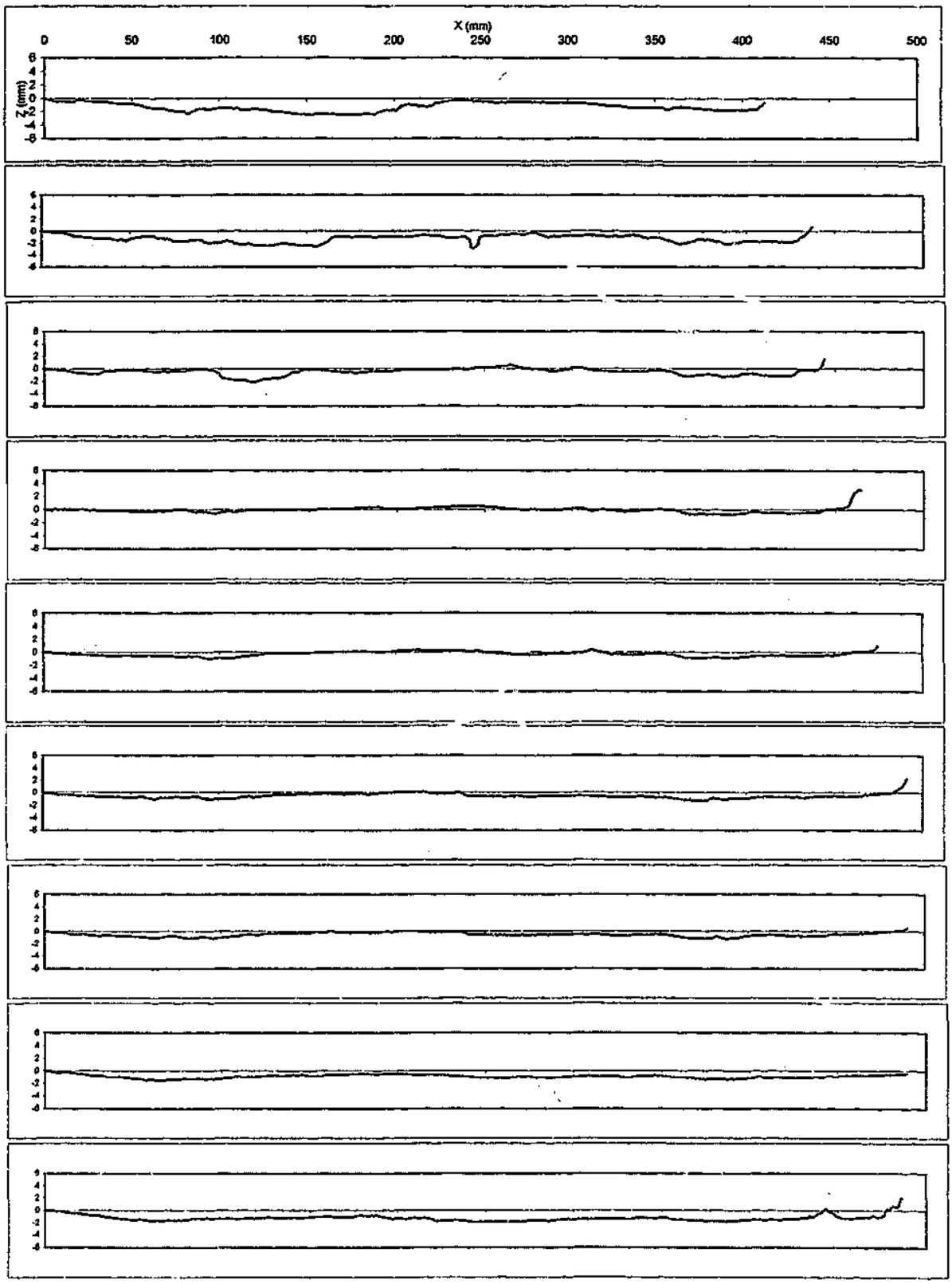

SILTSTONE SW, JOINT NEAR PERPENDICULAR TO BEDDING, PYRITE COATED

BLOCK 1, scanned at 10 mm intervals

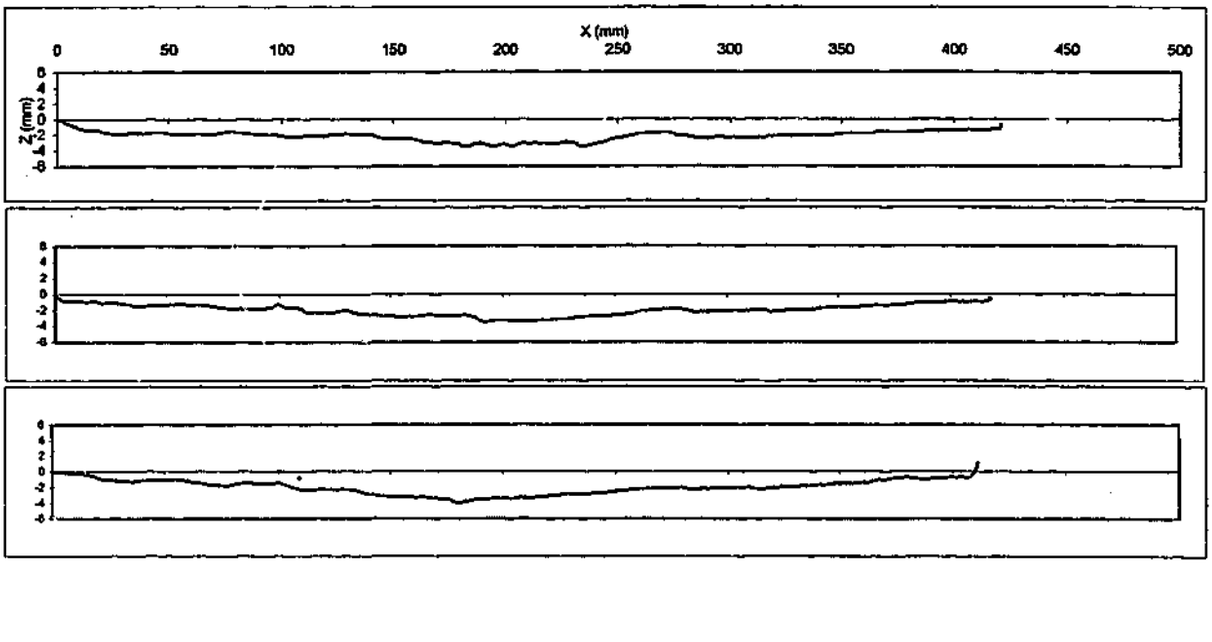

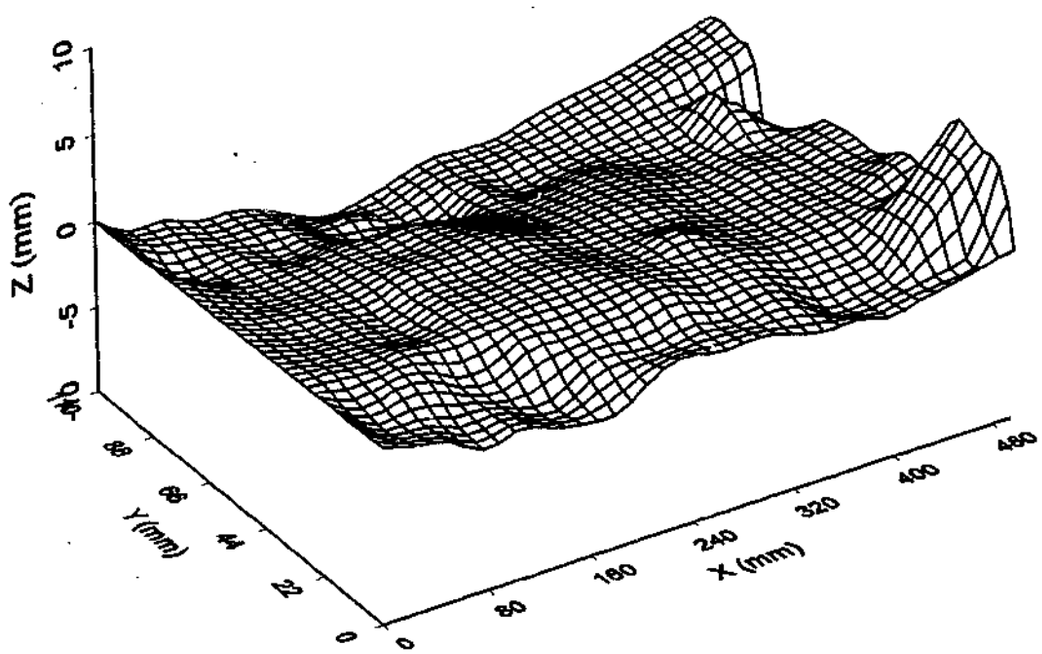

SILTSTONE SW, JOINT NEAR PERPENDICULAR TO BEDDING, PYRITE COATED

BLOCK 1, scanned at 10 mm intervals

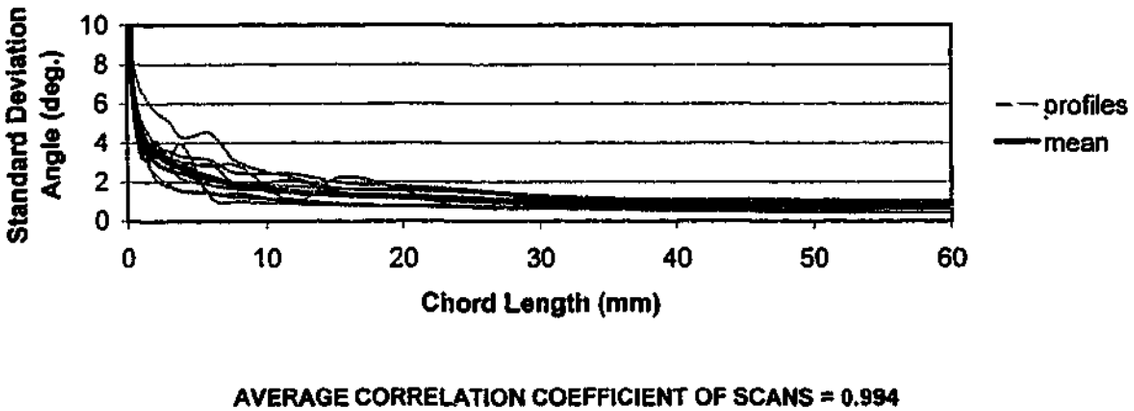

AVERAGE CORRELATION COEFFICIENT OF SCANS = 0.994

AVERAGE CORRELATION COEFFICIENT OF SCANS TO MEAN = 0.997

SILTSTONE SW, JOINT NEAR PERPENDICULAR TO BEDDING

BLOCK 1, scanned at 10mm intervals

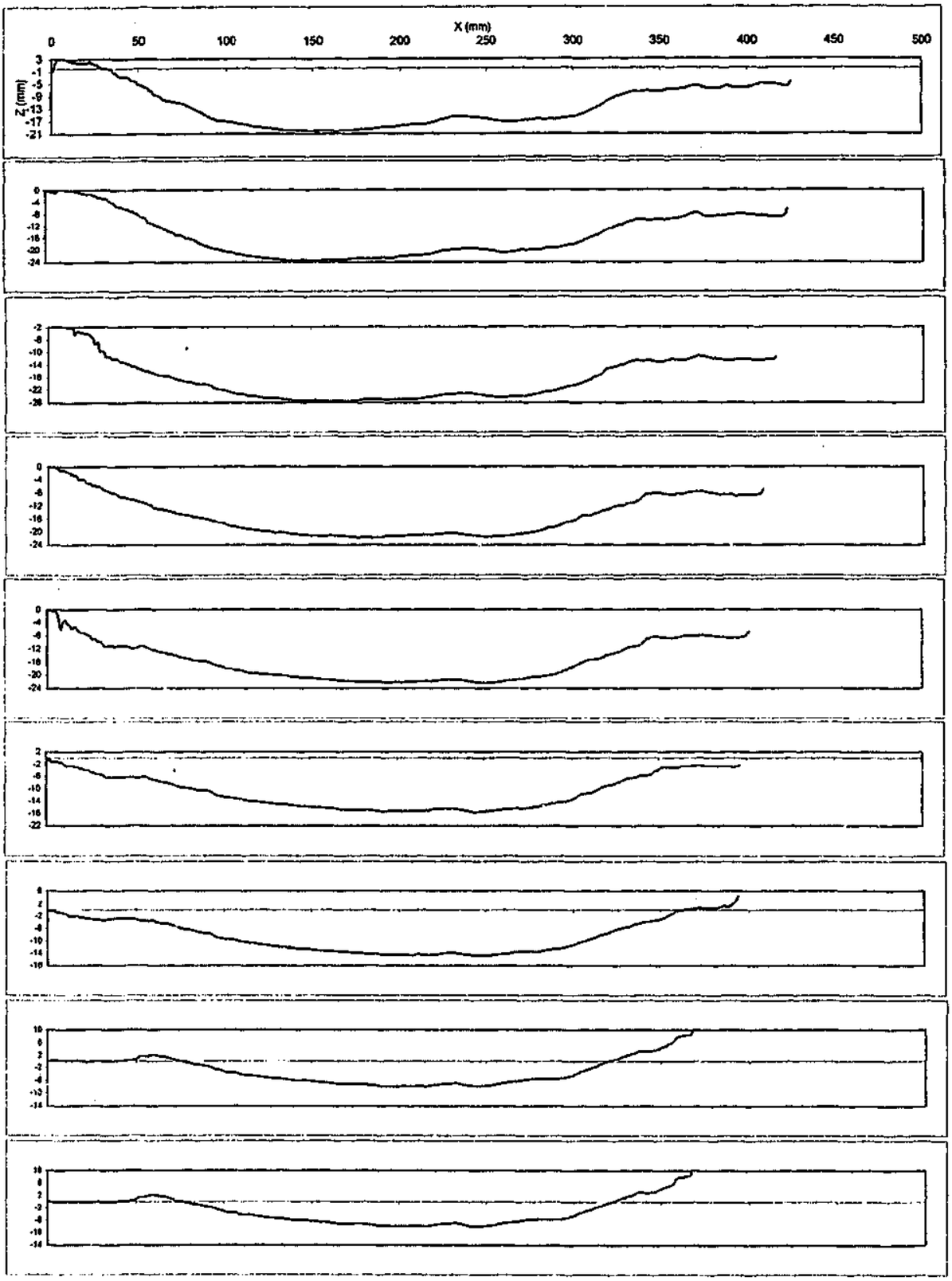

SILTSTONE SW, JOINT NEAR PERPENDICULAR TO BEDDING, PYRITE COATED

BLOCK 3, scanned at 10 mm intervals

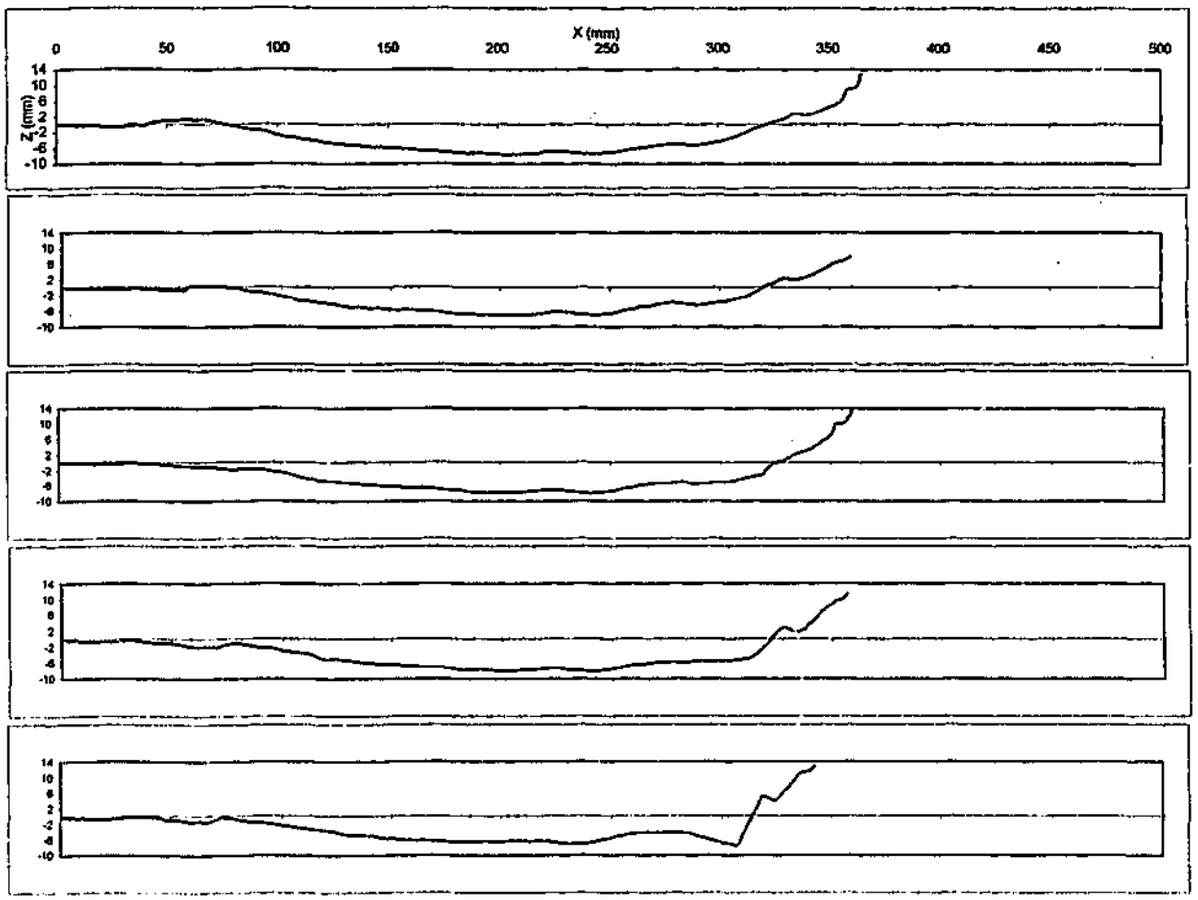

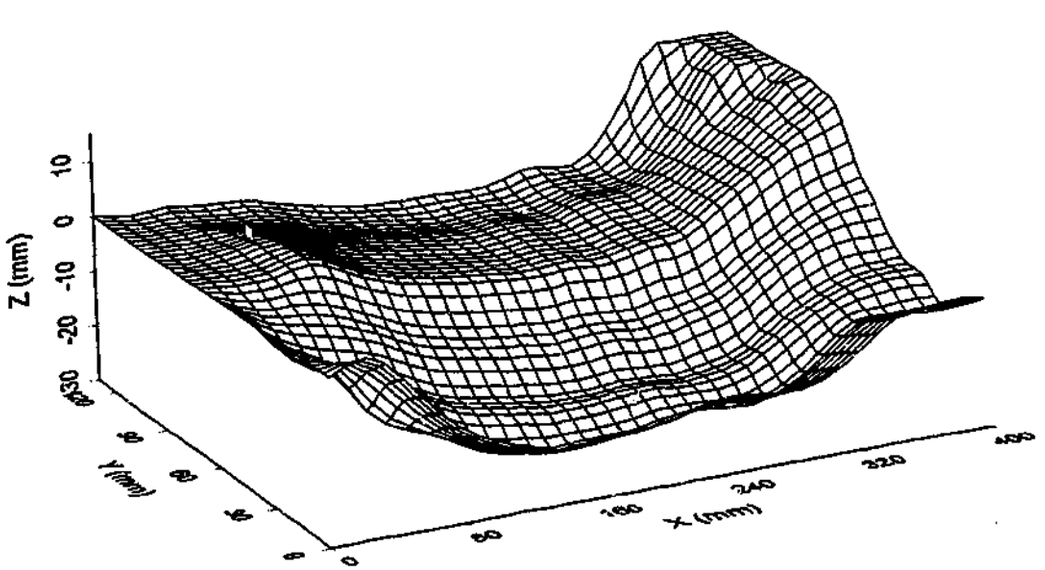

SILTSTONE SW, JOINT NEAR PERPENDICULAR TO BEDDING, PYRITE COATED

BLOCK 3, scanned at 10 mm intervals

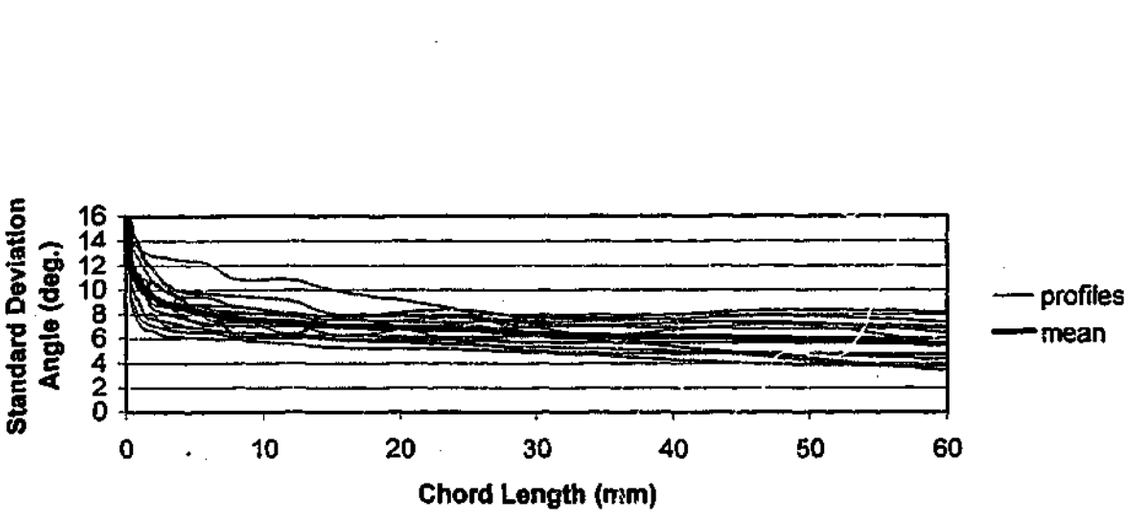

AVERAGE CORRELATION COEFFICIENT OF SCANS = 0.972

AVERAGE CORRELATION COEFFICIENT OF SCANS TO MEAN = 0.987

SILTSTONE SW, JOINT NEAR PERPENDICULAR TO BEDDING

BLOCK 3, scanned at 10 mm intervals

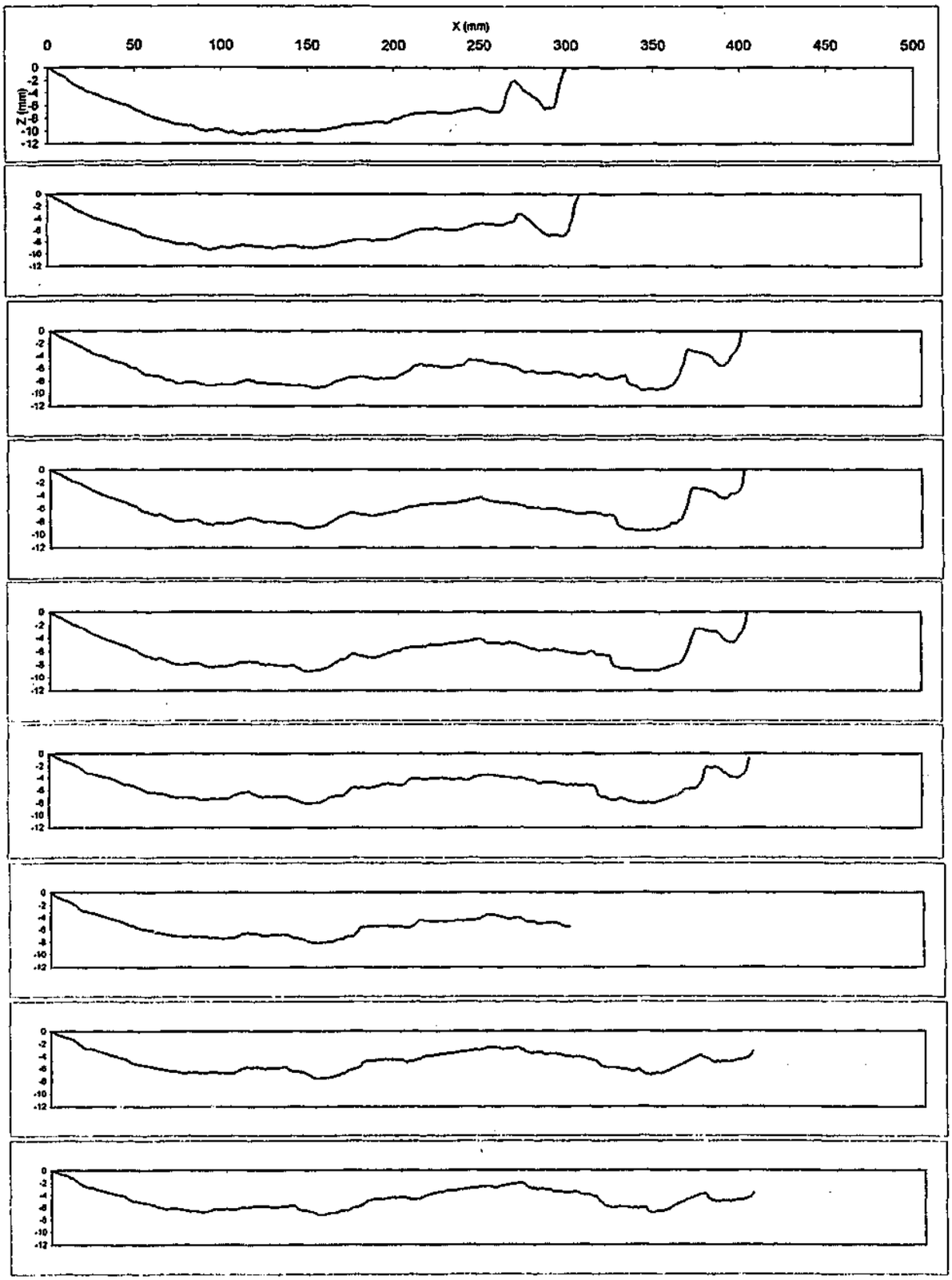

SILTSTONE SW, JOINT NEAR PERPENDICULAR TO BEDDING, PYRITE COATED

BLOCK 4 - scanned at 5mm intervals

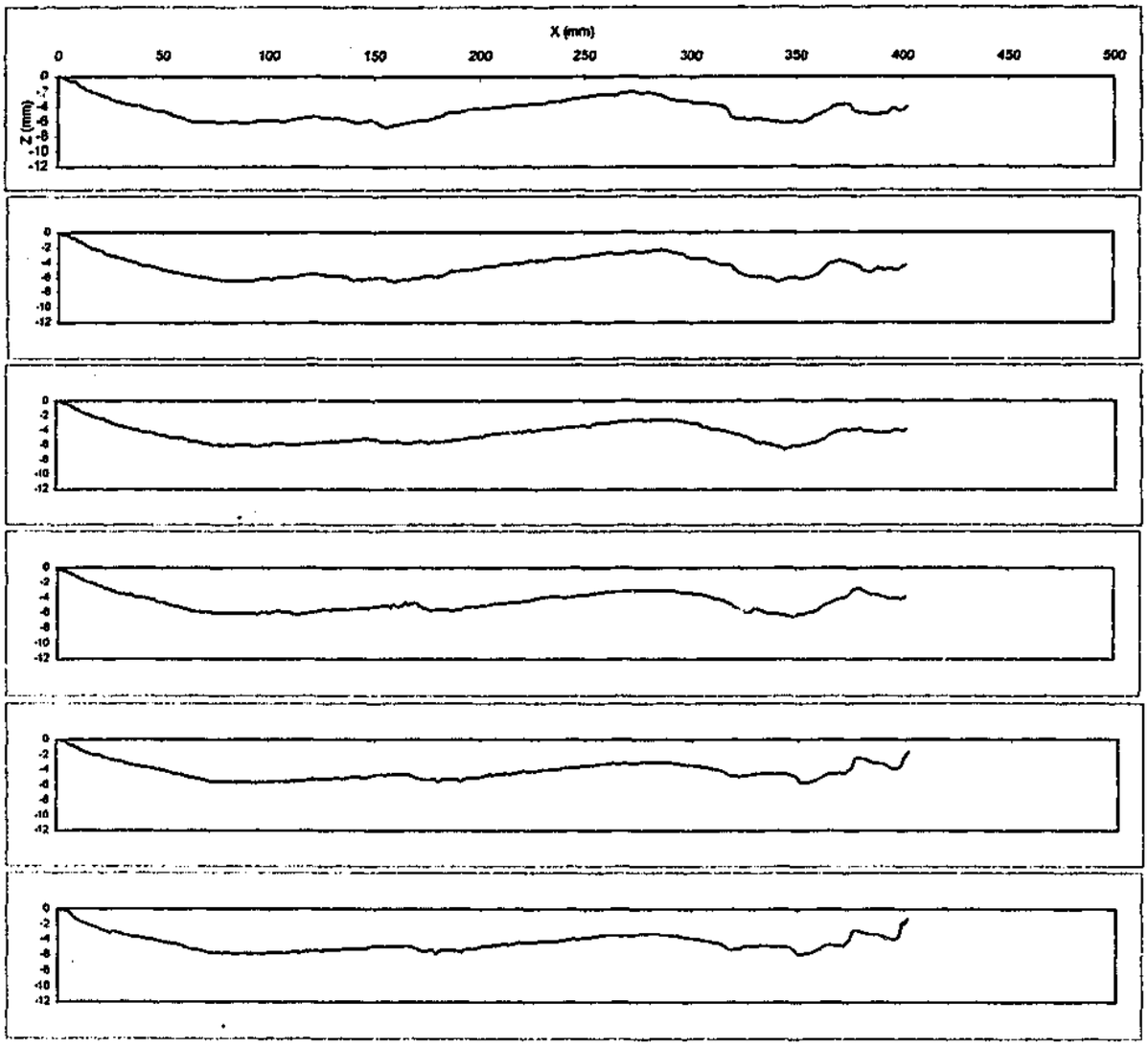

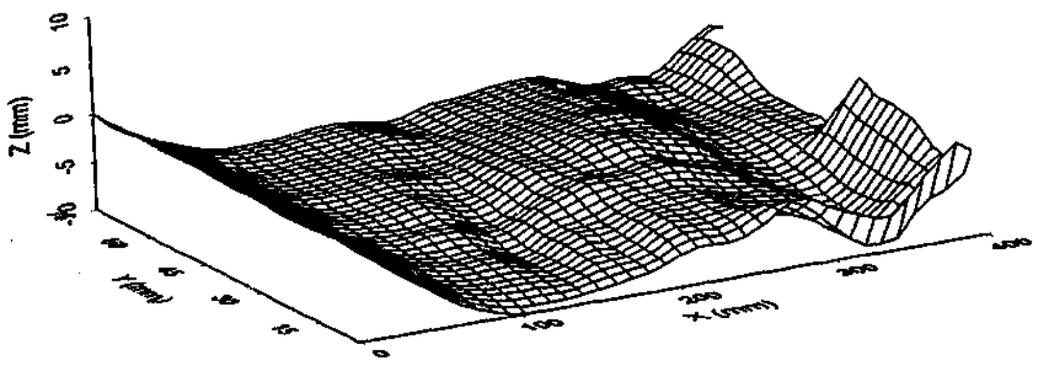

SILTSTONE SW, JOINT NEAR PERPENDICULAR TO BEDDING, PYRITE COATED

BLOCK 4 - scanned at 5mm intervals

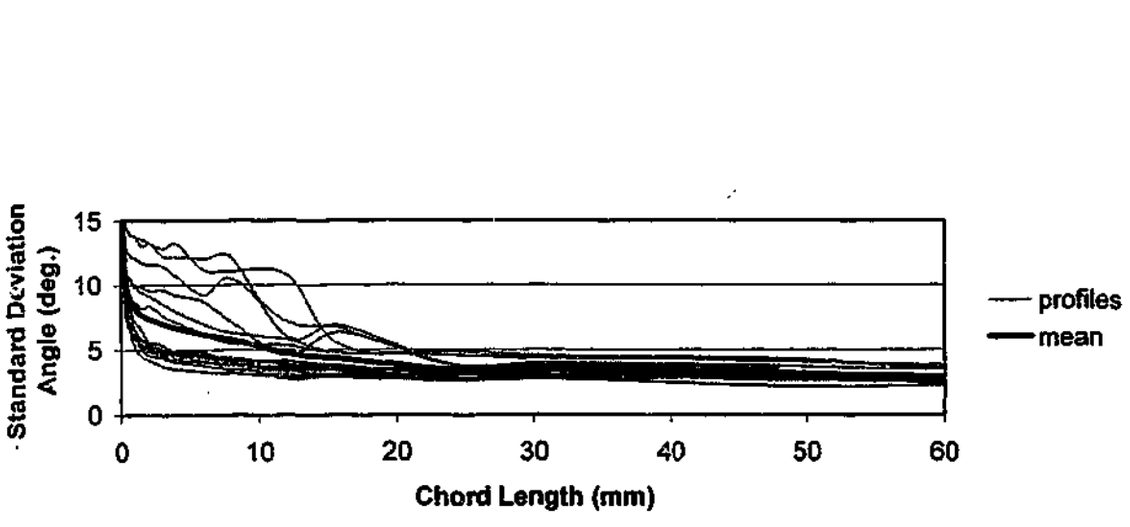

AVERAGE CORRELATION COEFFICIENT OF SCANS = 0.933

AVERAGE CORRELATION COEFFICIENT OF SCANS TO MEAN = 0.968

SILTSTONE SW, JOINT NEAR PERPENDICULAR TO BEDDING

BLOCK 4 - scanned at 5mm intervals

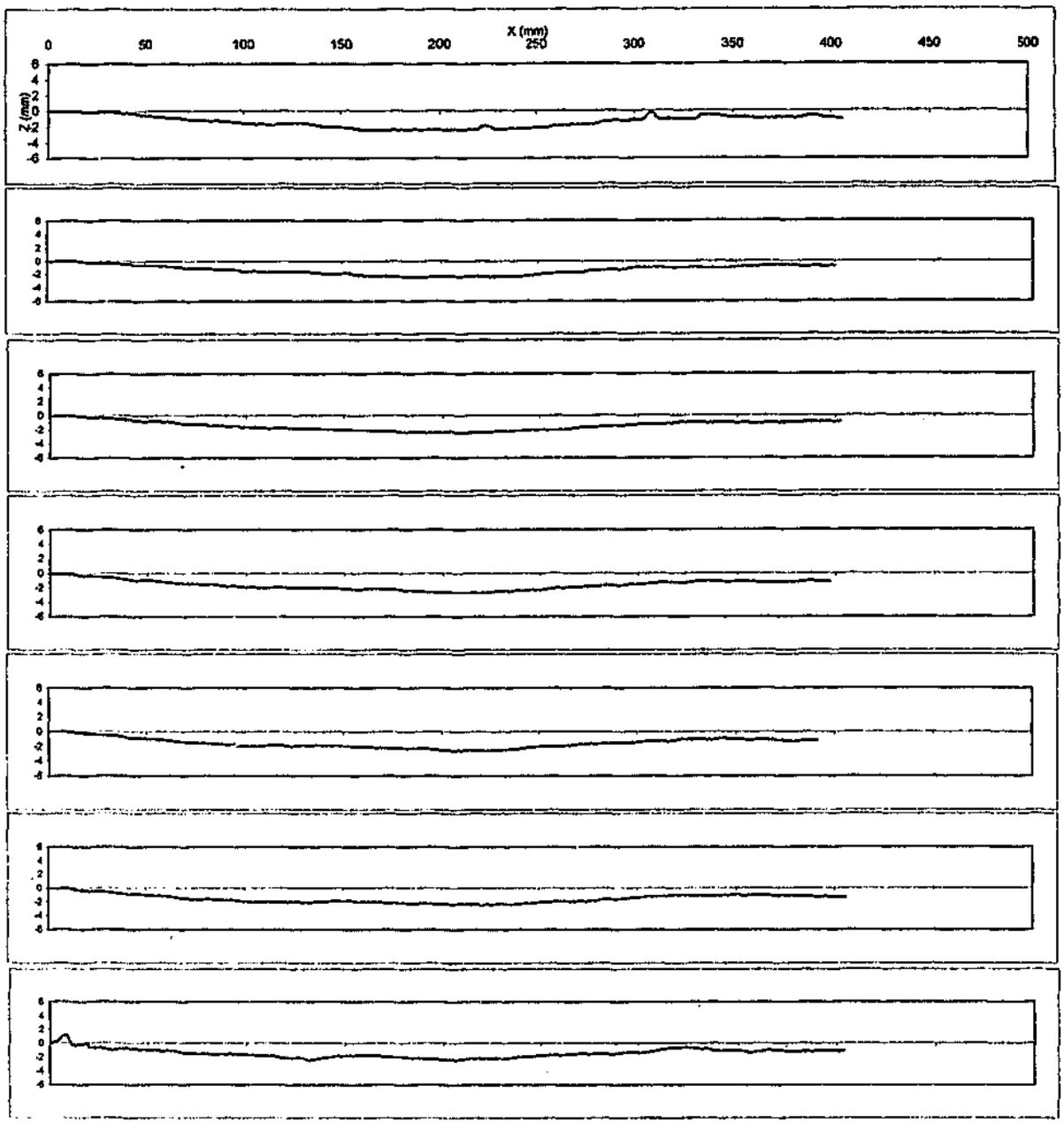

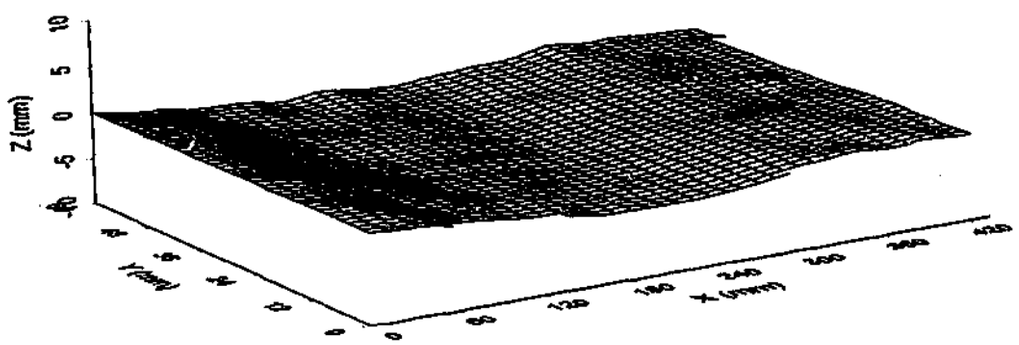

SILTSTONE SW, JOINT NEAR PERPENDICULAR TO BEDDING

BLOCK 5 - scanned at 10 mm intervals

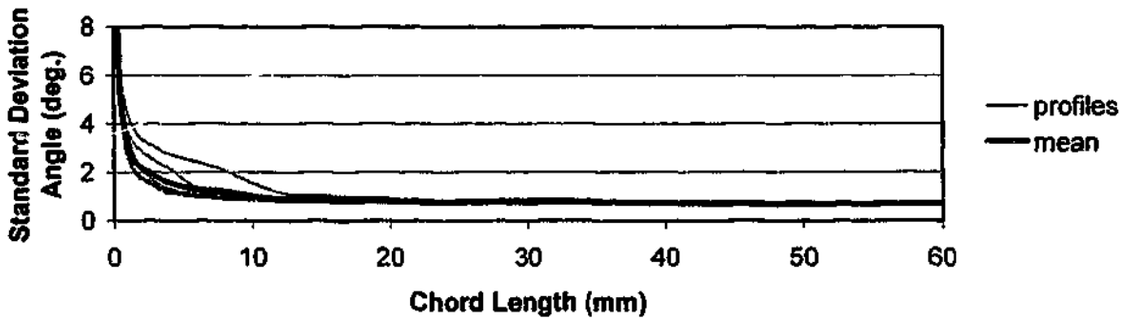

AVERAGE CORRELATION COEFFICIENT OF SCANS = 0.997

AVERAGE CORRELATION COEFFICIENT OF SCANS TO MEAN = 0.999

SILTSTONE SW, JOINT NEAR PERPENDICULAR TO BEDDING

BLOCK 5 - scanned at 10mm intervals

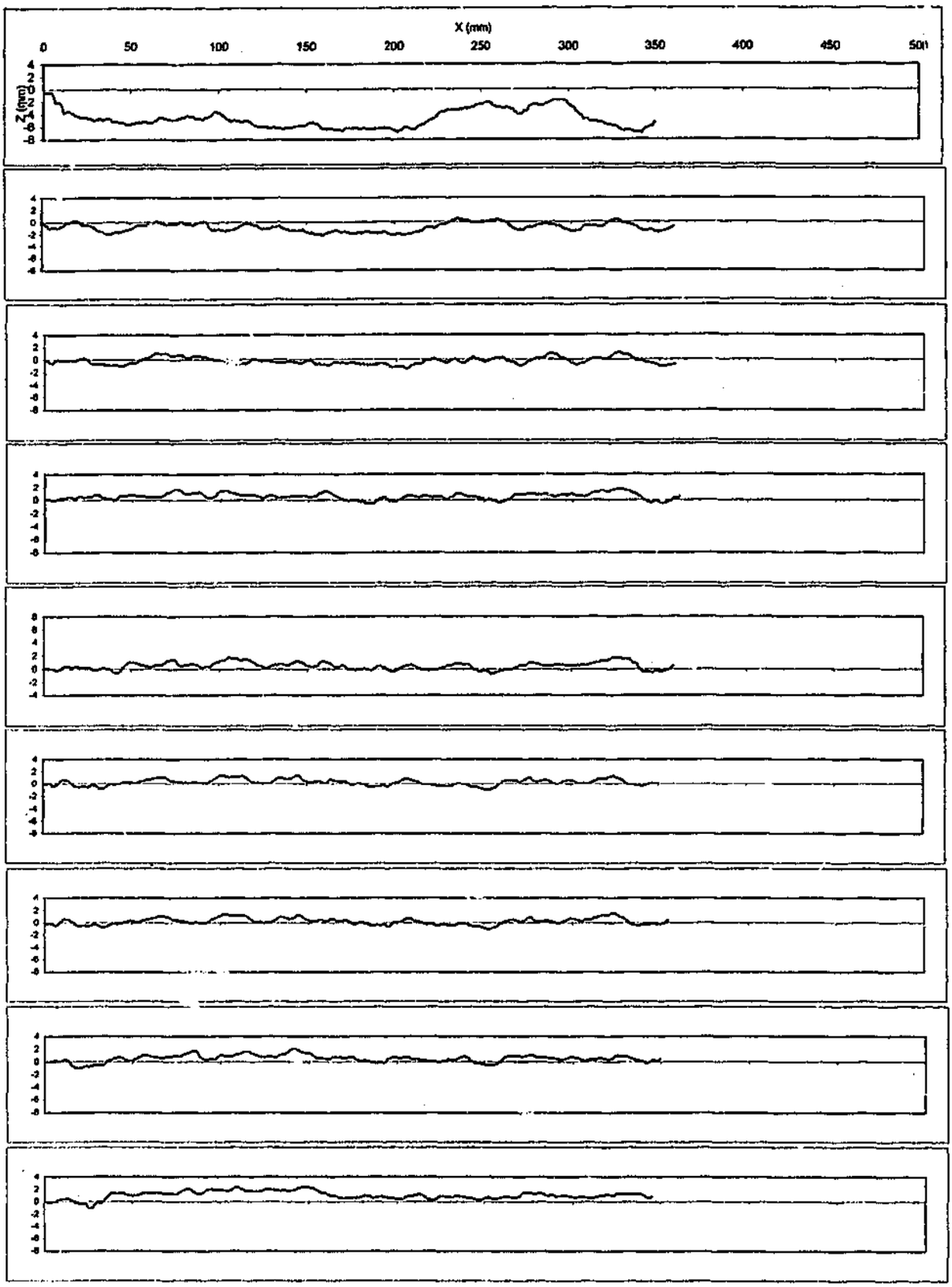

SILTSTONE SW, BEDDING JOINT

BLOCK 1, scanned at 5 mm intervals

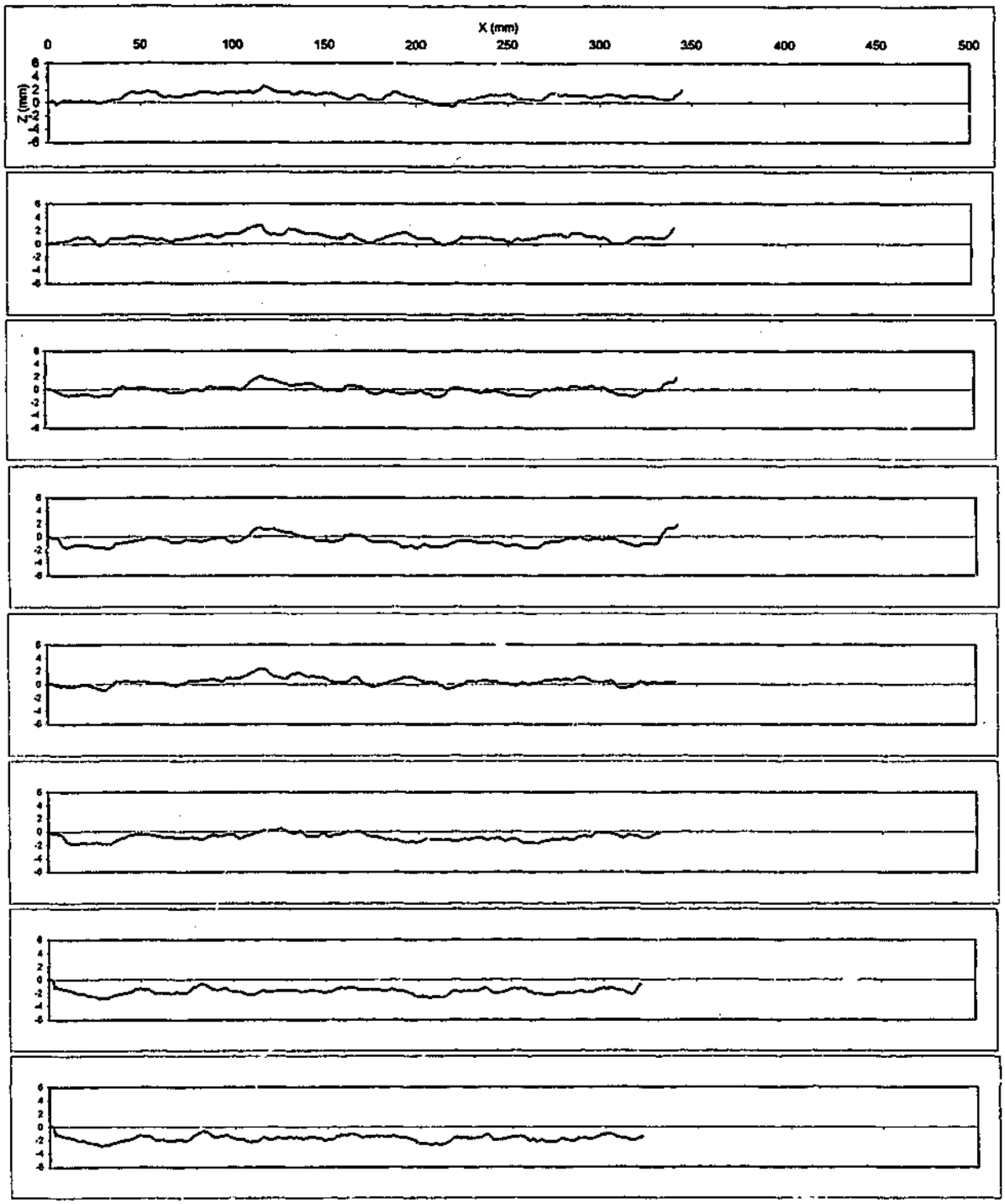

SILTSTONE SW, BEDDING JOINT

BLOCK 1, scanned at 5 mm intervals

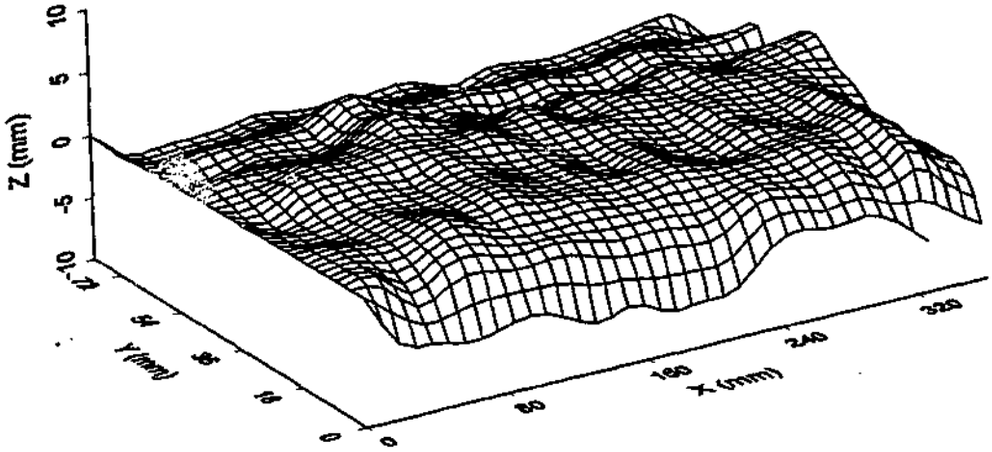

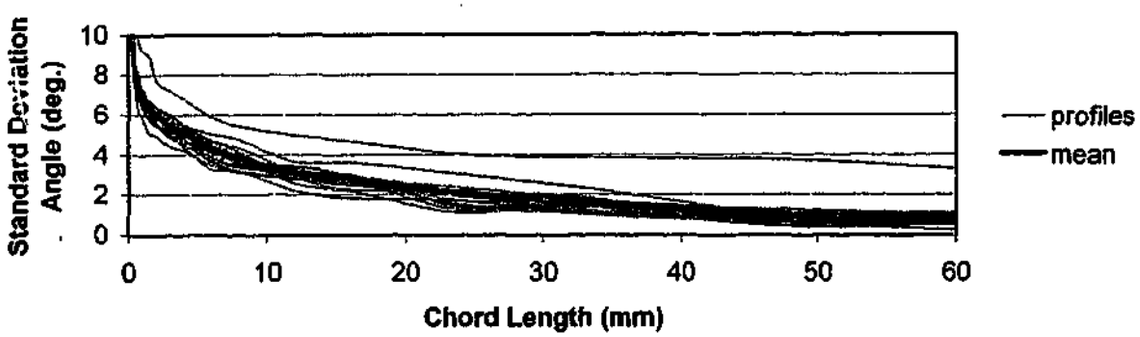

AVERAGE CORRELATION COEFFICIENT OF SCANS = 0.996

AVERAGE CORRELATION COEFFICIENT OF SCANS TO MEAN = 0.998

SILTSTONE SW, BEDDING JOINT

BLOCK 1, scanned at 5 mm intervals

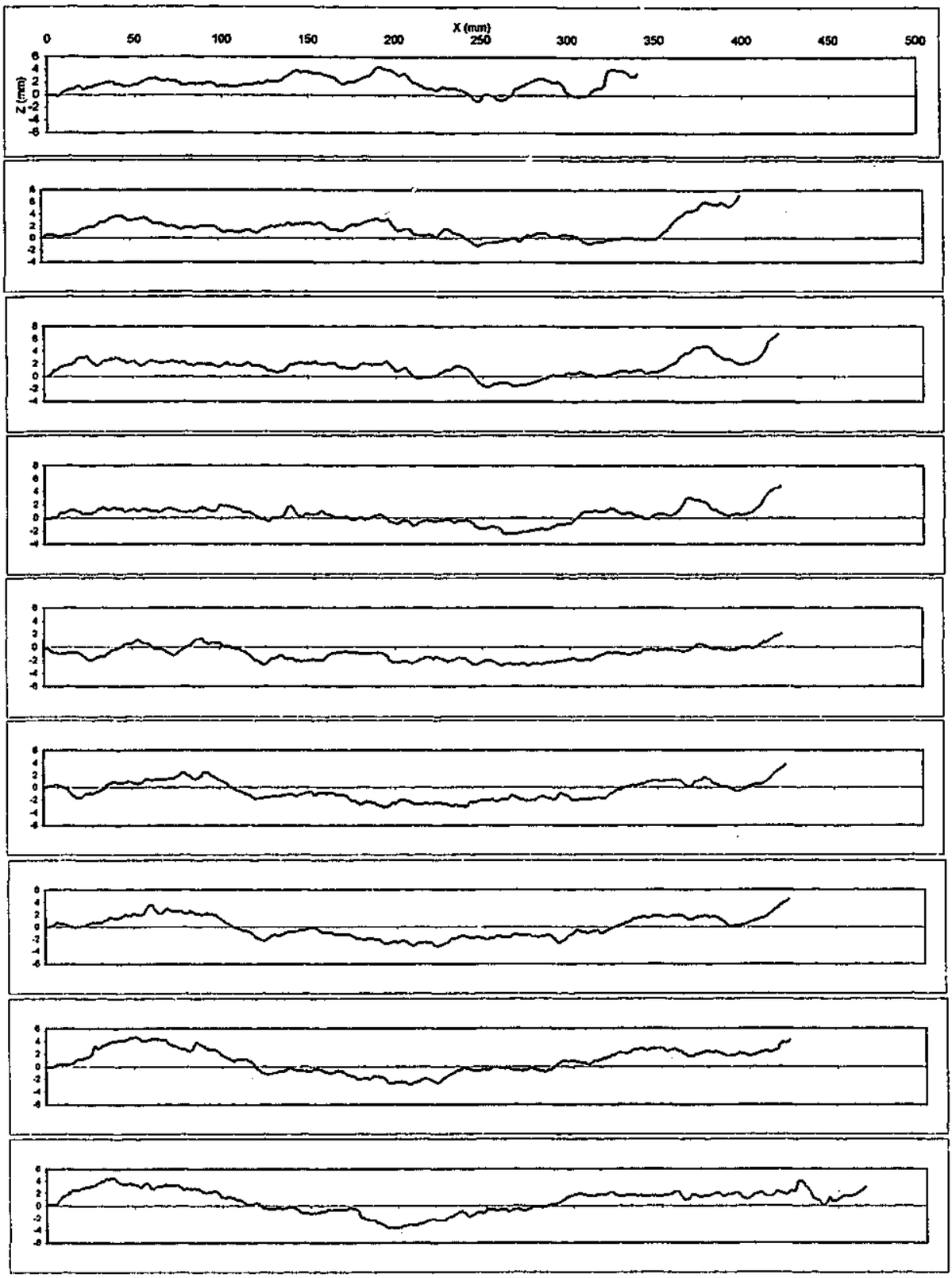

SILTSTONE SW, BEDDING JOINT

BLOCK 2, scanned at 10 mm intervals

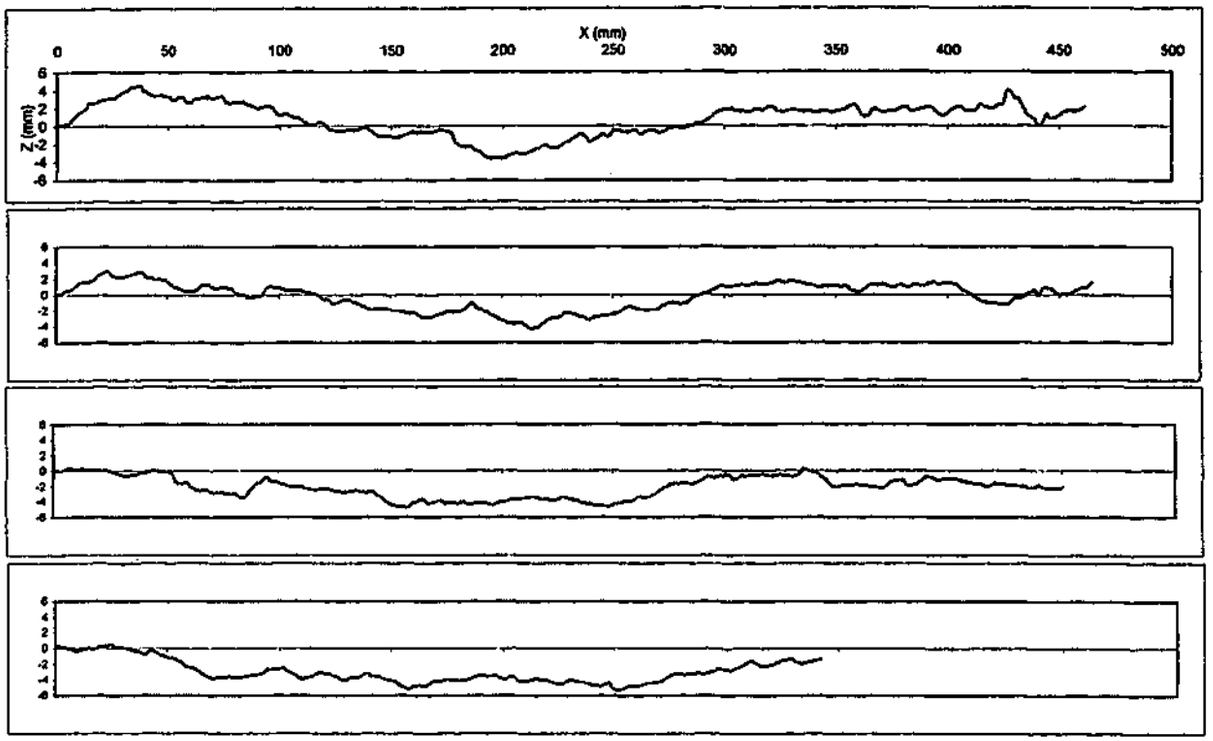

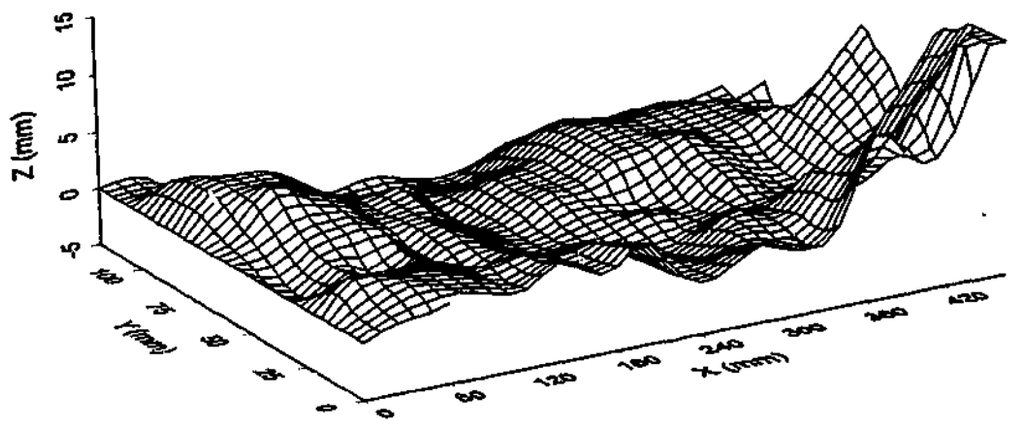

SILTSTONE SW, BEDDING JOINT

BLOCK 2, scanned at 10 mm intervals

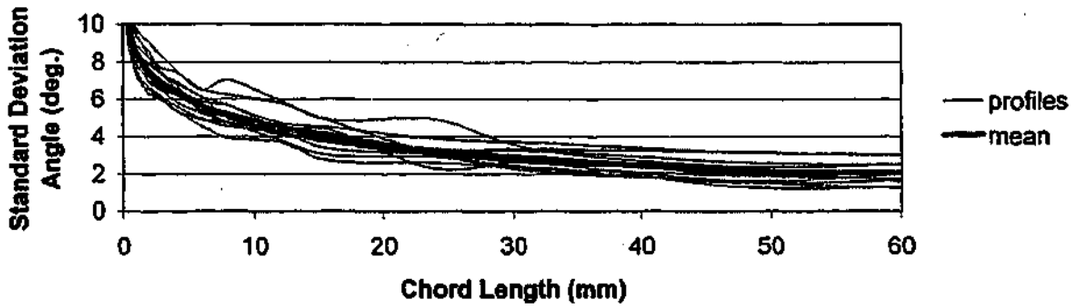

AVERAGE CORRELATION COEFFICIENT OF SCANS = 0.994

AVERAGE CORRELATION COEFFICIENT OF SCANS TO MEAN = 0.997

SILTSTONE SW, BEDDING JOINT

BLOCK 2, scanned at 10mm intervals

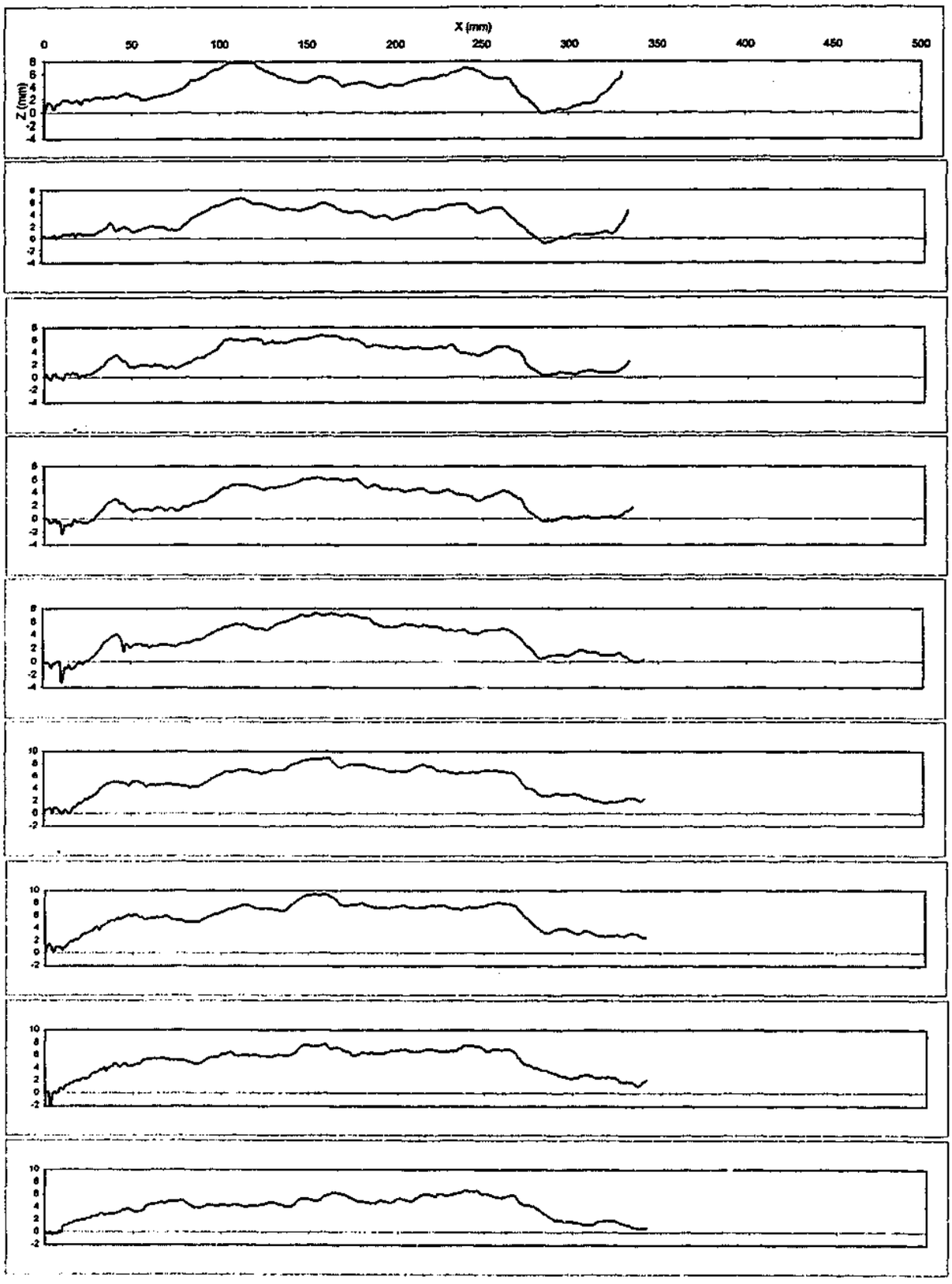

SILTSTONE SW, BEDDING JOINT, with limonite staining

BLOCK 3, scanned at 5 mm intervals

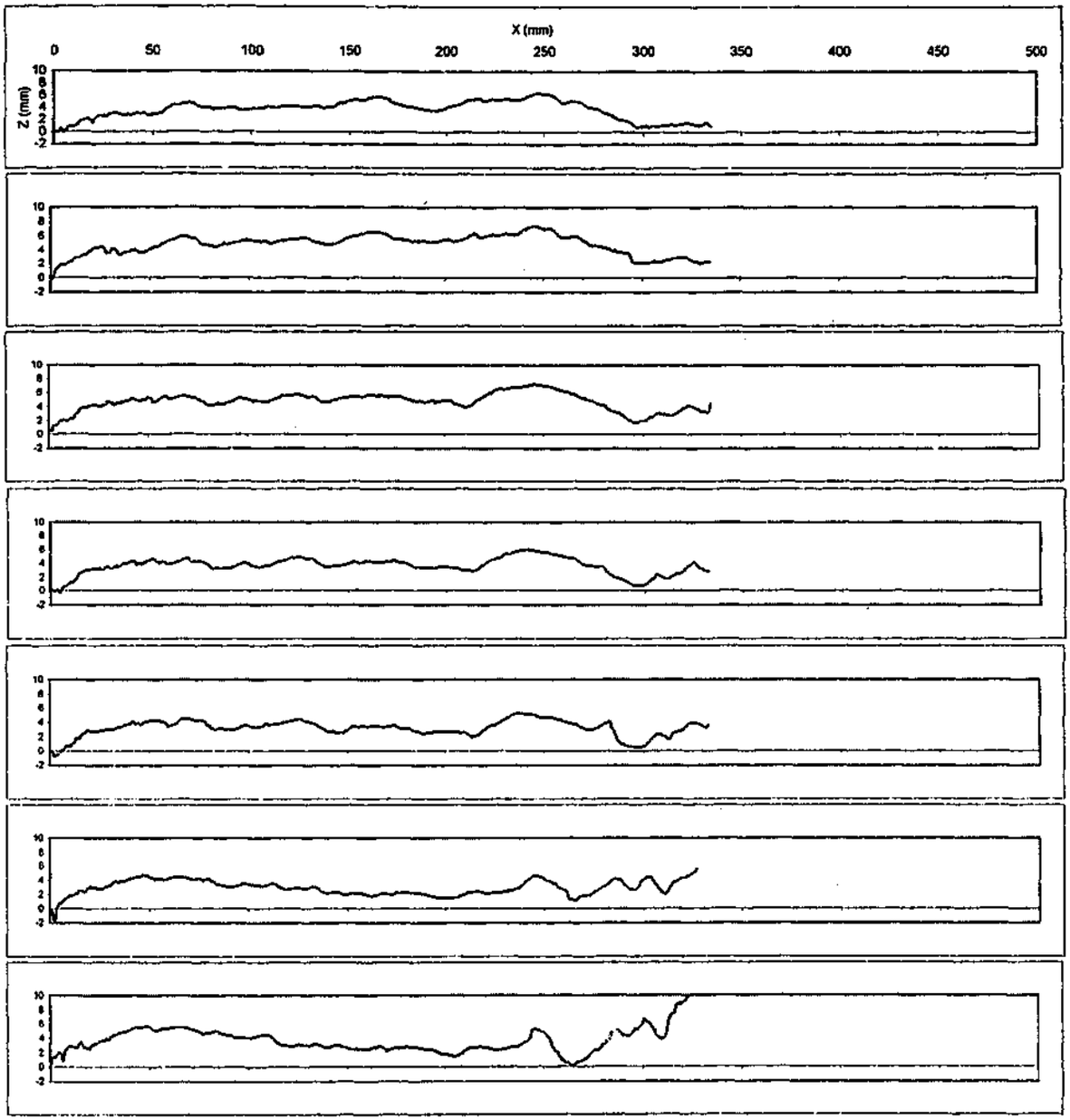

SILTSTONE SW, BEDDING JOINT, with limonite staining

BLOCK 3, scanned at 5 mm intervals

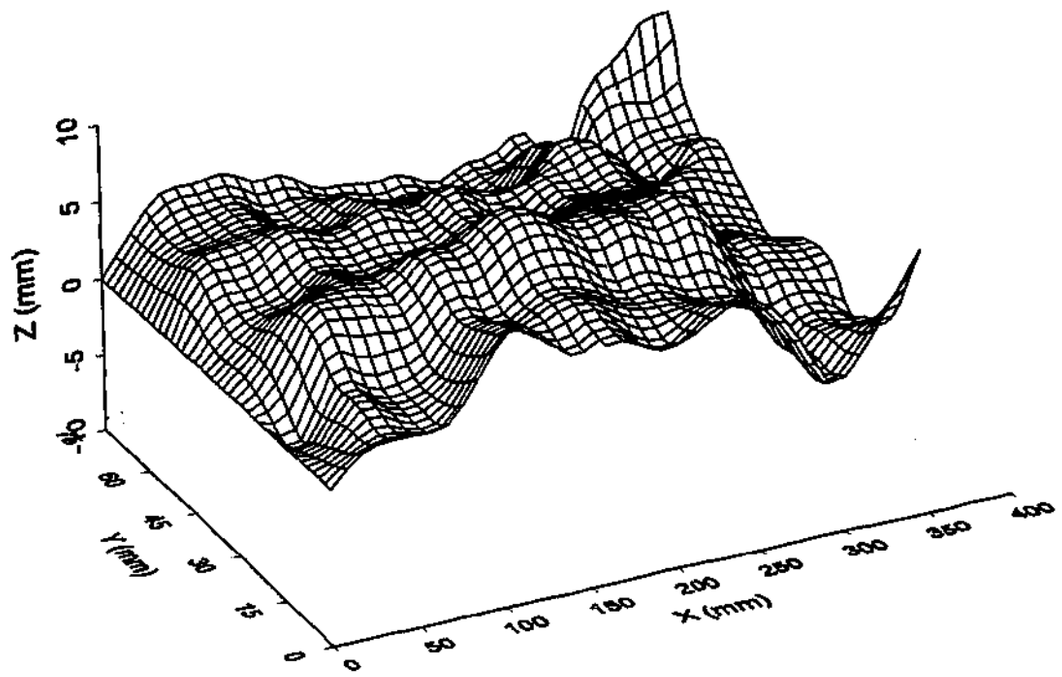

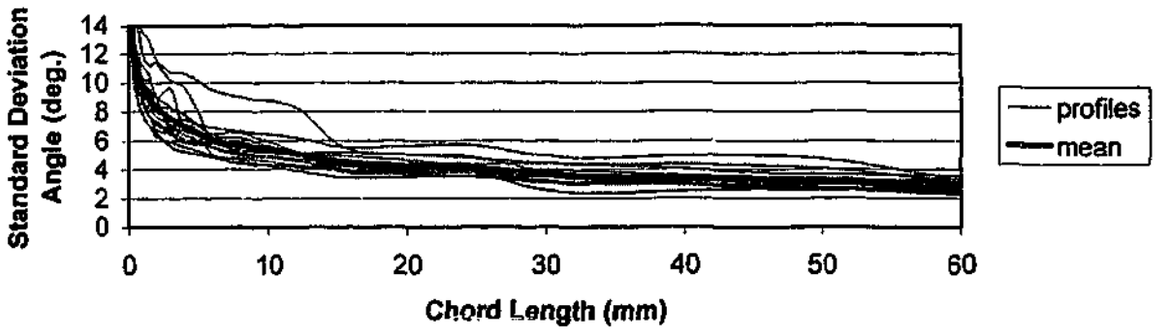

AVERAGE CORRELATION COEFFICIENT OF SCANS = 0.989

AVERAGE CORRELATION COEFFICIENT OF SCANS TO MEAN = 0.994

SILTSTONE SW, BEDDING JOINT, with limonite staining

BLOCK 3, scanned at 5 mm intervals

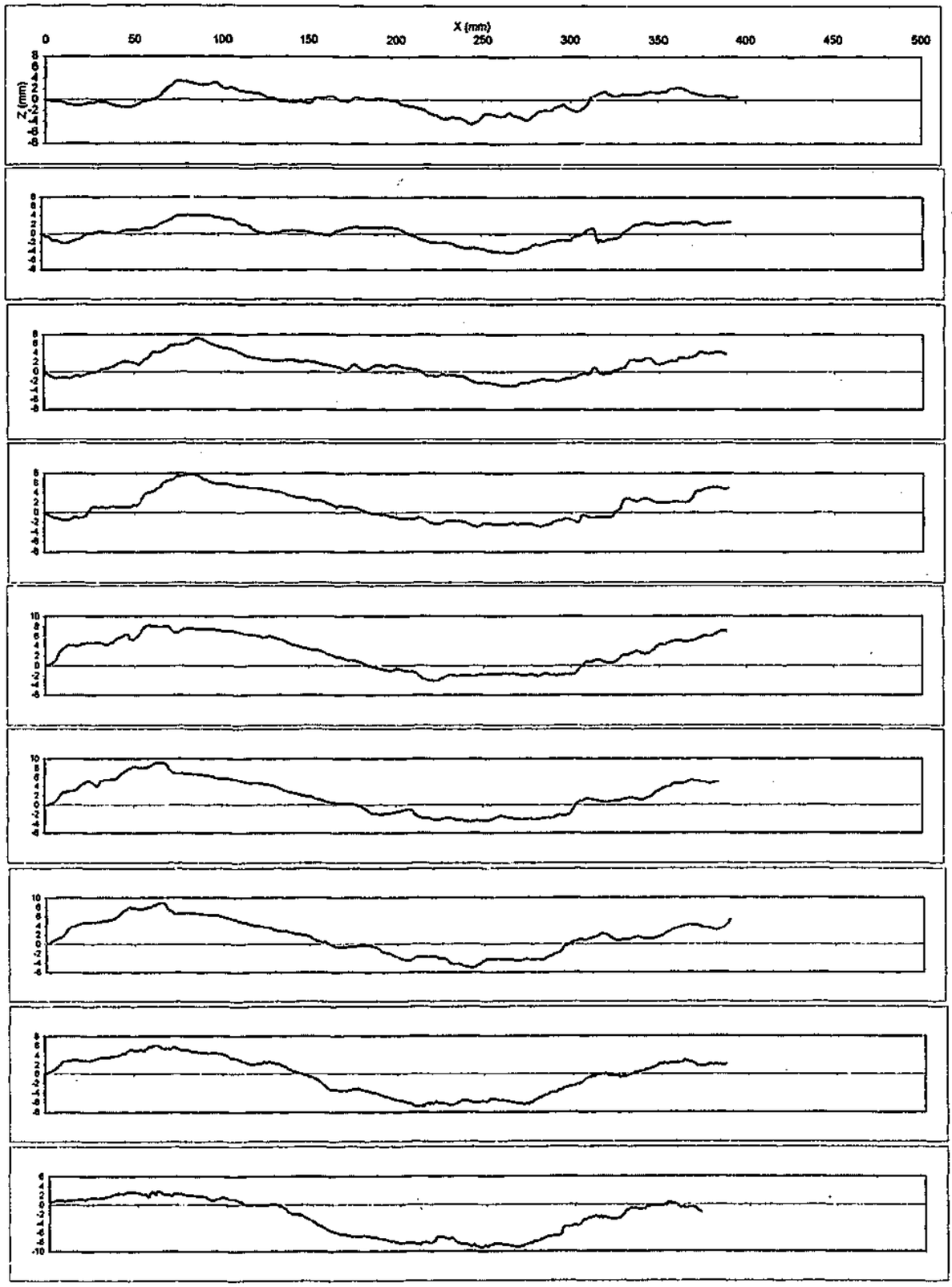

SILTSTONE SW, BEDDING JOINT, trace pyrite and carbonaceous coating

BLOCK 5 - scanned at 10mm intervals

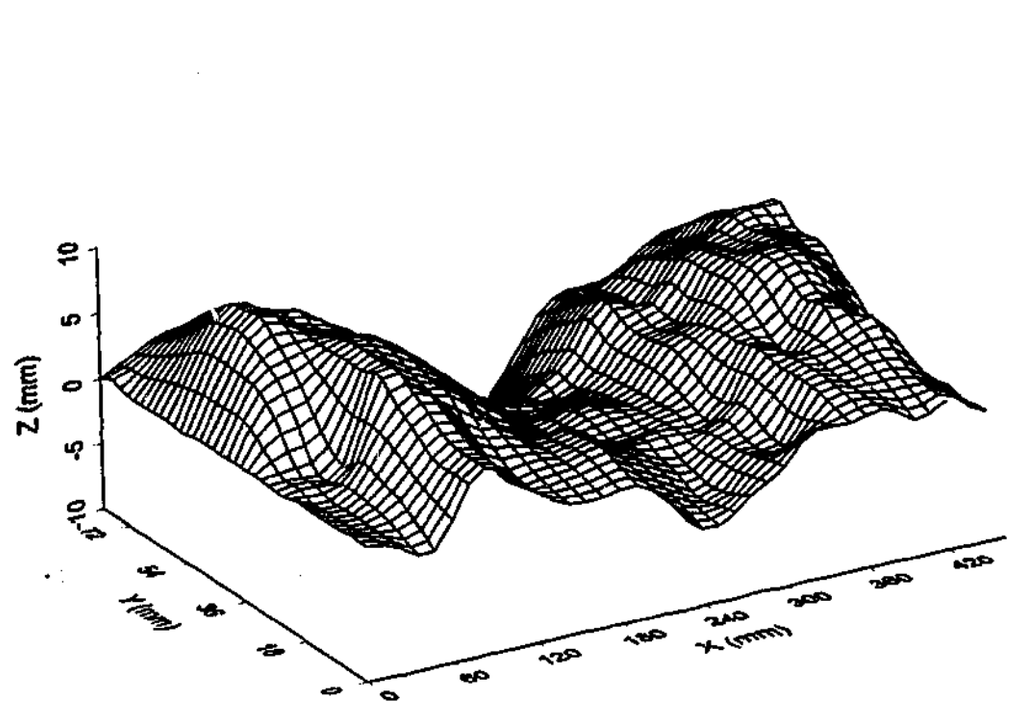

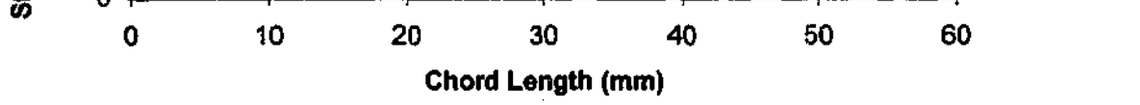

AVERAGE CORRELATION COEFFICIENT OF SCANS = 0.990

AVERAGE CORRELATION COEFFICIENT OF SCANS TO MEAN = 0.995

SILTSTONE SW, BEDDING JOINT, trace pyrite and carbonaceous coating

BLOCK 5 - scanned at 10mm intervals

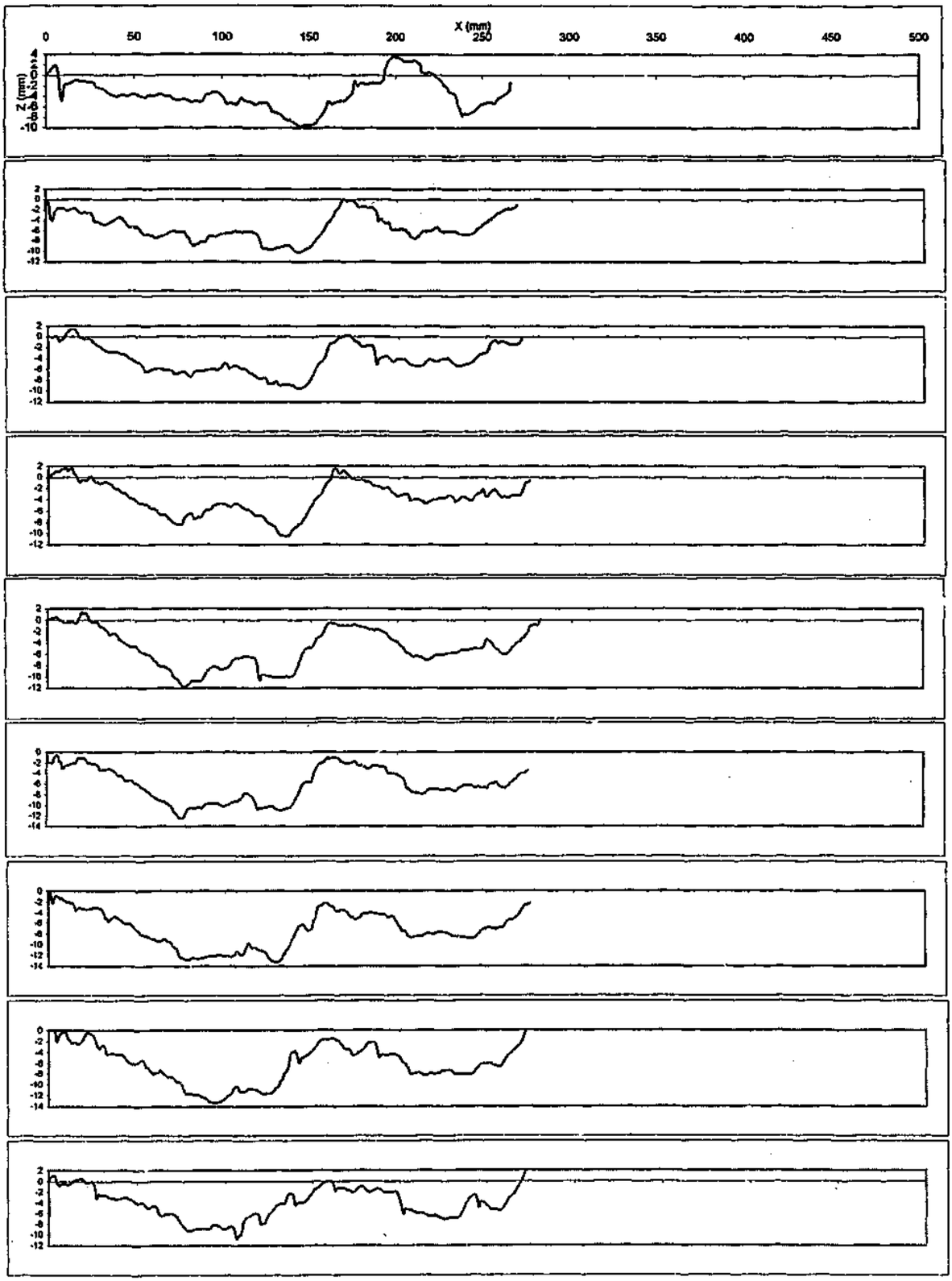

BASALT MW, JOINT, thick vesicular carbonaceous coating

BLOCK 1, scanned at 10 mm intervals

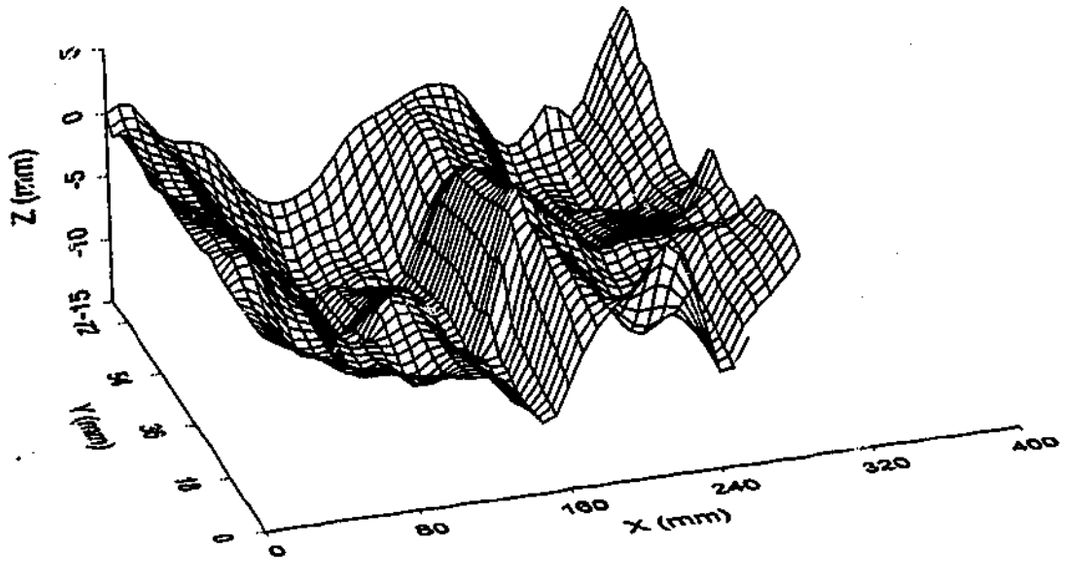

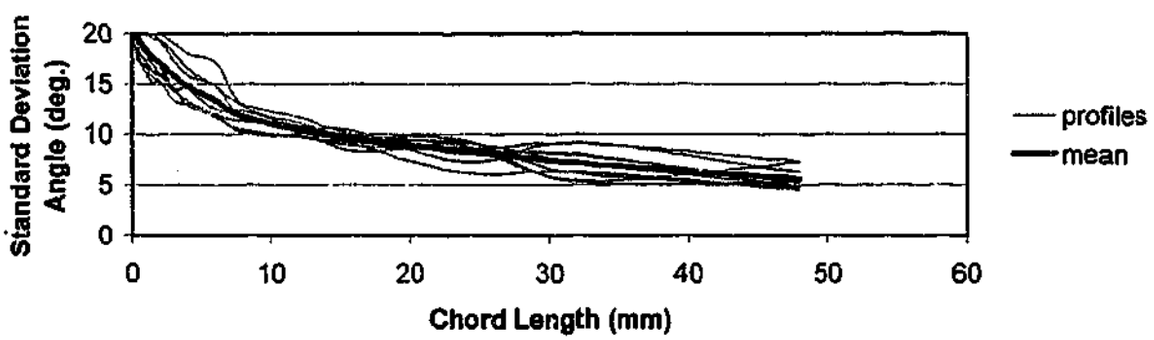

AVERAGE CORRELATION COEFFICIENT OF SCANS = 0.989

AVERAGE CORRELATION COEFFICIENT OF SCANS TO MEAN = 0.995

BASALT MW, JOINT, thick vesicular carbonaceous coating

BLOCK 1, scanned at 10 mm intervals

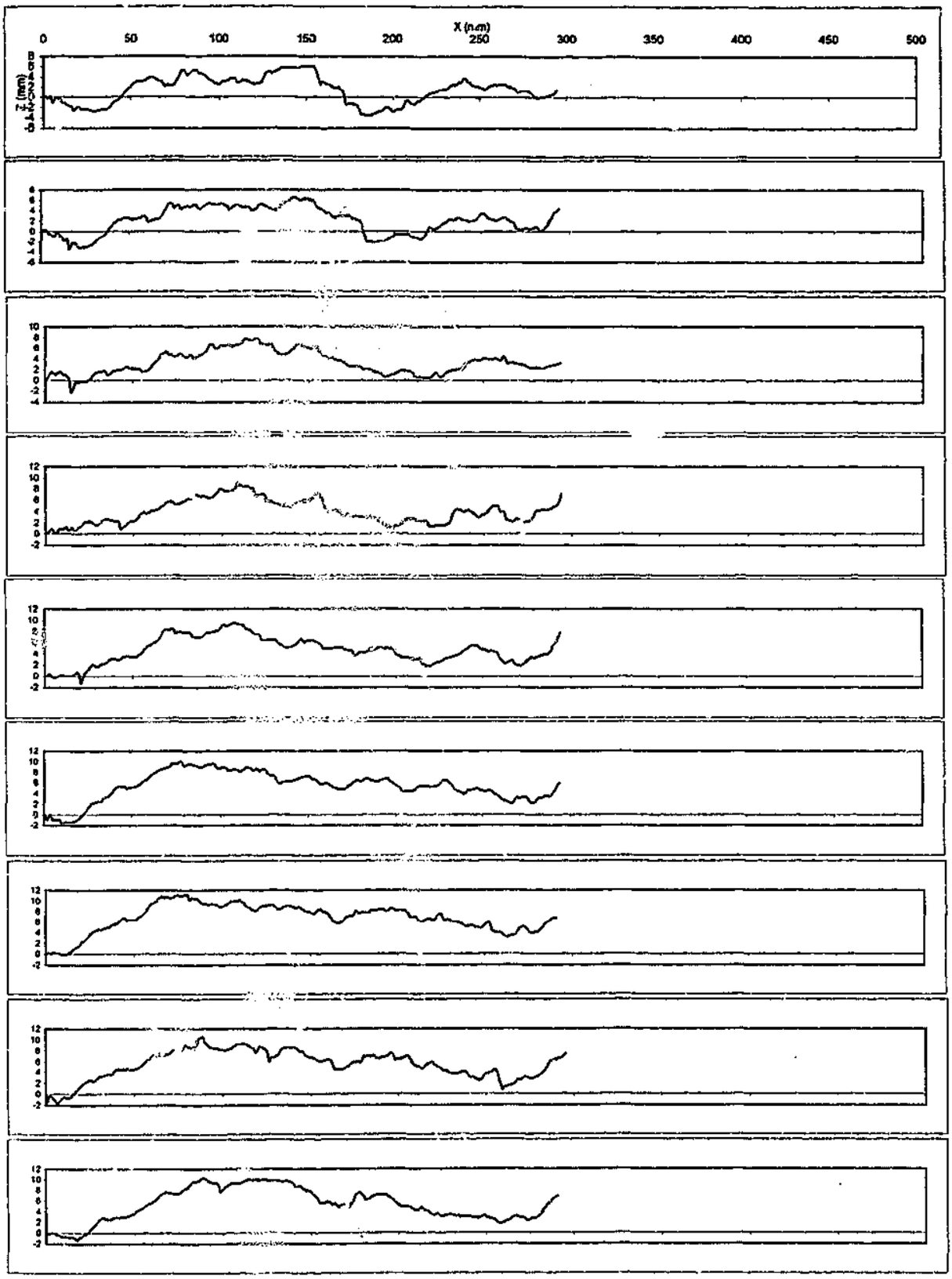

BASALT MW, JOINT, thick vesicular carbonaceous coating

BLOCK 1a, scanned at 10 mm intervals

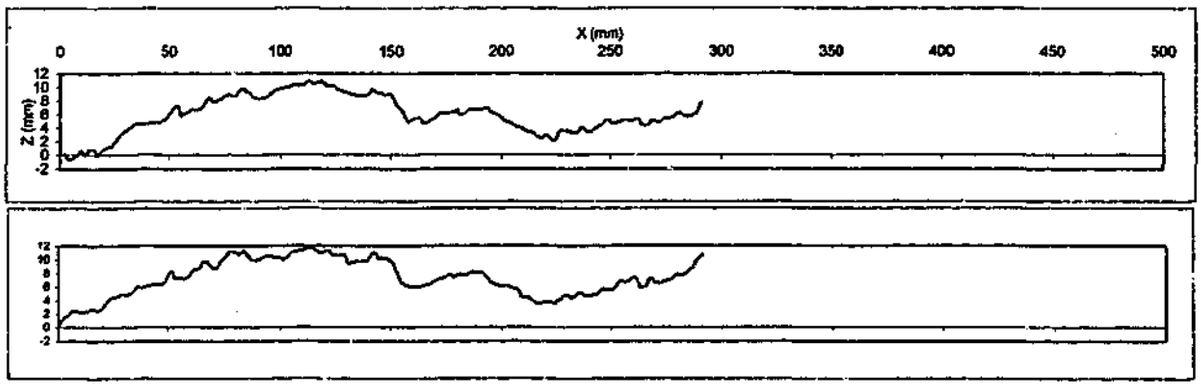

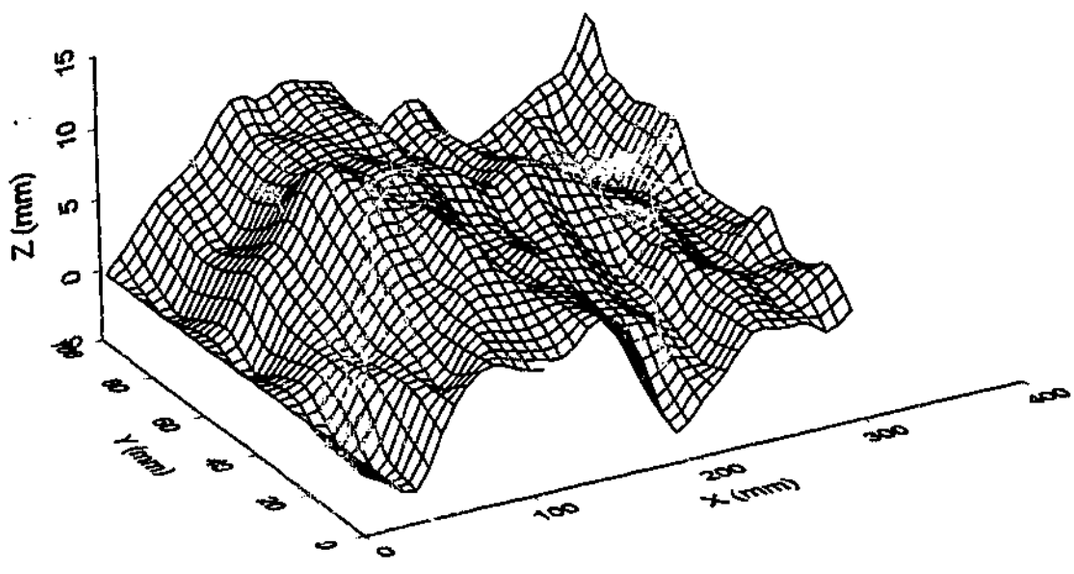

BASALT MW, JOINT, thick carbonaceous coating

BLOCK 1a, scanned at 10 mm intervals

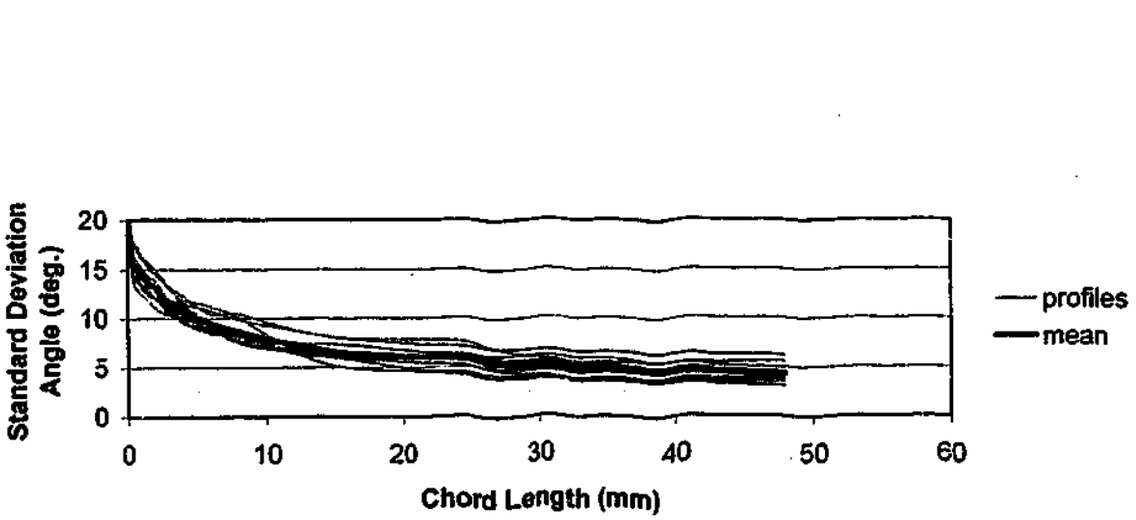

AVERAGE CORRELATION COEFFICIENT OF SCANS = 0.992

AVERAGE CORRELATION COEFFICIENT OF SCANS TO MEAN = 0.996

BASALT MW, JOINT, thick vesicular carbonaceous coating

BLOCK 1a - scanned at 10mm intervals

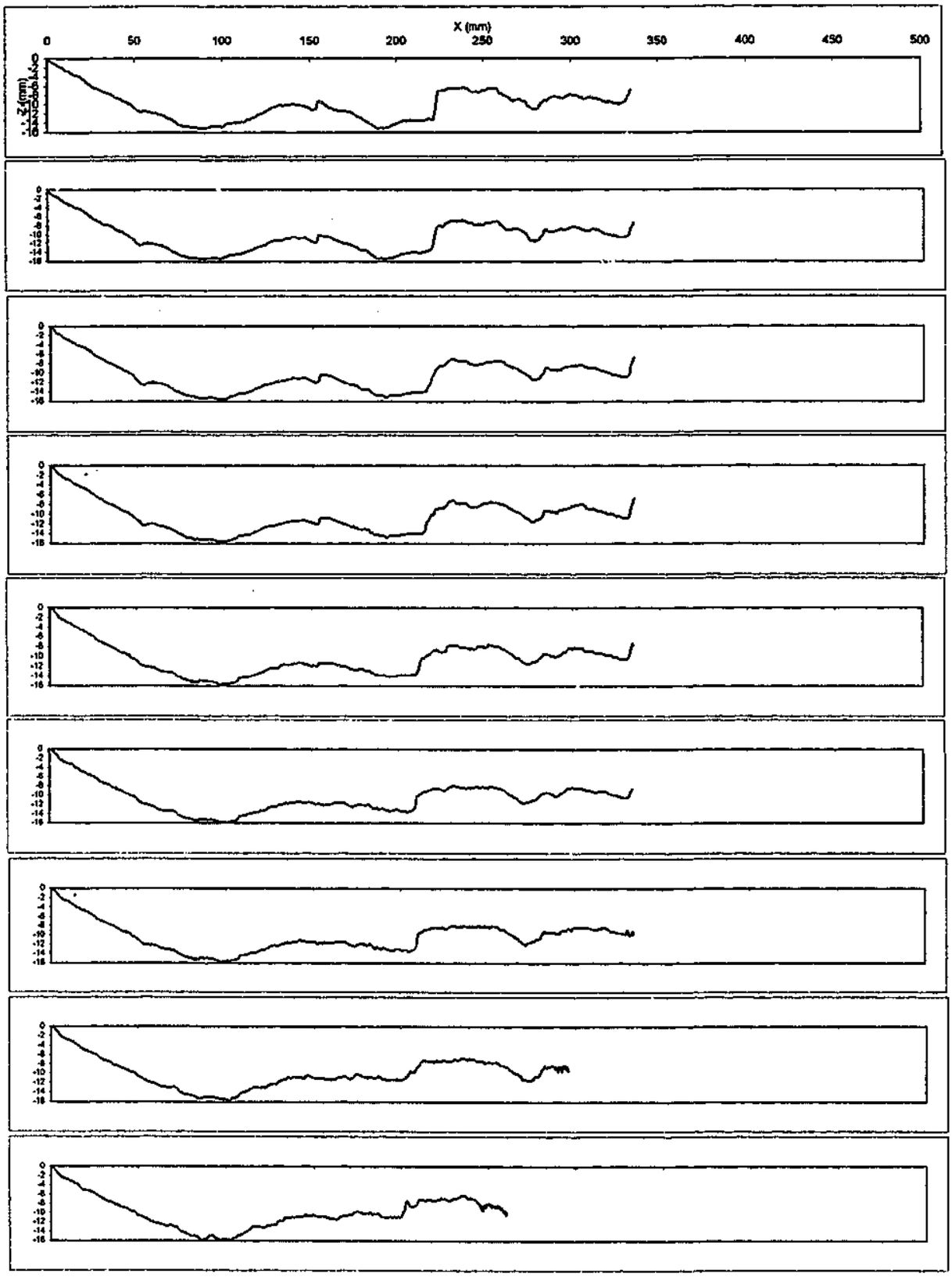

BASALT SW, JOINT, slight carbonaceous coating

BLOCK 2, scanned at 5 mm intervals

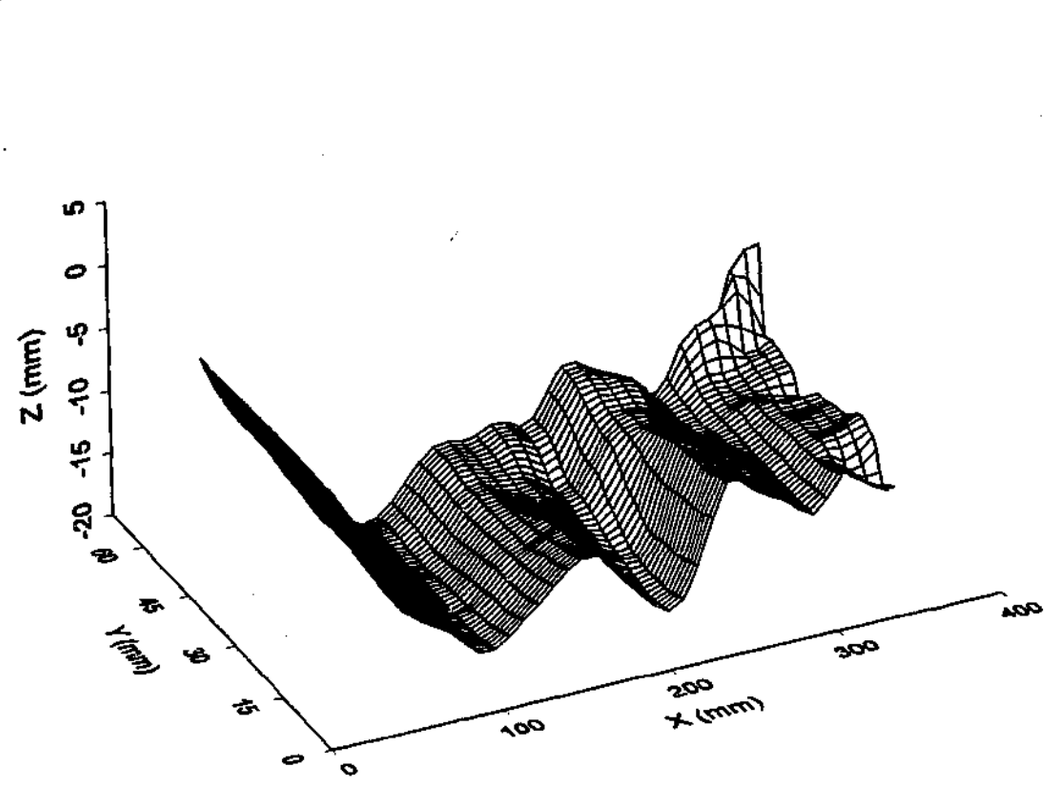

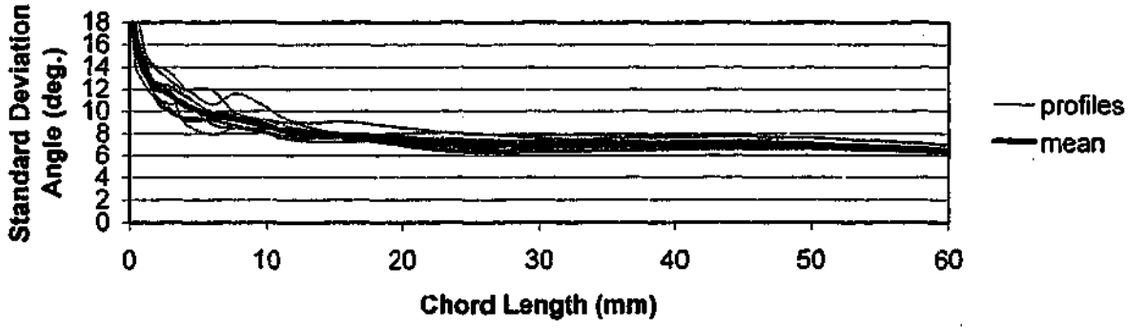

AVERAGE CORRELATION COEFFICIENT OF SCANS = 0.988

AVERAGE CORRELATION COEFFICIENT OF SCANS TO MEAN = 0.994

BASALT SW, JOINT, slight carbonaceous coating

BLOCK 2, scanned at 5 mm intervals

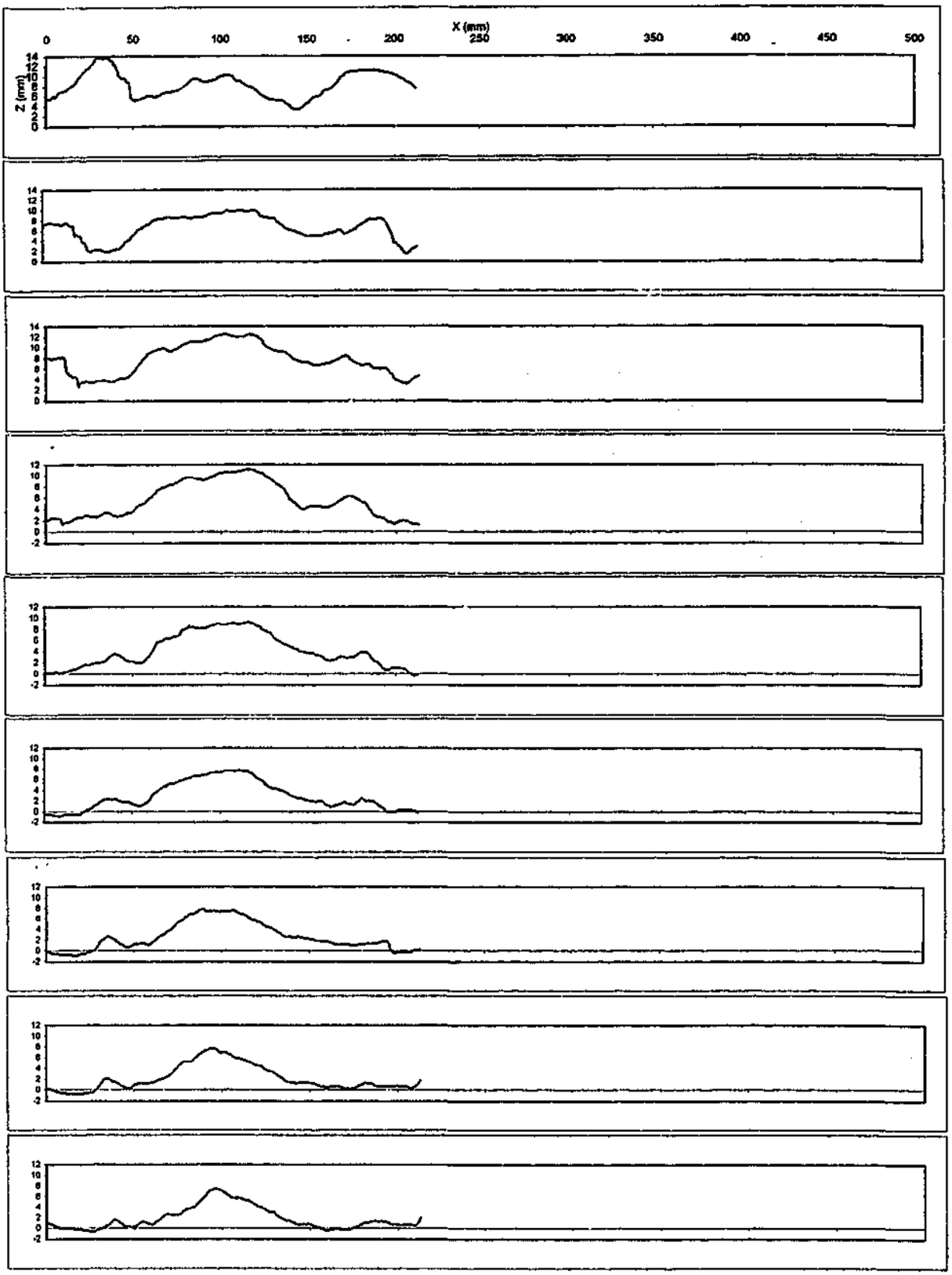

BASALT SW, JOINT, limonate stained

BLOCK 3, scanned at 10 mm intervals

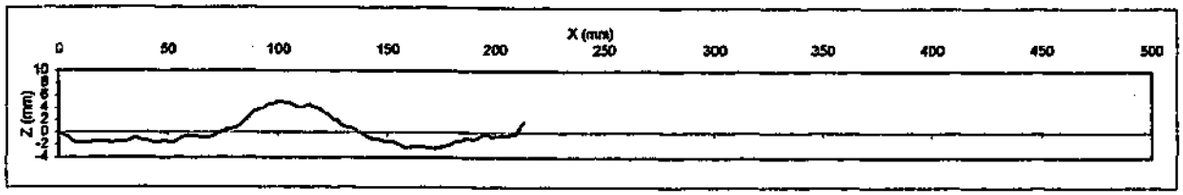

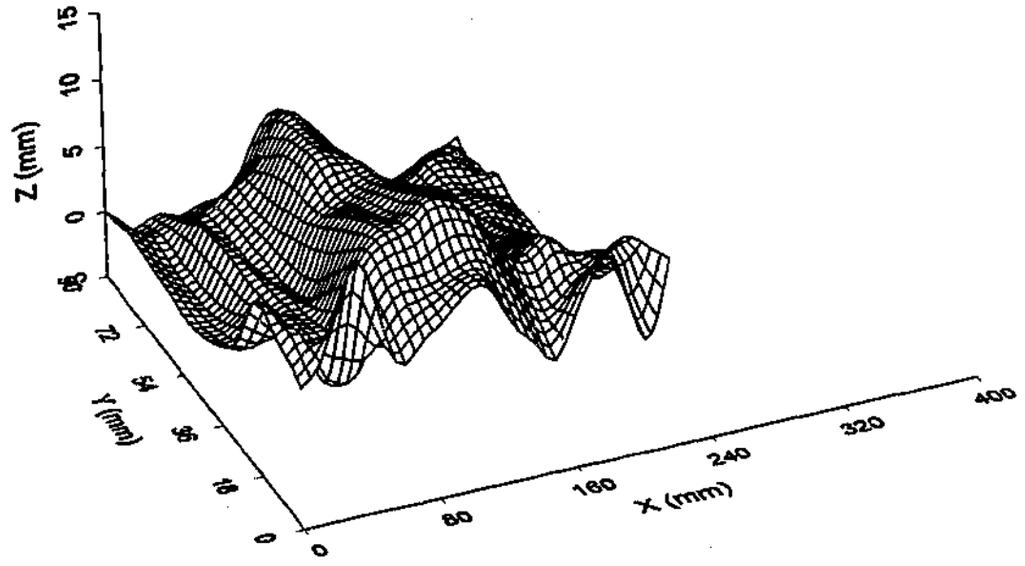

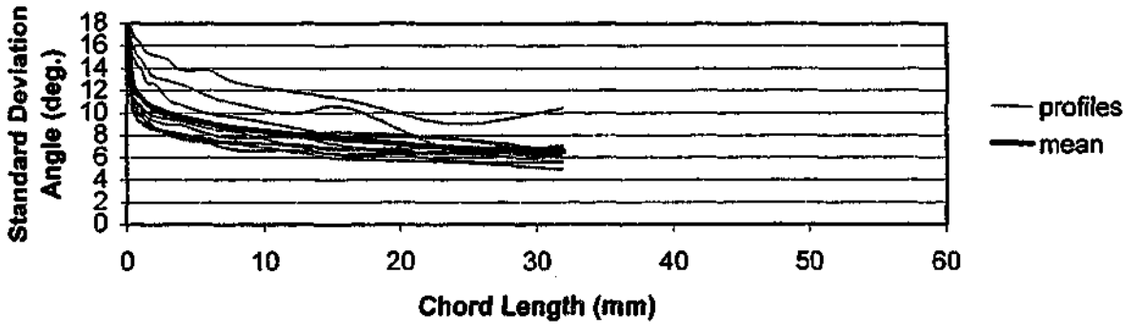

AVERAGE CORRELATION COEFFICIENT OF SCANS = 0.978

AVERAGE CORRELATION COEFFICIENT OF SCANS TO MEAN = 0.990

BASALT SW, JOINT, limonate stained

BLOCK 3, scanned at 10 mm intervals

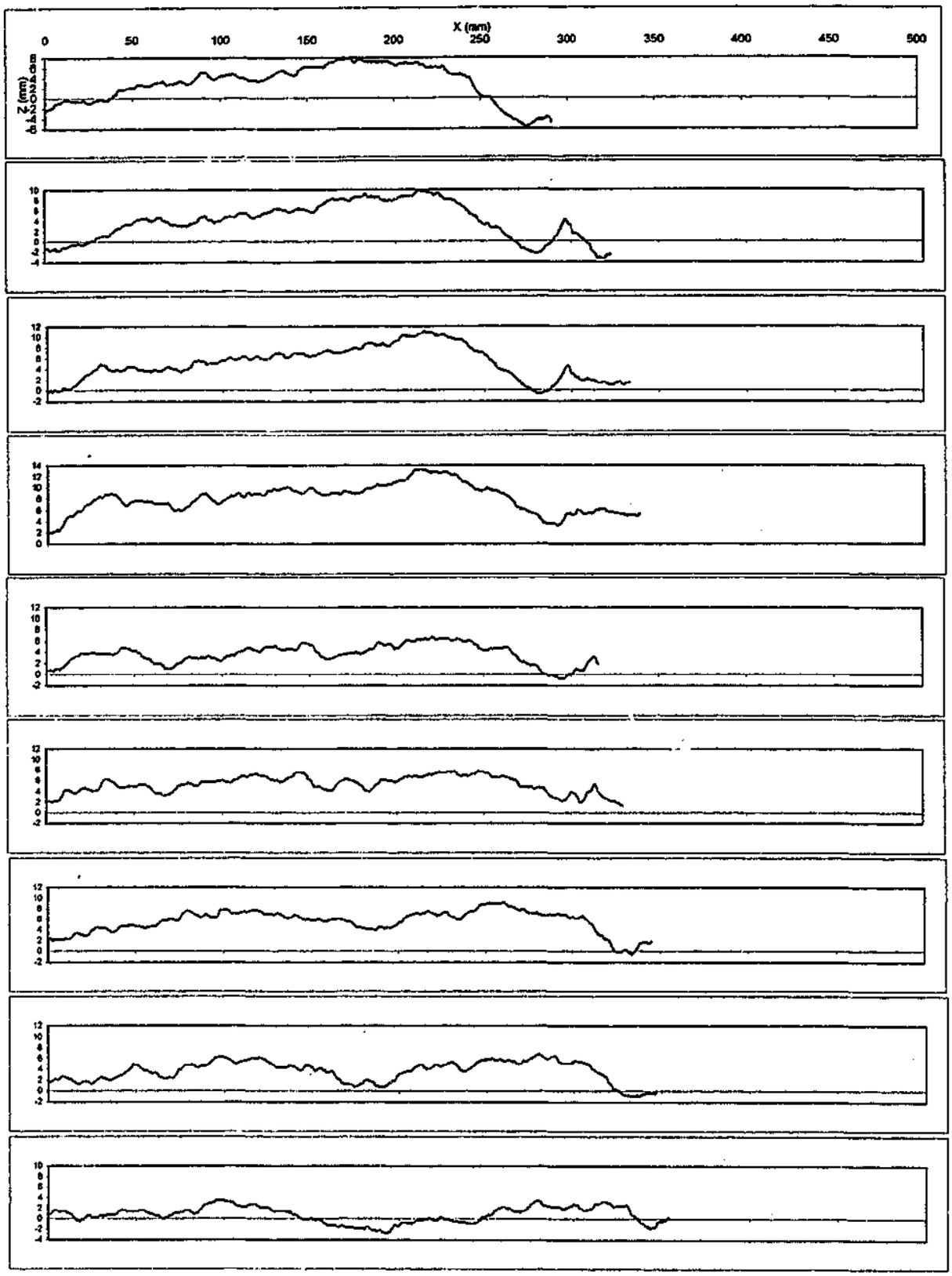

BASALT MW, JOINT, slight carbonaceous coating

BLOCK 4, scanned at 10 mm intervals

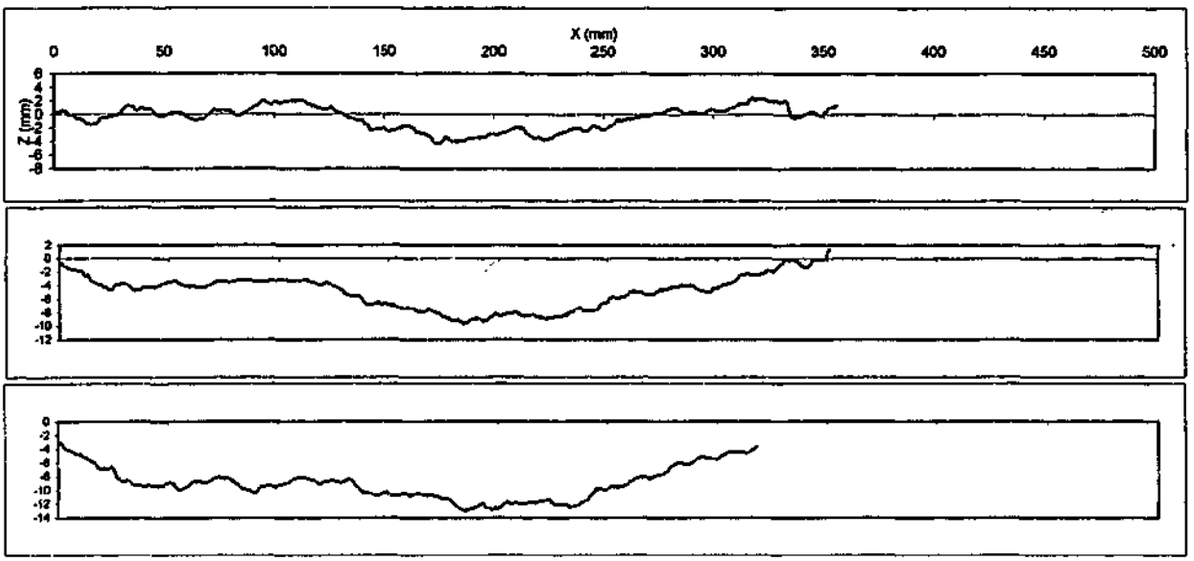

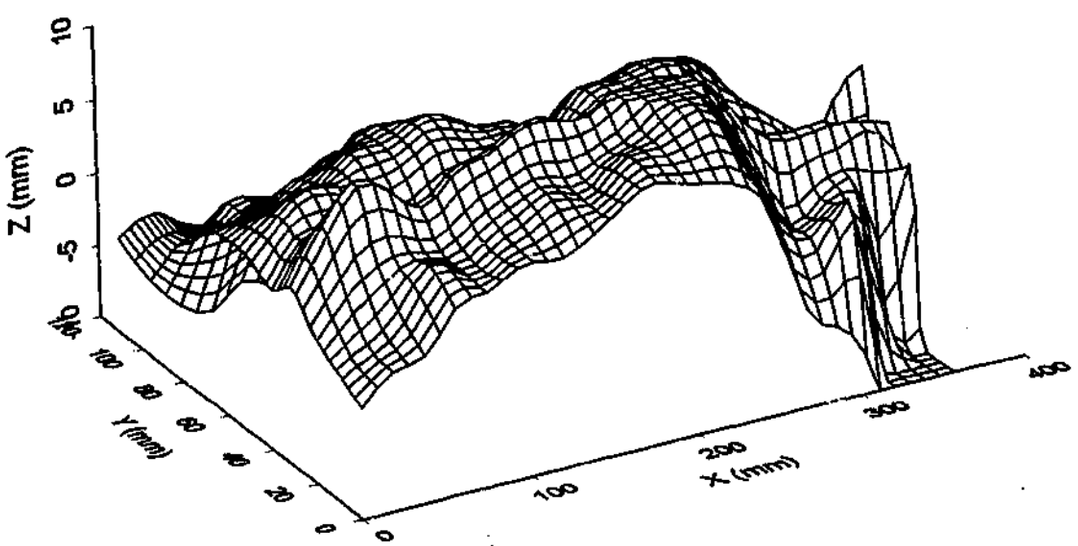

BASALT MW, JOINT, slight carbonaceous coating

BLOCK 4, scanned at 10 mm intervals

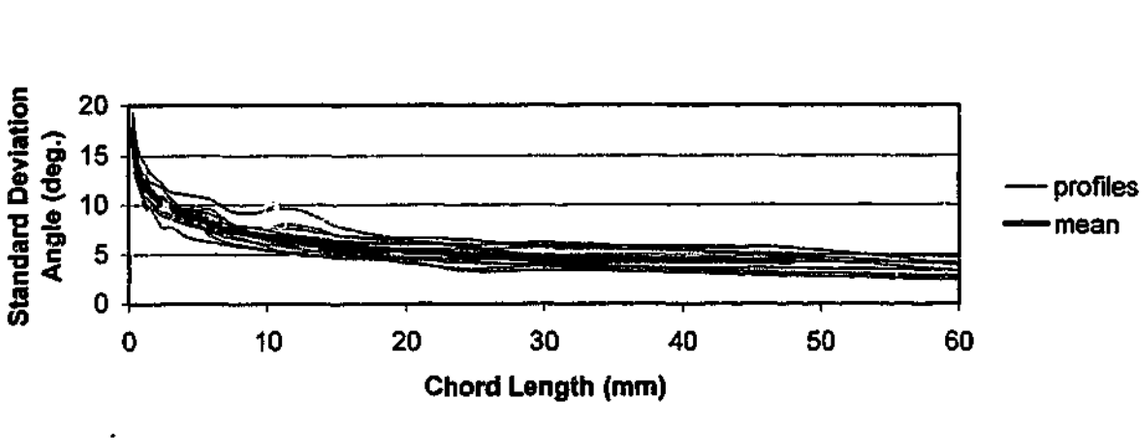

AVERAGE CORRELATION COEFFICIENT OF SCANS = 0.991

AVERAGE CORRELATION COEFFICIENT OF SCANS TO MEAN = 0.996

BASALT MW, JOINT, slight carbonaceous coating

BLOCK 4 - scanned at 10mm intervals

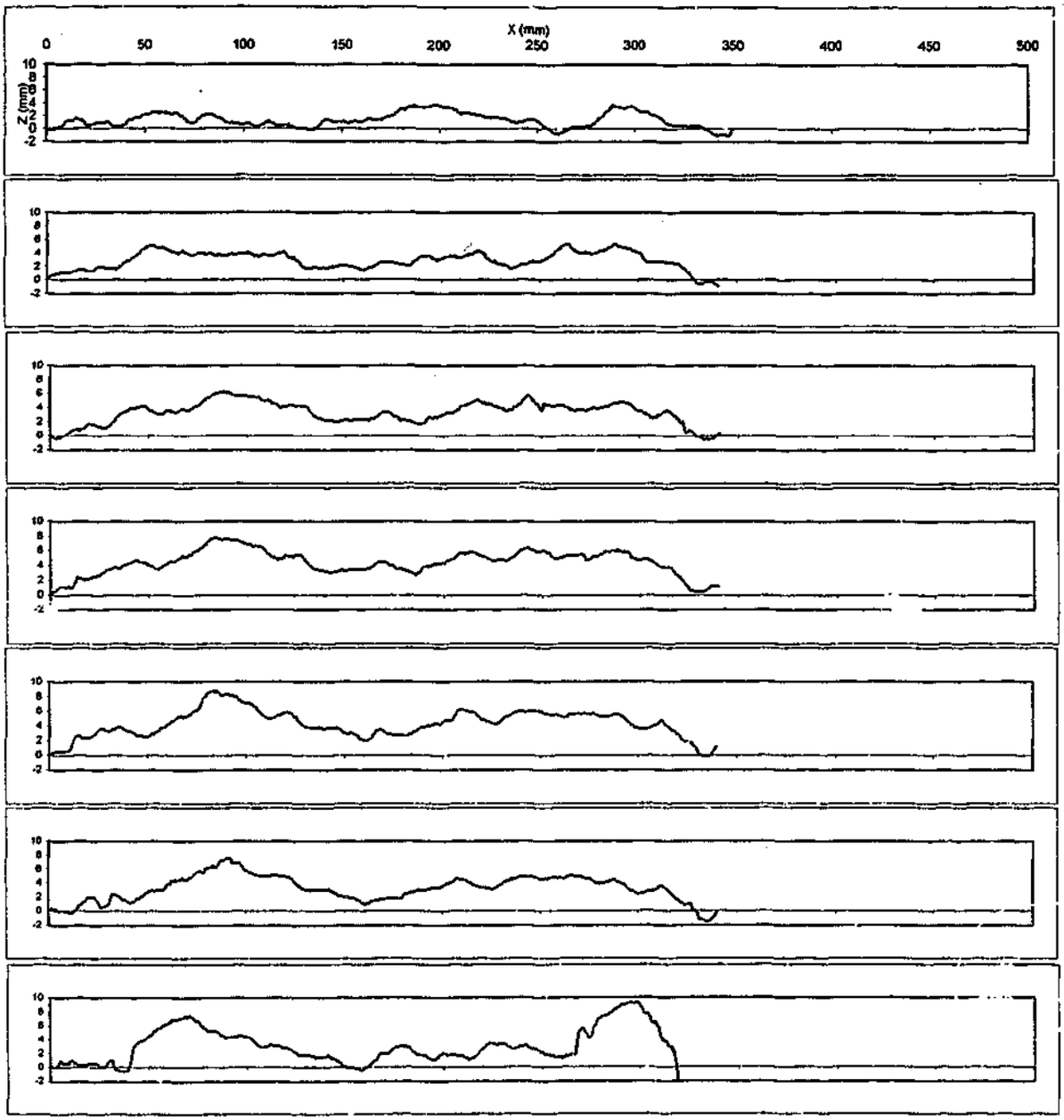

BASALT MW, JOINT, trace carbonaceous coating

BLOCK 5, scanned at 10 mm intervals

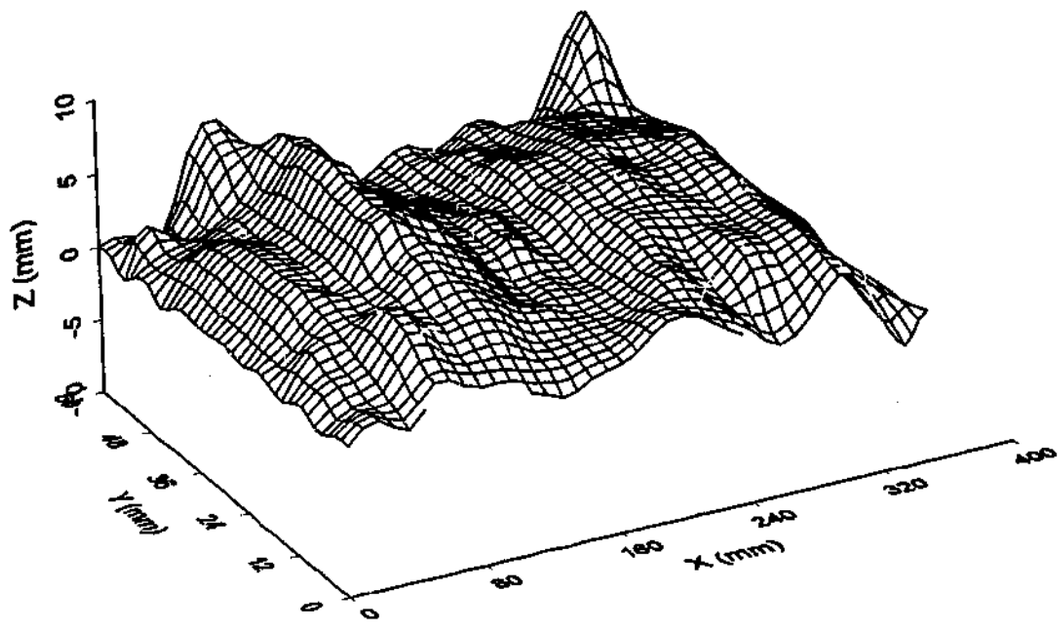

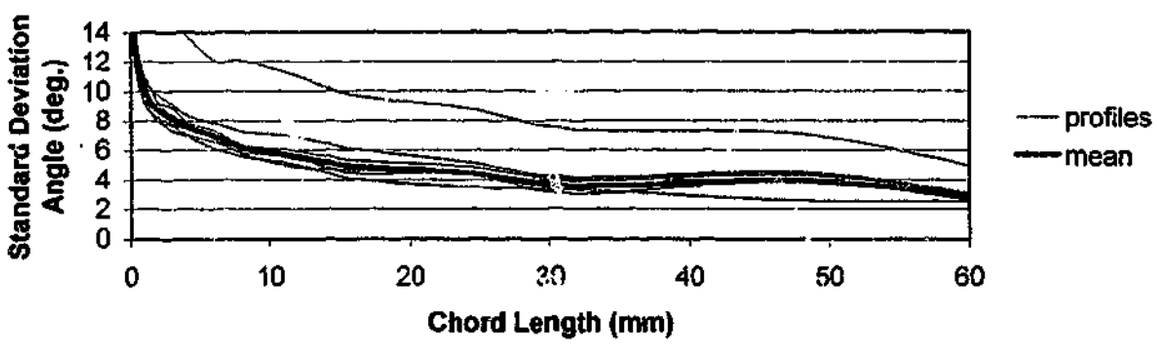

AVERAGE CORRELATION COEFFICIENT OF SCANS = 0.994

AVERAGE CORRELATION COEFFICIENT OF SCANS TO MEAN = 0.997

BASALT MW, JOINT, trace carbonaceous coating

BLOCK 5, scanned at 10 mm intervals

Scanned parallel to y-axis

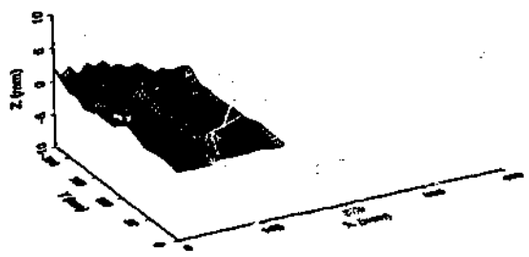

Scanned parallel to x-axis

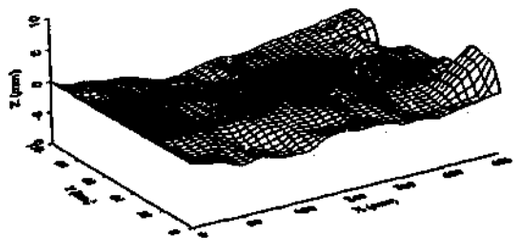

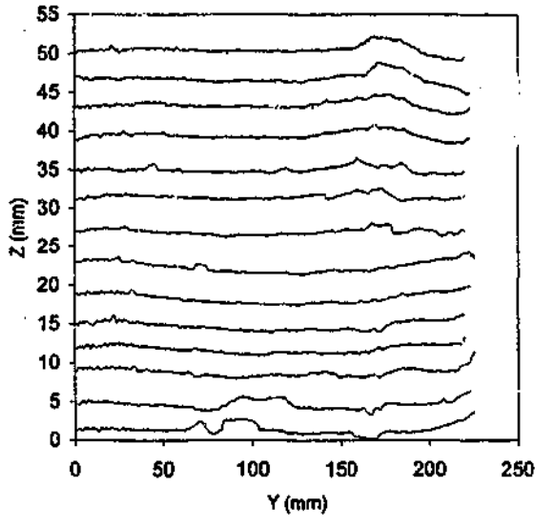

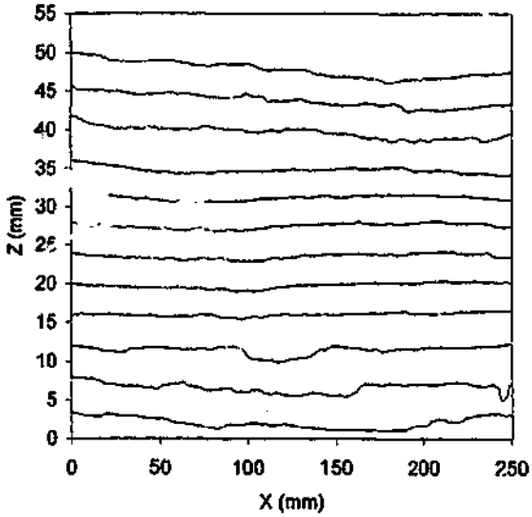

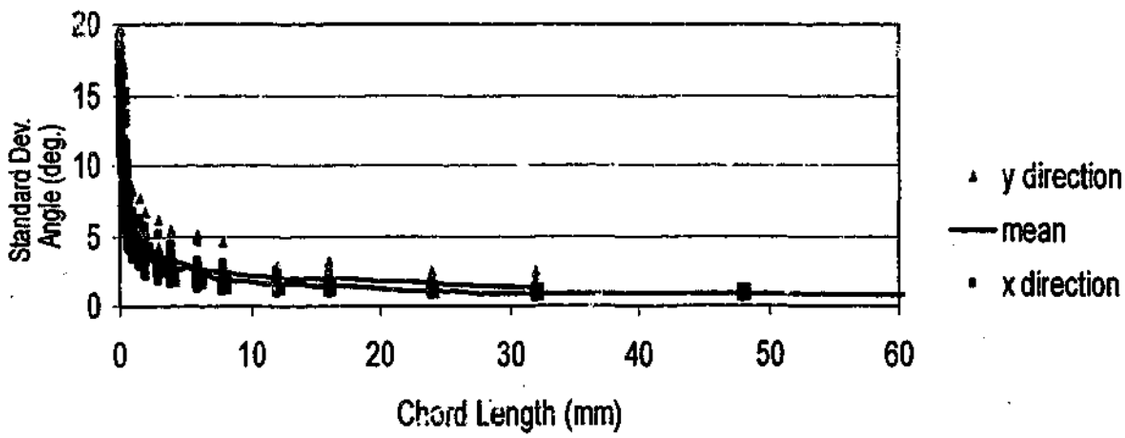

Correlation coefficient of mean statistics in Perpendicular Directions = 0.995

SILTSTONE SW, JOINT NEAR PERPENDICULAR TO BEDDING, PYRITE COATED

BLOCK 1

Scanned parallel to y-axis

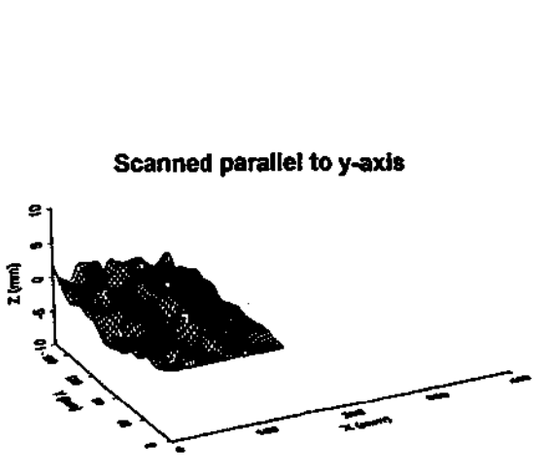

Scanned parallel to x-axis

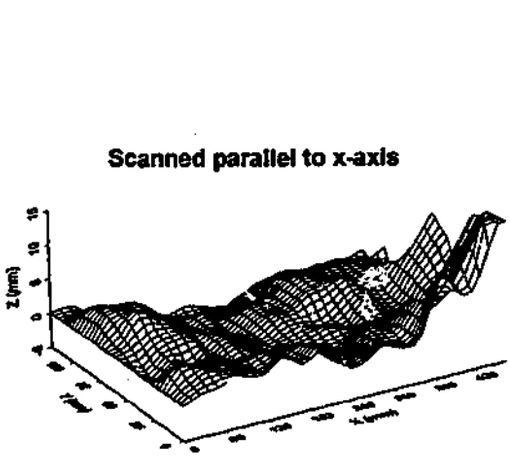

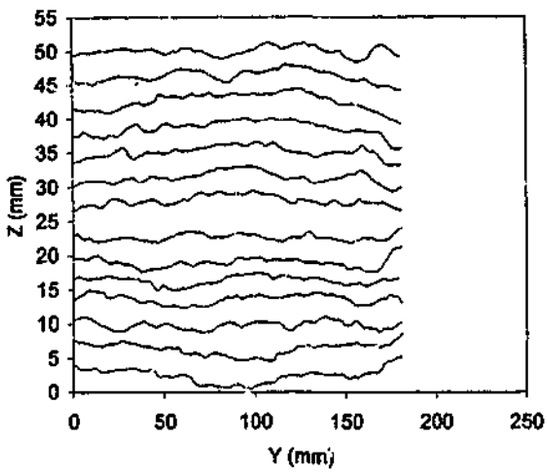

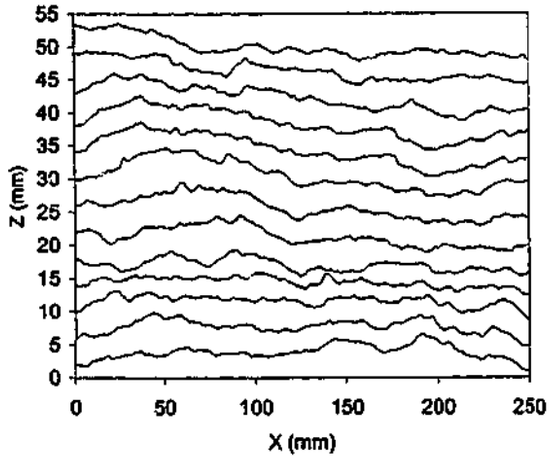

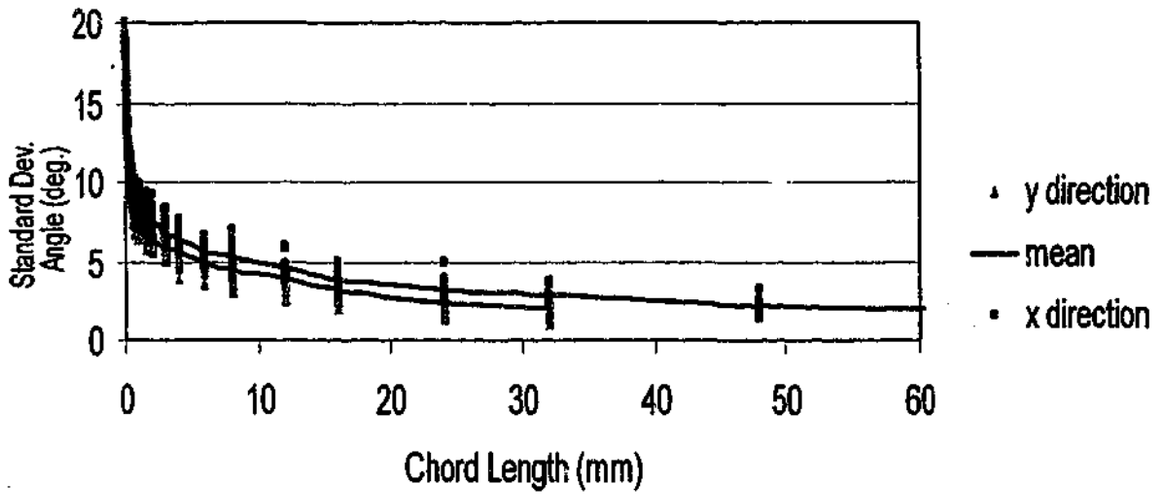

Correlation Coefficient of Mean Statistics in Perpendicular Directions = 0.996

SILTSTONE SW, BEDDING JOINT

BLOCK 2

Scanned parallel to y-axis

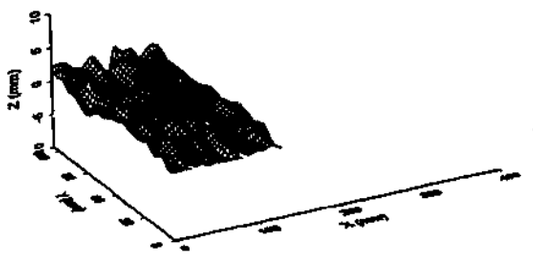

Scanned parallel to x-axis

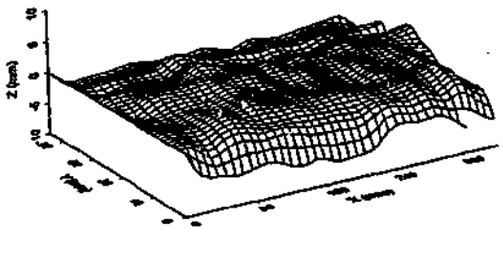

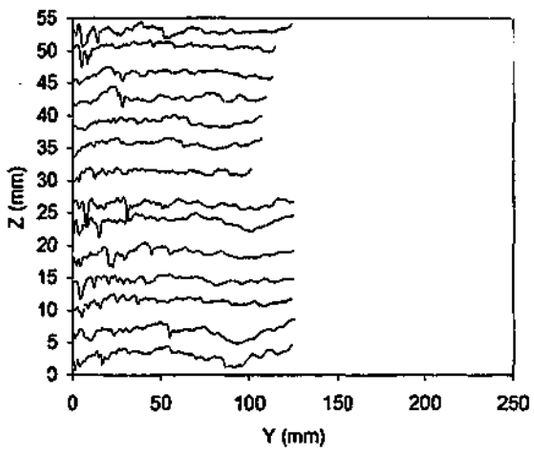

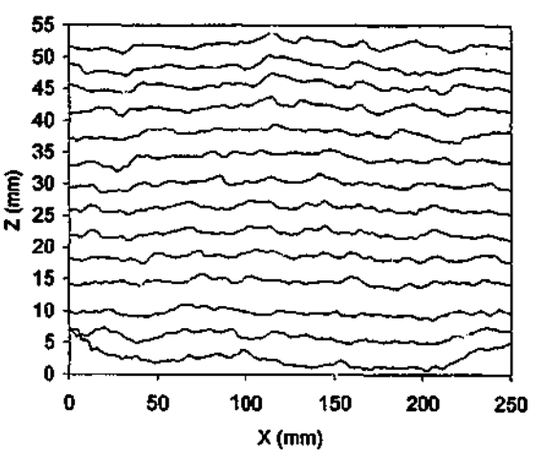

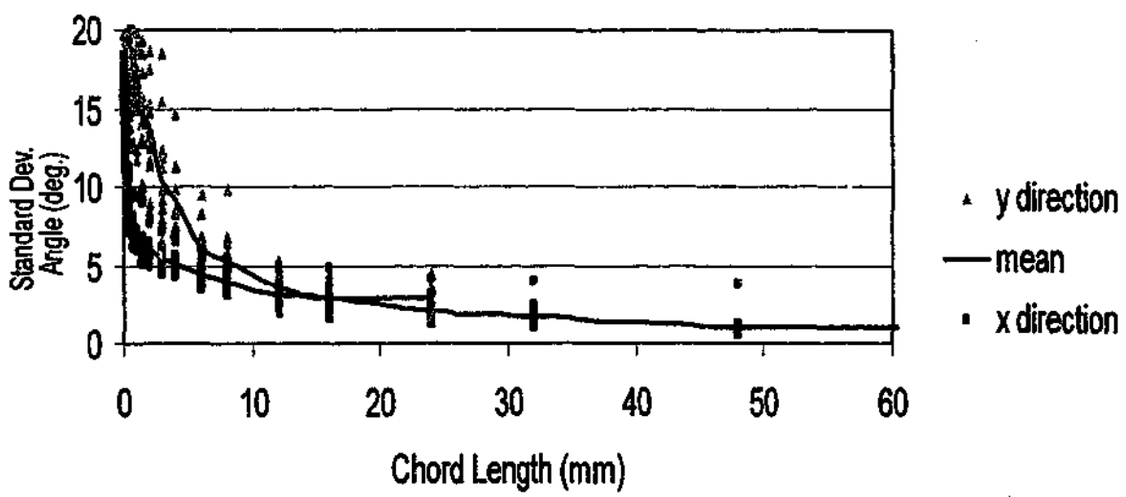

Correlation Coefficient of Mean Statistics in Perpendicular Directions = 0.939

SILTSTONE SW, BEDDING JOINT

BLOCK 1

Scanned parallel to y-axis

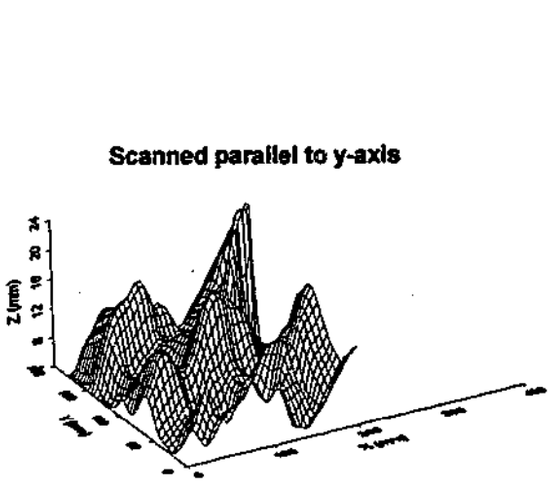

Scanned parallel to x-axis

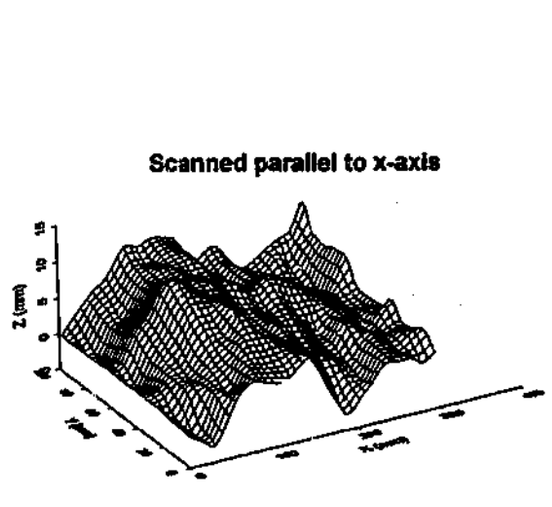

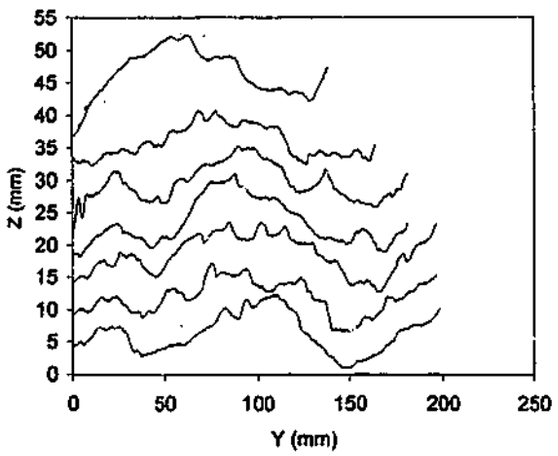

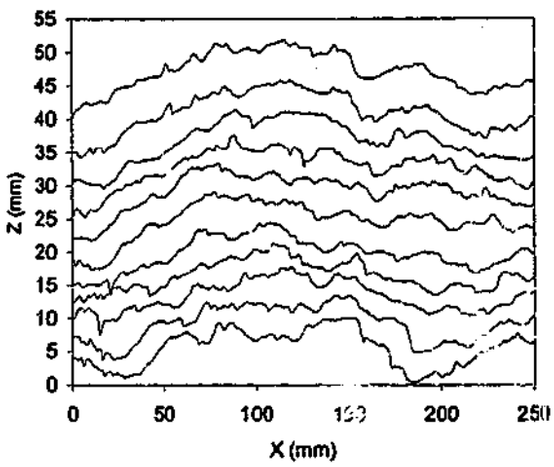

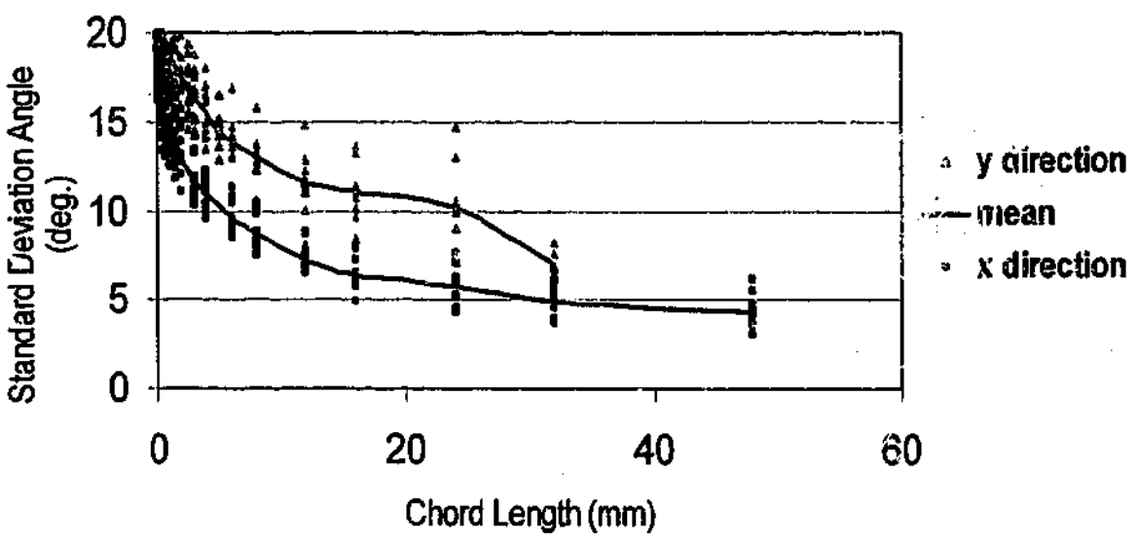

Correlation Coefficient of Mean Statistics in Perpendicular Directions = 0.996

BASALT MW, JOINT

BLOCK 1

Scanned parallel to y-axis

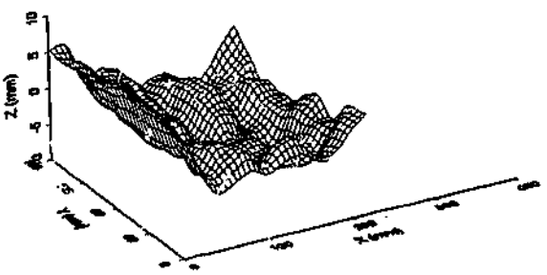

Scanned parallel to x-axis

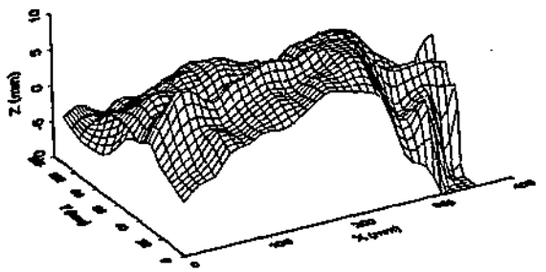

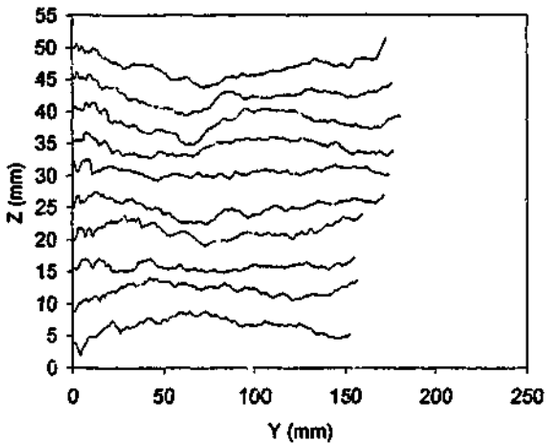

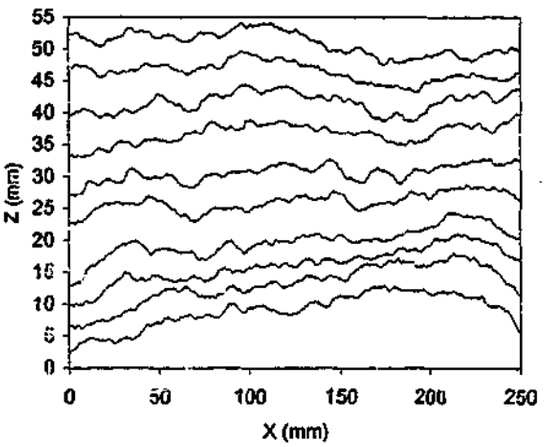

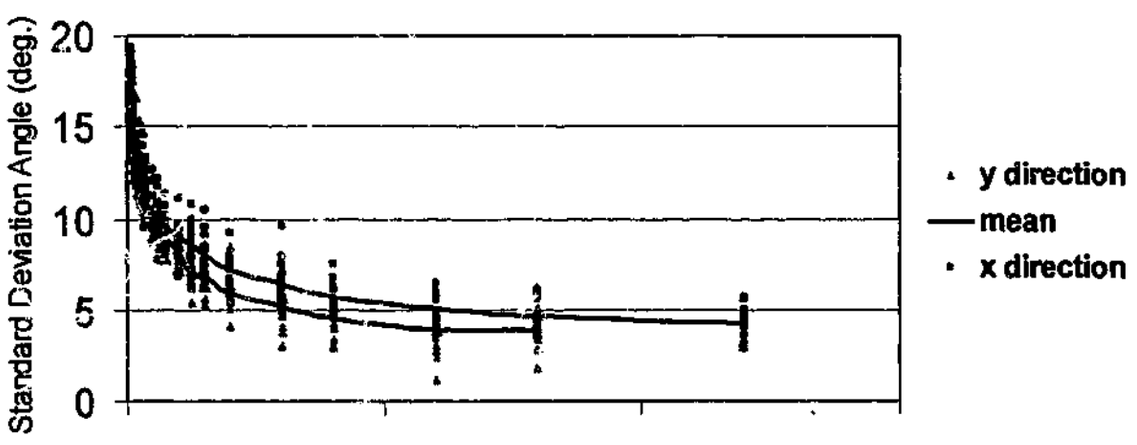

Correlation Coefficient of Mean Statistics in Perpendicular Directions = 0.996

BASALT/RAW, JOINT

BLOCK 4

APPENDIX B

LABORATORY CLASSIFICATION TEST RESULTS

Table of Contents – Appendix B

JOHNSTONE - UNIAXIAL TEST RESULTS

Sample	Saturated Moisture Content (%)	Uniaxial Compressive Strength (MPa)	Failure Mode	Average Young's Modulus (GPa)
1b-batch1	13.2	8.3	Tensile	-
3a-batch1	13.8	8.0	Tensile	0.80
3a-batch1	14.3	8.5	Shear	-
4b-batch1	14.0	7.6	Shear/tensile	0.85
7a-batch2	14.6	4.2	Shear/tensile	0.90
7a-batch2	14.0	4.6	Tensile	-
8a-batch2	13.0	5.1	Shear/tensile	-

SILTSTONE - UNIAXIAL TEST RESULTS

Block	Saturated Moisture Content (%)	Uniaxial Compressive Strength (MPa)	Failure Mode	Average Young's Modulus (GPa)
1	1.5	60.1	Shear	23.4
2	2.1	34.5	Tensile	6.1
3	1.4	56.6	Shear/tensile	46.8

BASALT - UNIAXIAL TEST RESULTS

Block	Saturated Moisture Content (%)	Uniaxial Compressive Strength (MPa)	Failure Mode	Average Young's Modulus (GPa)
1	2.9	128.3	Shear	61.8
1	2.9	111.7	Shear/tensile	70.6
5	2.1	126.0	Tensile	54.7
5	2.2	115.9	Shear	61.0

GRANITE - UNIAXIAL TEST RESULTS

Block	Saturated Moisture Content (%)	Uniaxial Compressive Strength (MPa)	Failure Mode	Average Young's Modulus (GPa)
1	0.4	168.5	Tensile	-
1	0.4	184.4	Tensile	58.8
1	0.4	180.8	Shear	63.3

SILTSTONE - TENSILE TEST RESULTS

Block	Saturated Moisture Content (%)	Tensile strength (MPa)
3	1.7	9.24
3	1.7	4.86
5	1.7	7.49
5	1.7	8.20
5	1.7	8.63

BASALT - TENSILE TEST RESULTS

Block	Saturated Moisture Content (%)	Tensile strength (MPa)
10	2.9	10.38
10	2.9	11.85

GRANITE - TENSILE TEST RESULTS

Block	Saturated Moisture Content (%)	Tensile strength (MPa)
1	0.4	10.50
1	0.4	9.70
1	0.4	9.38
1	0.4	10.75

DIRECT SHEAR TEST RESULTS TO DETERMINE SILTSTONE BASIC FRICTION ANGLE

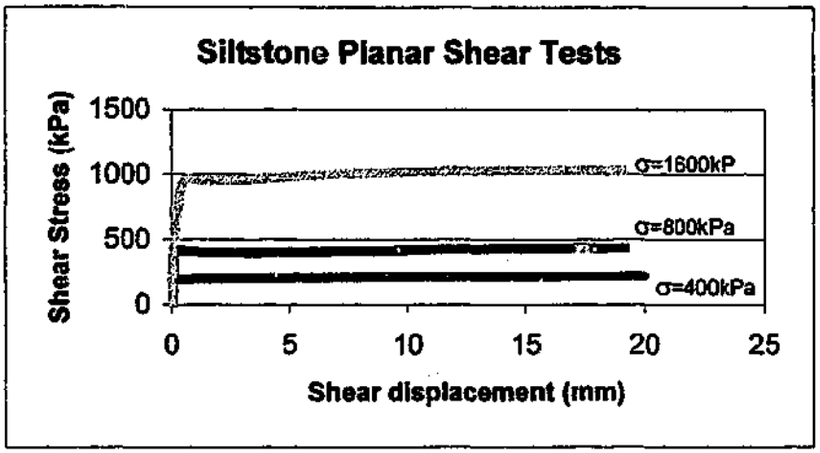

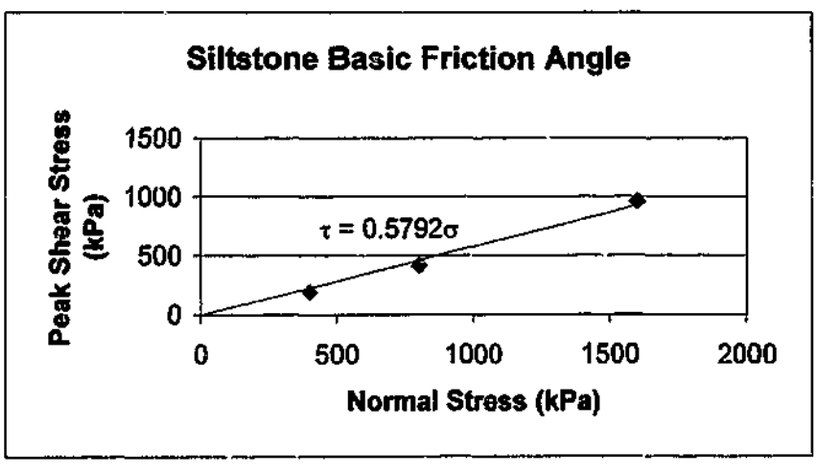

DIRECT SHEAR TEST RESULTS TO DETERMINE BASALT BASIC FRICTION ANGLE

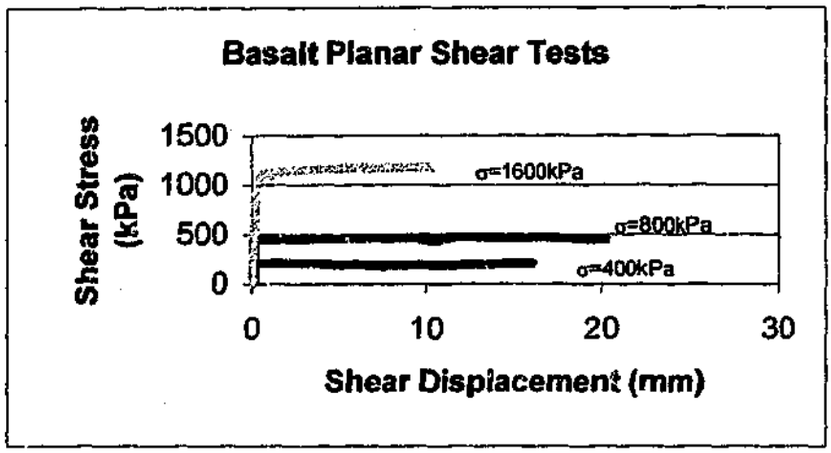

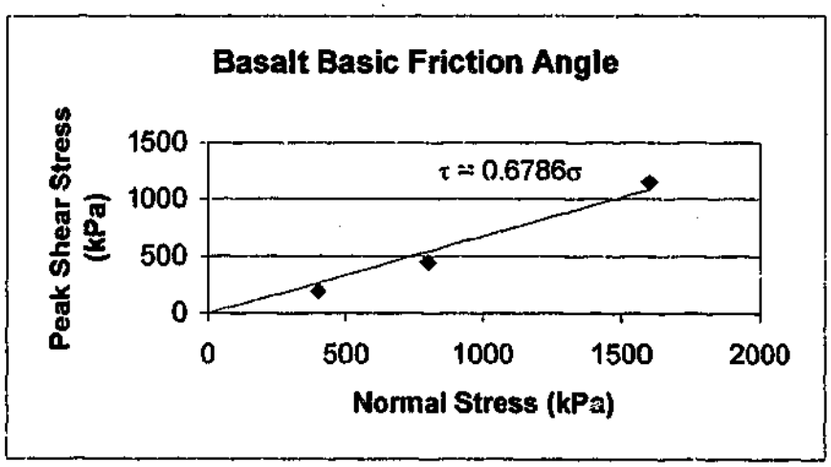

DIRECT SHEAR TEST RESULTS TO DETERMINE GRANITE BASIC FRICTION ANGLE

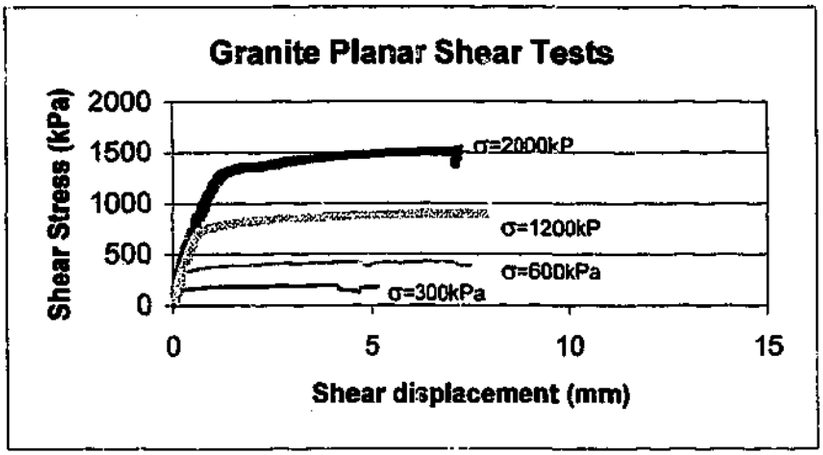

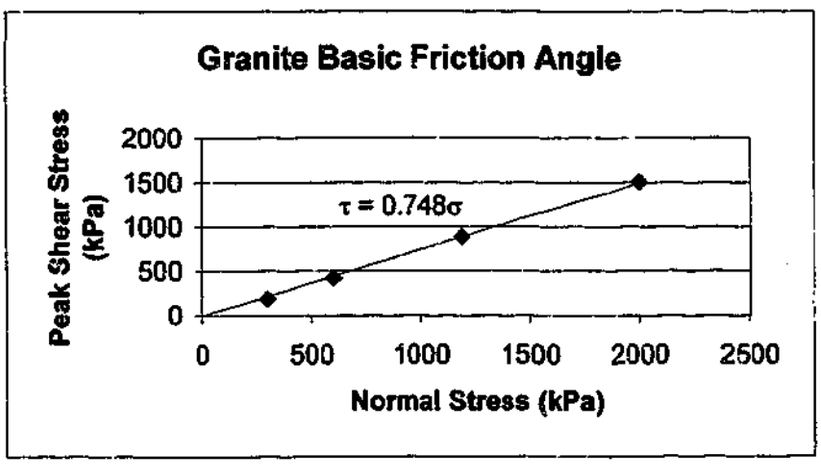

DIRECT SHEAR TEST RESULTS TO DETERMINE SILTSTONE PEAK FRICTION ANGLE

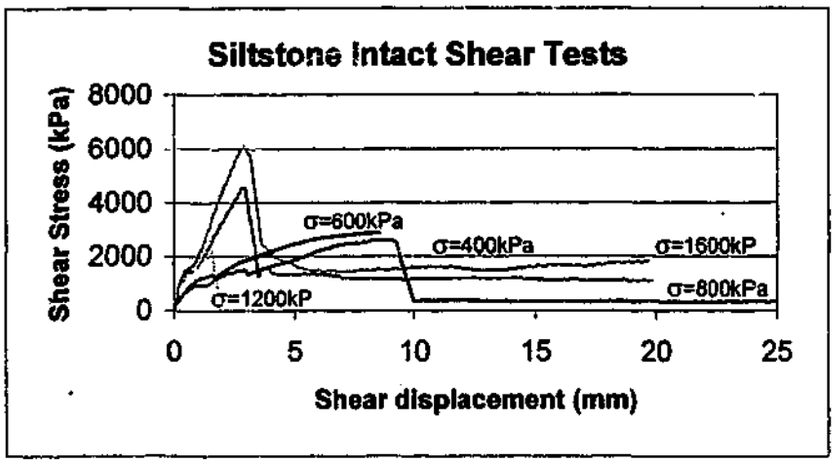

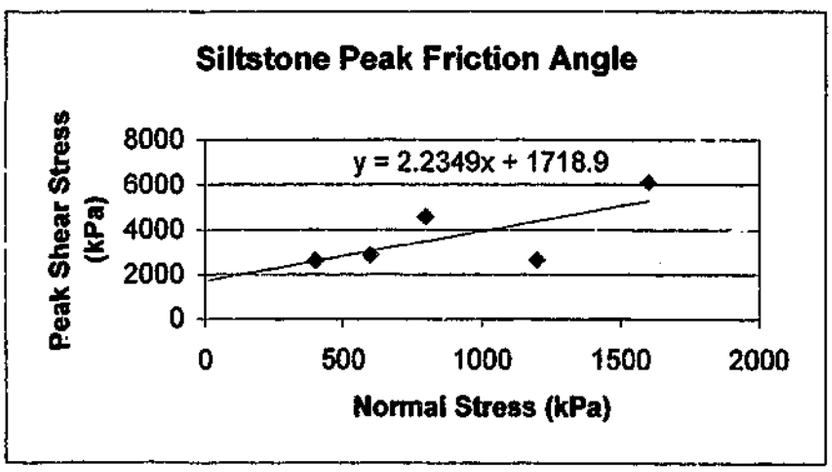

sheared parallel to bedding - σ = 600kPa, 1200kPa
sheared perpendicular to bedding - σ = 400kPa, 800kPa, 1600kPa

APPENDIX C

SPLIT SURFACES

Table of Contents – Appendix C

PROFILES AND STATISTICS OF SPLIT SURFACES

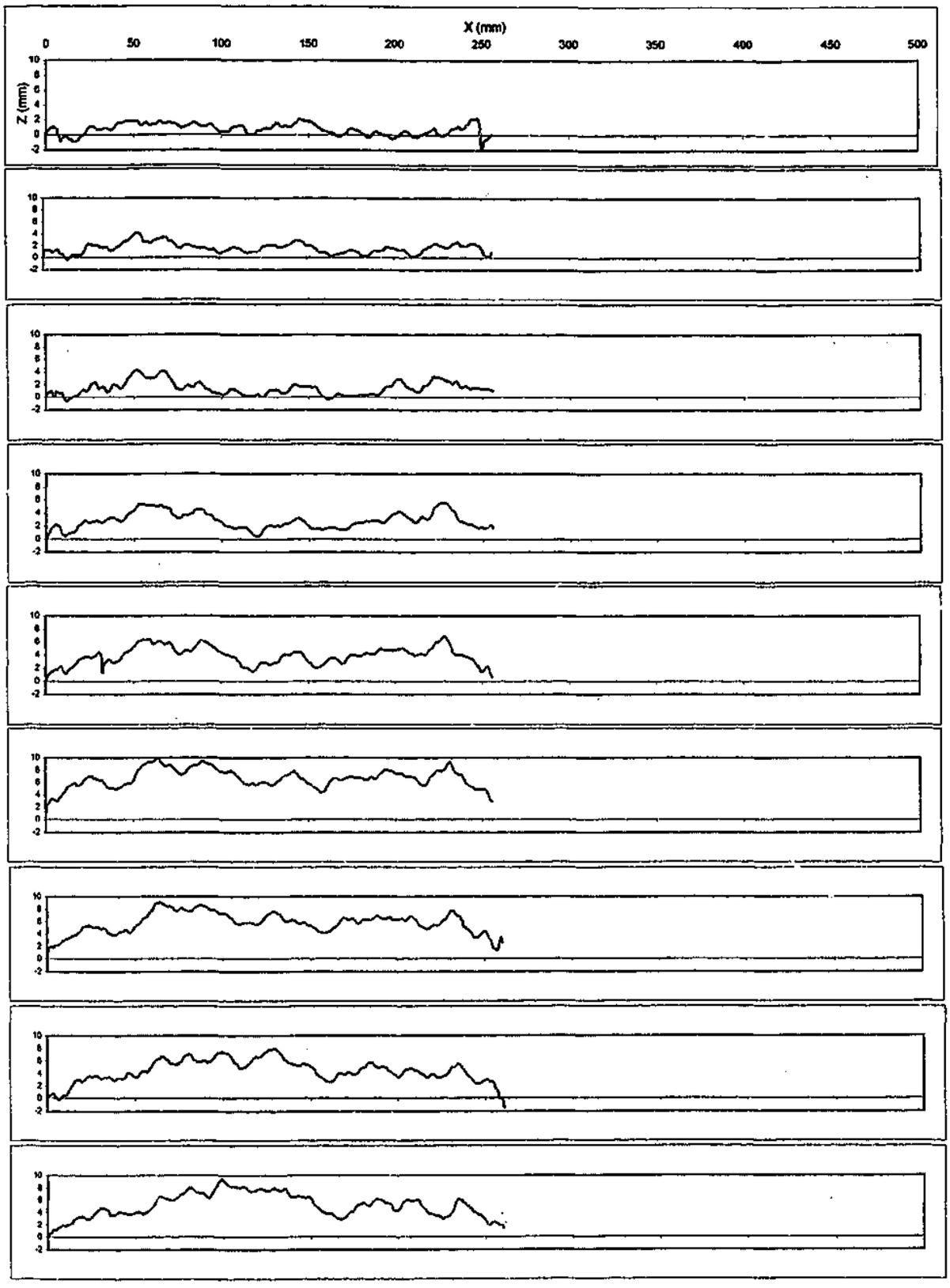

JOHNSTONE, SPLIT

BLOCK 1A

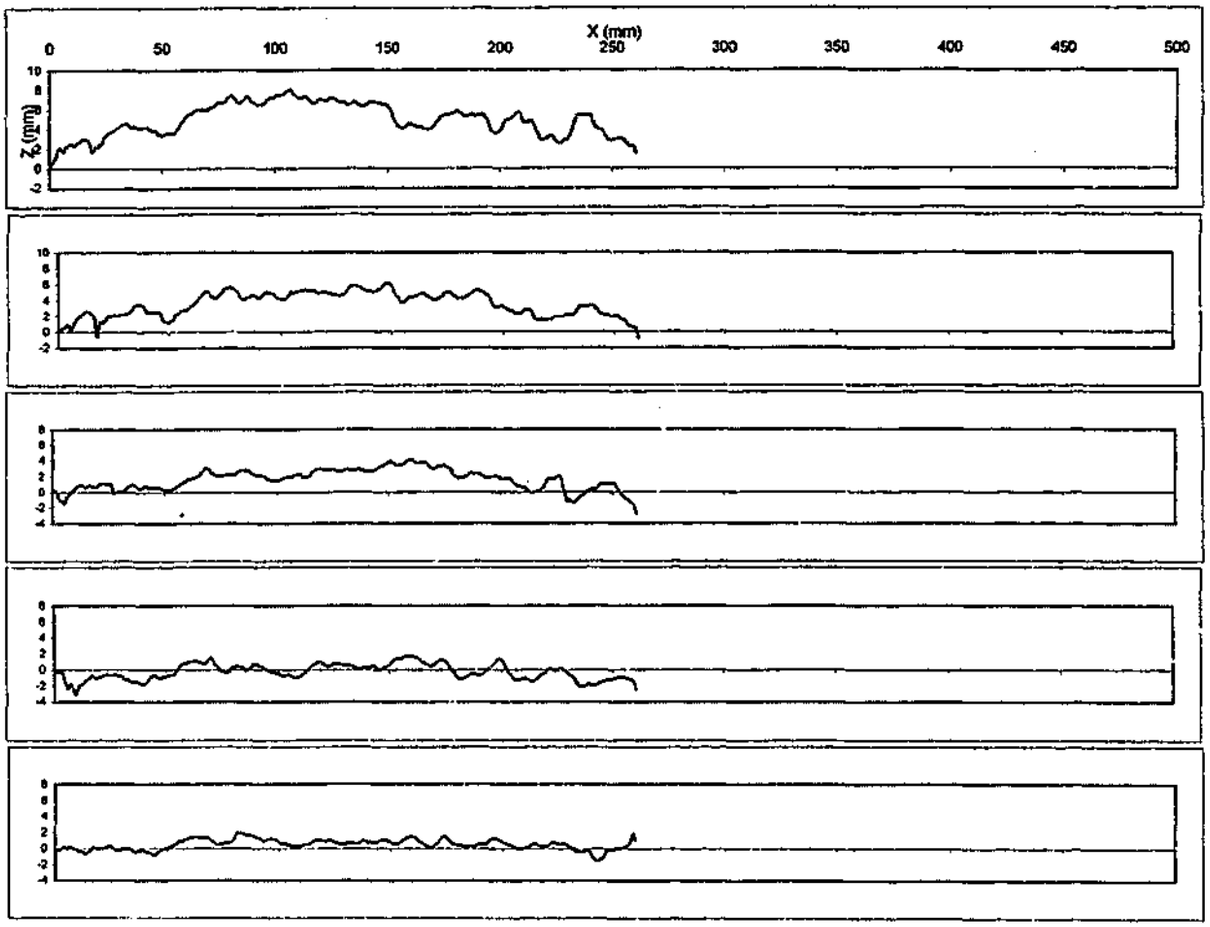

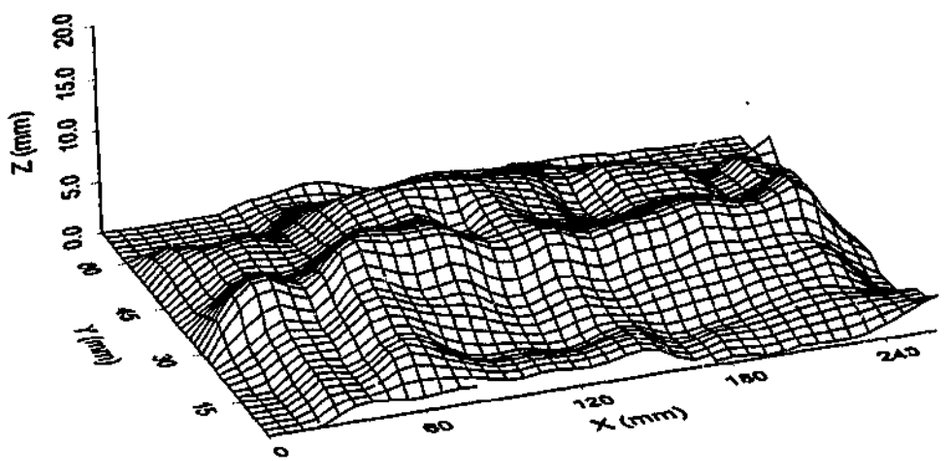

JOHNSTONE, SPLIT

BLOCK 1A

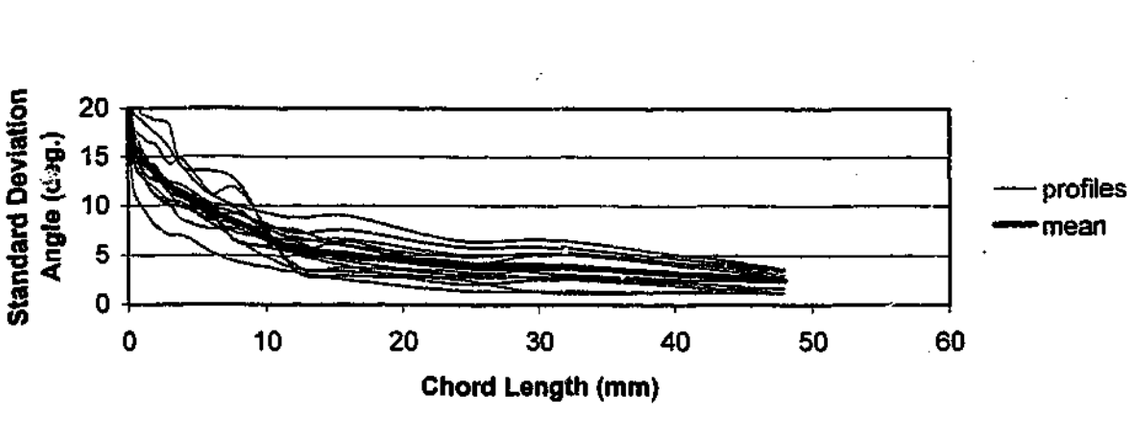

AVERAGE CORRELATION COEFFICIENT OF SCANS = 0.984

AVERAGE CORRELATION COEFFICIENT OF SCANS TO MEAN = 0.992

JOHNSTONE, SPLIT

BLOCK 1A

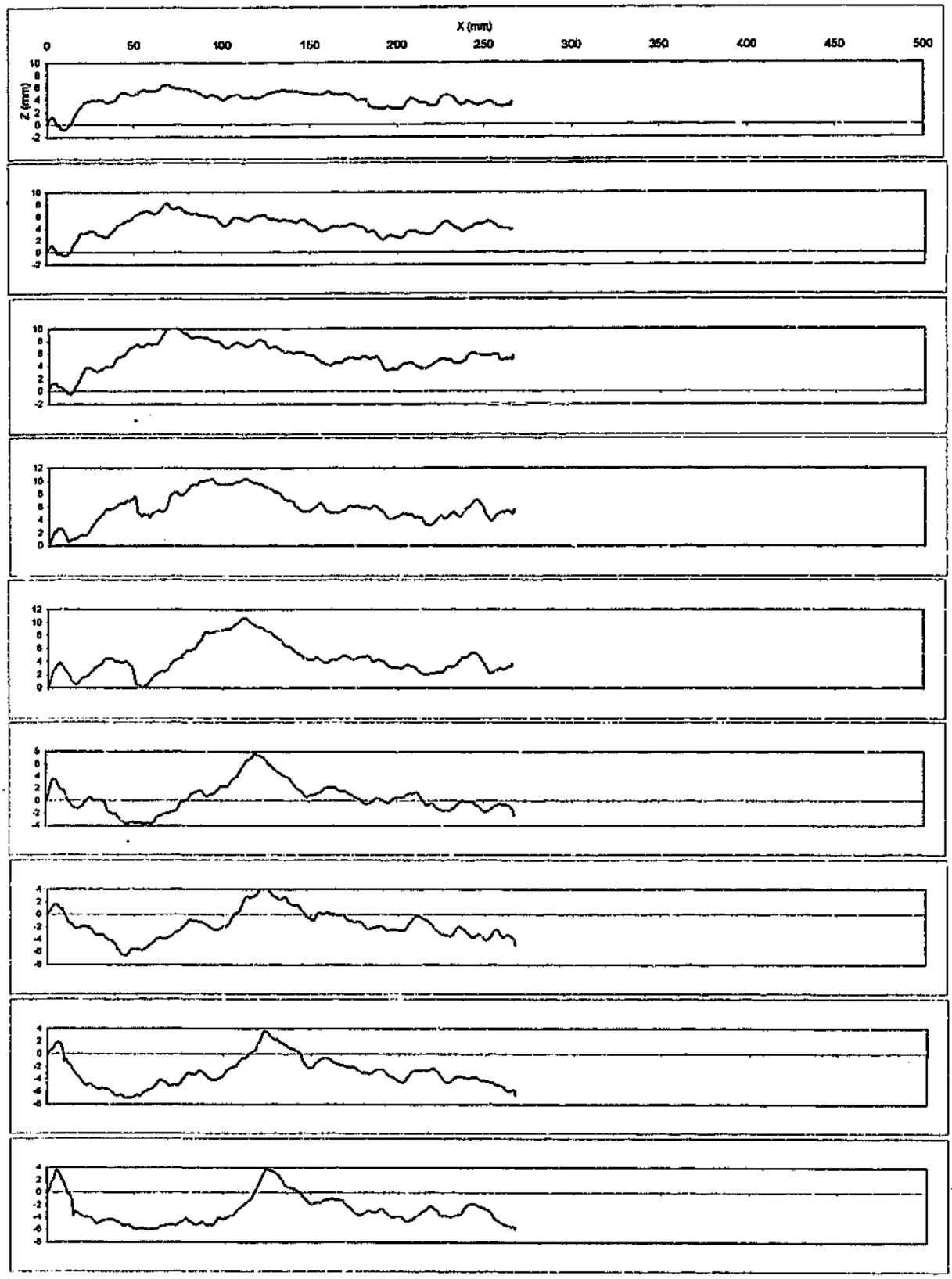

JOHNSTONE, SPLIT

BLOCK 1B

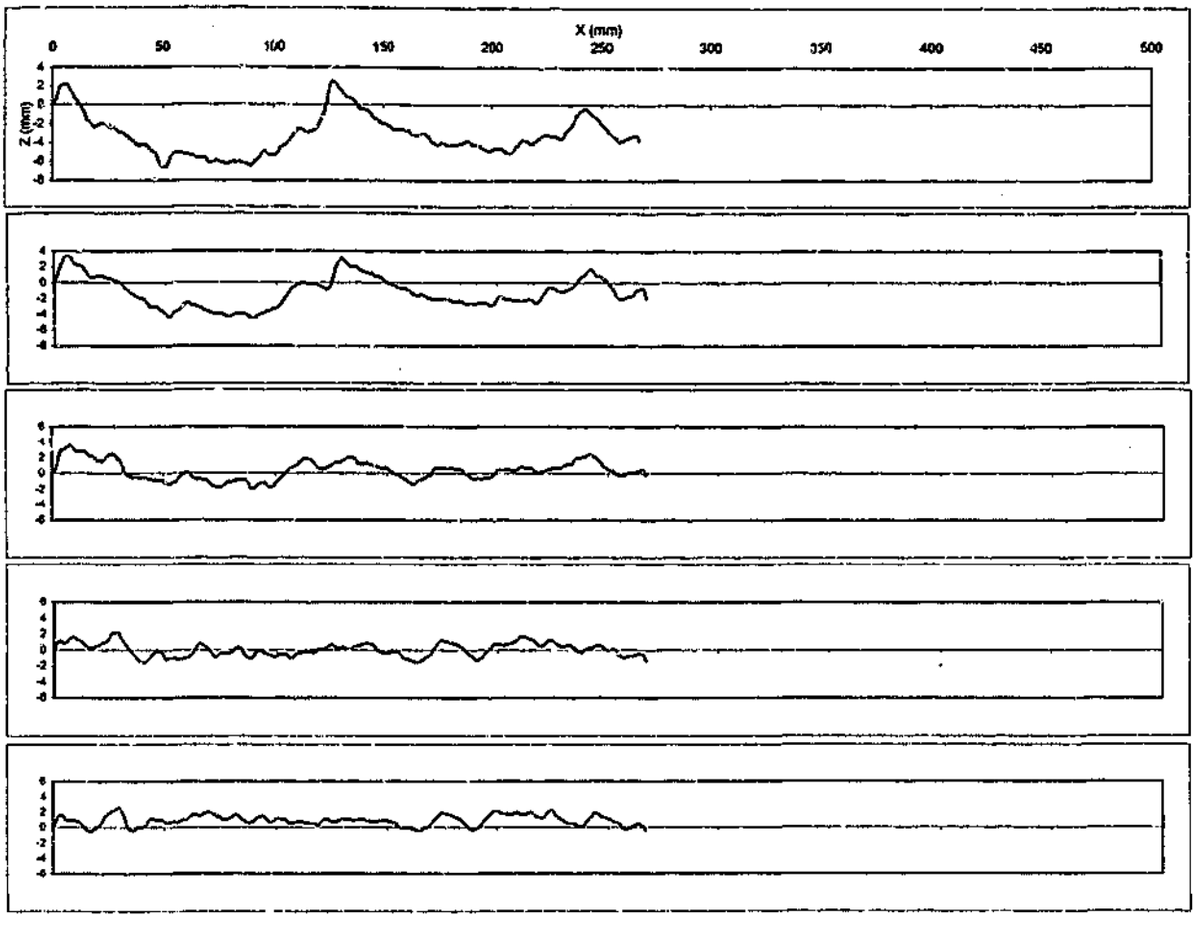

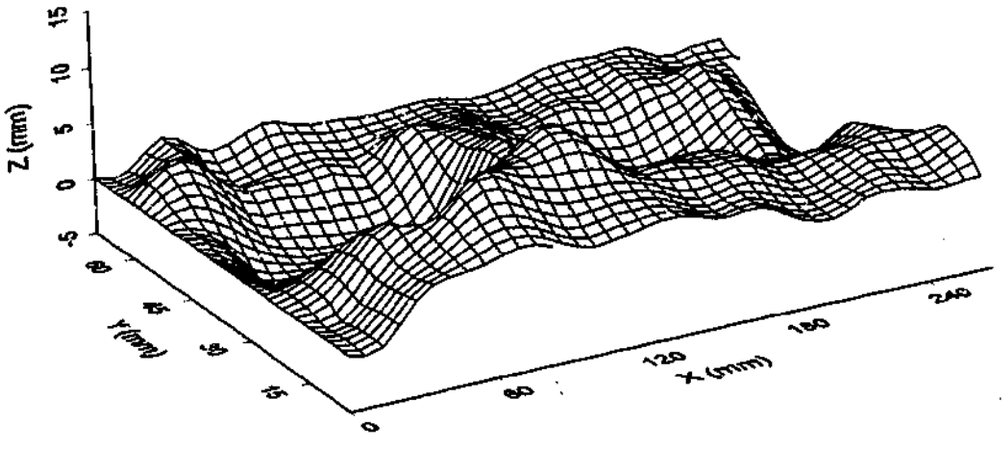

JOHNSTONE, SPLIT

BLOCK 1B

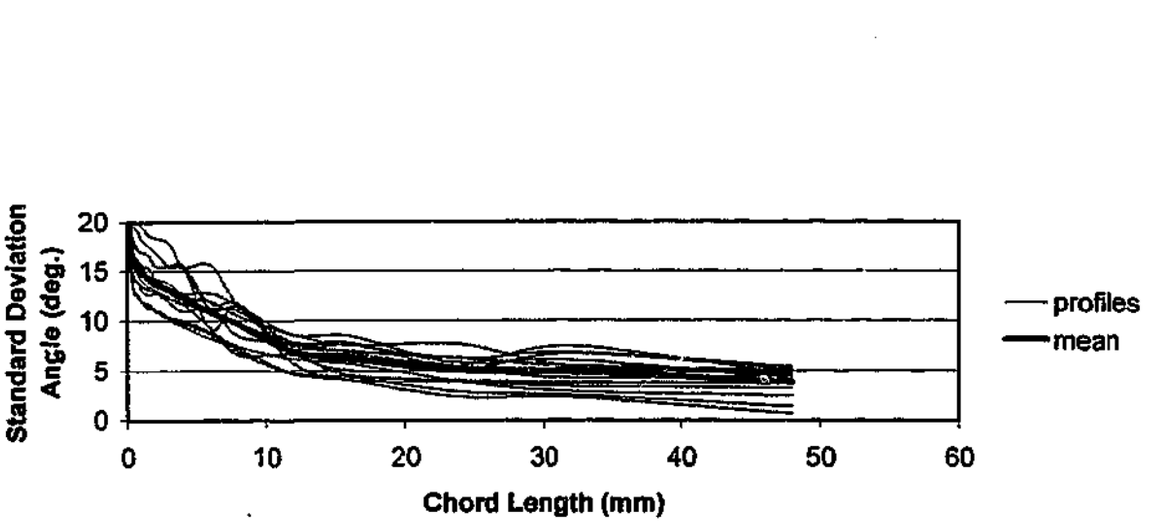

AVERAGE CORRELATION COEFFICIENT OF SCANS = 0.987

AVERAGE CORRELATION COEFFICIENT OF SCANS TO MEAN = 0.994

JOHNSTONE, SPLIT

BLOCK 1B

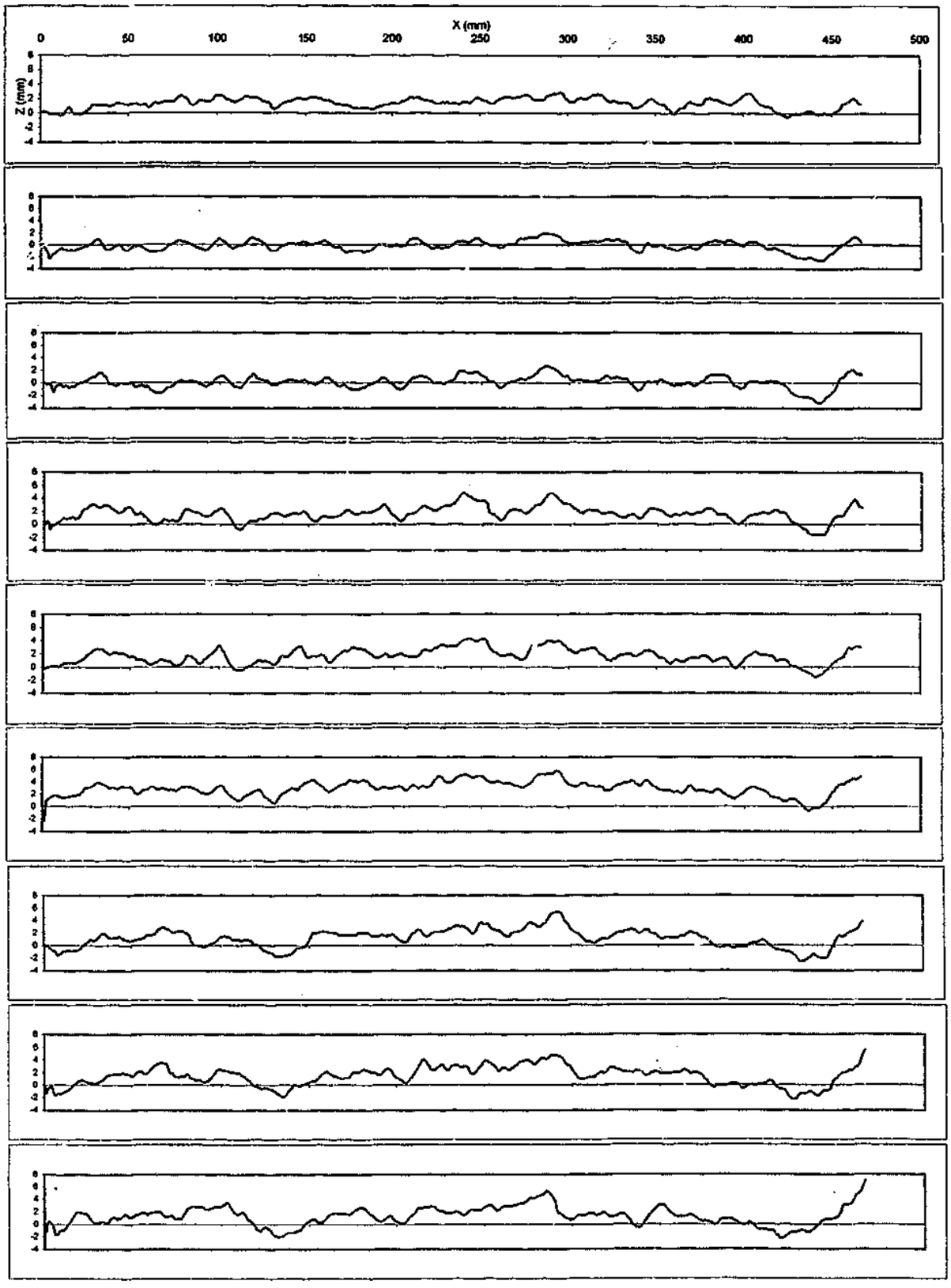

JOHNSTONE, SPLIT

BLOCK 2A

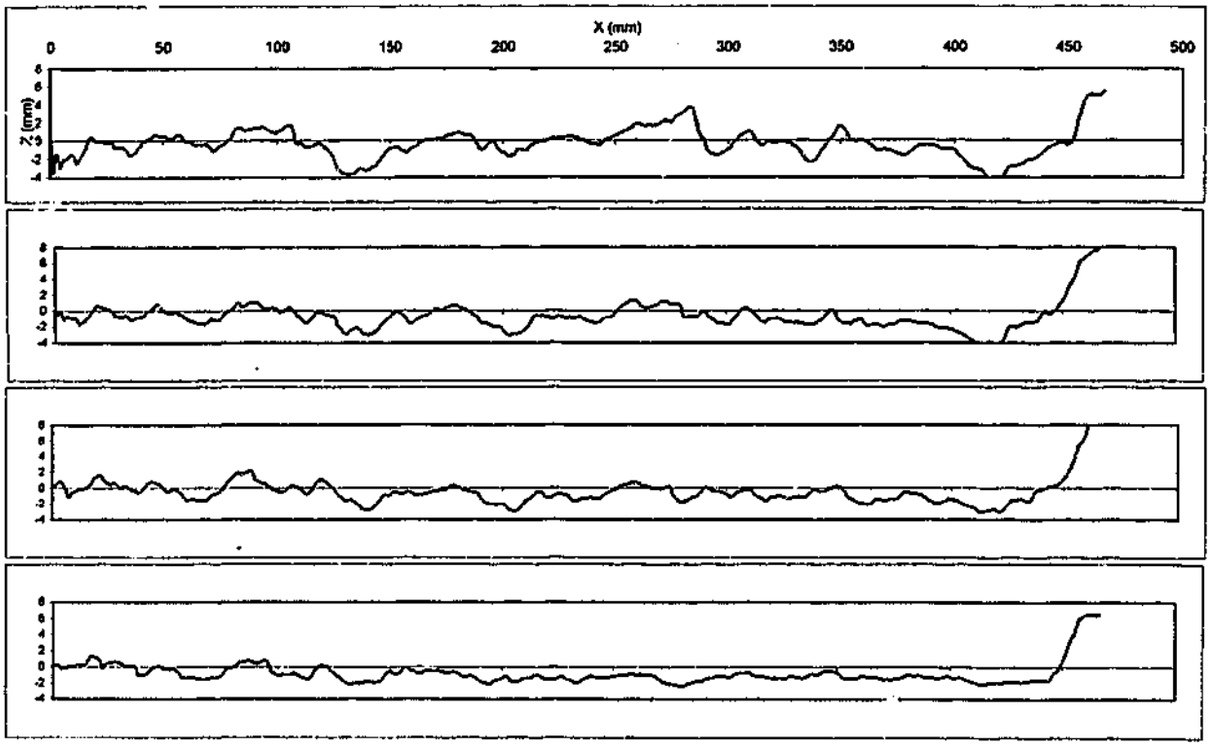

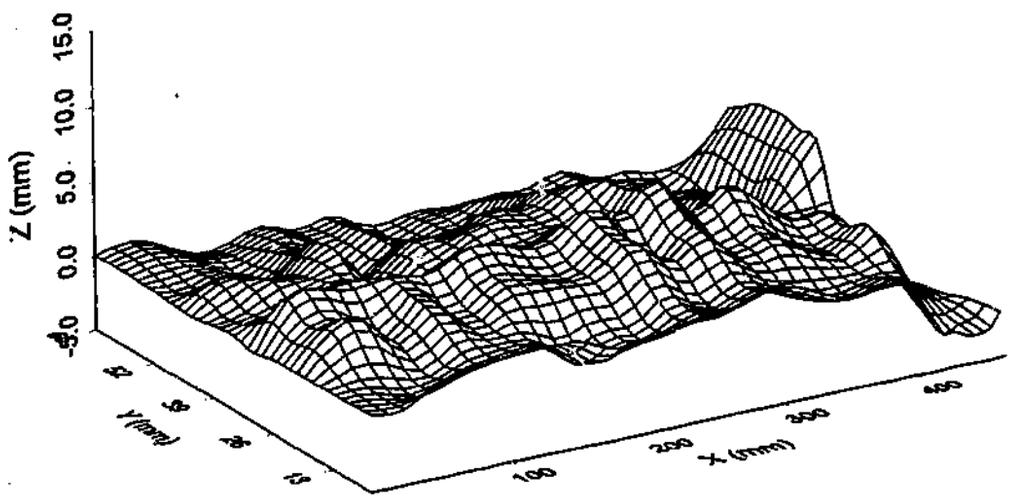

JOHNSTONE, SPLIT

BLOCK 2A

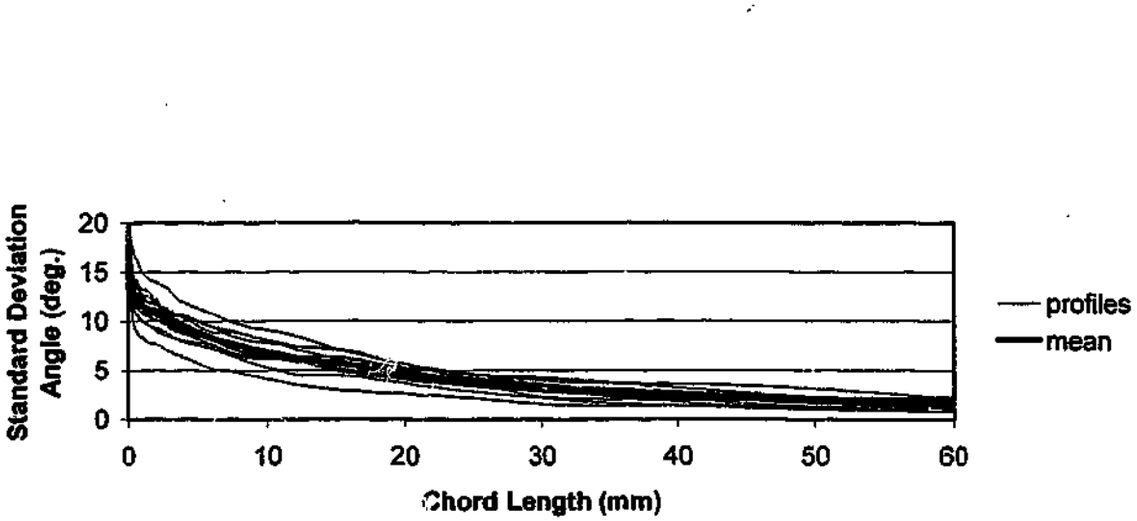

AVERAGE CORRELATION COEFFICIENT OF SCANS = 0.993

AVERAGE CORRELATION COEFFICIENT OF SCANS TO MEAN = 0.997

JOHNSTONE, SPLIT

BLOCK 2A

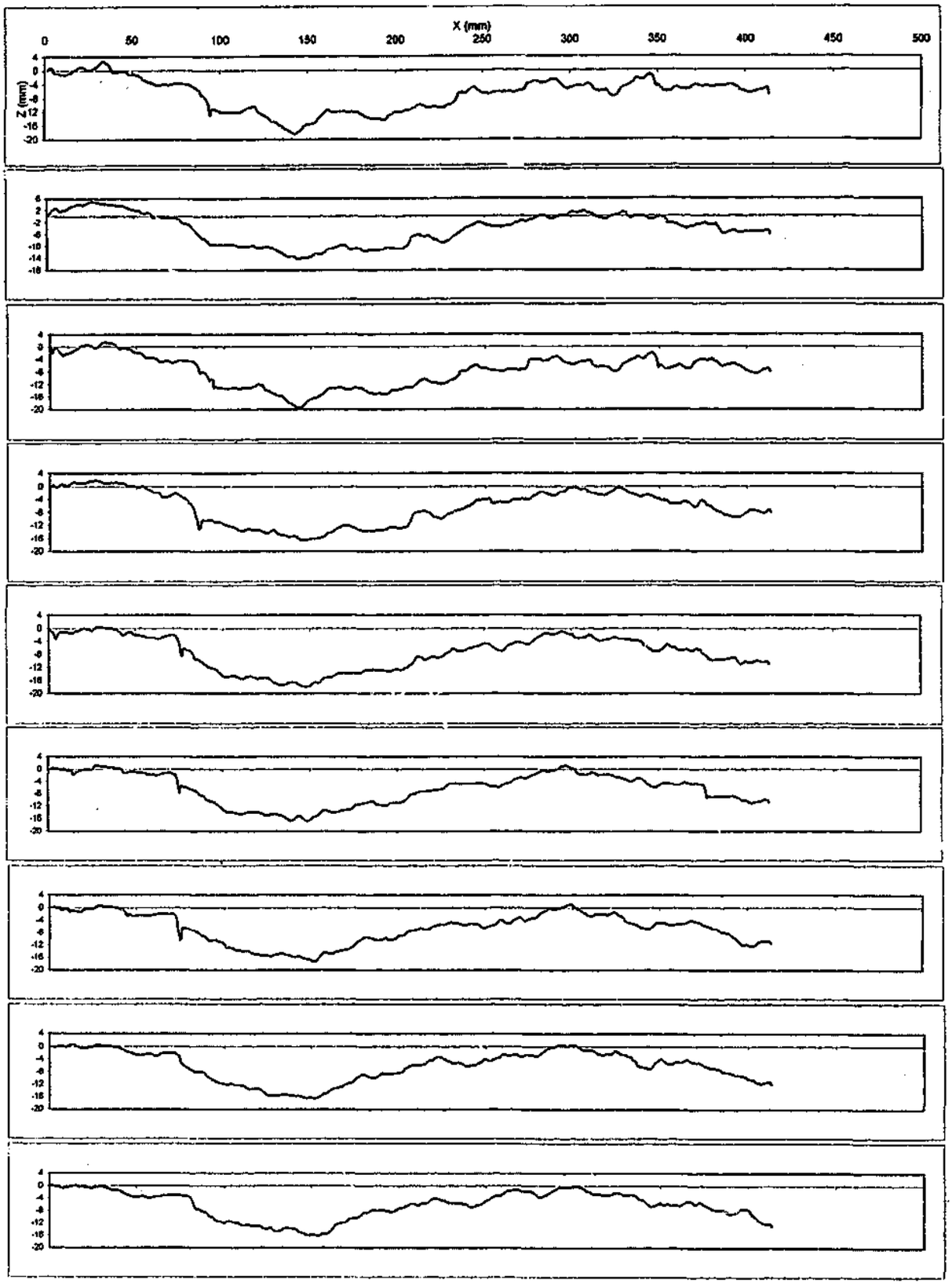

JOHNSTONE, SPLIT

BLOCK 2B

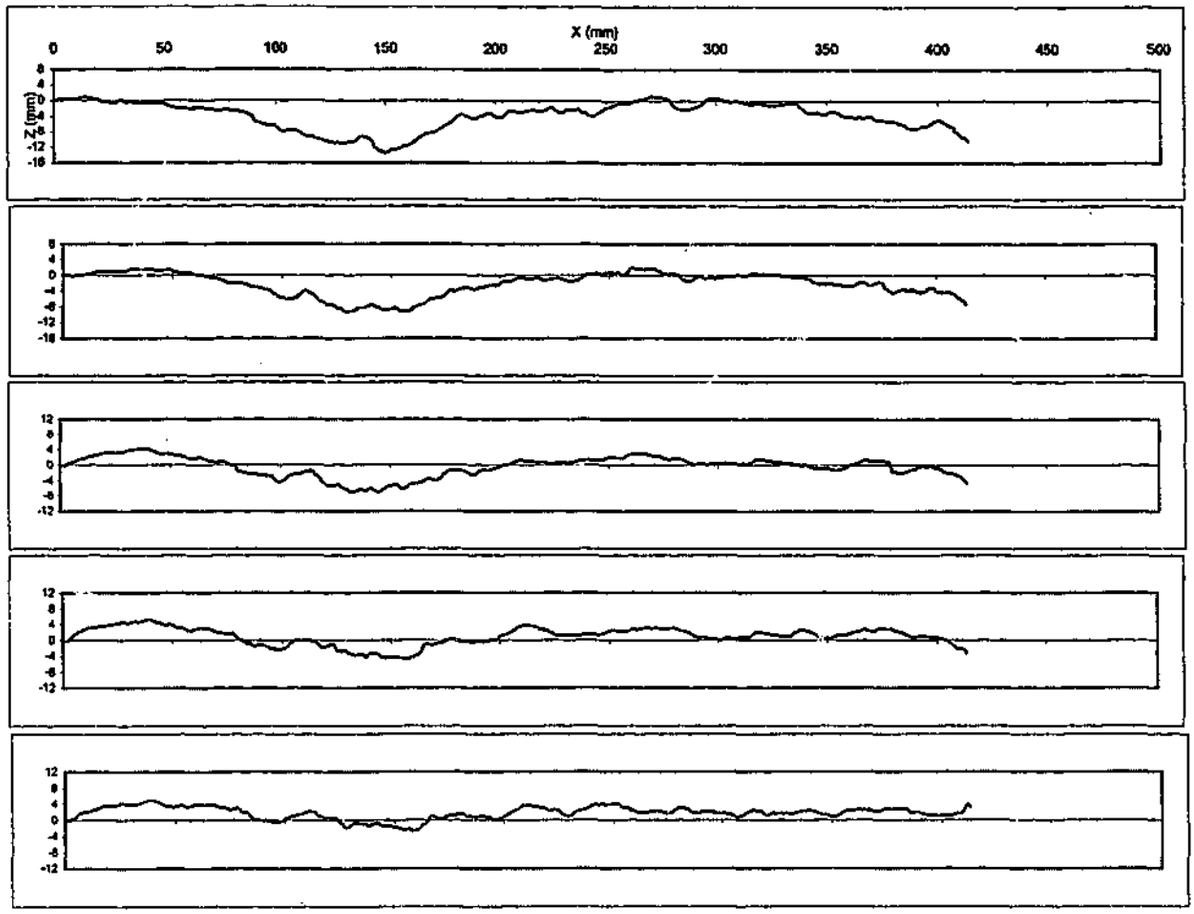

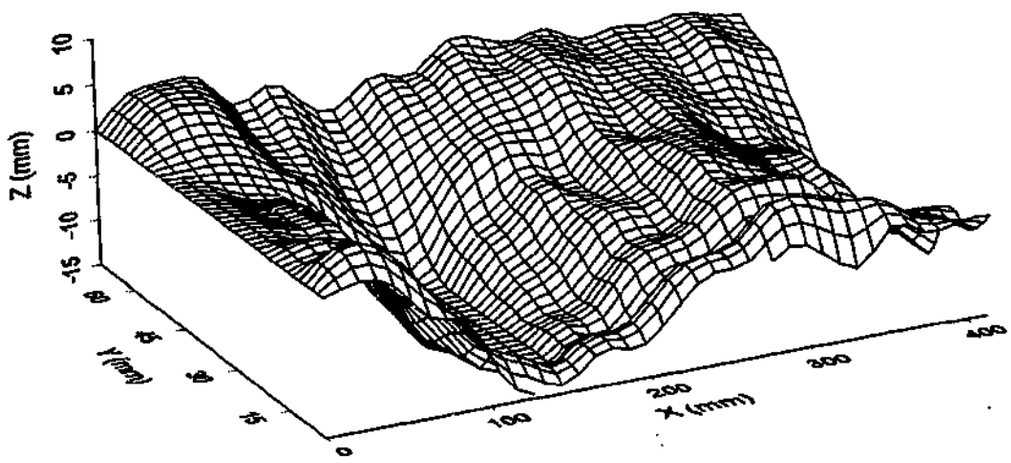

JOHNSTONE, SPLIT

BLOCK 2B

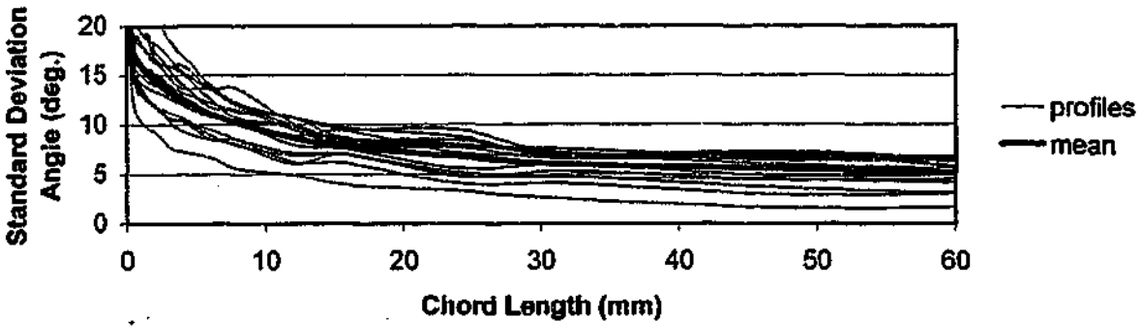

AVERAGE CORRELATION COEFFICIENT OF SCANS = 0.985

AVERAGE CORRELATION COEFFICIENT OF SCANS TO MEAN = 0.993

JOHNSTONE, SPLIT

BLOCK 2B

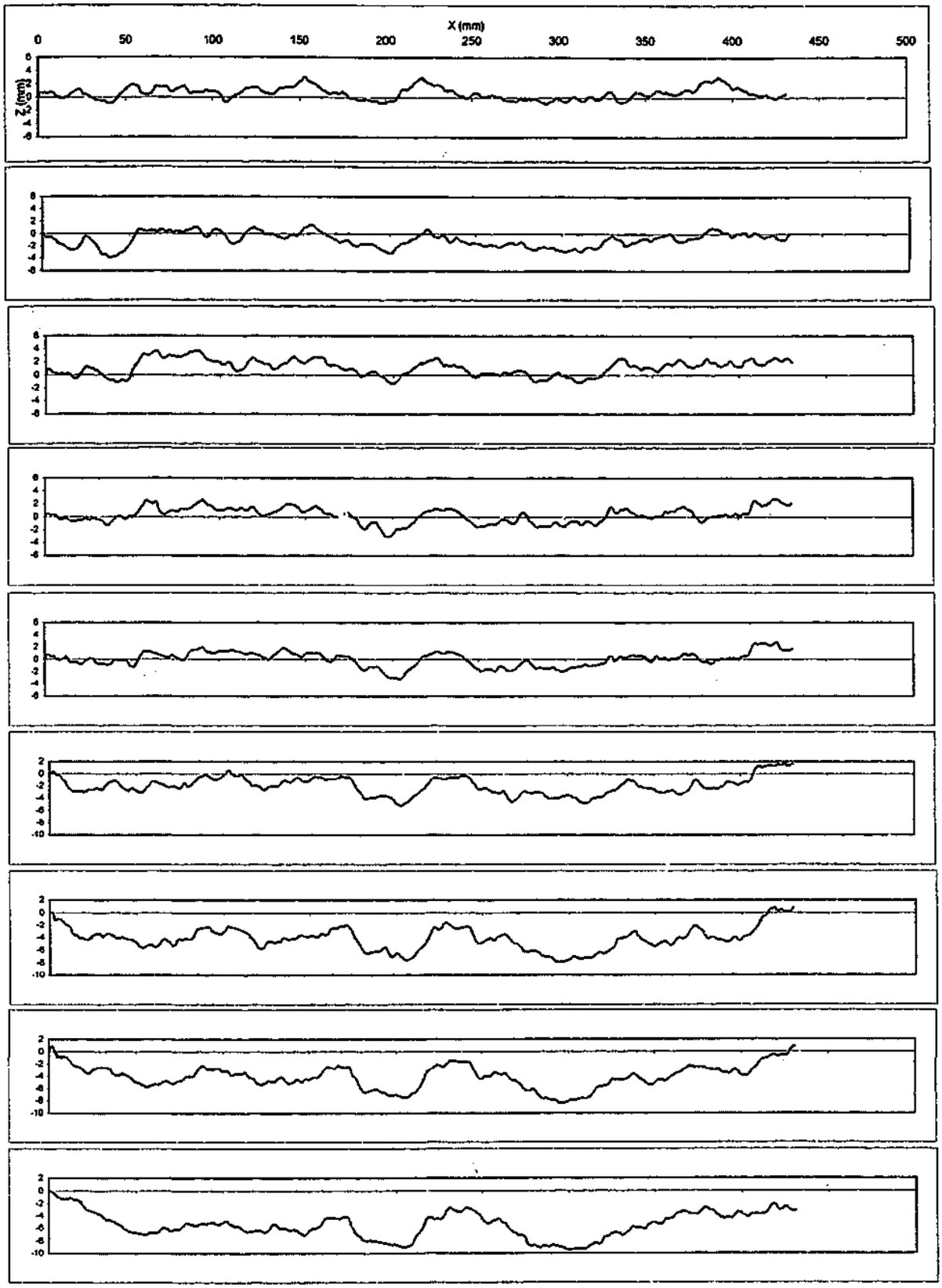

JOHNSTONE, SPLIT

BLOCK 3A

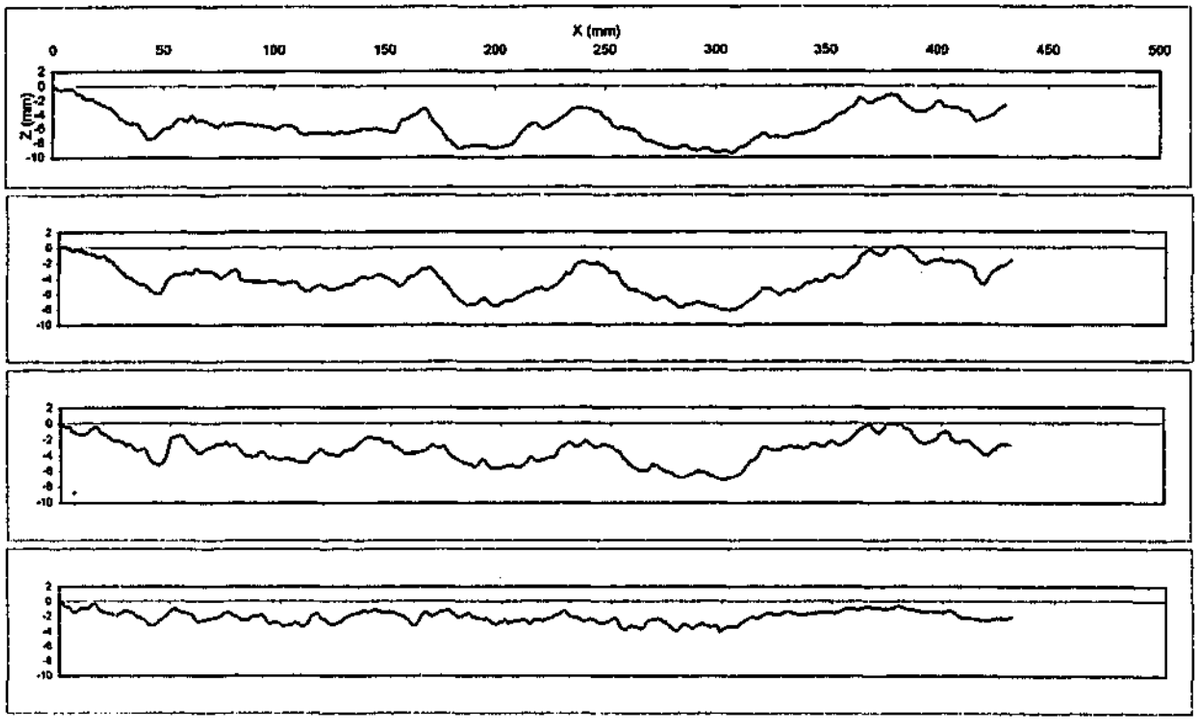

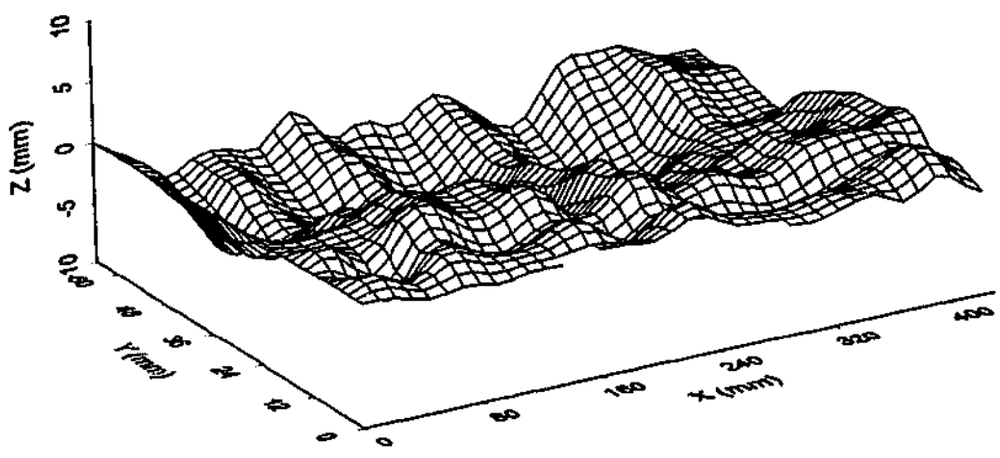

JOHNSTONE, SPLIT

BLOCK 3A

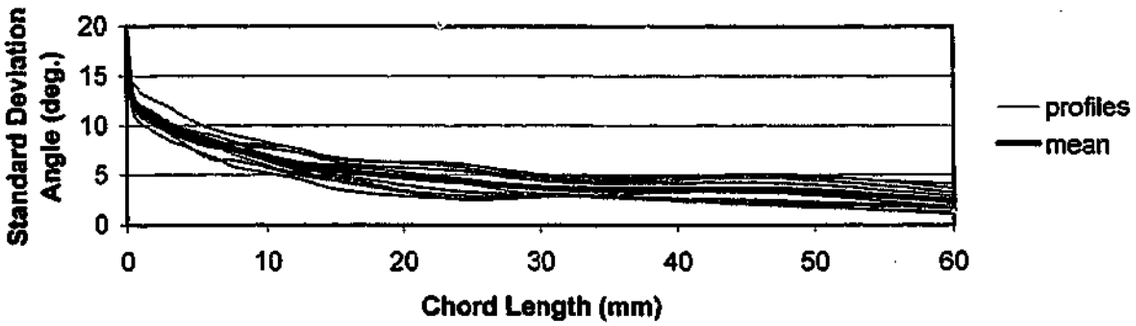

AVERAGE CORRELATION COEFFICIENT OF SCANS = 0.996

AVERAGE CORRELATION COEFFICIENT OF SCANS TO MEAN = 0.998

JOHNSTONE, SPLIT

BLOCK 3A

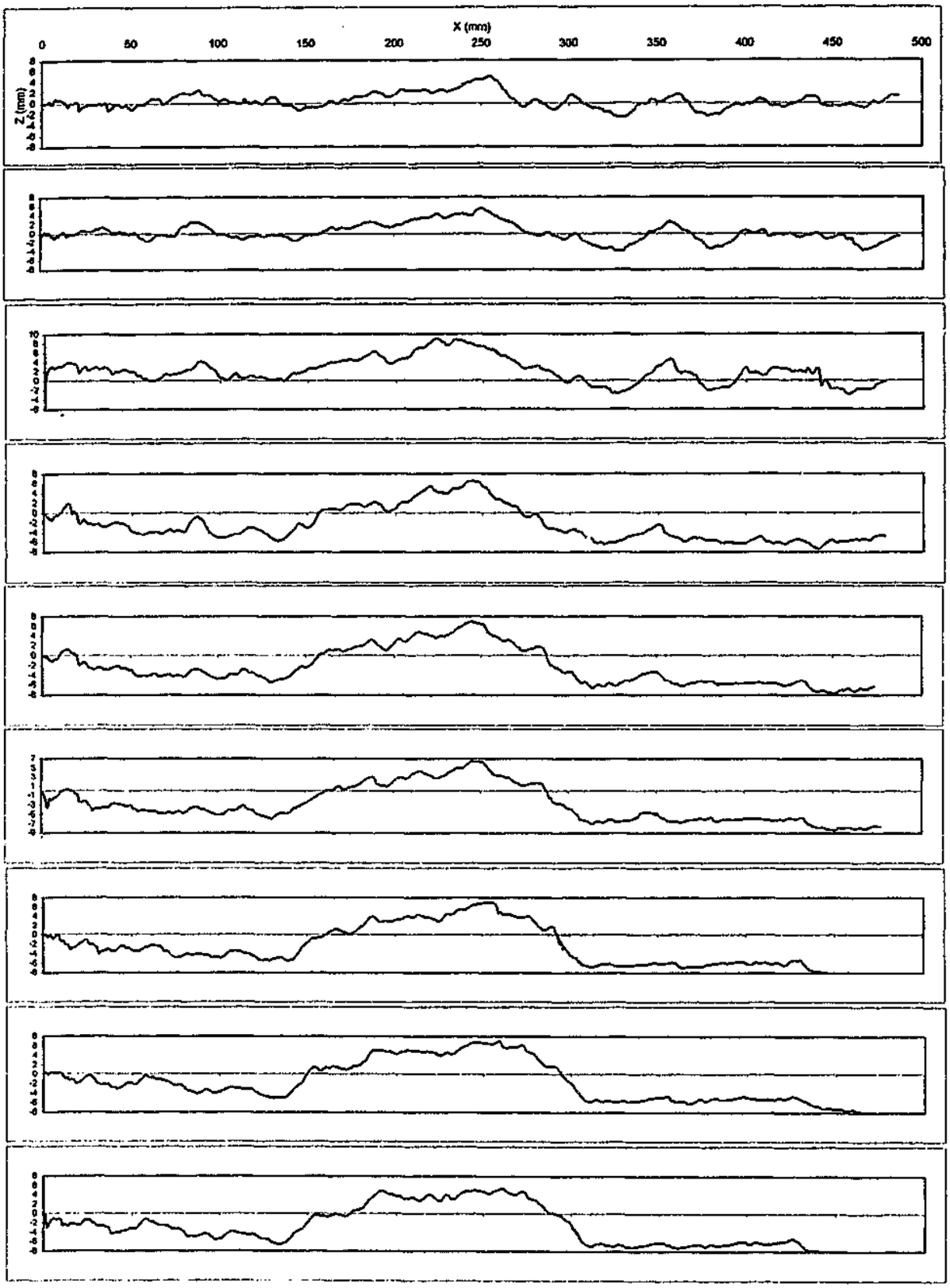

JOHNSTONE, SPLIT

BLOCK 3B

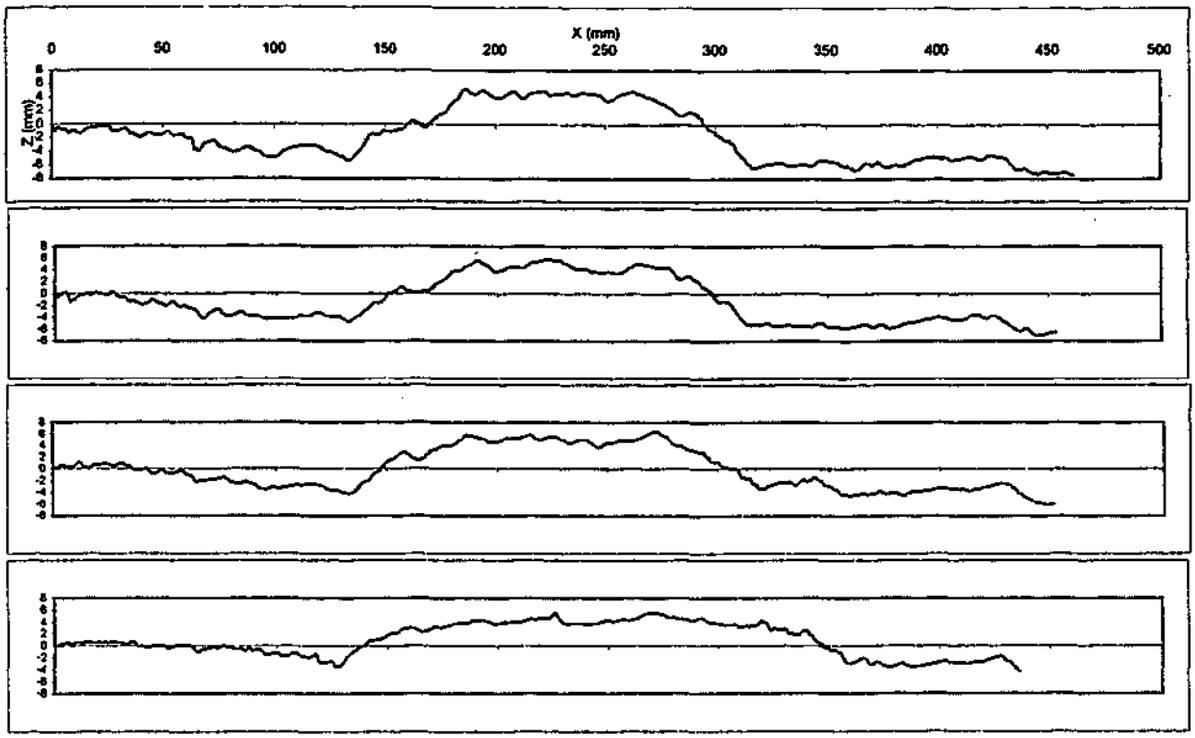

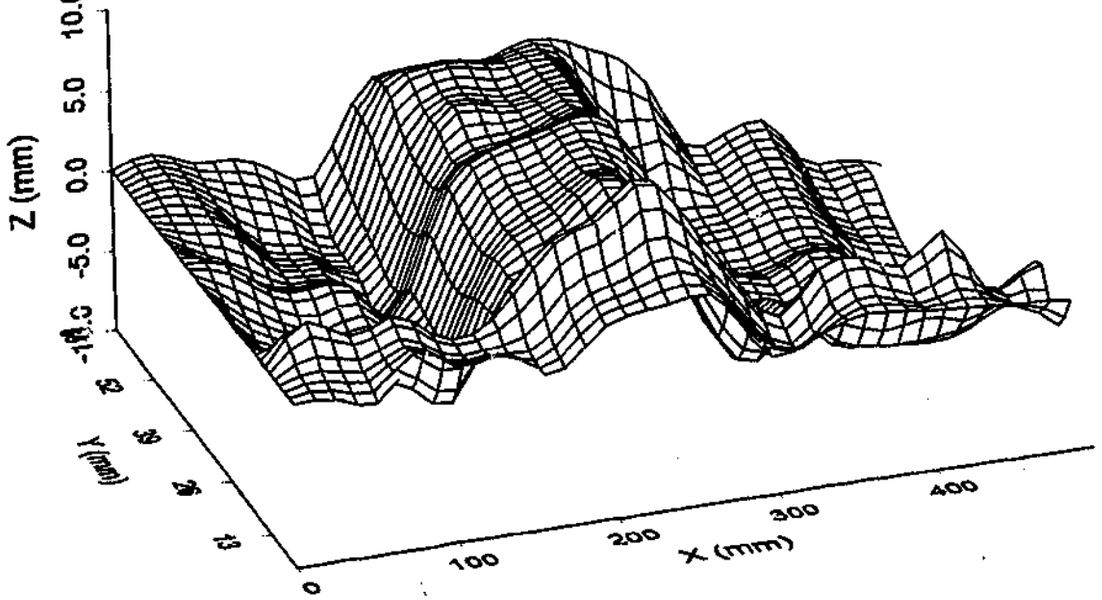

JOHNSTONE, SPLIT

BLOCK 3B

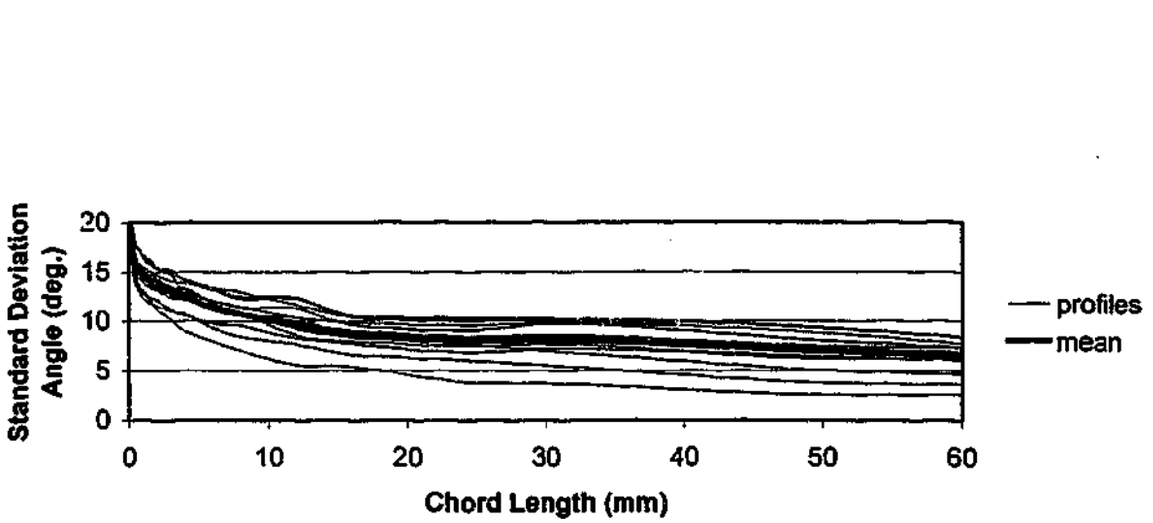

AVERAGE CORRELATION COEFFICIENT OF SCANS = 0.993

AVERAGE CORRELATION COEFFICIENT OF SCANS TO MEAN = 0.997

JOHNSTONE, SPLIT

BLOCK 3B

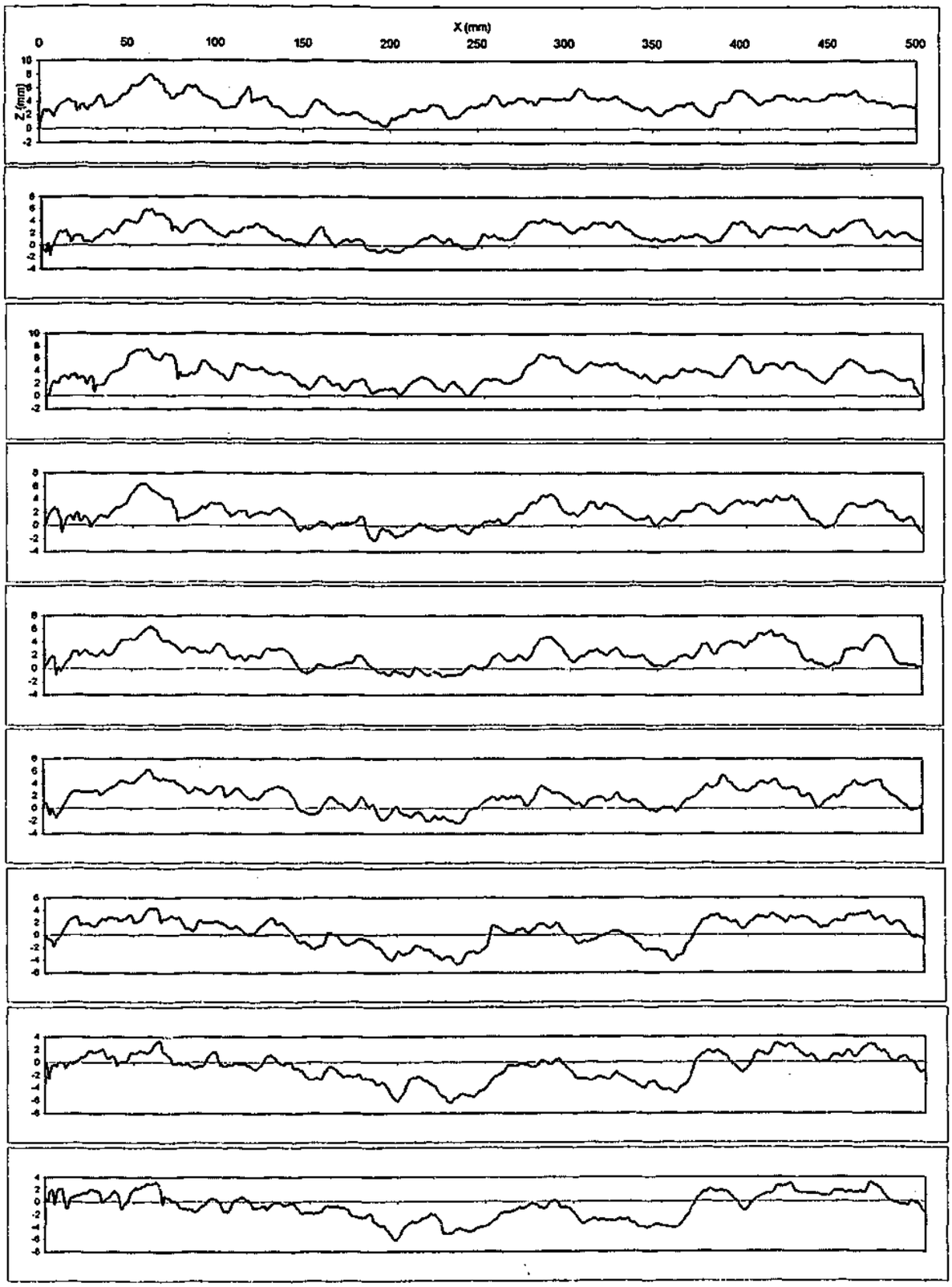

JOHNSTONE, SPLIT

BLOCK 4A

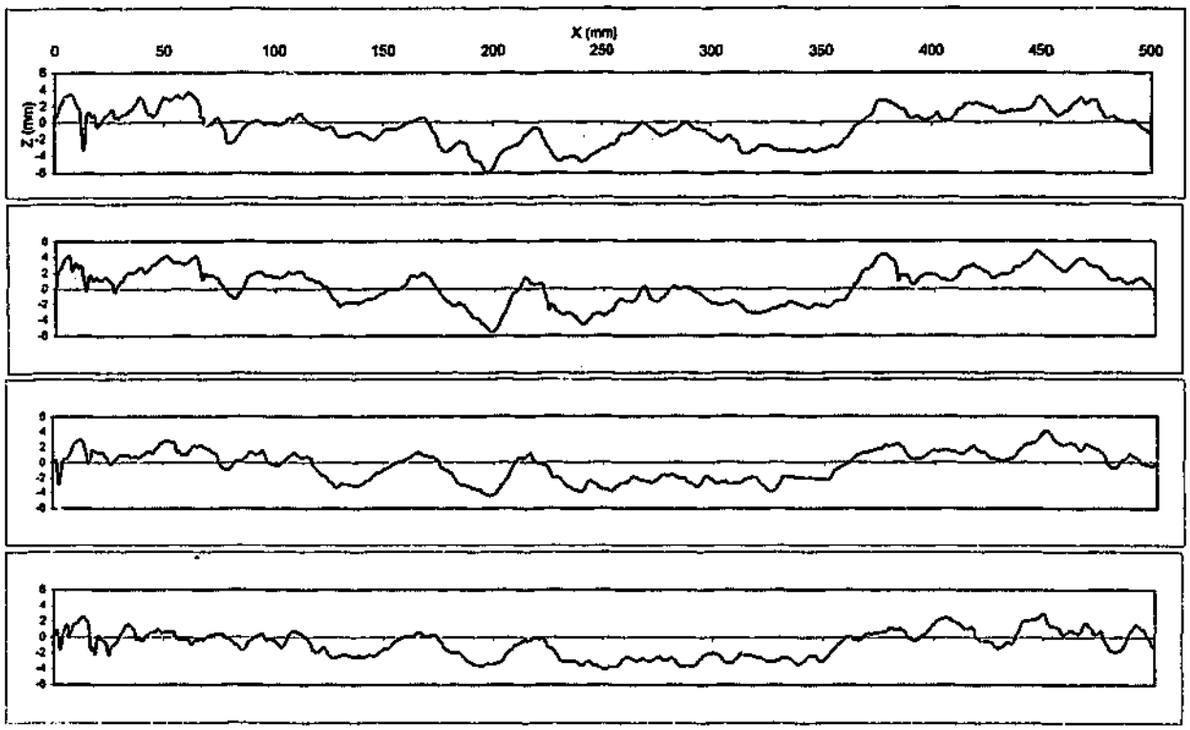

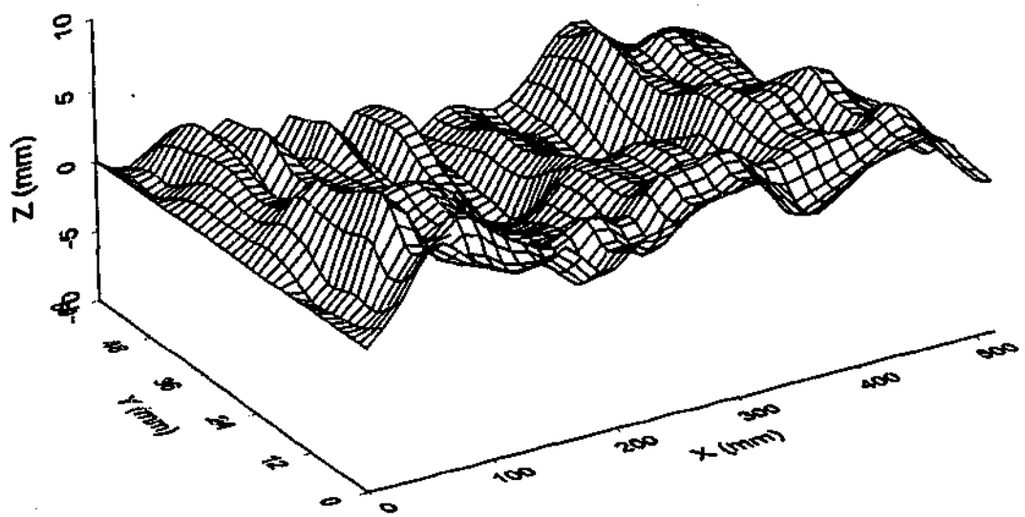

JOHNSTONE, SPLIT

BLOCK 4A

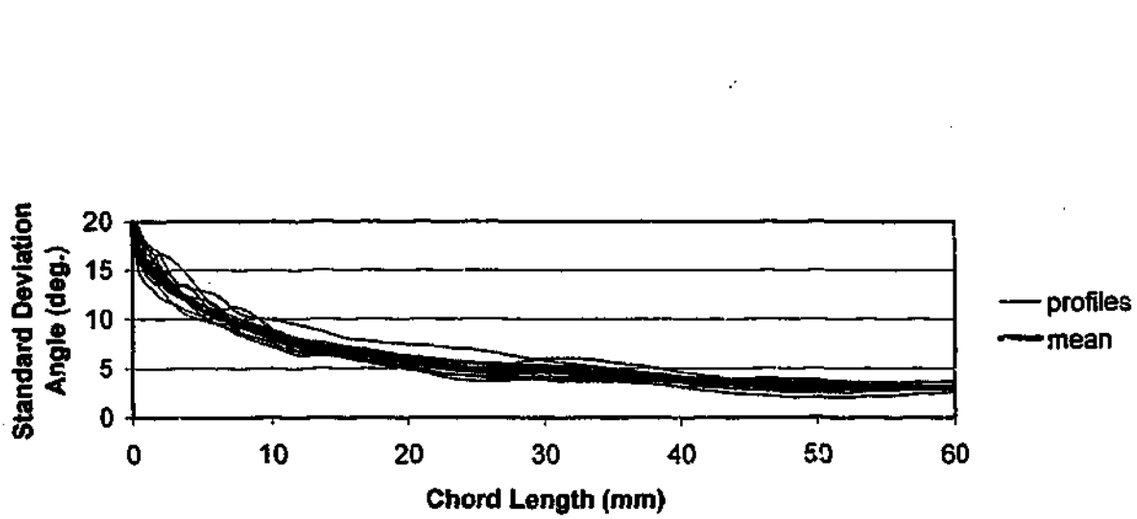

AVERAGE CORRELATION COEFFICIENT OF SCANS = 0.996

AVERAGE CORRELATION COEFFICIENT OF SCANS TO MEAN = 0.998

JOHNSTONE, SPLIT

BLOCK 4A

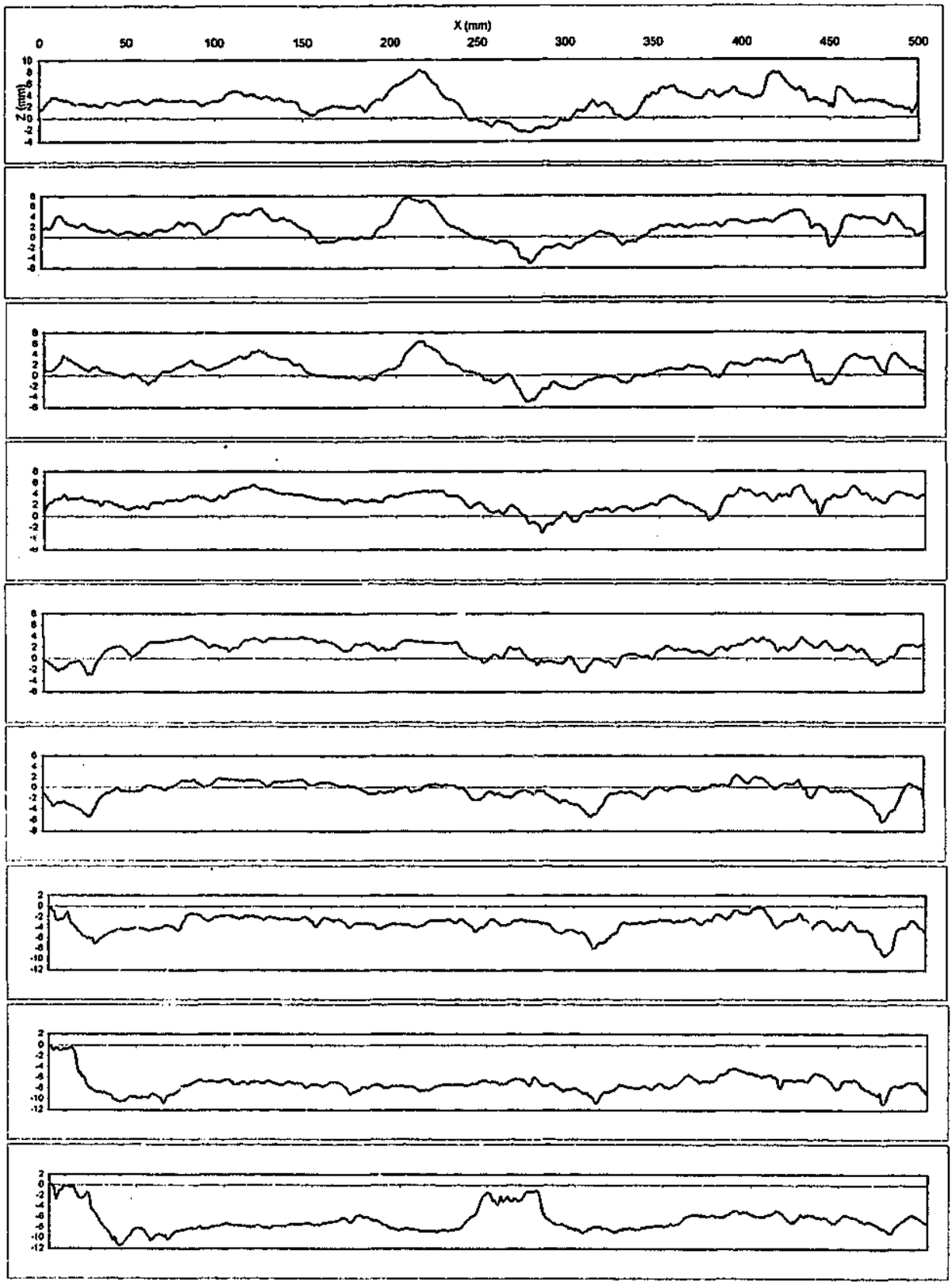

JOHNSTONE, SPLIT

BLOCK 6A

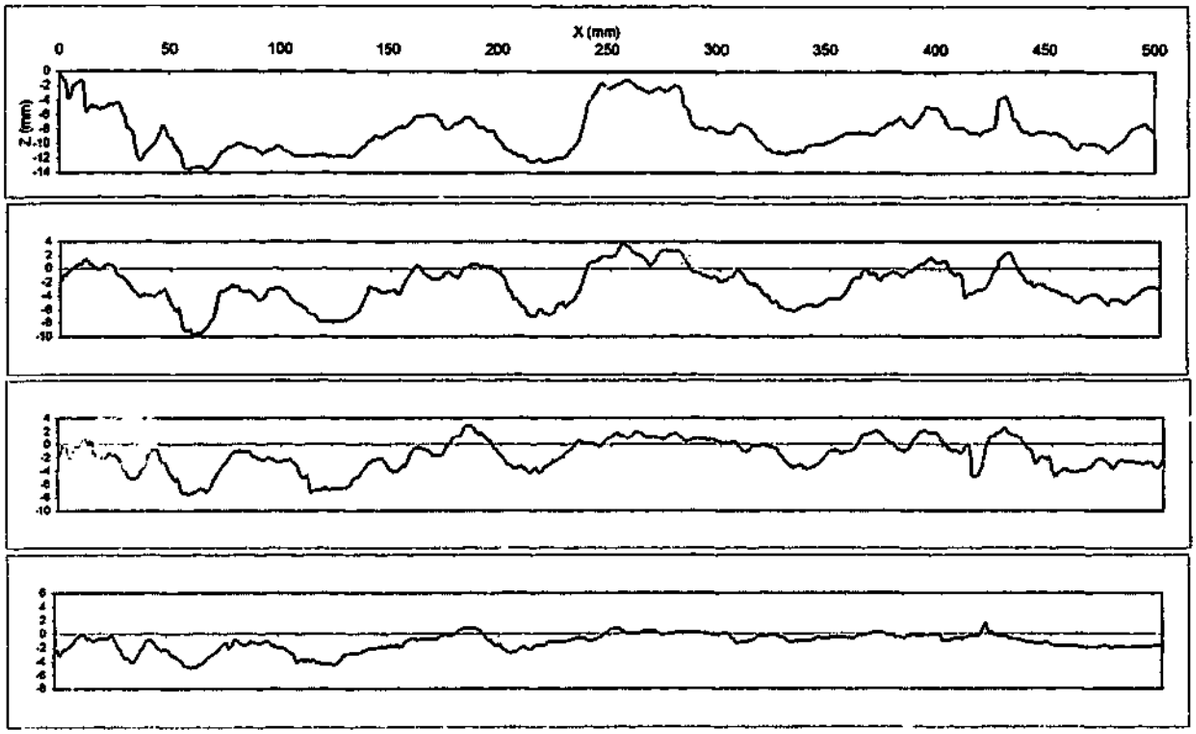

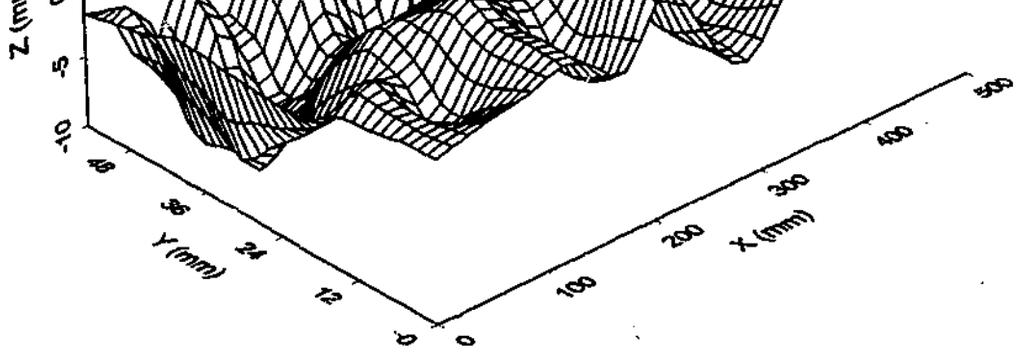

JOHNSTONE, SPLIT

BLOCK 6A

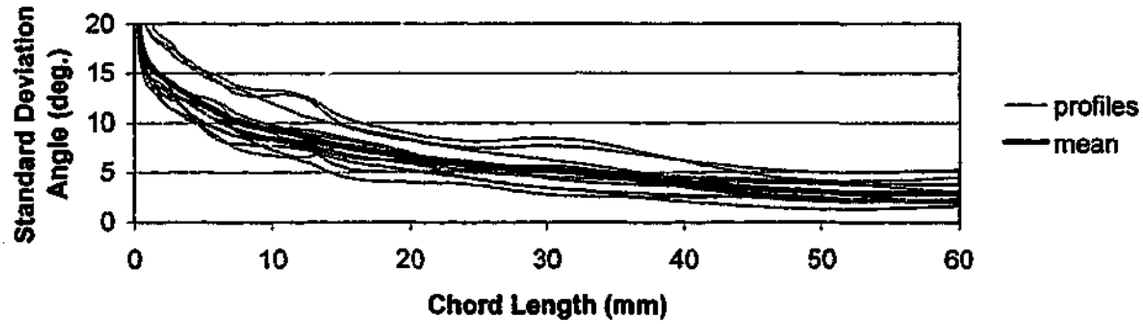

AVERAGE CORRELATION COEFFICIENT OF SCANS = 0.991

AVERAGE CORRELATION COEFFICIENT OF SCANS TO MEAN = 0.996

JOHNSTONE, SPLIT

BLOCK 6A

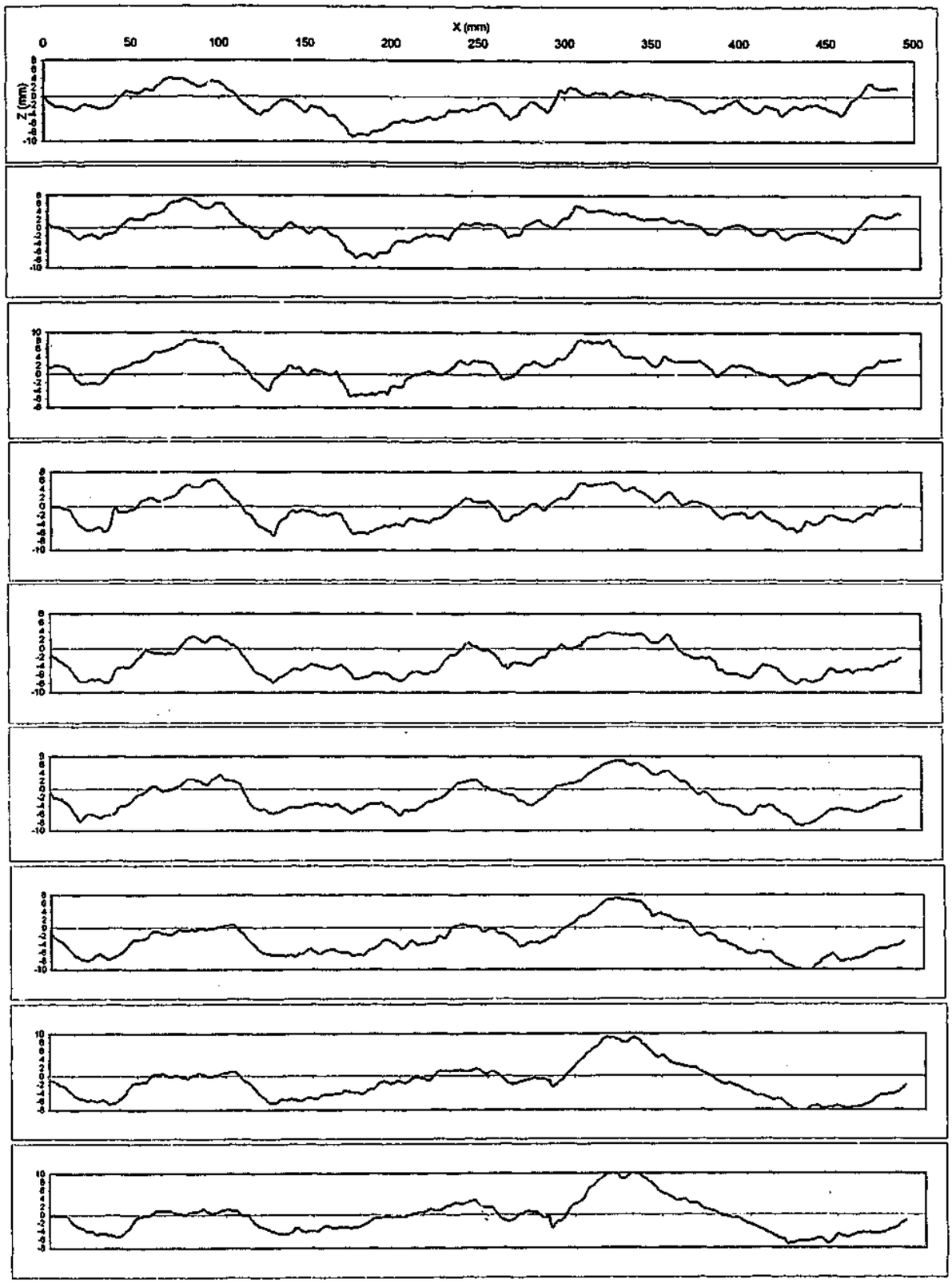

JOHNSTONE, SPLIT

BLOCK 7A

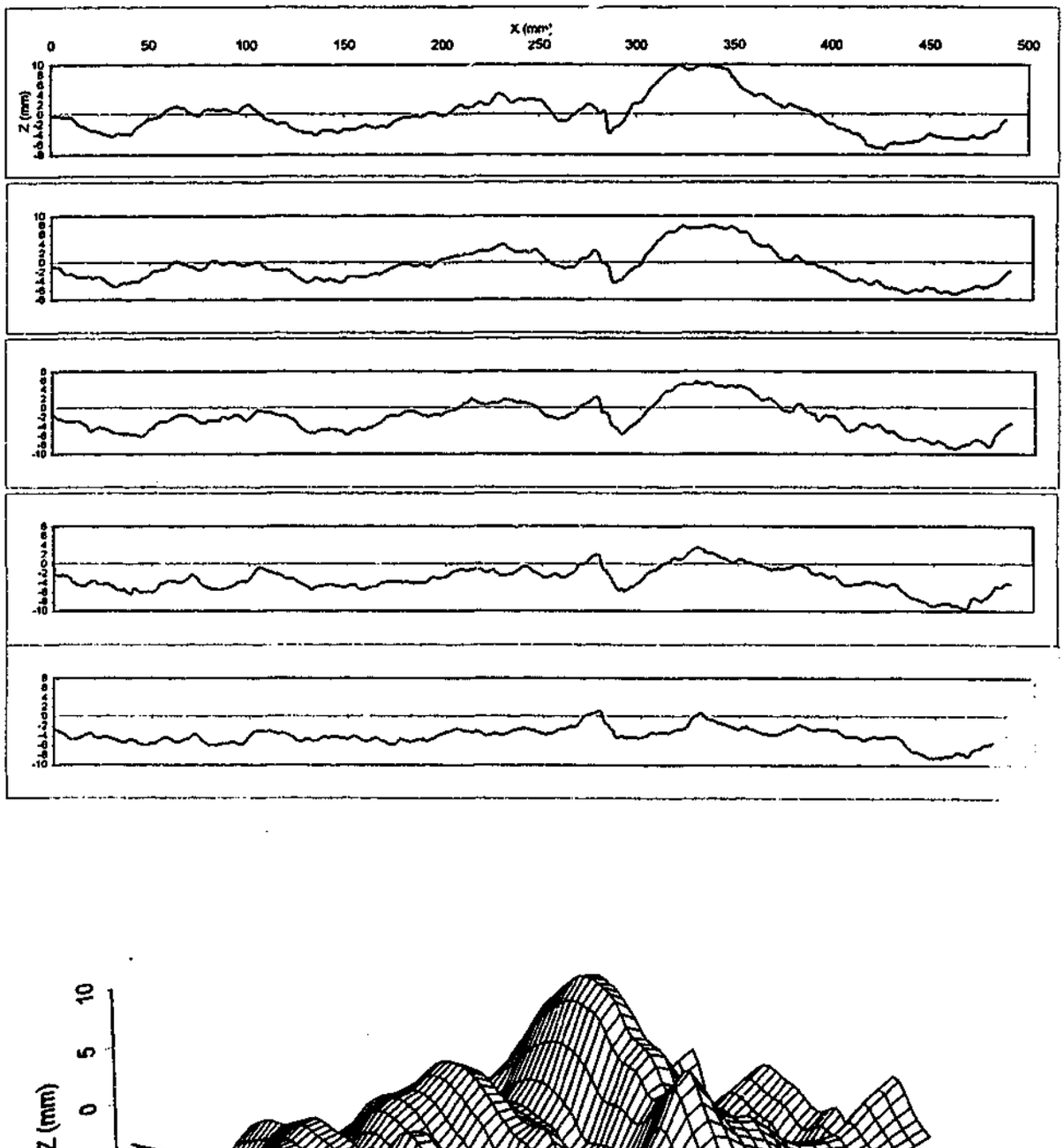

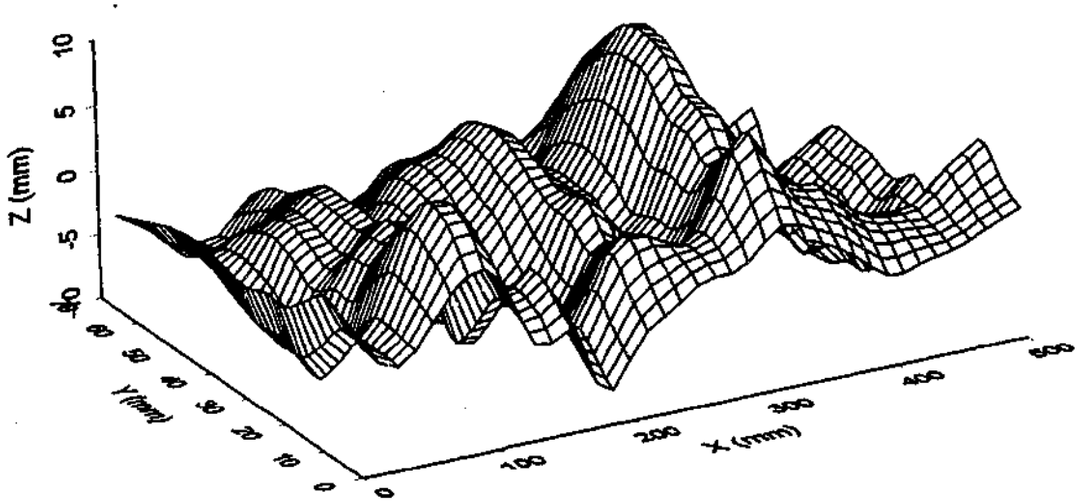

JOHNSTONE, SPLIT

BLOCK 7A

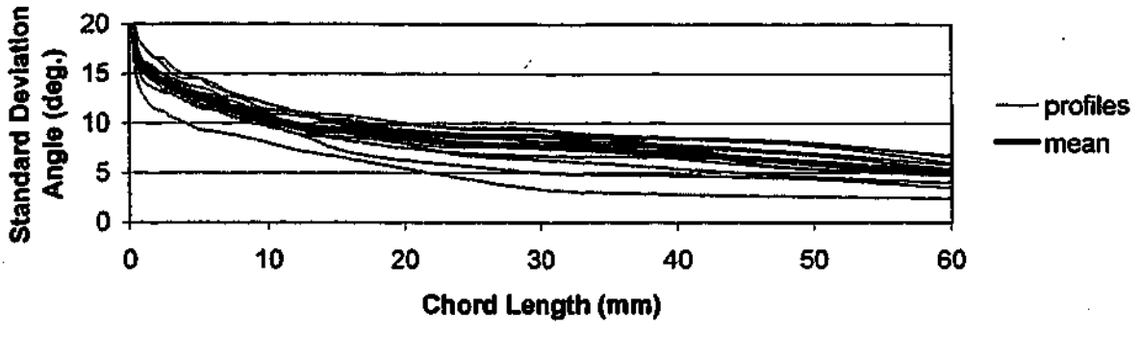

AVERAGE CORRELATION COEFFICIENT OF SCANS = 0.991

AVERAGE CORRELATION COEFFICIENT OF SCANS TO MEAN = 0.996

JOHNSTONE, SPLIT

BLOCK 7A

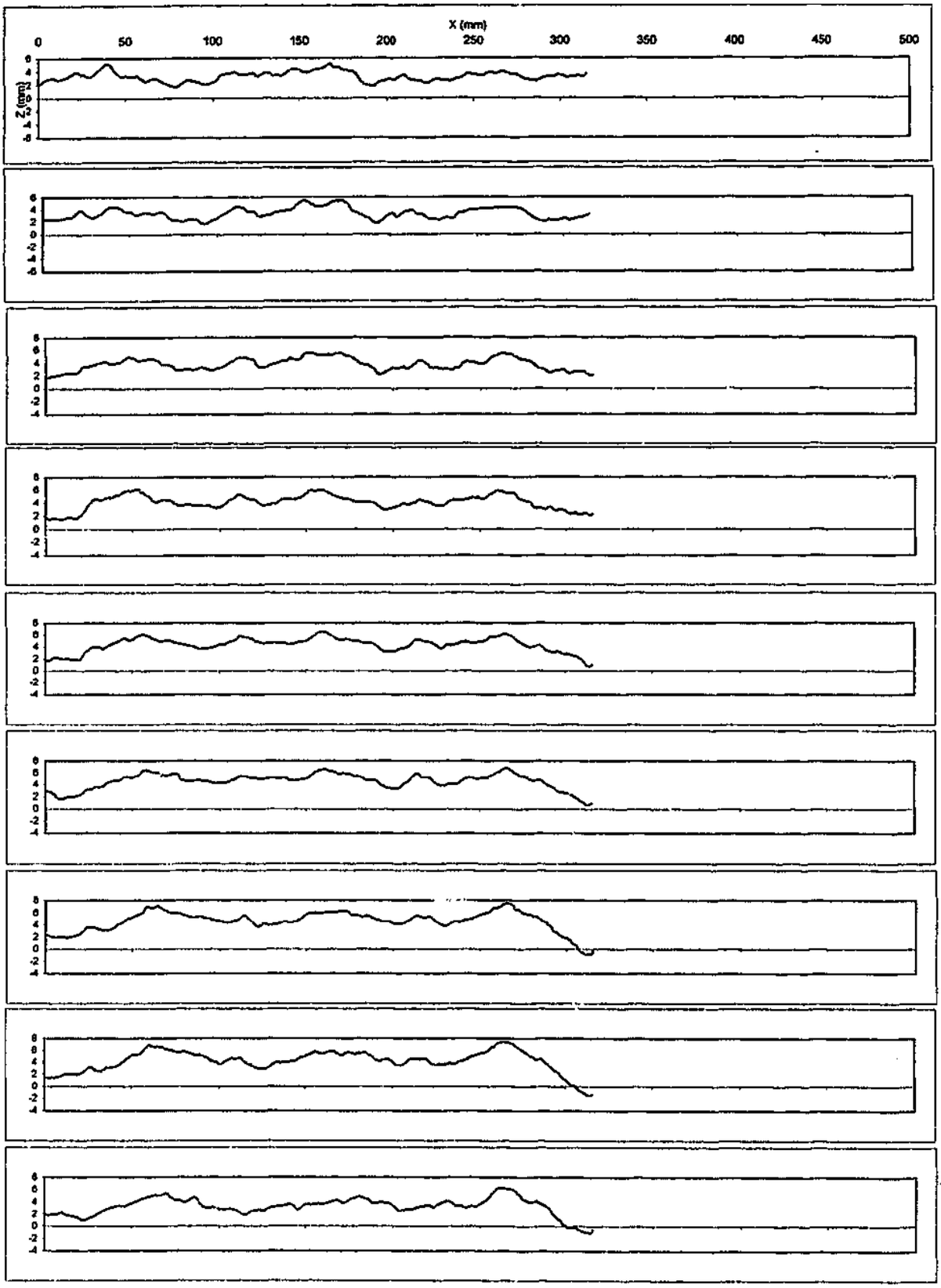

SANDSTONE, SPLIT

BLOCK 1

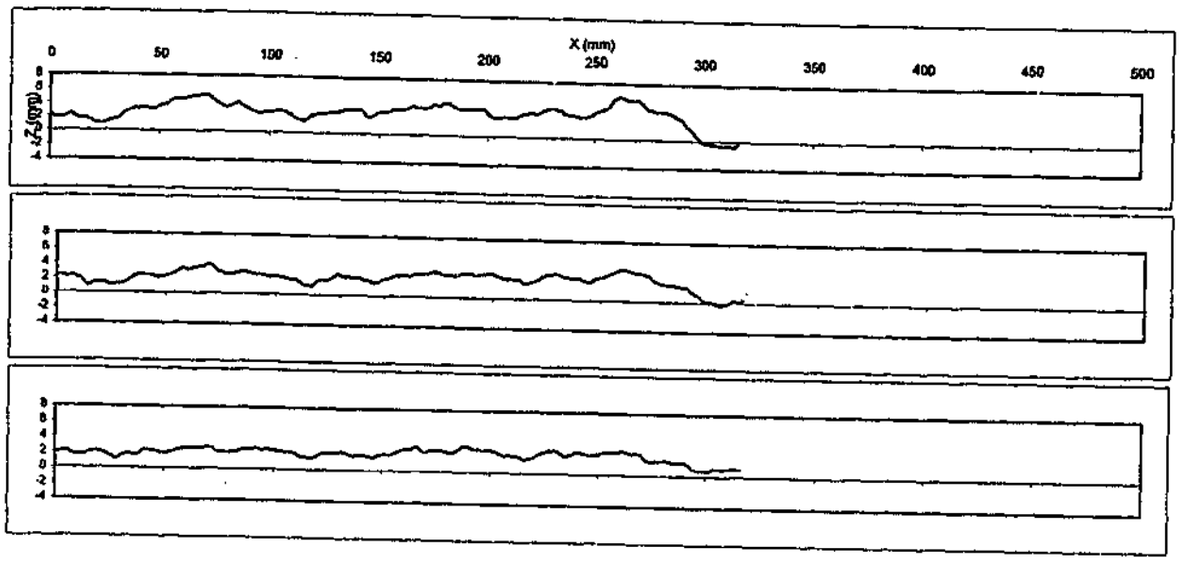

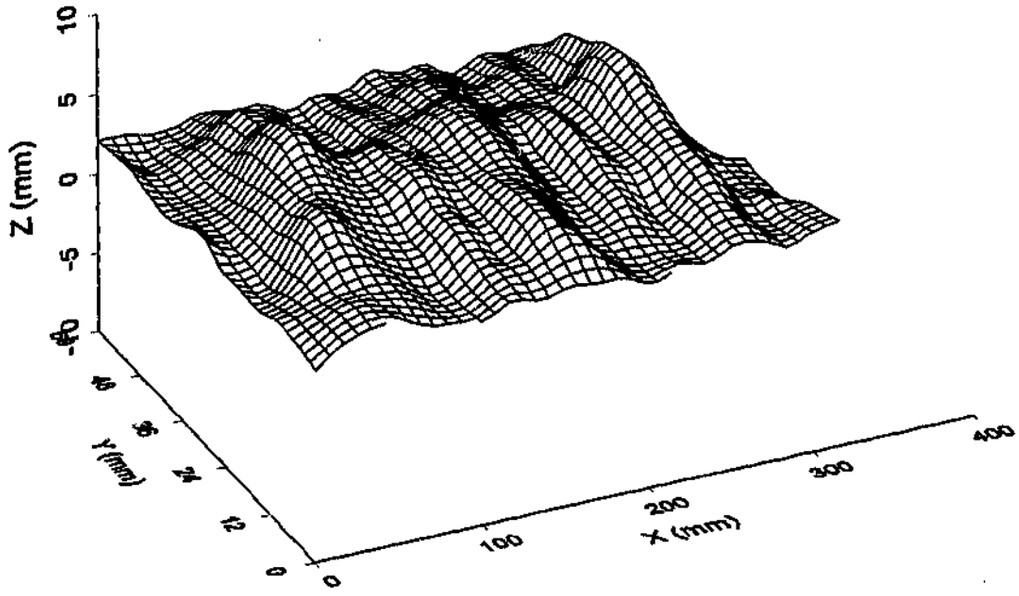

SANDSTONE, SPLIT

BLOCK 1

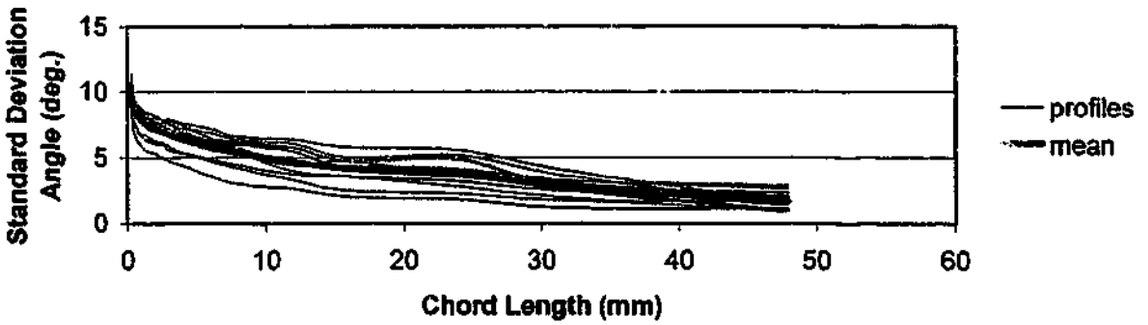

AVERAGE CORRELATION COEFFICIENT OF SCANS = 0.984

AVERAGE CORRELATION COEFFICIENT OF SCANS TO MEAN = 0.993

SANDSTONE, SPLIT

BLOCK 1

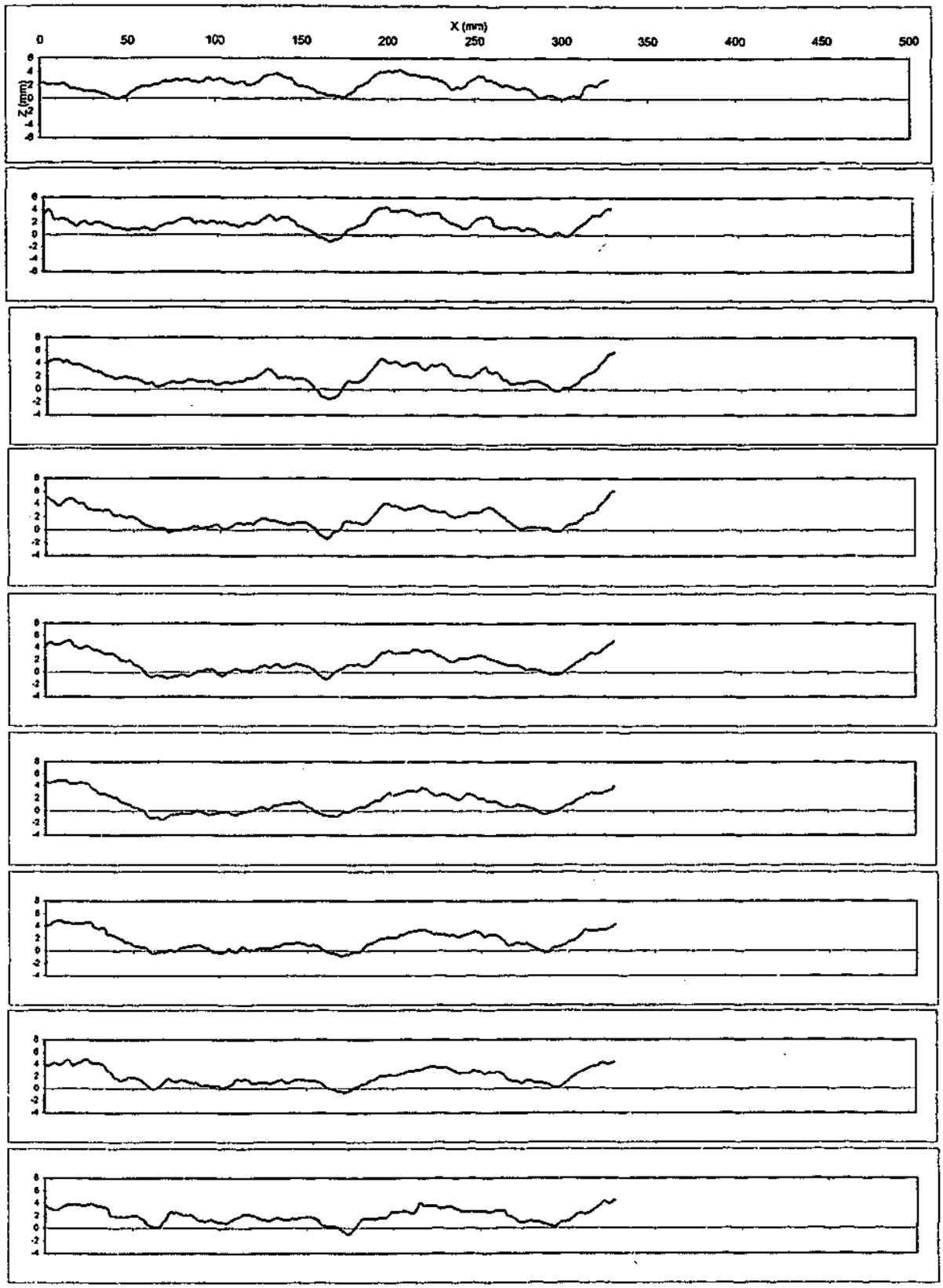

SANDSTONE, SPLIT

BLOCK 2

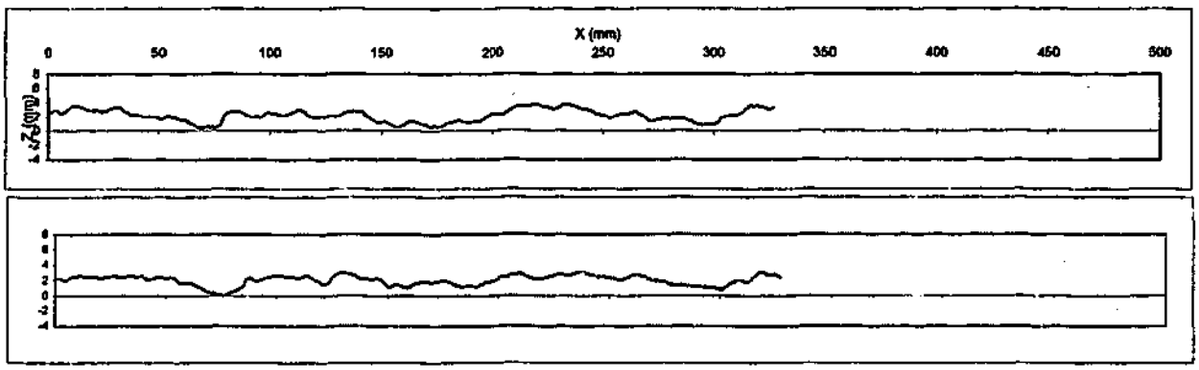

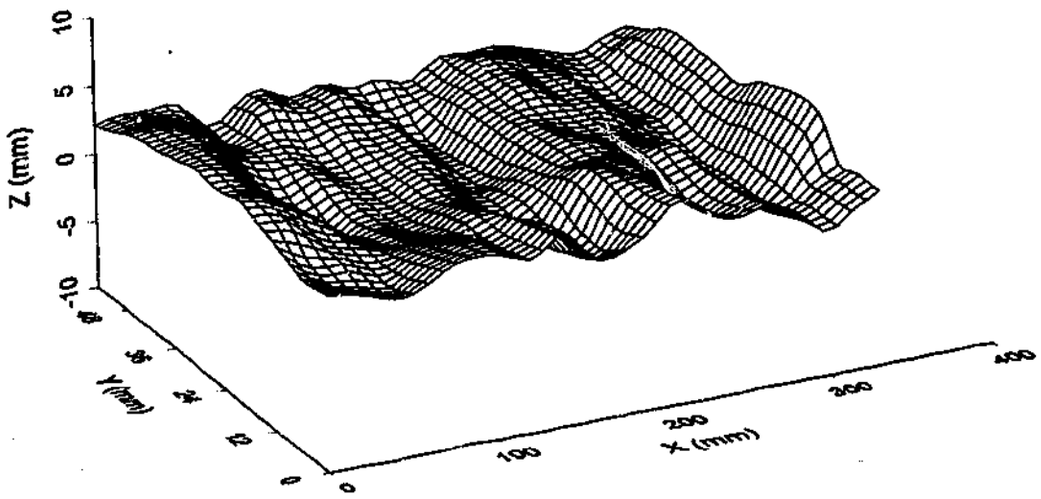

SANDSTONE, SPLIT

BLOCK 2

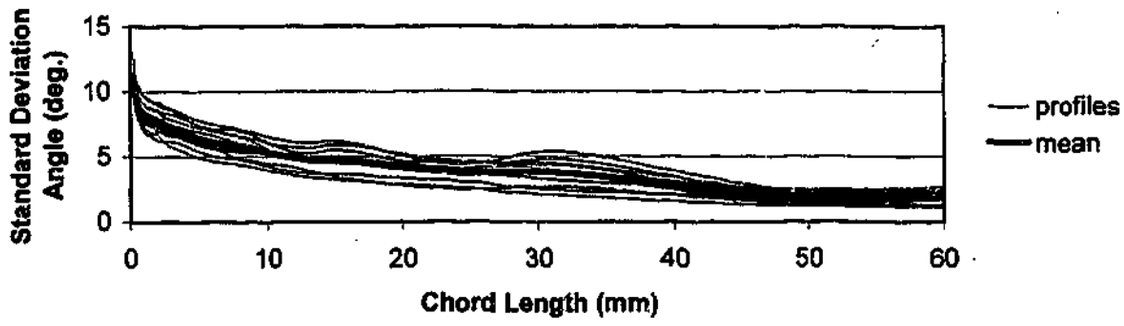

AVERAGE CORRELATION COEFFICIENT OF SCANS = 0.991

AVERAGE CORRELATION COEFFICIENT OF SCANS TO MEAN = 0.996

SANDSTONE, SPLIT

BLOCK 2

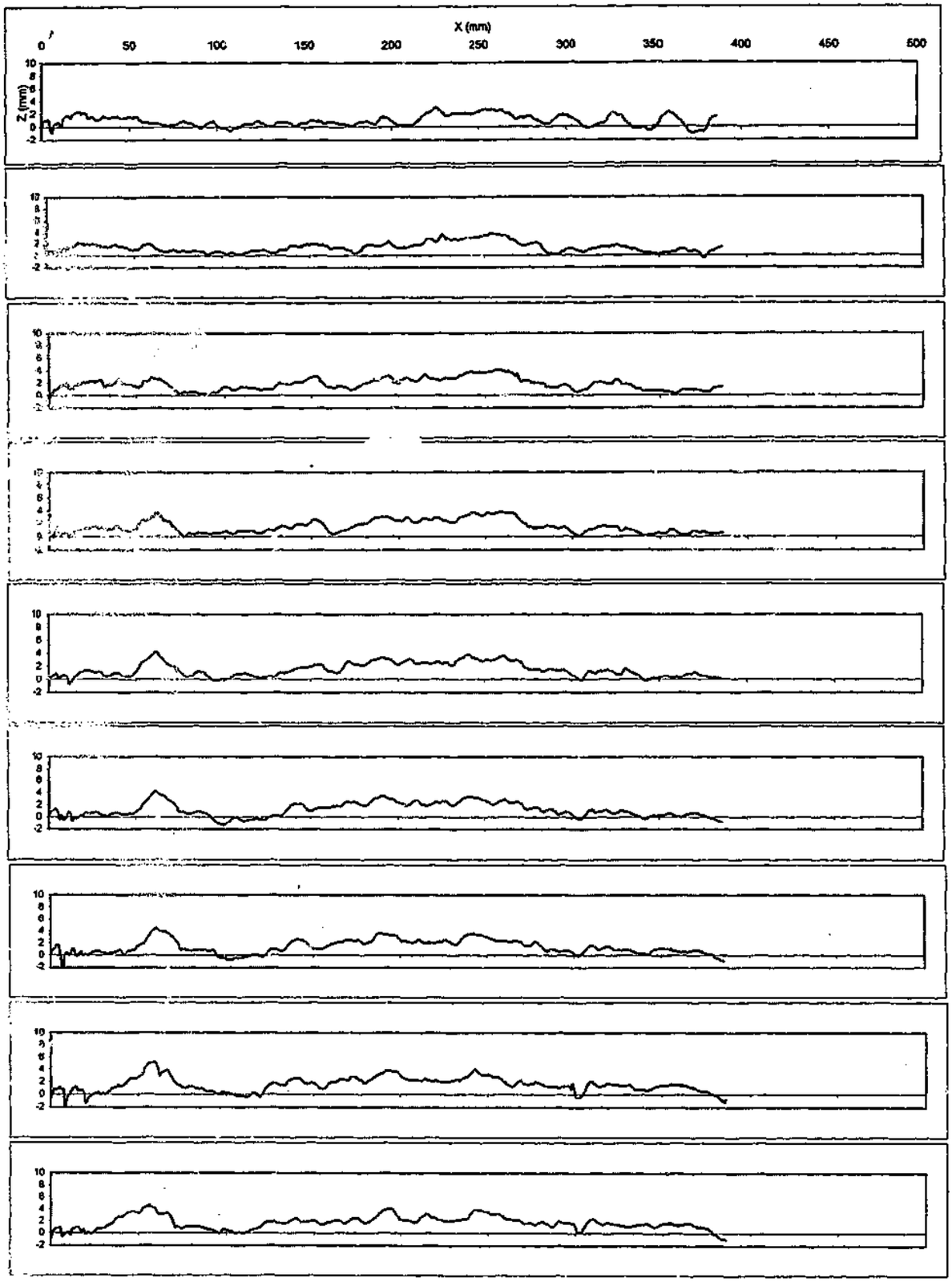

SILTSTONE SW, SPLIT 1

scanned at 5 mm intervals

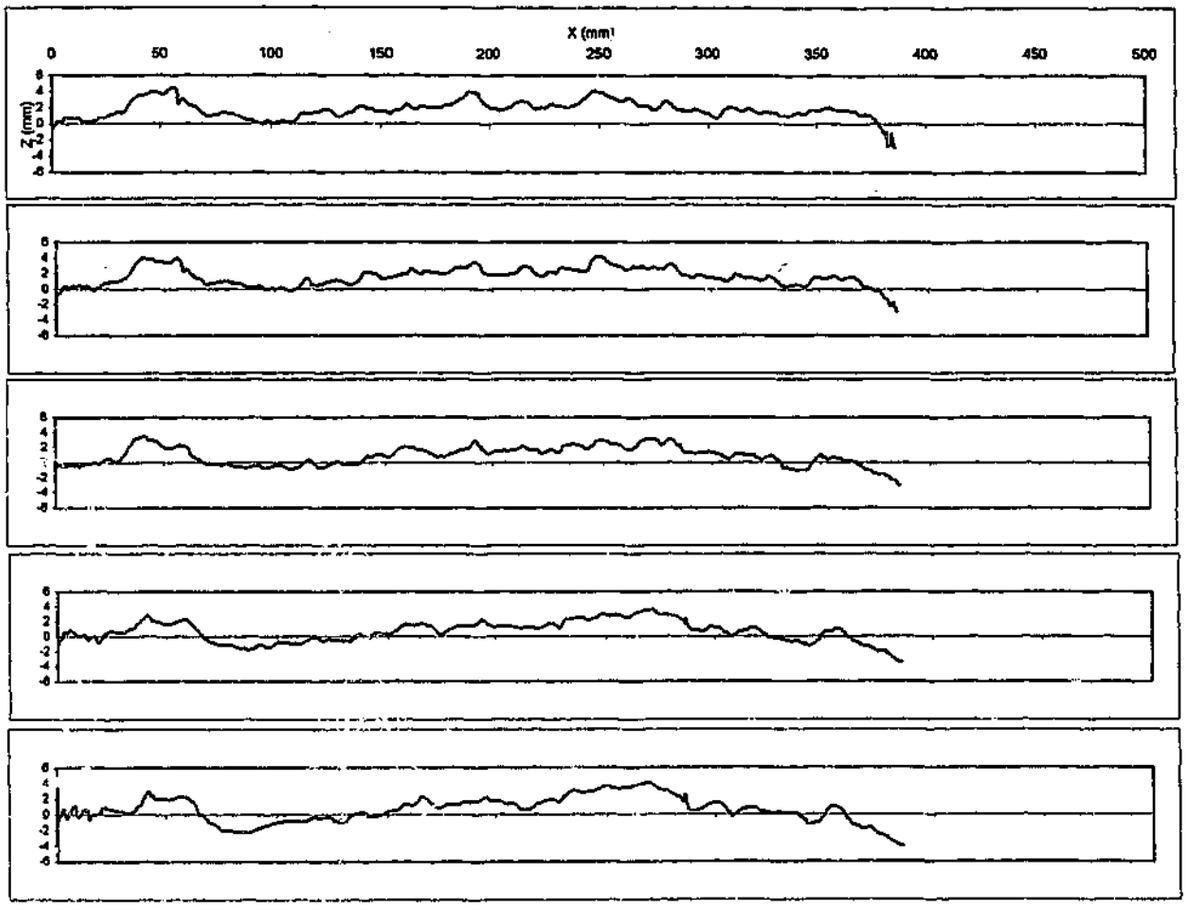

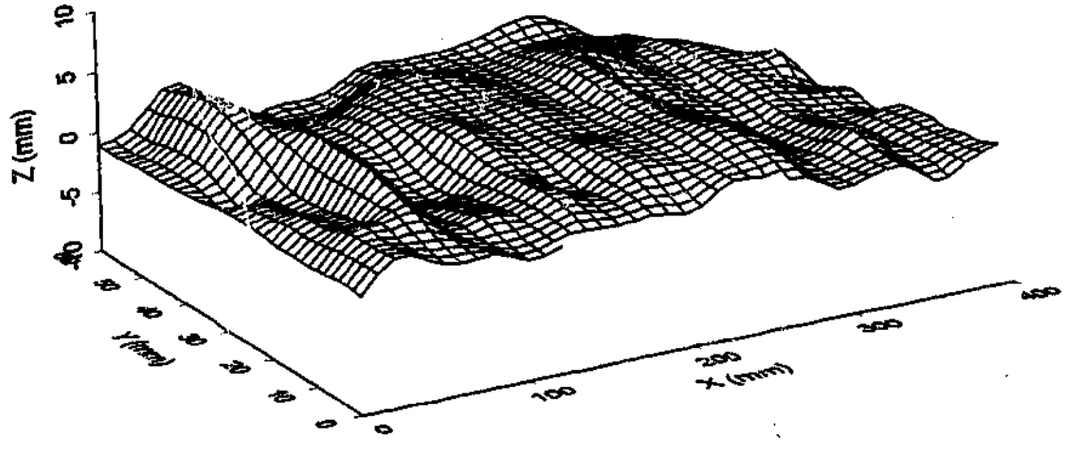

SILTSTONE SW, SPLIT 1

scanned at 5 mm intervals

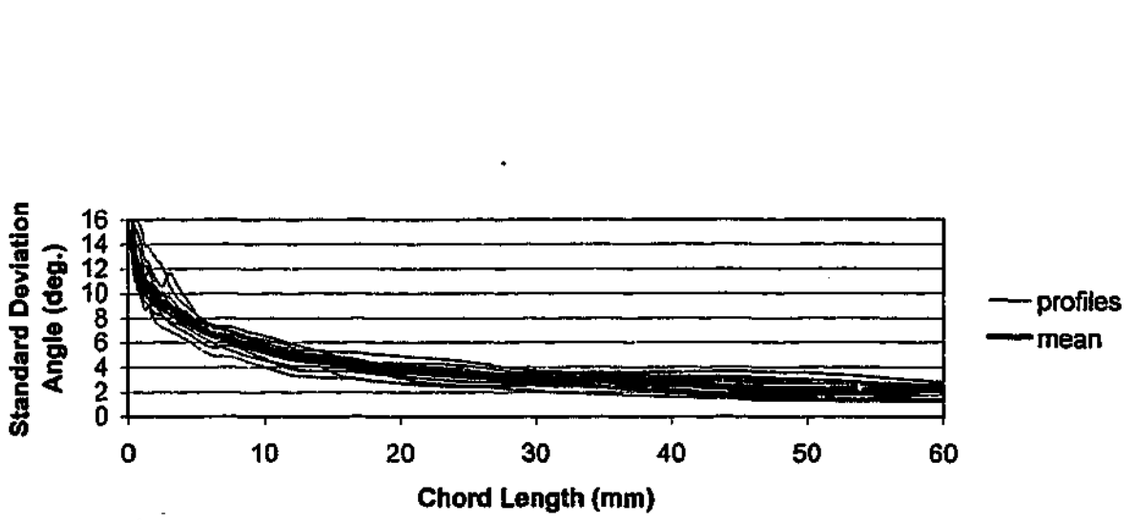

AVERAGE CORRELATION COEFFICIENT OF SCANS = 0.994

AVERAGE CORRELATION COEFFICIENT OF SCANS TO MEAN = 0.997

SILTSTONE SW, SPLIT

BLOCK 1

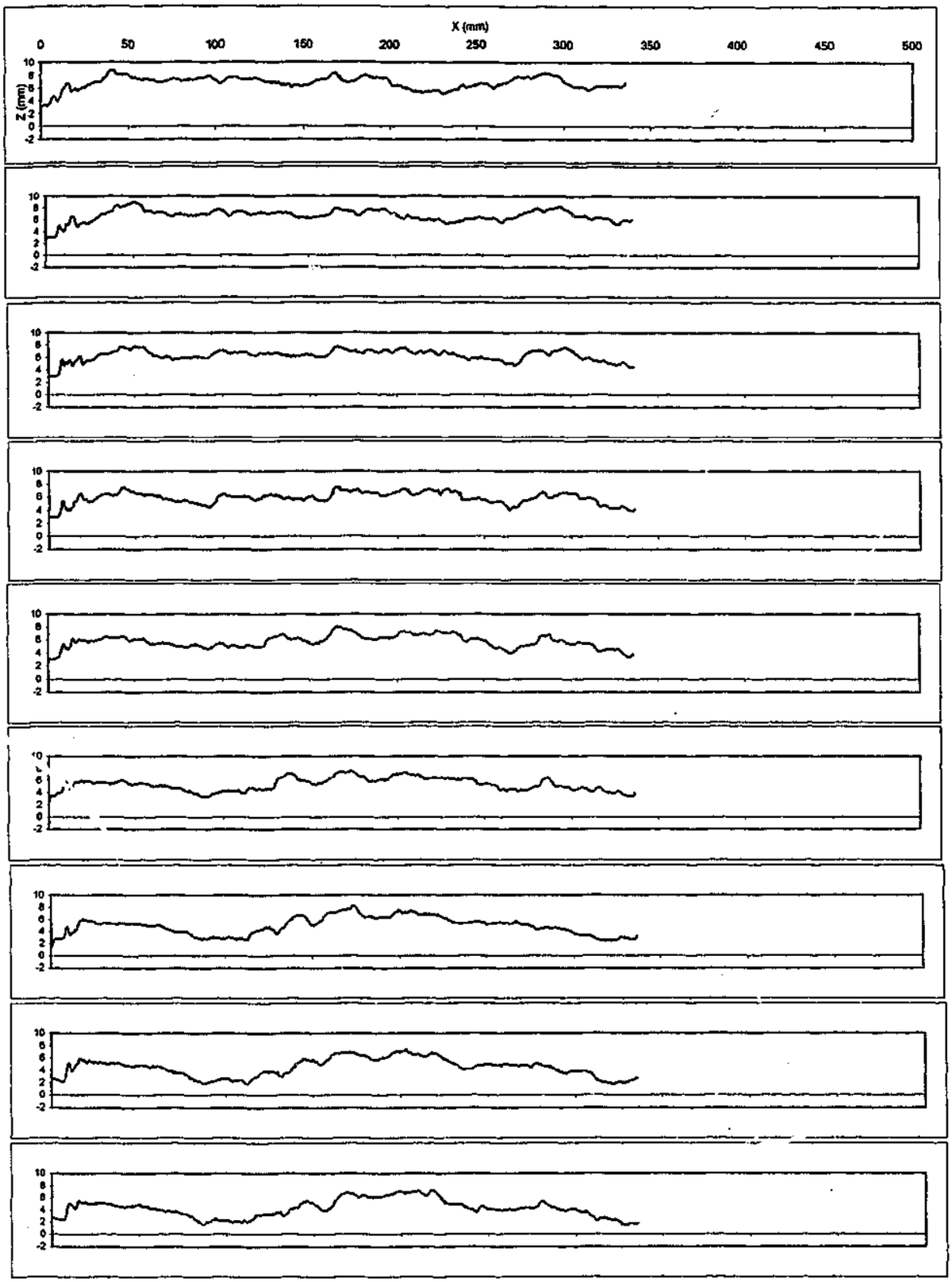

SILTSTONE SW, SPLIT 2

scanned at 5 mm intervals

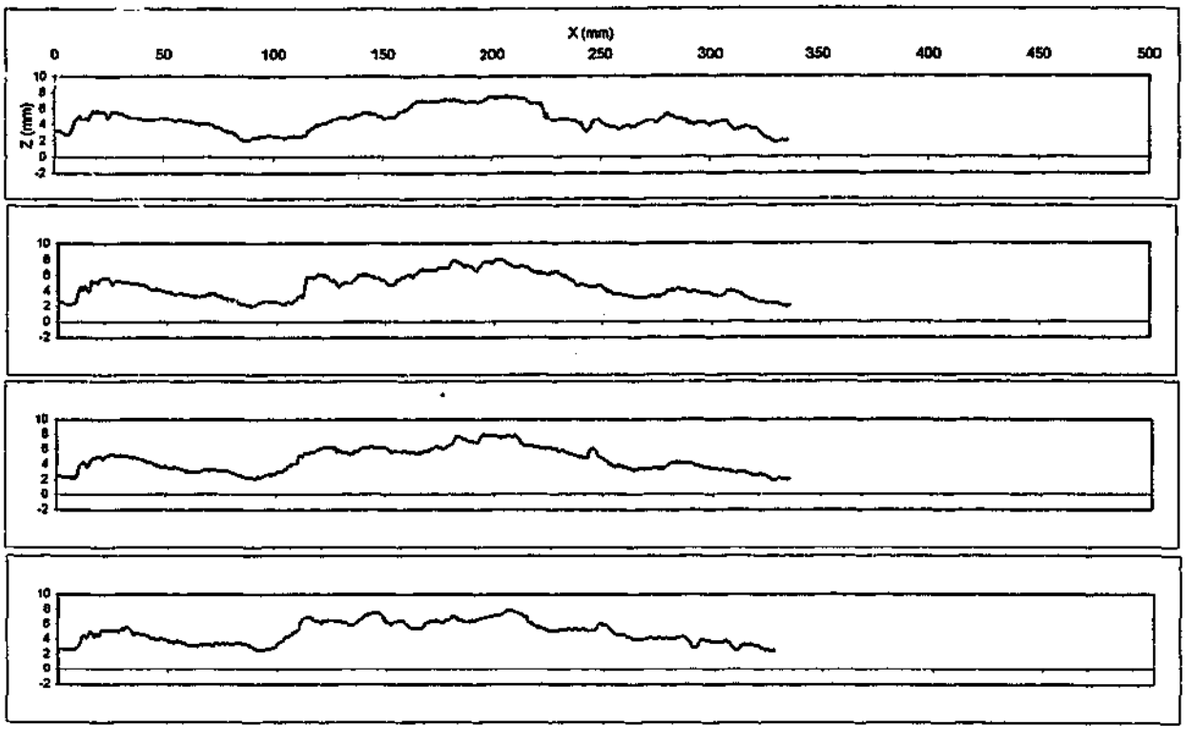

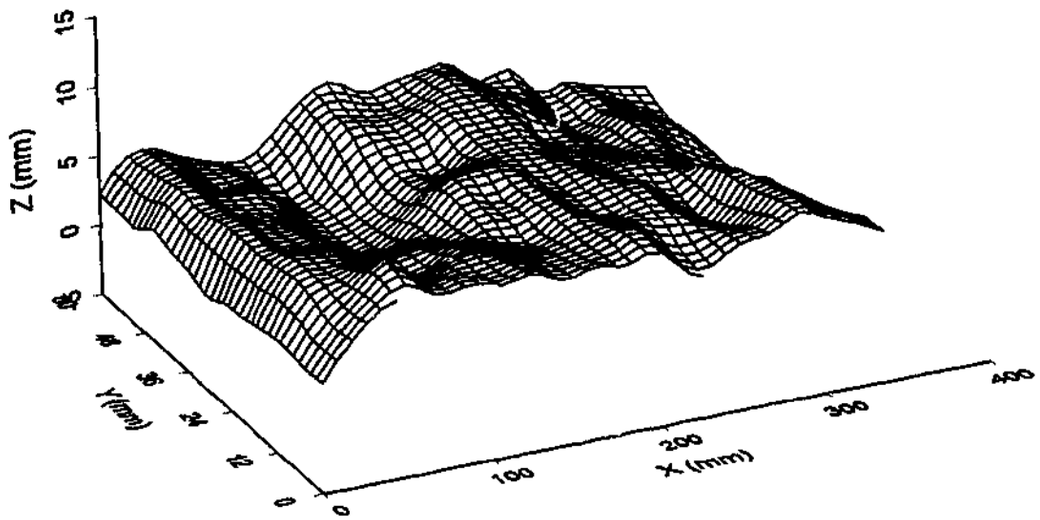

SILTSTONE SW, SPLIT 2

scanned at 5 mm intervals

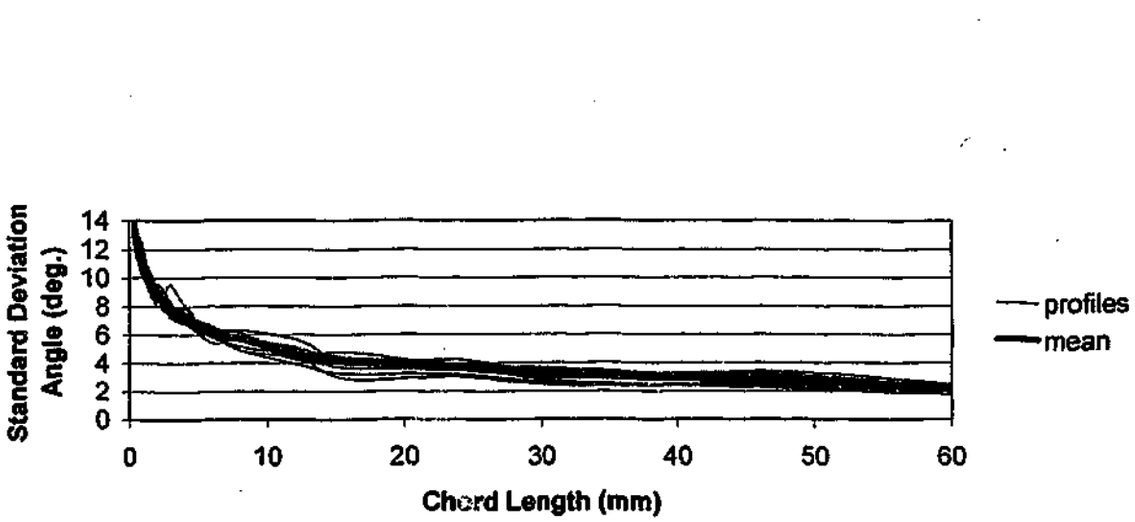

AVERAGE CORRELATION COEFFICIENT OF SCANS = 0.995

AVERAGE CORRELATION COEFFICIENT OF SCANS TO MEAN = 0.997

SILTSTONE SW, SPLIT

BLOCK 2

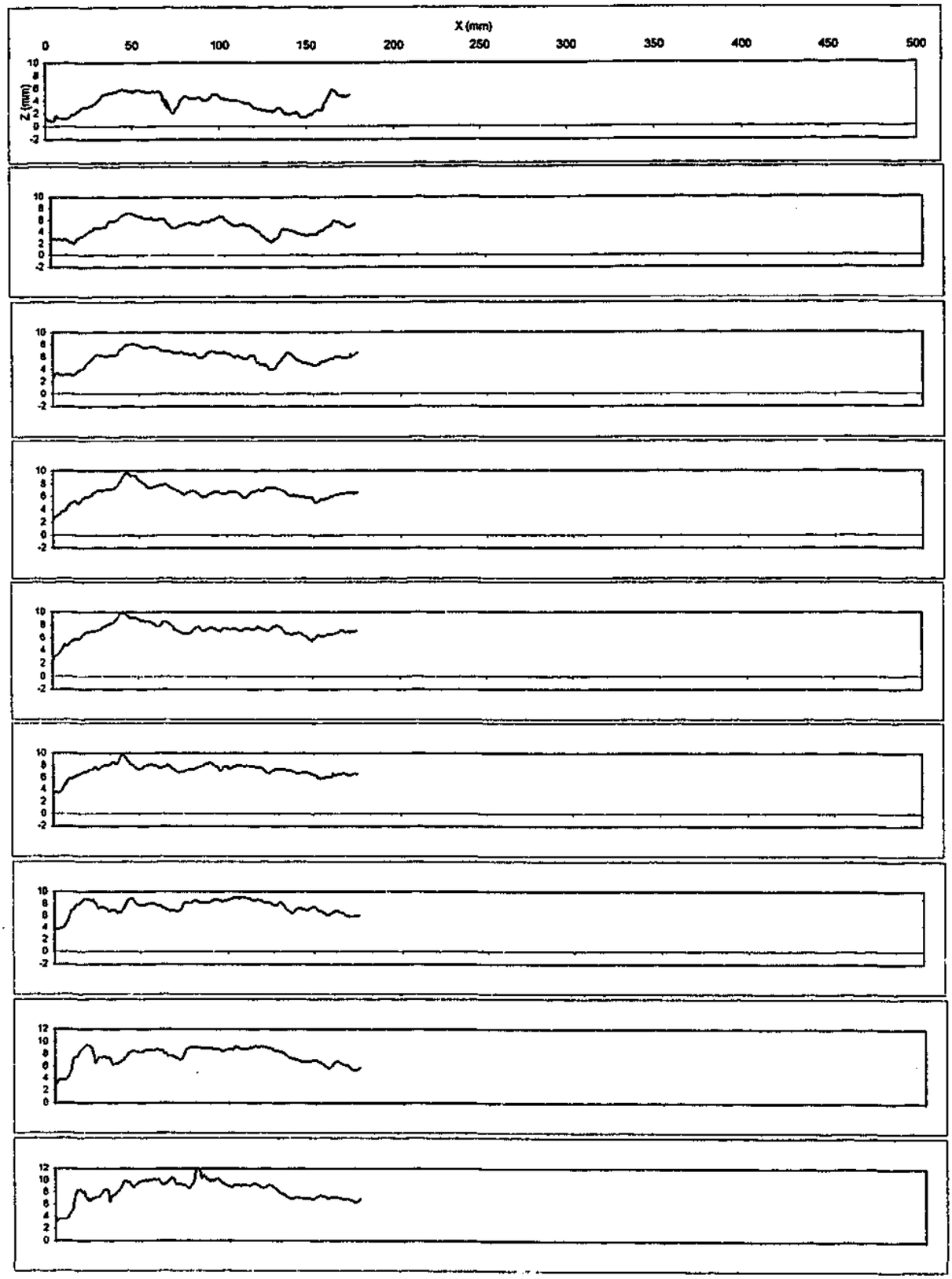

SILTSTONE SW, SPLIT 3

scanned at 5 mm intervals

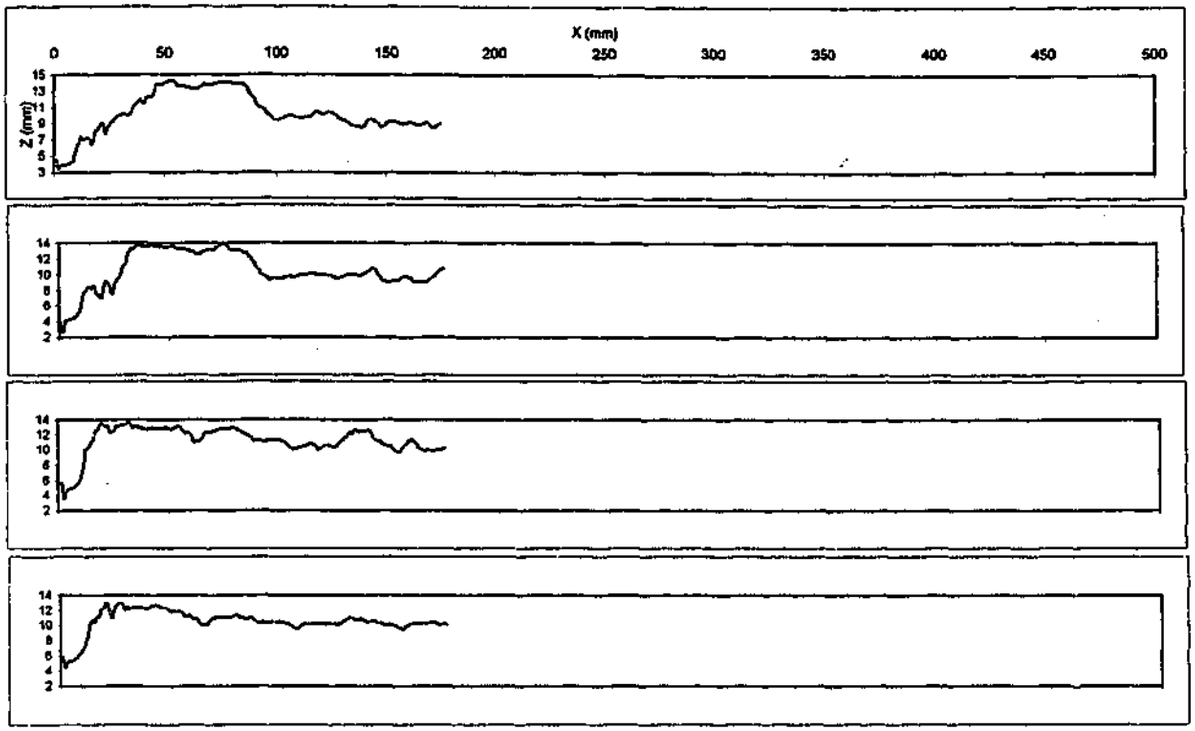

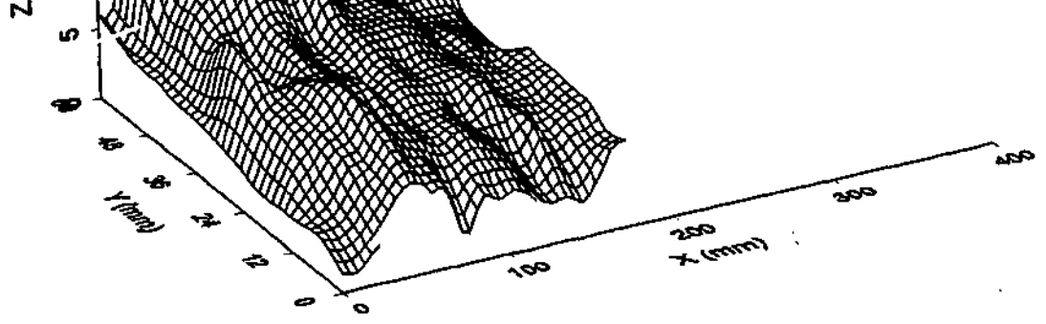

SILTSTONE SW, SPLIT 3

scanned at 5 mm intervals

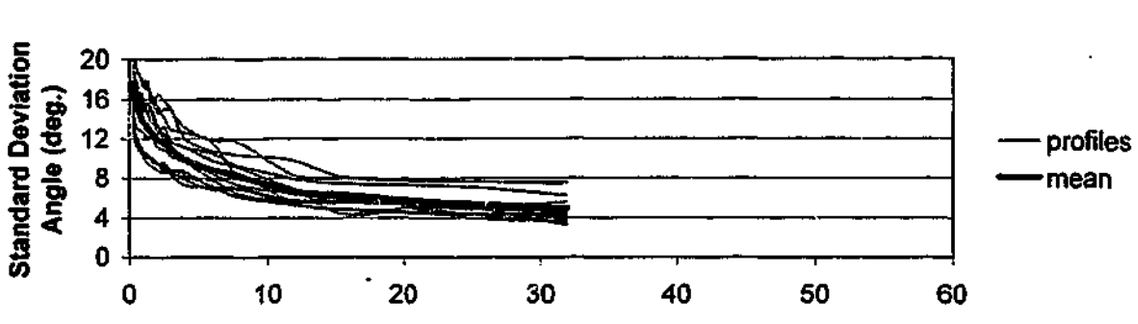

AVERAGE CORRELATION COEFFICIENT OF SCANS = 0.982

AVERAGE CORRELATION COEFFICIENT OF SCANS TO MEAN = 0.992

SILTSTONE SW, SPLIT

BLOCK 3

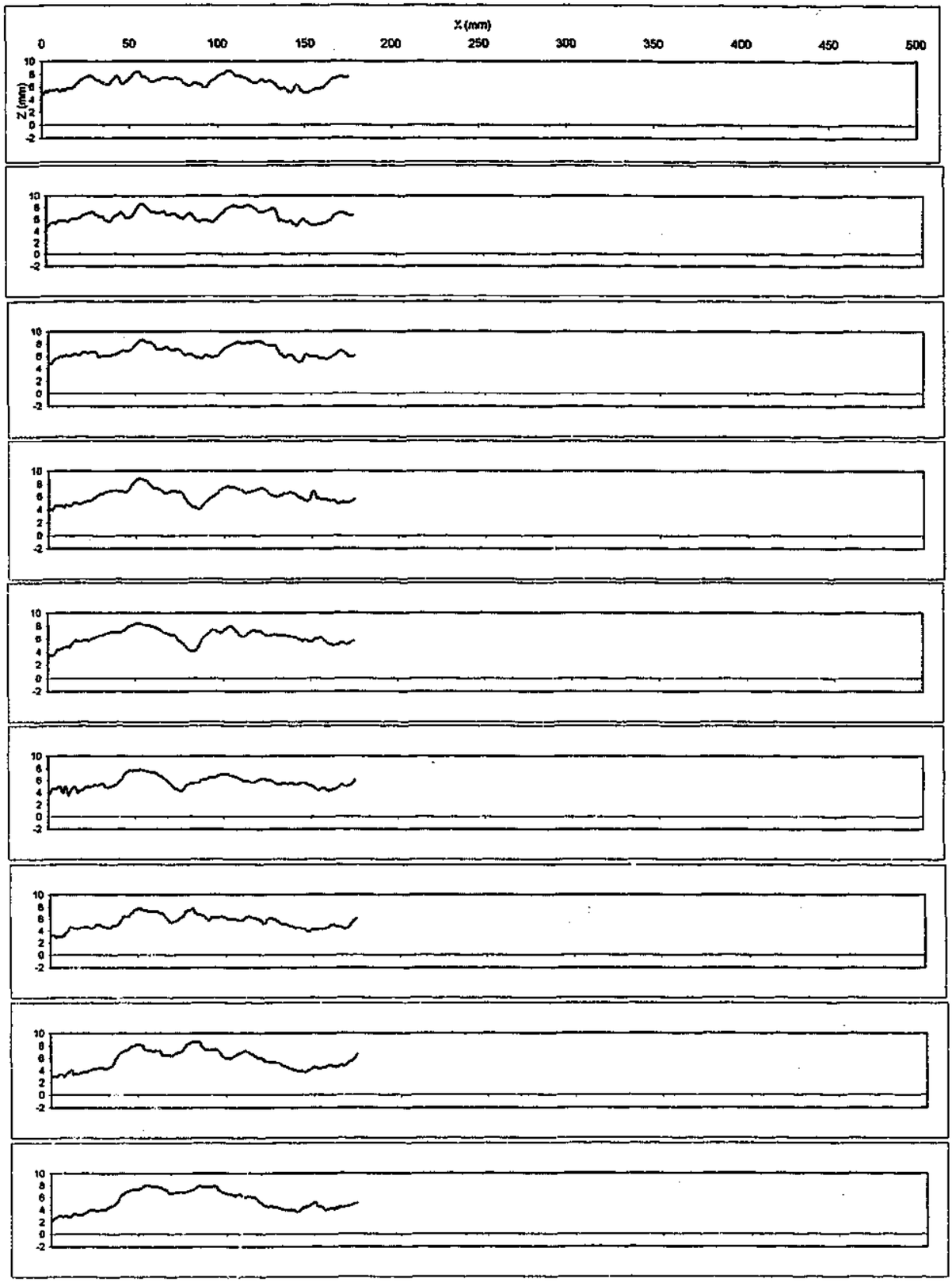

SILTSTONE SW, SPLIT 4

scanned at 5 mm intervals

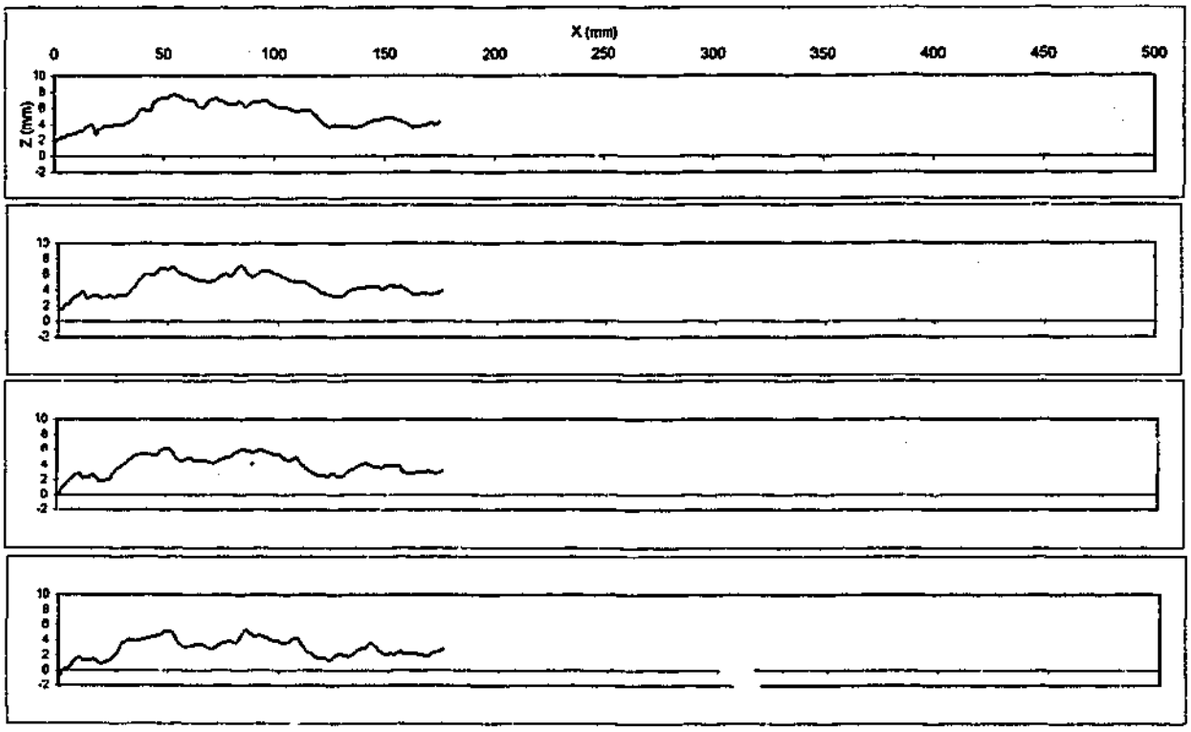

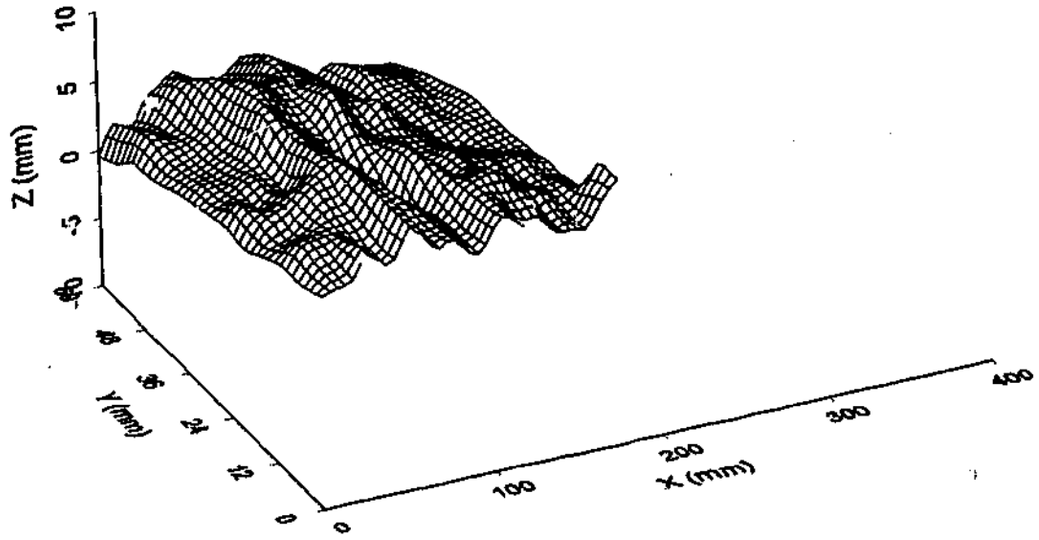

SILTSTONE SW, SPLIT 4

scanned at 5 mm intervals

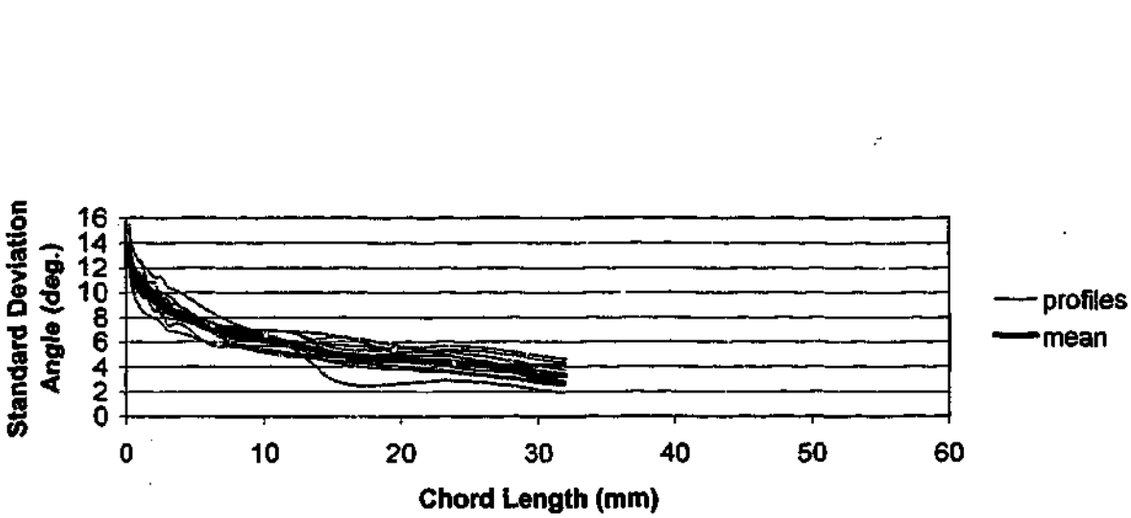

AVERAGE CORRELATION COEFFICIENT OF SCANS = 0.983

AVERAGE CORRELATION COEFFICIENT OF SCANS TO MEAN = 0.992

SILTSTONE SW, SPLIT

BLOCK 4

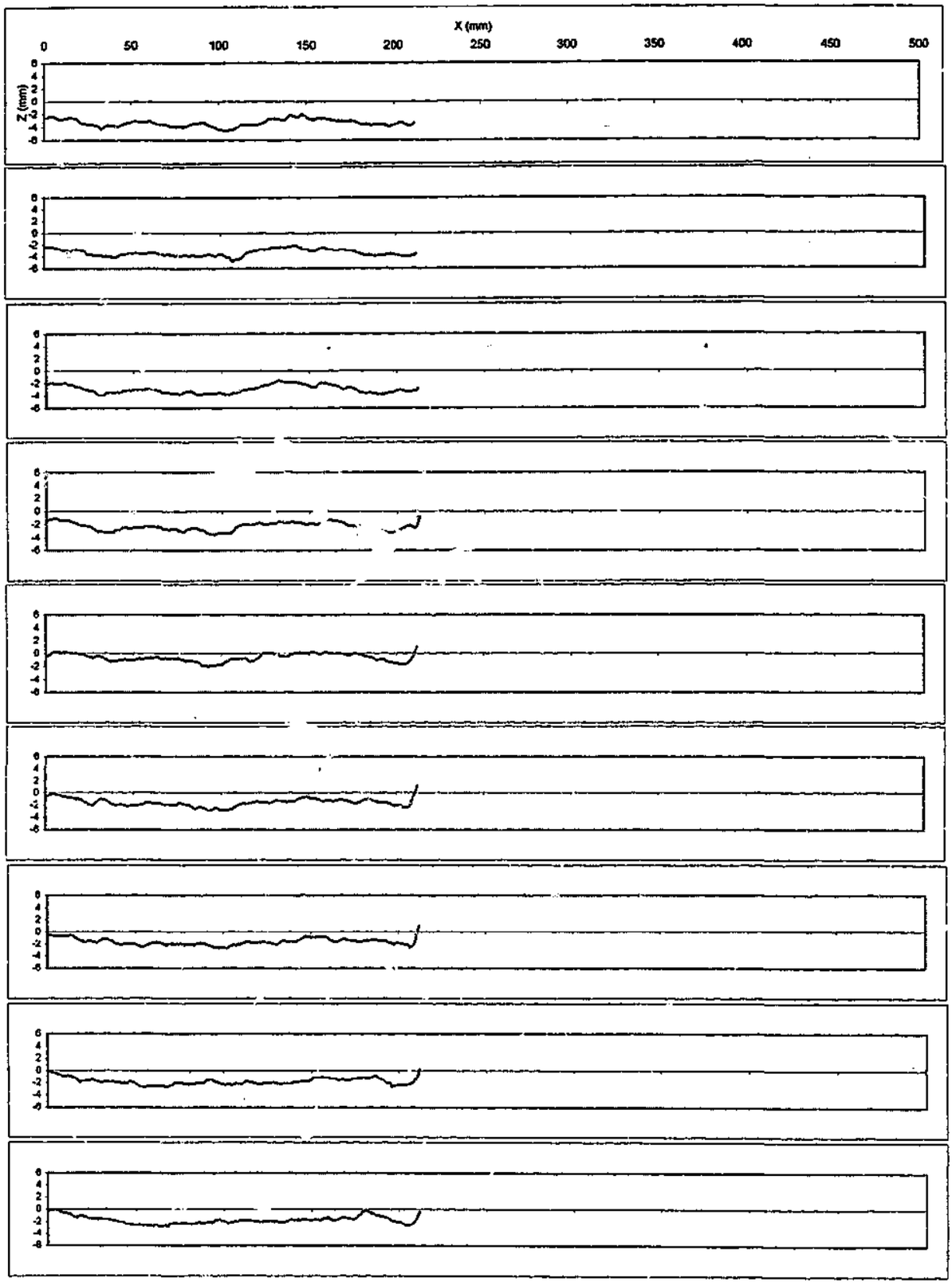

SILTSTONE SW, SHEAR SPLIT 5

scanned at 5 mm intervals

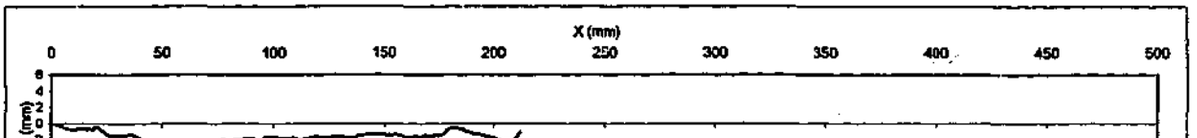

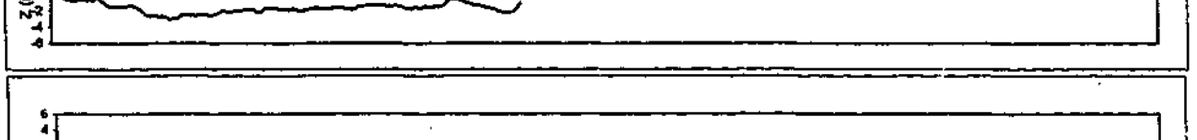

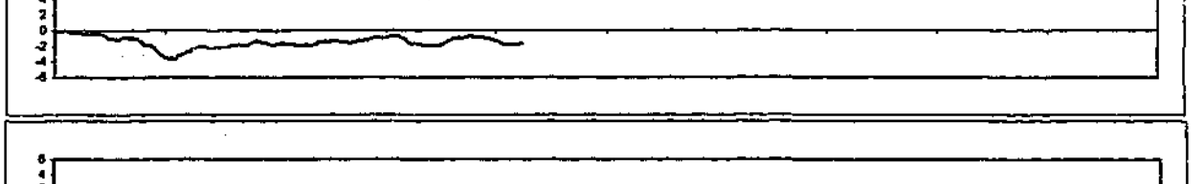

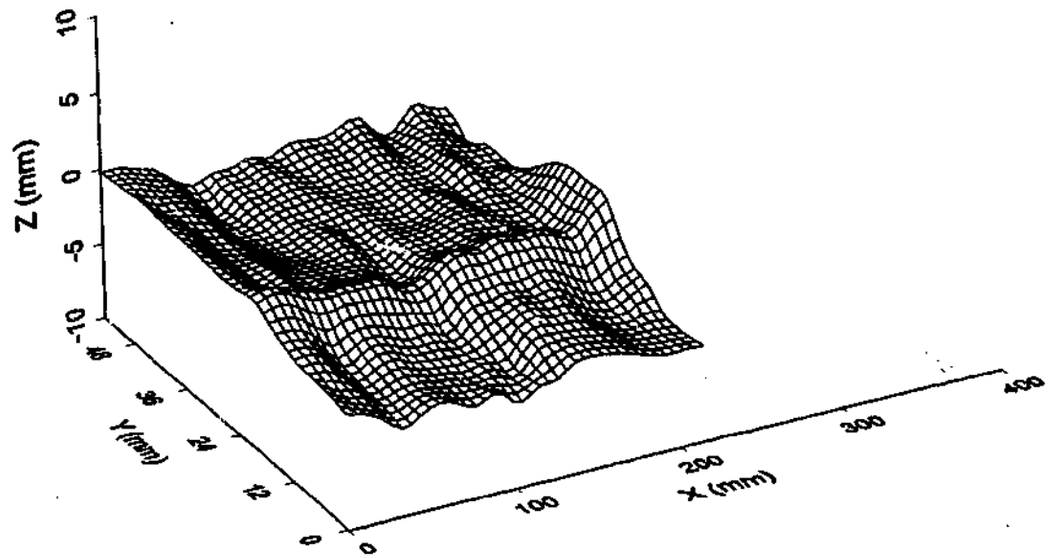

SILTSTONE SW, SHEAR SPLIT 5

scanned at 5 mm intervals

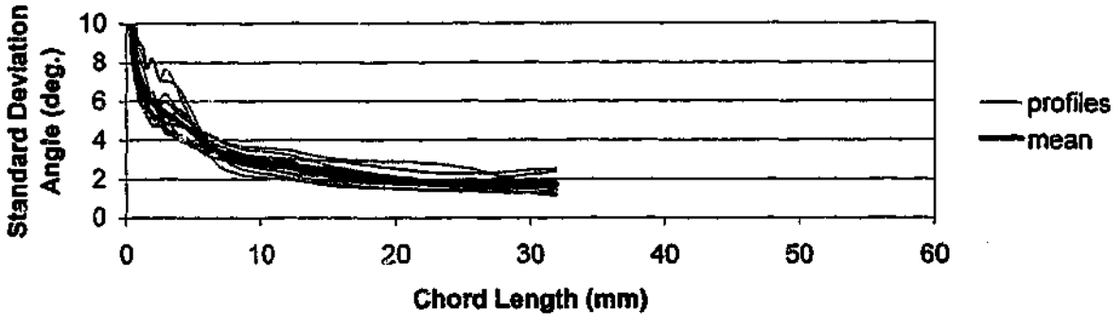

AVERAGE CORRELATION COEFFICIENT OF SCANS = 0.983

AVERAGE CORRELATION COEFFICIENT OF SCANS TO MEAN = 0.992

SILTSTONE SW, SHEAR SPLIT

BLOCK 5

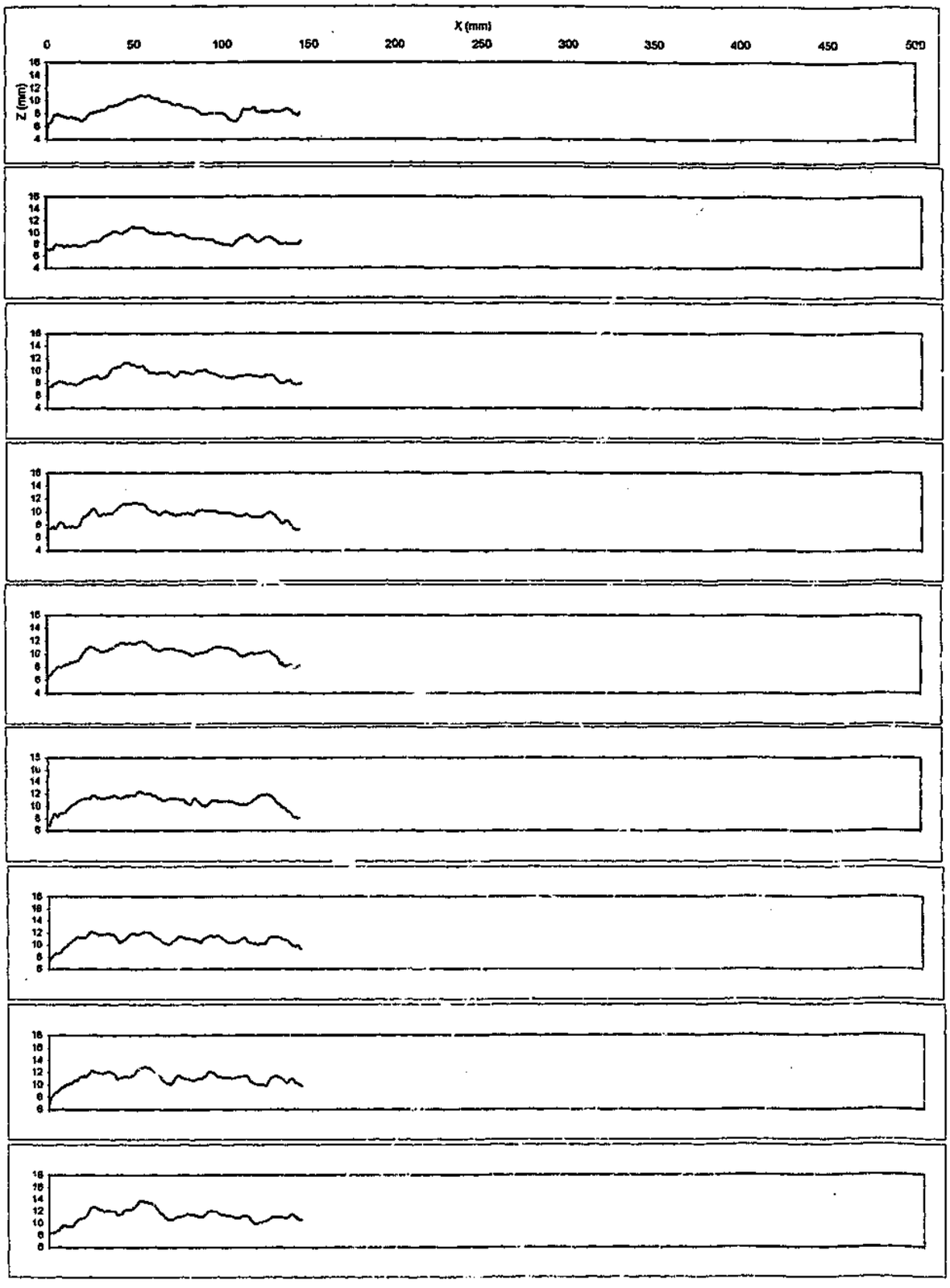

SILTSTONE SW, SPLIT 6

scanned at 5 mm intervals

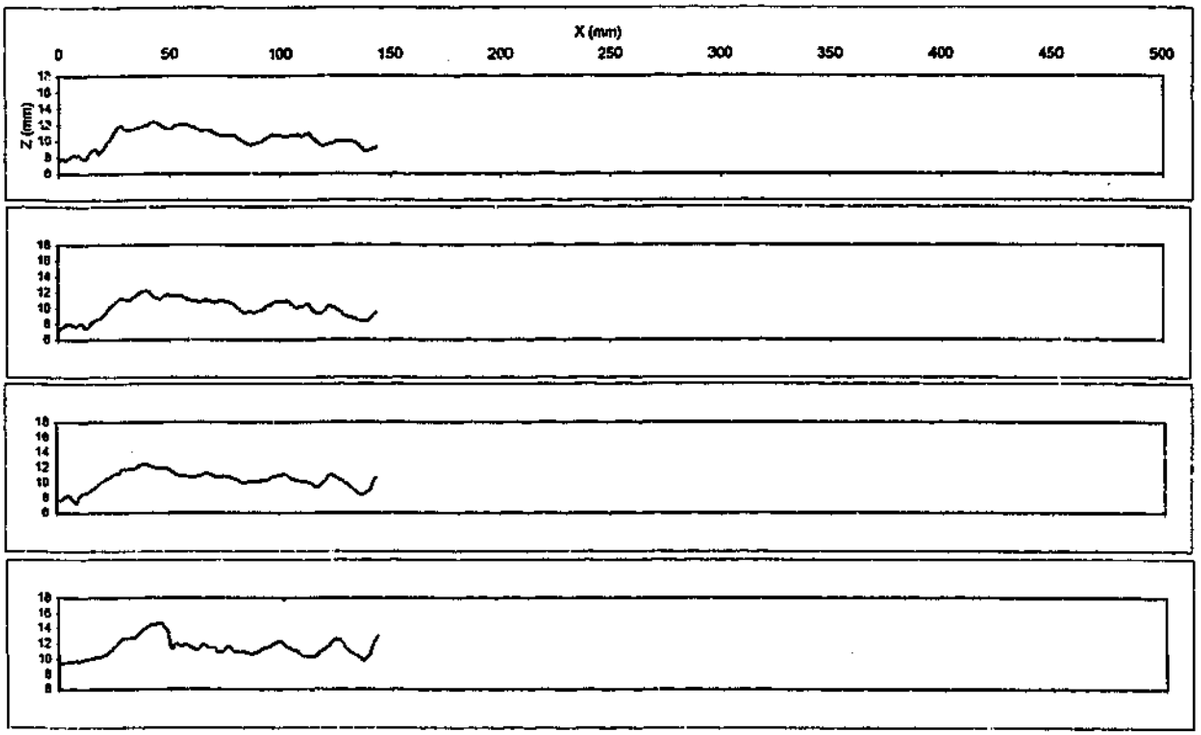

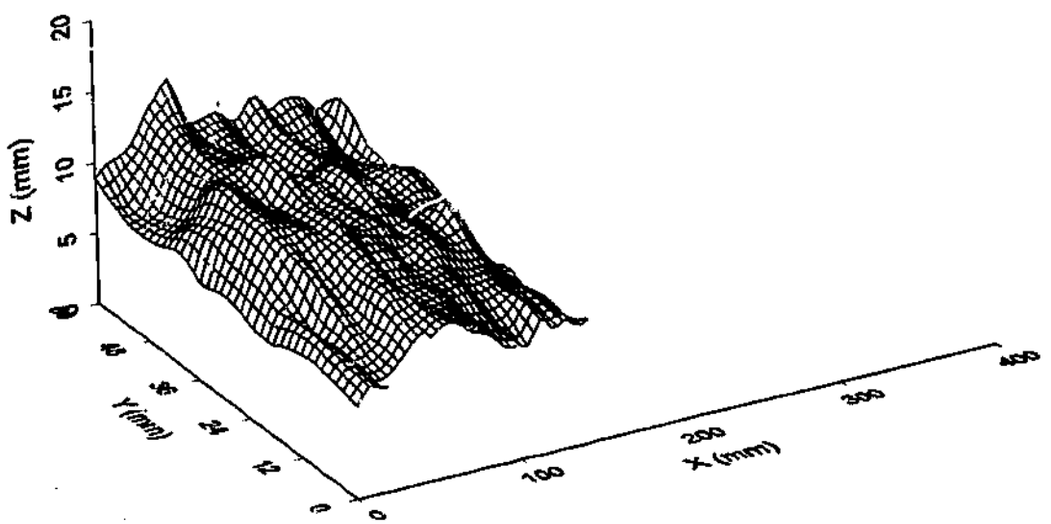

SILTSTONE SW, SPLIT 6

scanned at 5 mm intervals

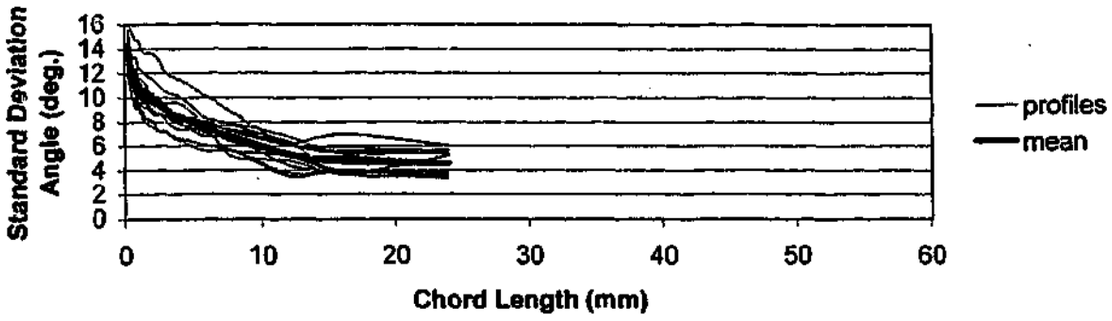

AVERAGE CORRELATION COEFFICIENT OF SCANS = 0.981

AVERAGE CORRELATION COEFFICIENT OF SCANS TO MEAN = 0.991

SILTSTONE SW, SPLIT

BLOCK 6

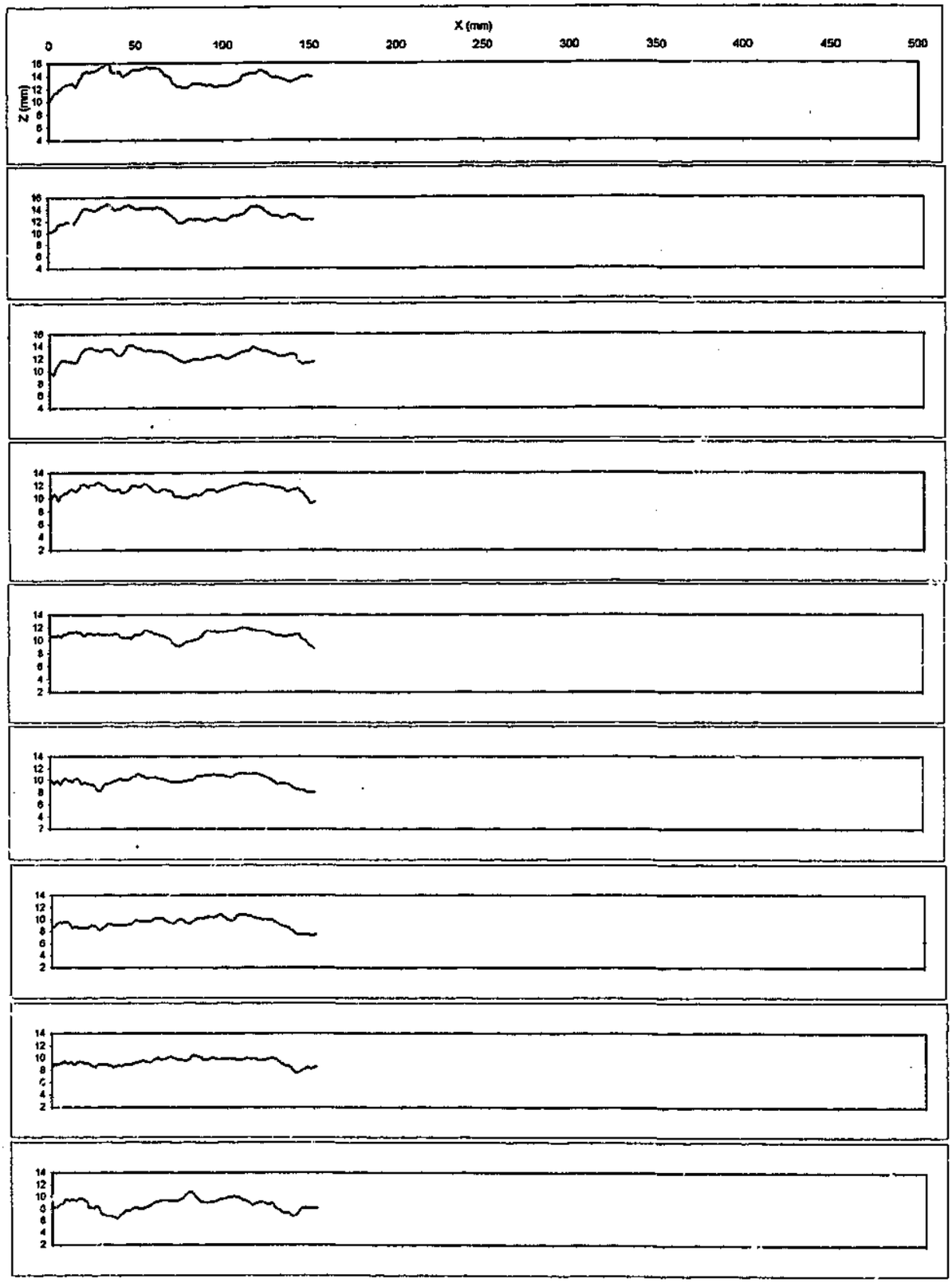

SILTSTONE SW, SPLIT 7

scanned at 5 mm intervals

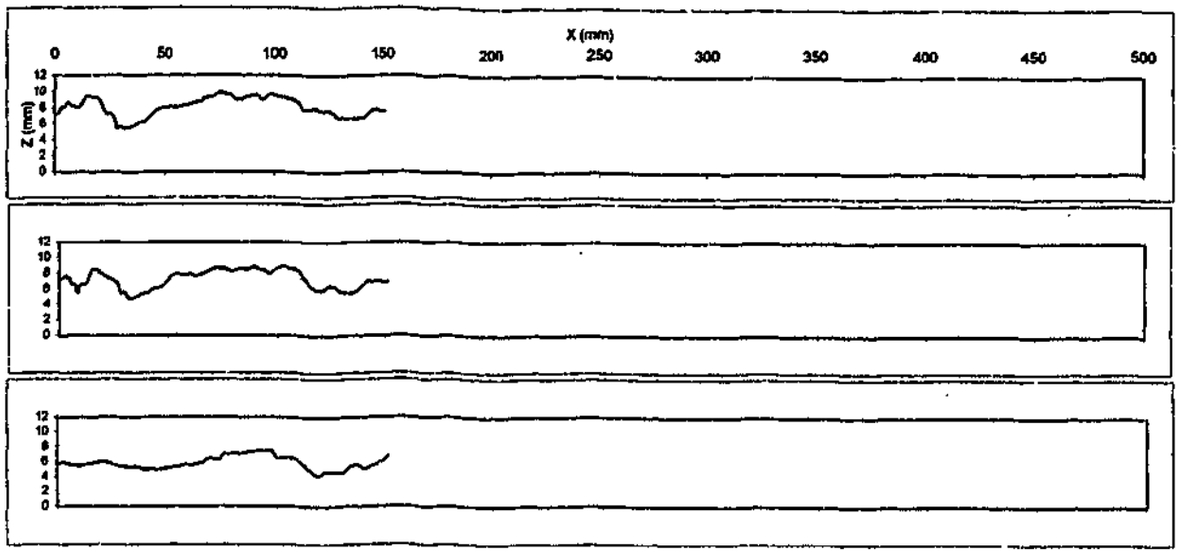

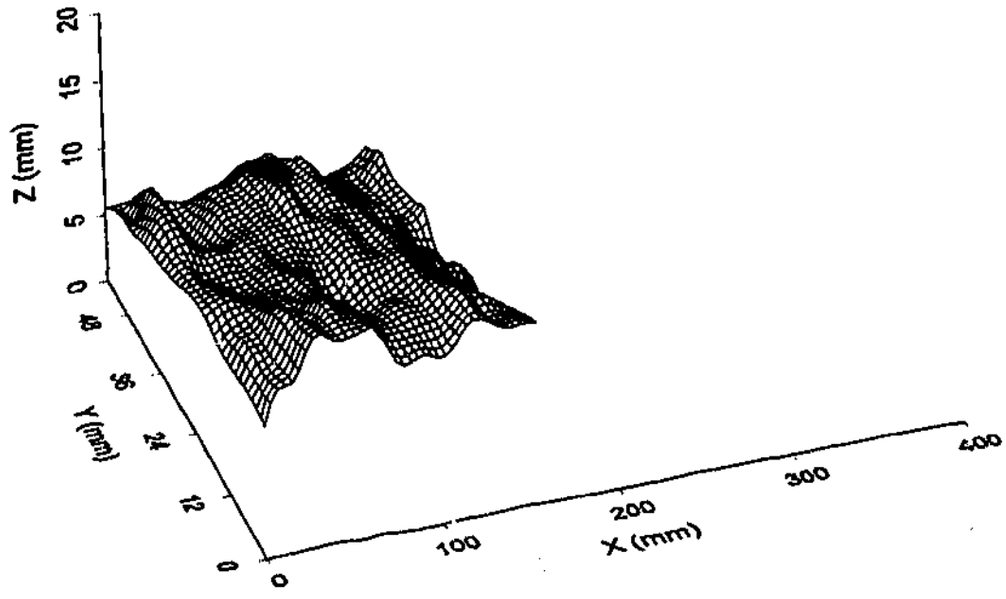

SILTSTONE SW, SPLIT 7

scanned at 5 mm intervals

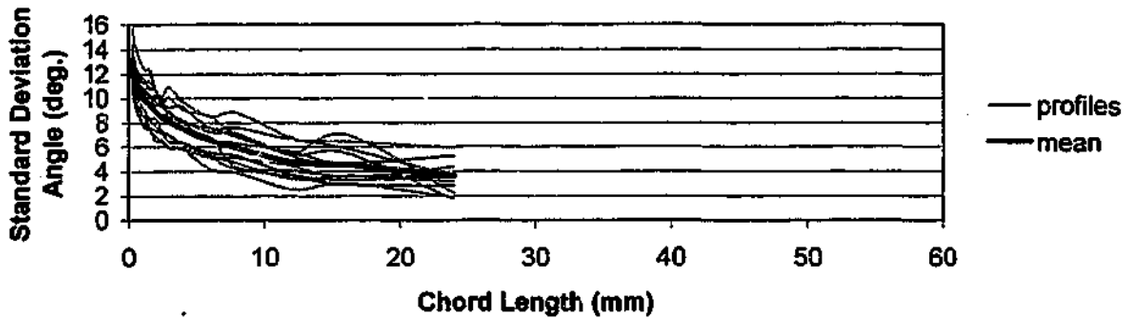

AVERAGE CORRELATION COEFFICIENT OF SCANS = 0.976

AVERAGE CORRELATION COEFFICIENT OF SCANS TO MEAN = 0.989

SILTSTONE SW, SPLIT

BLOCK 7

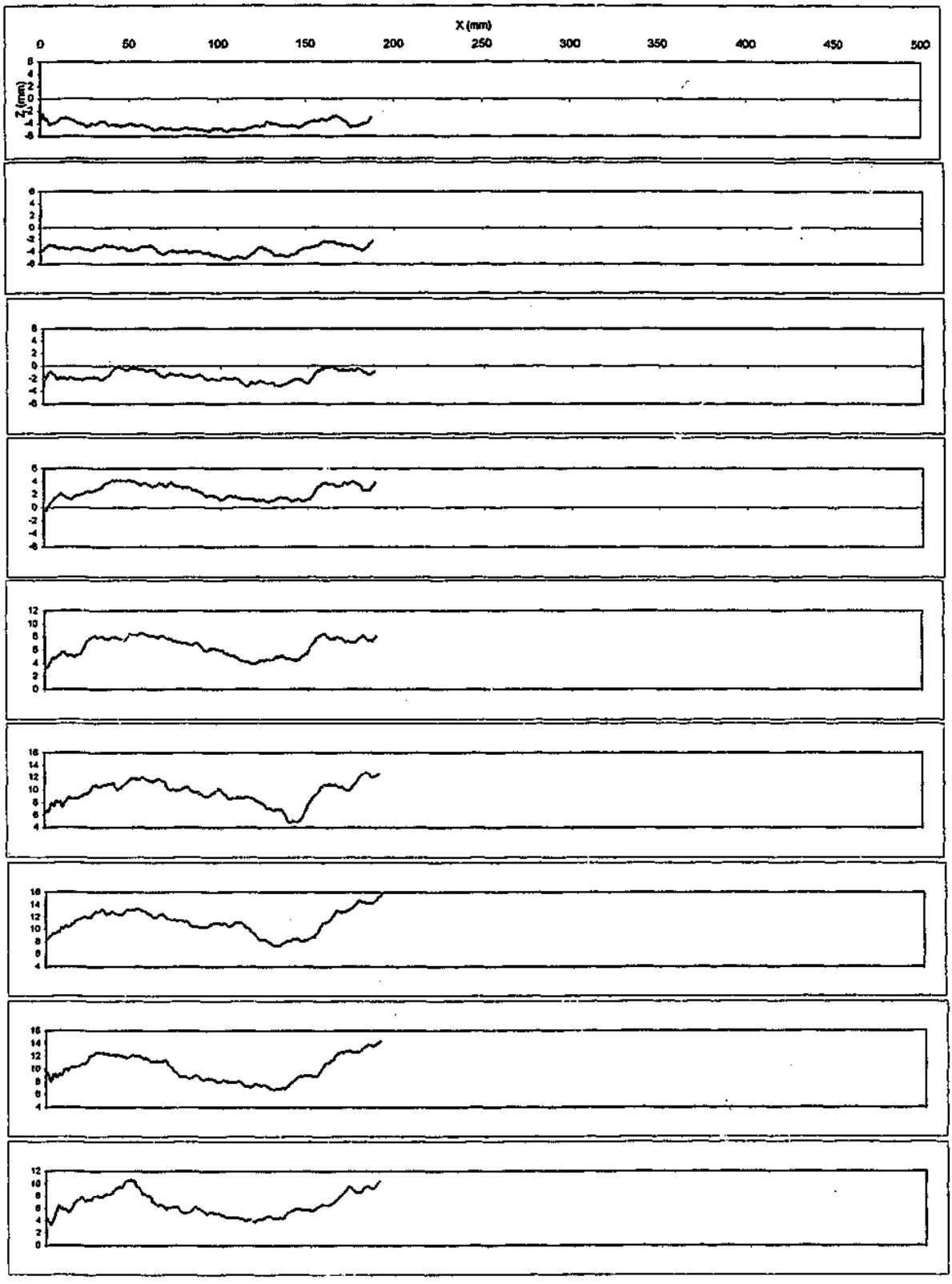

BASALT MW, SPLIT 1

scanned at 10mm intervals

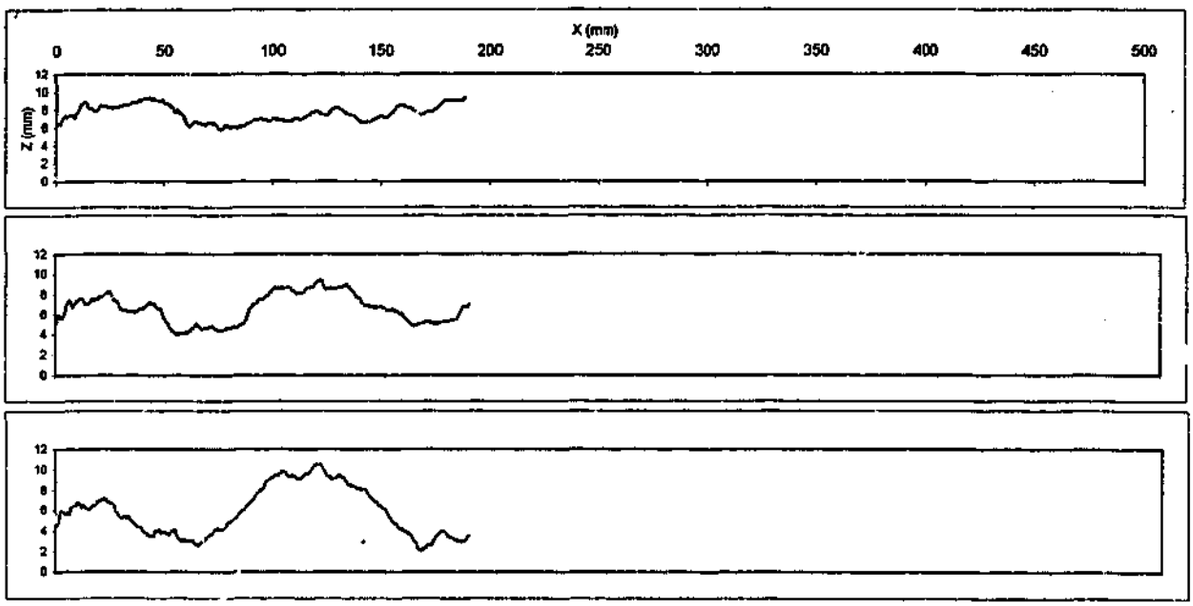

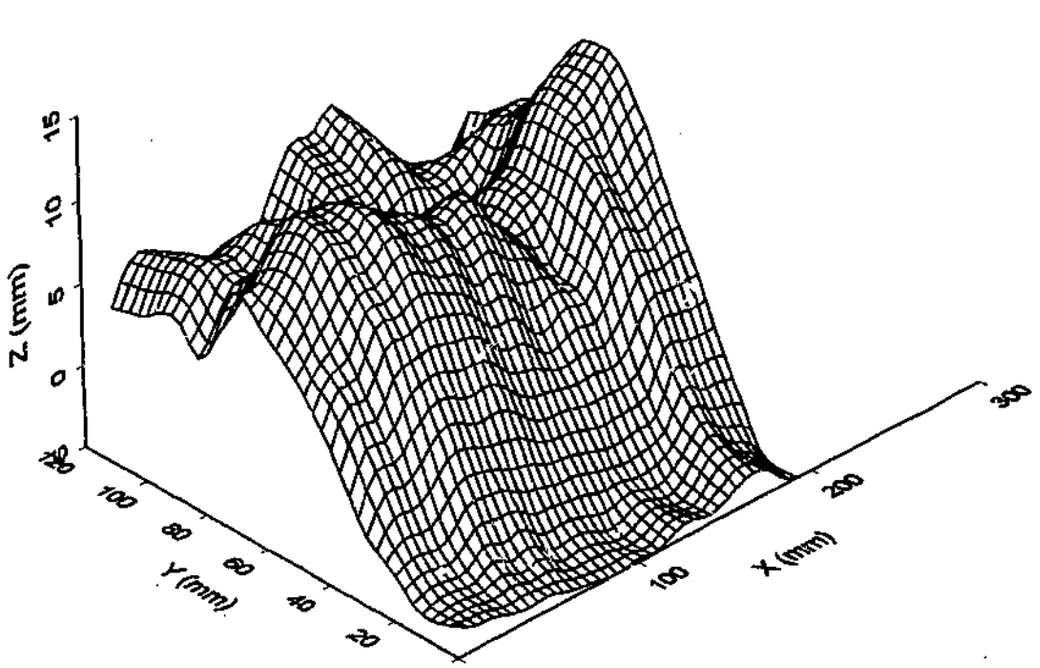

BASALT MW, SPLIT 1

scanned at 10 mm intervals

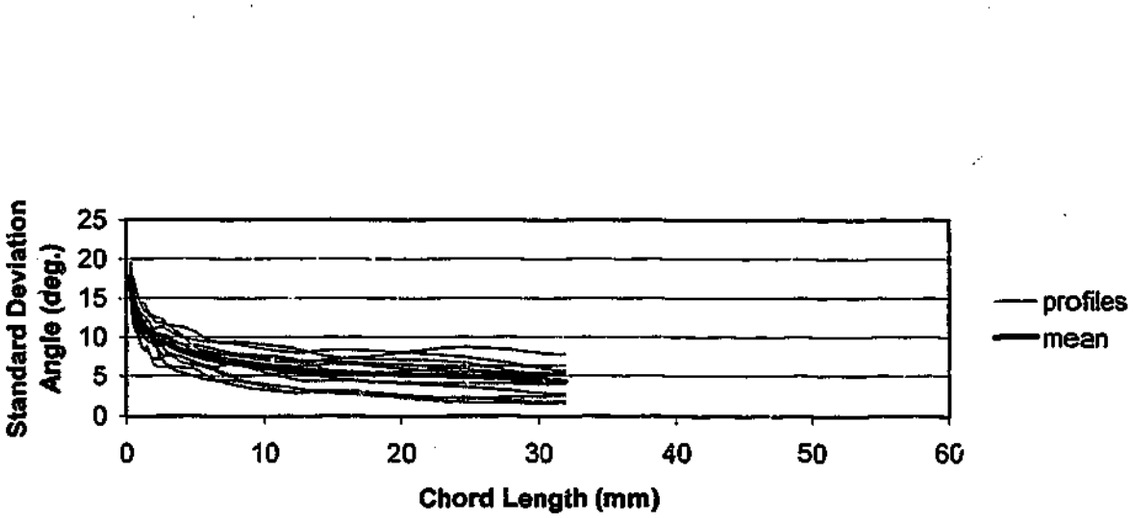

AVERAGE CORRELATION COEFFICIENT OF SCANS = 0.991

AVERAGE CORRELATION COEFFICIENT OF SCANS TO MEAN = 0.996

BASALT MW, SPLIT 1

scanned at 10 mm intervals

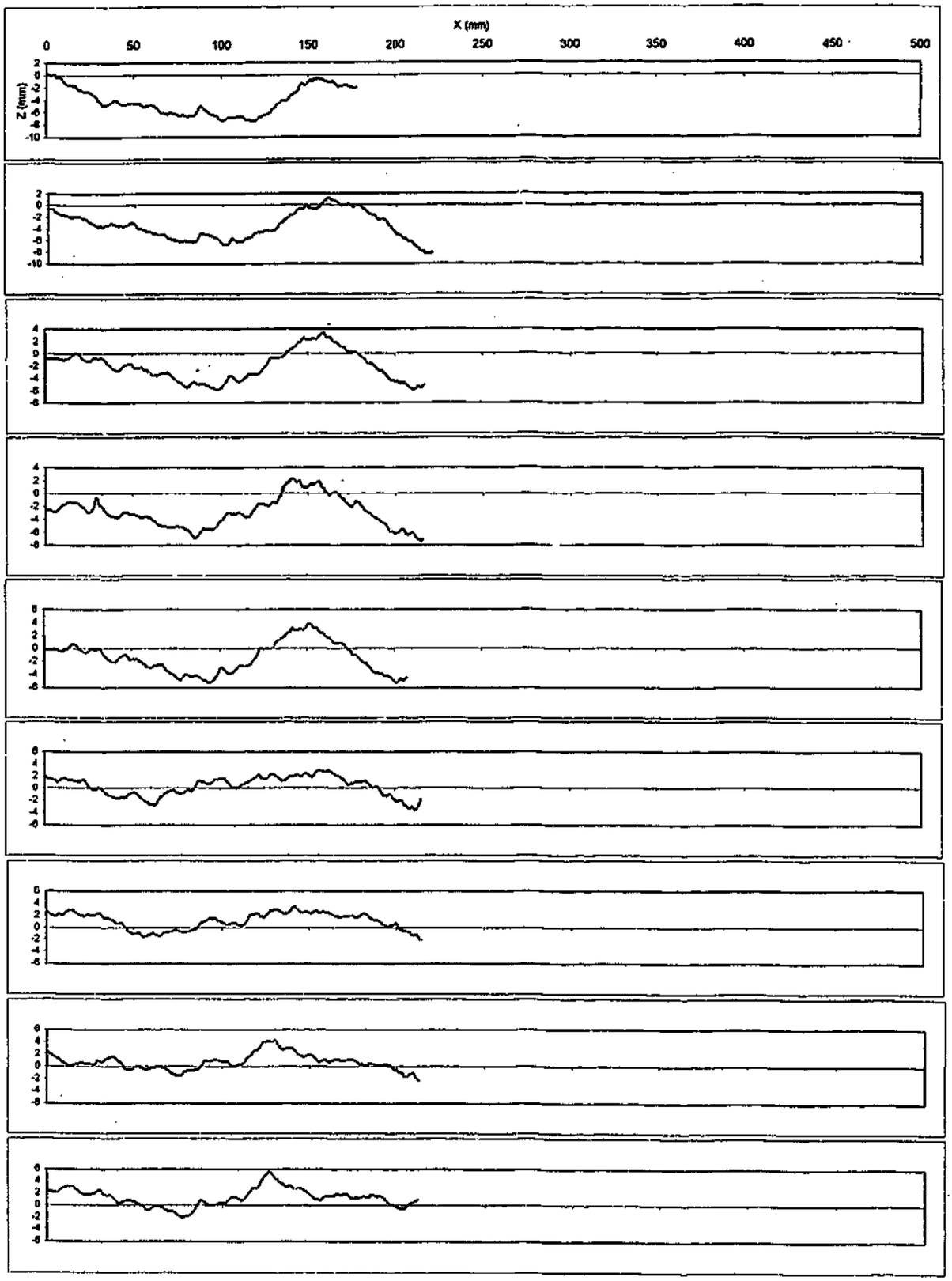

BASALT MW, SPLIT 2

scanned at 10mm intervals

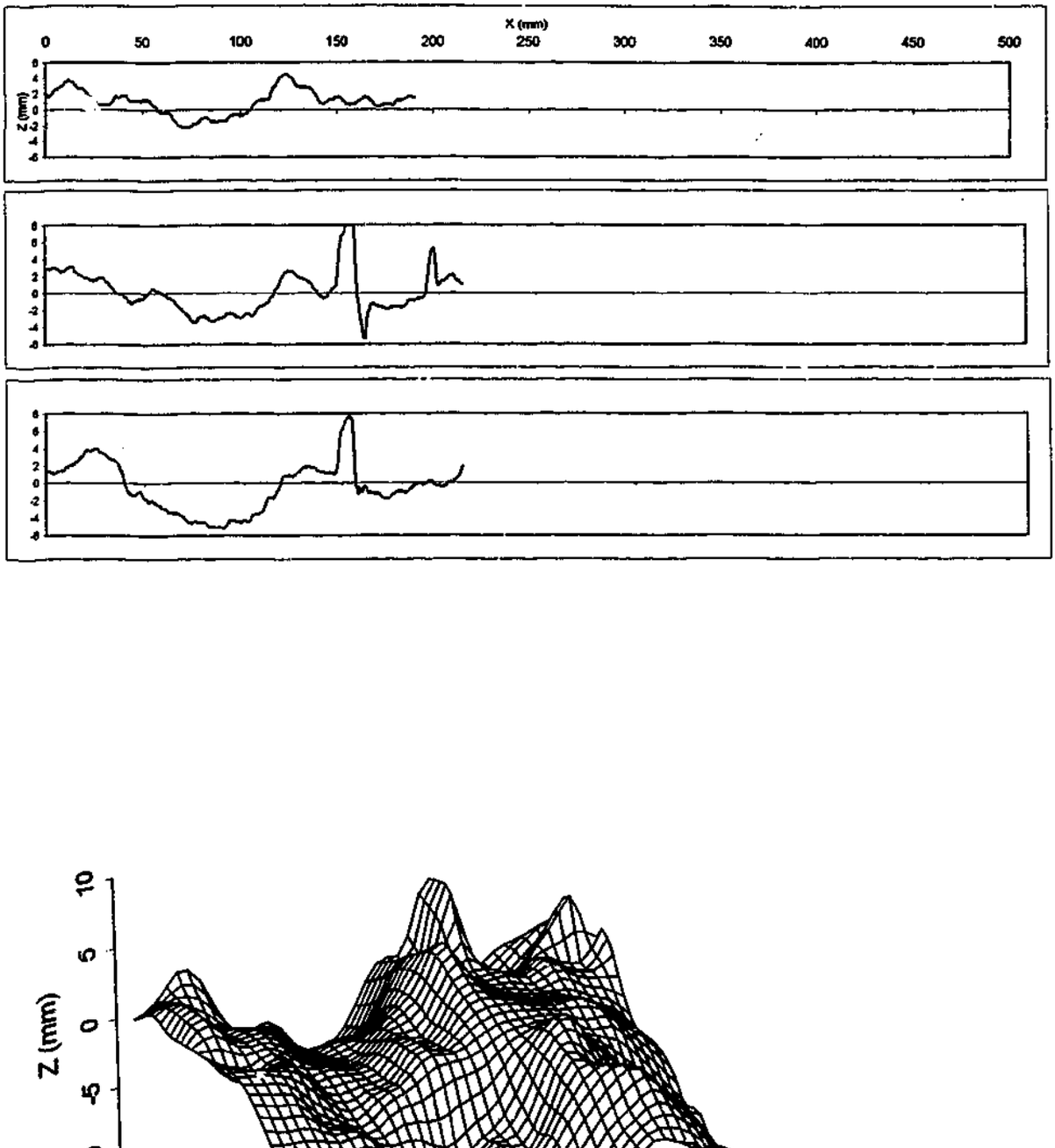

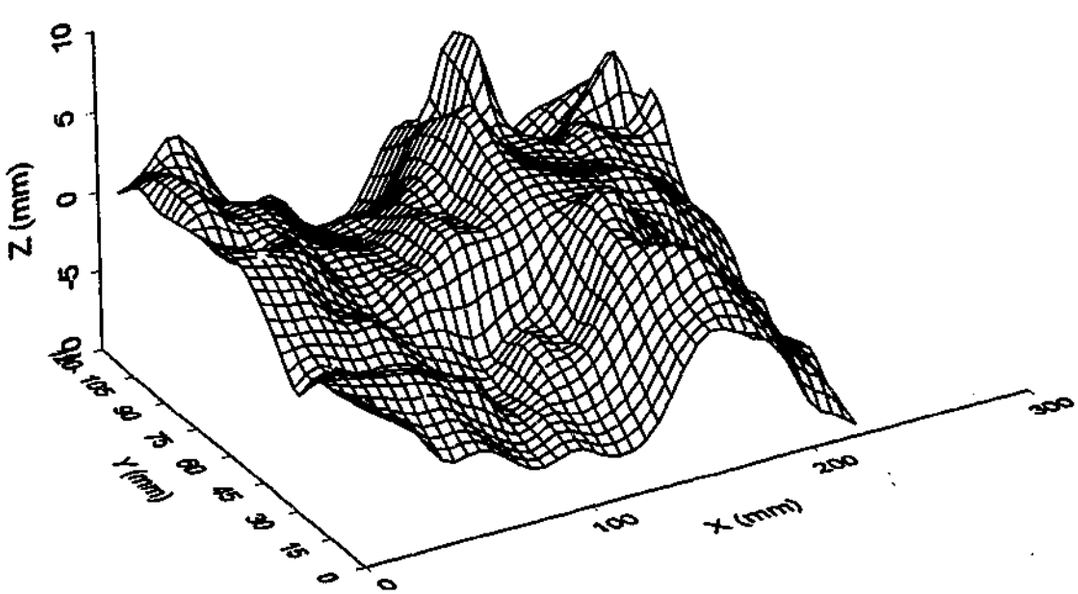

BASALT MW, SPLIT 2

scanned at 10 mm intervals

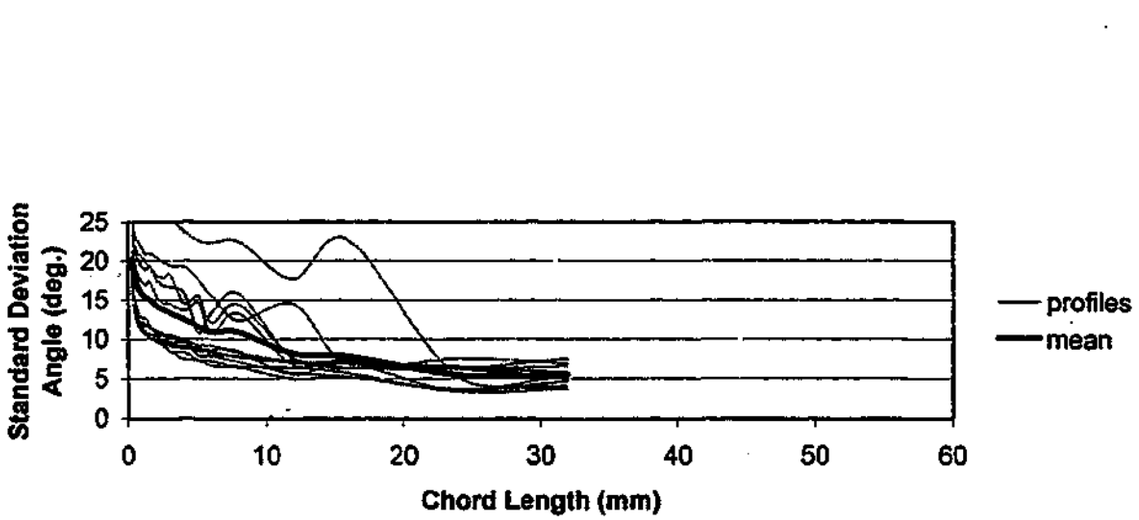

AVERAGE CORRELATION COEFFICIENT OF SCANS = 0.947

AVERAGE CORRELATION COEFFICIENT OF SCANS TO MEAN = 0.975

BASALT MW, SPLIT 2

scanned at 10 mm intervals

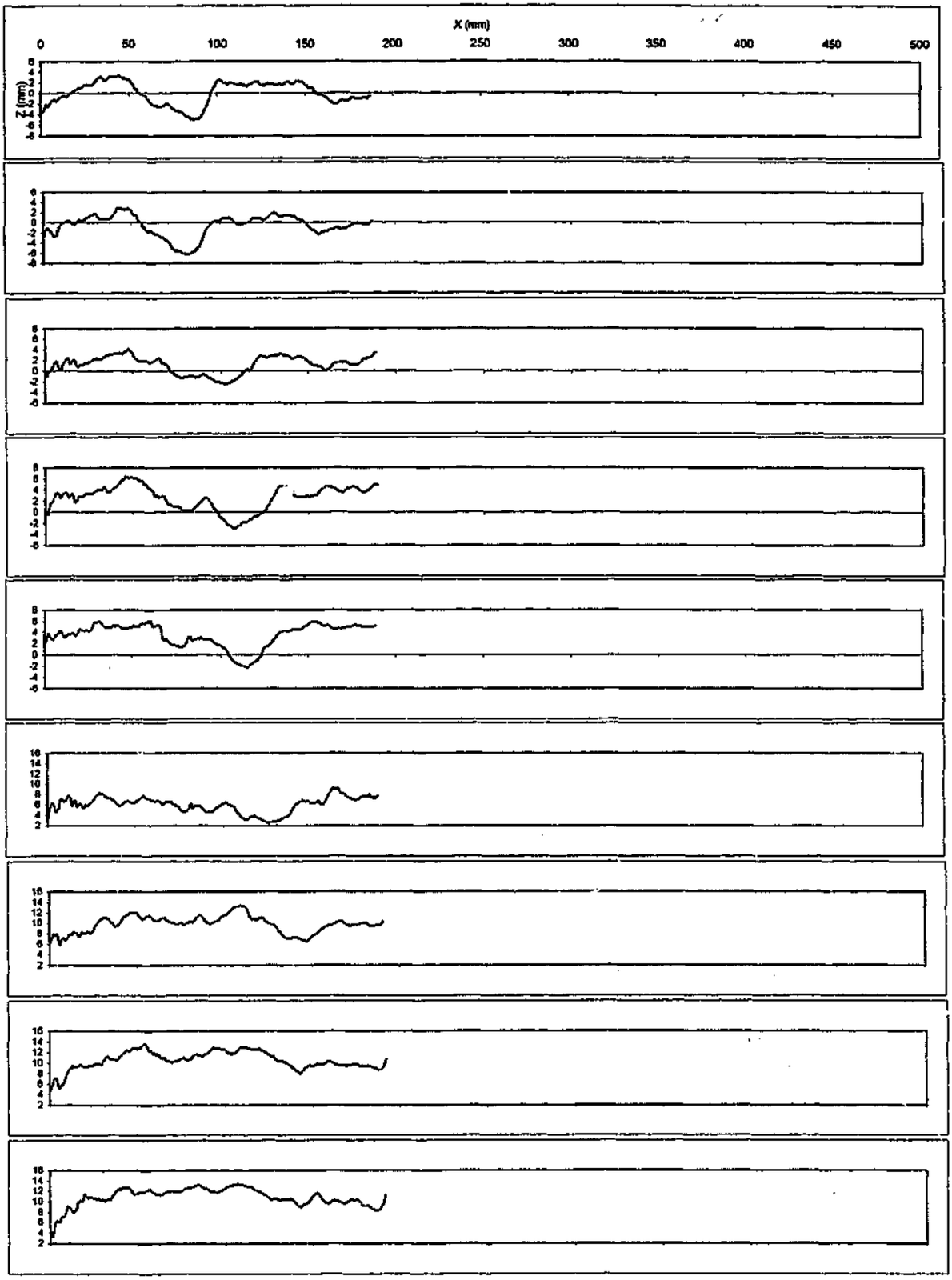

BASALT MW, SPLIT 3

scanned at 10mm intervals

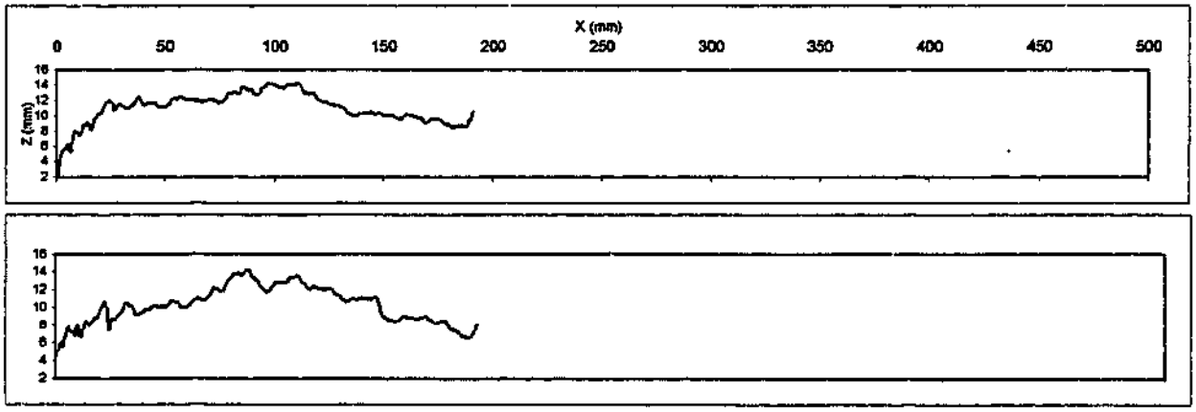

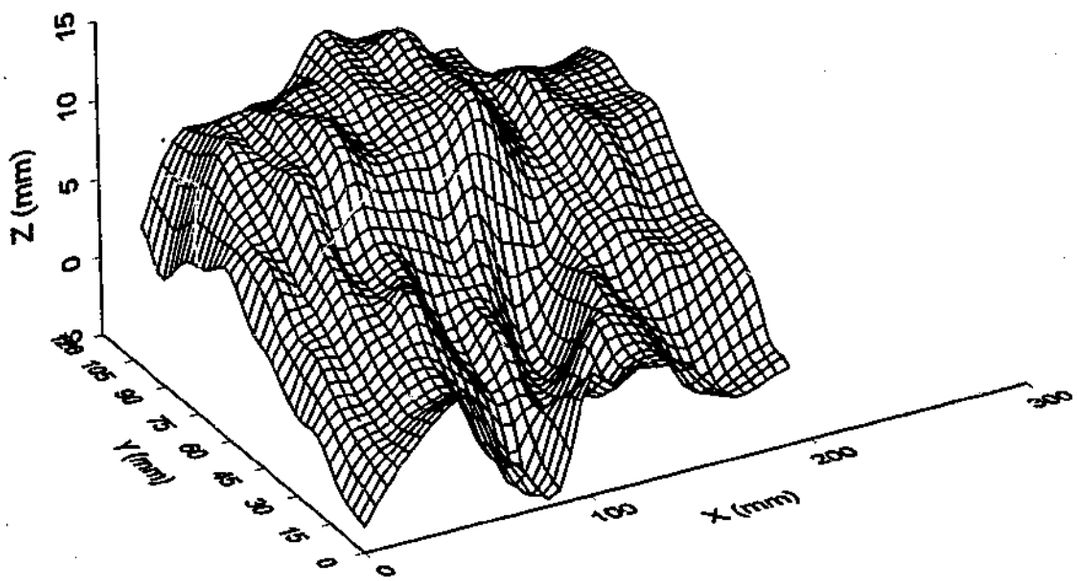

BASALT MW, SPLIT 3

scanned at 10 mm intervals

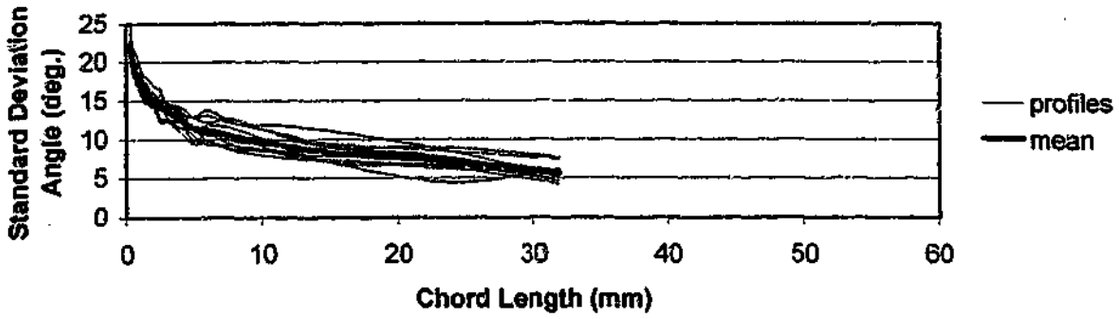

AVERAGE CORRELATION COEFFICIENT OF SCANS = 0.985

AVERAGE CORRELATION COEFFICIENT OF SCANS TO MEAN = 0.993

BASALT MW, SPLIT 3

scanned at 10 mm intervals

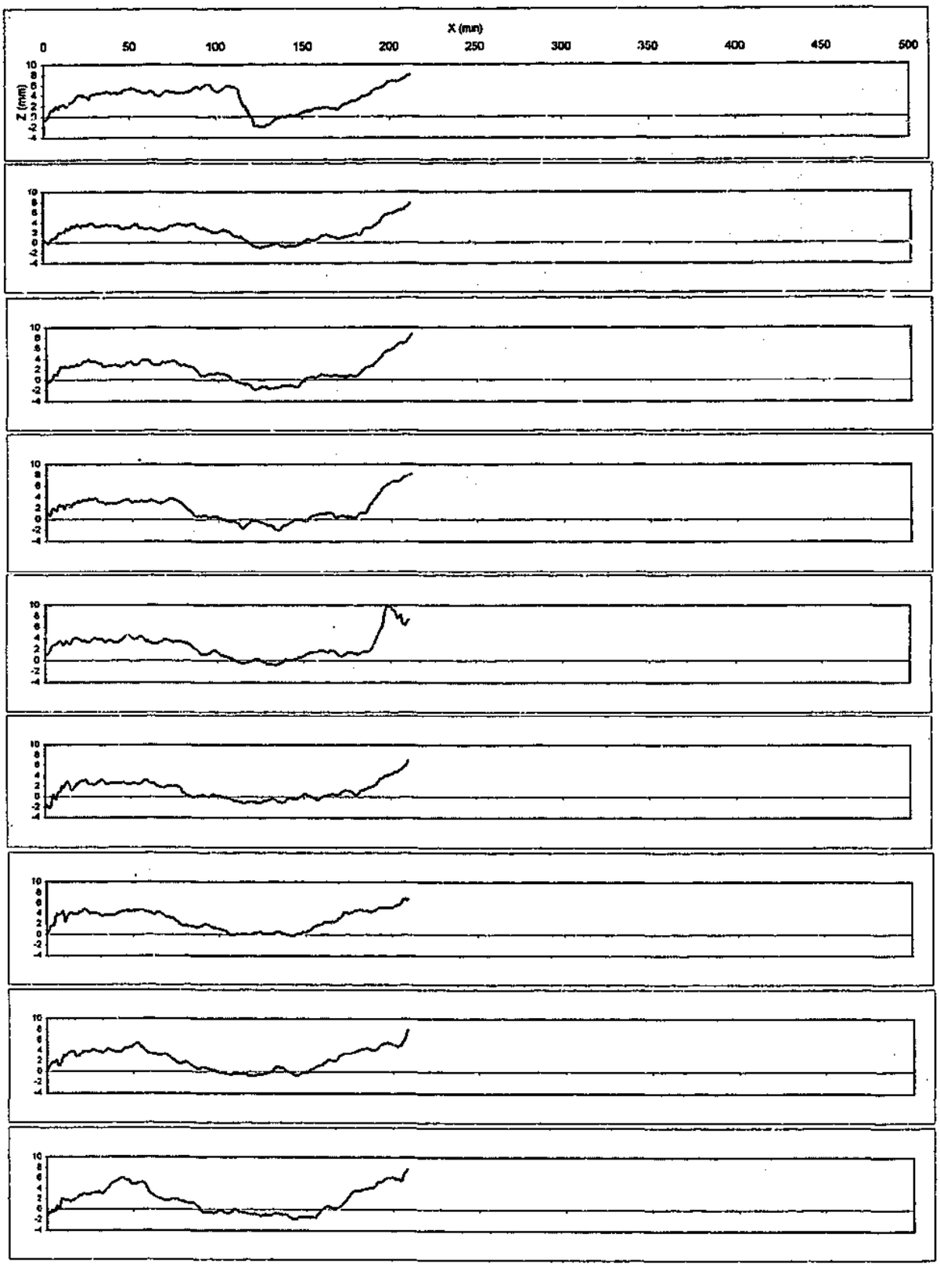

BASALT MW, SPLIT 4

scanned at 10mm intervals

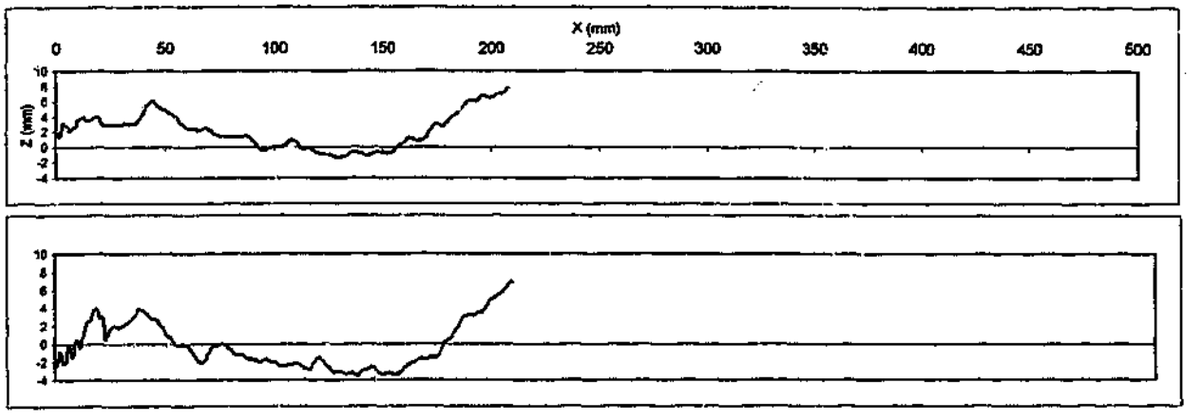

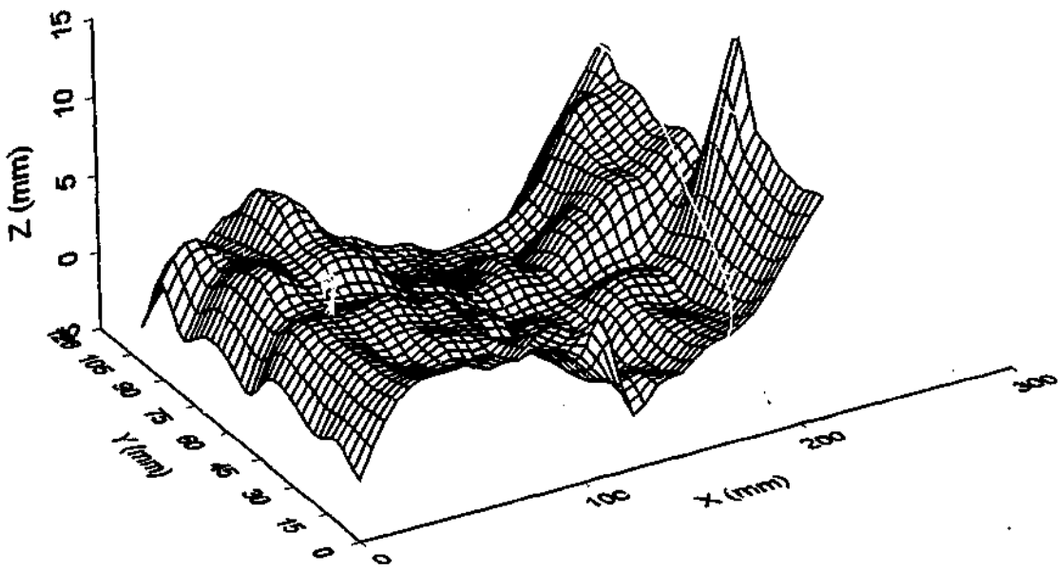

BASALT MW, SPLIT 4

scanned at 10 mm intervals

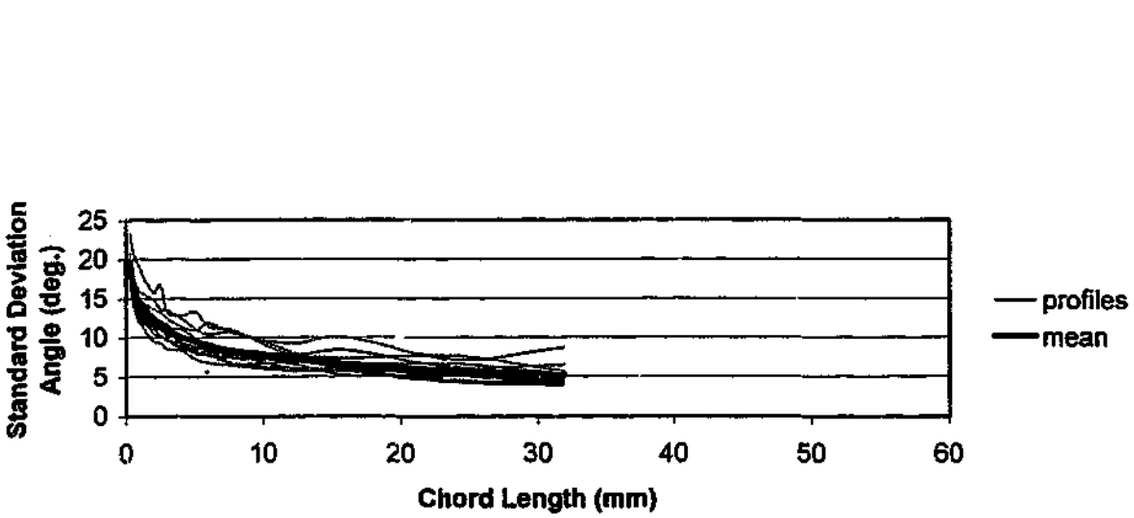

AVERAGE CORRELATION COEFFICIENT OF SCANS = 0.986

AVERAGE CORRELATION COEFFICIENT OF SCANS TO MEAN = 0.994

BASALT MW, SPLIT 4

scanned at 10 mm intervals

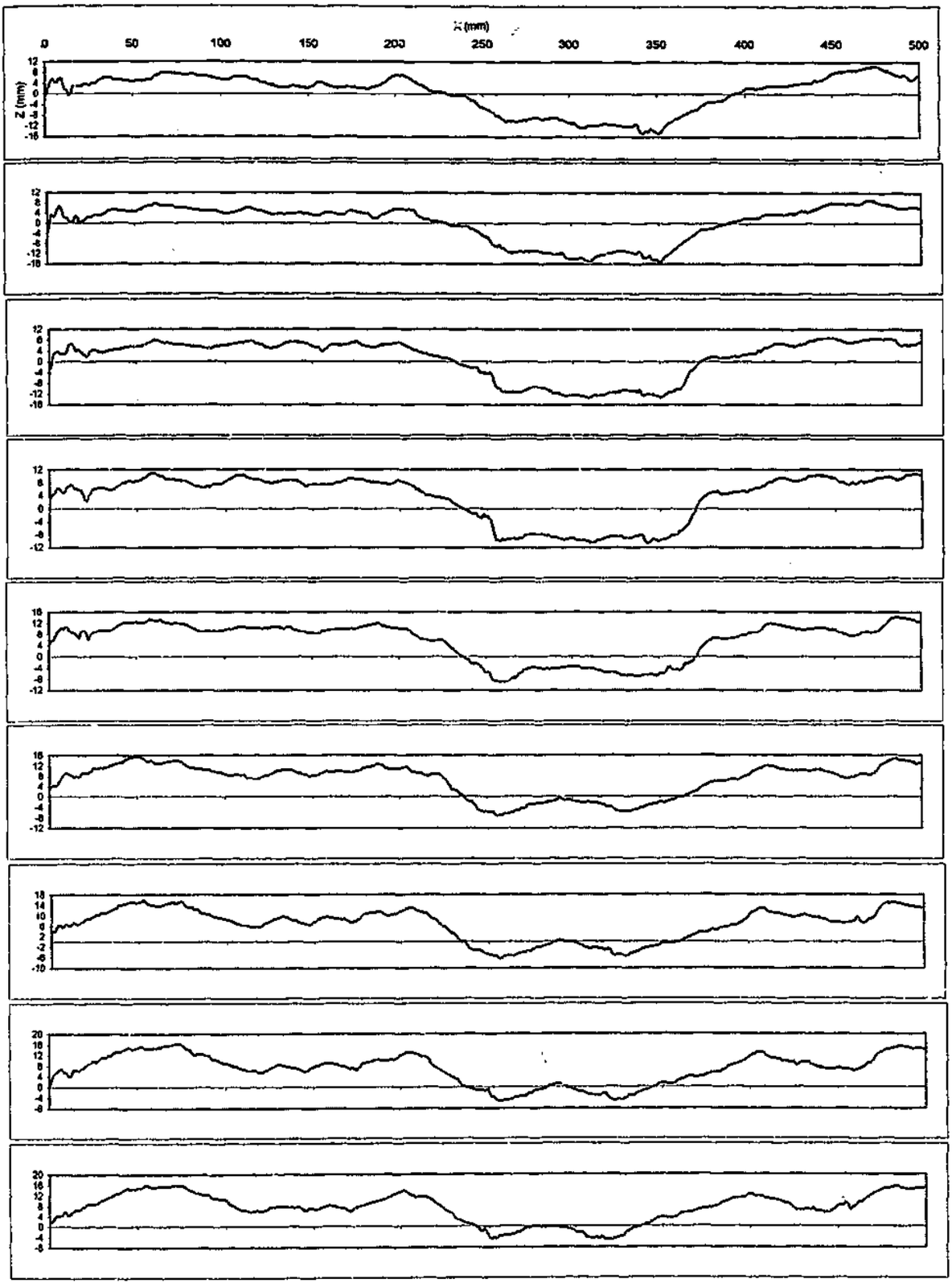

GRANITE SW, SPLIT 1

scanned at 5 mm intervals

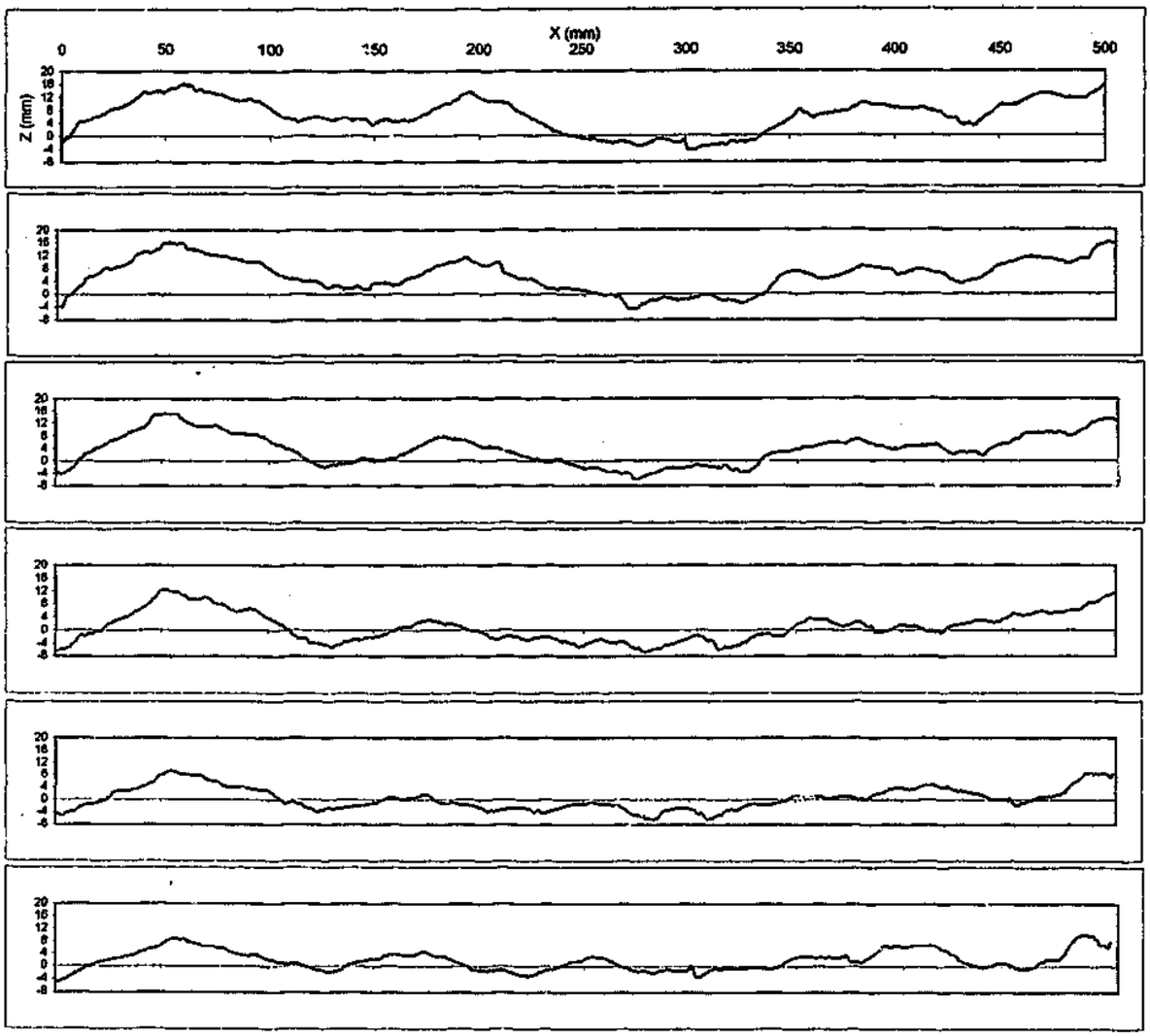

GRANITE SW, SPLIT 1

scanned at 5 mm intervals

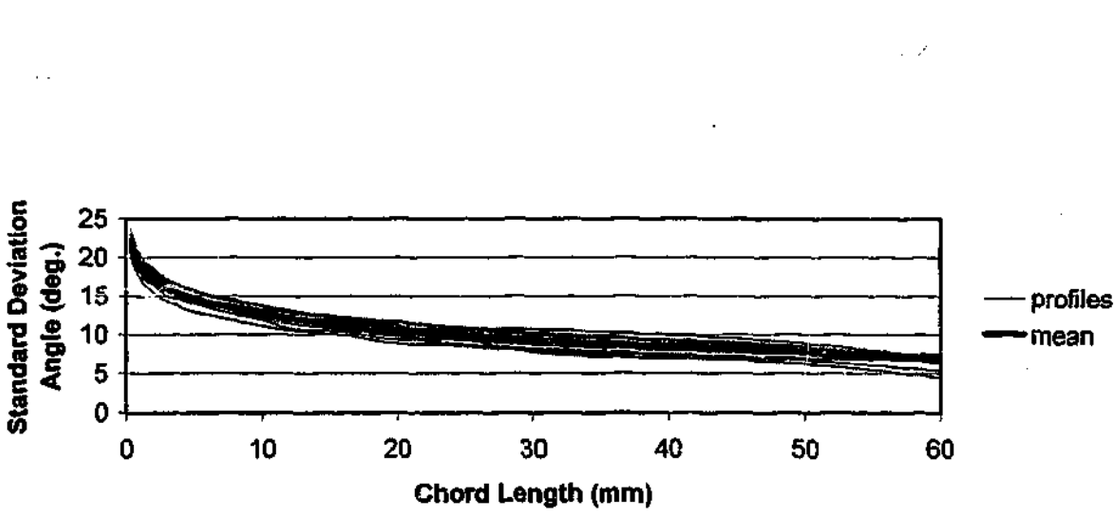

AVERAGE CORRELATION COEFFICIENT OF SCANS = 0.992

AVERAGE CORRELATION COEFFICIENT OF SCANS TO MEAN = 0.996

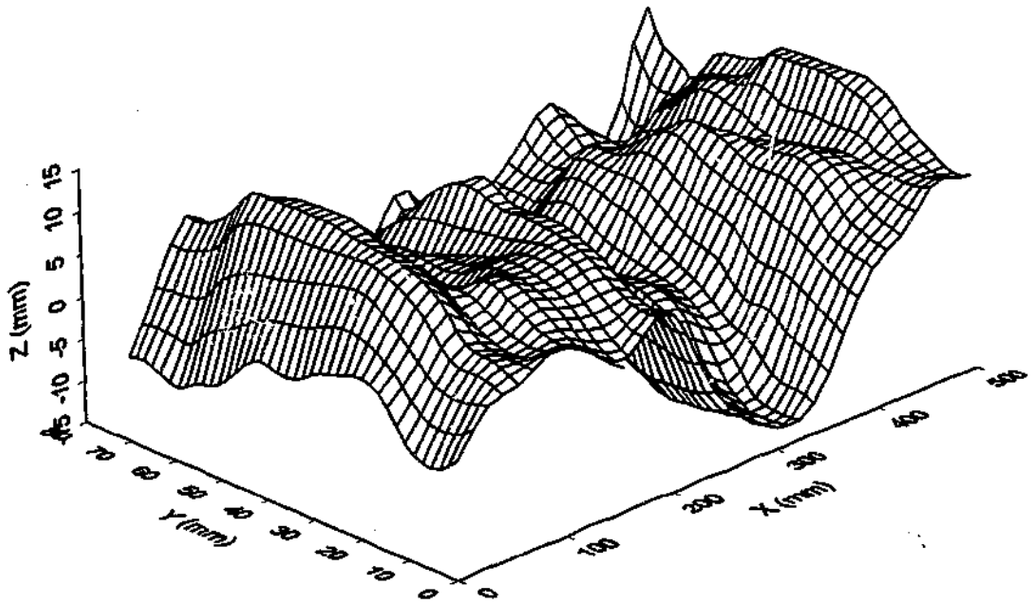

GRANITE SW, SPLIT 1

scanned at 5mm intervals

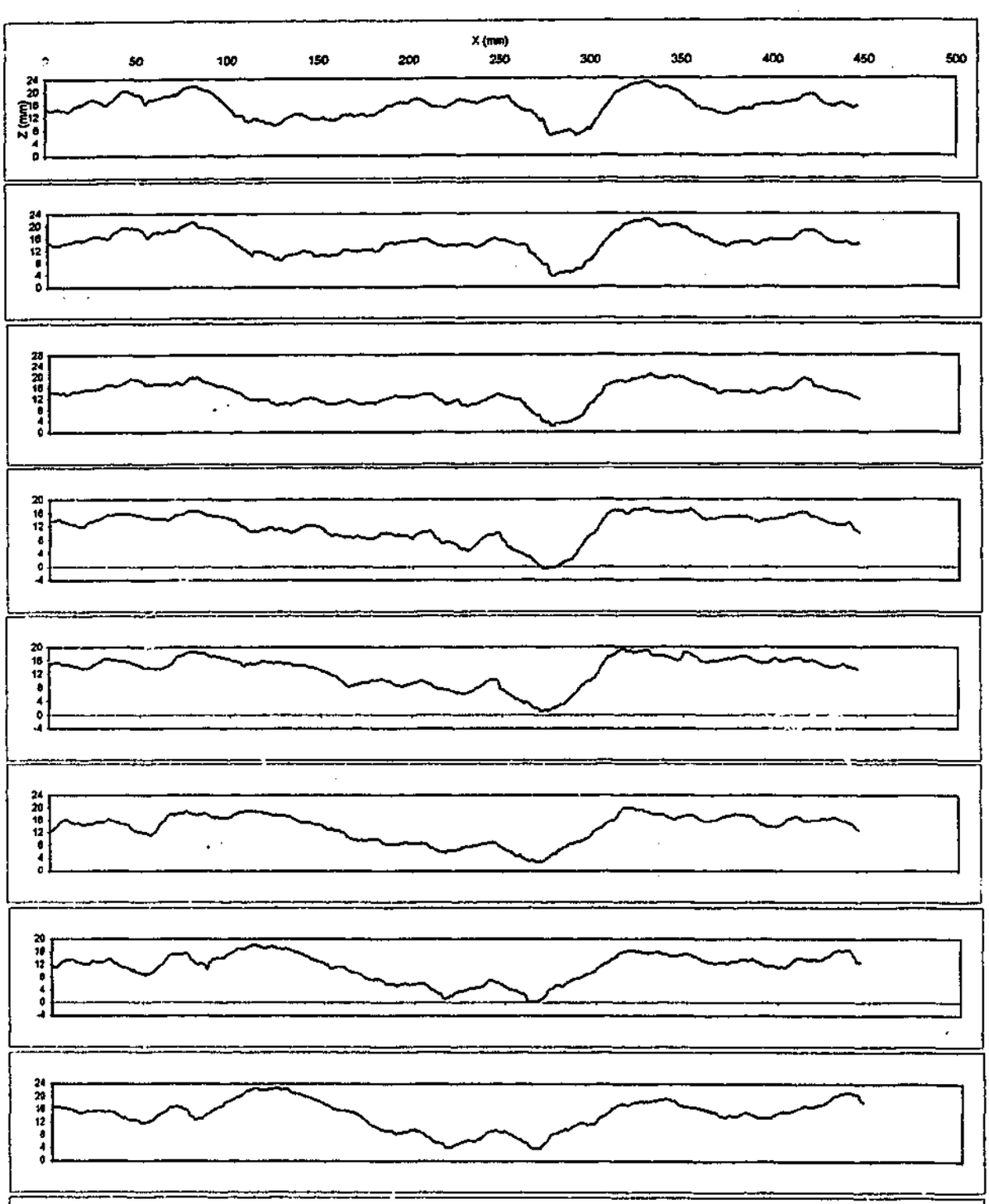

GRANITE SW, SPLIT 2

scanned at 5mm intervals

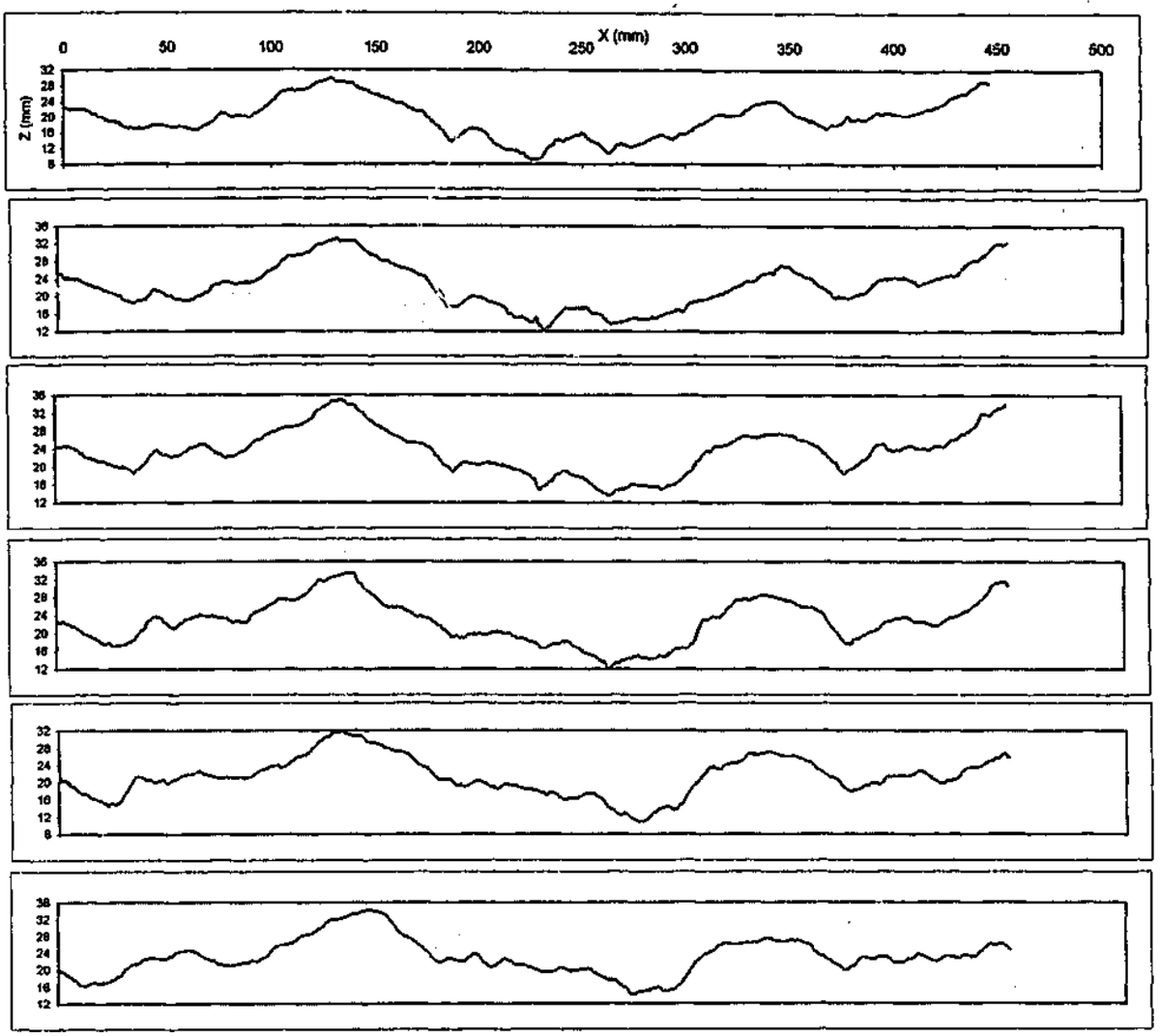

GRANITE SW, SPLIT 2

scanned at 5 mm intervals

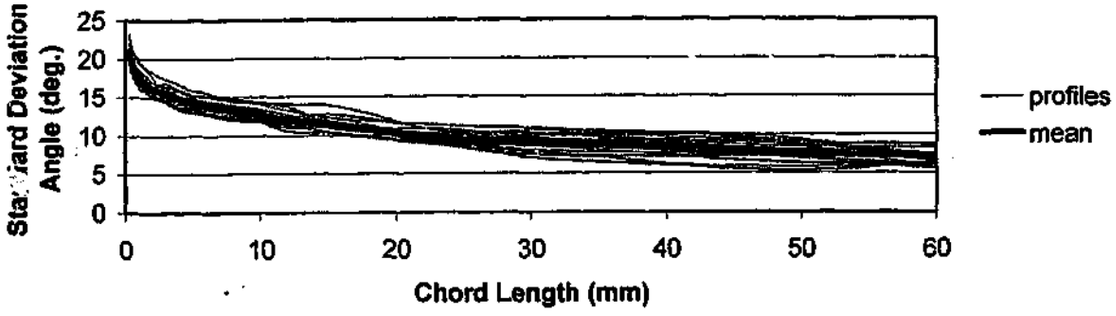

AVERAGE CORRELATION COEFFICIENT OF SCANS = 0.991

AVERAGE CORRELATION COEFFICIENT OF SCANS TO MEAN = 0.996

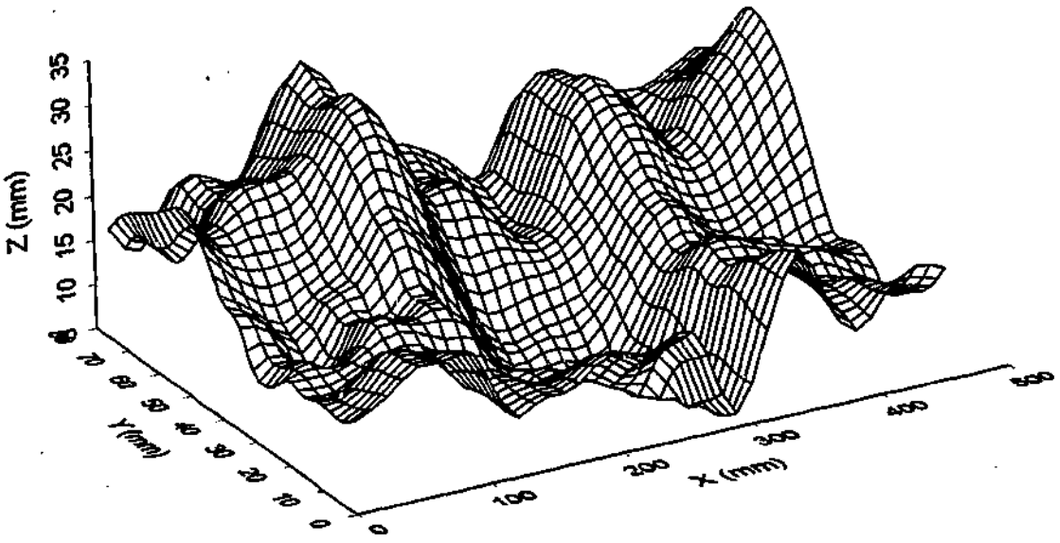

GRANITE SW, SPLIT 2

scanned at 5mm intervals

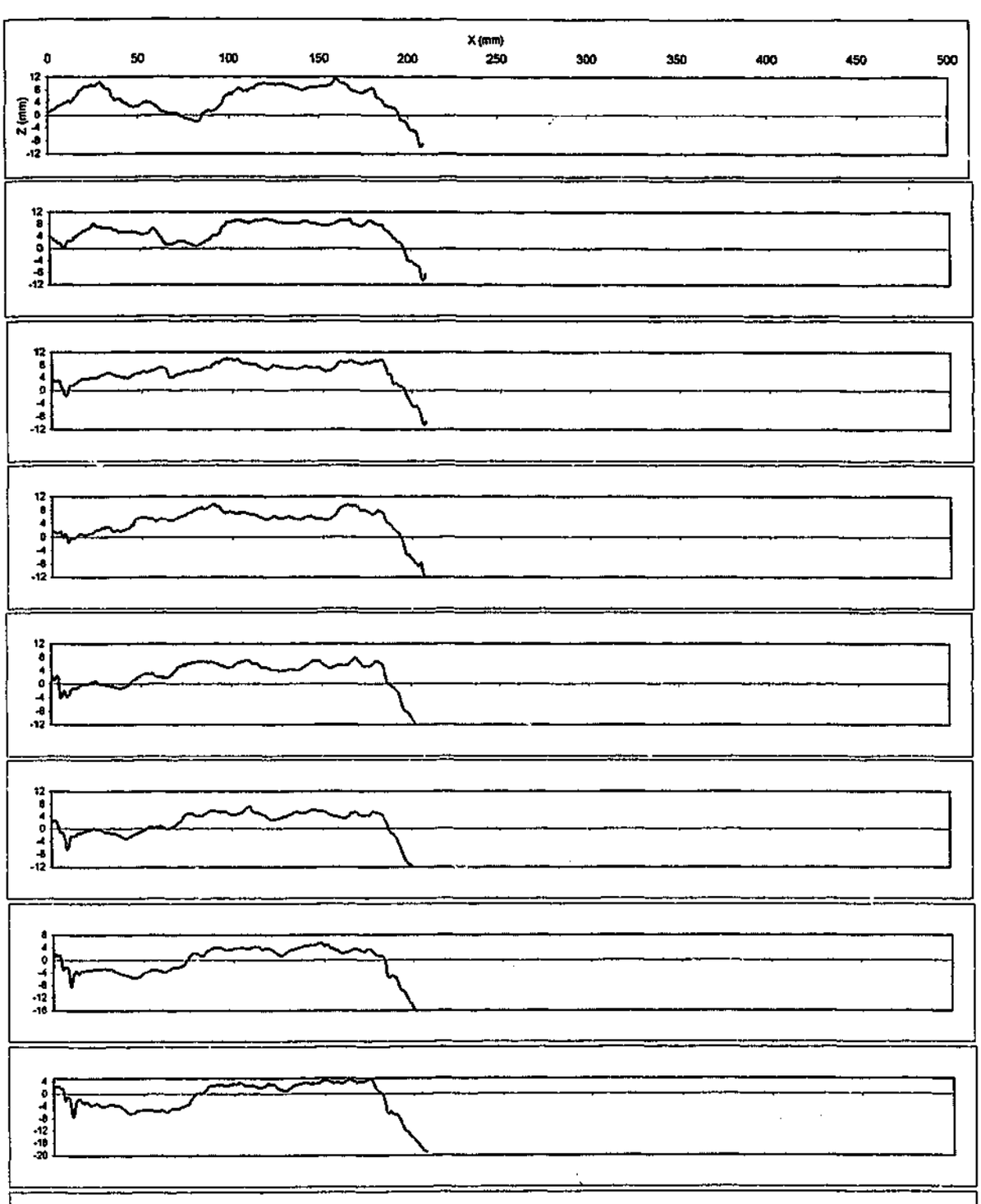

GRANITE SW, SPLIT 3

scanned at 5mm intervals

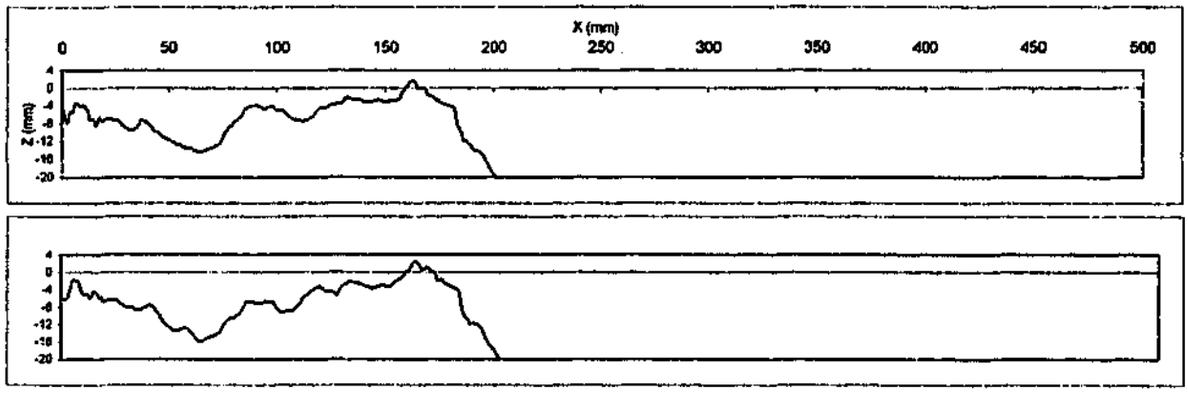

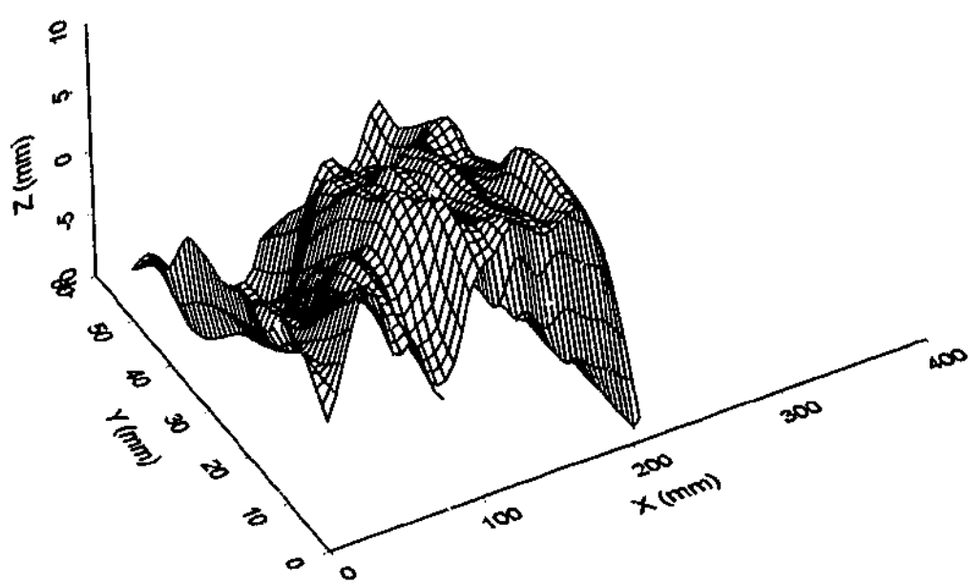

GRANITE SW, SPLIT 3

scanned at 5 mm intervals

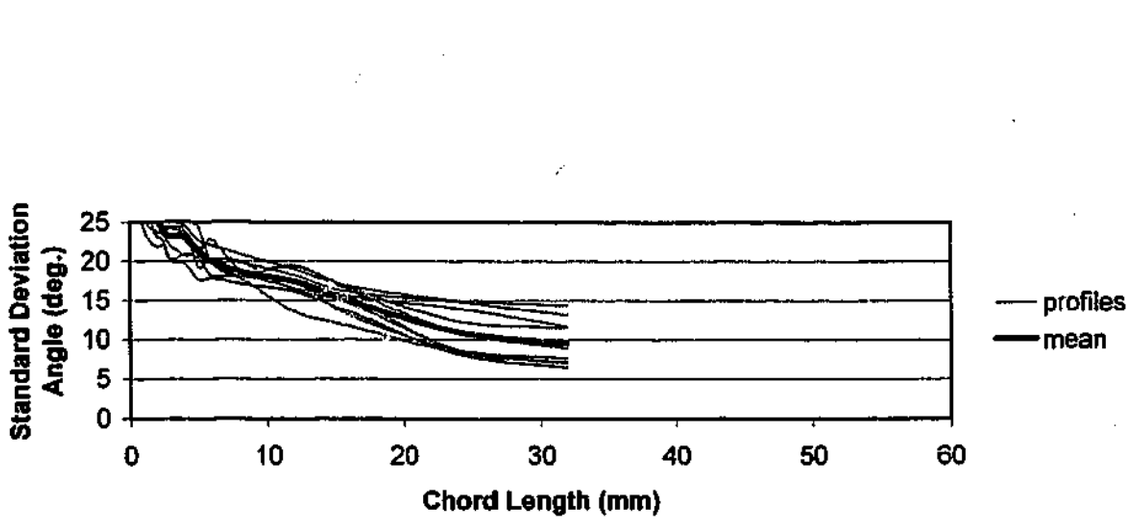

AVERAGE CORRELATION COEFFICIENT OF SCANS = 0.992

AVERAGE CORRELATION COEFFICIENT OF SCANS TO MEAN = 0.996

GRANITE SW, SPLIT 3

scanned at 5mm intervals

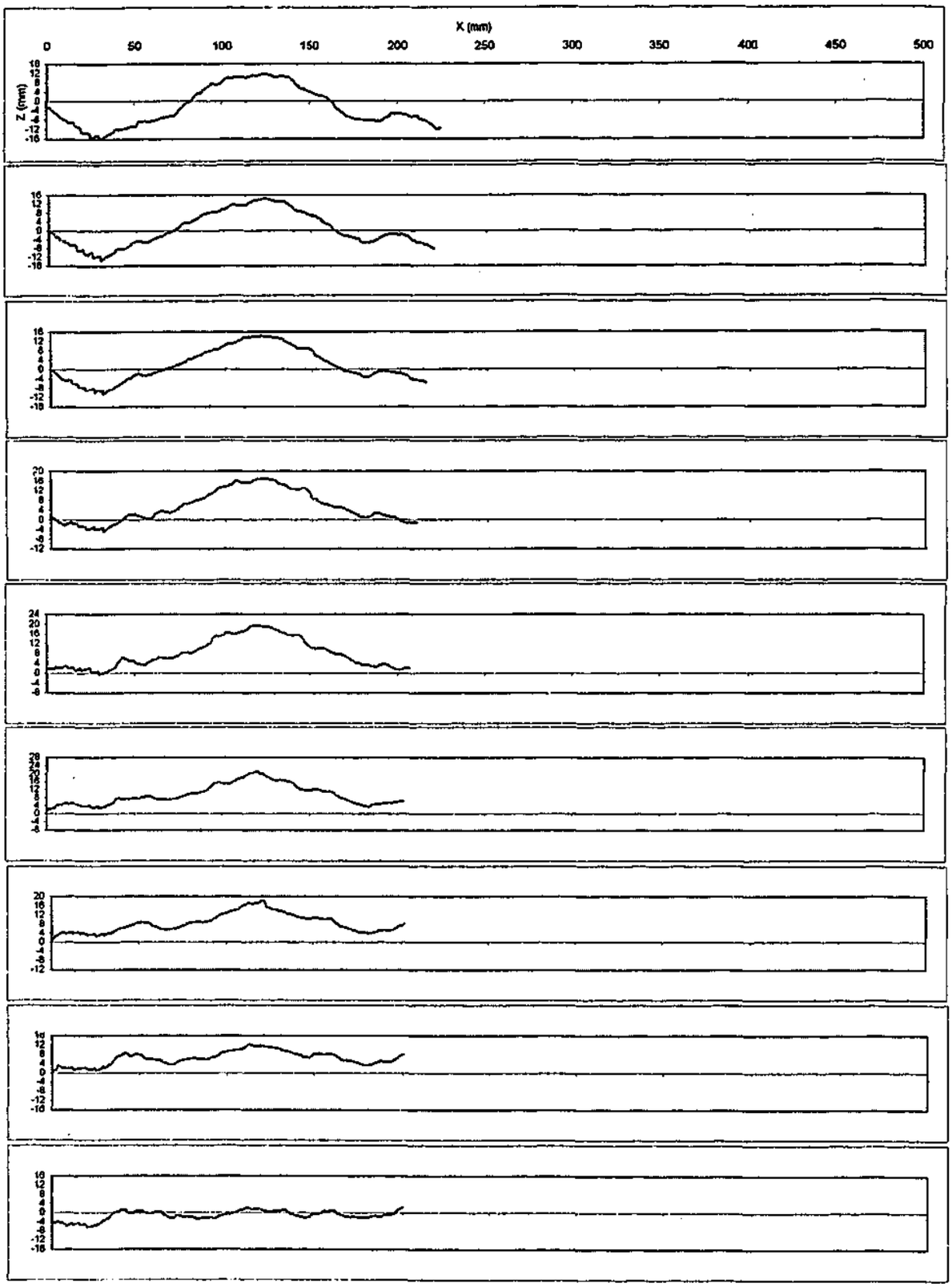

GRANITE SW, SPLIT 4

scanned at 5mm intervals

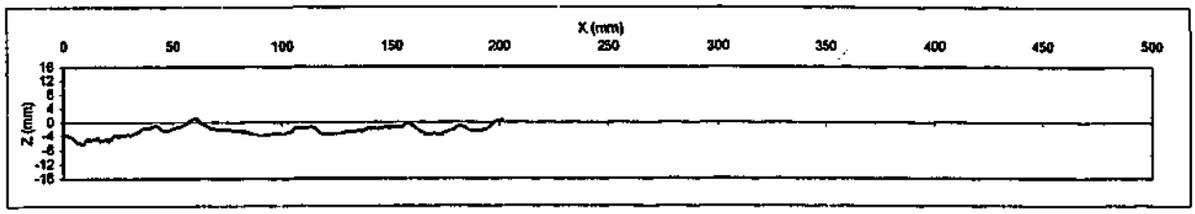

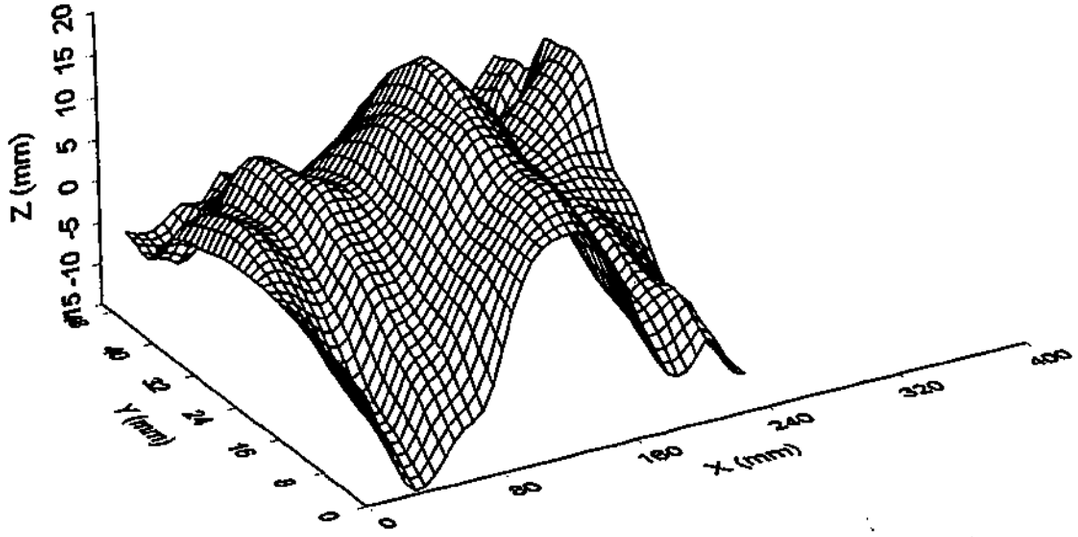

GRANITE SW, SPLIT 4

scanned at 5 mm intervals

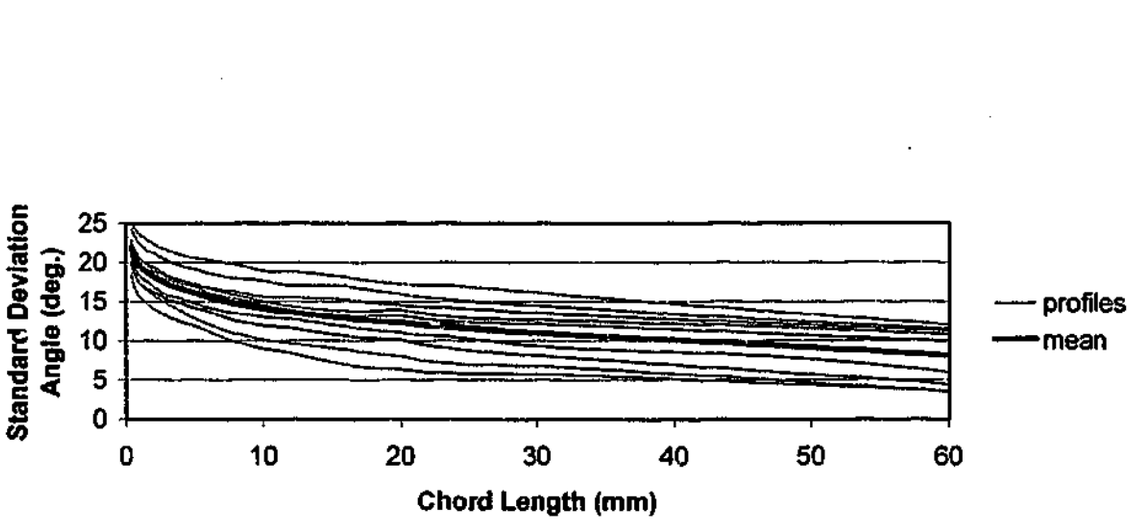

AVERAGE CORRELATION COEFFICIENT OF SCANS = 0.992

AVERAGE CORRELATION COEFFICIENT OF SCANS TO MEAN = 0.996

GRANITE SW, SPLIT 4

scanned at 5mm intervals

APPENDIX D

LABORATORY DIRECT SHEAR TEST RESULTS

Table of Contents – Appendix D

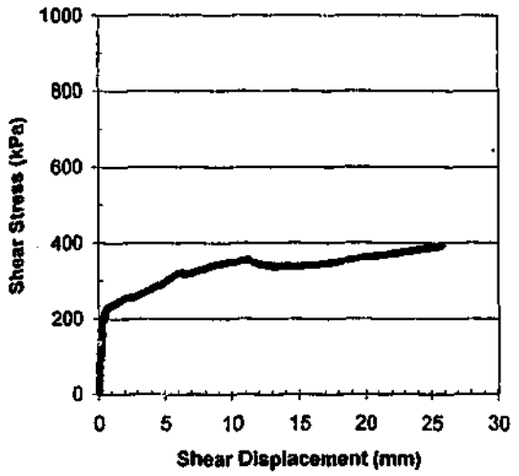

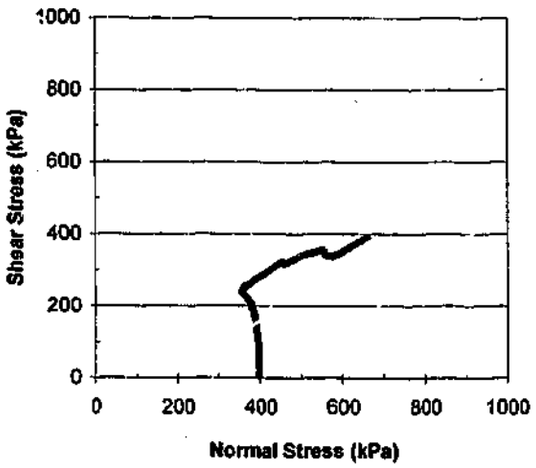

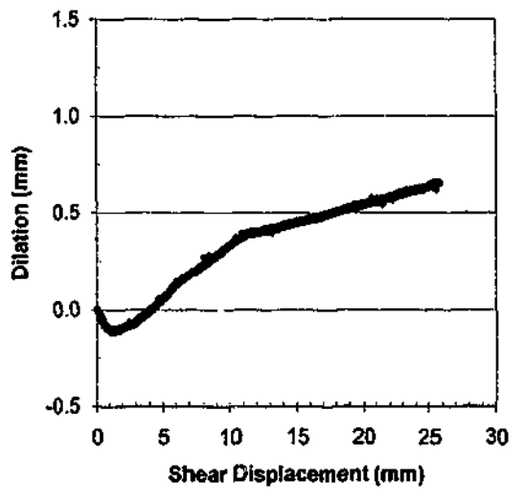

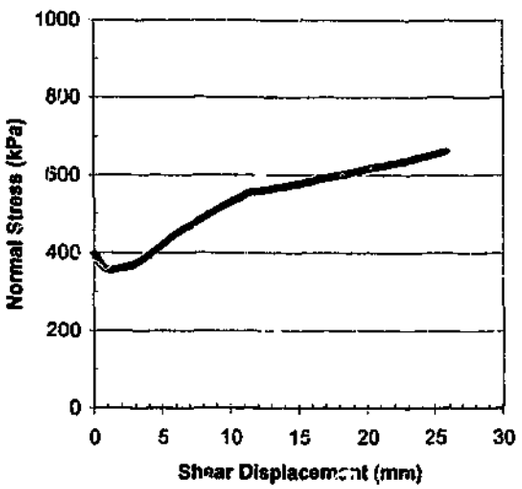

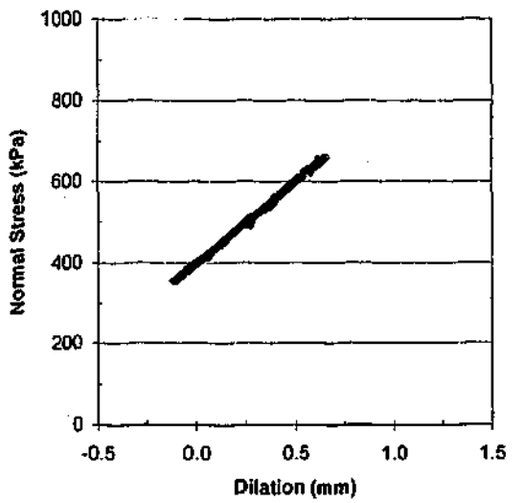

Test No:	**JF8_12**
Test Date: 23/6/00	
JOHNSTONE	
Profile :	**2-D cut profile of centre profile of JS_4a cut @ 12mm chords**
Shear Rate = 0.5 mm/min	
Initial Normal Stress (kPa):	**400**
Normal Stiffness (kPa/mm):	**400**

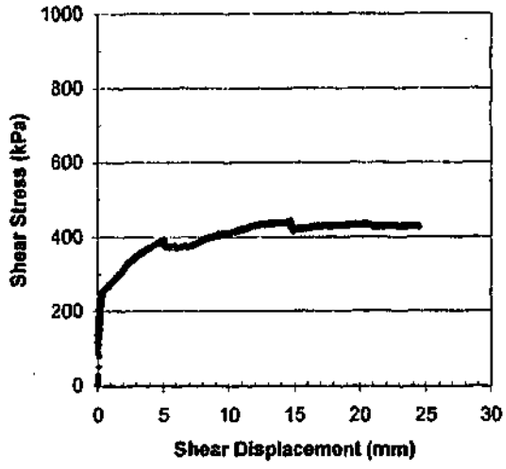

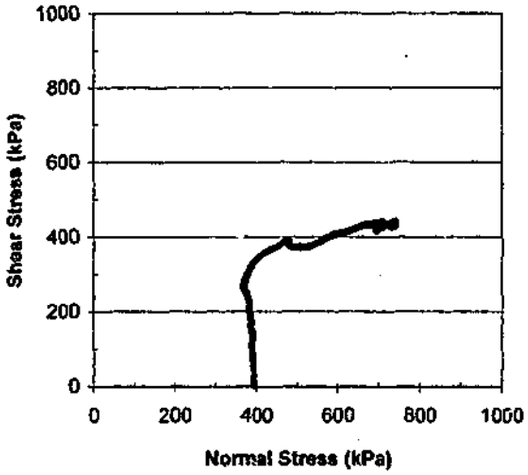

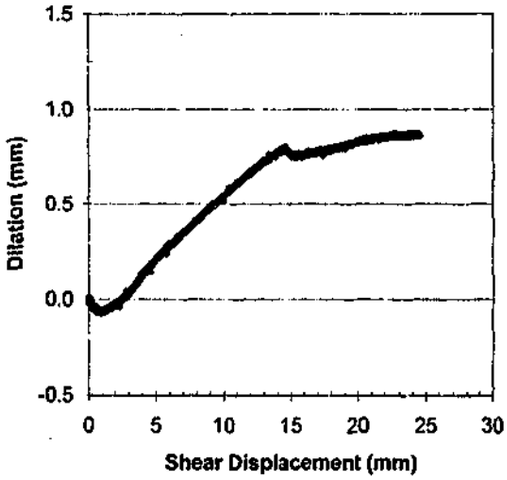

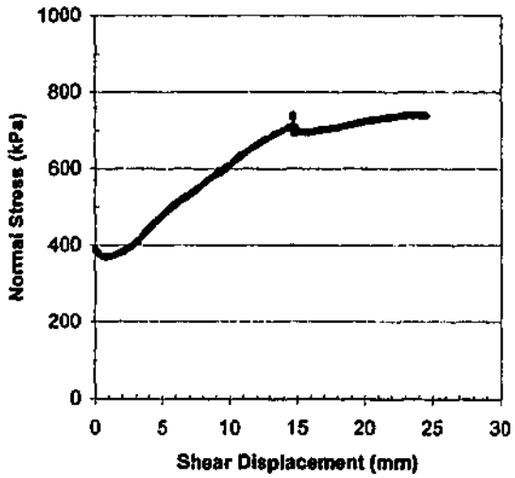

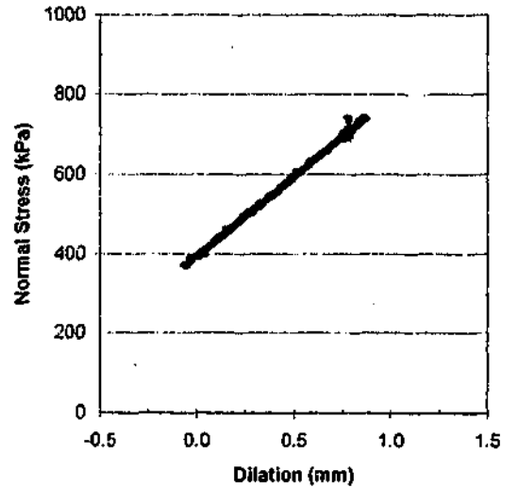

Test No:	JF12_3
Test Date: 11/4/00	
JOHNSTONE	
Profile : 2-D cut profile of centre profile of split JS_3a @ 3mm chords	
Shear Rate = 0.5 mm/min	
Initial Normal Stress (kPa):	400
Normal Stiffness (kPa/mm):	400

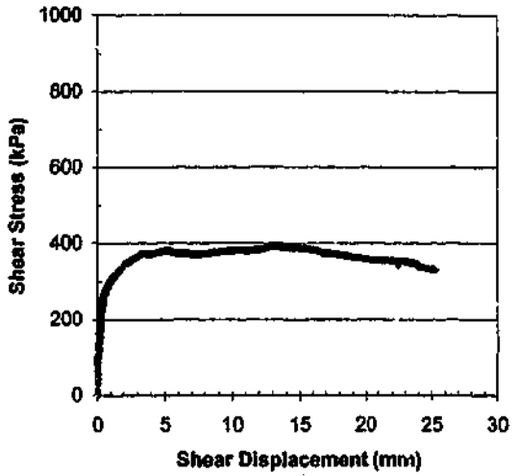

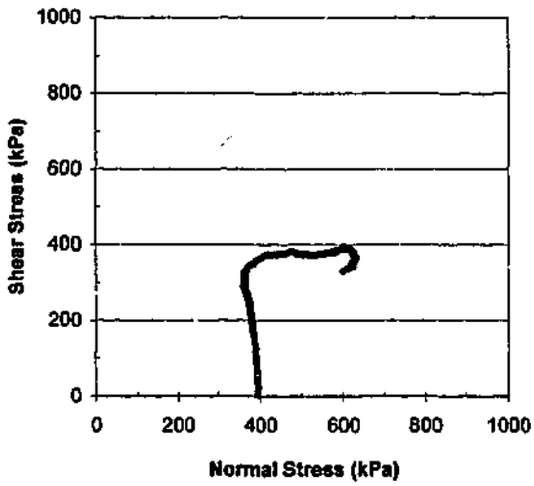

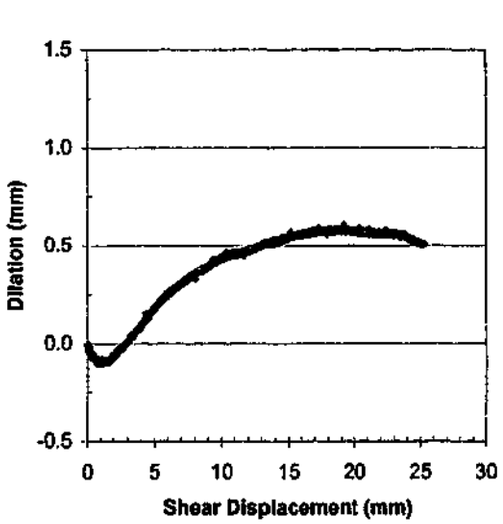

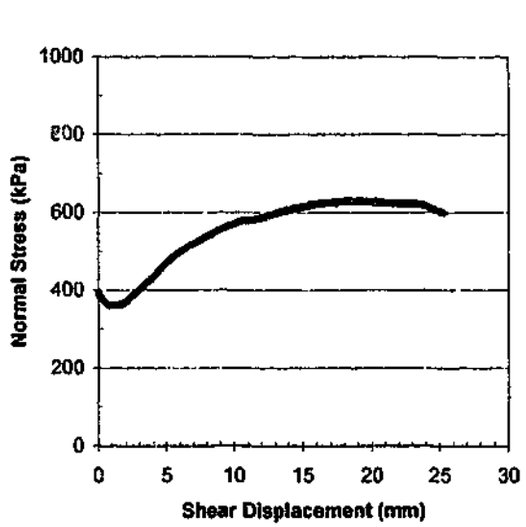

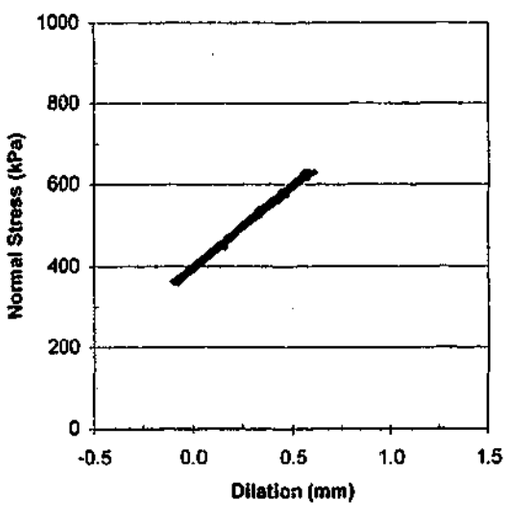

Test No:	JF15a_3
Test Date: 16/5/00	
JOHNSTONE	
Profile : 2-D cut profile of centre profile of JS_4a cut @ 3mm chords	
Shear Rate = 0.5 mm/min	
Initial Normal Stress (kPa):	400
Normal Stiffness (kPa/mm):	400

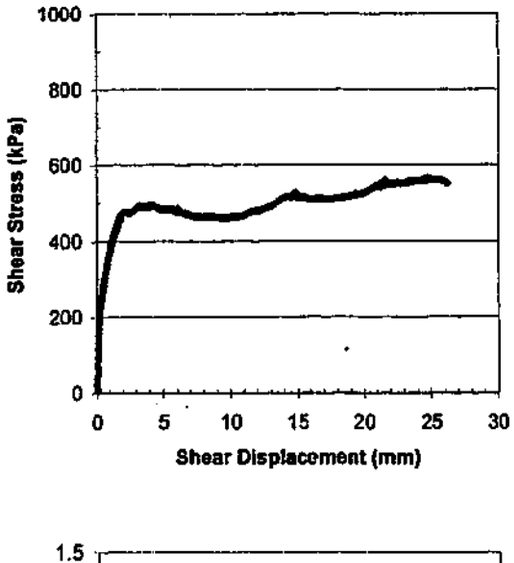

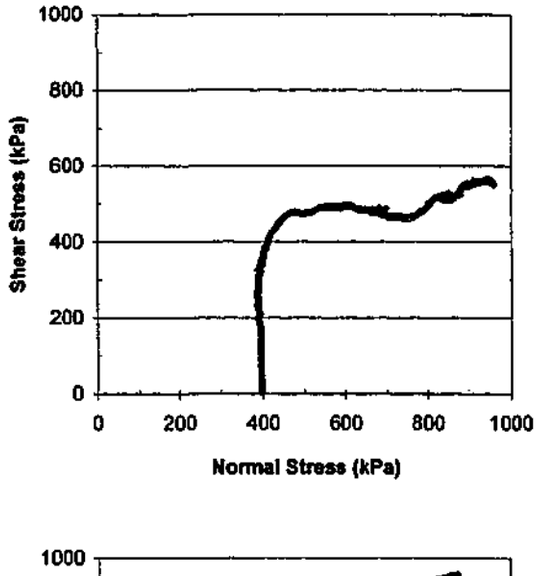

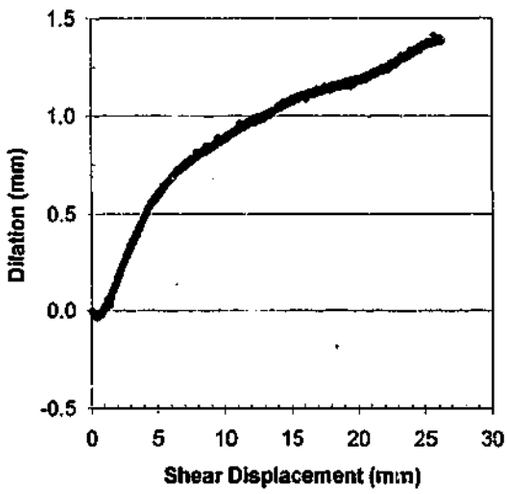

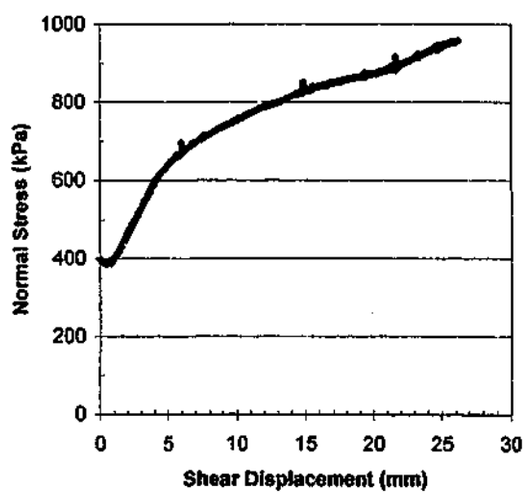

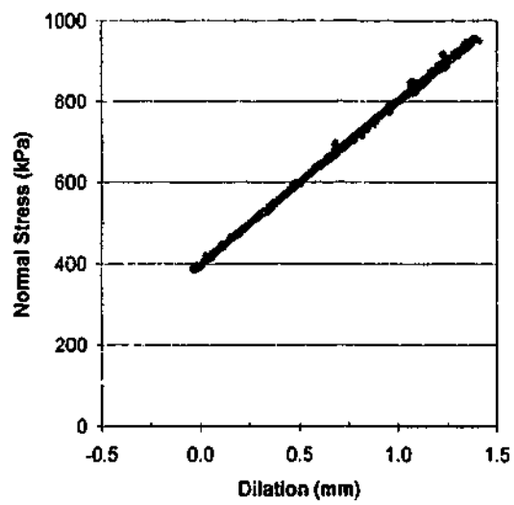

Test No:	**JF15_3**
Test Date: 15/8/00	
JOHNSTONE	
Profile :	**2-D cut profile using split JS_3a statistically represented with power function @ 3mm chords**
Shear Rate = 0.5 mm/min	
Initial Normal Stress (kPa):	**400**
Normal Stiffness (kPa/mm):	**400**

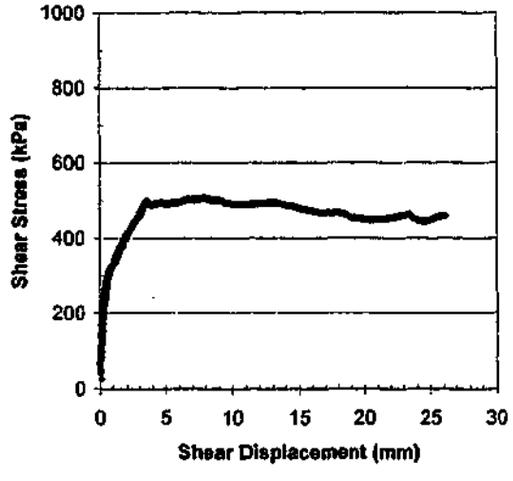

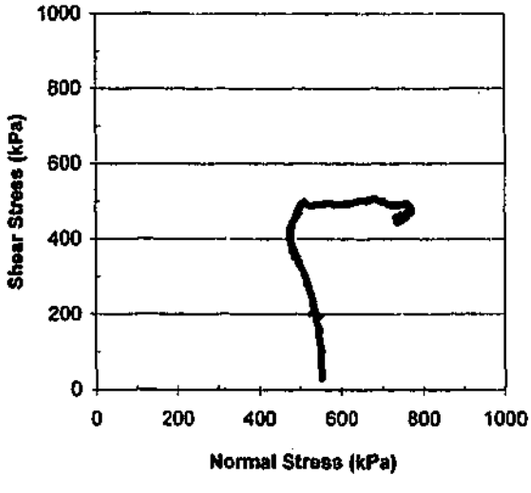

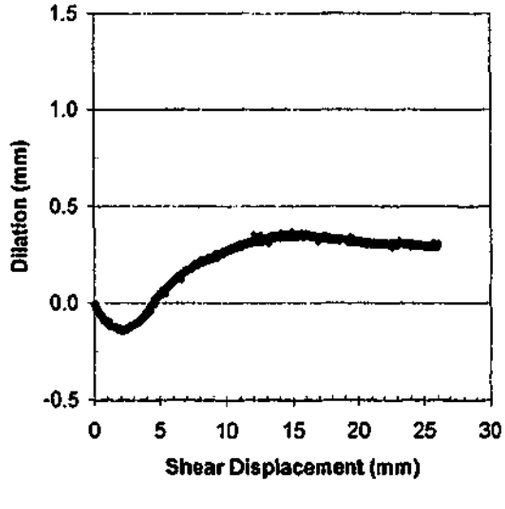

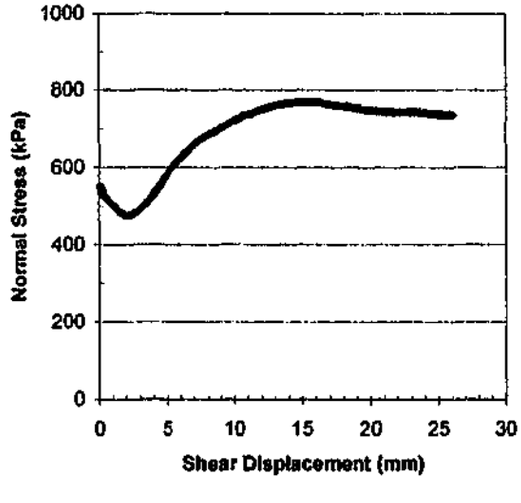

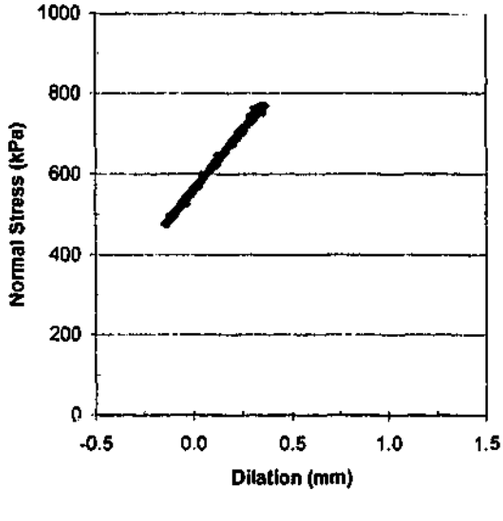

Test No:	JF21_3
Test Date: 18/4/00	
JOHNSTONE	
Profile : 2-D cut profile using split JS_3b statistically represented with power function @ 3mm chords	
Shear Rate = 0.5 mm/min	
Initial Normal Stress (kPa):	560
Normal Stiffness (kPa/mm):	600

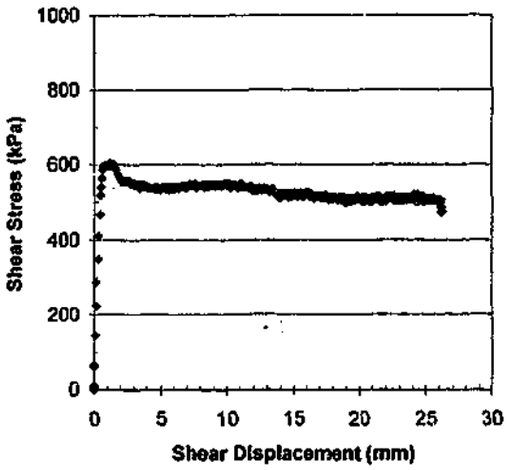

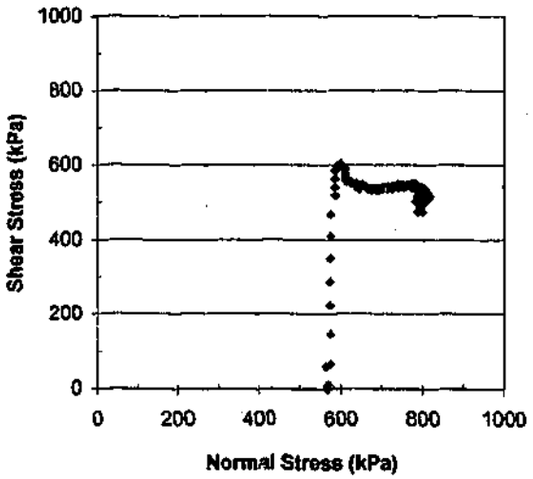

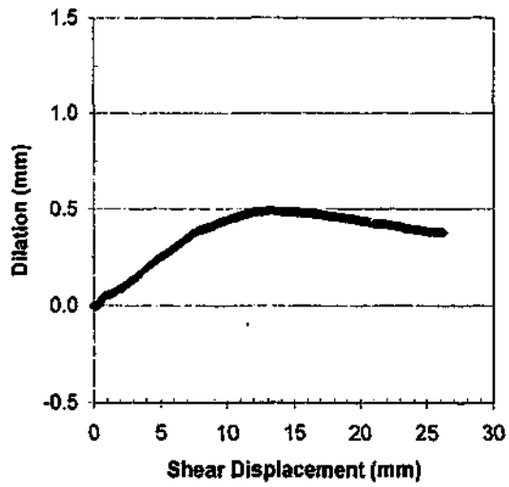

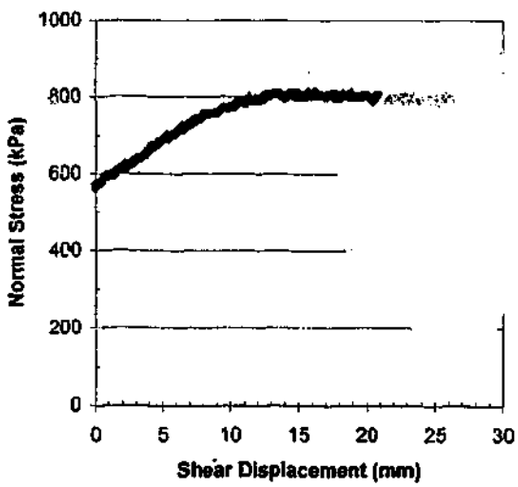

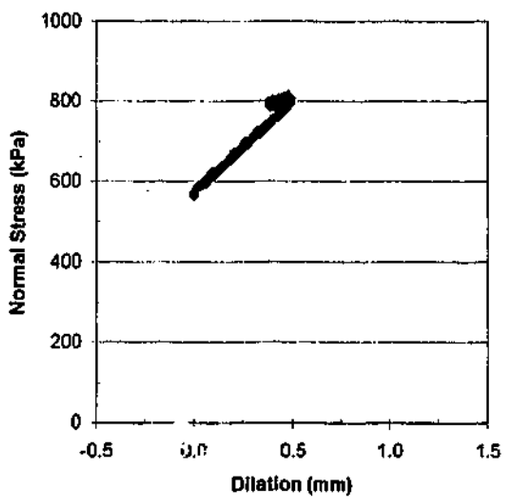

Test No:	JS_1a
Test Date: 4/11/98	
JOHNSTONE	
Profile : Split	
Shear Rate = 0.5 mm/min	
Initial Normal Stress (kPa):	600
Normal Stiffness (kPa/mm):	400

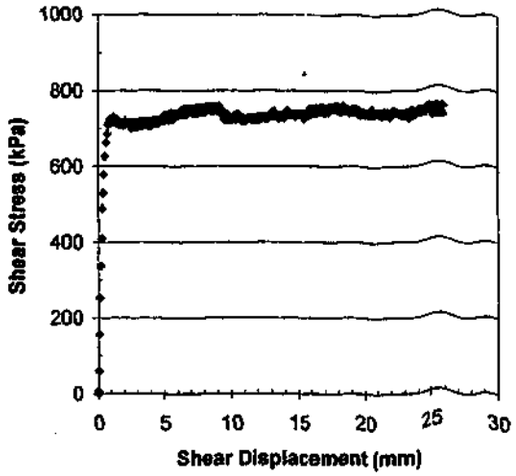

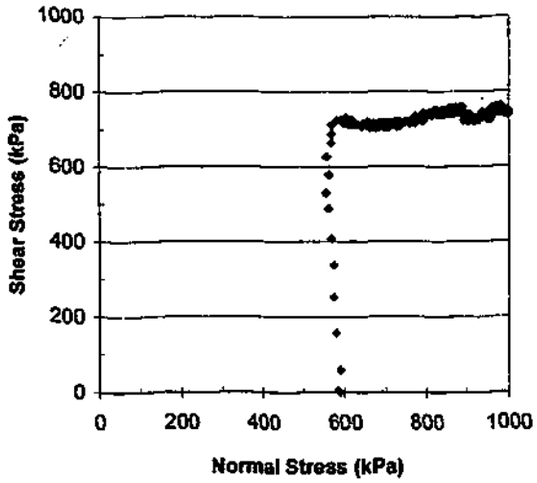

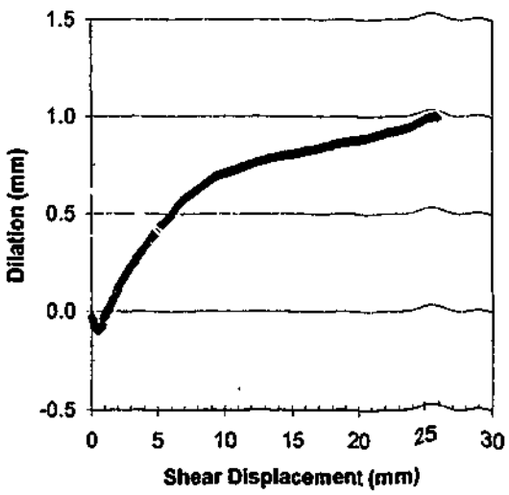

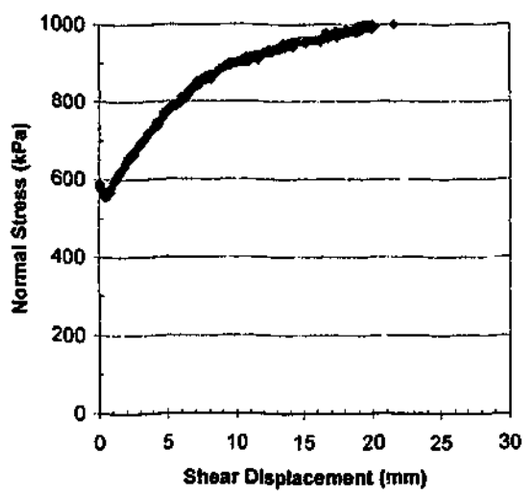

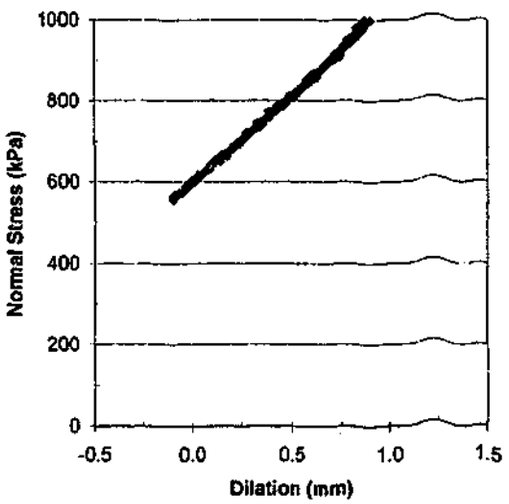

Test No:	JS_1b
Test Date: 5/11/98	
JOHNSTONE	
Profile : Split	
Shear Rate = 0.5 mm/min	
Initial Normal Stress (kPa):	600
Normal Stiffness (kPa/mm):	400

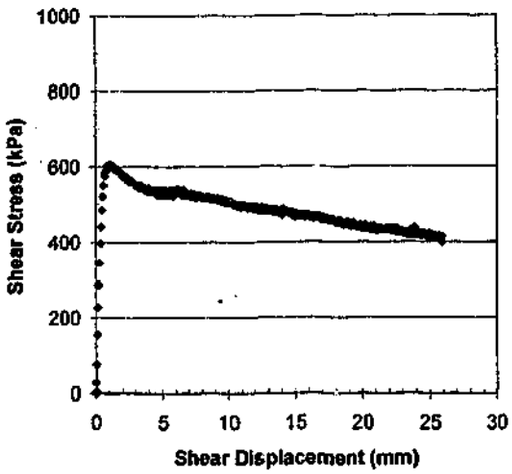

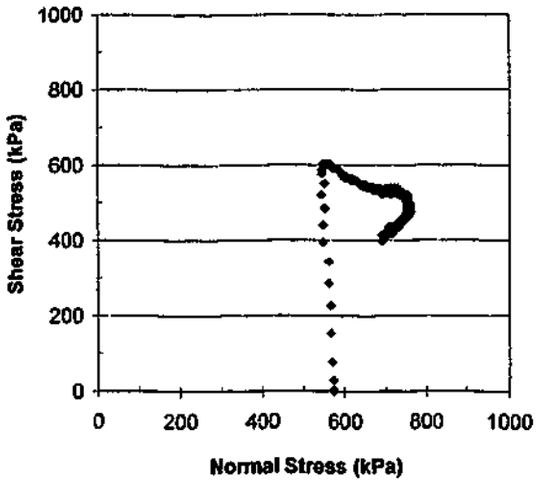

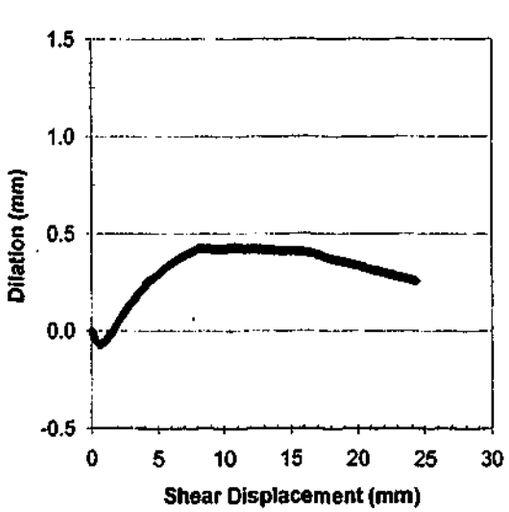

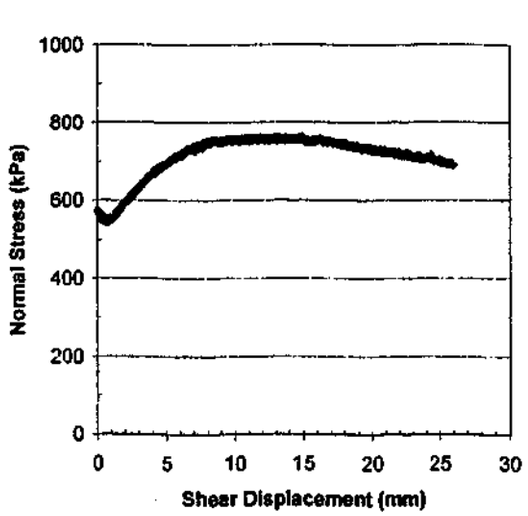

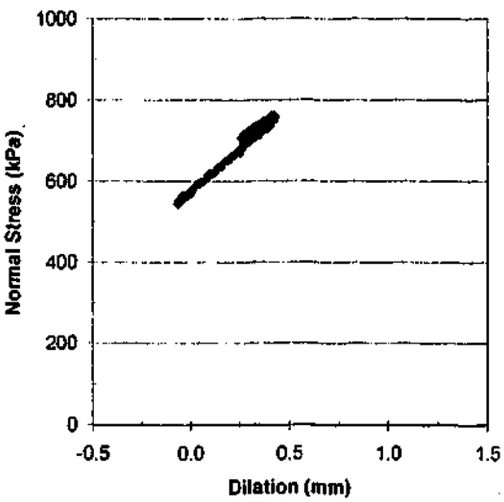

Test No:	JS_2a
Test Date: 6/11/98	
JOHNSTONE	
Profile : Split	
Shear Rate = 0.5 mm/min	
Initial Normal Stress (kPa):	600
Normal Stiffness (kPa/mm):	400

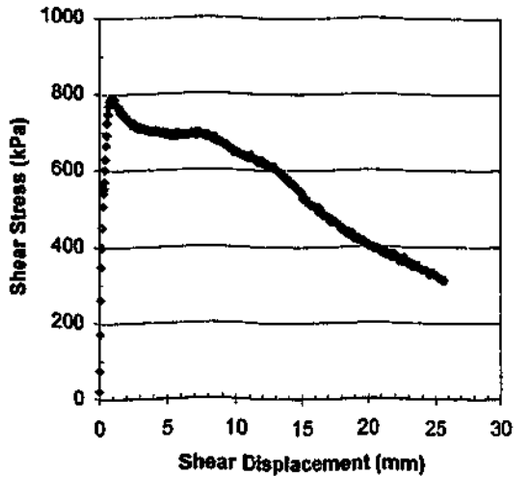

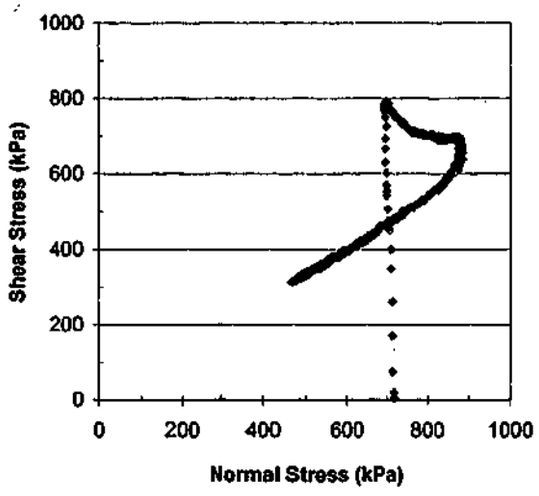

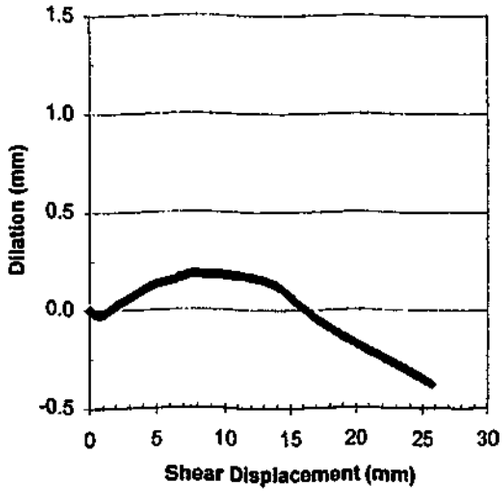

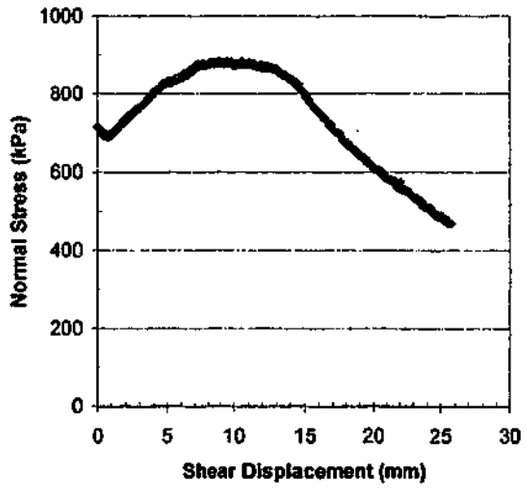

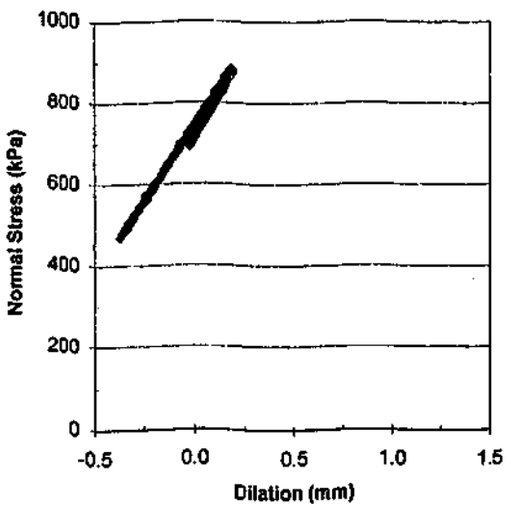

Test No:	JS_2b
Test Date:19/11/98	
JOHNSTONE	
Profile : Split	
Shear Rate = 0.5 mm/min	
Initial Normal Stress (kPa):	700
Normal Stiffness (kPa/mm):	800
Failure of sample setup during testing	

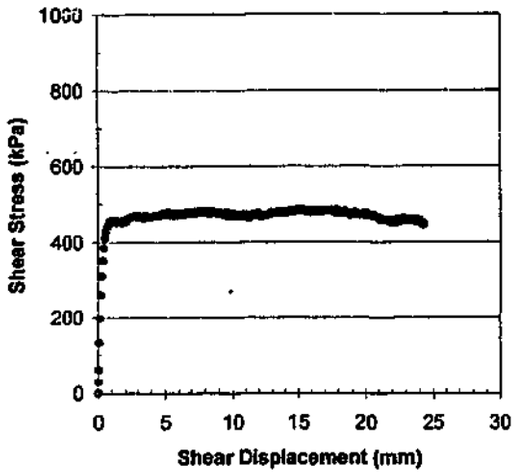

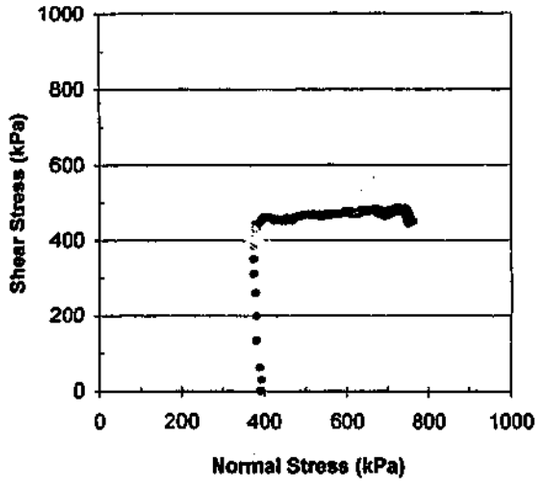

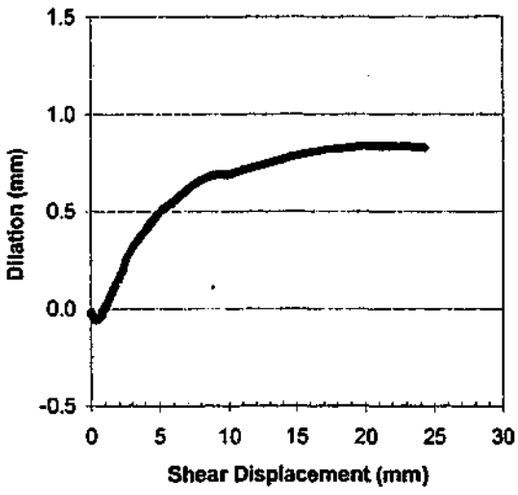

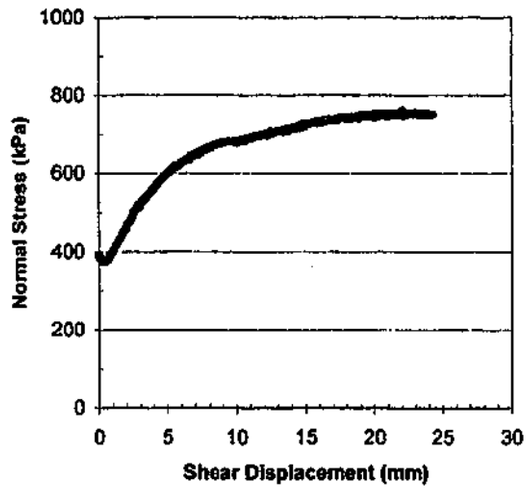

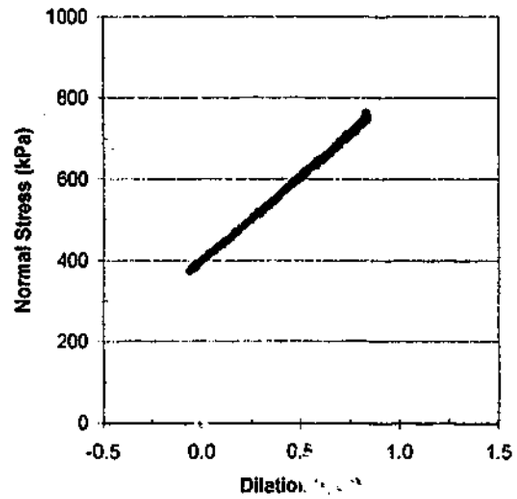

Test No:	JS_3a
Test Date	18/11/98
JOHNSTONE	
Profile : Split	
Shear Rate = 0.5 mm/min	
Initial Normal Stress (kPa):	400
Normal Stiffness (kPa/mm):	400

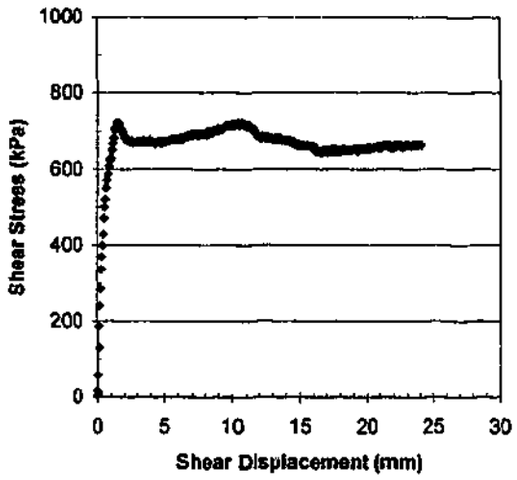

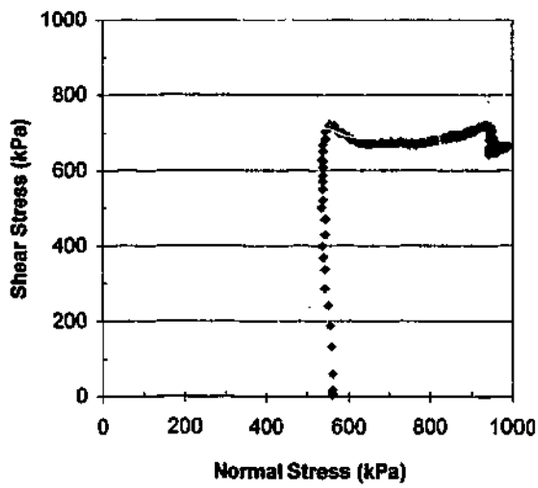

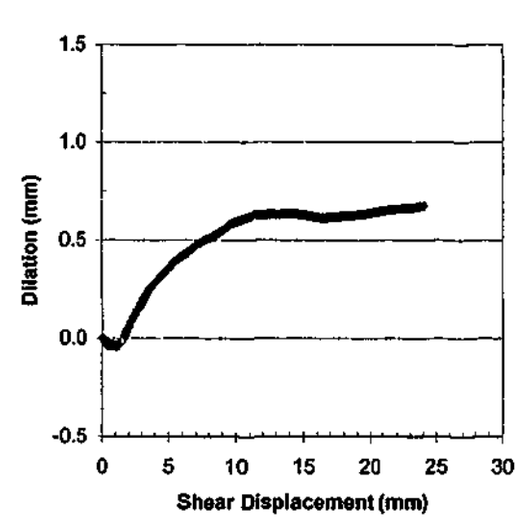

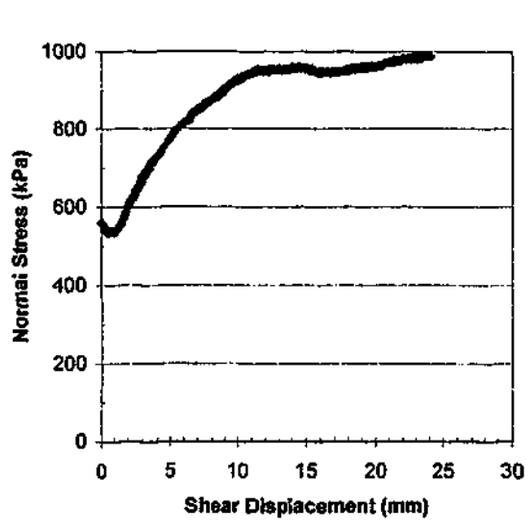

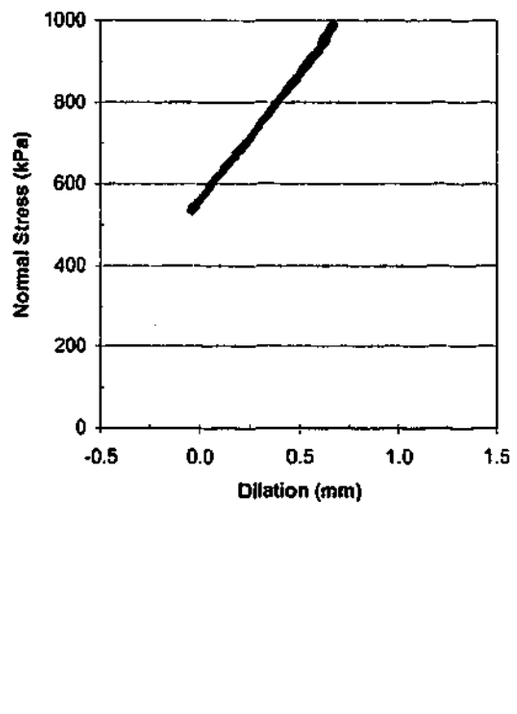

Test No:	JS_3b
Test Date	2/12/98
JOHNSTONE	
Profile : Split	
Shear Rate = 0.5 mm/min	
Initial Normal Stress (kPa):	560
Normal Stiffness (kPa/mm):	600

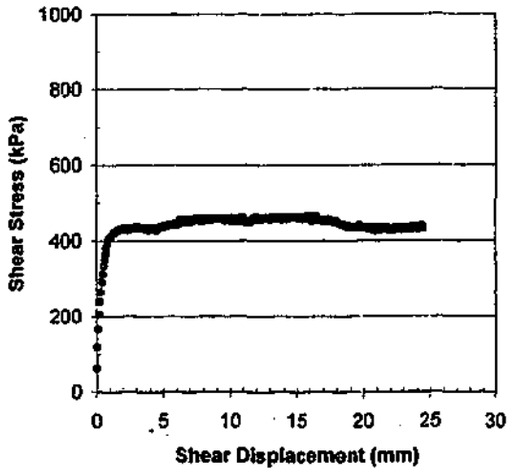

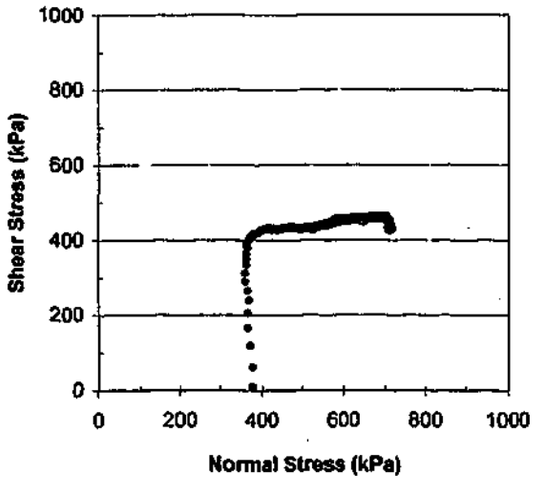

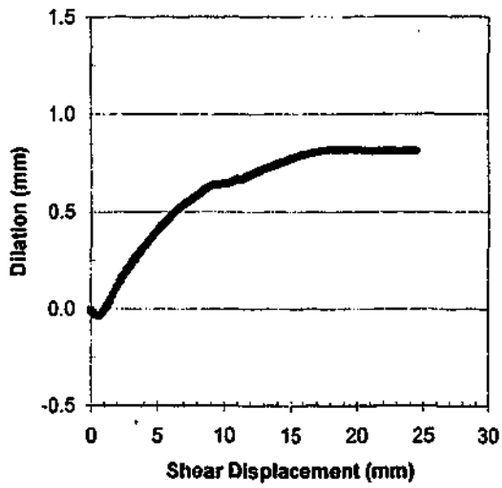

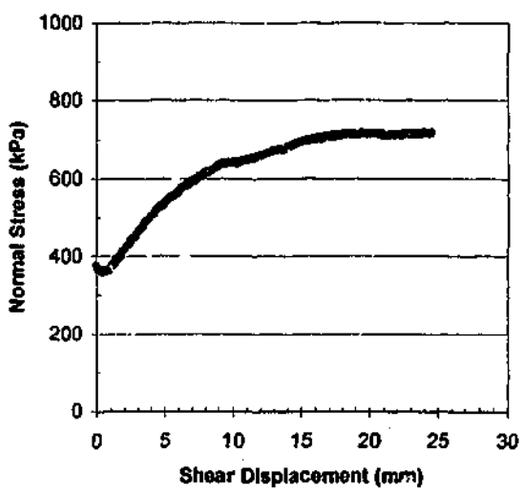

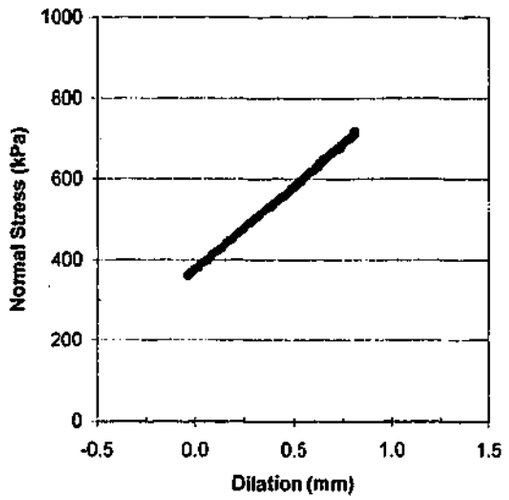

Test No:	JS_4a
Test Date	1/12/93
JOHNSTONE	
Profile : Split	
Shear Rate = 0.5 mm/min	
Initial Normal Stress (kPa):	400
Normal Stiffness (kPa/mm):	400

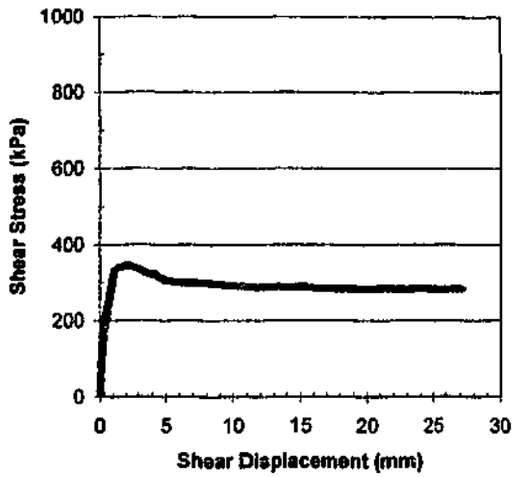

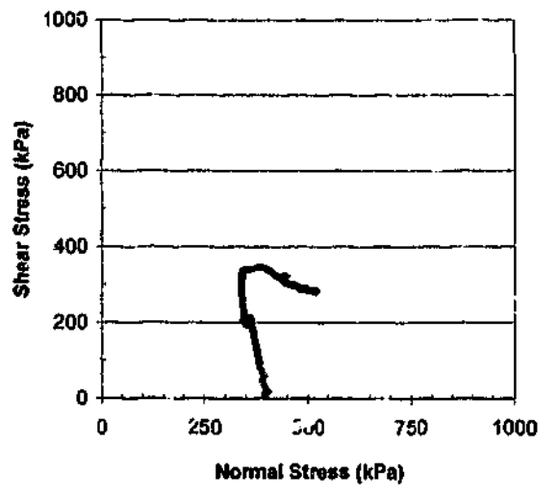

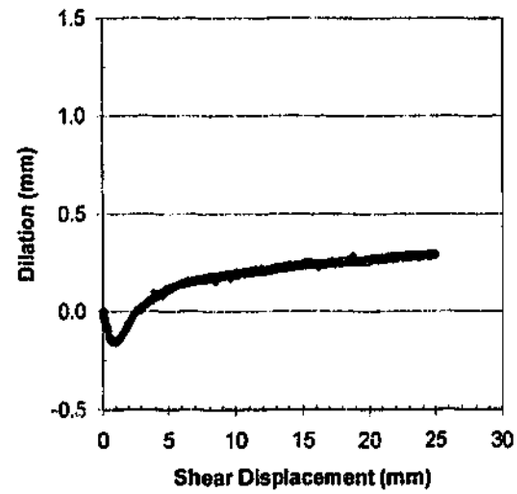

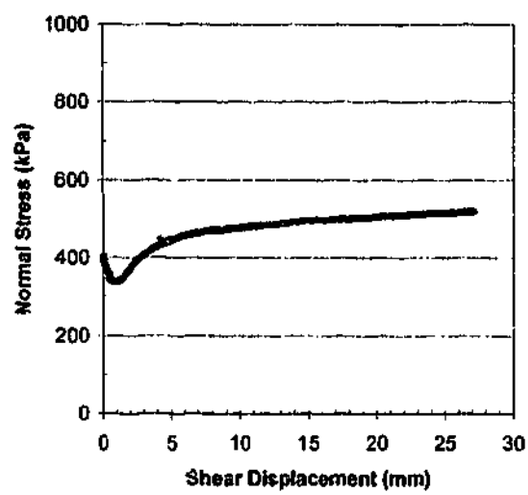

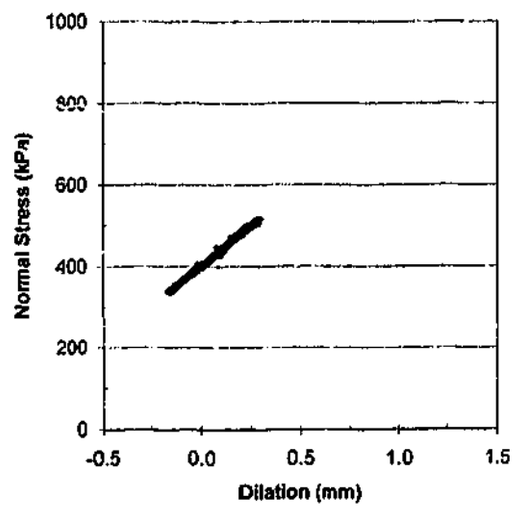

Test No:	JS_6a
Test Date: 21/3/00	
JOHNSTONE	
Profile : Split	
Shear Rate = 0.5 mm/min	
Initial Normal Stress (kPa):	400
Normal Stiffness (kPa/mm):	400

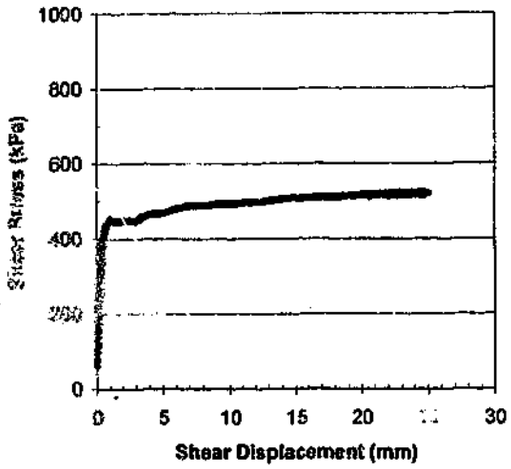

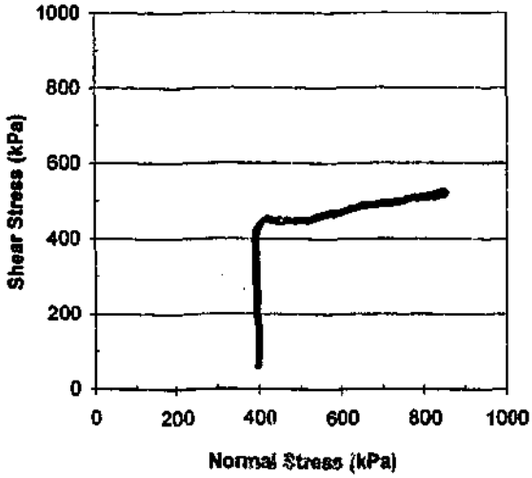

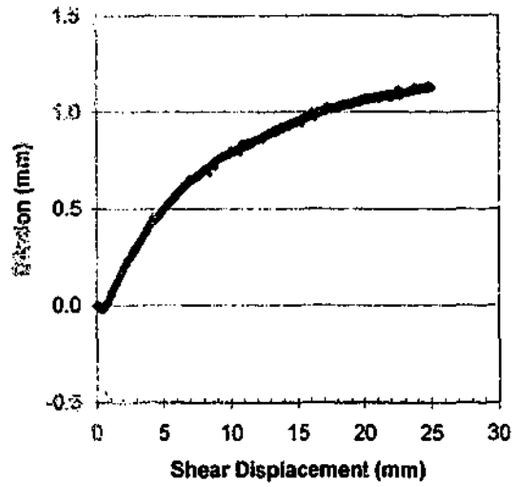

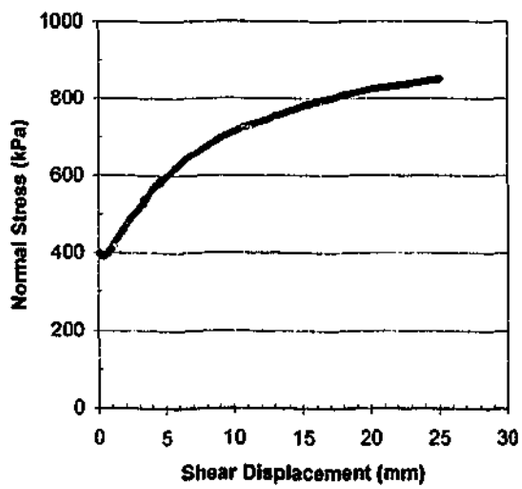

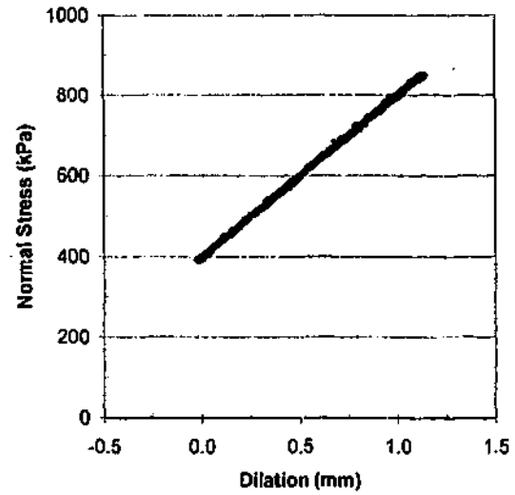

Test No:	JS_7a
Test Date: 3/10/00	
JOHNSTONE	
Profile : Split	
Shear Rate = 0.5 mm/min	
Initial Normal Stress (kPa):	400
Normal Stiffness (kPa/mm):	400

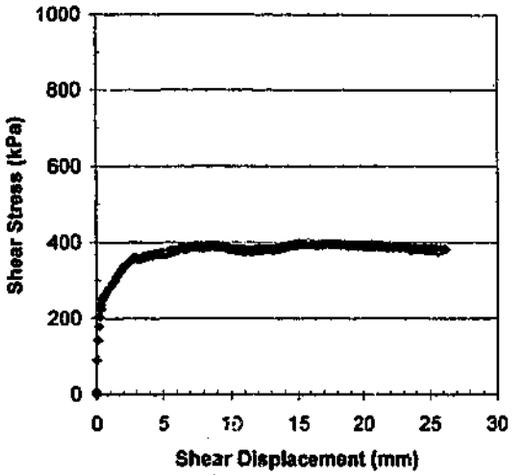

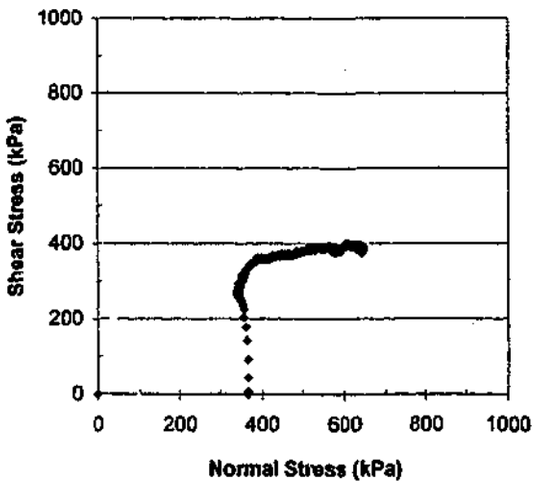

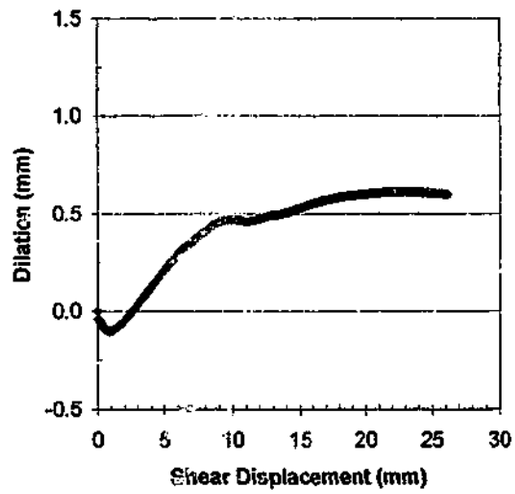

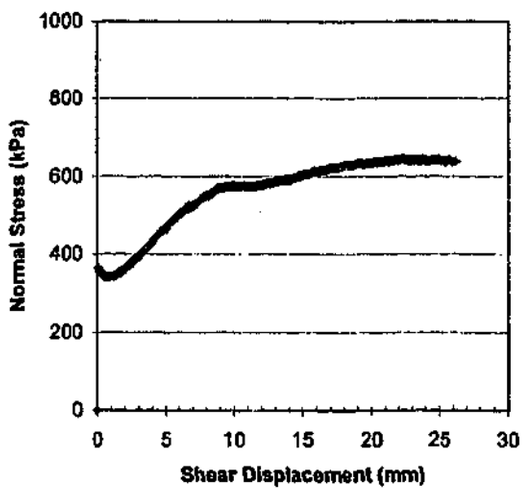

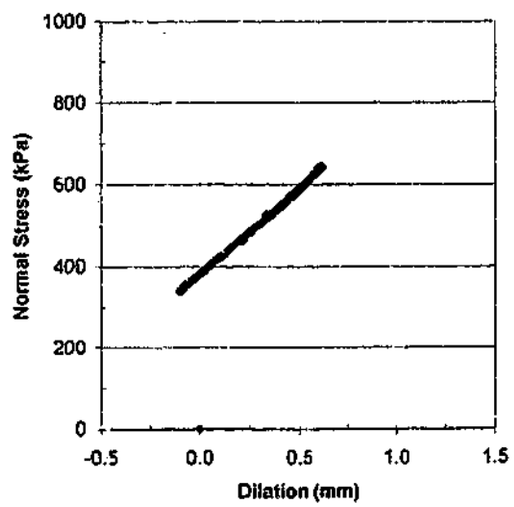

Test No:	**JC3a_stat6**
Test Date: 9/12/98	
JOHNSTONE	
Profile : 2-D cut version of split JS_3a statistically represented @ 6mm chords	
Shear Rate = 0.5 mm/min	
Initial Normal Stress (kPa):	**400**
Normal Stiffness (kPa/mm):	**400**

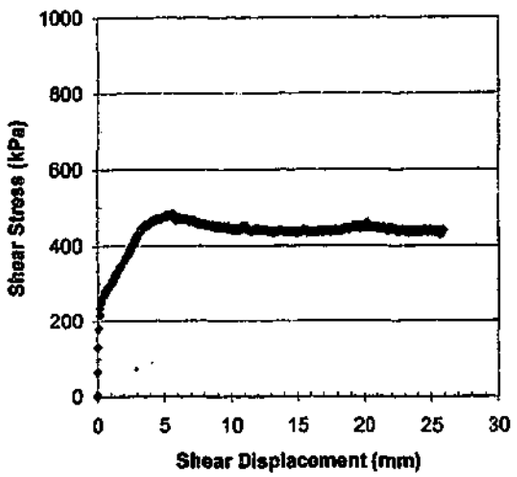

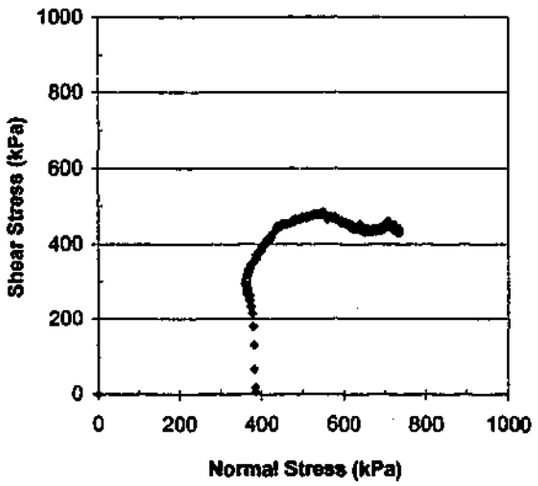

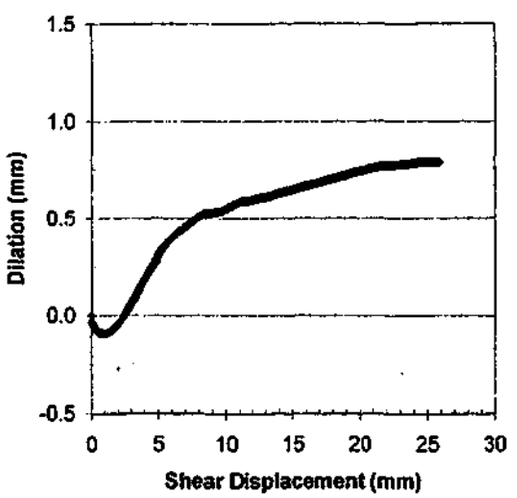

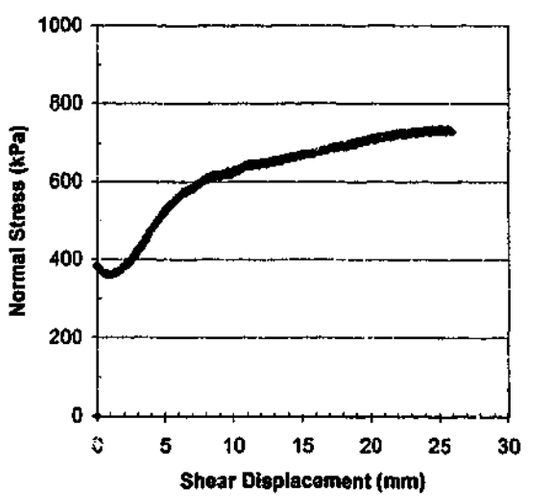

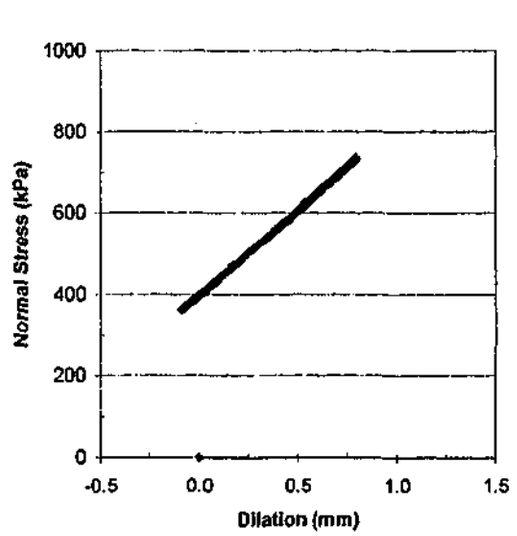

Test No:	JC4a_6
Test Date: 8/12/98	
JOHNSTONE	
Profile : 2-D cut profile of centre profile of JS_4a cut @ 4mm chords	
Shear Rate = 0.5 mm/min	
Initial Normal Stress (kPa):	400
Normal Stiffness (kPa/mm):	400

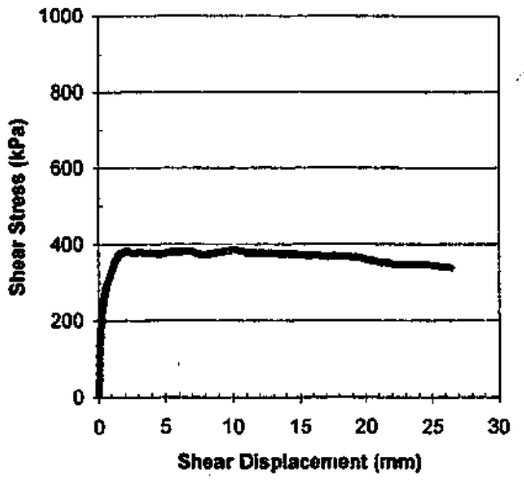

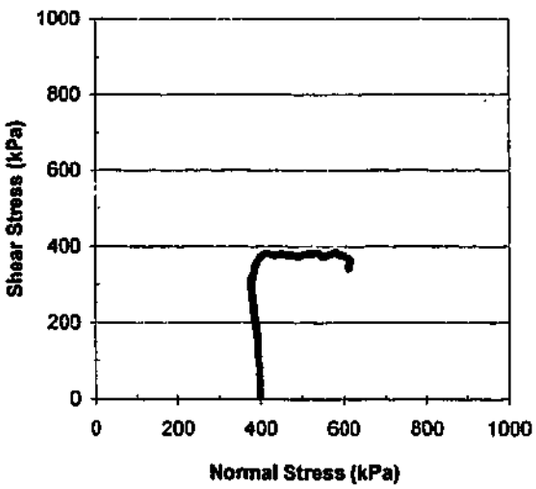

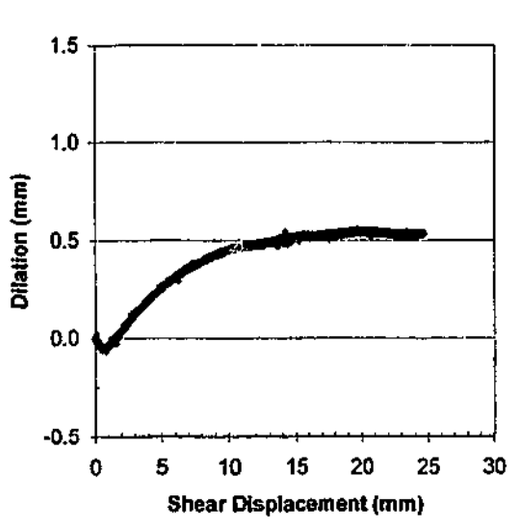

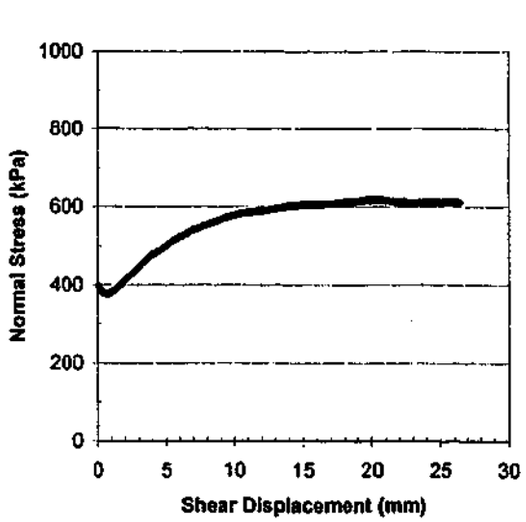

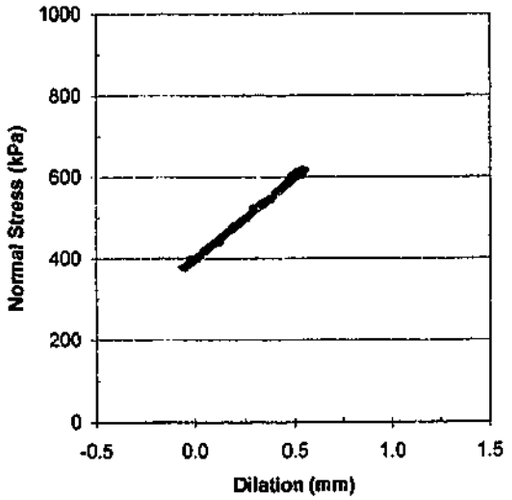

Test No:	**JC6a_3**
Test Date: 6/9/00	
JOHNSTONE	
Profile : 2-D cut profile at centre profile of JS_3_ cut @ 3mm chords	
Shear Rate = 0.5 mm/min	
Initial Normal Stress (kPa):	**400**
Normal Stiffness (kPa/mm):	**400**

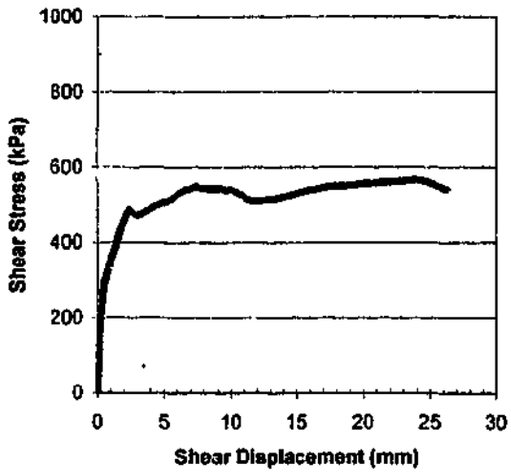

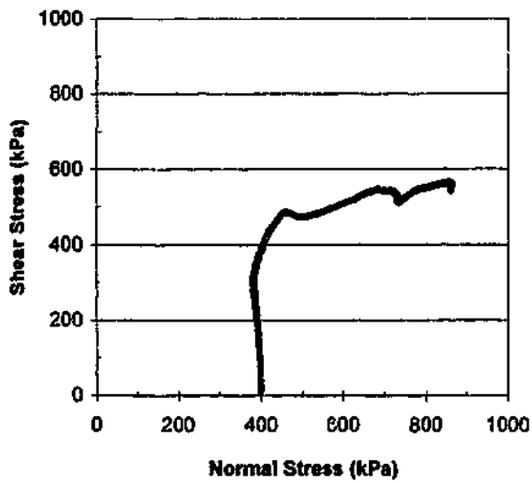

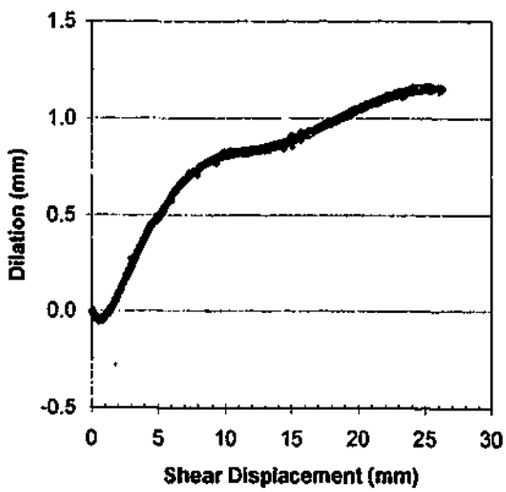

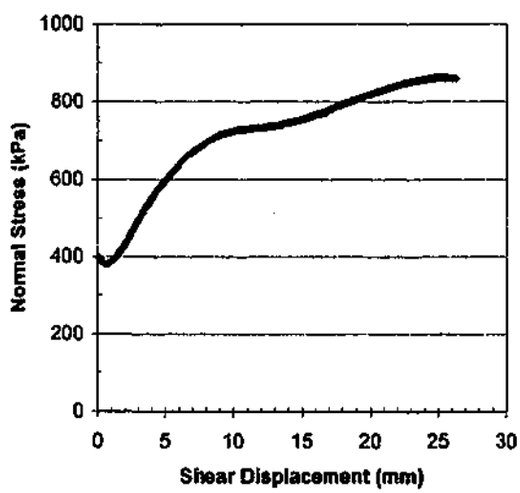

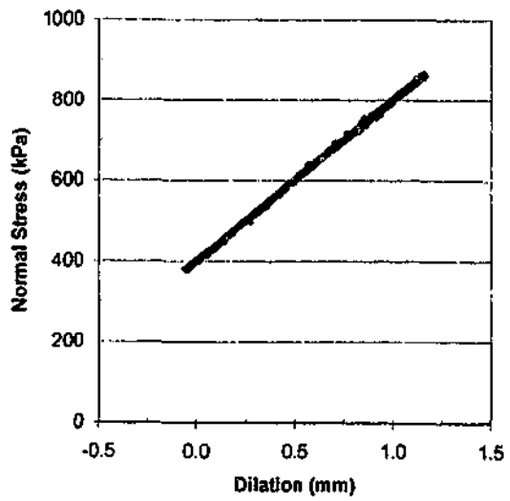

Test No:	JC6a_pow4
Test Date: 5/9/00	
JOHNSTONE	
Profile : 2-D cut profile using split JS_6a statistically represented with a power function @ 4mm chords	
Shear Rate = 0.5 mm/min	
Initial Normal Stress (kPa):	400
Normal Stiffness (kPa/mm):	400

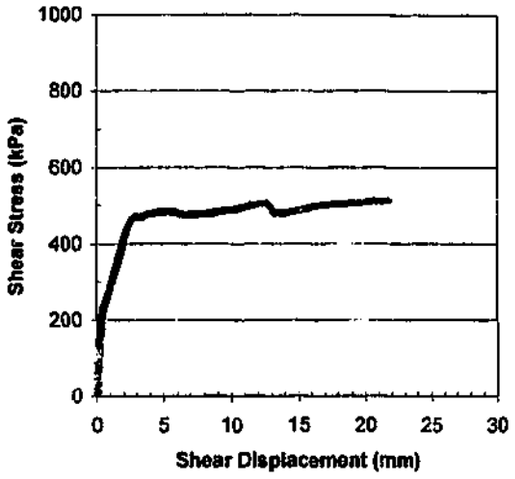

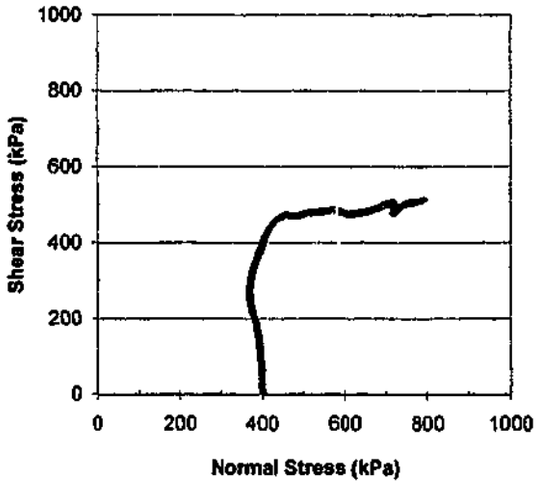

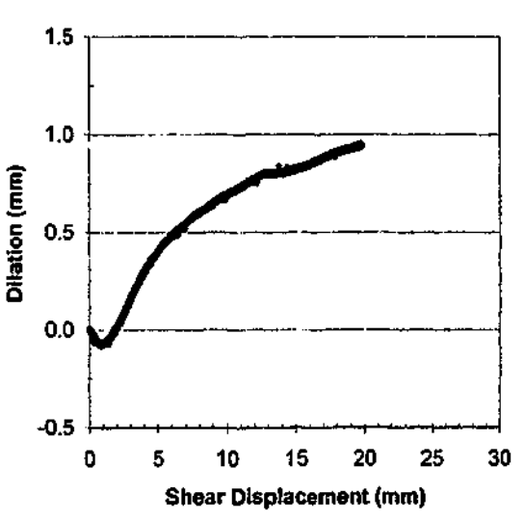

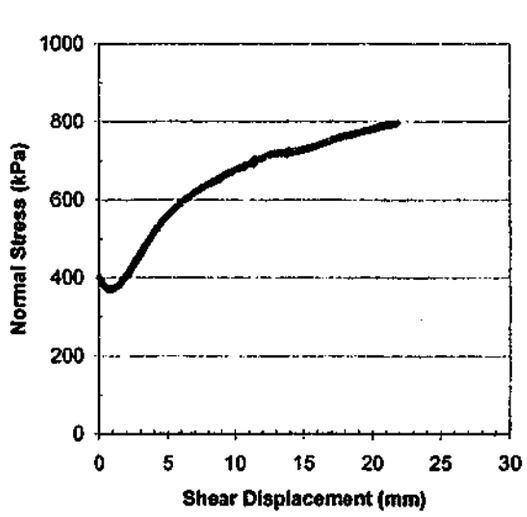

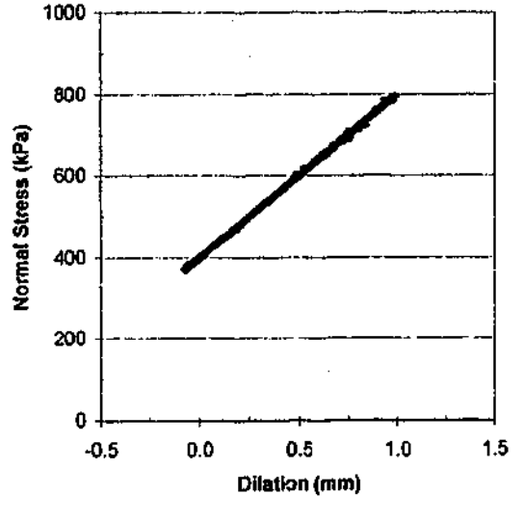

Test No:	**JC7a_4**
Test Date: 31/10/00	
JOHNSTONE	
Profile : 2-D cut version of centre profile of JS_7a cut @ 4mm chords	
Shear Rate = 0.5 mm/min	
Initial Normal Stress (kPa):	**400**
Normal Stiffness (kPa/mm):	**400**

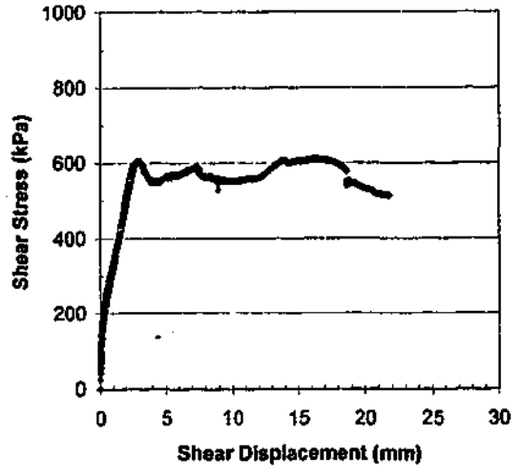

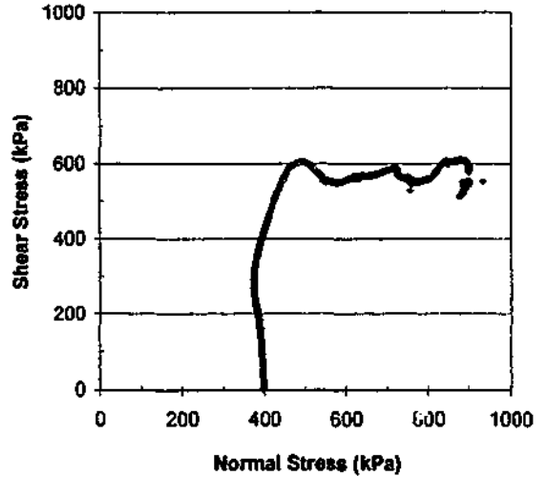

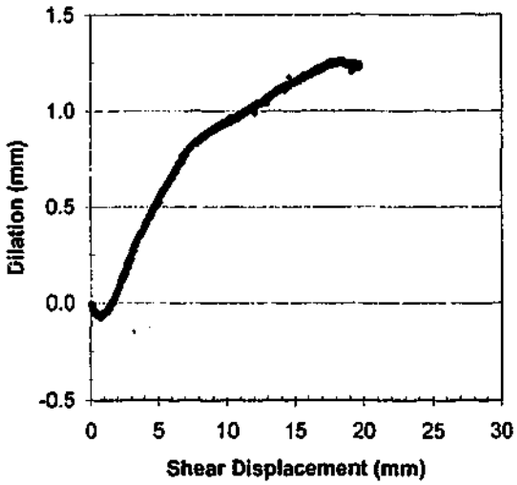

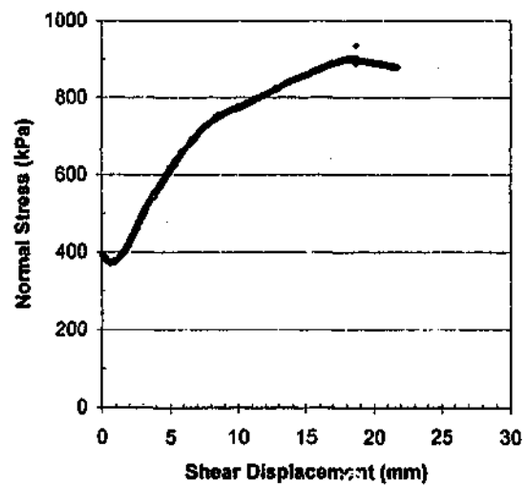

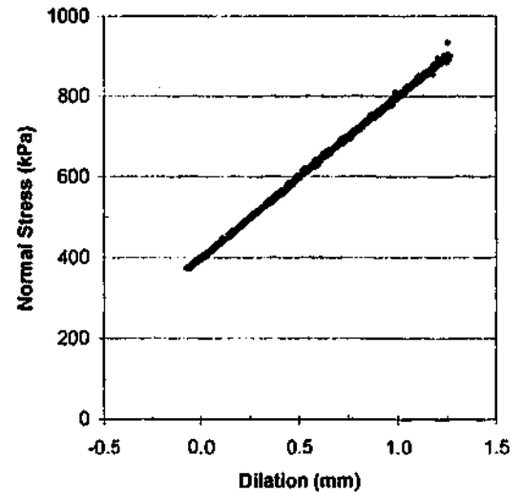

Test No:	JC7a_log4
Test Date: 1/11/00	
JOHNSTONE	
Profile : 2-D version of split JS_7a statistically represented with log function @ 4mm chords	
Shear Rate = 0.5 mm/min	
Initial Normal Stress (kPa):	400
Normal Stiffness (kPa/mm):	400

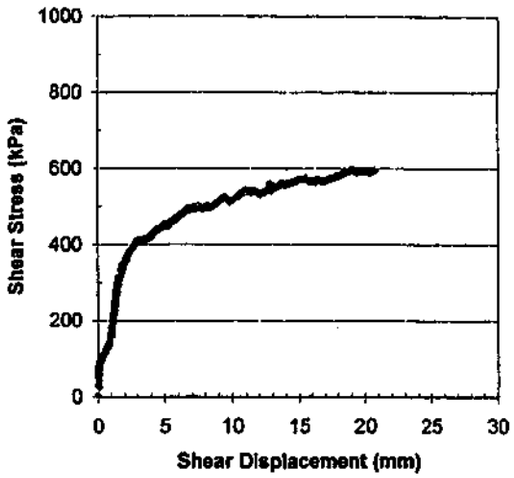

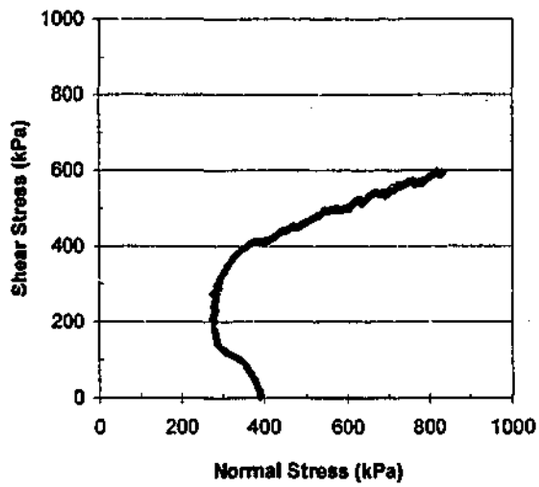

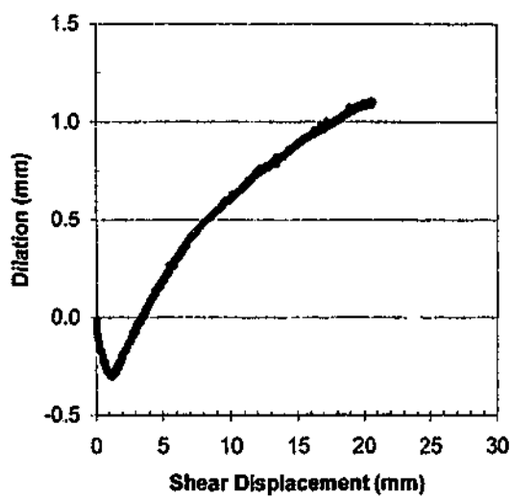

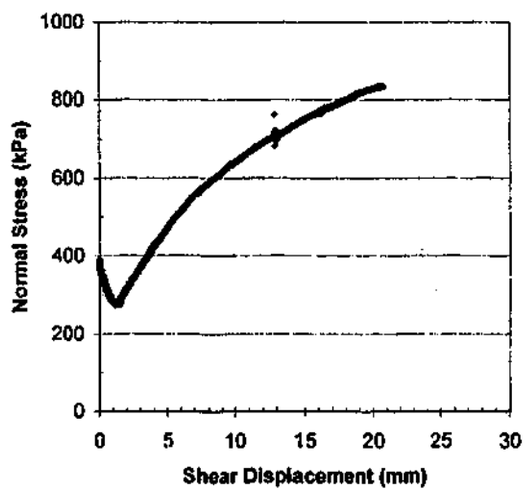

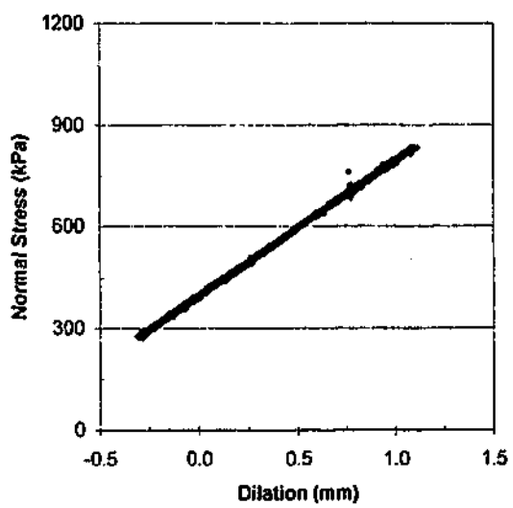

Test No:	SS_1
Test Date: 8/7/99	
SANDSTONE	
Profile : Split	
Shear Rate = 0.5 mm/min	
Initial Normal Stress (kPa):	400
Normal Stiffness (kPa/mm):	400

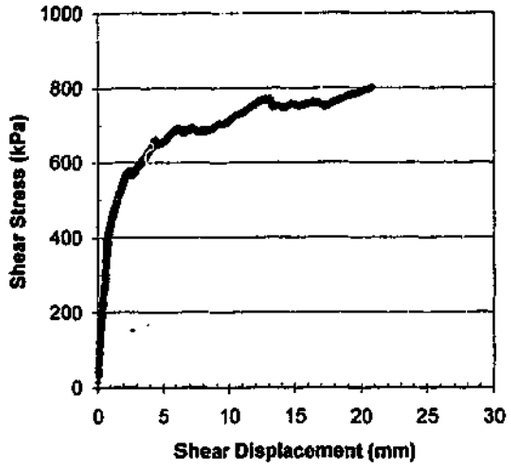

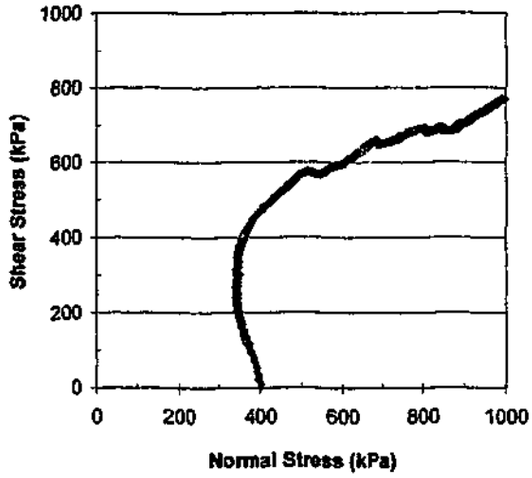

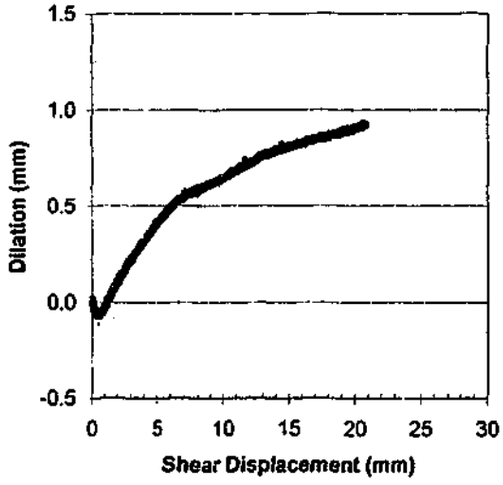

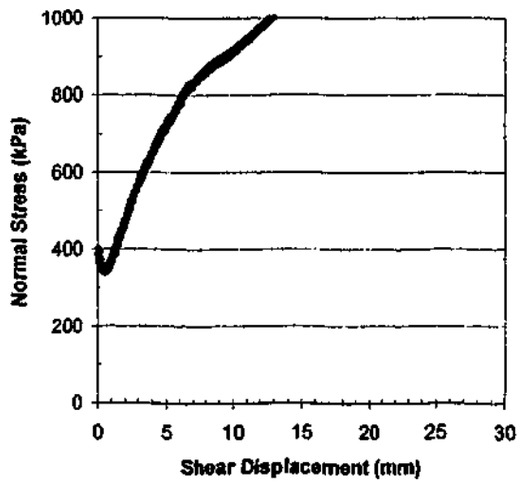

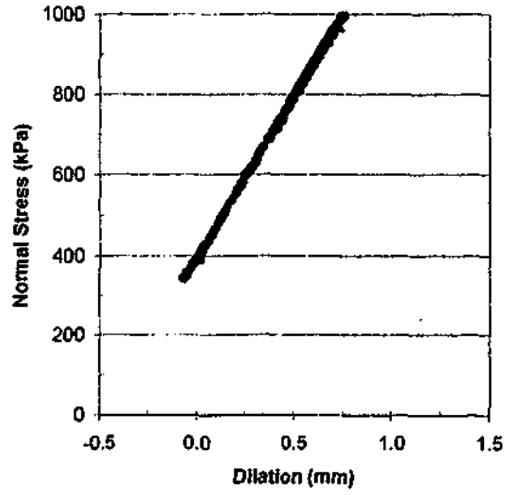

Test No:	SS_2
Test Date: 9/7/99	
SANDSTONE	
Profile : Split	
Shear Rate = 0.5 mm/min	
Initial Normal Stress (kPa):	400
Normal Stiffness (kPa/mm):	800

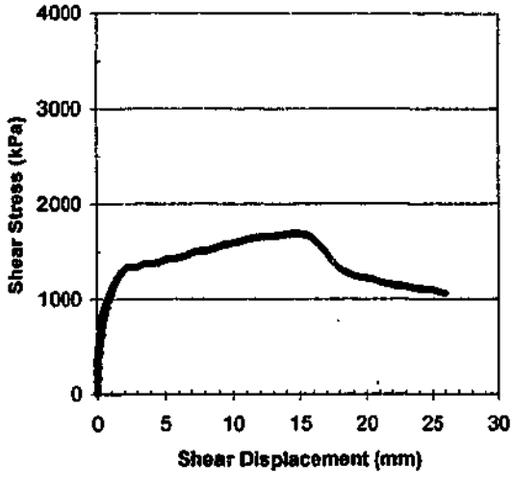

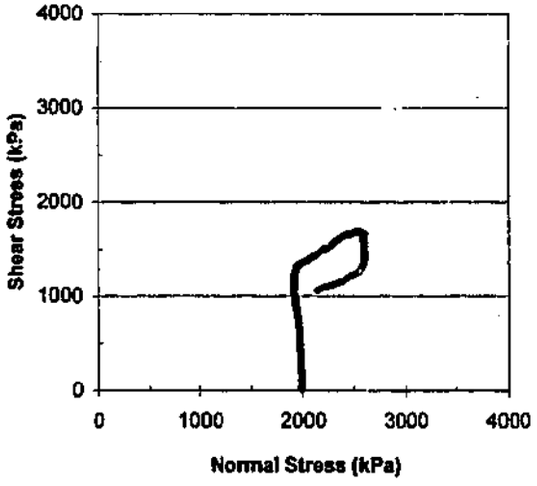

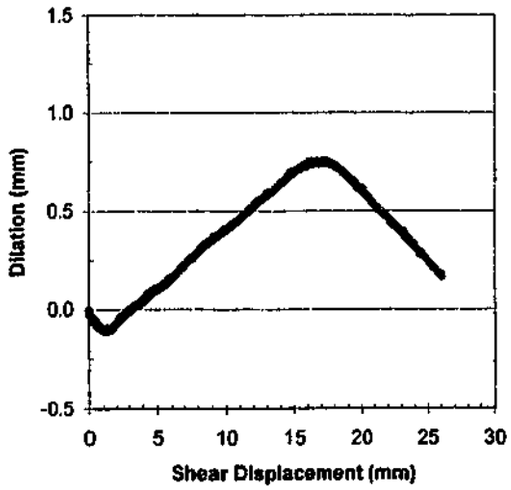

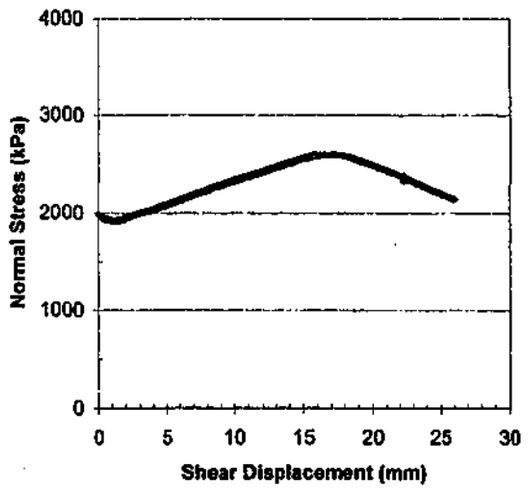

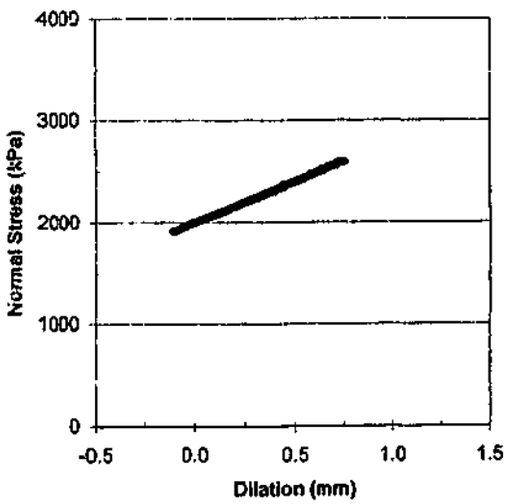

Test No:	MR5a_16
Test Date: 2/7/99	
SILTSTONE	
Profile : regular 6deg. X 16mm	
Shear Rate = 0.5 mm/min	
Initial Normal Stress (kPa):	2000
Normal Stiffness (kPa/mm):	800

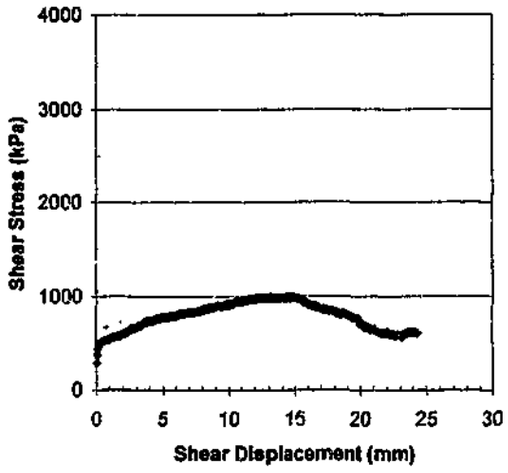

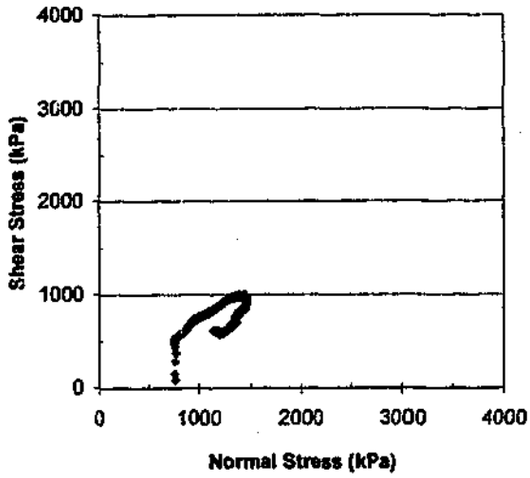

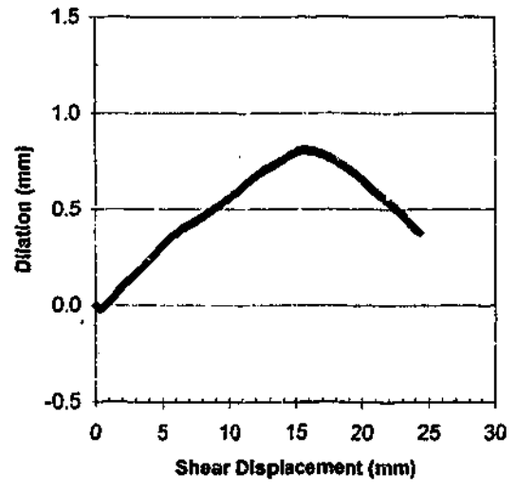

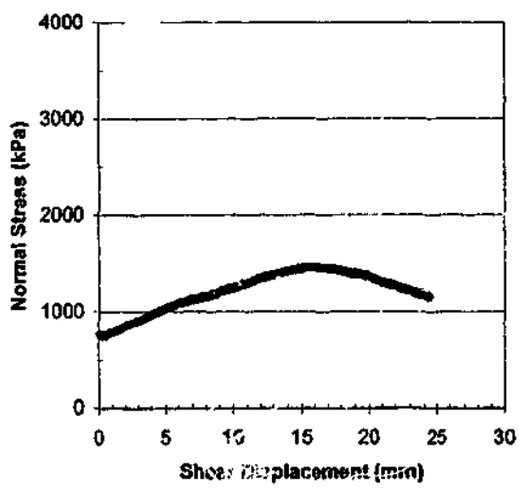

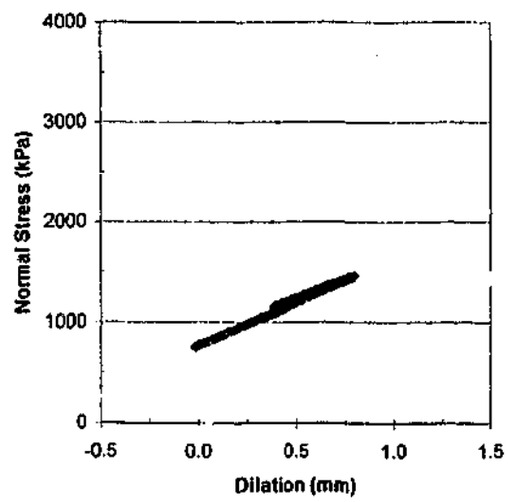

Test No:	MR5_16
Test Date: 16/12/98	
SILTSTONE	
Profile : Regular 5deg. X 16mm	
Shear Rate = 0.6 mm/min	
Initial Normal Stress (kPa):	800
Normal Stiffness (kPa/mm):	800

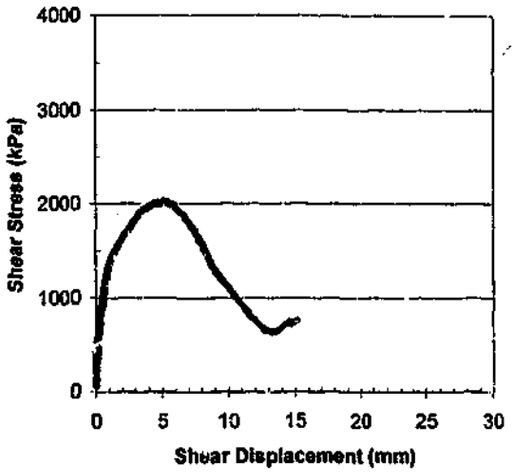

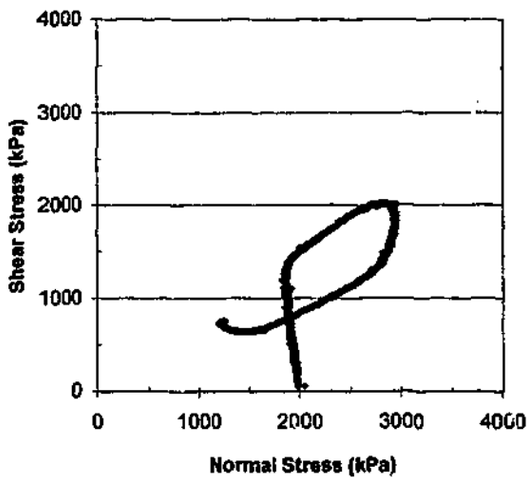

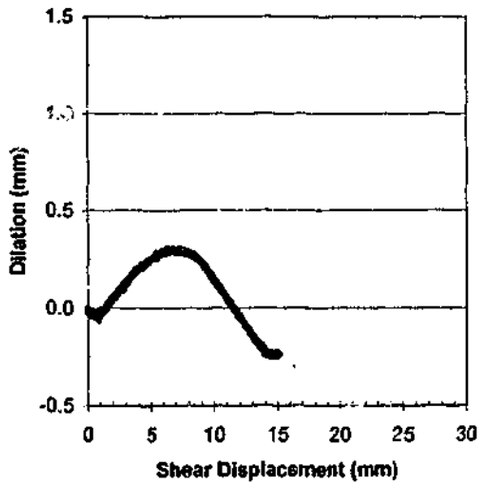

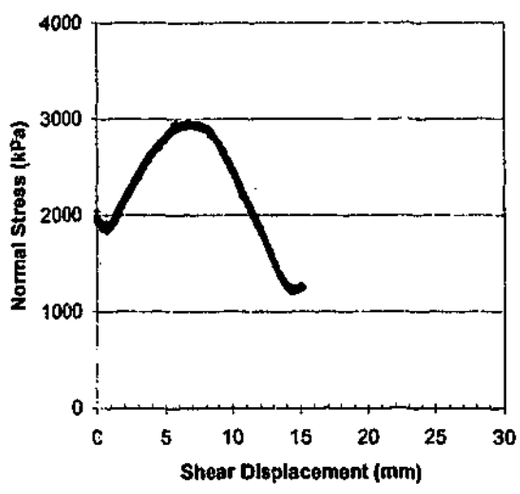

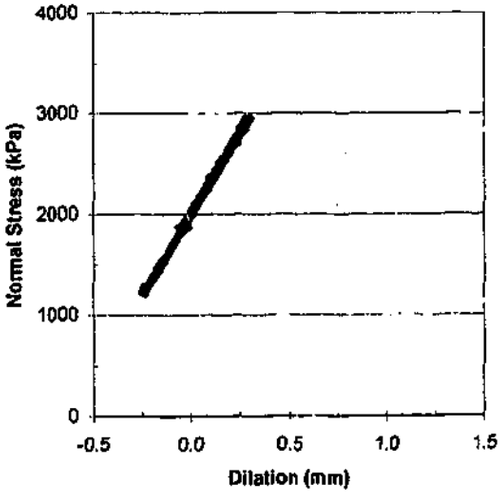

Test No:	**MR10_8**
Test Date: 3/10/00	
SILTSTONE	
Profile :	**regular 10deg. X 8mm**
Shear Rate = 0.5 mm/min	
Initial Normal Stress (kPa):	**2000**
Normal Stiffness (kPa/mm):	**3200**

sample setup moved during shear test

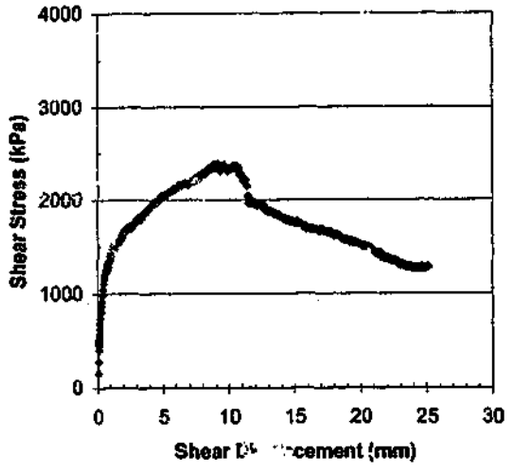

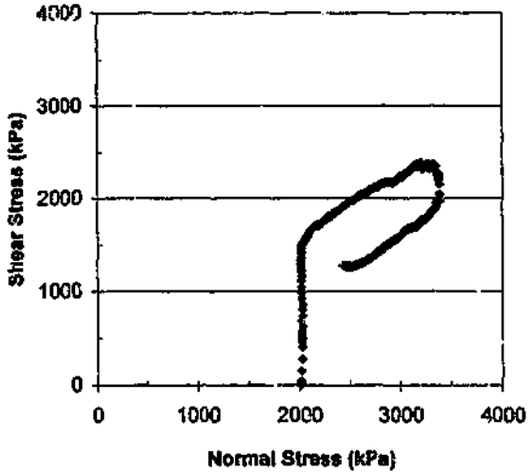

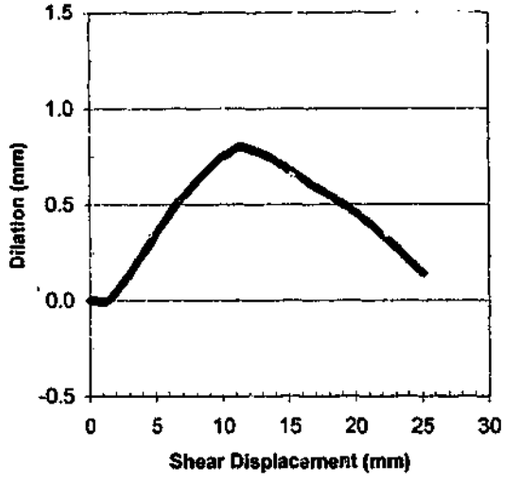

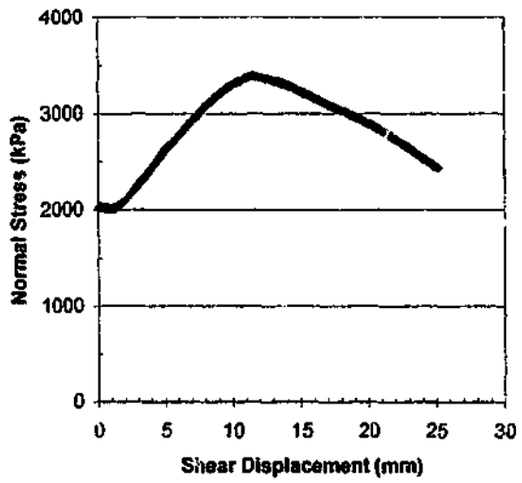

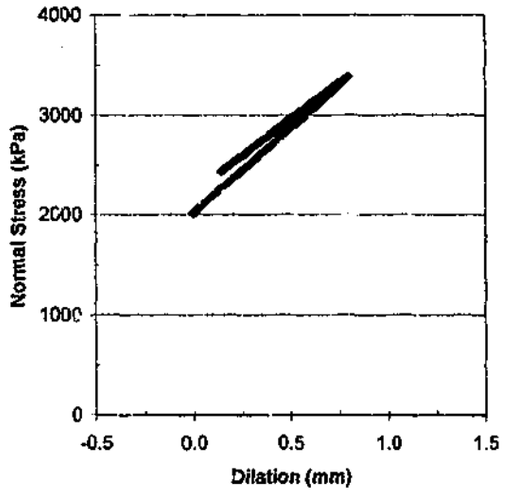

Test No:	MR10_16
Test Date	19/01/99
SILTSTONE	
Profile : Regular 10deg. X 16mm	
Shear Rate = 0.5 mm/min	
Initial Normal Stress (kPa):	2000
Normal Stiffness (kPa/mm):	1600

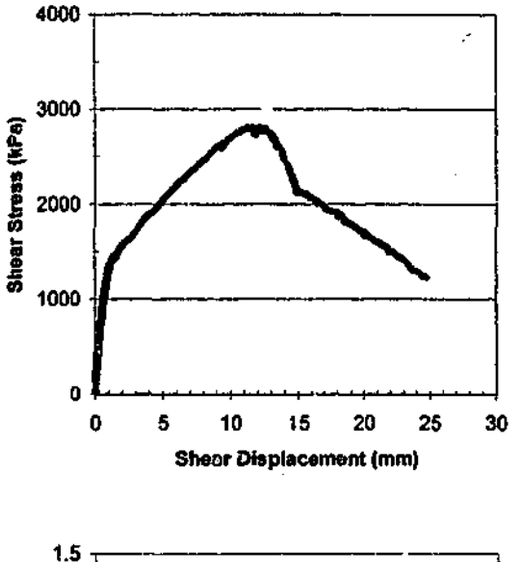

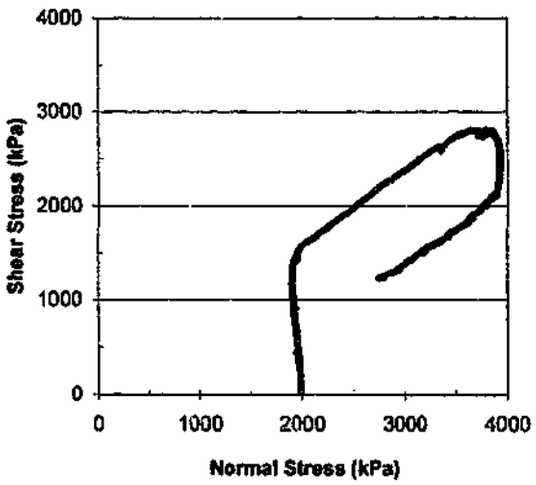

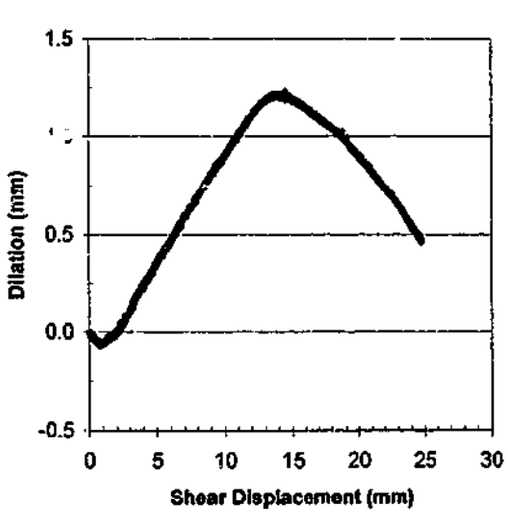

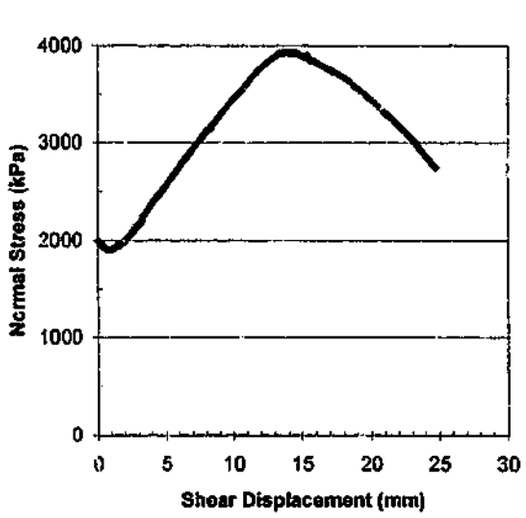

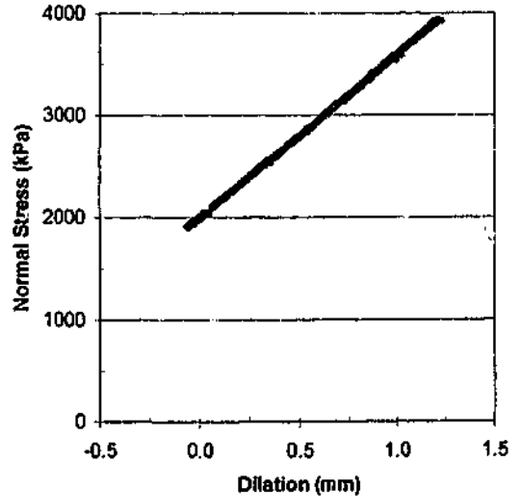

Test No:	MR10a_16
Test Date: 30/10/00	
SILTSTONE	
Profile : regular 10deg. X 16mm	
Shear Rate = 0.5 mm/min	
Initial Normal Stress (kPa):	2000
Normal Stiffness (kPa/mm):	1600

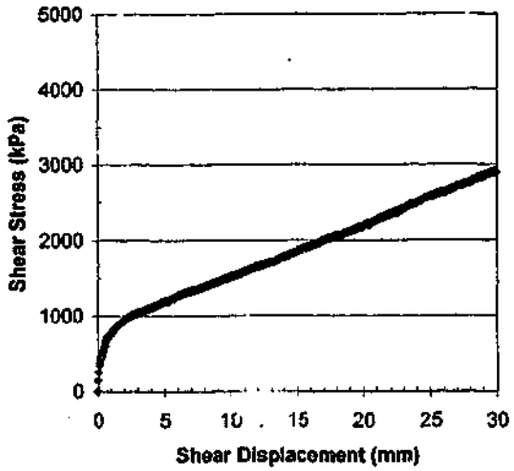

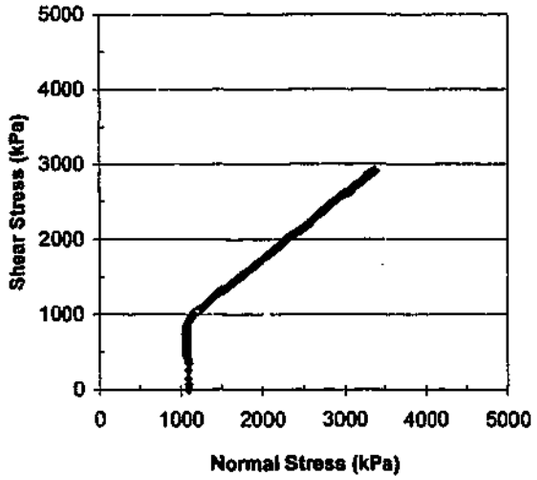

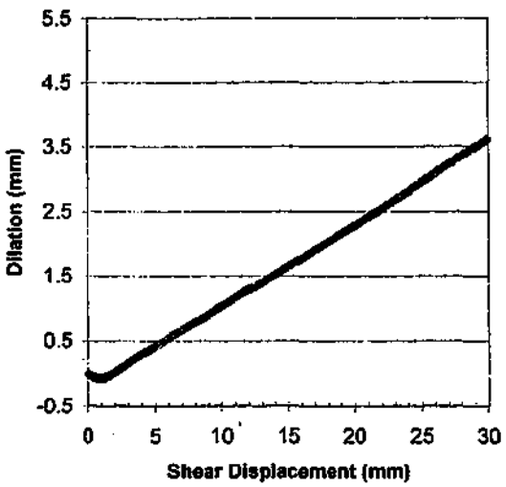

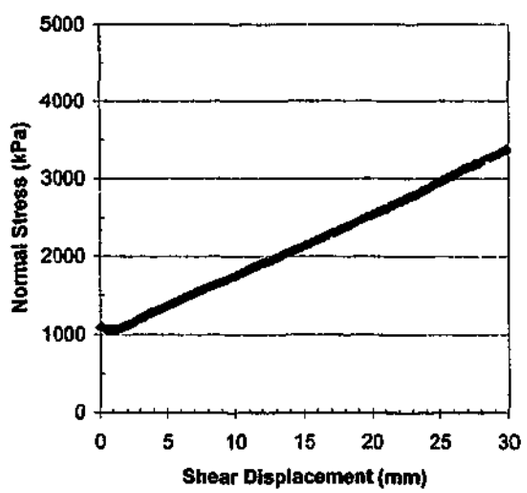

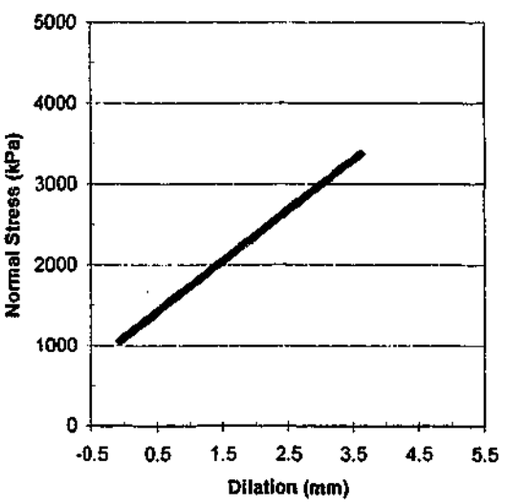

Test No:	MR10_48
Test Date	21/01/99
SILTSTONE	
Profile : Regular 10deg. X 48mm	
Shear Rate = 0.5 mm/min	
Initial Normal Stress (kPa):	1200
Normal Stiffness (kPa/mm):	600

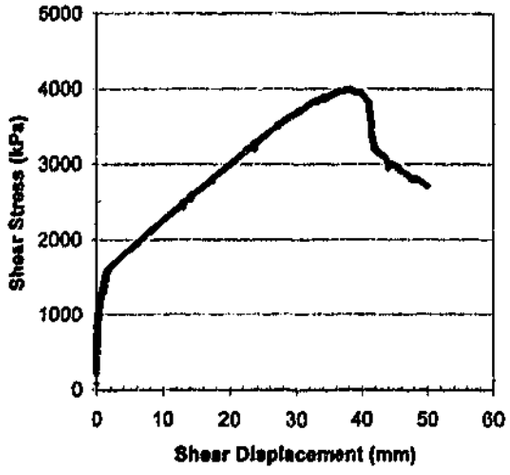

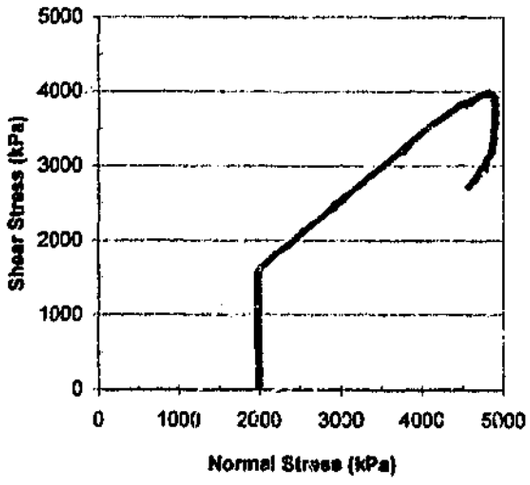

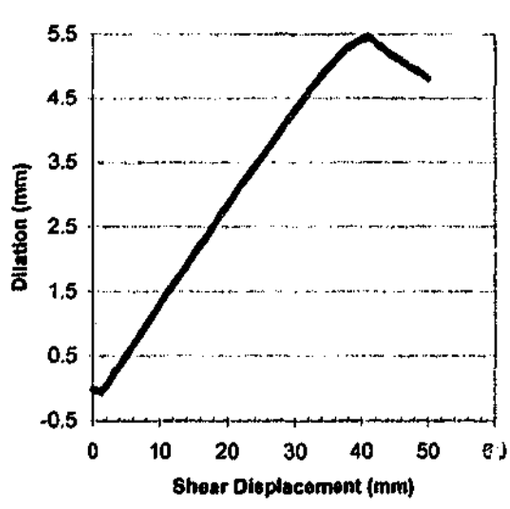

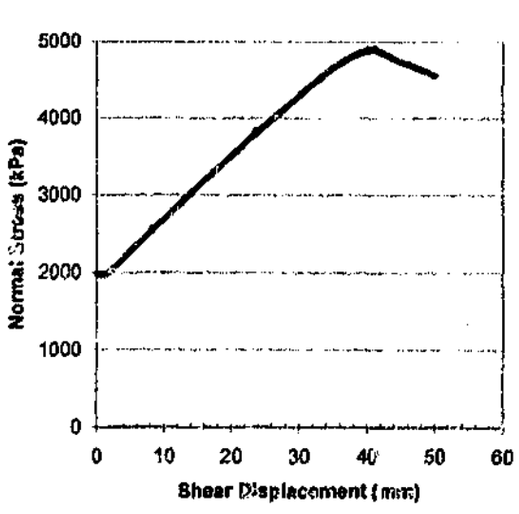

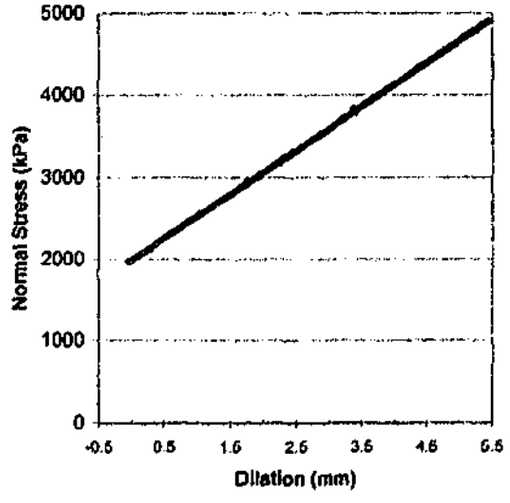

Test No:	MR10a_48
Test Date: 4/9/09	
SILTSTONE	
Profile :	regular 10deg. X 48mm
Shear Rate = 0.6 mm/min	
Initial Normal Stress (kPa):	2000
Normal Stiffness (kPa/mm):	533

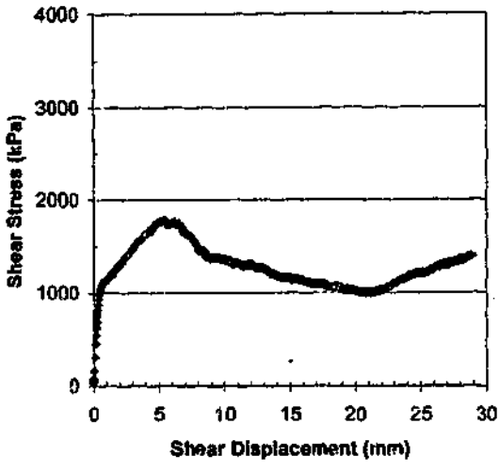

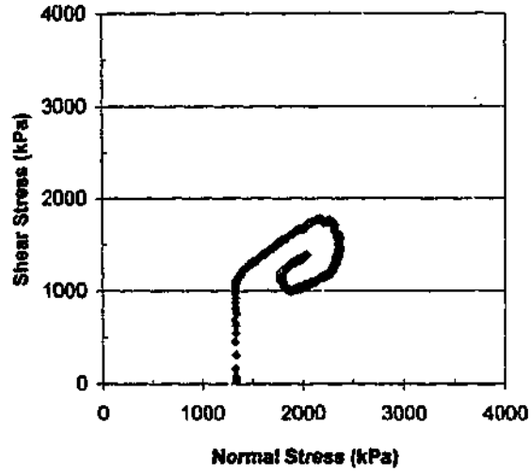

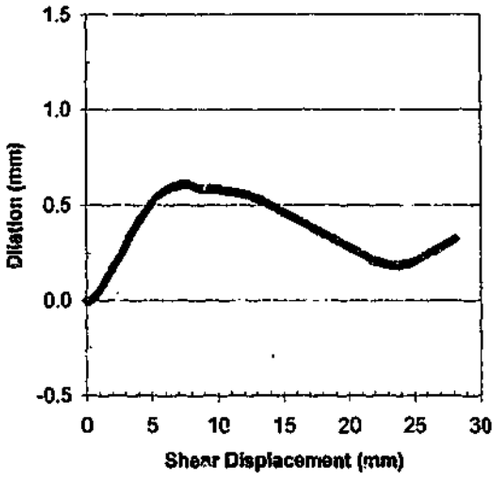

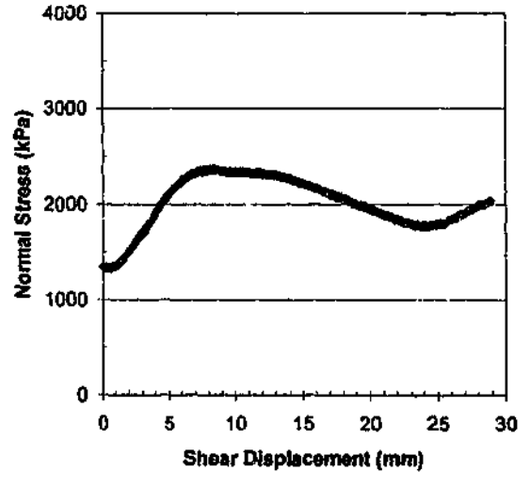

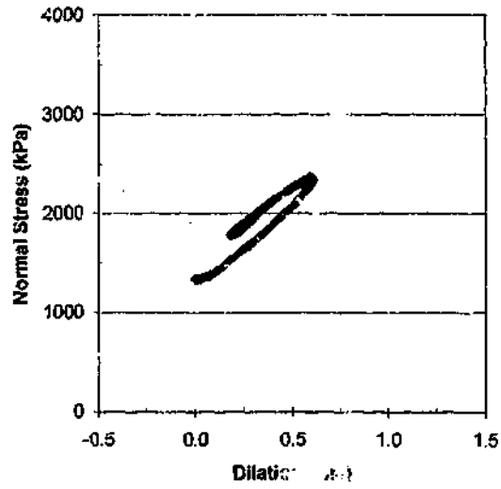

Test No:	MR15_16
Test Date: 14/1/99	
SILTSTONE	
Profile : Regular 15deg. X 16mm	
Shear Rate = 0.5 mm/min	
Initial Normal Stress (kPa):	1600
Normal Stiffness (kPa/mm):	1600

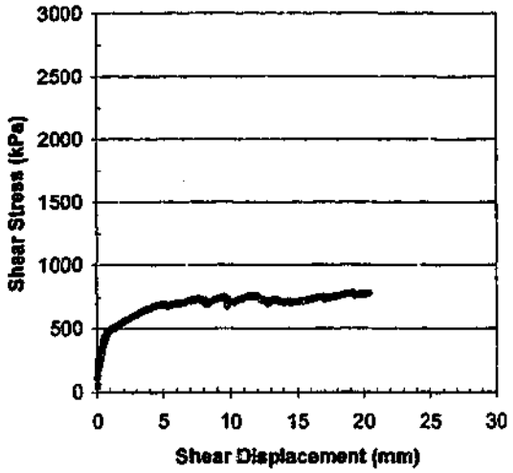

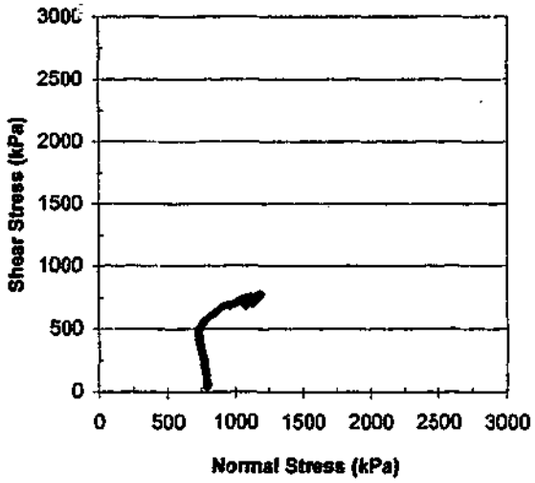

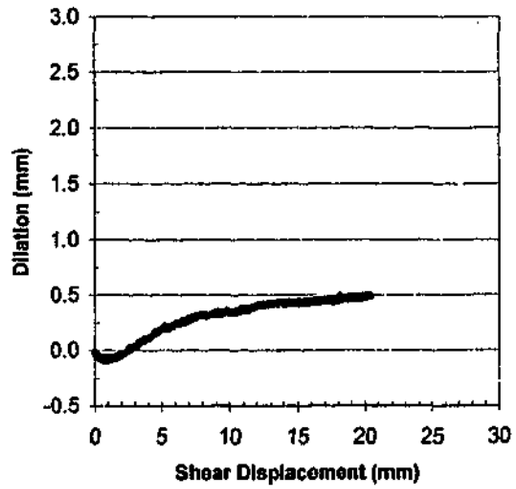

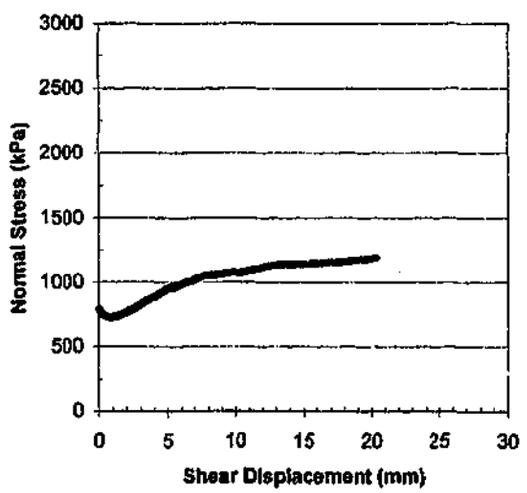

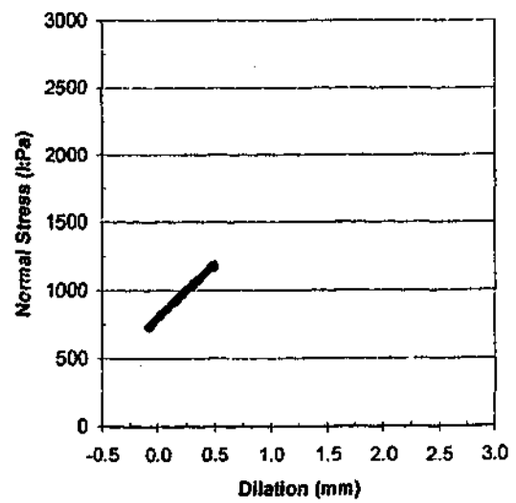

Test No:	MF5_5
Test Date: 9/6/99	
SILTSTONE	
Profile : Fractal s=5deg, 5mm chord	
Shear Rate = 0.5 mm/min	
Initial Normal Stress (kPa):	800
Normal Stiffness (kPa/mm):	800

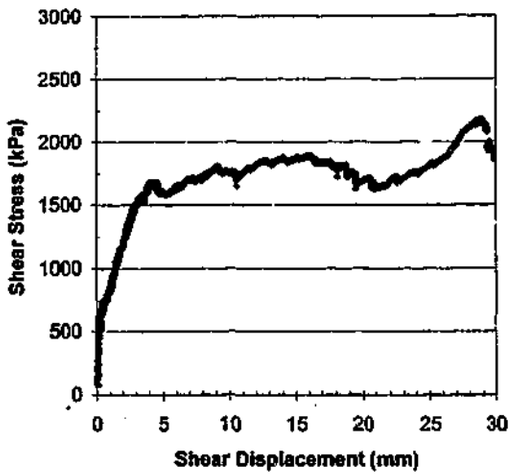

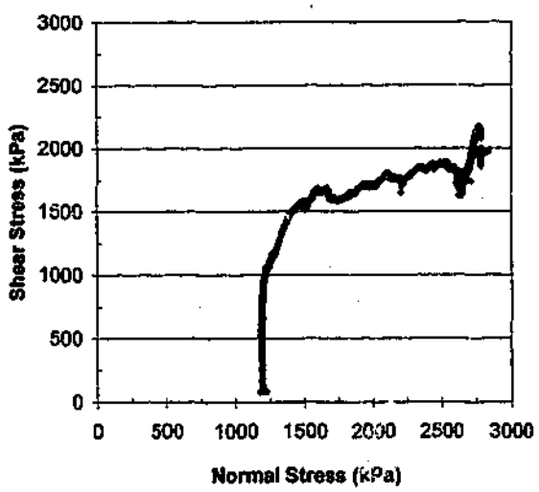

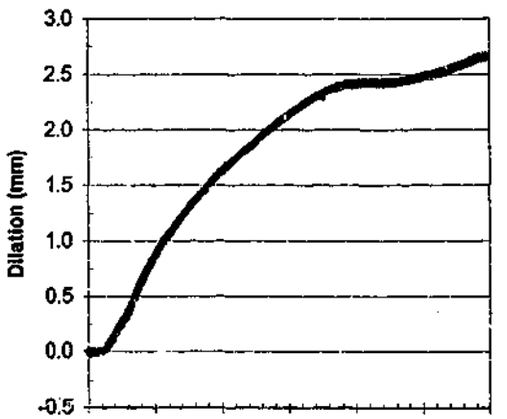

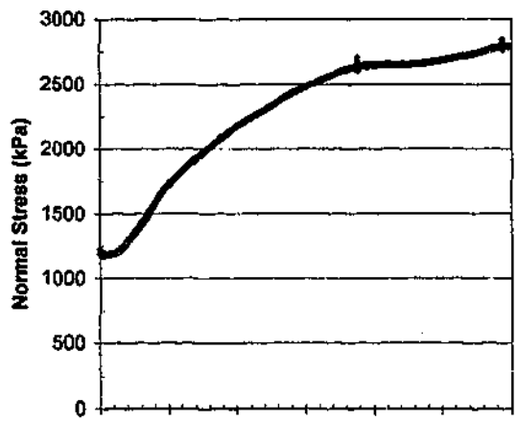

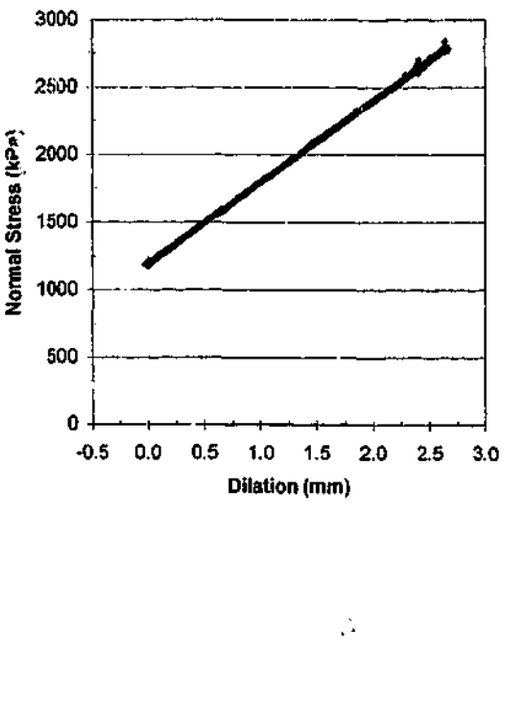

Test No:	MF10_5
Test Date: 7/6/99	
SILTSTONE	
Profile : Fractal s=10deg, 5mm chord	
Shear Rate = 0.5 mm/min	
Initial Normal Stress (kPa):	1200
Normal Stiffness (kPa/mm):	600

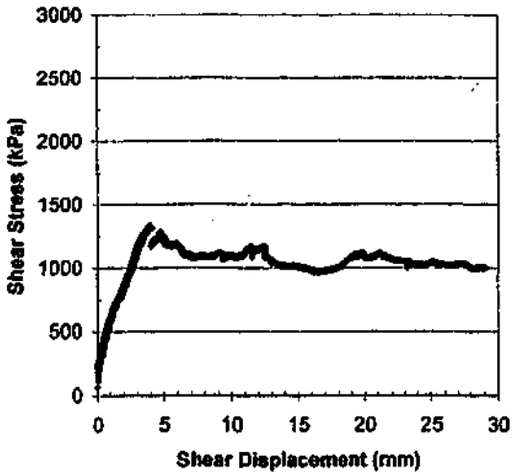

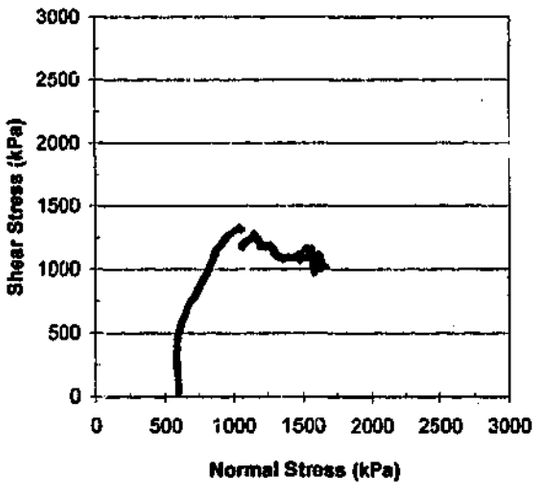

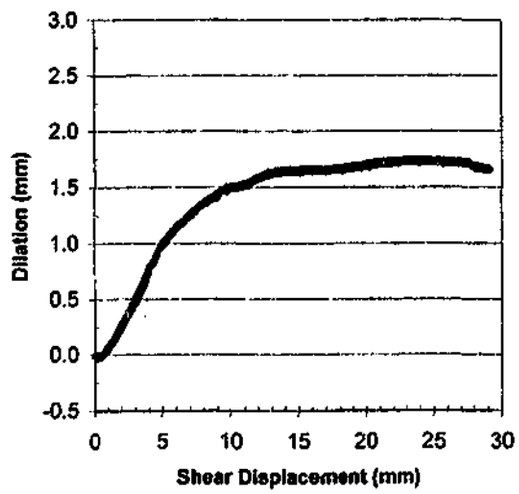

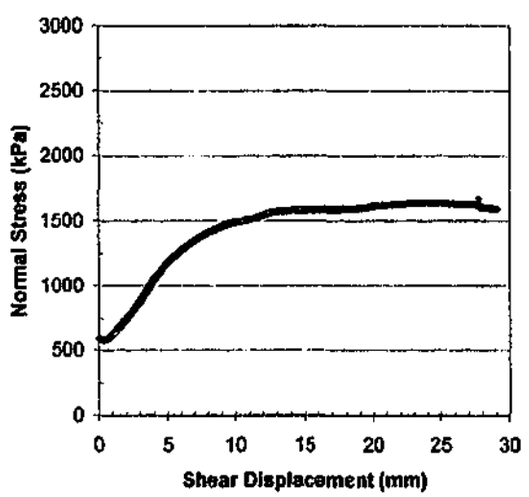

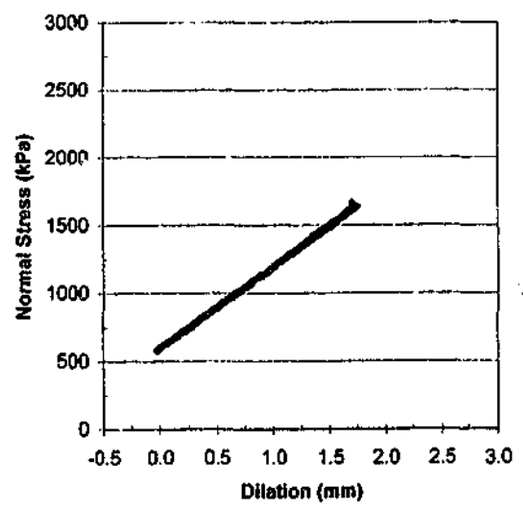

Test No:	MF10a_5
Test Date: 11/6/99	
SILTSTONE	
Profile : Fractal s=10deg, 6mm chord	
Shear Rate = 0.5 mm/min	
Initial Normal Stress (kPa):	600
Normal Stiffness (kPa/mm):	600

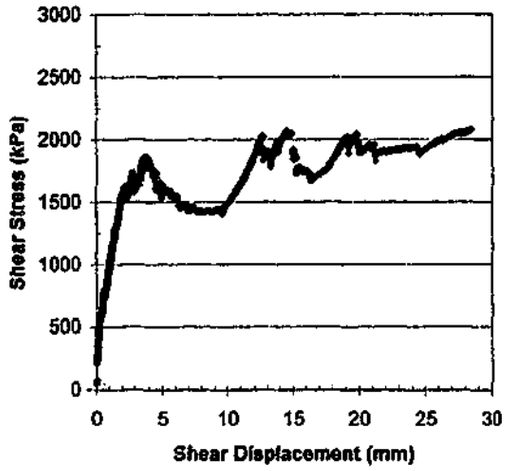

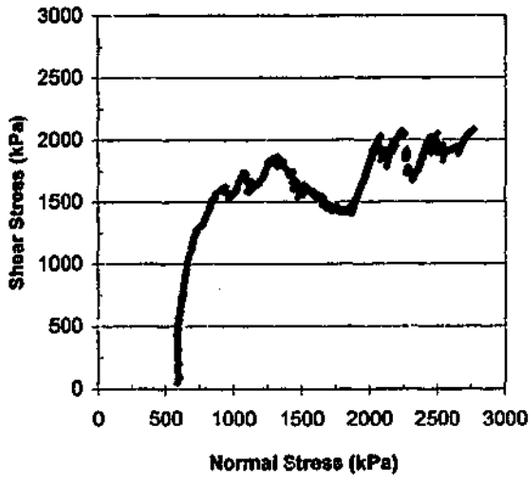

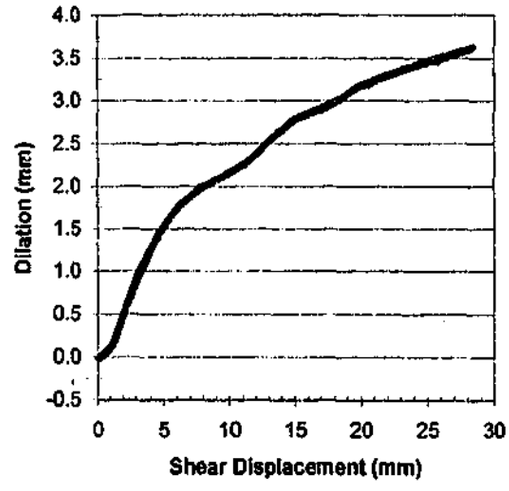

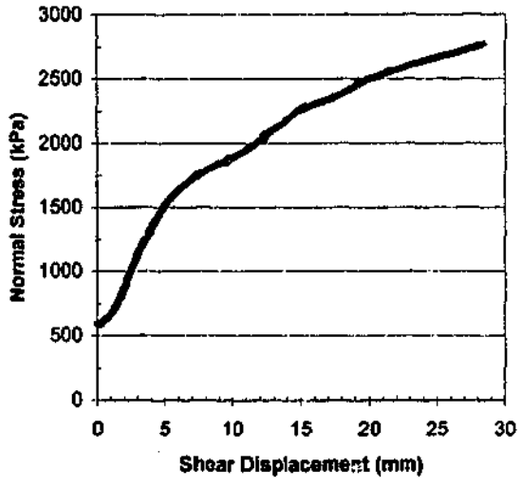

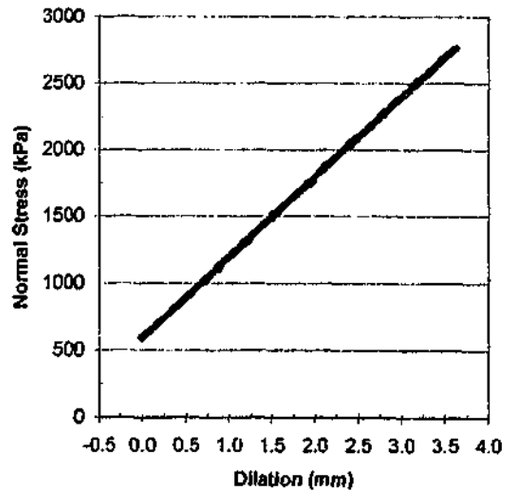

Test No:	MF15_5
Test Date: 15/6/99	
SILTSTONE	
Profile : Fractal s=15deg, 5mm chord	
Shear Rate = 0.5 mm/min	
Initial Normal Stress (kPa):	600
Normal Stiffness (kPa/mm):	600

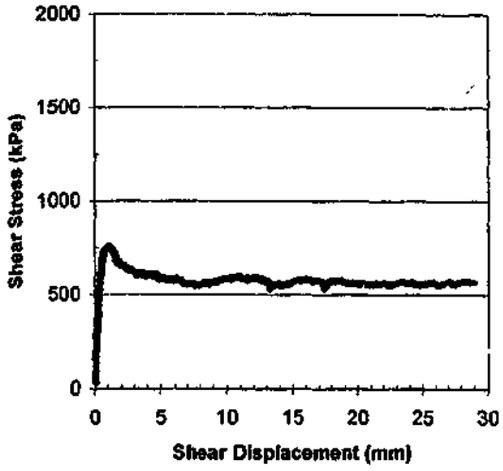

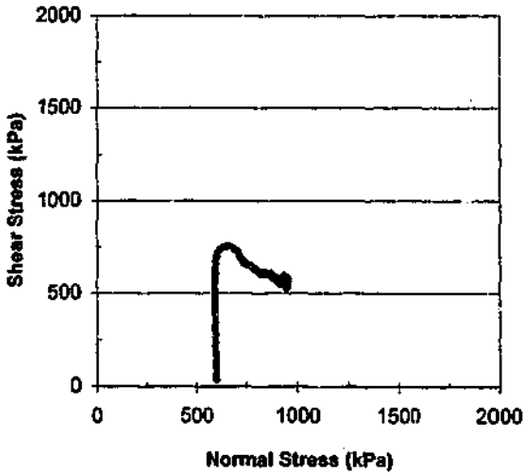

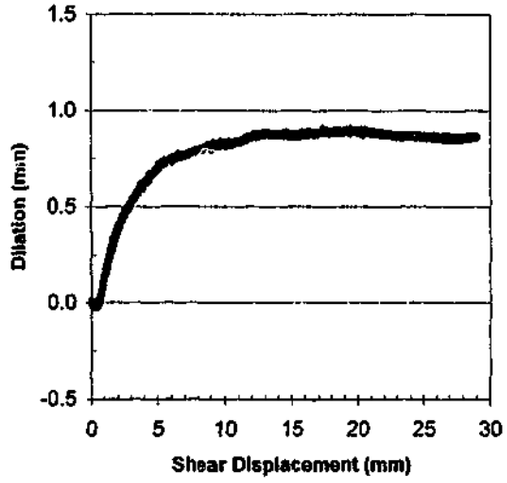

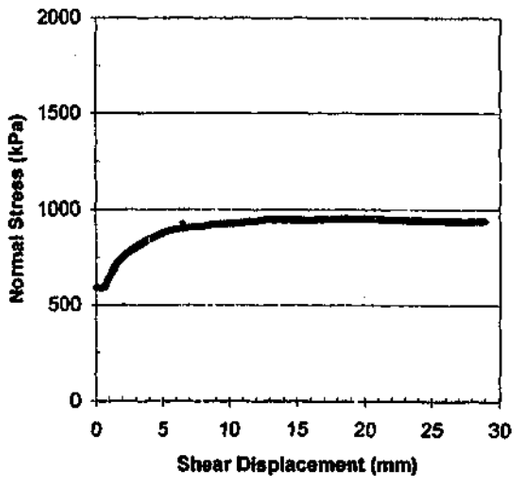

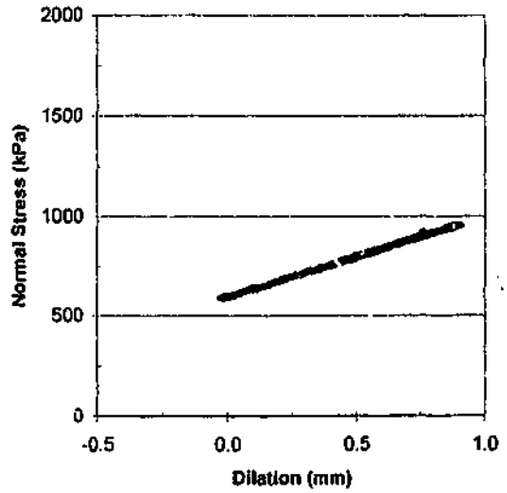

Test No:	MS_1
Test Date:	31/8/99
SILTSTONE	
Profile : Split	
Shear Rate = 0.5 mm/min	
Initial Normal Stress (kPa):	600
Normal Stiffness (kPa/mm):	400

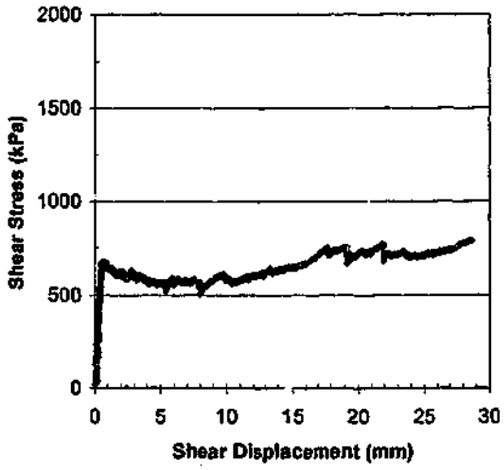

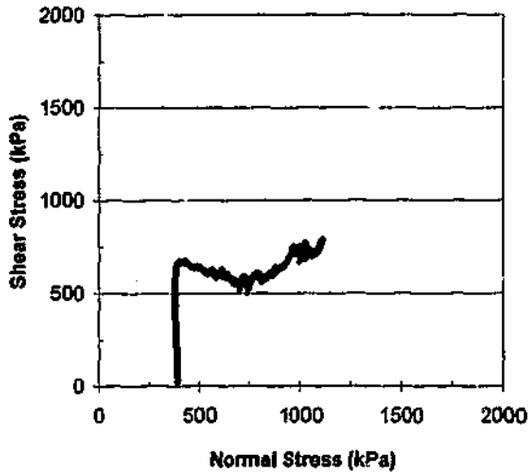

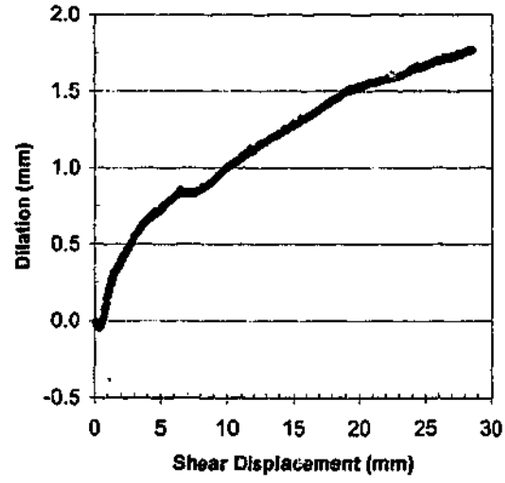

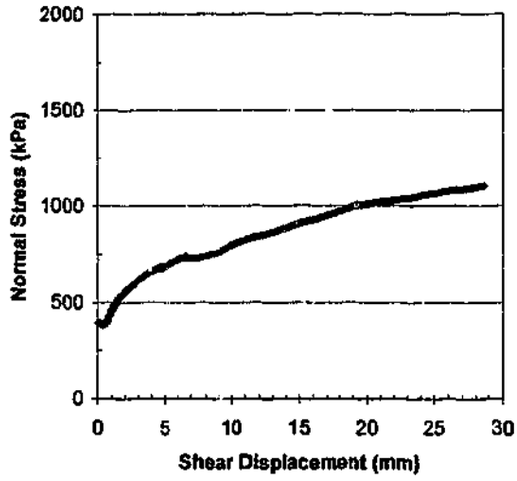

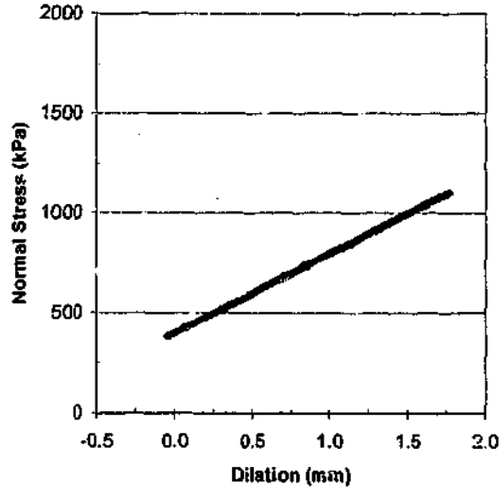

Test No:	MS_2
Test Date: 18/6/99	
SILTSTONE	
Profile : Split	
Shear Rate = 0.5 mm/min	
Initial Normal Stress (kPa):	400
Normal Stiffness (kPa/mm):	400

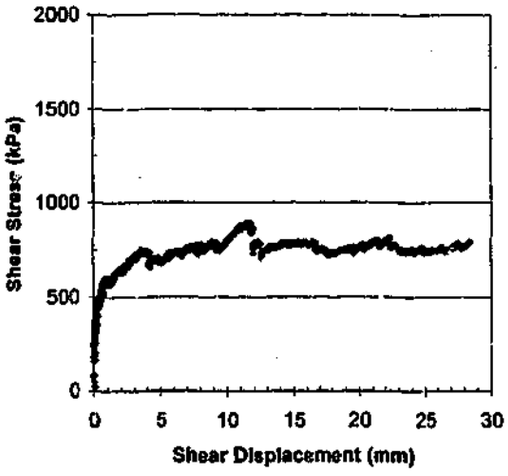

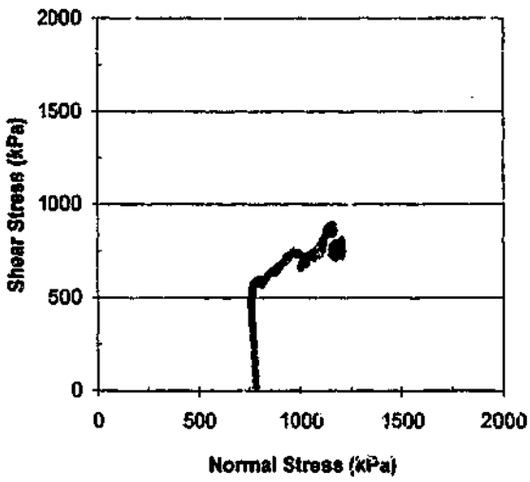

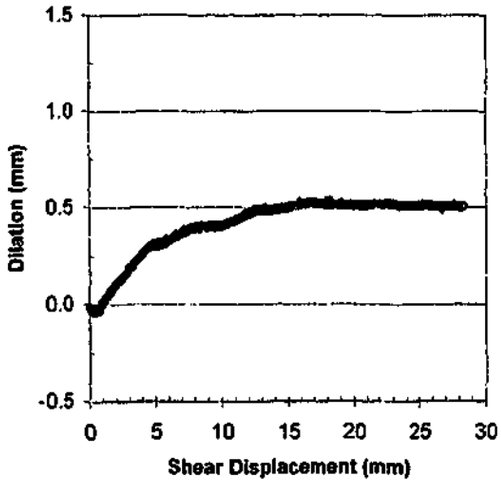

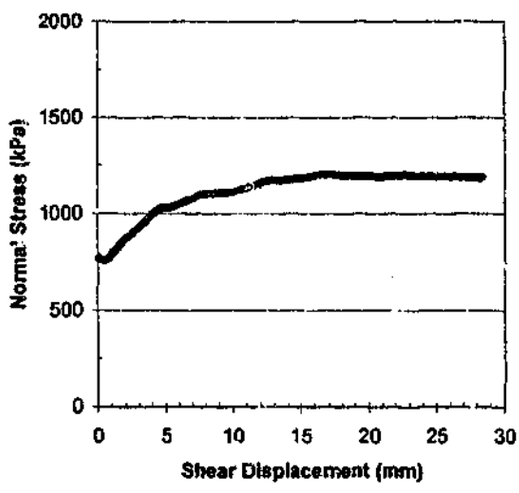

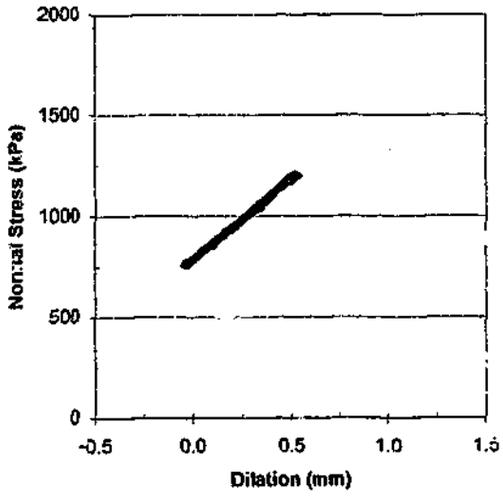

Test No:	MS_3
Test Date: 23/6/99	
SILTSTONE	
Profile : Split	
Shear Rate = 0.5 mm/min	
Initial Normal Stress (kPa):	800
Normal Stiffness (kPa/mm):	800

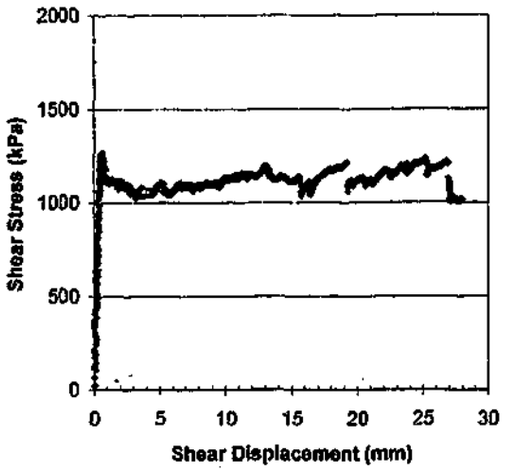

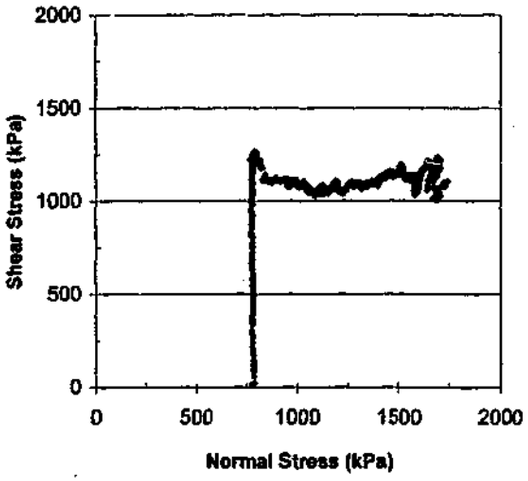

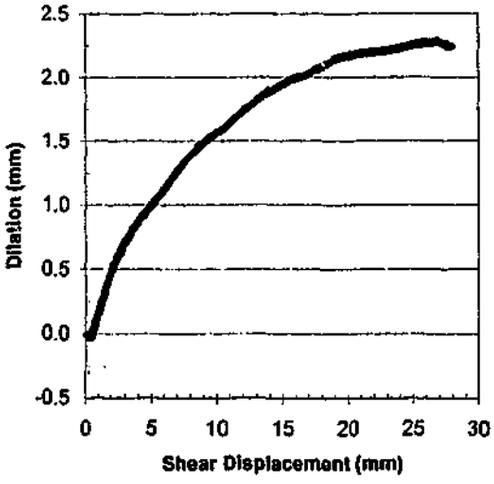

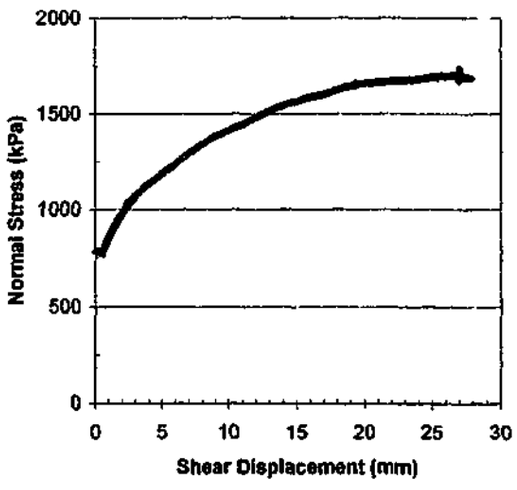

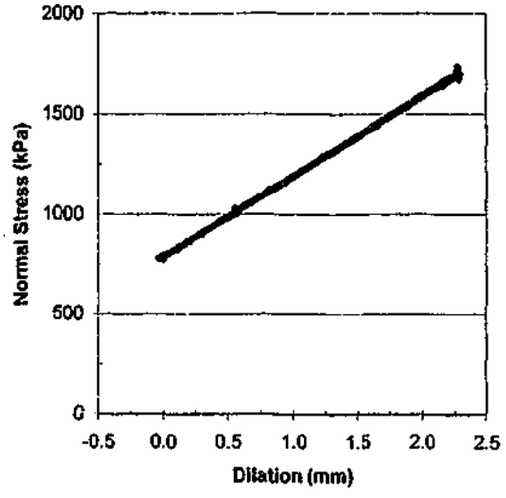

Test No:	MS_4
Test Date: 25/6/99	
SILTSTONE	
Profile : Split	
Shear Rate = 0.5 mm/min	
Initial Normal Stress (kPa):	800
Normal Stiffness (kPa/mm):	400

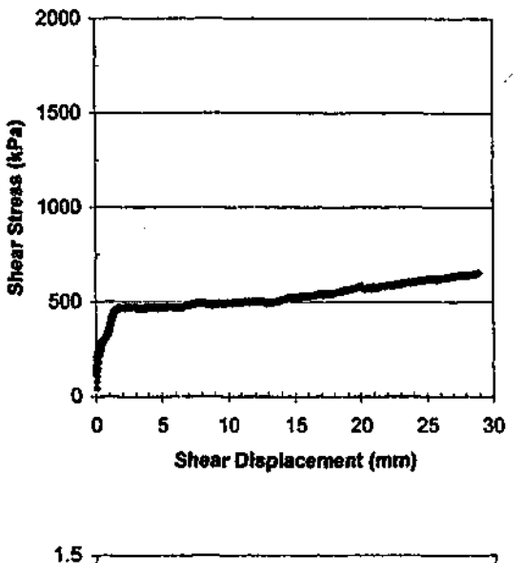

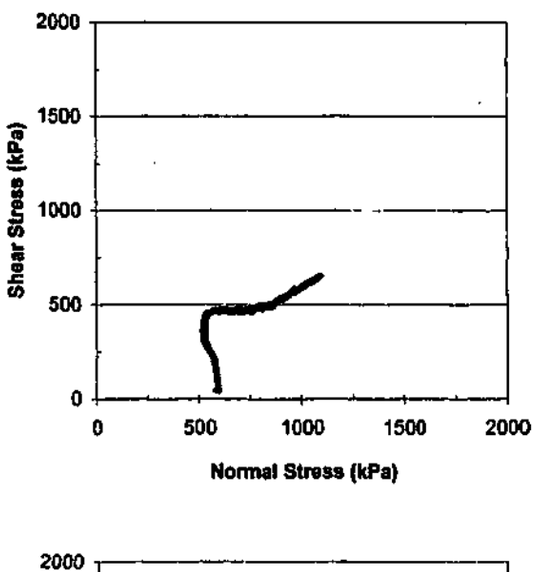

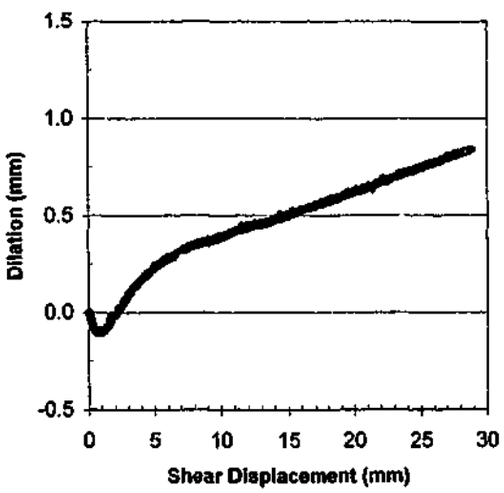

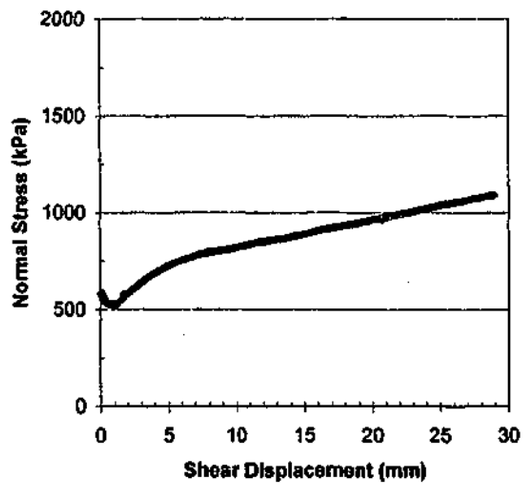

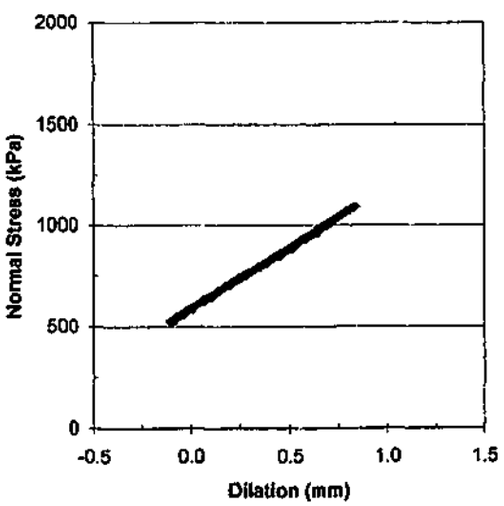

Test No:	MS_5
Test Date: 15/7/99	
SILTSTONE	
Profile : Split	
Shear Rate = 0.5 mm/min	
Initial Normal Stress (kPa):	600
Normal Stiffness (kPa/mm):	600

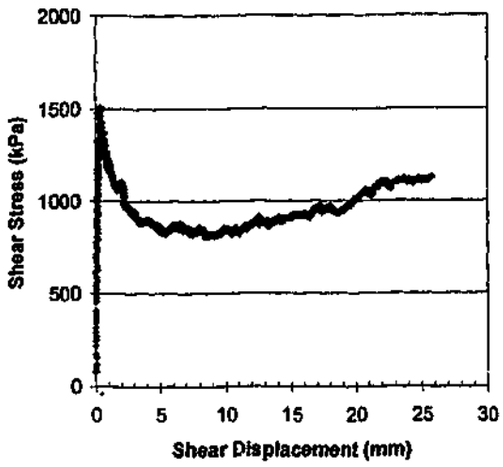

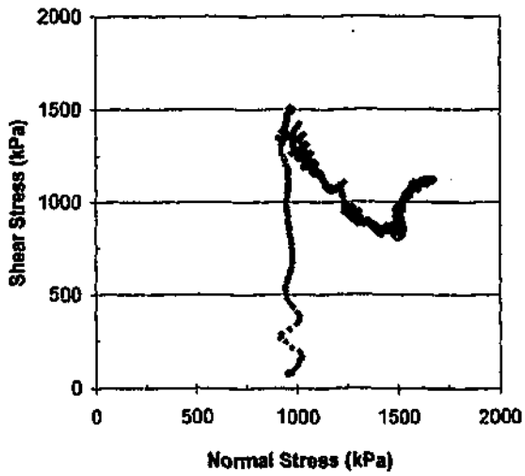

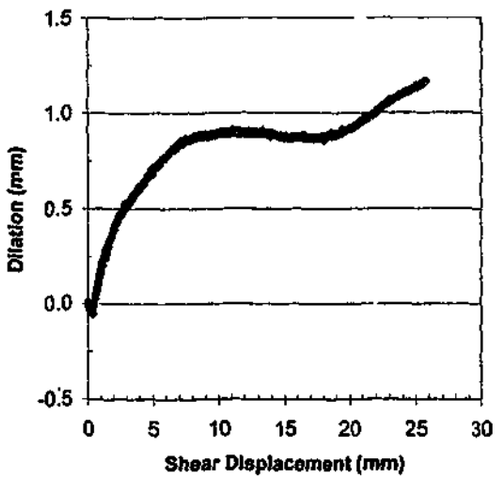

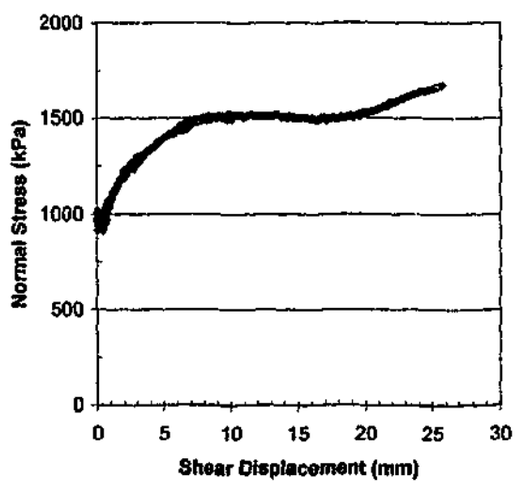

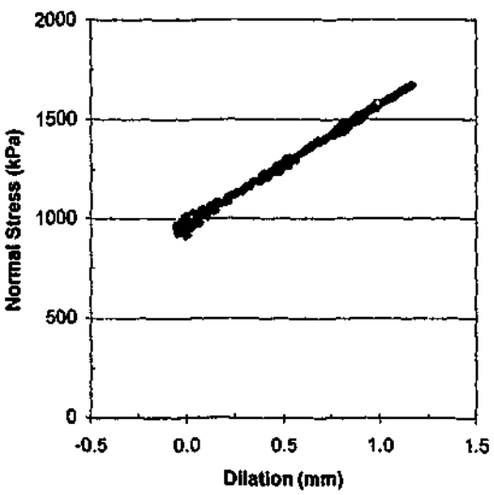

Test No:	MS_6
Test Date: 30/6/99	
SILTSTONE	
Profile : Split	
Shear Rate = 0.5 mm/min	
Initial Normal Stress (kPa):	1000
Normal Stiffness (kPa/mm):	600

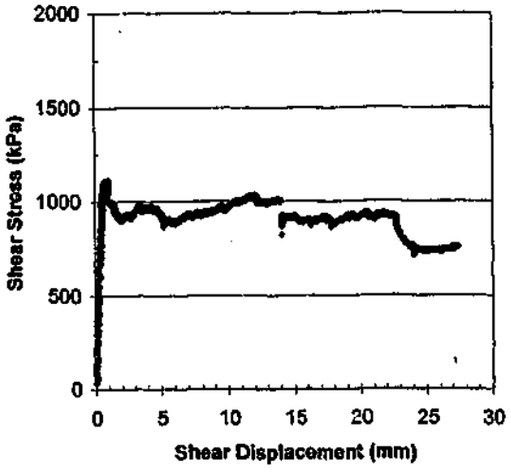

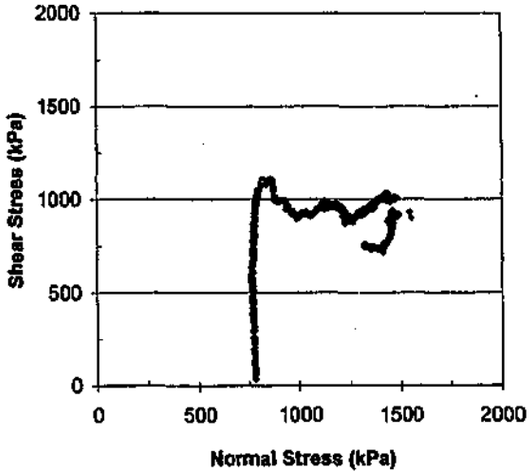

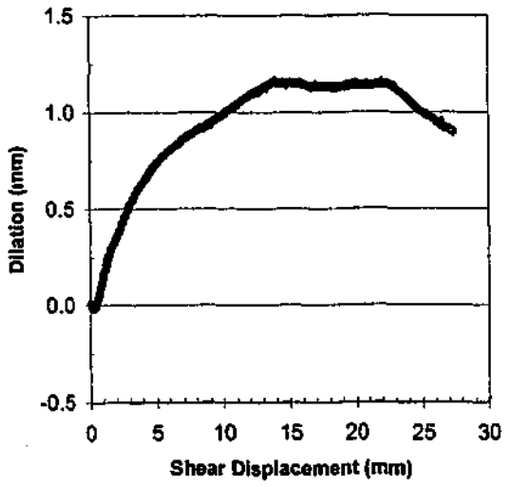

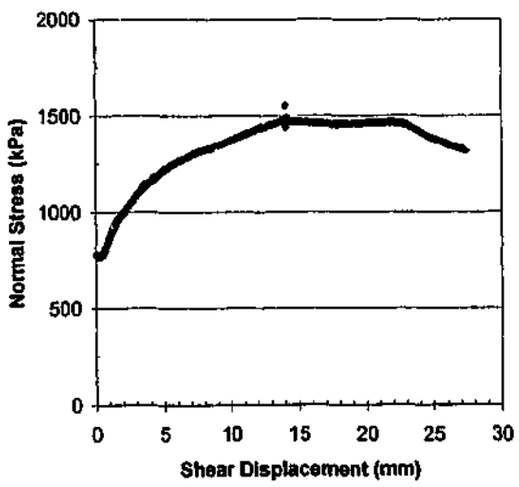

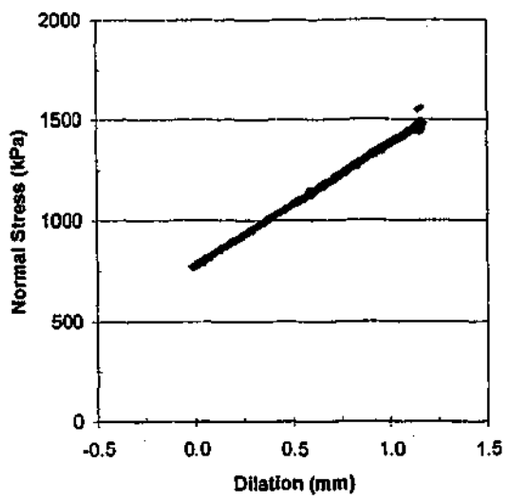

Test No:	MS_7
Test Date: 28/6/99	
SILTSTONE	
Profile : Split	
Shear Rate = 0.5 mm/min	
Initial Normal Stress (kPa):	800
Normal Stiffness (kPa/mm):	600

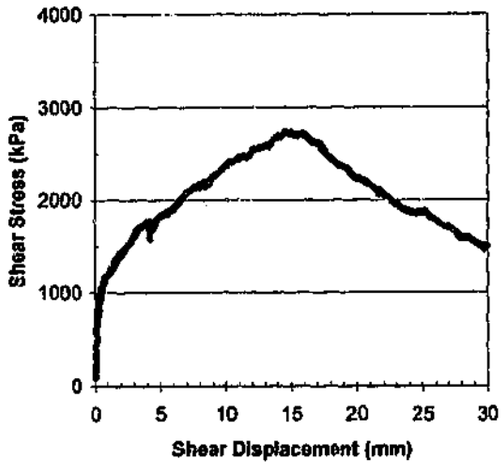

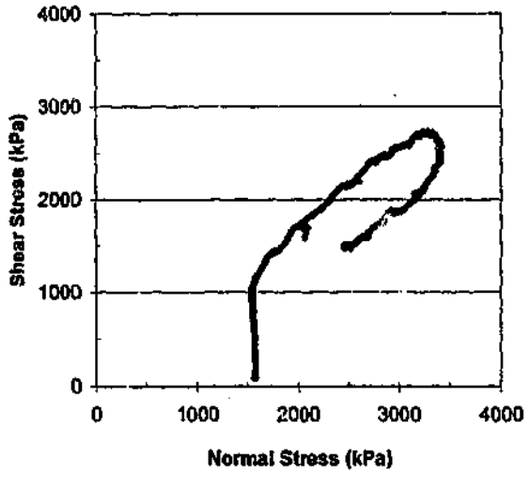

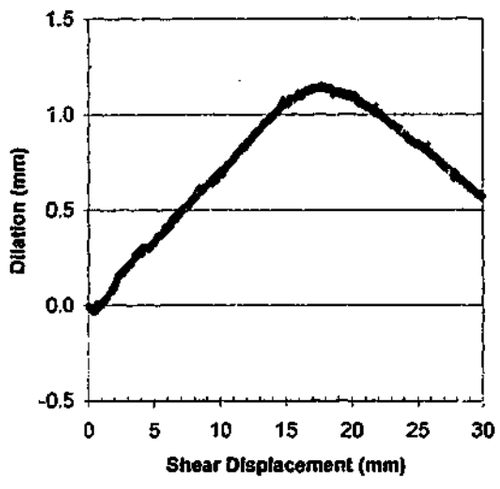

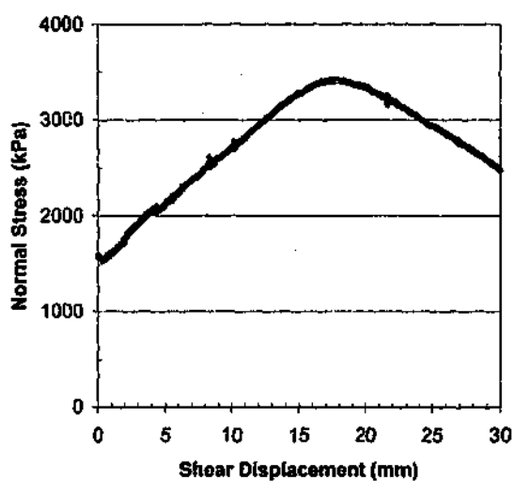

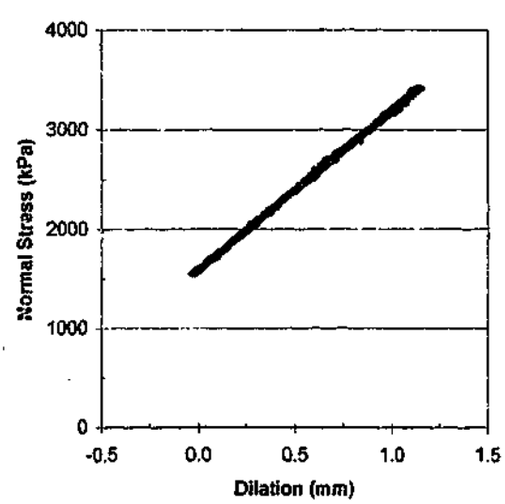

Test No:	BR5_16
Test Date: 7/2/00	
BASALT	
Profile : Regular 5deg. X 16mm	
Shear Rate = 0.5 mm/min	
Initial Normal Stress (kPa):	1600
Normal Stiffness (kPa/mm):	1600

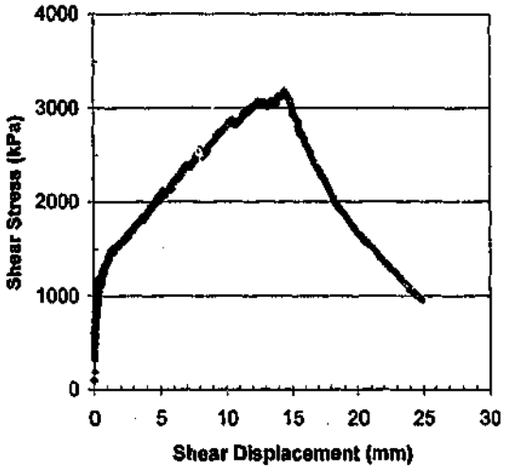

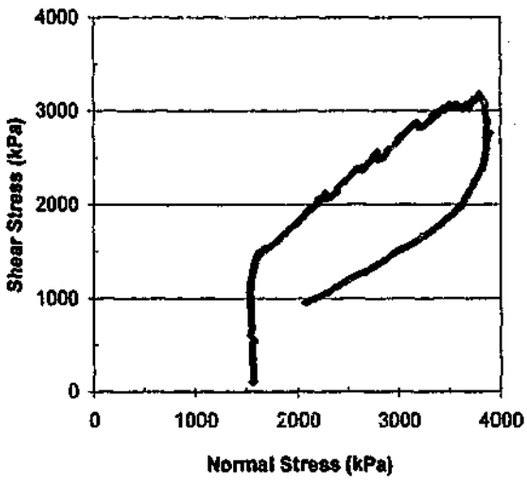

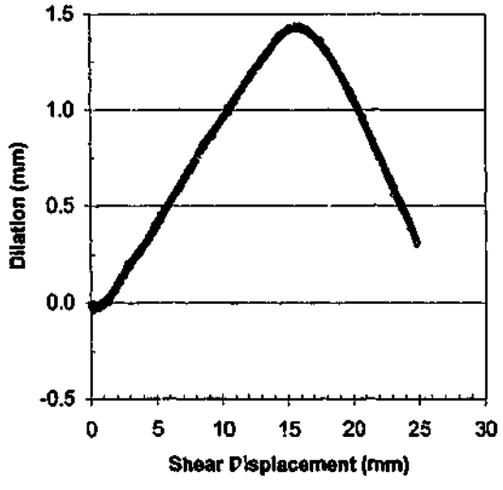

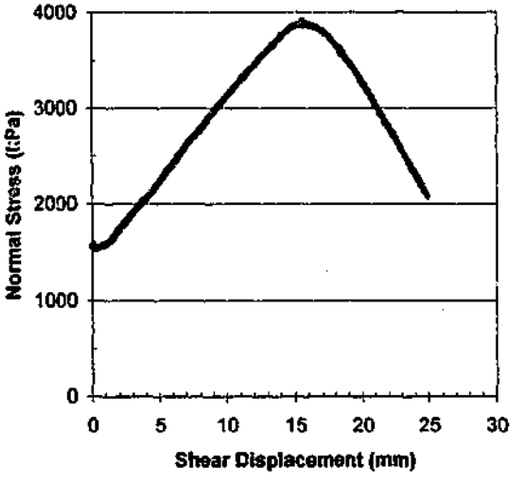

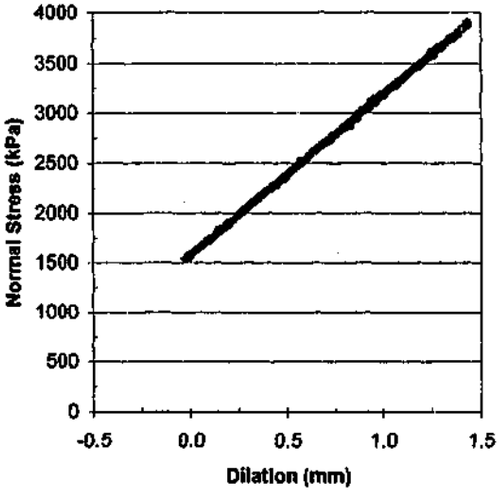

Test No:	BR10_16
Test Date: 9/2/00	
BASALT	
Profile : Regular 10deg. X 16mm	
Shear Rate = 0.5 mm/min	
Initial Normal Stress (kPa):	1600
Normal Stiffness (kPa/mm):	1600

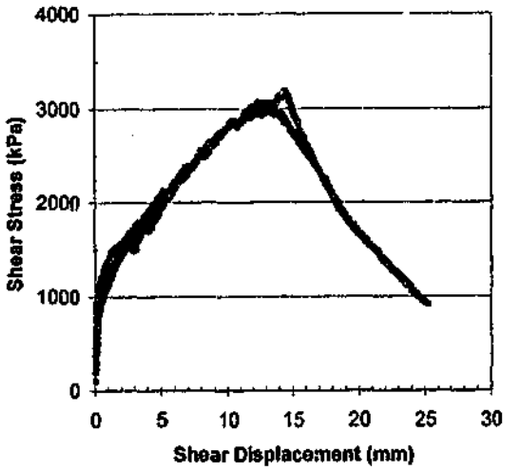

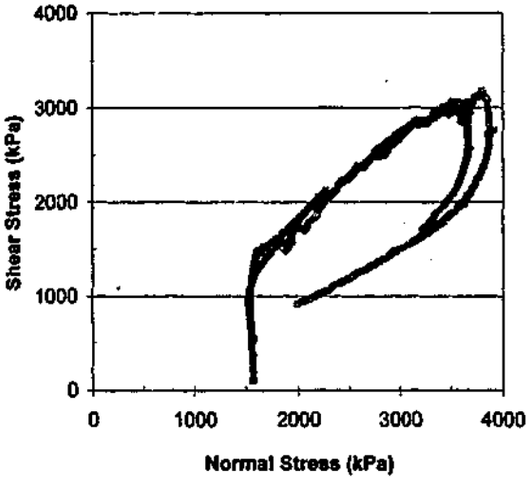

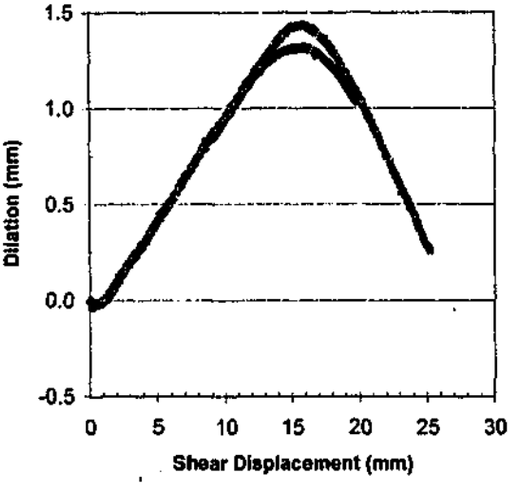

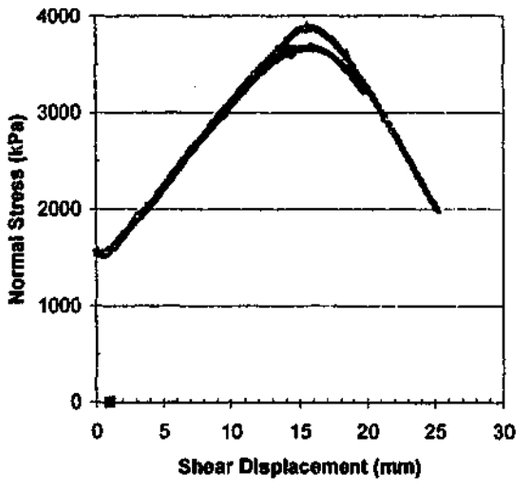

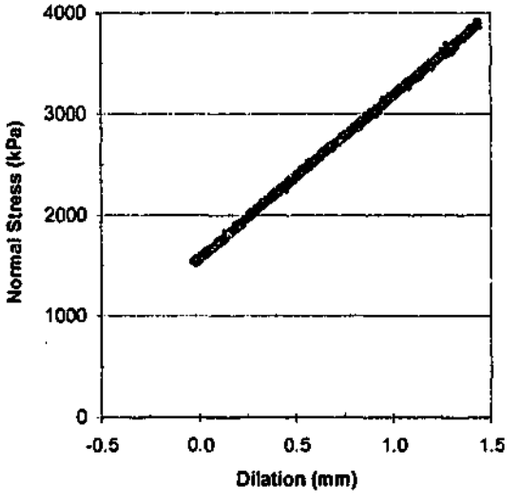

Test No:	BR10_16
Test Date: 9/2/00	
BASALT	
Profile : Retesting Regular 10^0 x 16mm	
Shear Rate = 0.5 mm/min	
Initial Normal Stress (kPa):	1600
Normal Stiffness (kPa/mm):	1600

1st test — Retest

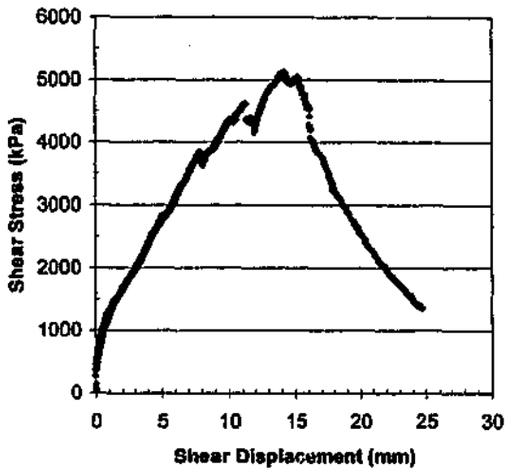

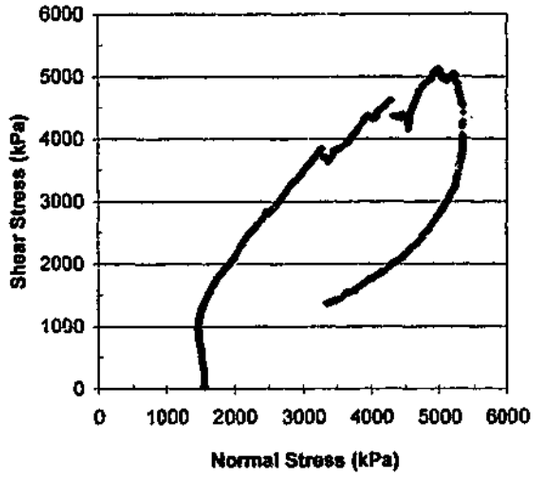

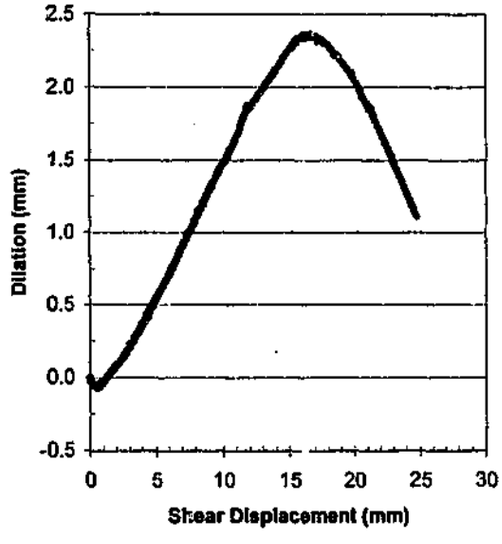

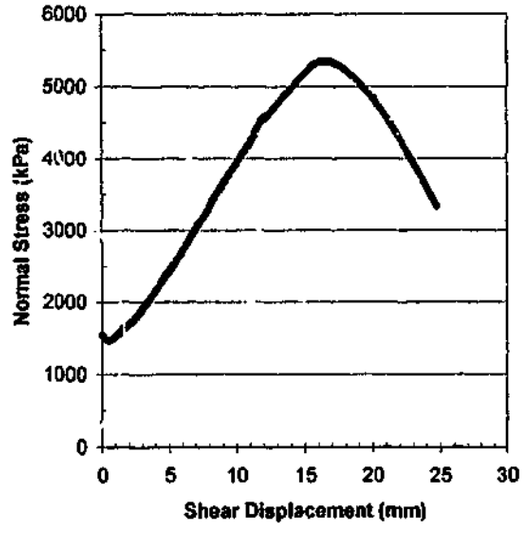

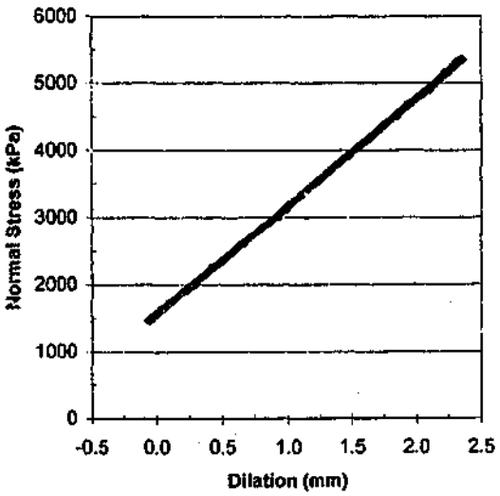

Test No:	BR15_16
Test Date: 11/2/00	
BASALT	
Profile : Regular 15deg. X 16mm	
Shear Rate = 0.5 mm/min	
Initial Normal Stress (kPa):	1600
Normal Stiffness (kPa/mm):	1600

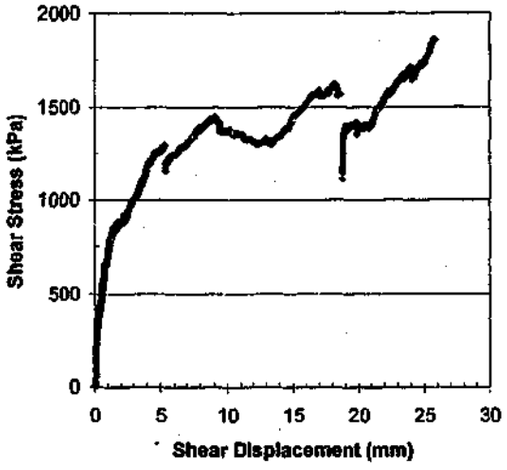

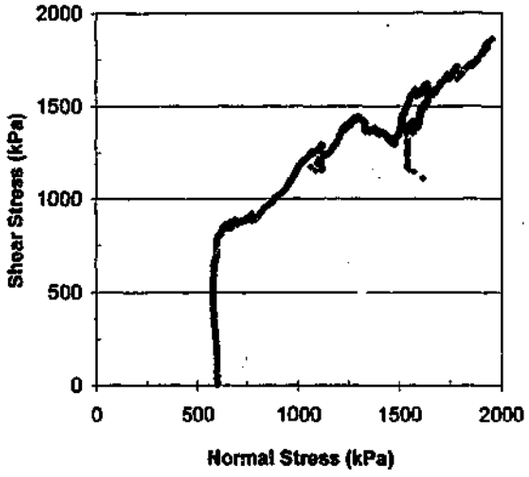

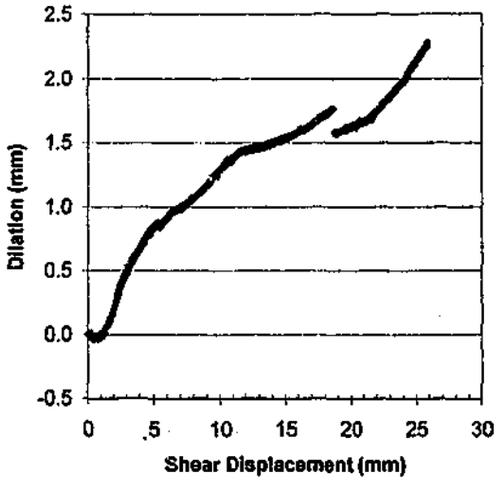

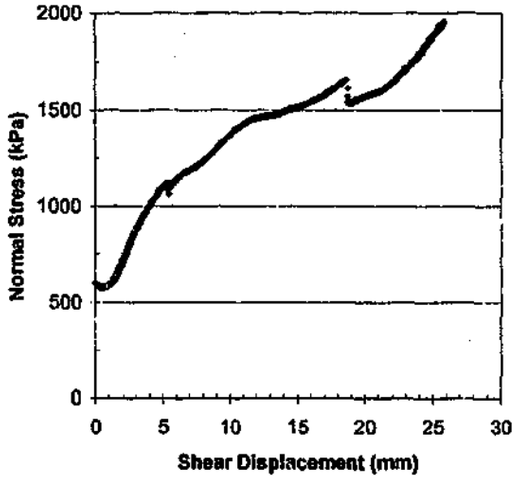

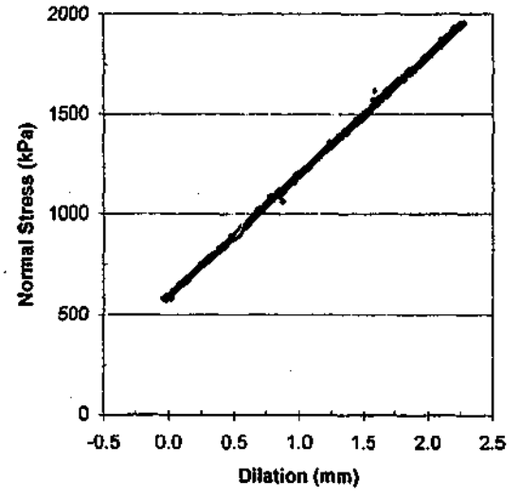

Test No:	BF10_5
Test Date: 11/8/00	
BASALT	
Profile : Fractal s=10deg, 5mm chord	
Shear Rate = 0.5 mm/min	
Initial Normal Stress (kPa):	600
Normal Stiffness (kPa/mm):	600

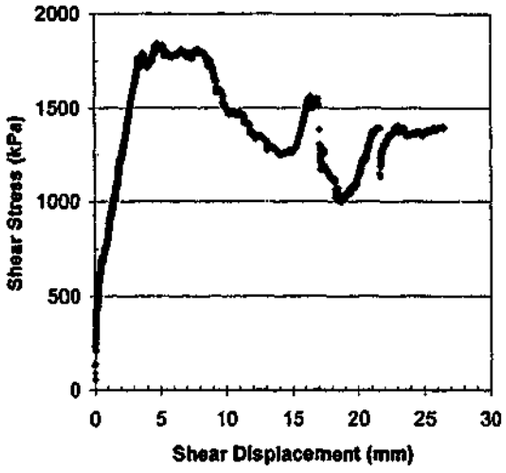

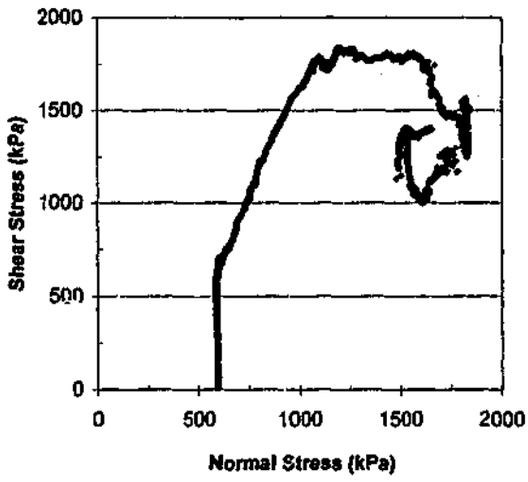

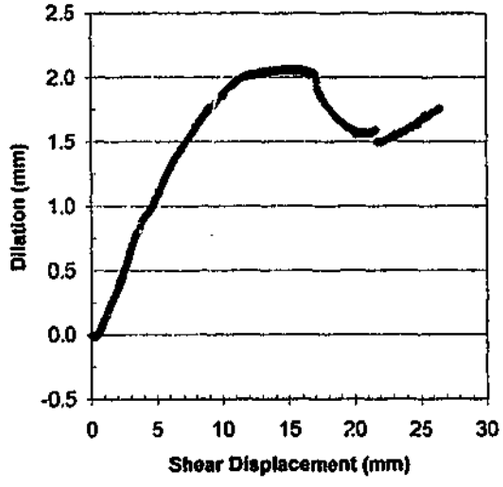

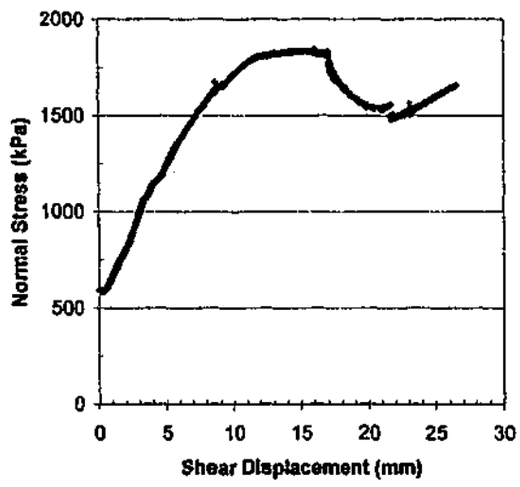

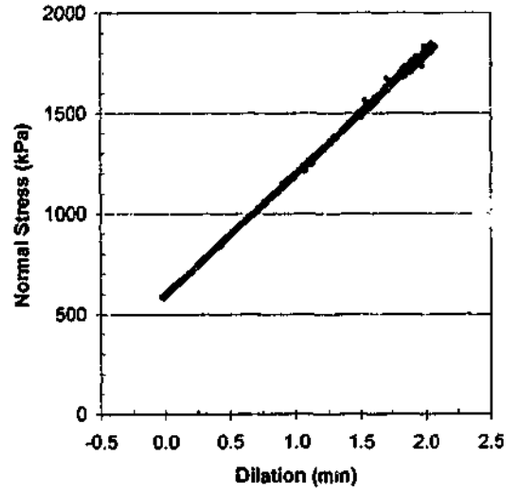

Test No:	BF15_5
Test Date: 14/8/00	
EASALT	
Profile : Fractal s=15deg, 5mm chord	
Shear Rate = 0.5 mm/min	
Initial Normal Stress (kPa):	600
Normal Stiffness (kPa/mm):	600

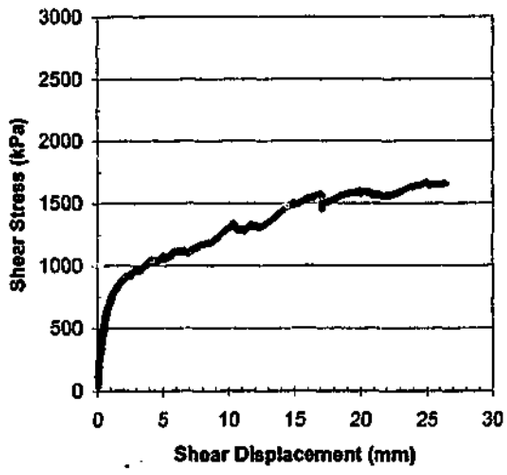

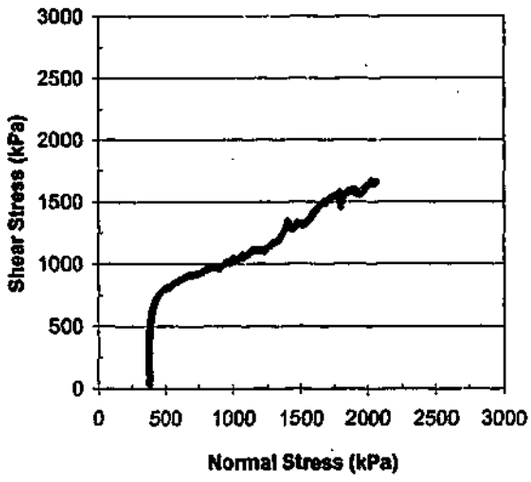

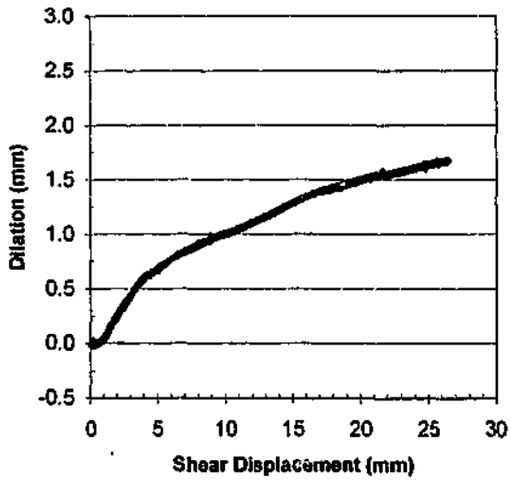

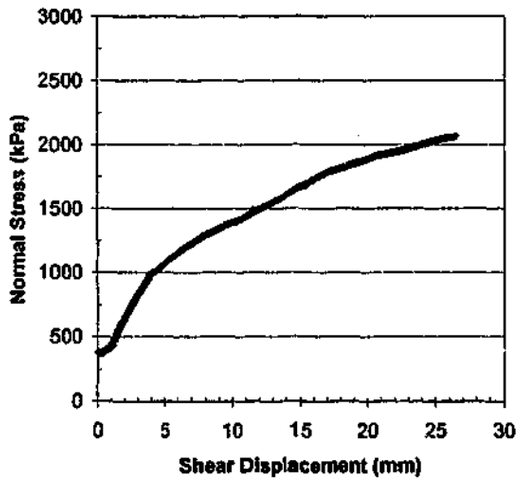

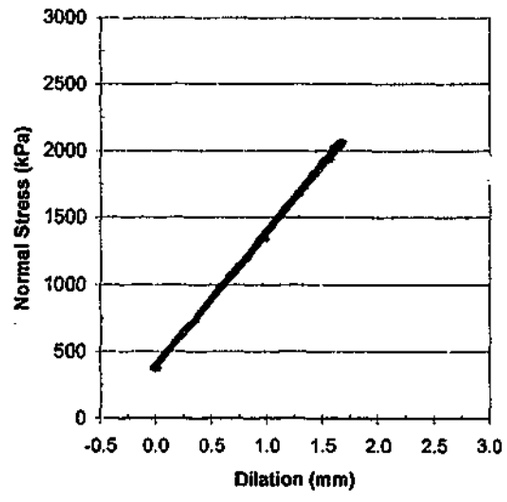

Test No:	BS_1
Test Date: 22/5/00	
BASALT	
Profile : Split	
Shear Rate = 0.5 mm/min	
Initial Normal Stress (kPa):	400
Normal Stiffness (kPa/mm):	1000

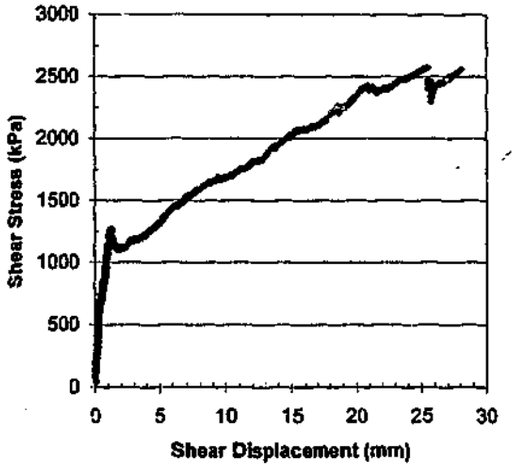

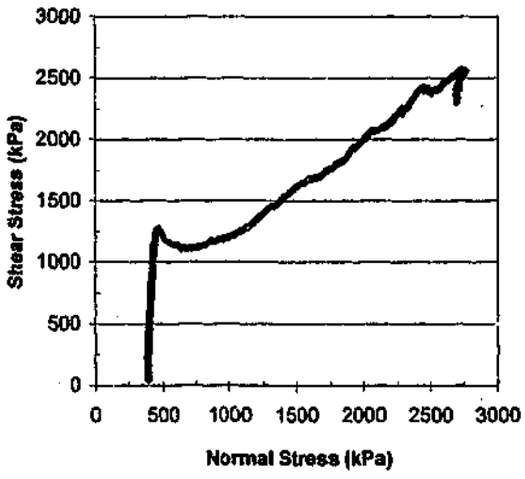

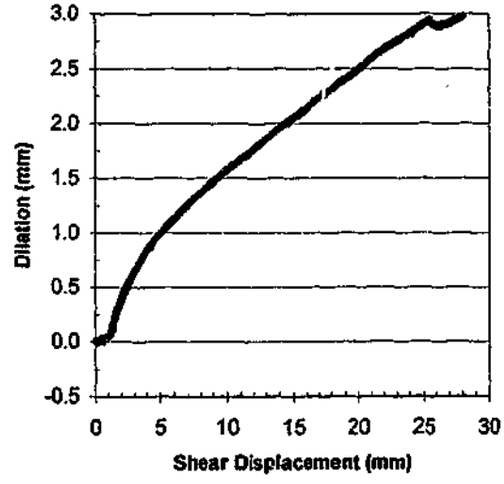

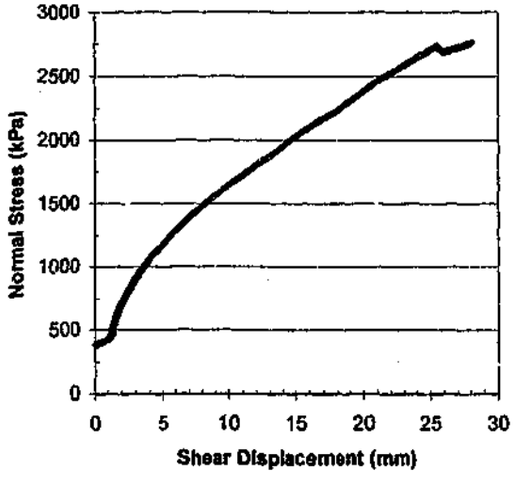

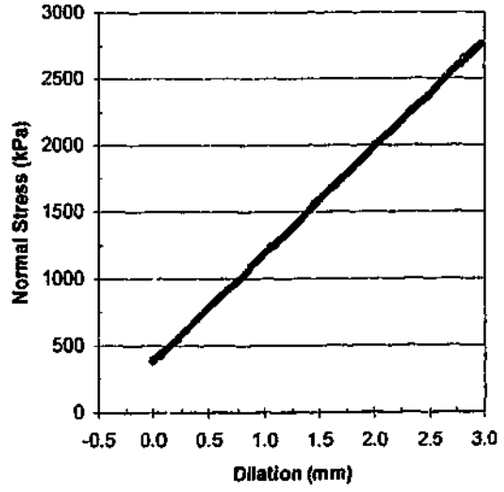

Test No:	BS_2
Test Date: 26/5/00	
BASALT	
Profile : Split	
Shear Rate = 0.5 mm/min	
Initial Normal Stress (kPa):	400
Normal Stiffness (kPa/mm):	800

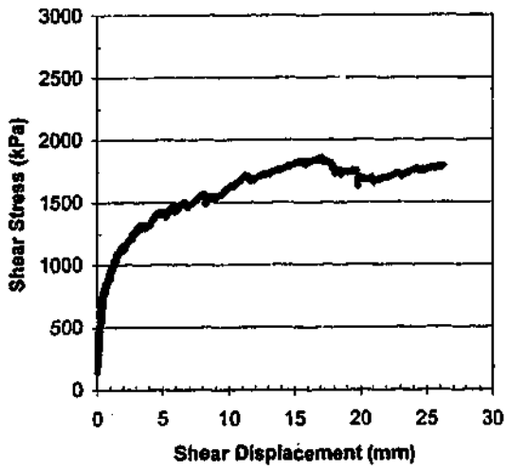

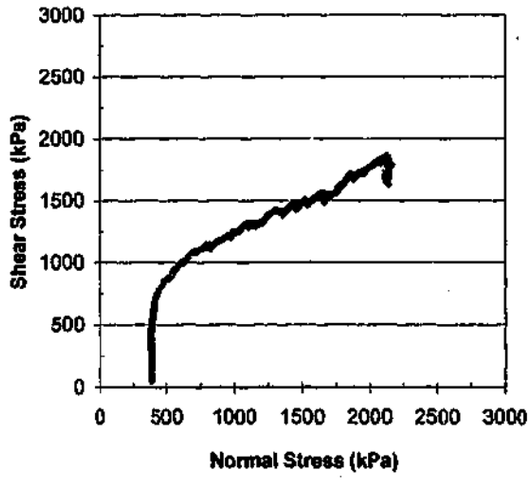

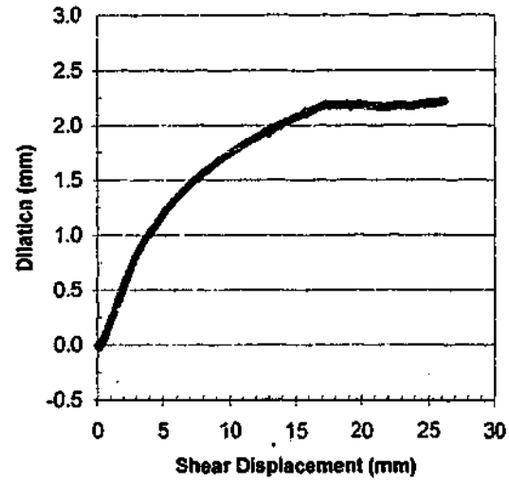

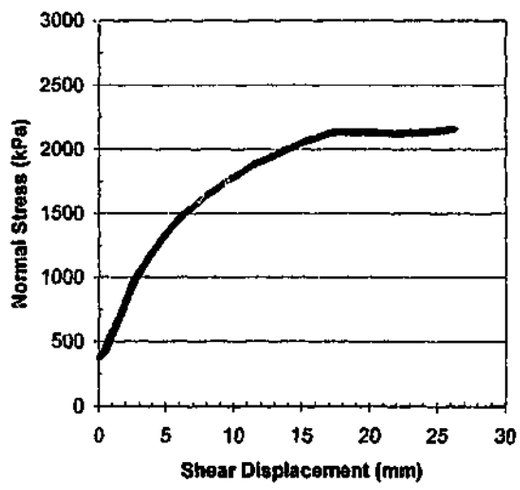

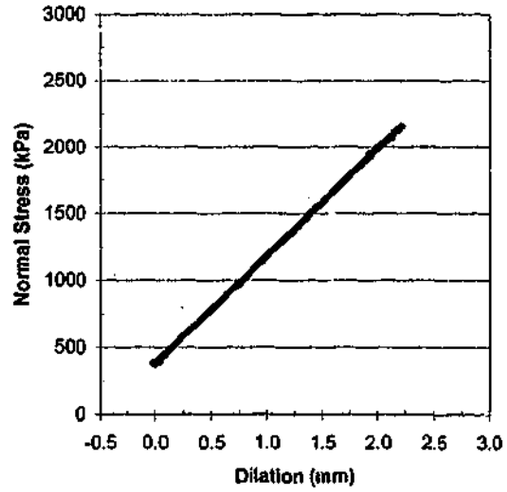

Test No:	BS_3
Test Date: 29/5/00	
BASALT	
Profile : Split	
Shear Rate = 0.5 mm/min	
Initial Normal Stress (kPa):	400
Normal Stiffness (kPa/mm):	800

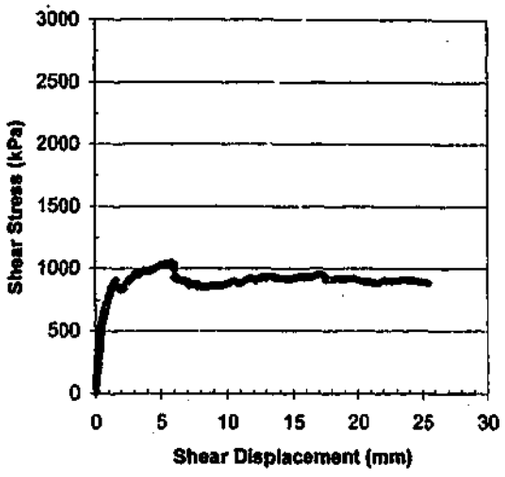

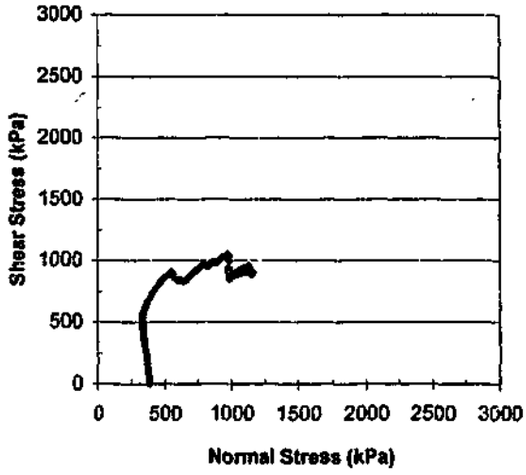

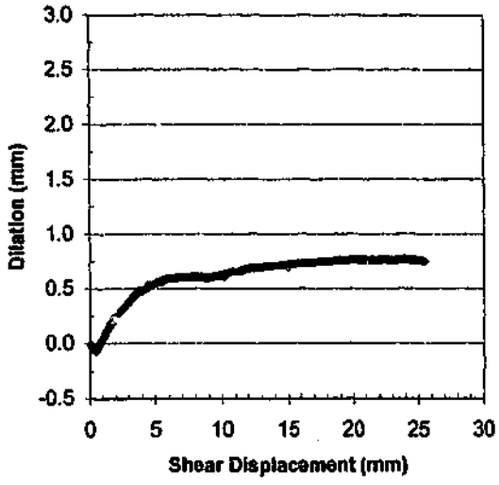

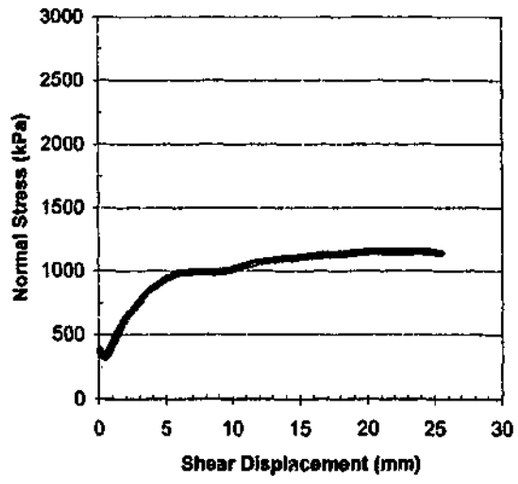

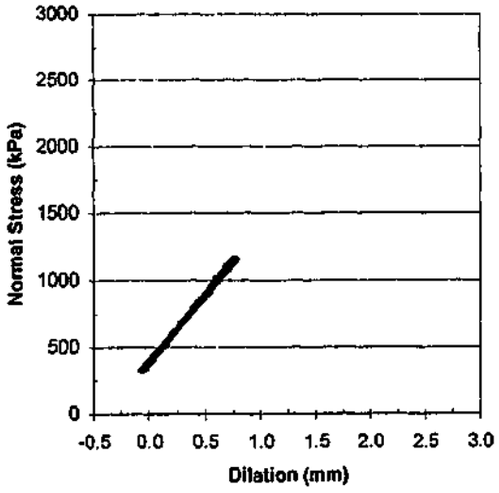

Test No:	BS_4
Test Date: 2/6/00	
BASALT	
Profile : Split	
Shear Rate = 0.5 mm/min	
Initial Normal Stress (kPa):	400
Normal Stiffness (kPa/mm):	1000

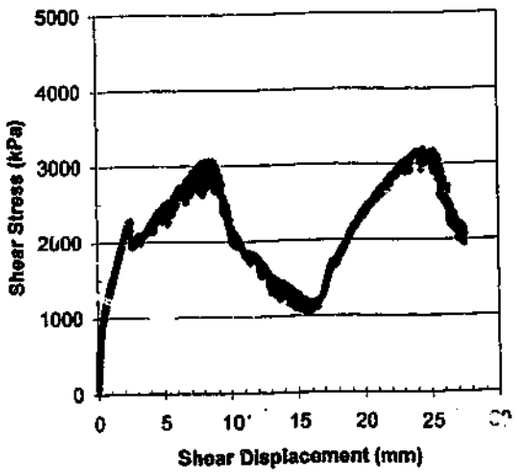

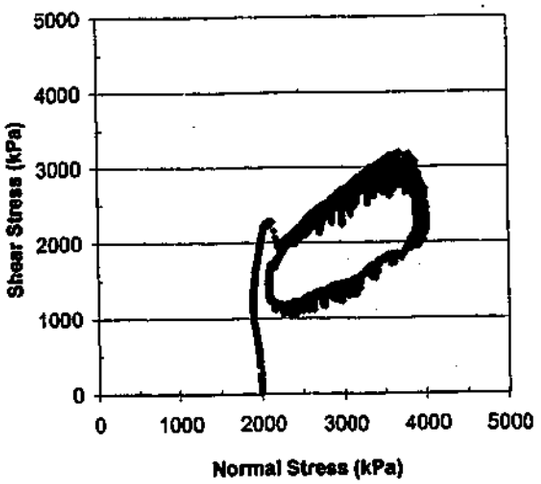

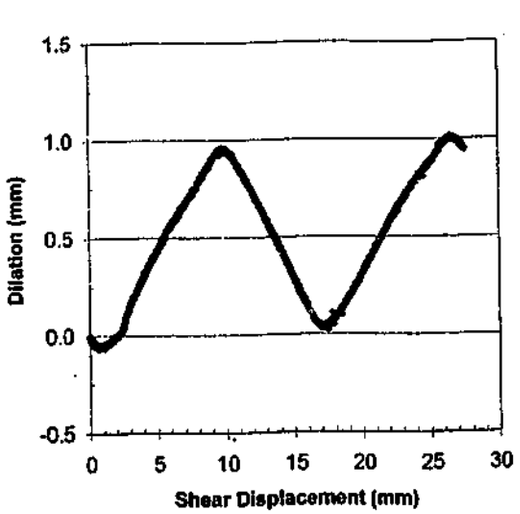

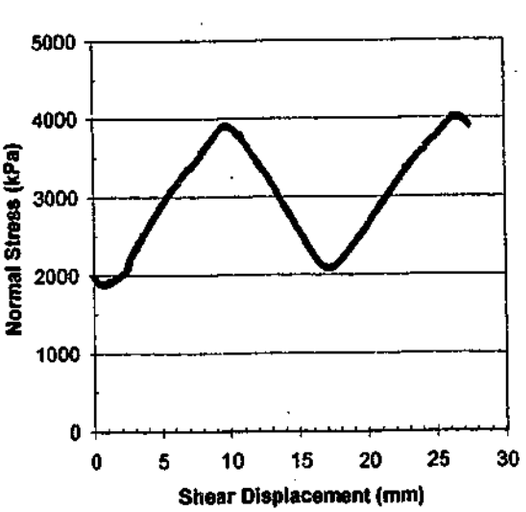

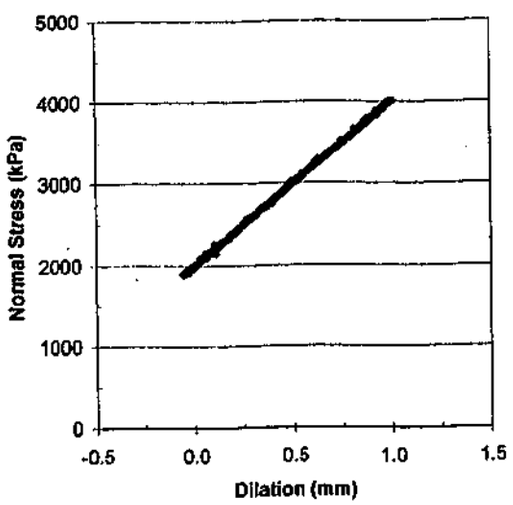

Test No:	GR10_8
Test Date: 11/9/00	
GRANITE	
Profile : Regular 10deg. X 8mm	
Shear Rate = 0.5 mm/min	
Initial Normal Stress (kPa):	2000
Normal Stiffness (kPa/mm):	2000

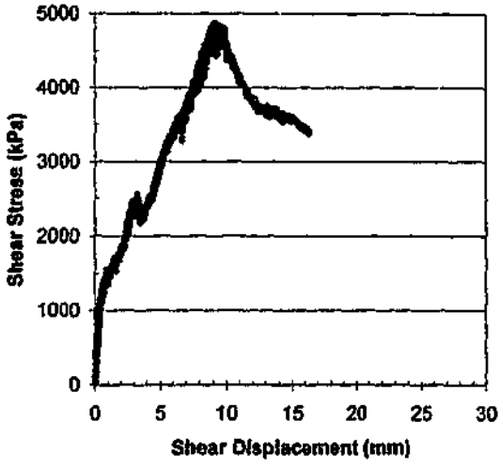

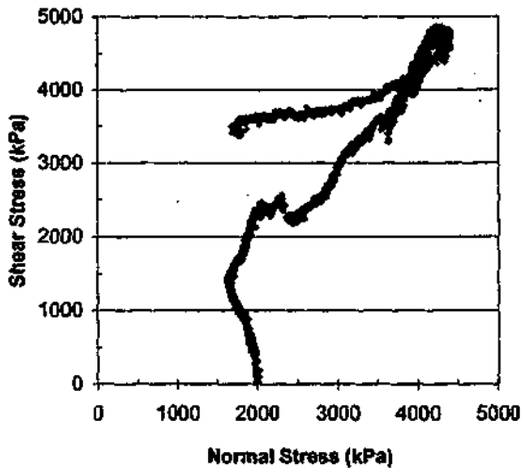

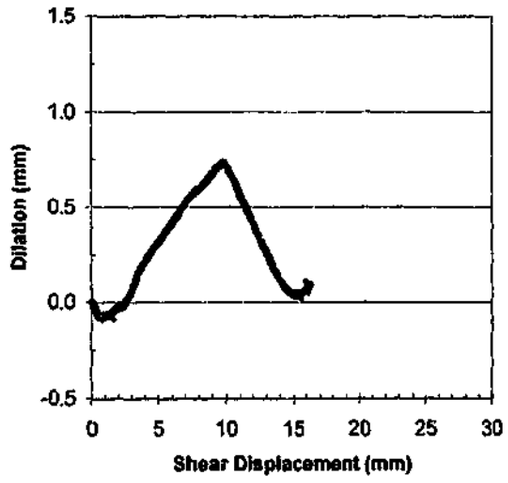

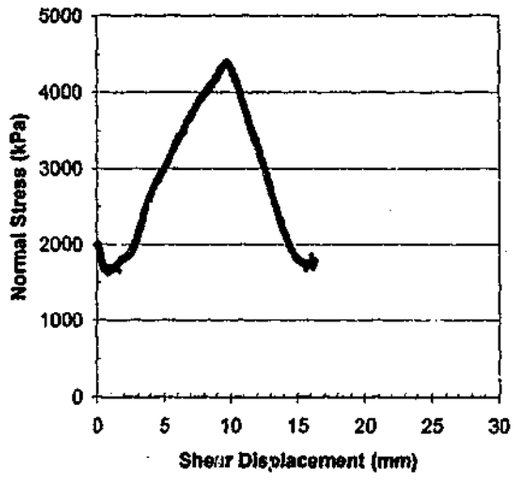

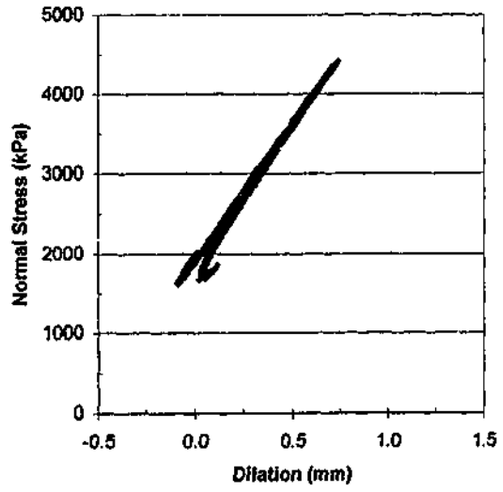

Test No:	GR10a_8
Test Date: 8/9/00	
GRANITE	
Profile : Regular 10deg. X 8mm	
Shear Rate = 0.5 mm/min	
Initial Normal Stress (kPa):	2000
Normal Stiffness (kPa/mm):	4000

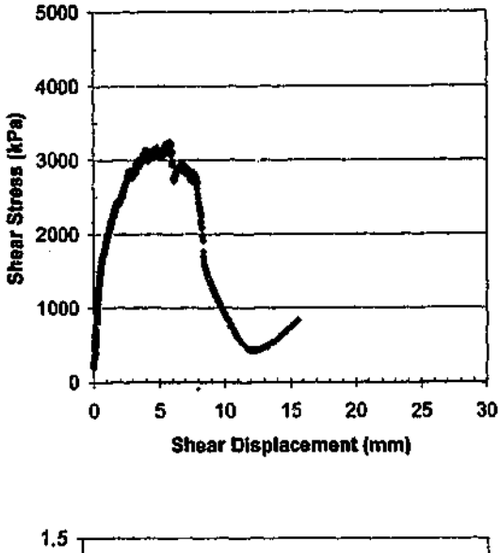

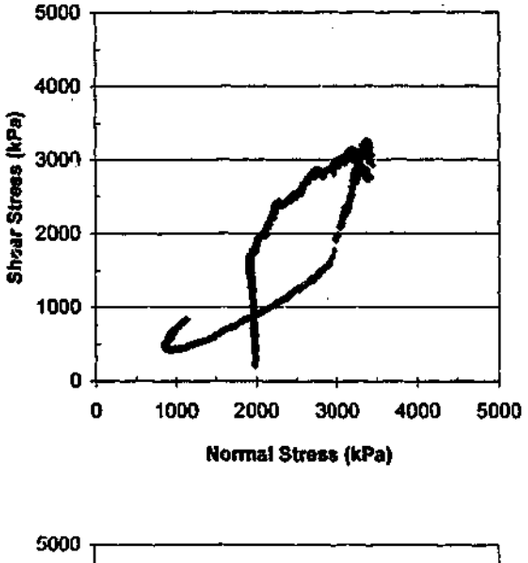

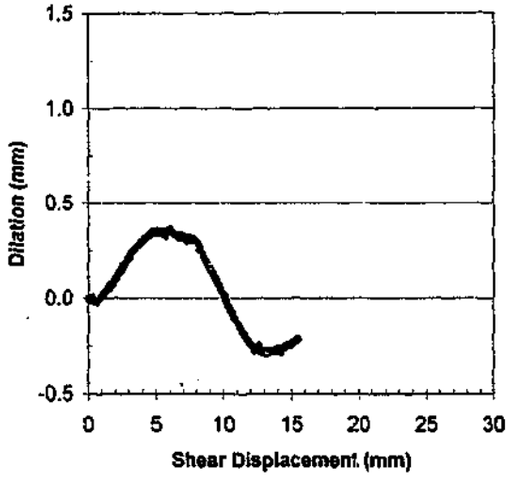

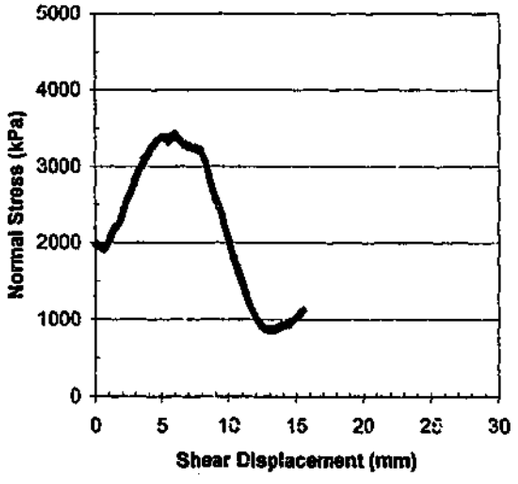

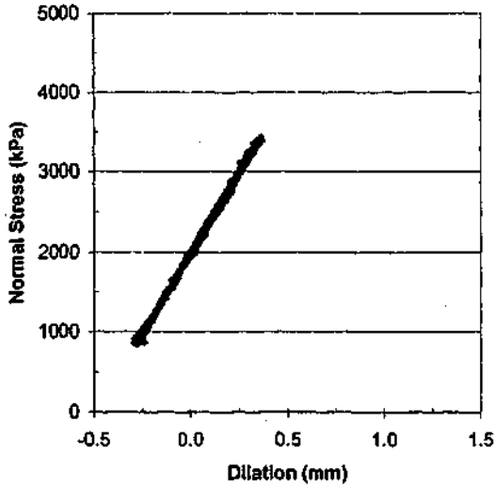

Test No:	GR20_8
Test Date: 9/8/00	
GRANITE	
Profile : Regular 20deg. X 8mm	
Shear Rate = 0.5 mm/min	
Initial Normal Stress (kPa):	2000
Normal Stiffness (kPa/mm):	4000

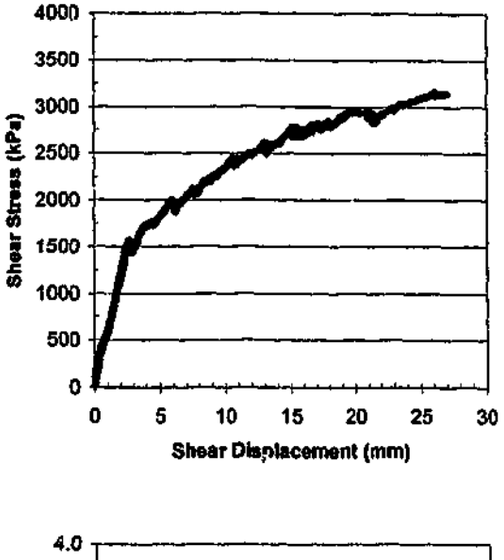

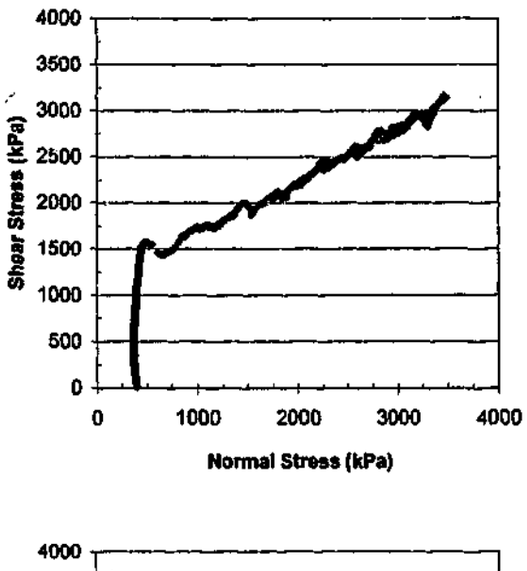

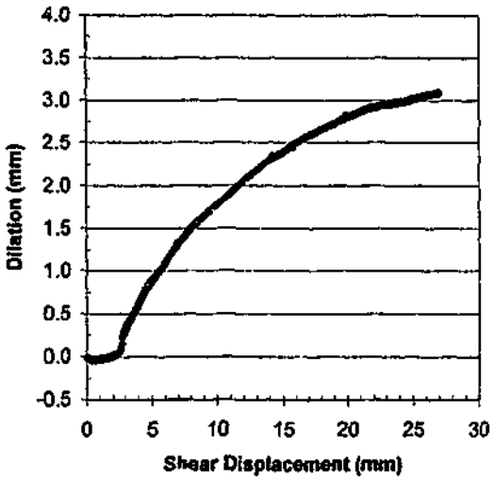

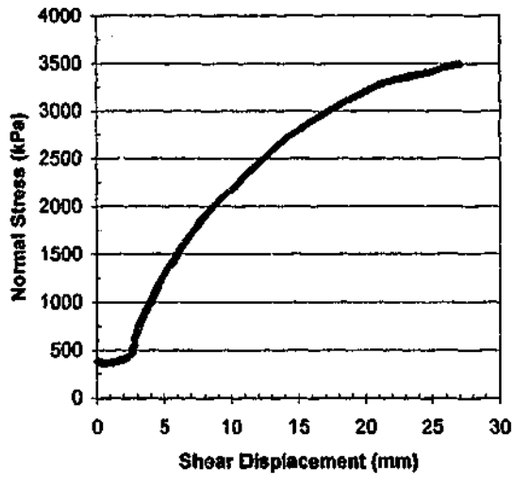

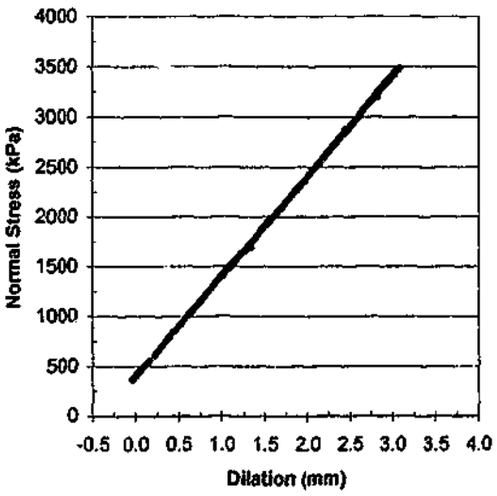

Test No:	GS_1
Test Date: 15/5/00	
GRANITE	
Profile : Split	
Shear Rate = 0.5 mm/min	
Initial Normal Stress (kPa):	400
Normal Stiffness (kPa/mm):	1000

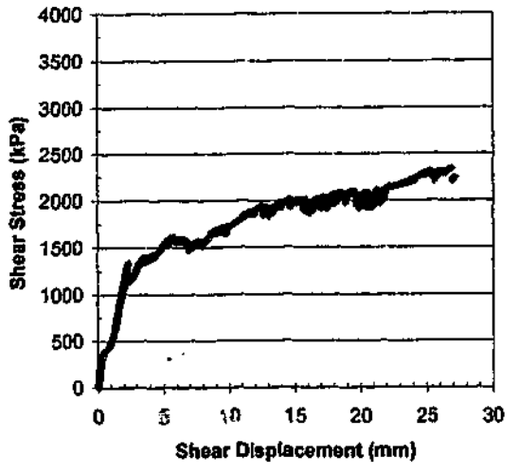

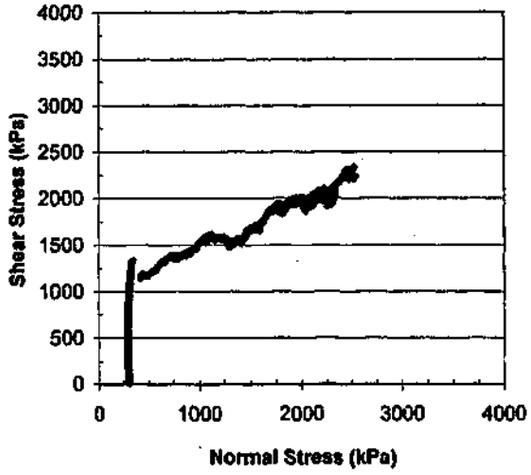

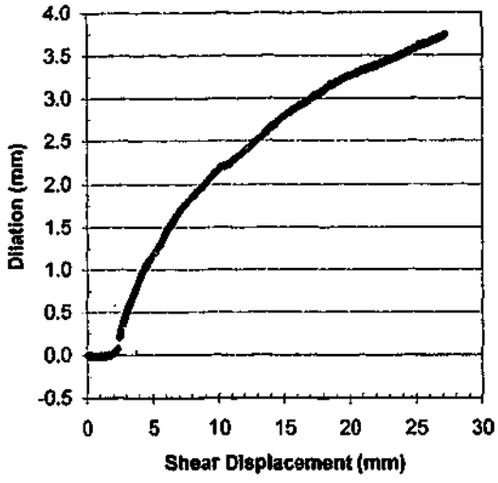

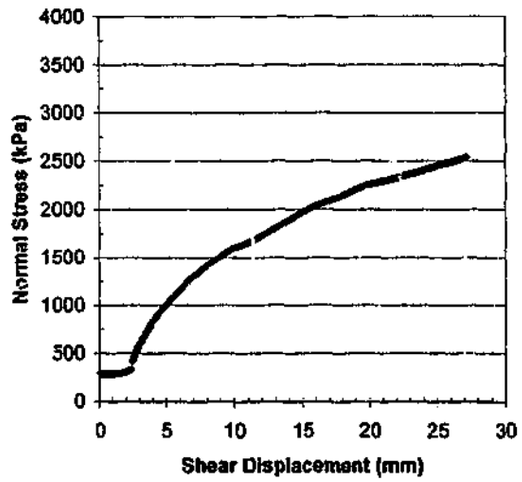

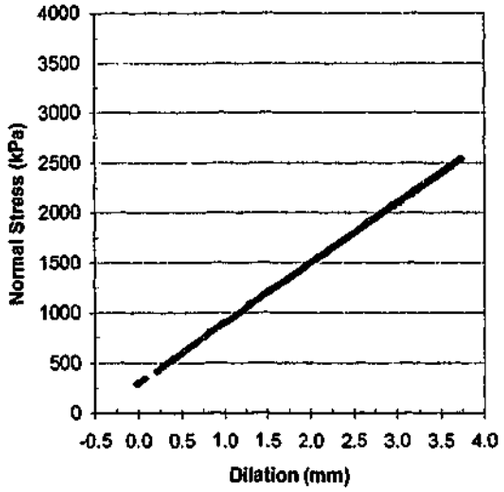

Test No:	GS_2
Test Date: 4/8/00	
GRANITE	
Profile : Split	
Shear Rate = 0.5 mm/min	
Initial Normal Stress (kPa):	300
Normal Stiffness (kPa/mm):	600

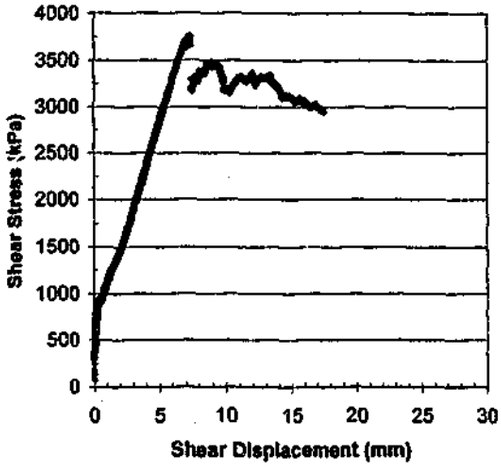

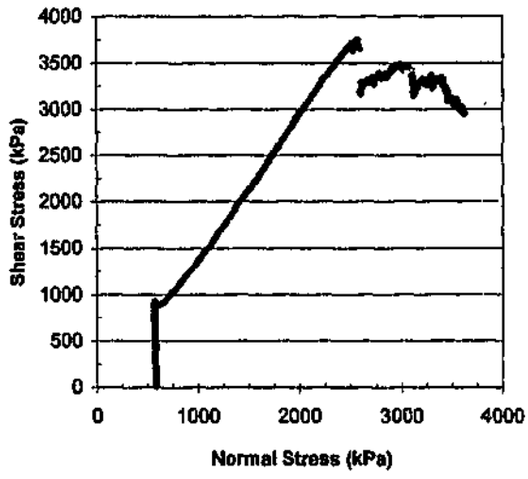

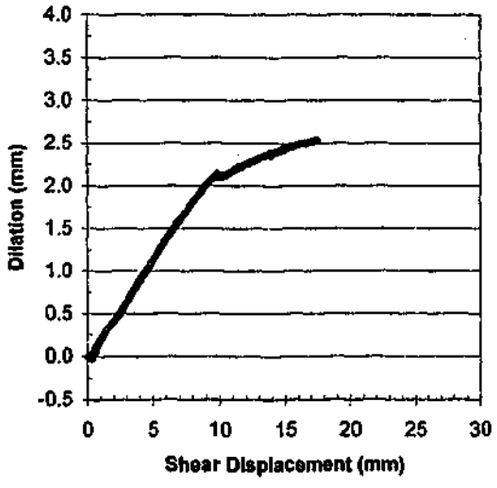

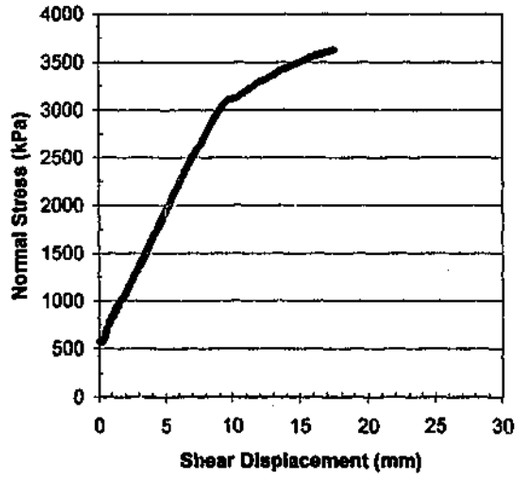

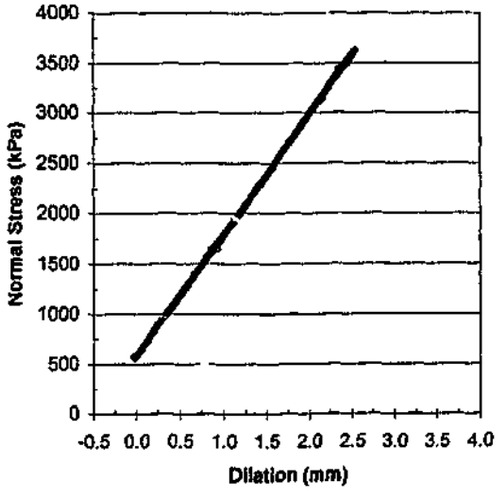

Test No:	GS_3
Test Date: 19/5/00	
GRANITE	
Profile : Split	
Shear Rate = 0.5 mm/min	
Initial Normal Stress (kPa):	600
Normal Stiffness (kPa/mm):	1200

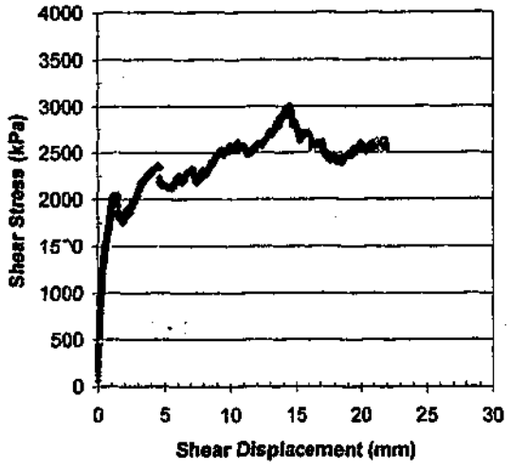

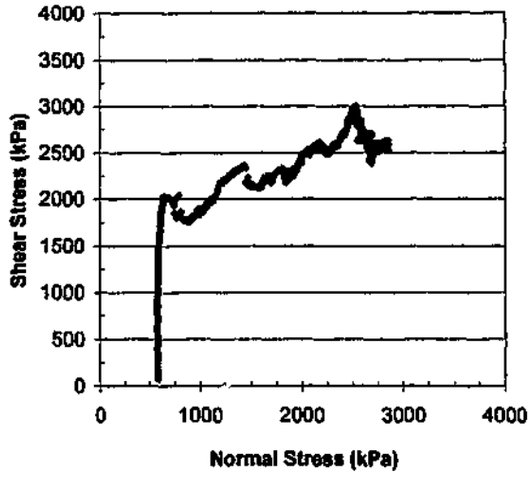

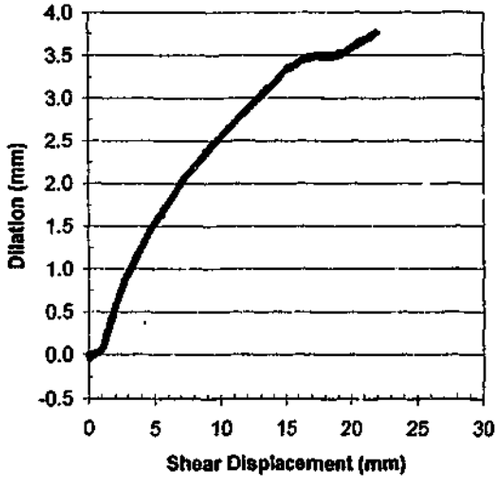

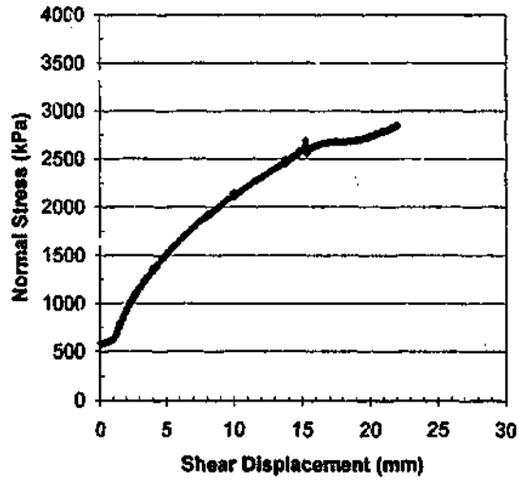

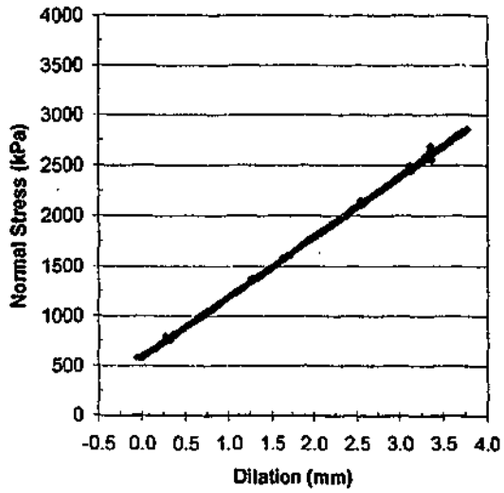

Test No:	GS_4
Test Date: 7/8/00	
GRANITE	
Profile : Split	
Shear Rate = 0.5 mm/min	
Initial Normal Stress (kPa):	600
Normal Stiffness (kPa/mm):	600

APPENDIX E

STATISTICAL DISTRIBUTION OF JOINT SURFACE STATISTICS

MATHEMATICAL DESCRIPTION OF JOINT SURFACE STATISTICS

REPRODUCTION OF JOINT SURFACE STATISTICS USING MODIFIED MIDPOINT DISPLACEMENT METHOD

Table of Contents – Appendix E

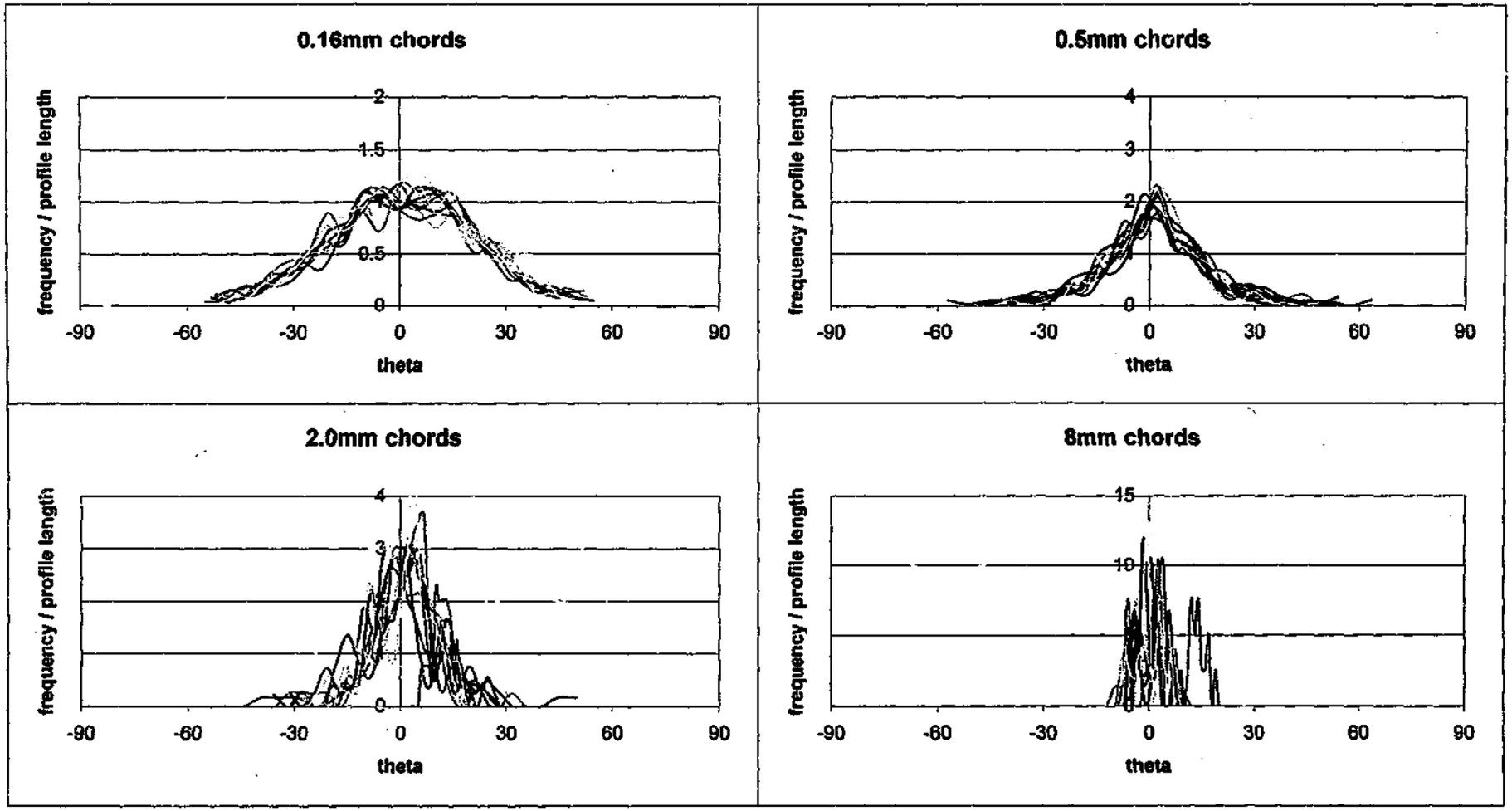

Siltstone Bedding Joint 1 - all profiles, 5deg bins

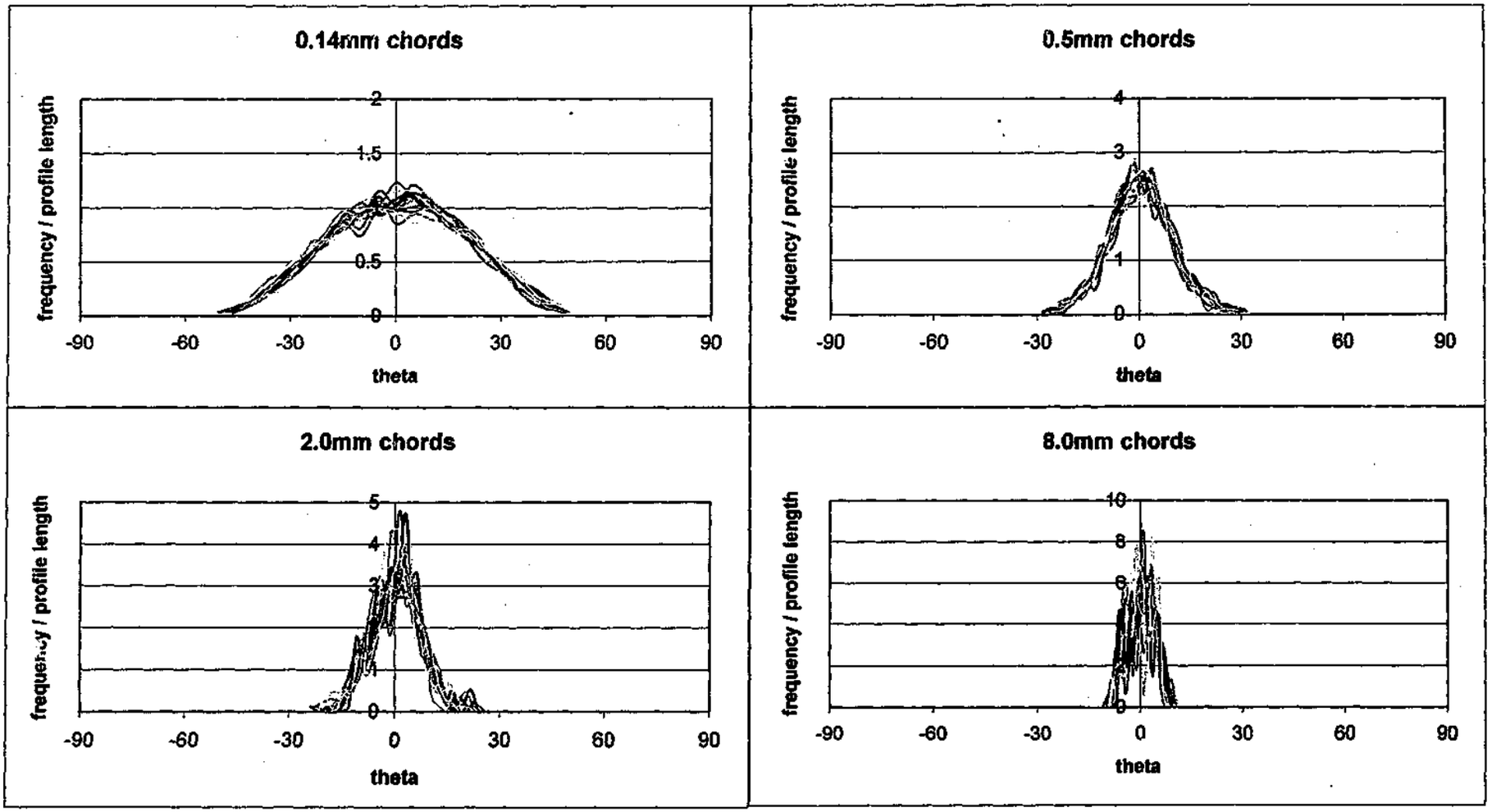

Siltstone Bedding Joint 2 - all profiles, 5deg bins

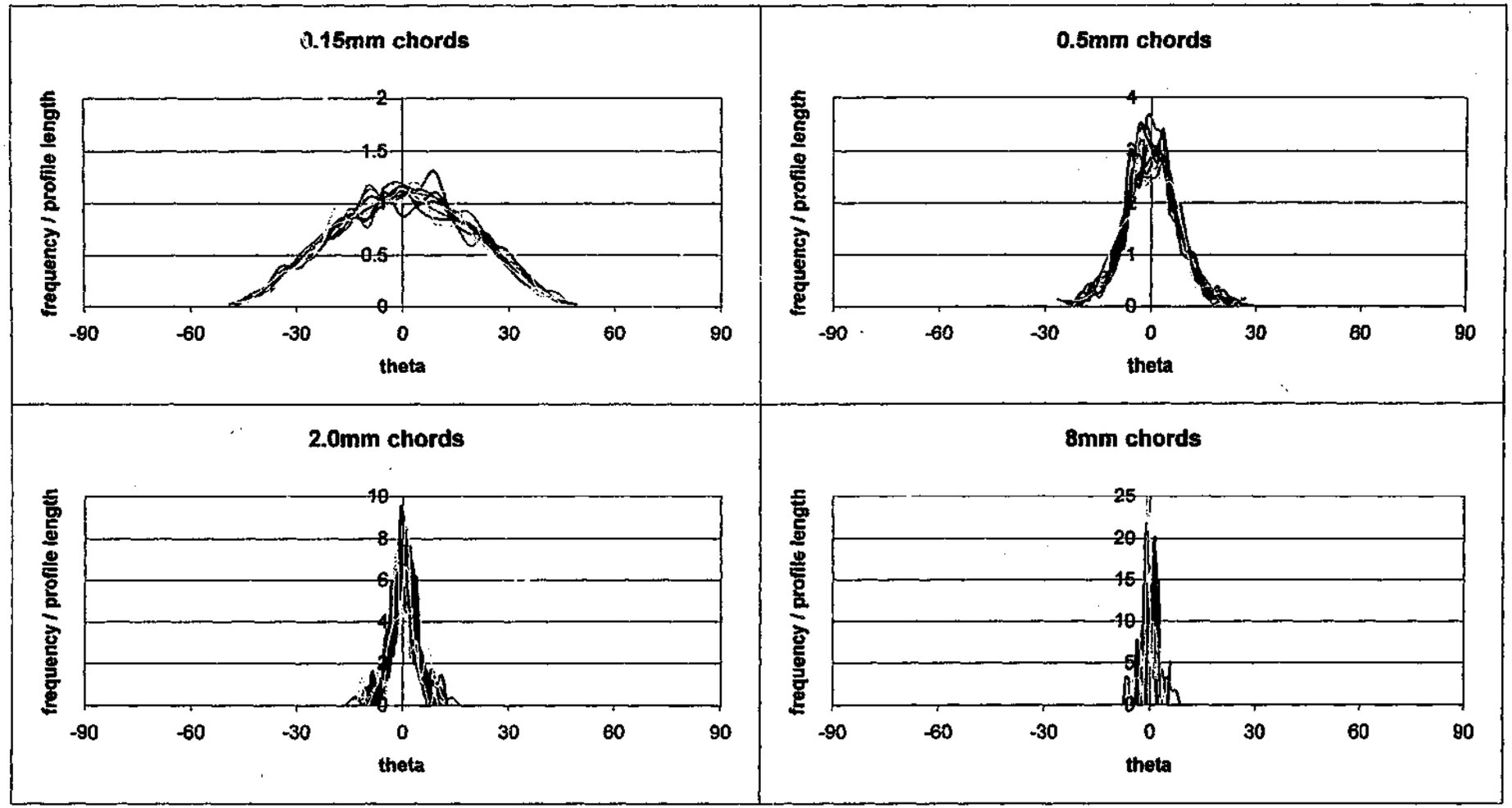

Siltstone Joint 1 - all profiles, 5deg bins

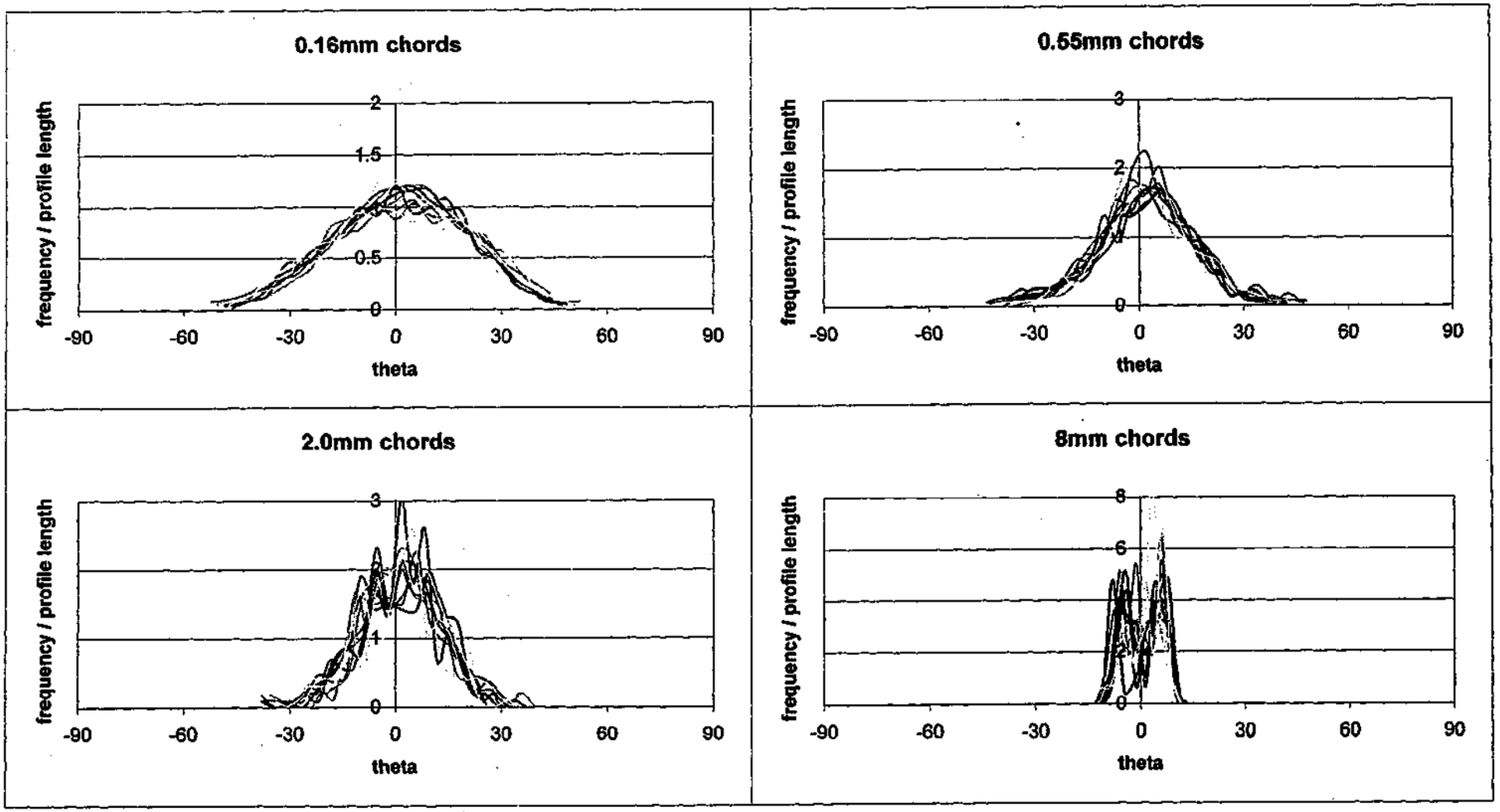

Basalt Joint 1a - all profiles, 5deg bins

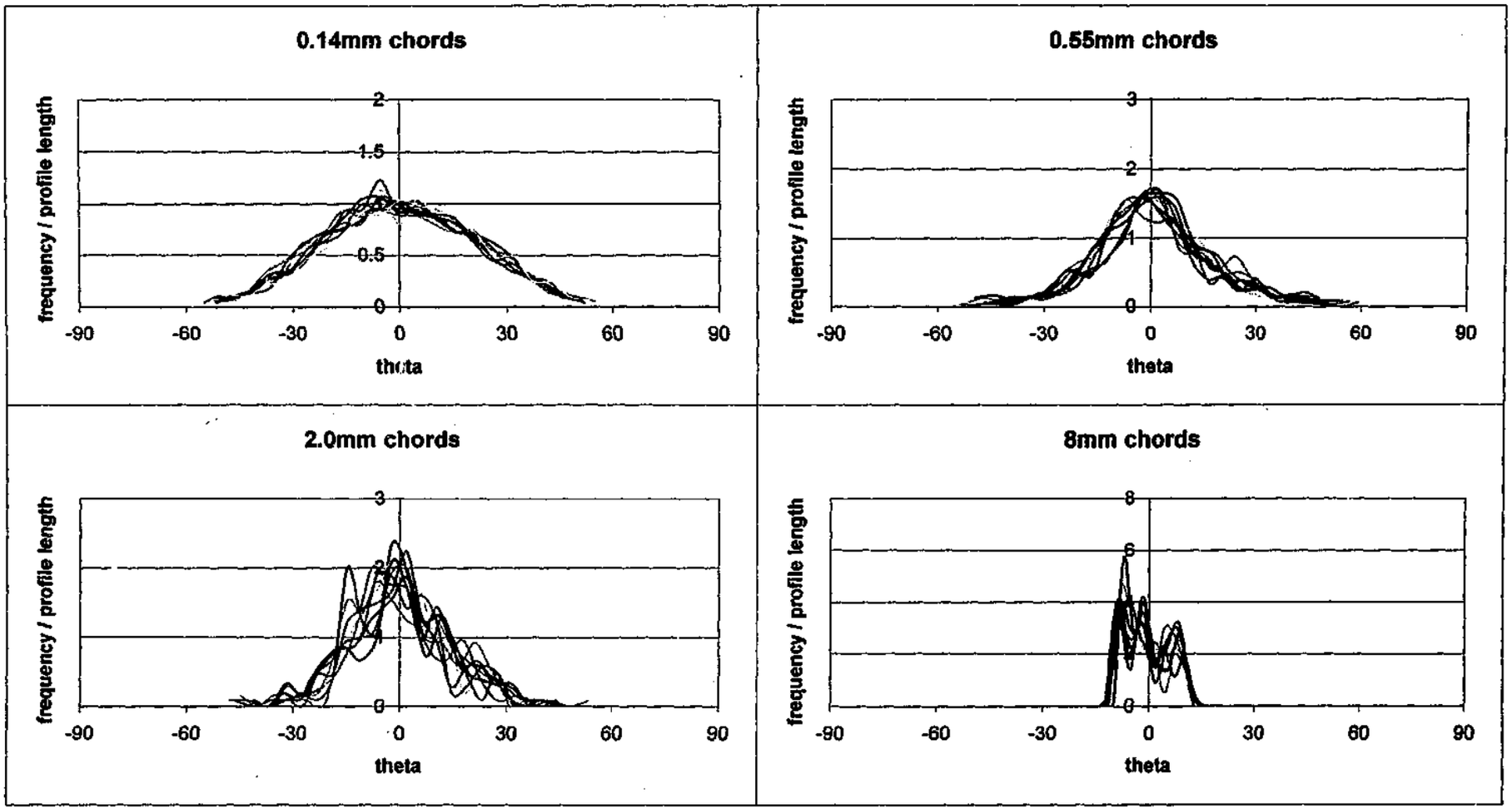

Basalt Joint 1 - all profiles, 5deg bins

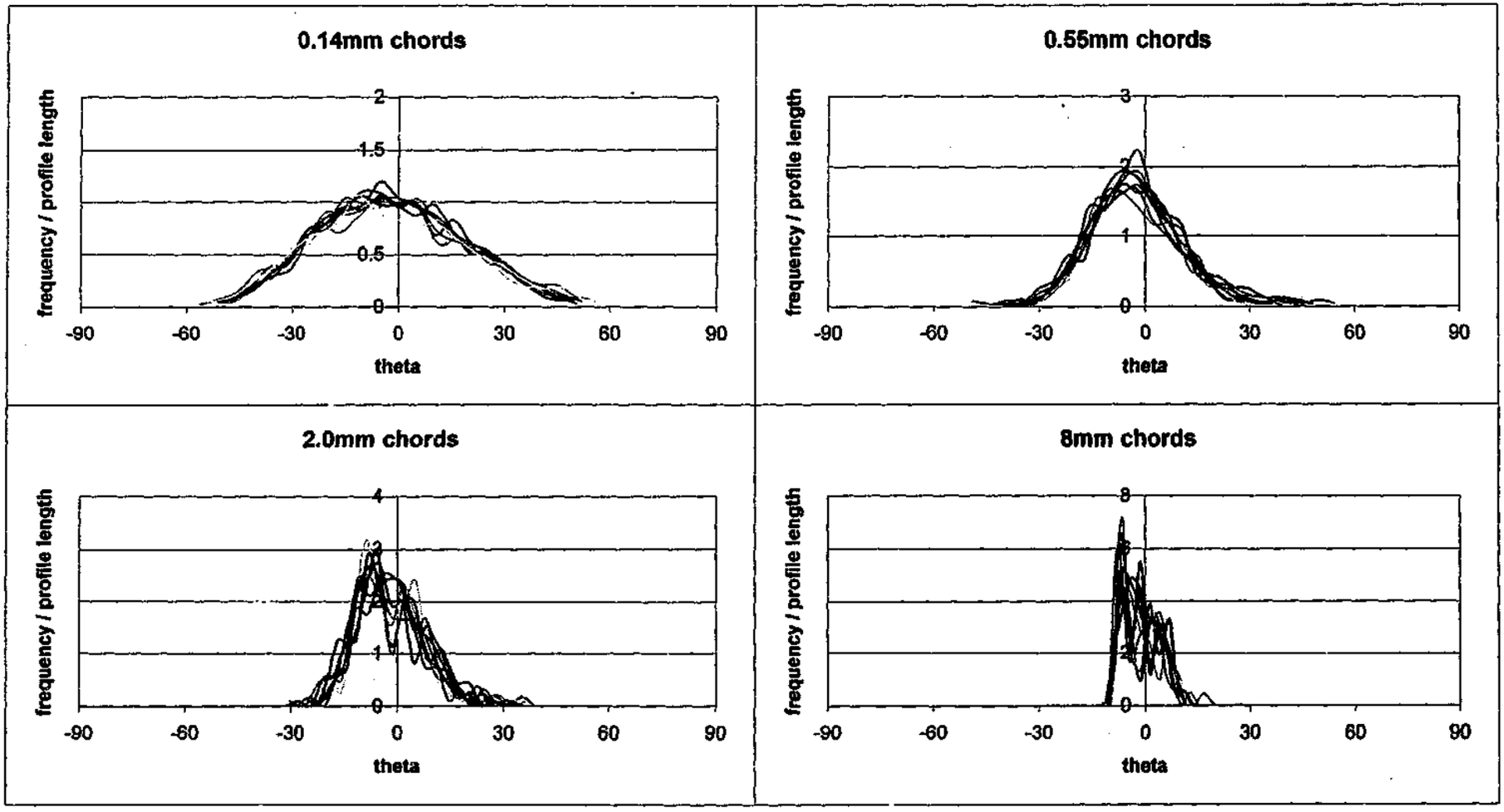

Basalt Joint 2 - all profiles, 5deg bins

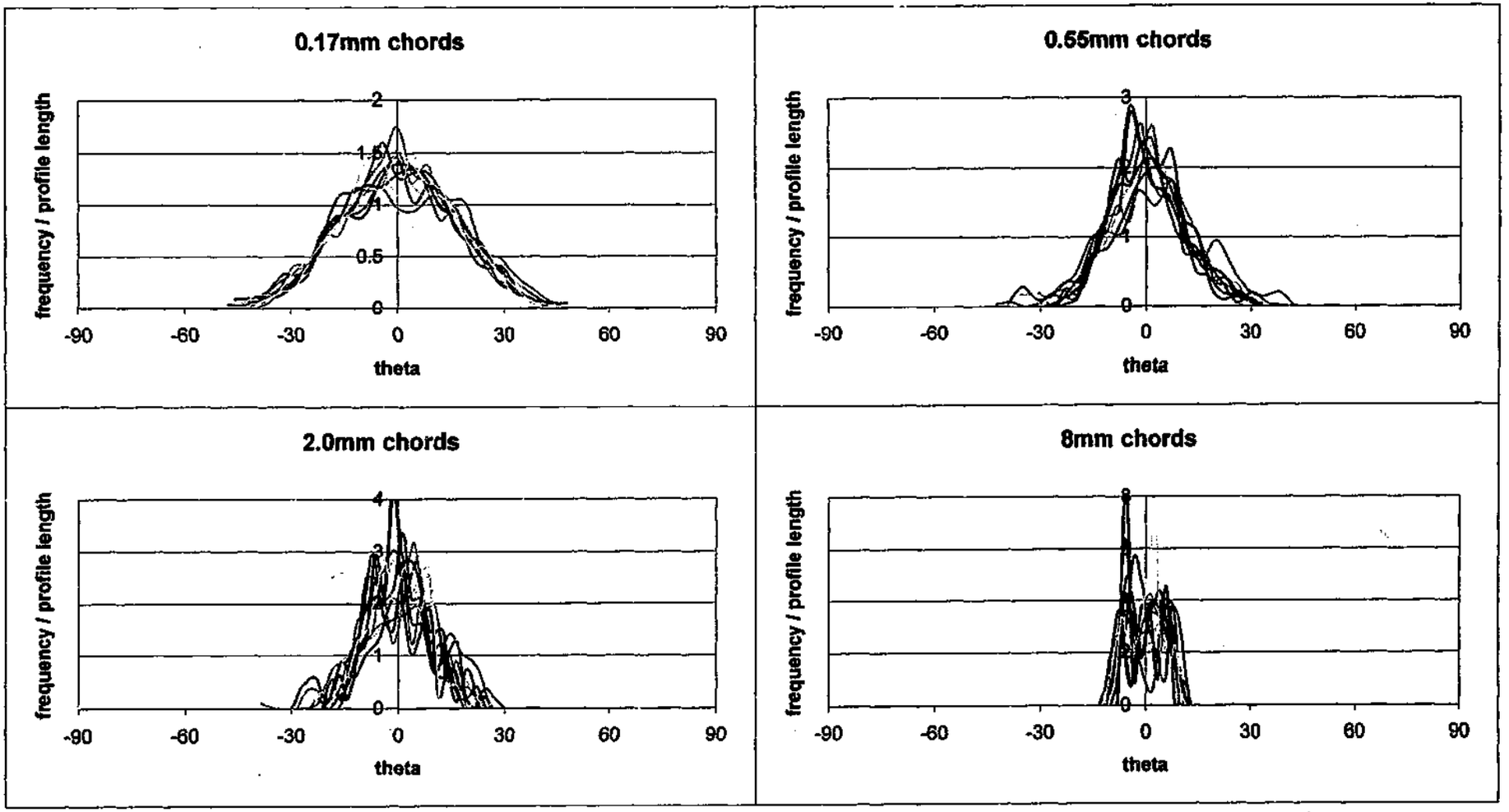

Basalt Joint 3 - all profiles, 5deg bins

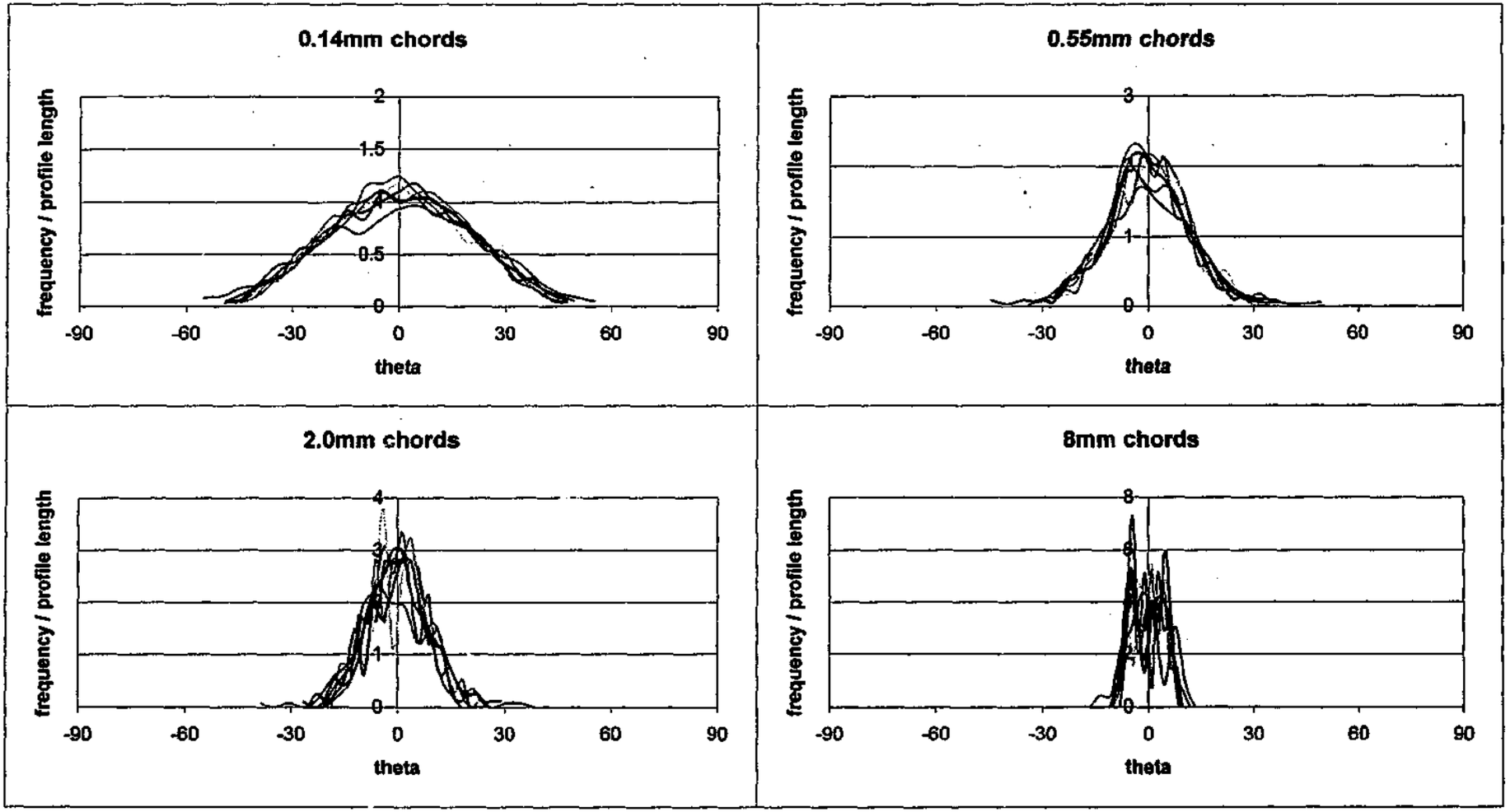

Basalt Joint 5 - all profiles, 5deg bins

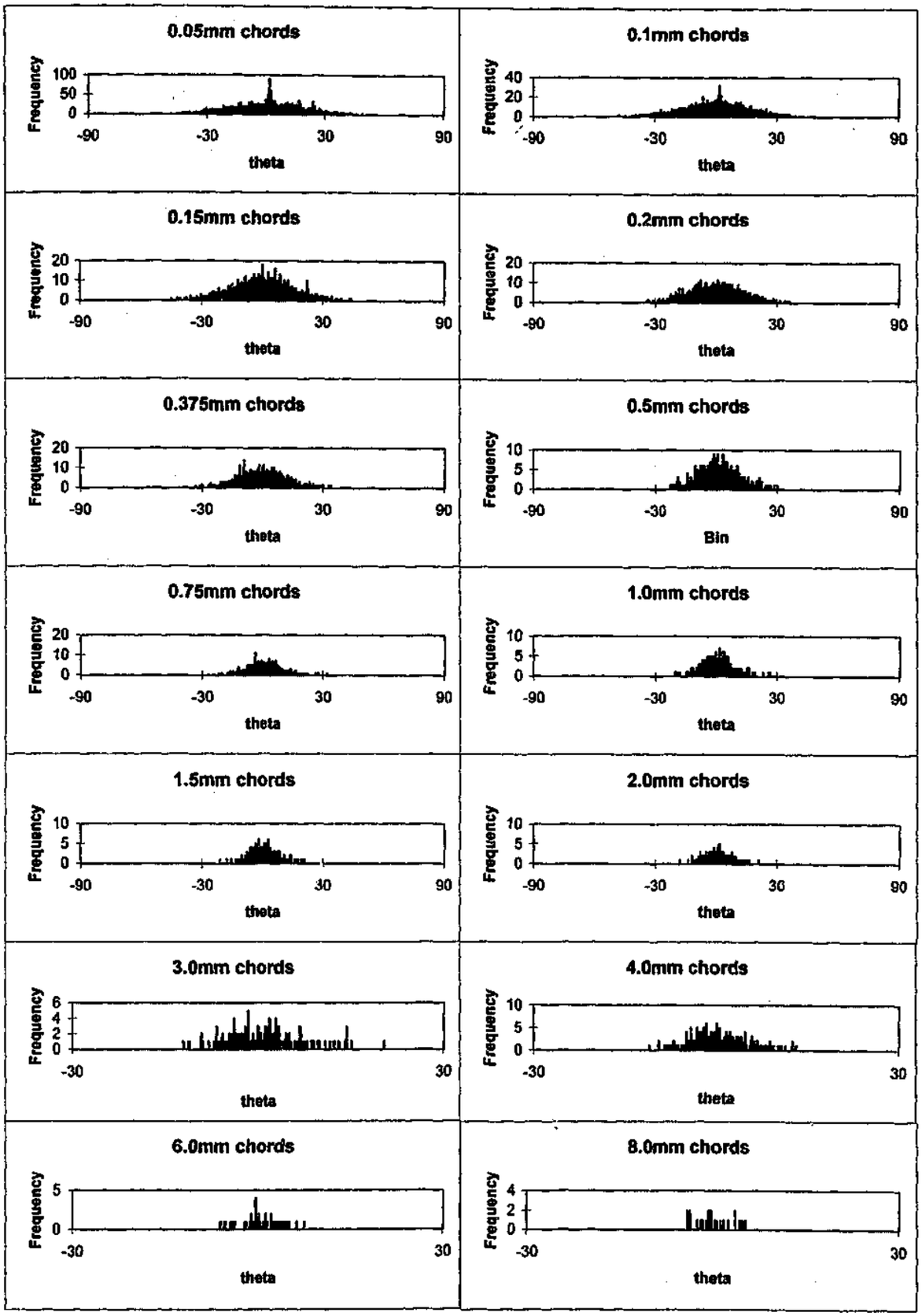

SILTSTONE BEDDING JOINT 1 - *profile h*, 0.1deg bins

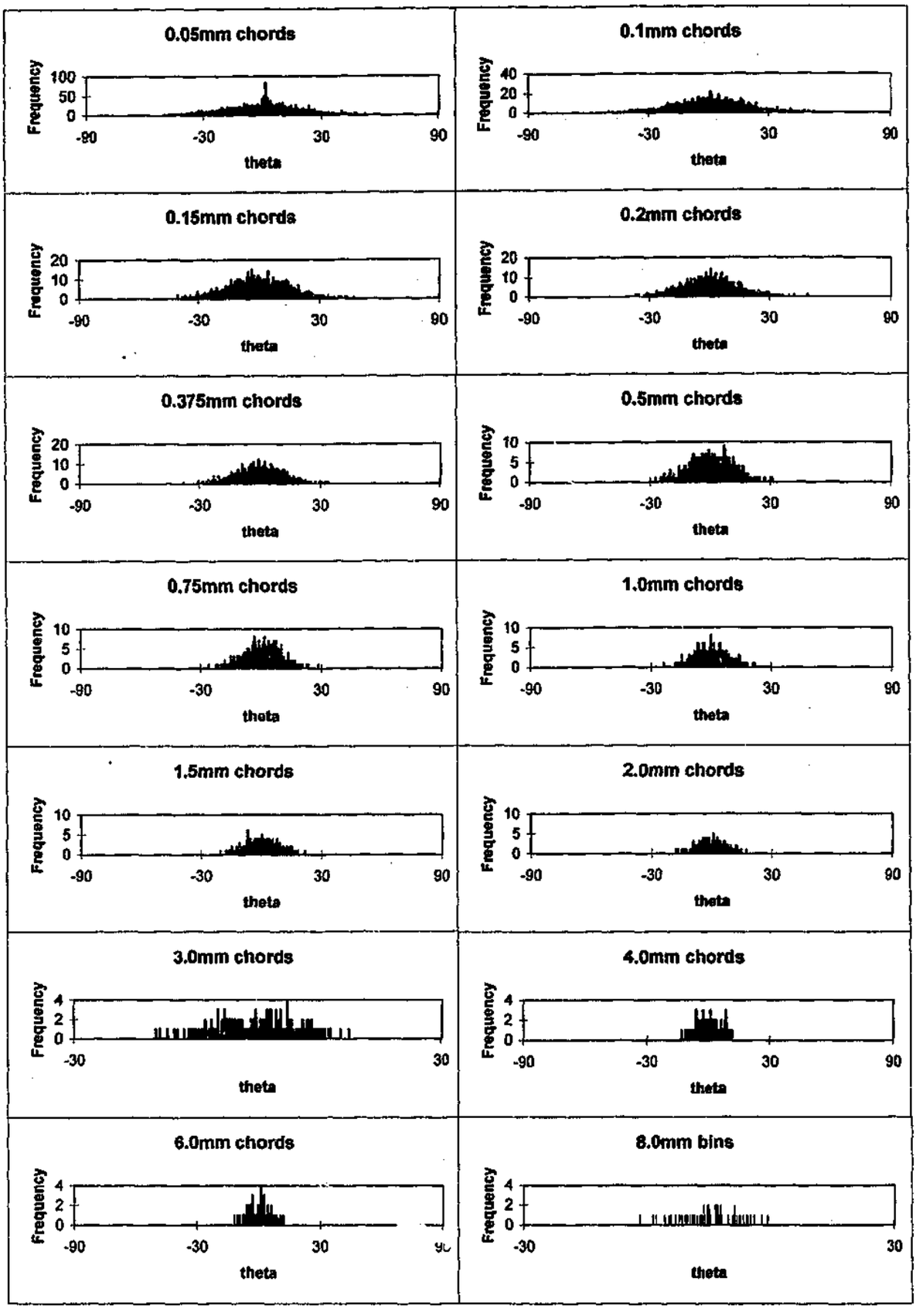

SILTSTONE BEDDING JOINT 1 - *profile k, 0.1deg bins*

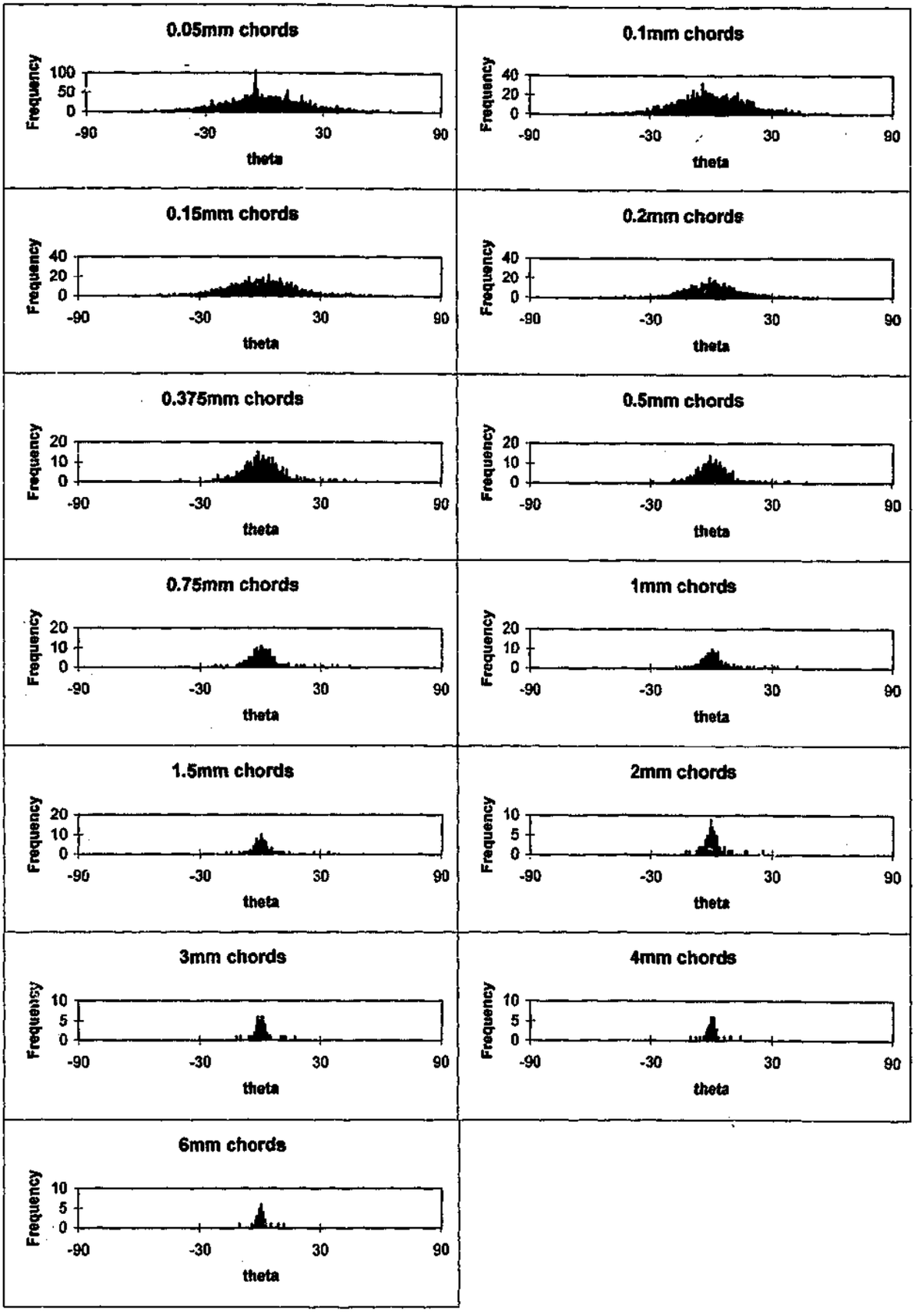

SILTSTONE JOINT 1 - profile e, 0.1deg bins

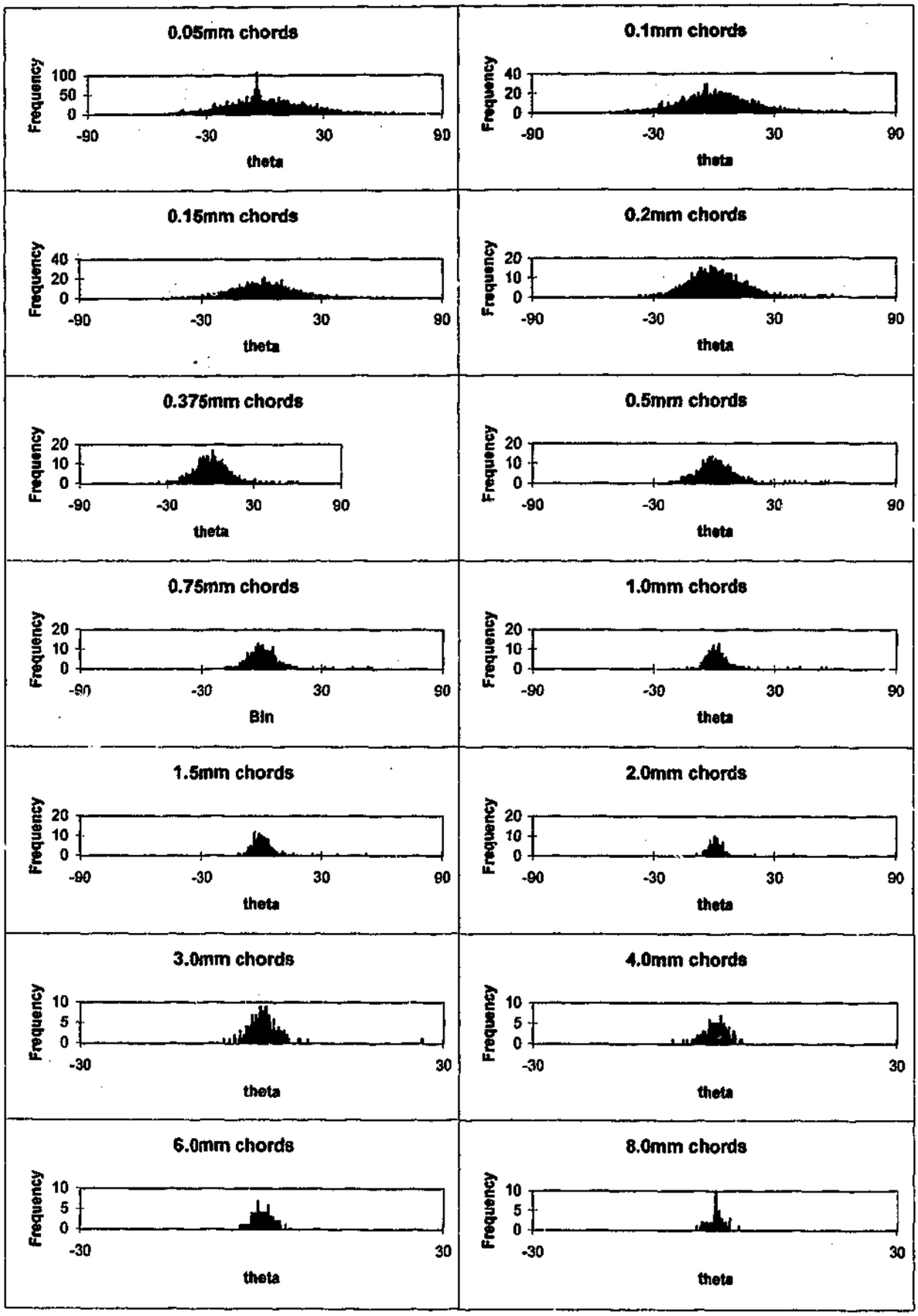

SILTSTONE JOINT 1 - profile f, 0.1deg bins

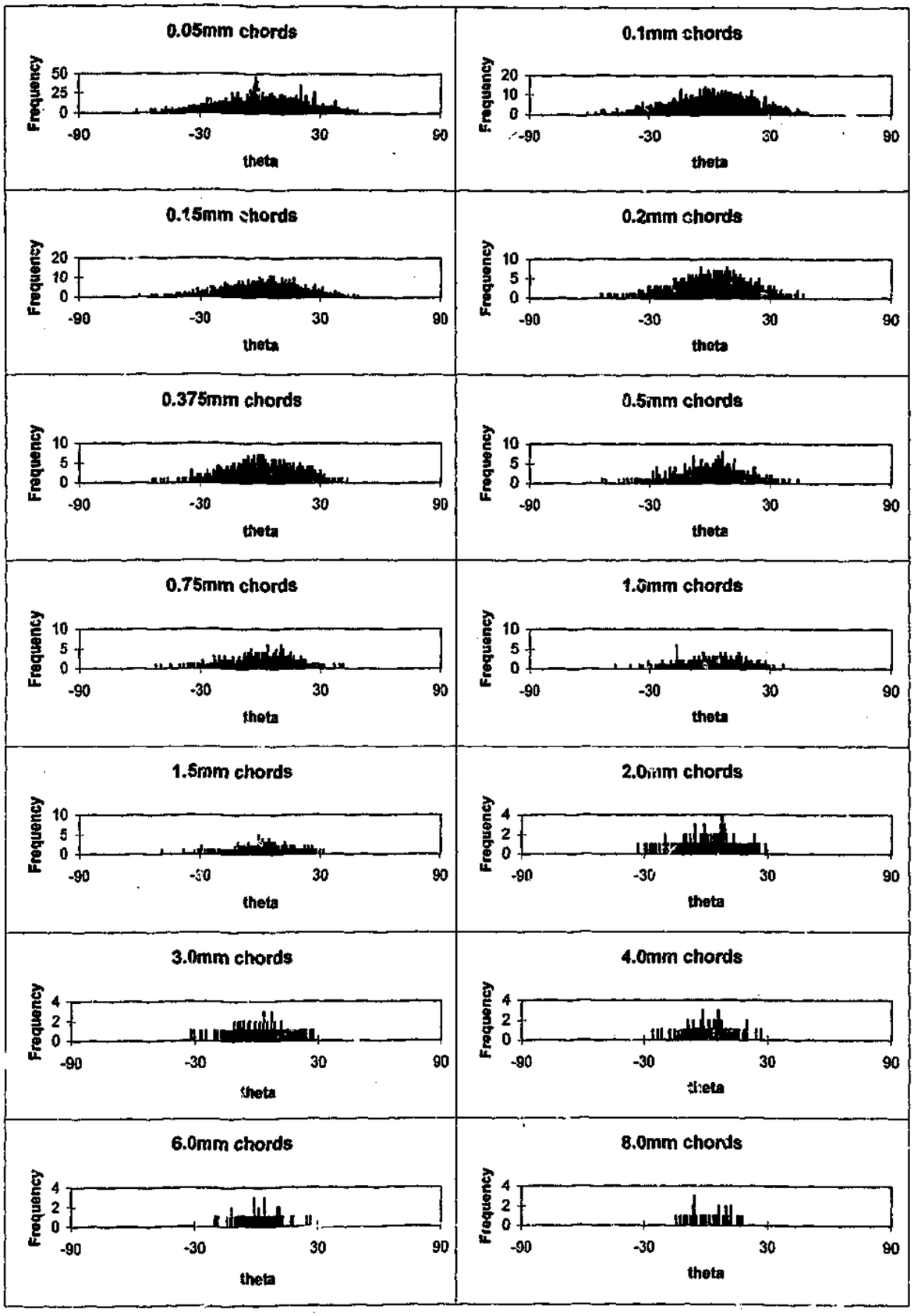

BASALT JOINT 1a - profile f, 0.1deg bins

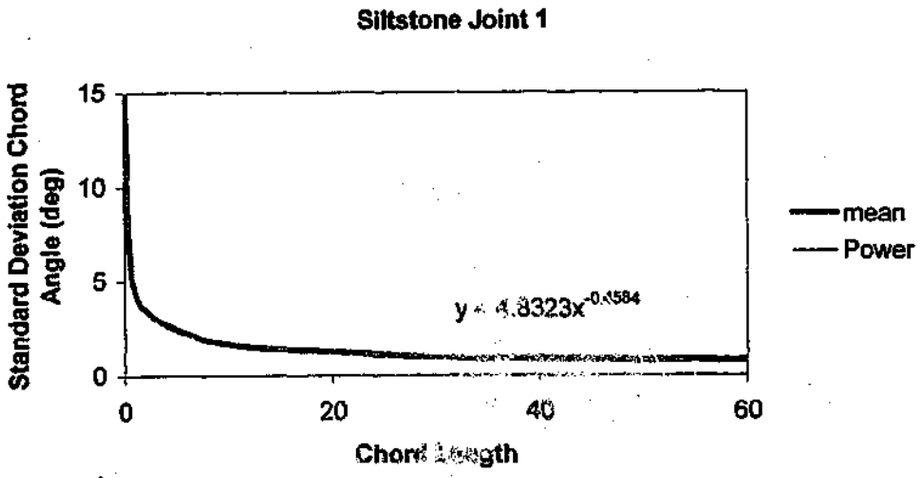

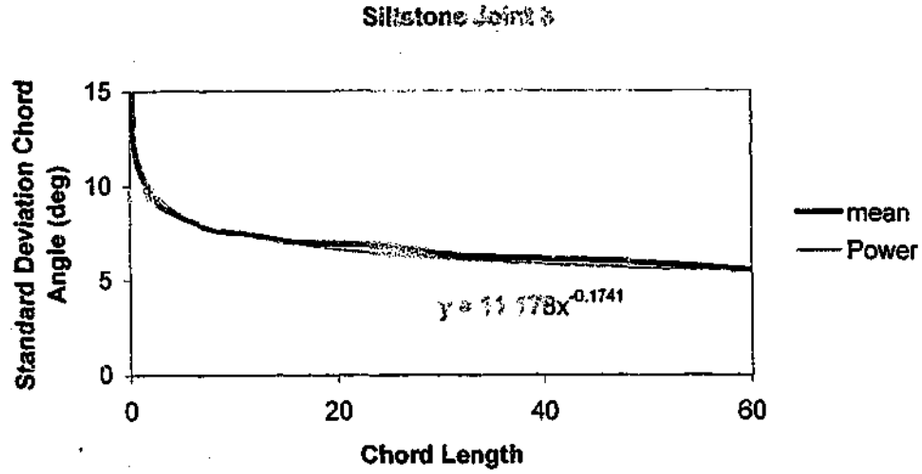

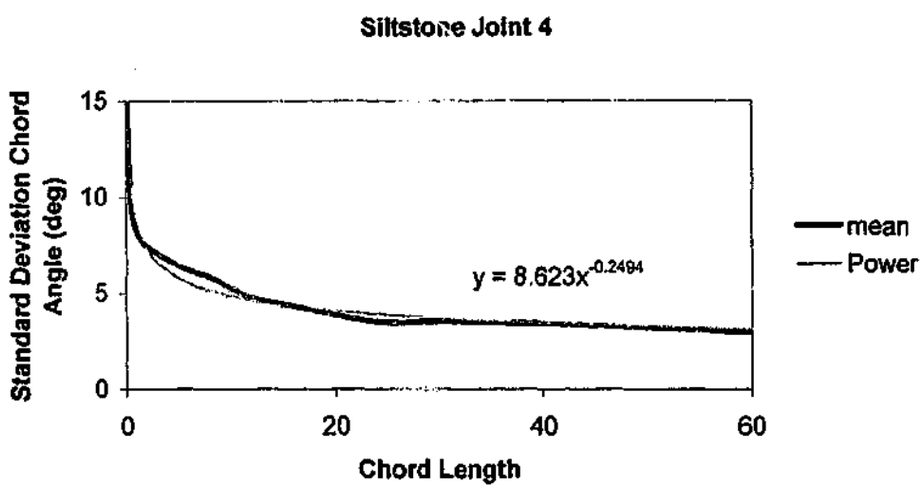

Natural Siltstone Joints - Mean Standard Deviation of Chord Angle Statistics Described by a Power Function

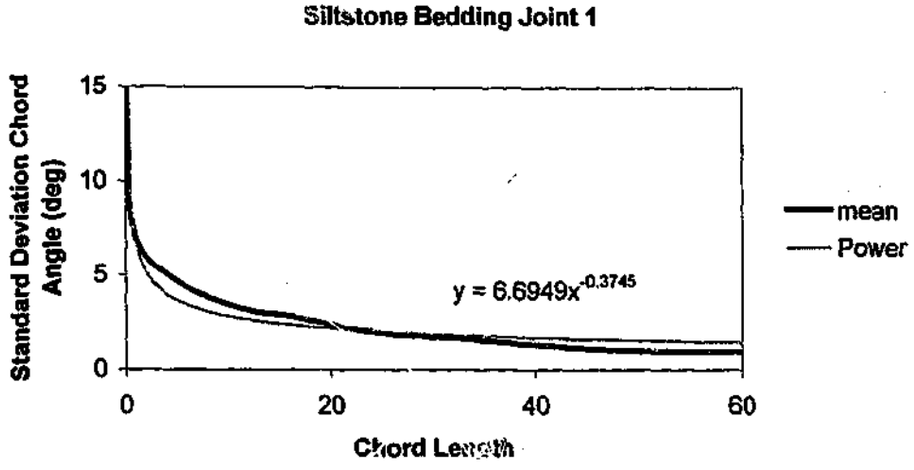

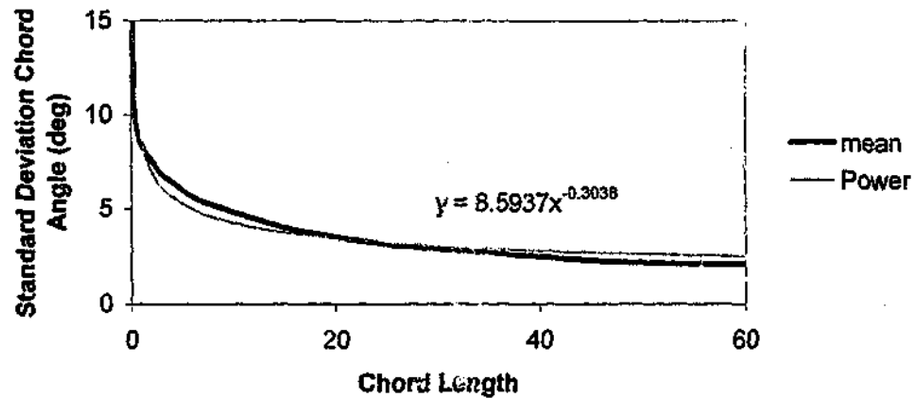

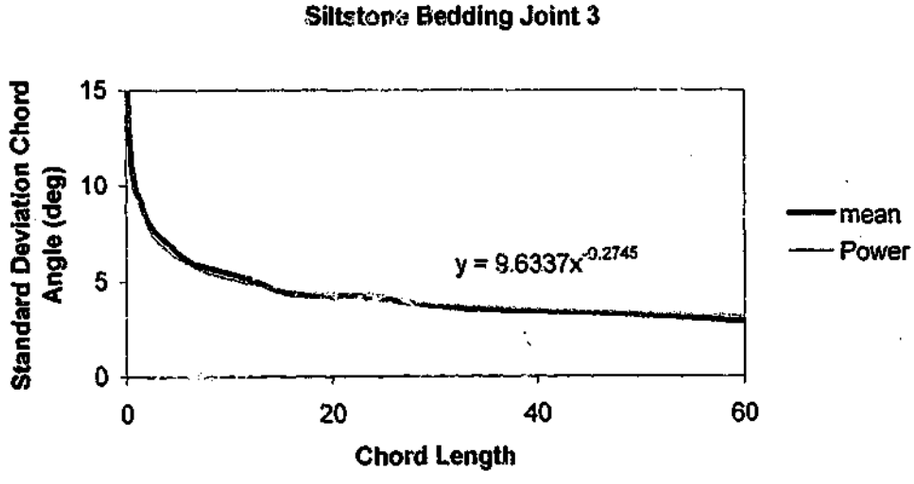

Natural Siltstone Bedding Joints - Mean Standard Deviation of Chord Angle Statistics Described by a Power Function

Basalt Joint 1

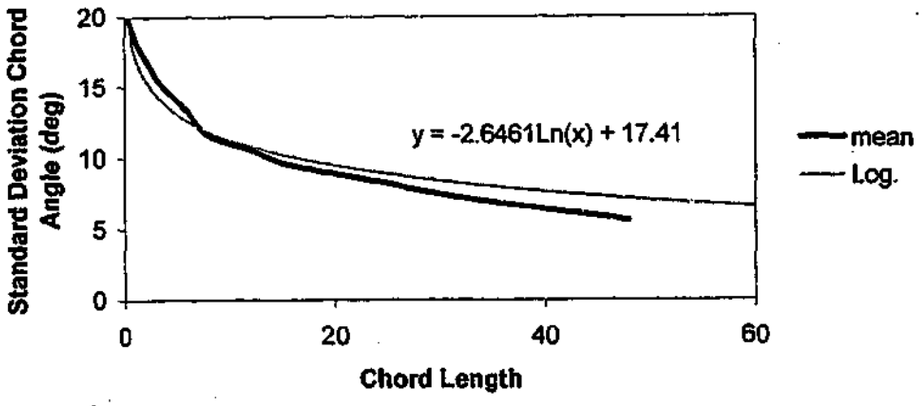

Basalt Joint 1a

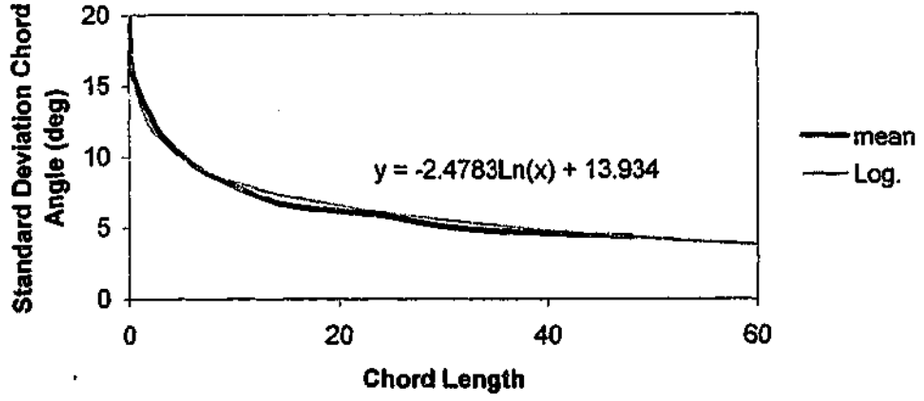

Basalt Joint 2

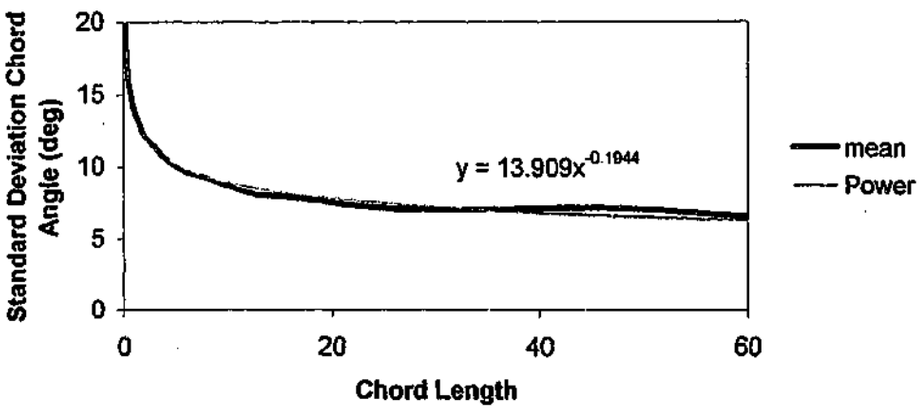

Natural Basalt Joints - Mean Standard Deviation of Chord

Angle Statistics Described by a Power or Logarithmic Function

Basalt Joint 3

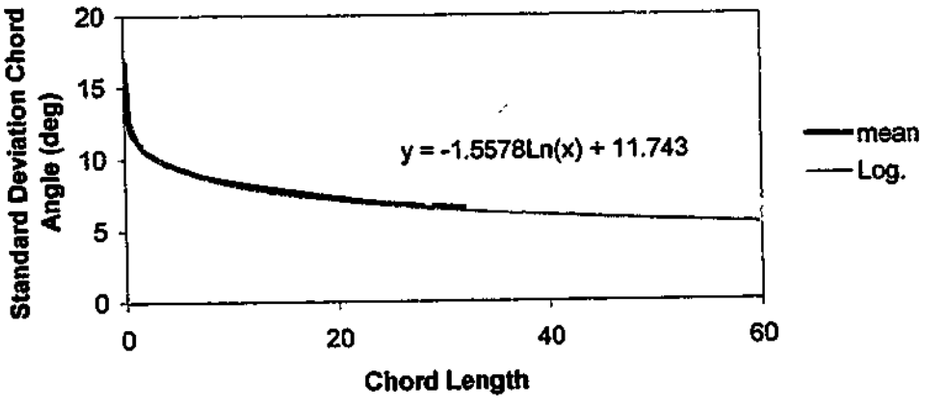

Basalt Joint 4

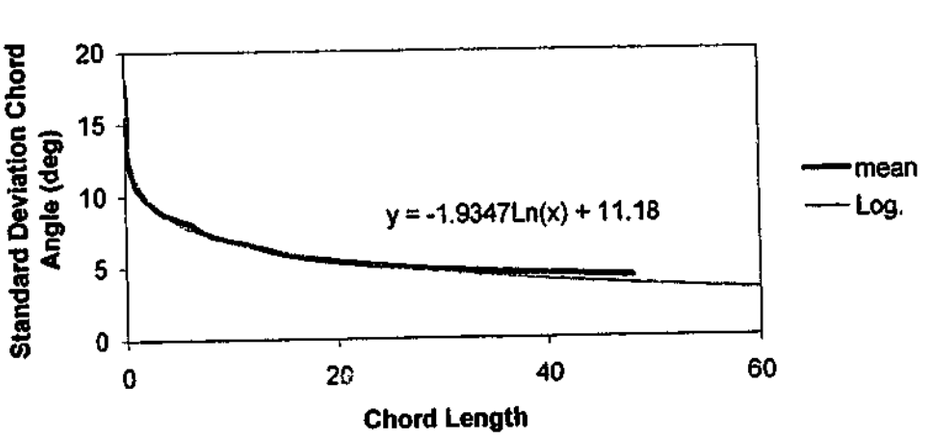

Basalt Joint 5

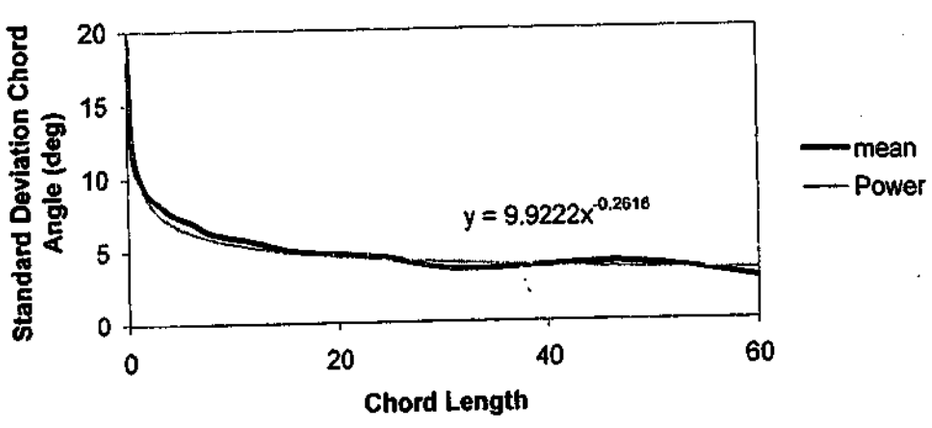

Natural Basalt Joints - Mean Standard Deviation of Chord Angle Statistics Described by a Power or Logarithmic Function

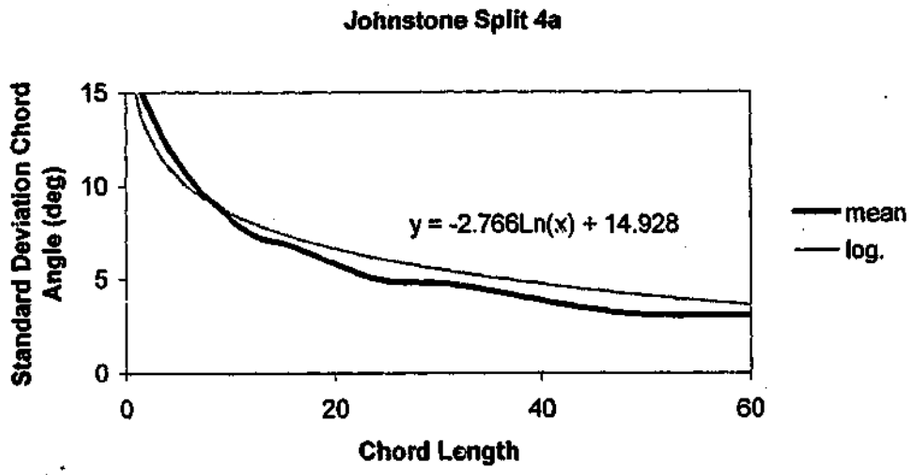

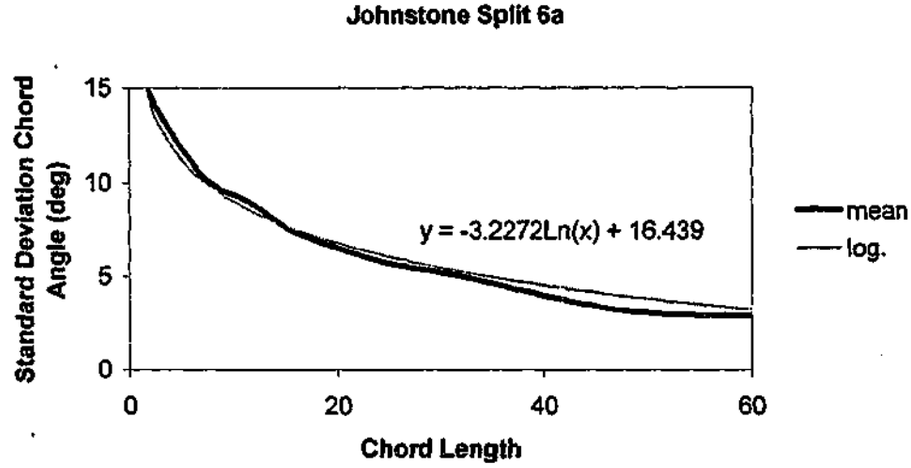

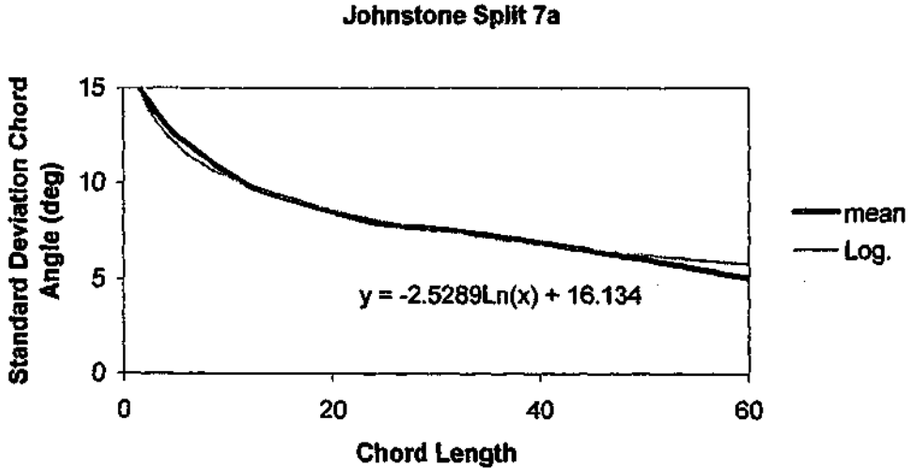

Johnstone Split Surfaces - Mean Standard Deviation of Chord Angle Statistics Described by a Logarithmic Function

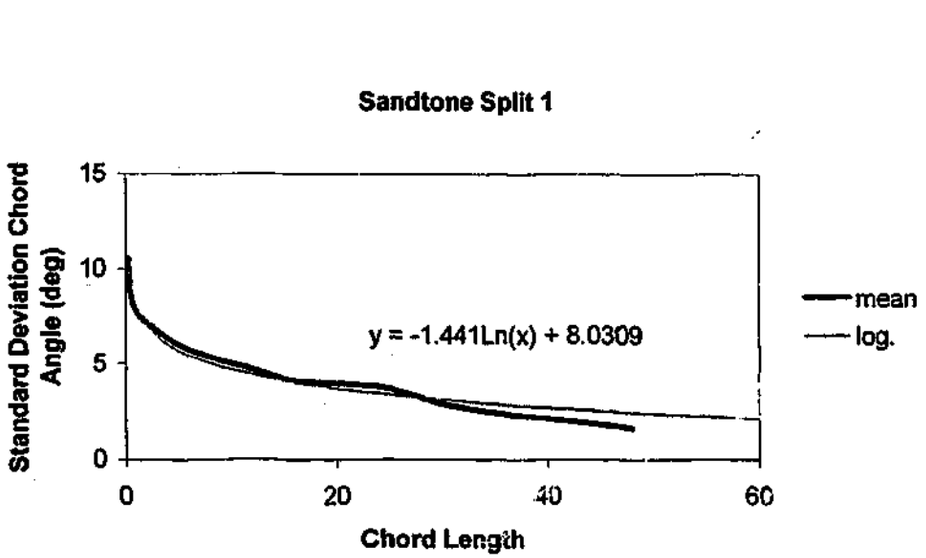

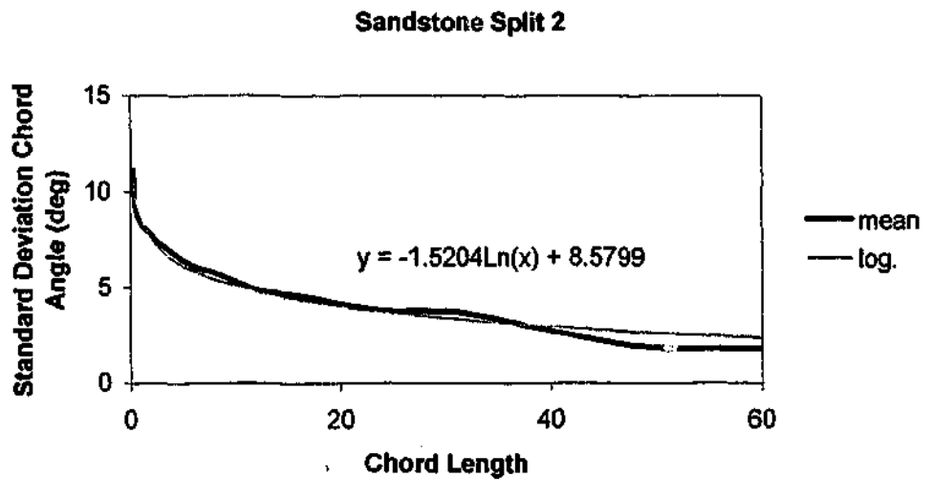

Sandstone Split Surfaces - Mean Standard Deviation of

Chord Angle Statistics Described by a Logarithmic Function

Siltstone Split 1

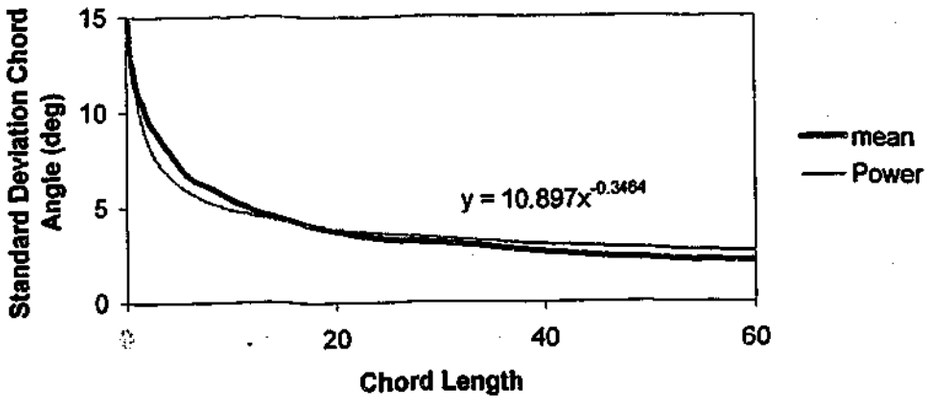

Siltstone Split 2

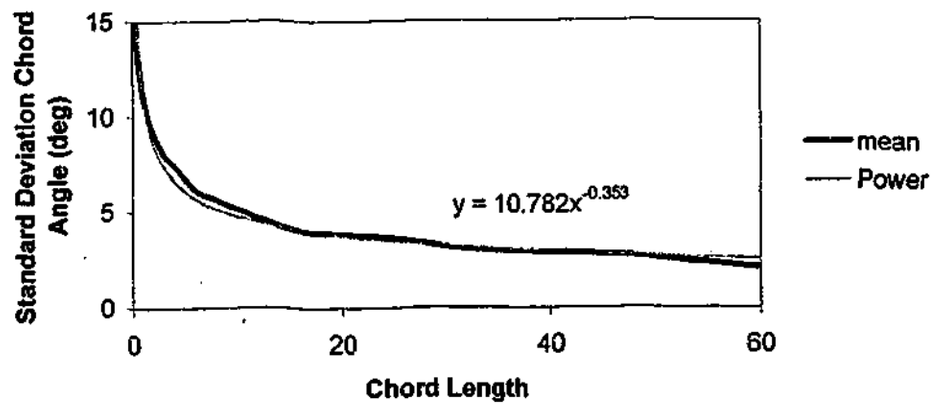

Siltstone Split 3

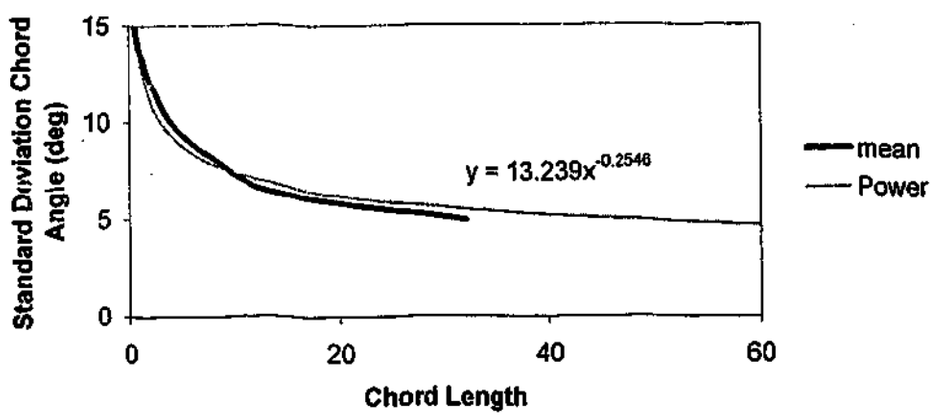

Siltstone Split Surfaces - Mean Standard Deviation of Chord Angle Statistics Described by a Power Function

Basalt Split 1

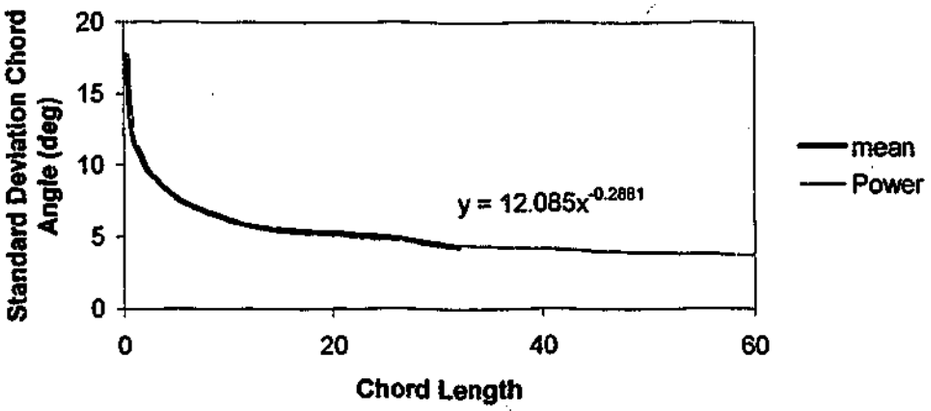

Basalt Split 2

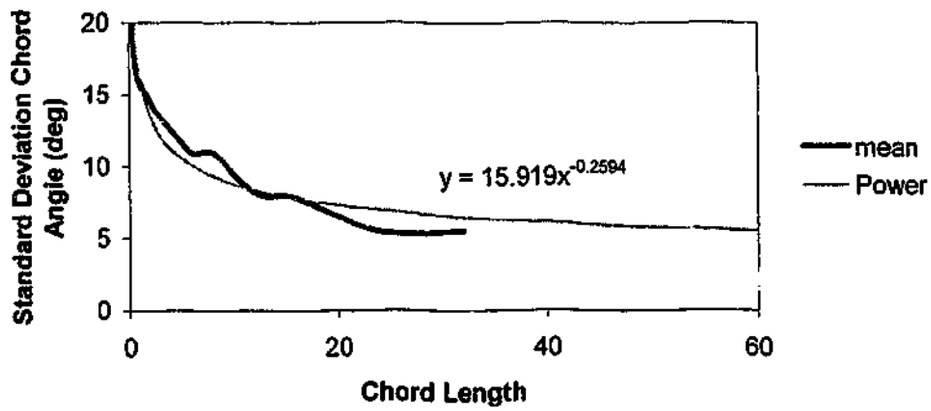

Basalt Split 3

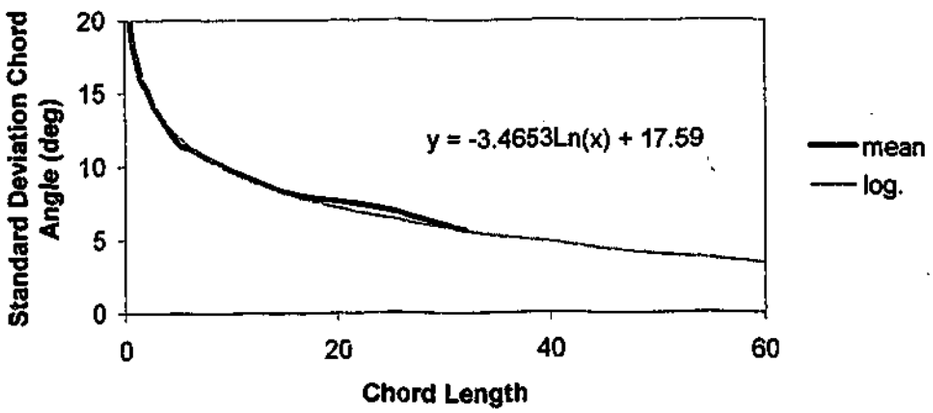

Basalt Split Surfaces - Mean Standard Deviation of Chord Angle Statistics Described by a Logarithmic or Power Function

Granite Split 1

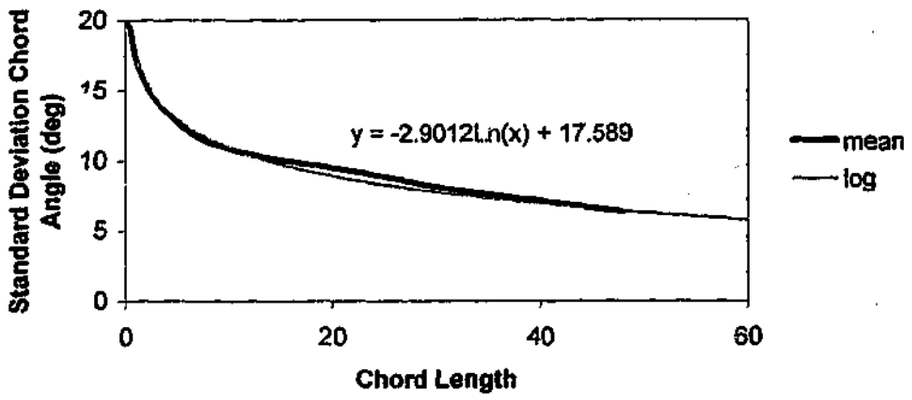

Granite Split 2

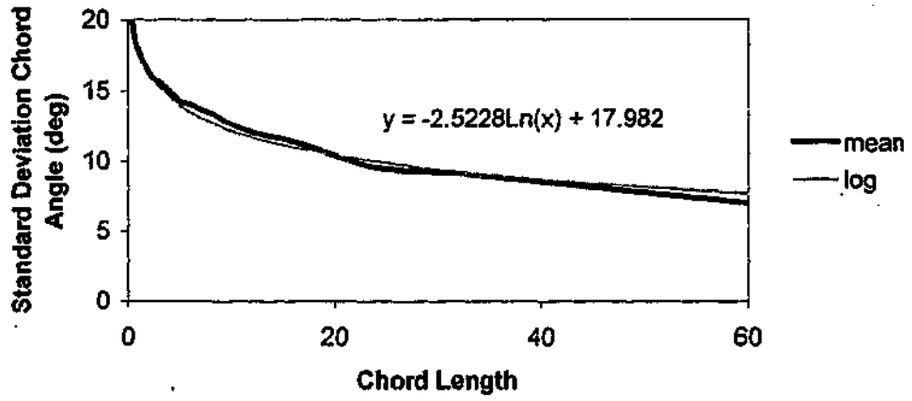

Granite Split 4

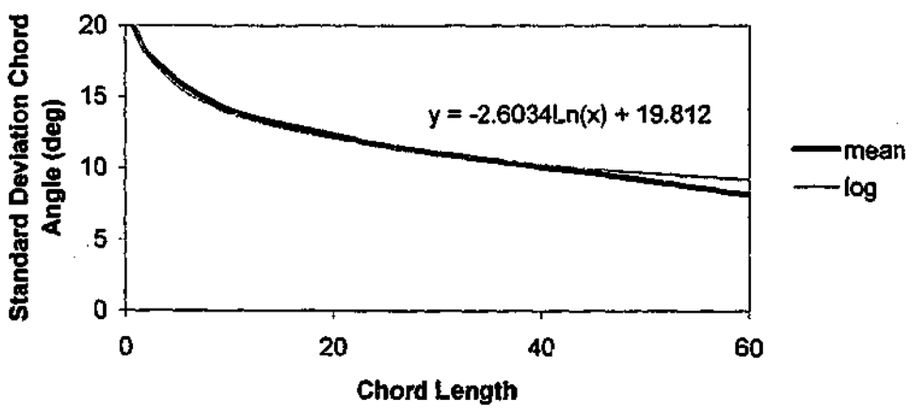

Granite Split Surfaces - Mean Standard Deviation of Chord Angle Statistics Described by a Logarithmic Function

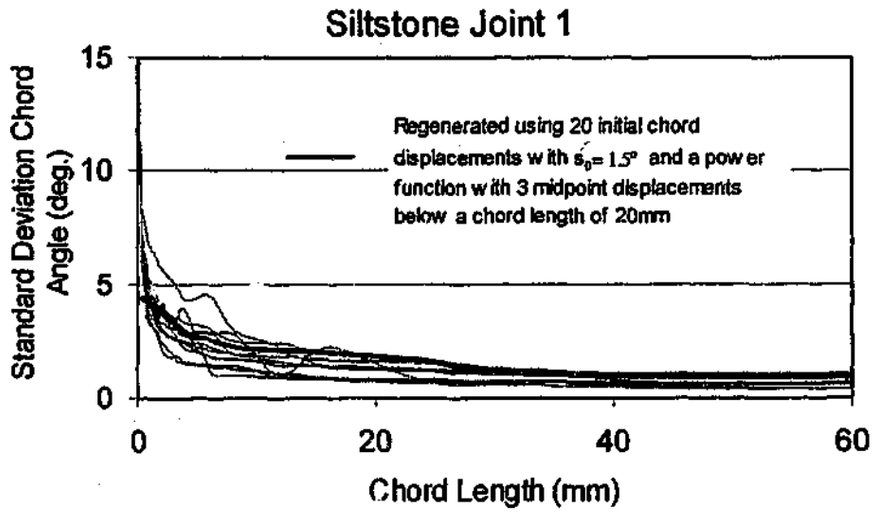

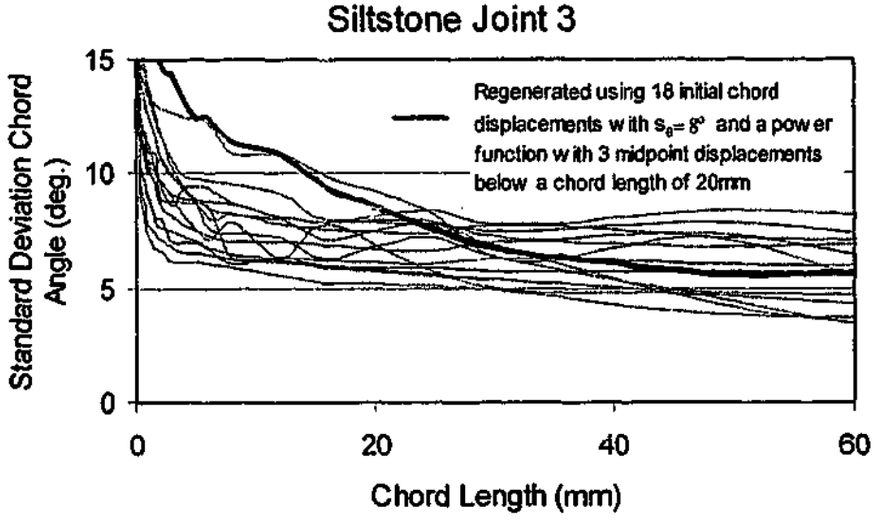

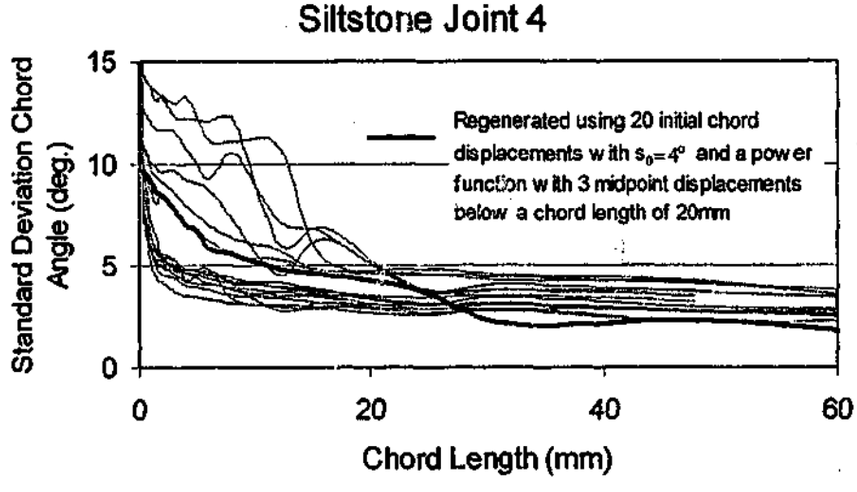

Natural Siltstone Joints - Mean Standard Deviation of Chord Angle Statistics Used to Regenerate Profile

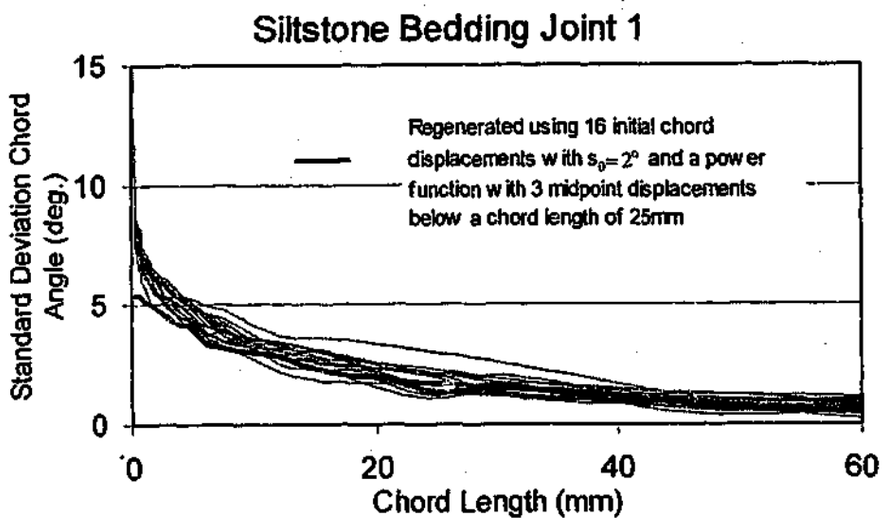

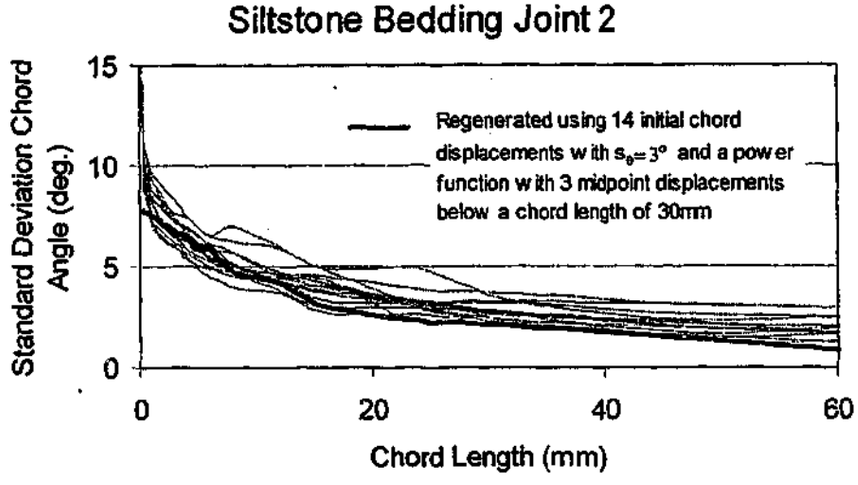

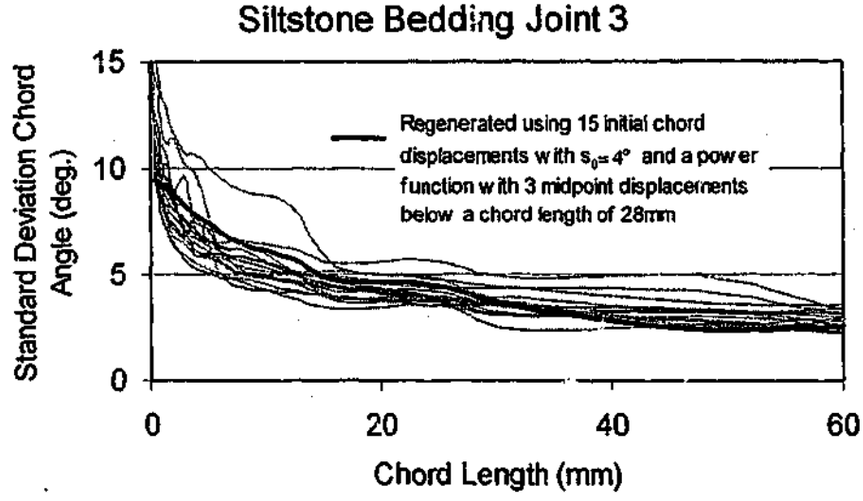

Natural Siltstone Bedding Joints - Mean Standard Deviation of Chord Angle Statistics Used to Regenerate Profile

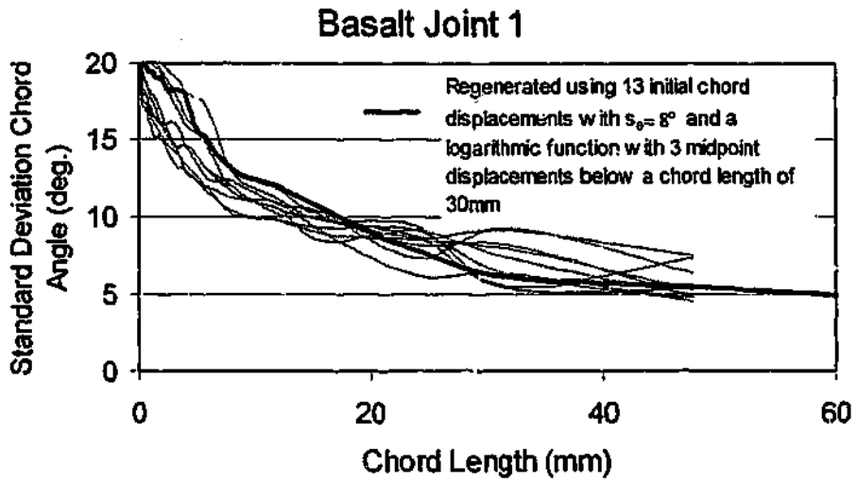

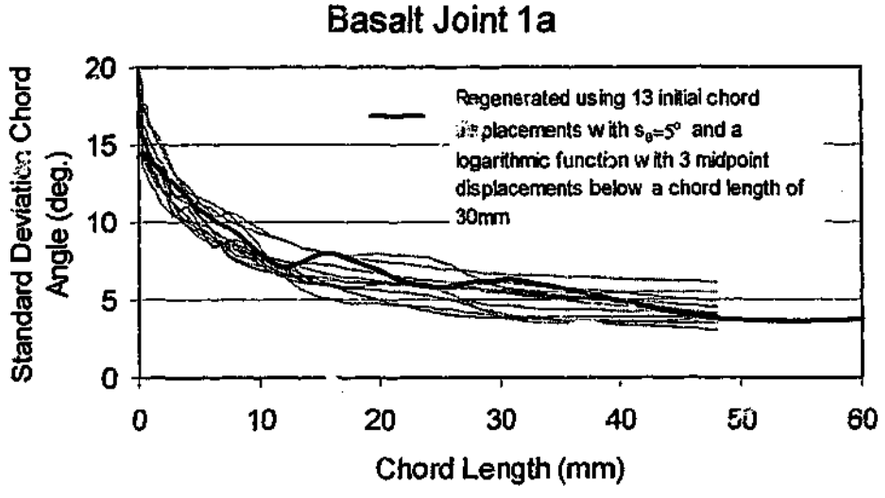

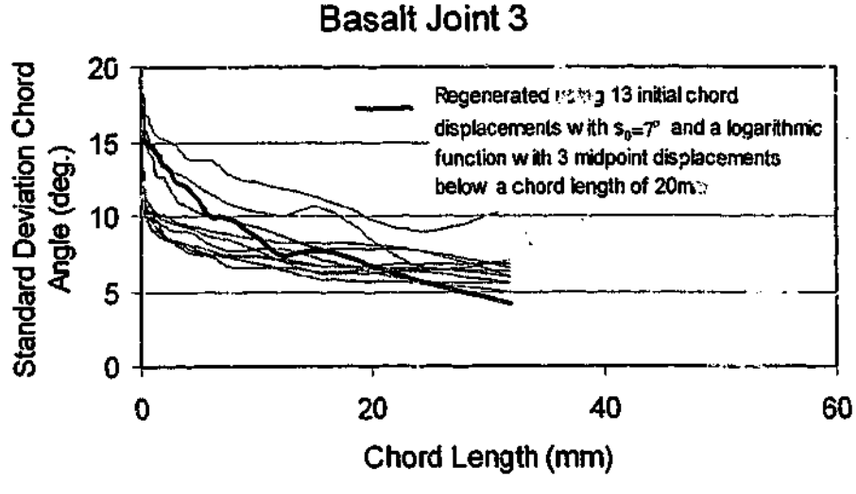

Natural Basalt Joints - Mean Standard Deviation of Chord

Angle Statistics Used to Regenerate Profile

APPENDIX F

PREDICTIONS OF JOINT SHEAR BEHAVIOUR

Table of Contents – Appendix F

Johnstone Direct Shear Test Predictions

In this section the predictions produced using the program Rocket are compared with direct shear tests conducted on Johnstone samples. The prediction have been presented in 4 graphs :

- shear stress vs. shear displacement
- shear stress vs. normal stress
- dilation vs. shear displacement
- normal stress vs. shear displacement

The shear and normal stress values are average stress values calculated for the contacting area of the surface. Each graph shows the laboratory test results together with one prediction if the profile has a single chord length, or three predictions at different chord lengths for irregular profiles. As shown in Figure 9.1, when three predictions at different chord lengths are used, an envelope of shear response can be drawn onto the graph. For visual simplicity this envelope has not been drawn on the graphs in the appendix.

The following parameters were used in the predictions:

Parameter	Adopted value
Young's Modulus	900MPa
Poisson's Ratio	0.25
Intact Friction Angle Batch 1	35°
Intact Friction Angle Batch 2	34°
Residual Friction Angle	24.5°
Cohesion Batch 1	1500kPa
Cohesion Batch 2	1050kPa
Joint Normal Stiffness – water-jet surface	6.0MPa/mm
Joint Normal Stiffness – split surface	5.4MPa/mm
Failure Stress	1.38 * Sokolovsky failure stress

Johnstone Fractal Profile JF8_12 Prediction of Shear Response

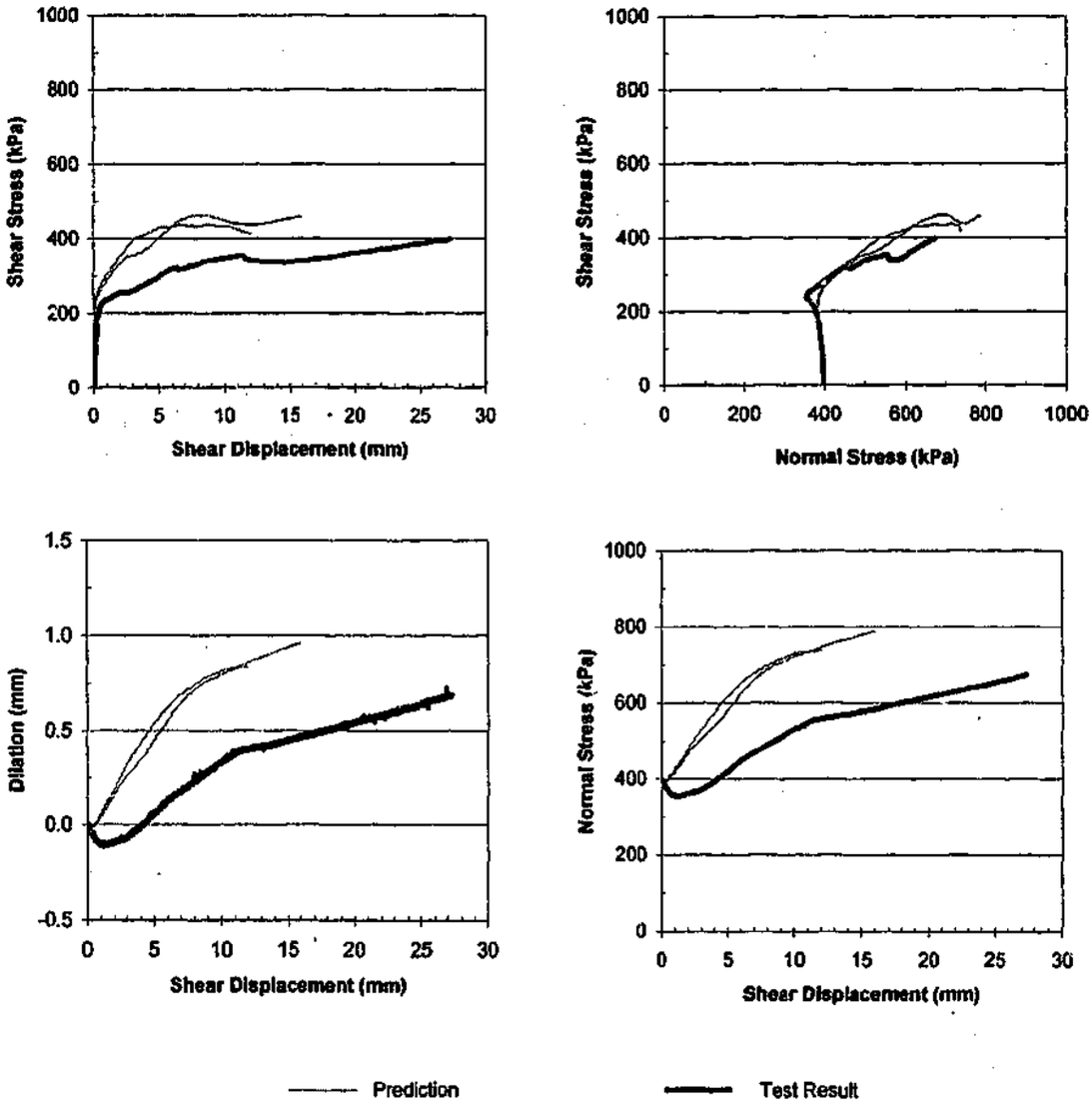

Sample : JF8_12

Sokolovsky Factor = 1.38

Johnstone Batch 2

Initial Normal Stress (kPa): 400

Normal Stiffness (kPa/mm): 400

Chord Lengths Used For Predictions : 12mm, 16mm

Johnstone Fractal Profile JF12_3 Prediction of Shear Response

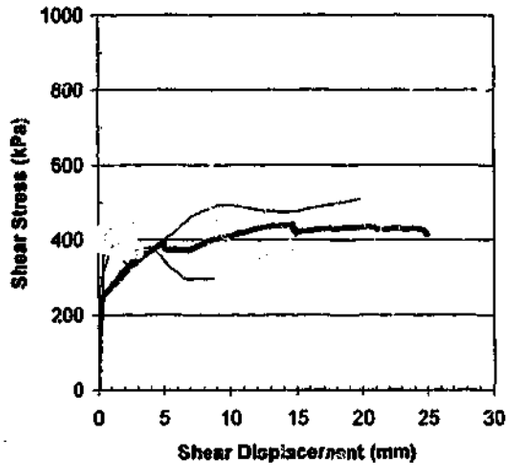

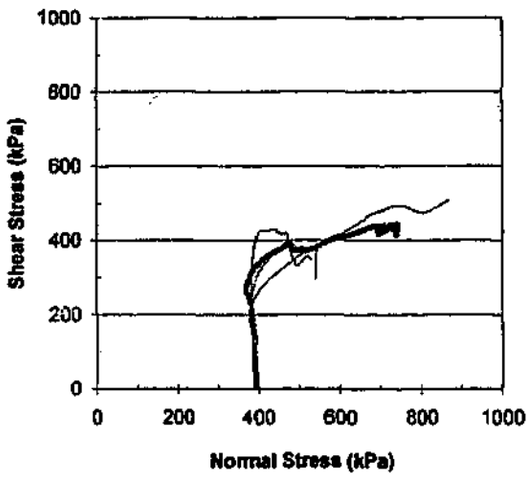

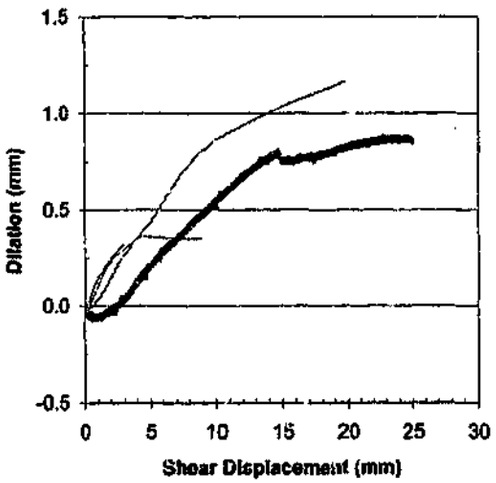

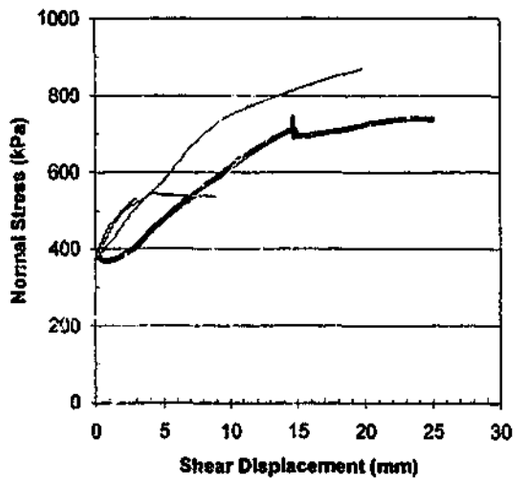

Prediction Test Result

Sample : JF12_3

Sokolovsky Factor = 1.38

Johnstone Batch 2

Initial Normal Stress (kPa): 400

Normal Stiffness (kPa/mm): 400

Chord Lengths Used For Predictions : 3mm, 9mm, 20mm

Johnstone Fractal Profile JF15a_3 Prediction of Shear Response

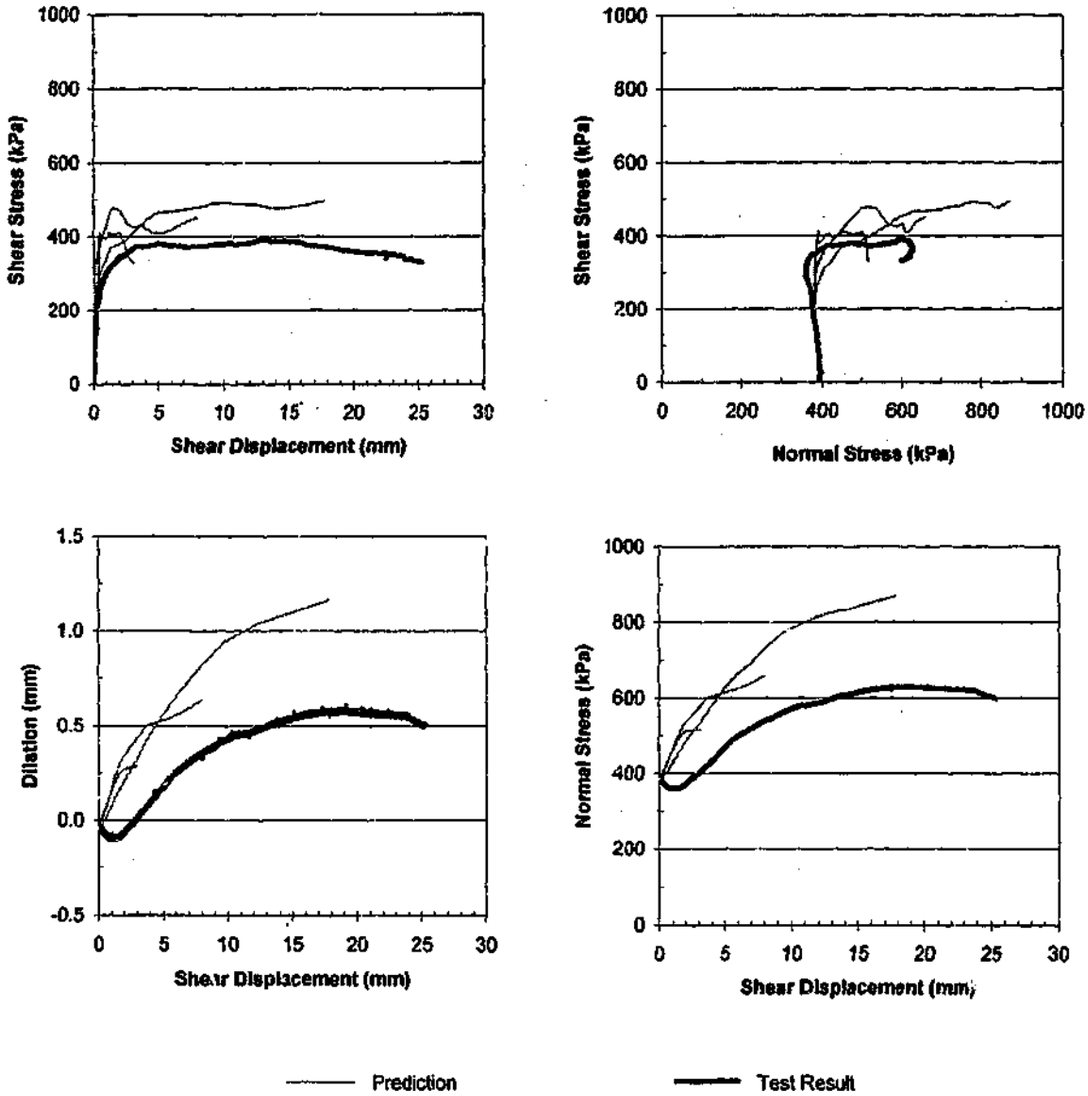

Sample : JF15a_3

Sokolovsky Factor = 1.38

Johnstone Batch 2

Initial Normal Stress (kPa): 400

Normal Stiffness (kPa/mm): 400

Chord Lengths Used For Predictions : 3.1mm, 8mm, 18mm

Johnstone Fractal Profile JF15_3 Prediction of Shear Response

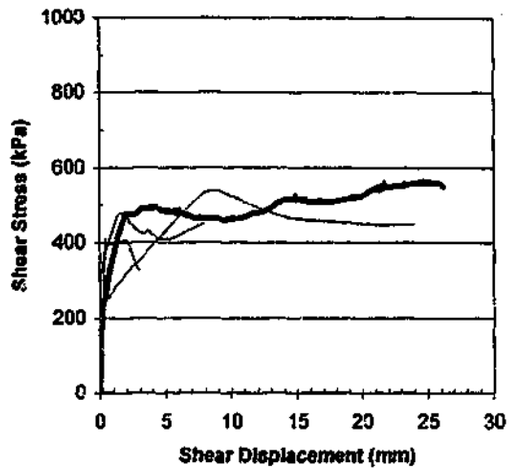

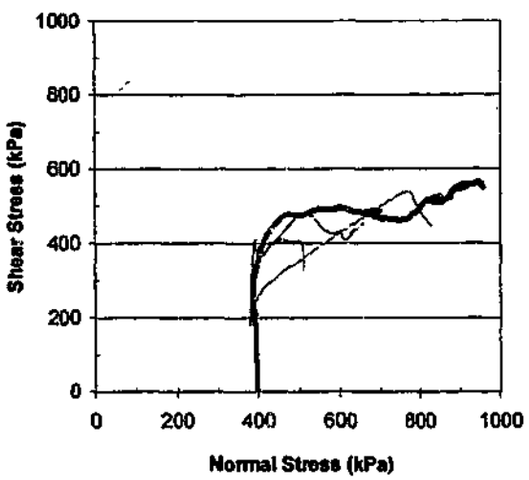

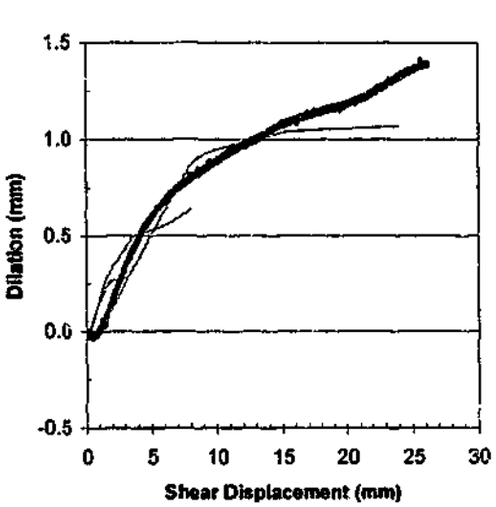

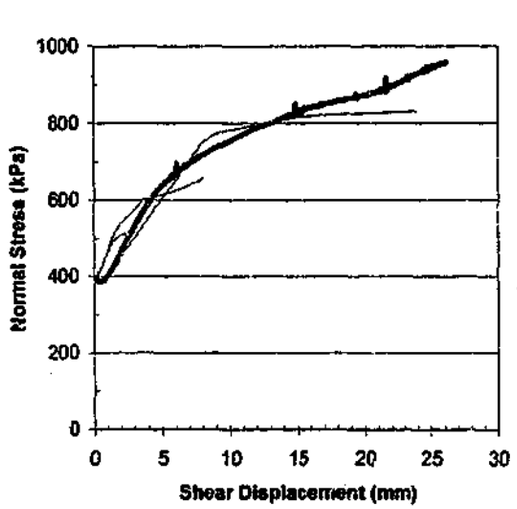

Prediction — Test Result

Sample : JF15_3

Sokolovsky Factor = 1.39

Johnstone Batch 3

Initial Normal Stress (kPa): 400

Normal Stiffness (kPa/mm): 400

Chord Lengths Used For Predictions : 3mm, 8mm, 24mm

Johnstone Fractal Profile JF21_3 Prediction of Shear Response

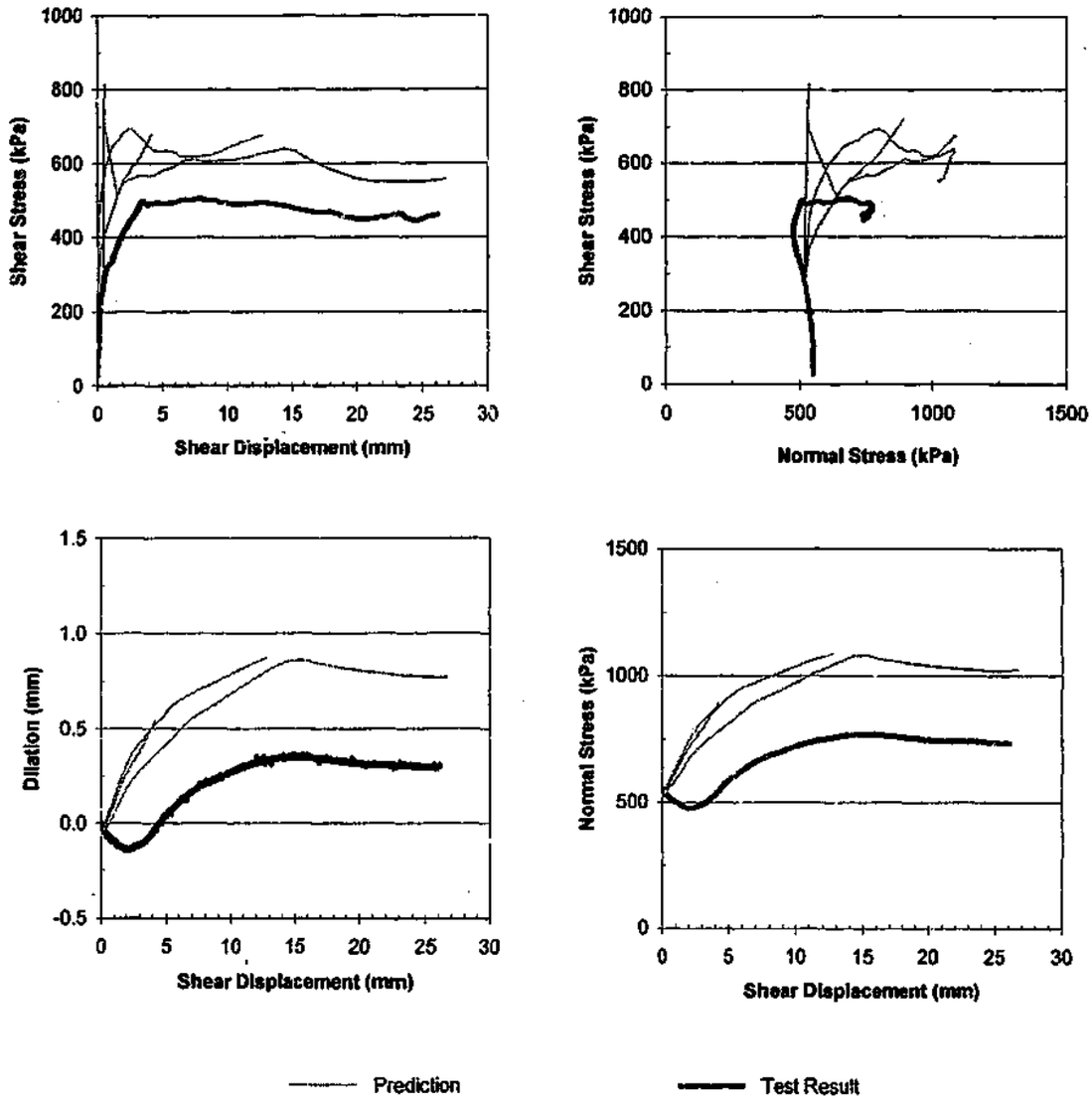

Sample : JF21_3

Sokolovsky Factor = 1.38

Johnstone Batch 2

Initial Normal Stress (kPa): **560**

Normal Stiffness (kPa/mm): **600**

Chord Lengths Used For Predictions : 4.3mm, 13mm, 27mm

Johnstone Split Surface JS_1a Prediction of Shear Response

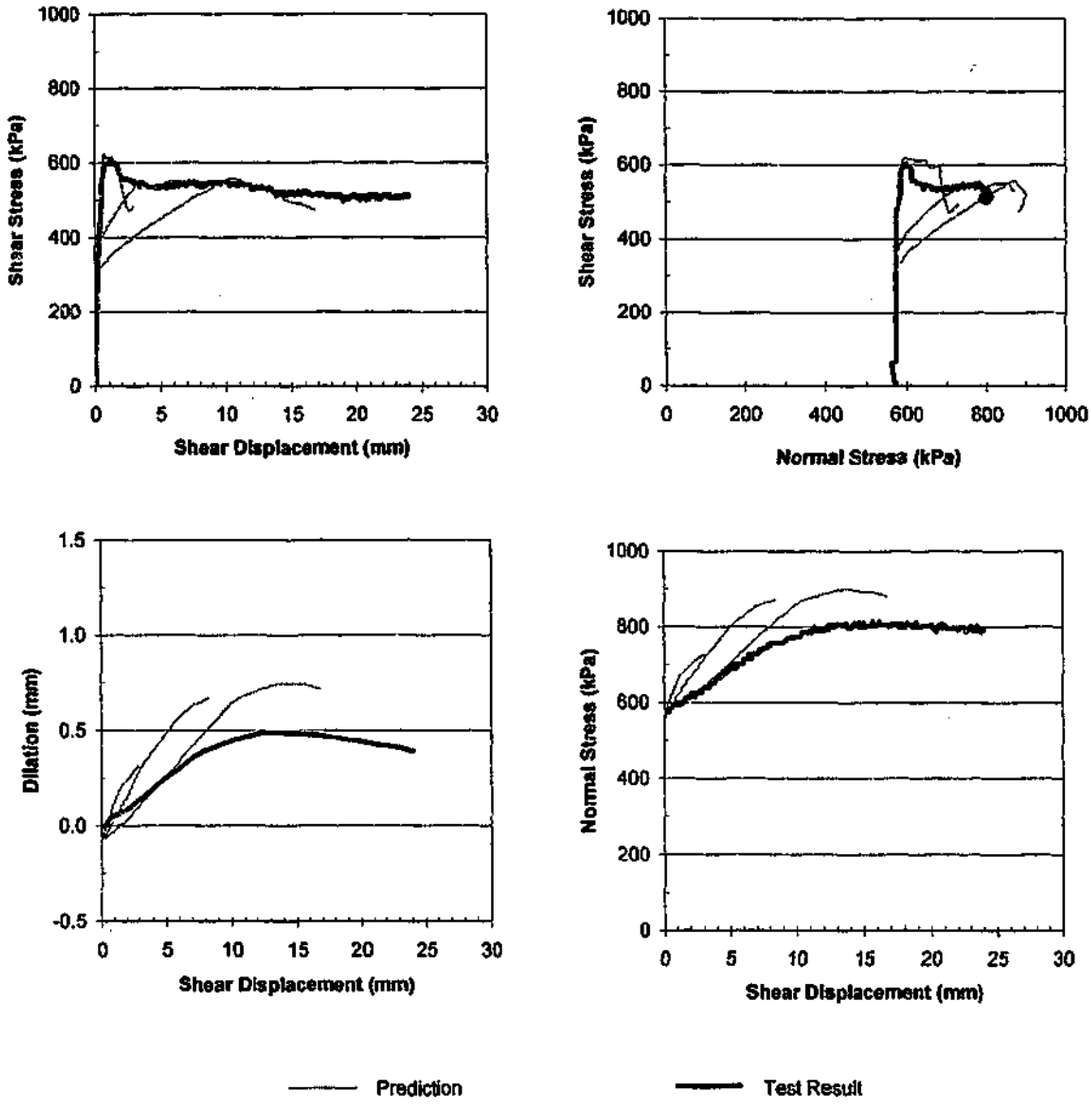

Sample : JS_1a

Sokolovsky Factor = 1.38

Johnstone Batch 1

Initial Normal Stress (kPa): **600**

Normal Stiffness (kPa/mm): **400**

Chord Lengths Used For Predictions : 3mm, 8.5mm, 17mm

Johnstone Split Surface JS_1b Prediction of Shear Response

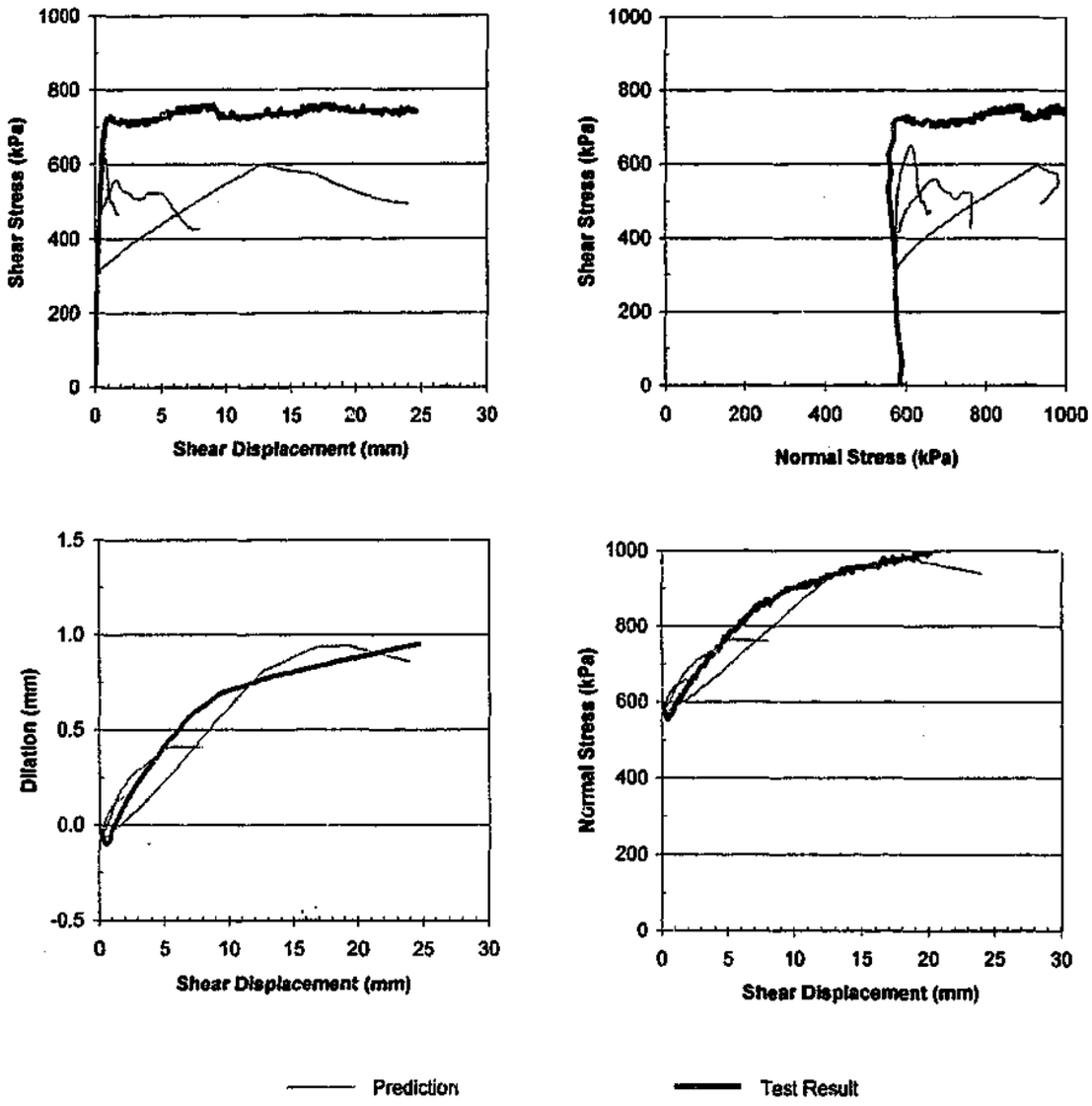

Sample : JS_1b

Sokolovsky Factor = 1.38

Johnstone Batch 1

Initial Normal Stress (kPa): 600

Normal Stiffness (kPa/mm): 400

Chord Lengths Used For Predictions : 1.9mm, 8mm, 24mm

Johnstone Split Surface JS_2a Prediction of Shear Response

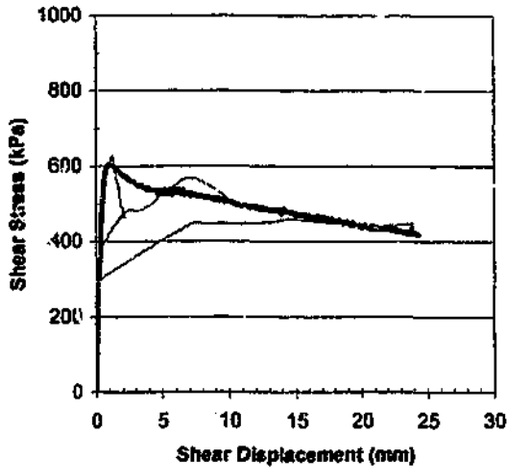

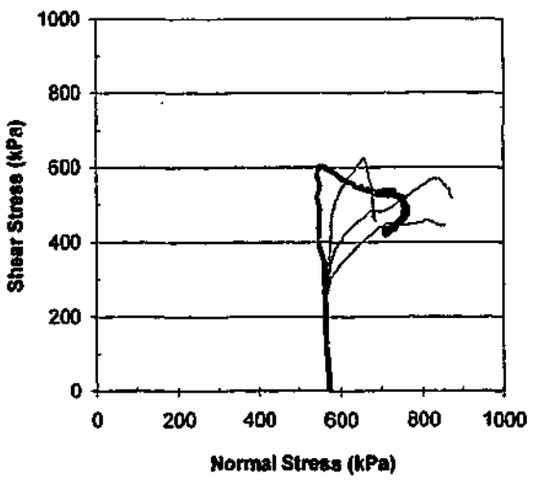

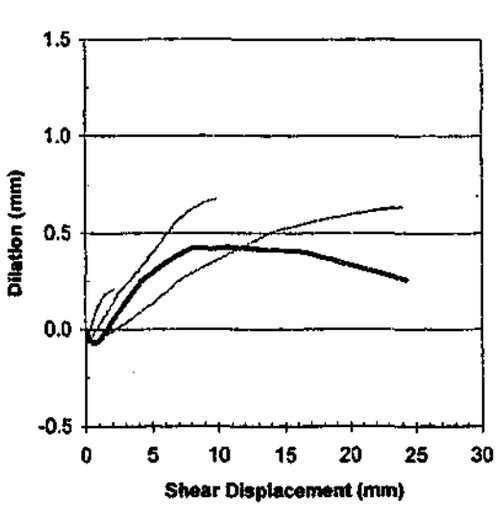

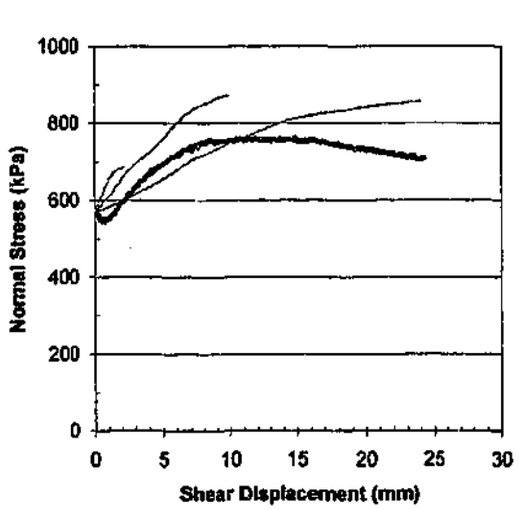

Prediction — Test Result

Sample : JS_2a

Sokolovsky Factor = 1.38

Johnstone Batch 1

Initial Normal Stress (kPa): 600

Normal Stiffness (kPa/mm): 400

Chord Lengths Used For Predictions : 2.2mm, 10mm, 24mm

Johnstone Split Surface JS_3a Prediction of Shear Response

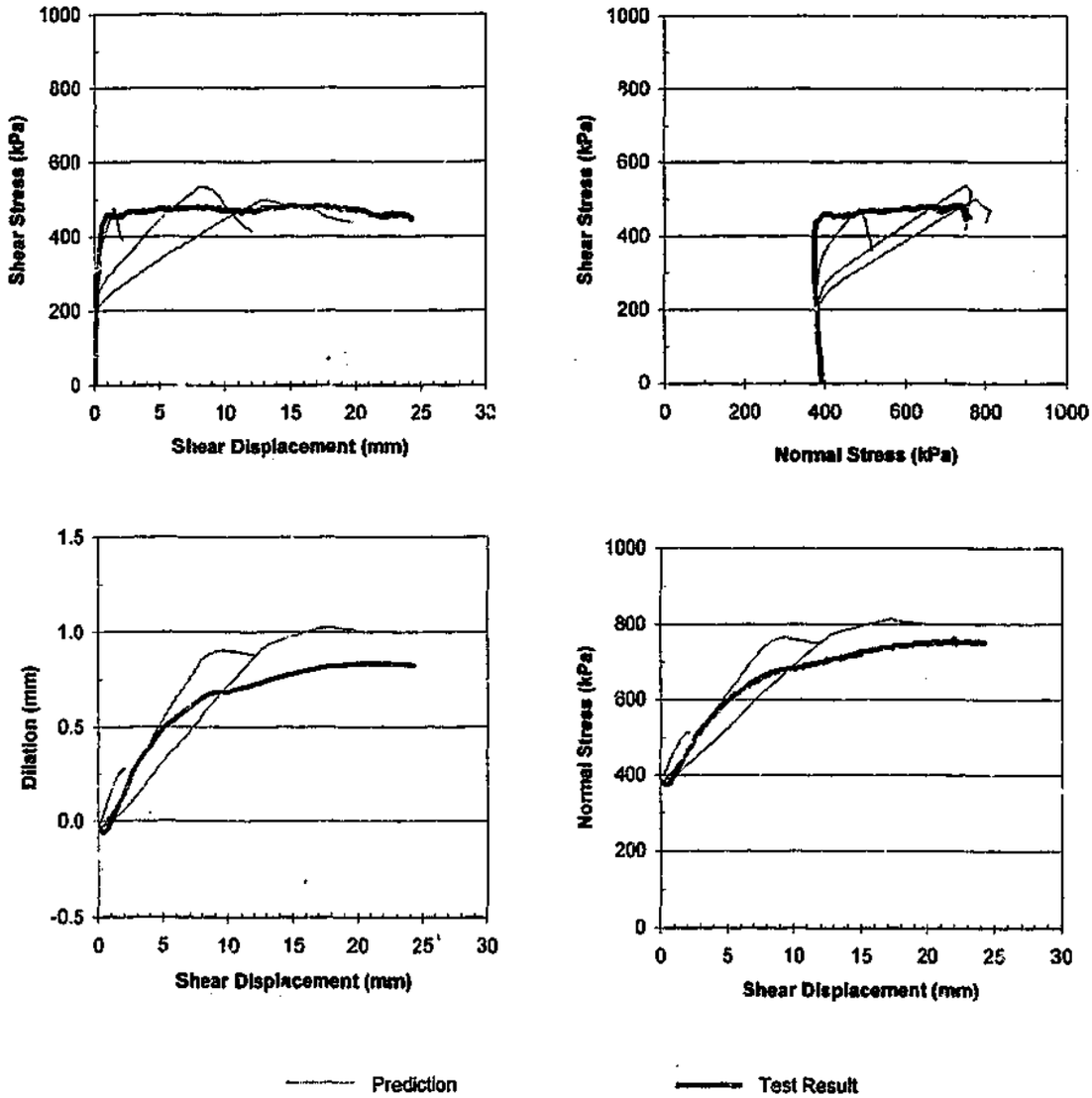

Sample : JS_3a

Sokolovsky Factor = 1.38

Johnstone Batch 1

Initial Normal Stress (kPa): **400**

Normal Stiffness (kPa/mm): **400**

Chord Lengths Used For Predictions : 2.2mm, 12mm, 20mm

Johnstone Split Surface JS_3b Prediction of Shear Response

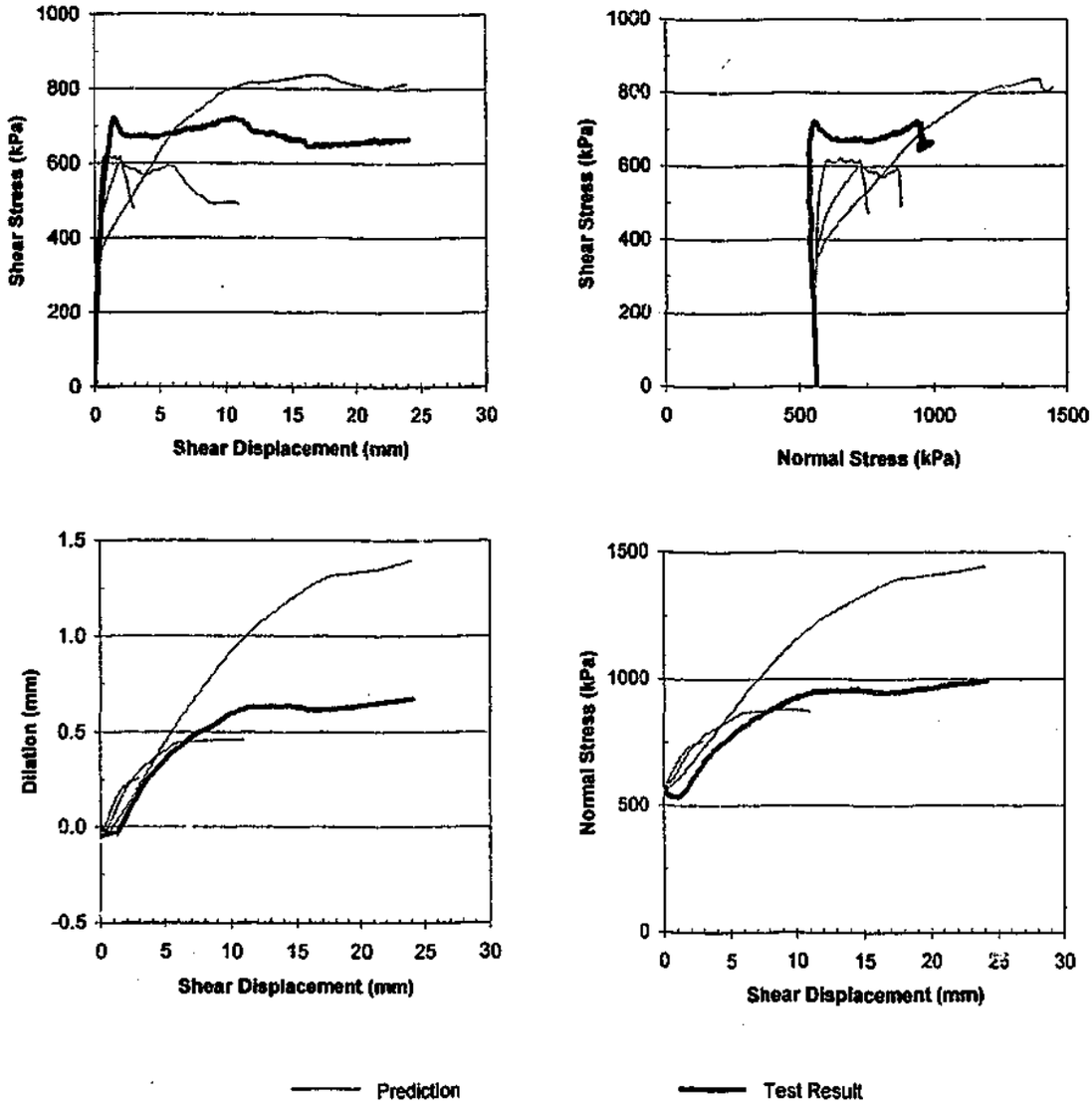

Sample : JS_3b

Sokolovsky Factor = 1.38

Johnstone Batch 1

Initial Normal Stress (kPa): **560**

Normal Stiffness (kPa/mm): **600**

Chord Lengths Used For Predictions : 3mm, 11mm, 24mm

Johnstone Split Surface JS_4a Prediction of Shear Response

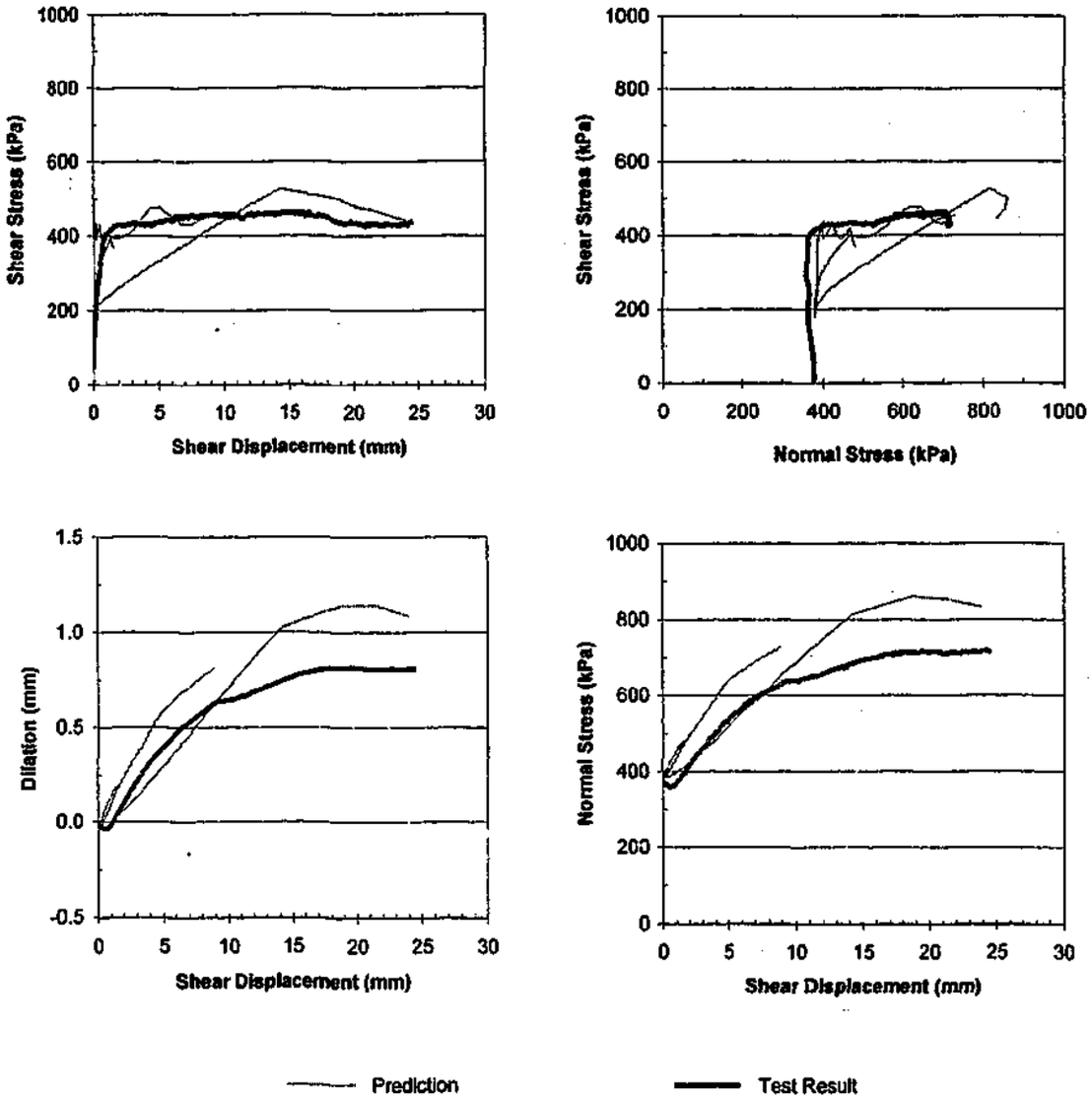

Sample : JS_4a

Sokolovsky Factor = 1.38

Johnstone Batch 1

Initial Normal Stress (kPa): 400

Normal Stiffness (kPa/mm): 400

Chord Lengths Used For Predictions : 1.6mm, 9mm, 24mm

Johnstone Split Surface JS_6a Prediction of Shear Response

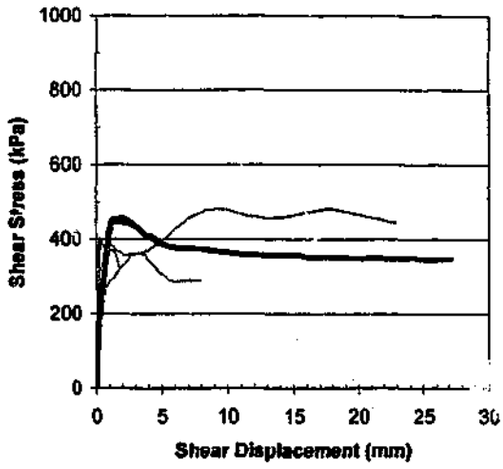

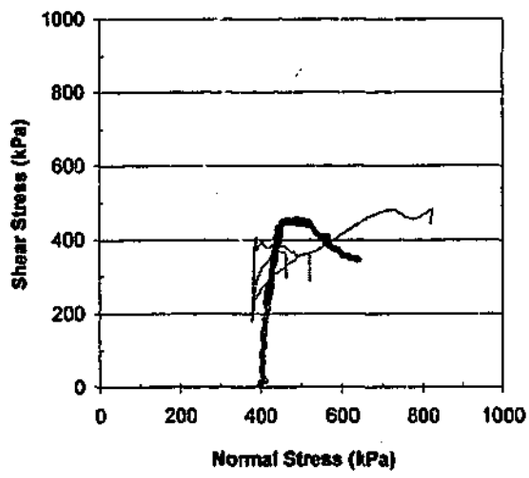

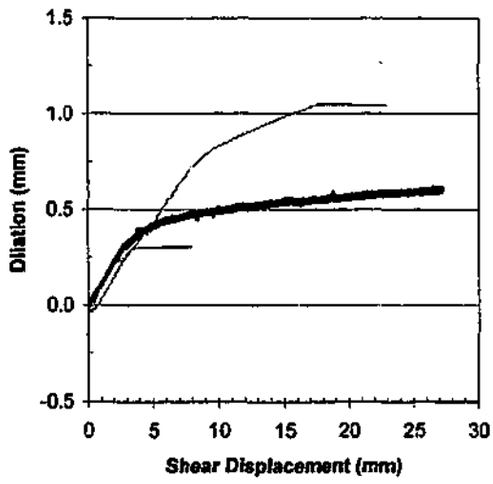

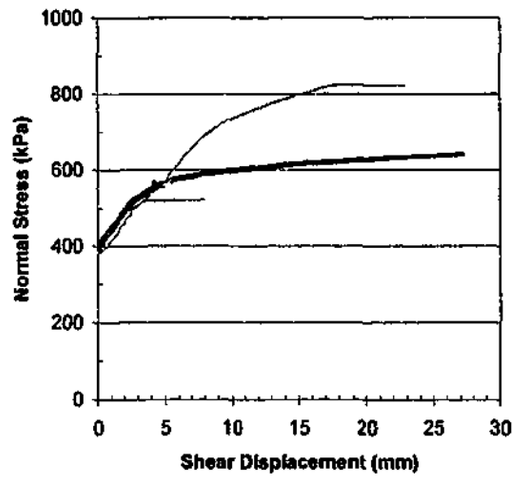

Prediction Test Result

Sample : JS_6a

Sokolovsky Factor = 1.38

Johnstone Batch 2

Initial Normal Stress (kPa): 40[illegible]

Normal Stiffness (kPa/mm): 400

Chord Lengths Used For Predictions : 1.7mm, 8mm, 18mm

Johnstone Split Surface JS_7a Prediction of Shear Response

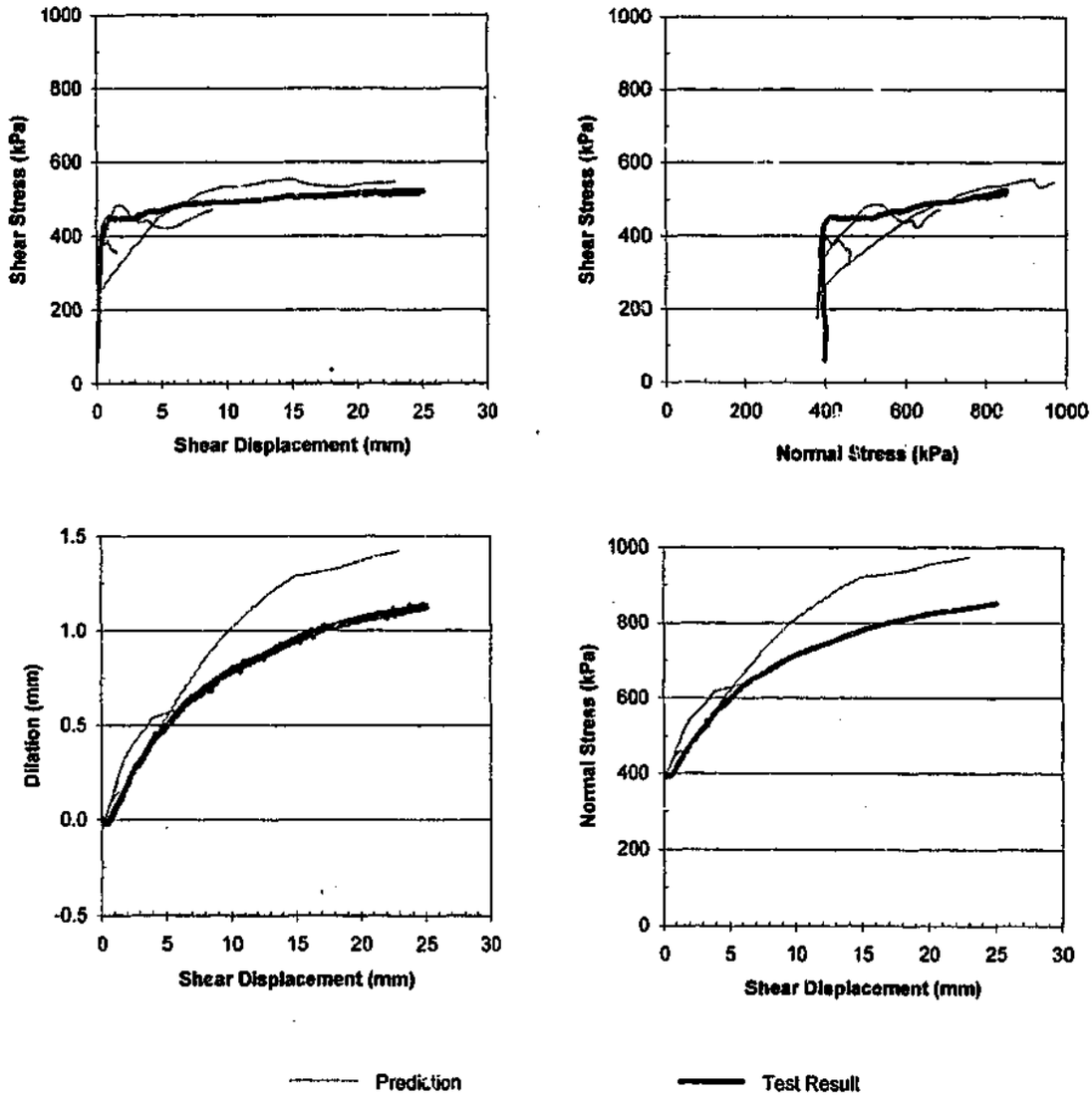

Sample : JS_7a

Sokolovsky Factor = 1.38

Johnstone Batch 2

Initial Normal Stress (kPa): 400

Normal Stiffness (kPa/mm): 400

Chord Lengths Used For Predictions : 1.5mm, 9mm, 23mm

Sandstone Direct Shear Test Predictions

In this section the predictions produced using the program Rocket are compared with direct shear tests conducted on sandstone samples.

The following parameters were used in the predictions:

Parameter	Adopted value
Young's Modulus	3200MPa
Poisson's Ratio	0.1
Intact Friction Angle	50°
Residual Friction Angle	32°
Cohesion	2200kPa
Joint Normal Stiffness – split surface	2.1MPa/mm
Failure Stress	1.26 * Sokolovsky failure stress

Sandstone Split Surface SS_1 Prediction of Shear Response

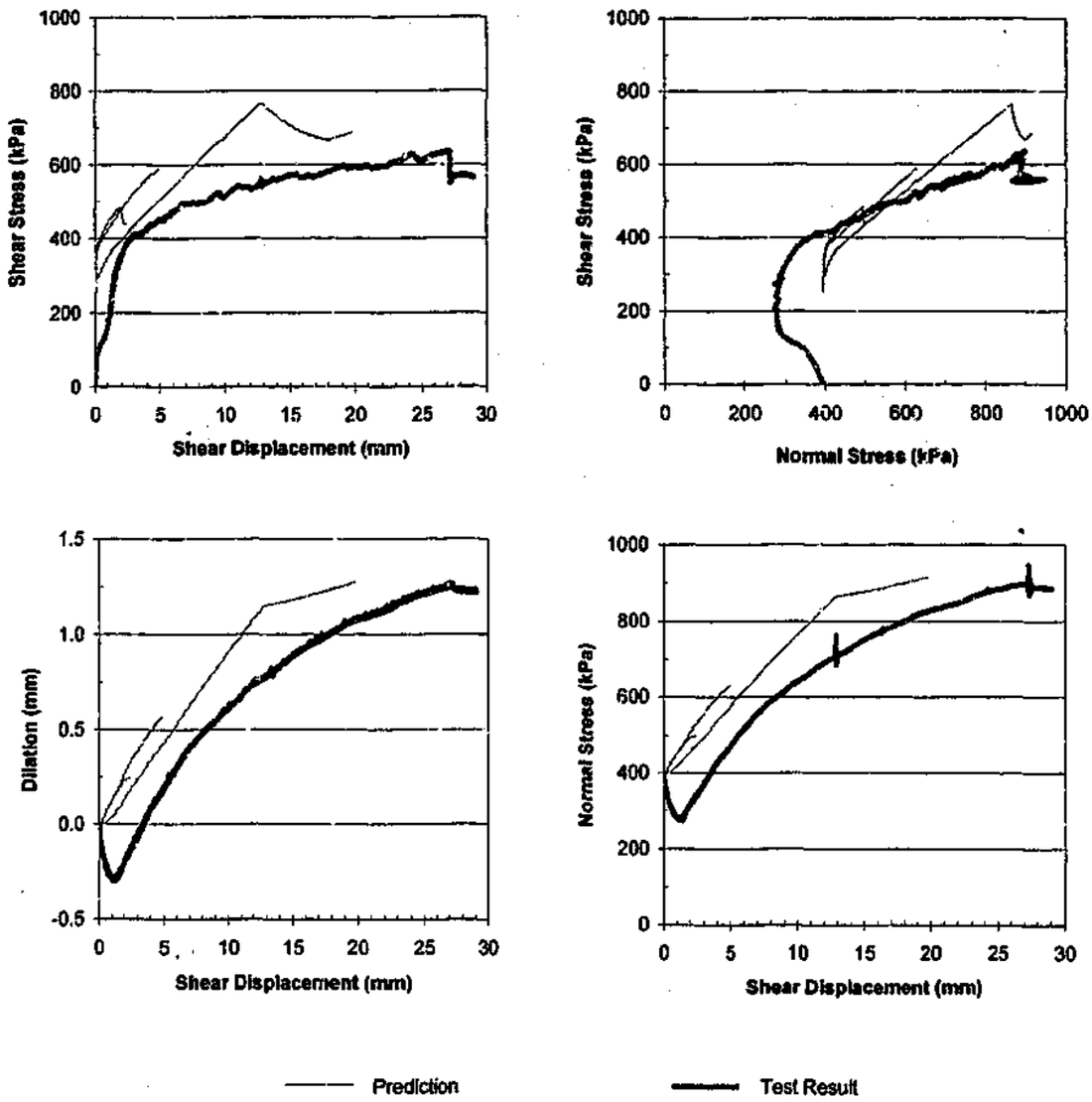

Sample : SS_1

Sokolovsky Factor = 1.26

Initial Normal Stress (kPa): **400**

Normal Stiffness (kPa/mm): **400**

Chord Lengths Used For Predictions : 2.5mm, 5mm, 20mm

Sandstone Split Surface Shear Response Prediction

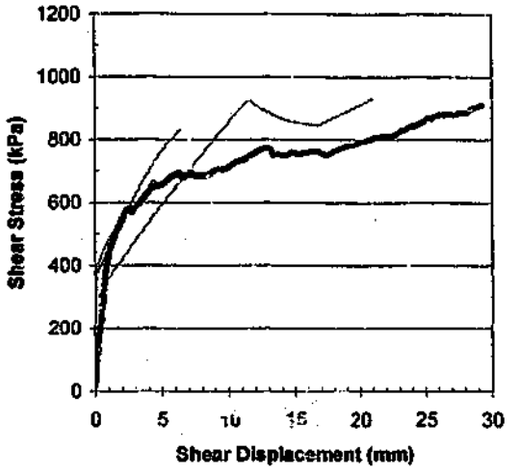

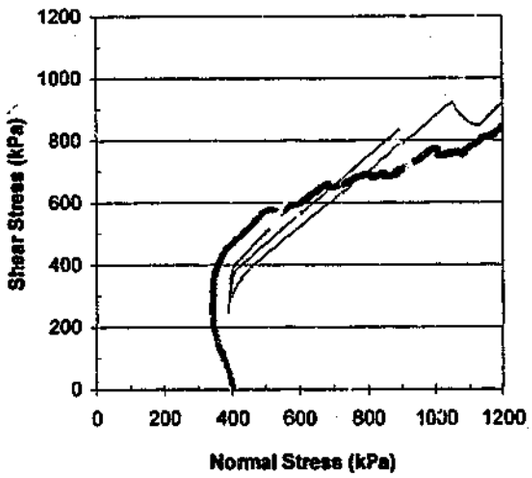

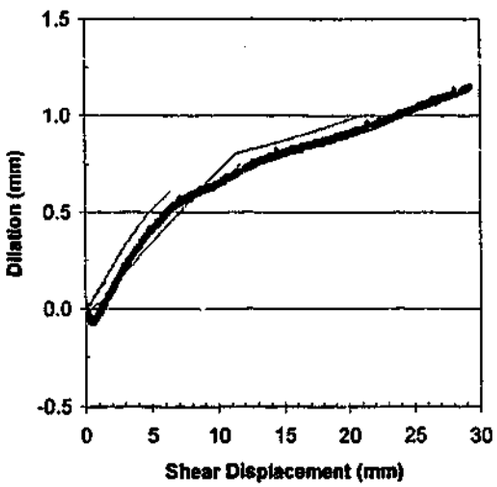

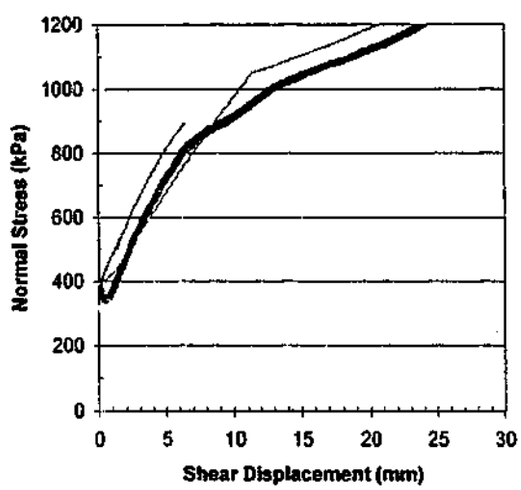

Prediction Test Result

Sample : SS_2

Sokolovsky Factor = 1.26

Initial Normal Stress (kPa): 400

Normal Stiffness (kPa/mm): 800

Chord Lengths Used For Predictions : 1.5mm, 6.5mm, 21mm

Siltstone Direct Shear Test Predictions

In this section the predictions produced using the program Rocket are compared with direct shear tests conducted on siltstone samples.

The following parameters were used in the predictions:

Parameter	Adopted value
Young's Modulus	25.4GPa
Poisson's Ratio	0.15
Intact Friction Angle	40°
Residual Friction Angle	28.5°
Cohesion	12MPa
Joint Normal Stiffness – water-jet surface	6.2MPa/mm
Joint Normal Stiffness – split surface	3.9MPa/mm
Failure Stress – shear along bedding	30MPa
Failure Stress - shear through matrix	55MPa

Siltstone Regular Triangular Profile MR5_16 Prediction of Shear Response

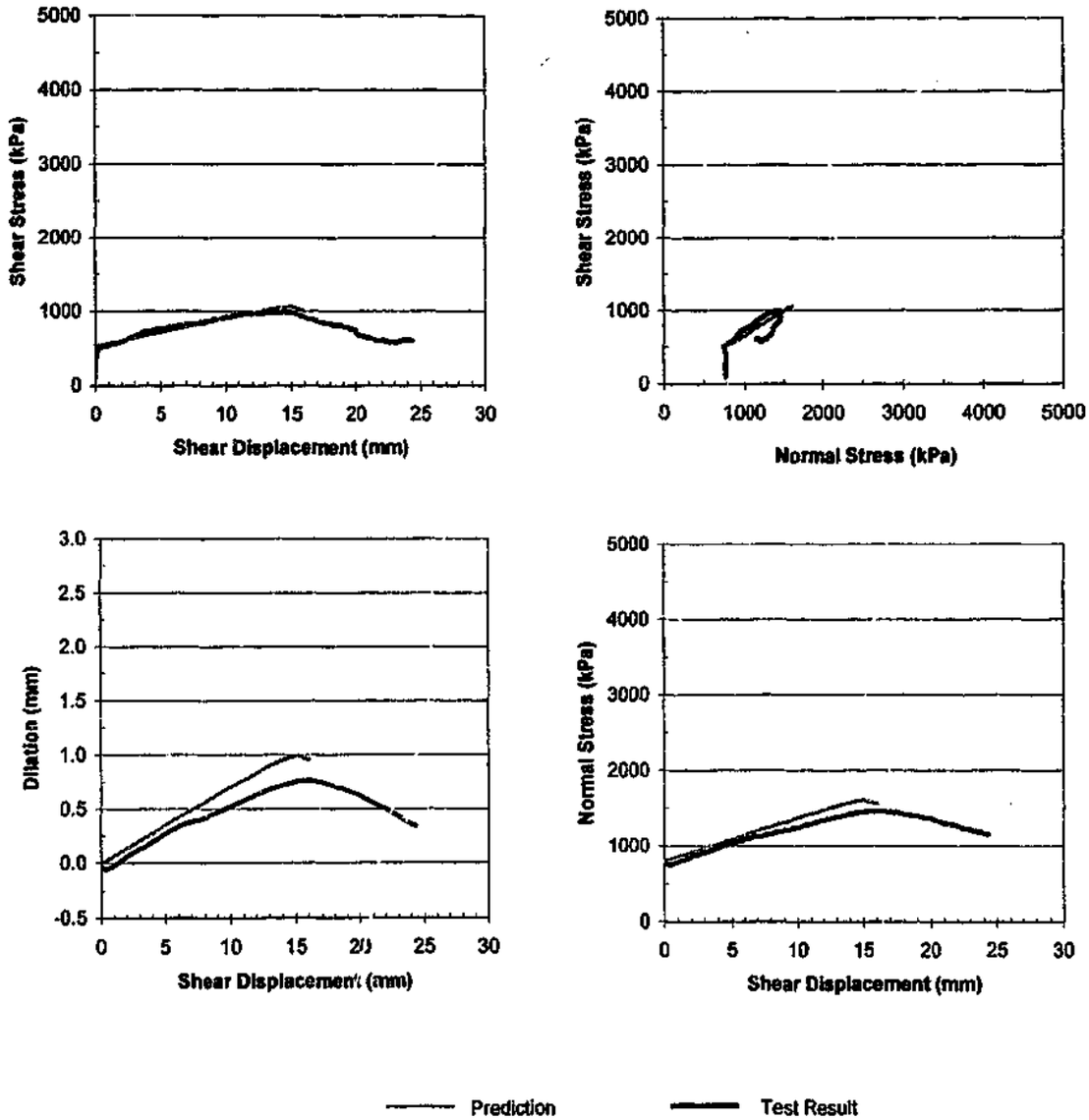

Sample : MR5_16

Failure Stress = UCS bedding

Initial Normal Stress (kPa): **800**

Normal Stiffness (kPa/mm): **800**

Siltstone Regular Triangular Profile MR5a_16 Prediction of Shear Response

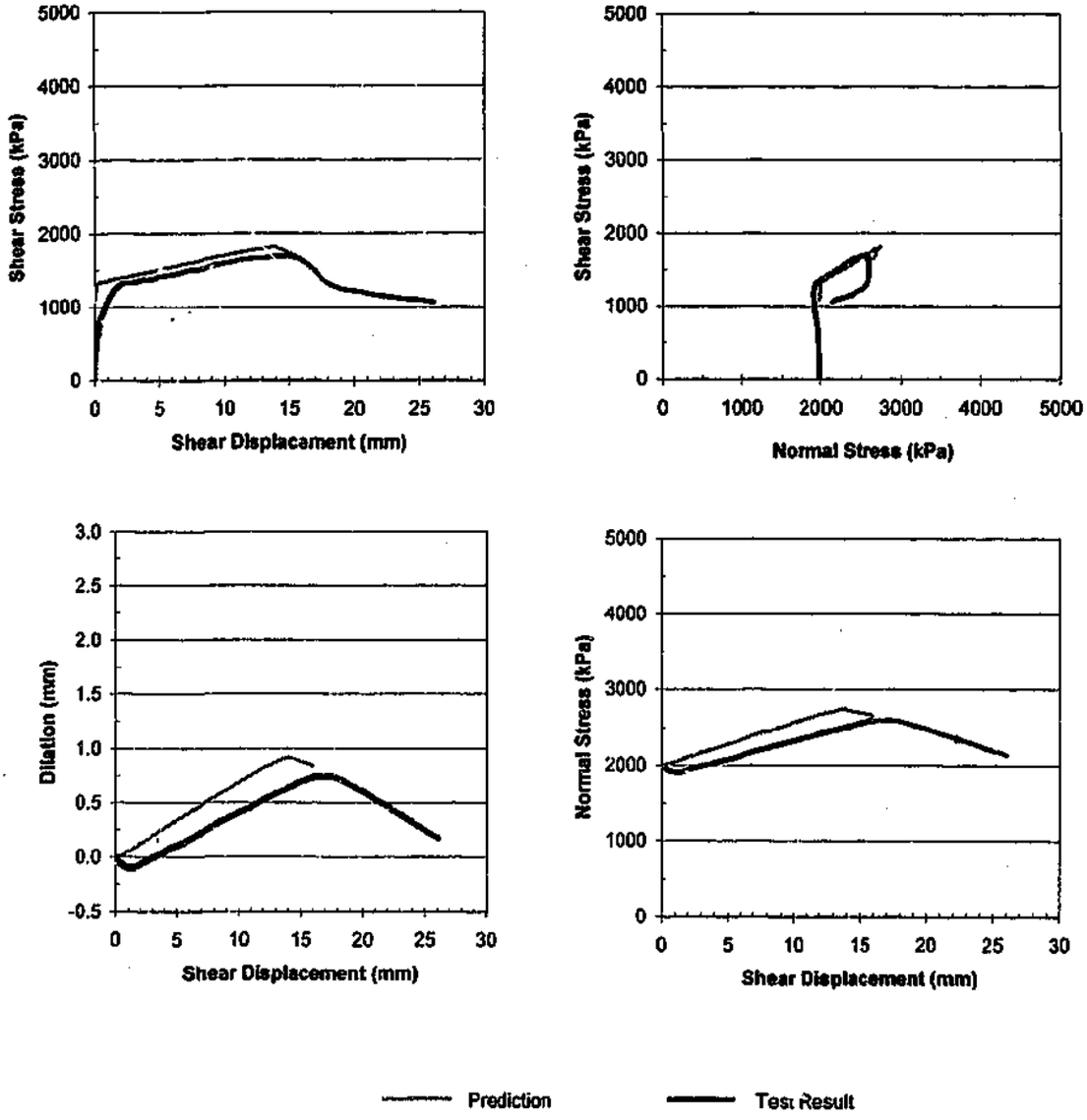

Sample : MR5a_16

Failure Stress = UCS bedding

Initial Normal Stress (kPa): **2000**

Normal Stiffness (kPa/mm): **800**

Siltstone Regular Triangular Profile MR10a_16 Prediction of Shear Response

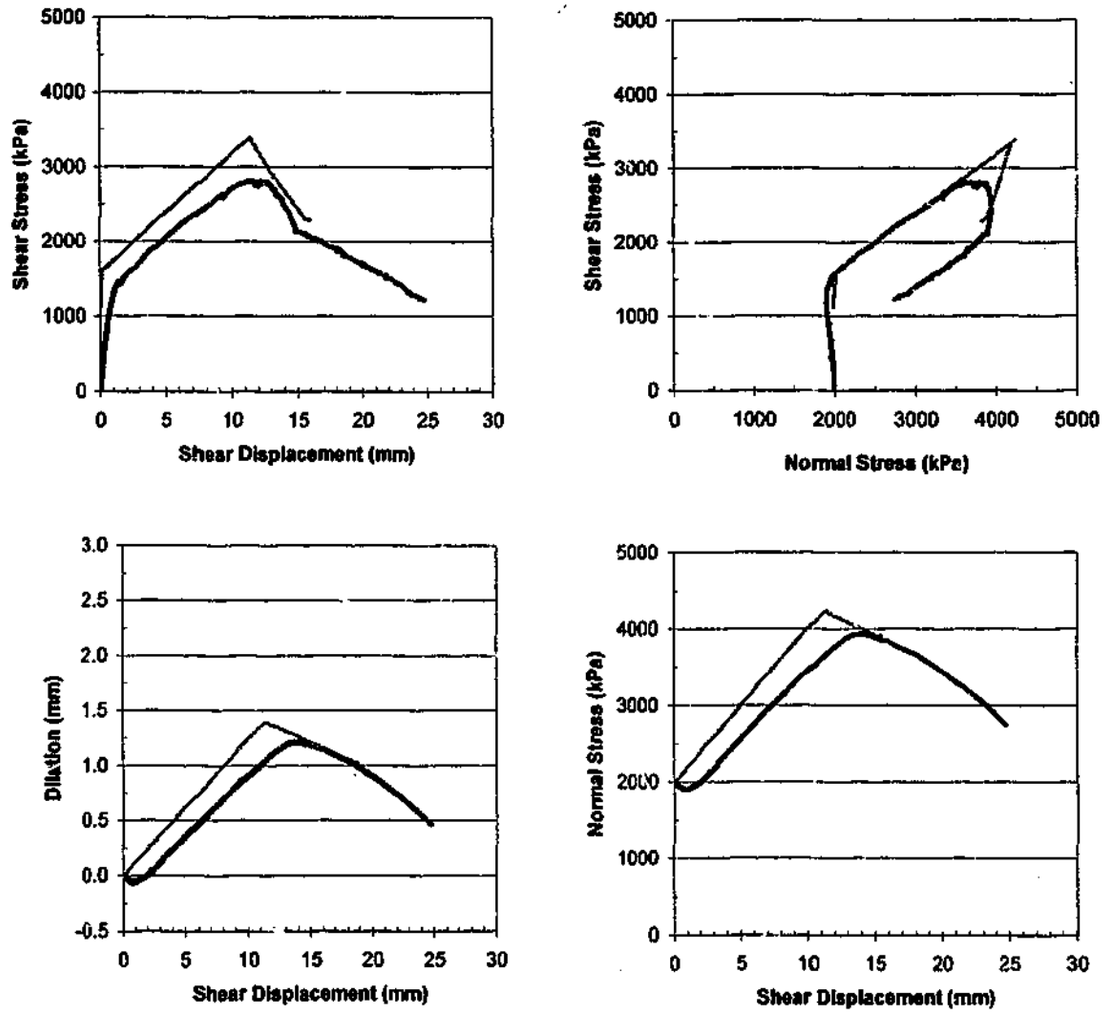

Sample : MR10a_16

Failure Stress = UCS bedding

Initial Normal Stress (kPa): 2000

Normal Stiffness (kPa/mm): 1600

Siltstone Regular Triangular Profile MR10a_48 Prediction of Shear Response

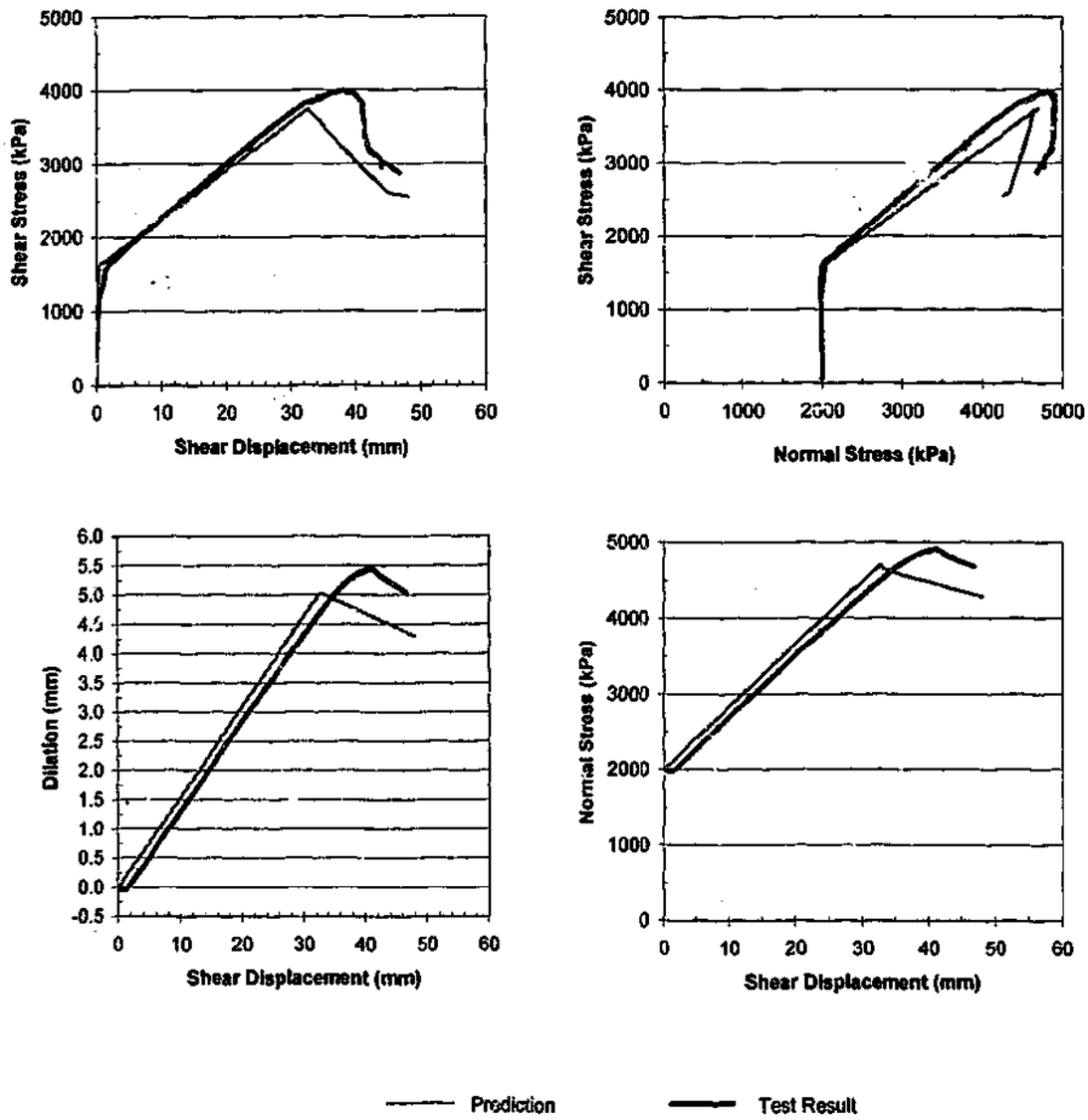

Sample : MR10a_48

Failure Stress = UCS bedding

Initial Normal Stress (kPa): **2000**

Normal Stiffness (kPa/mm): **533**

Siltstone Regular Triangular Profile MR15_16 Prediction of Shear Response

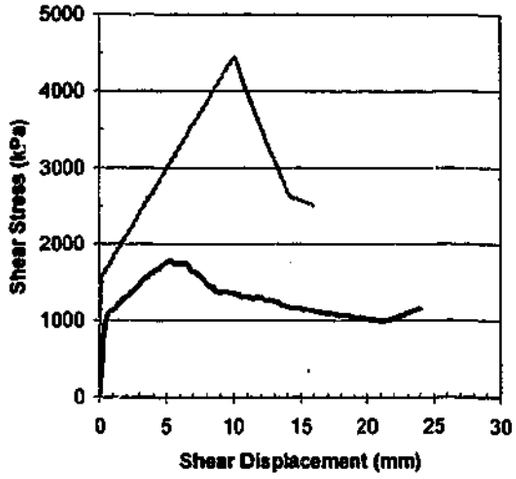

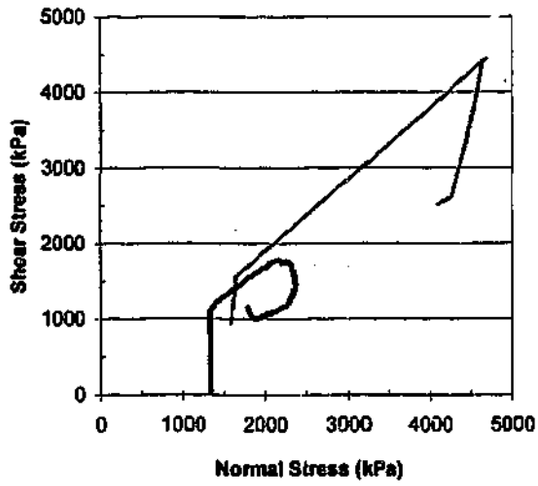

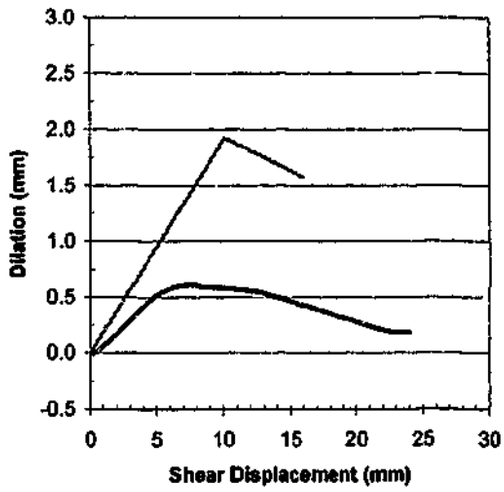

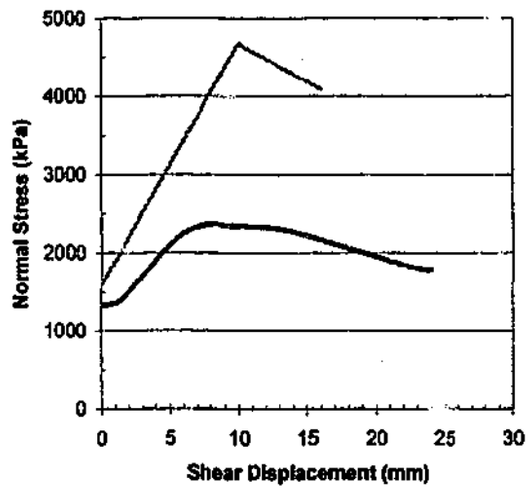

Prediction Test Result

Sample : MR15_16

Failure Stress = UCS bedding

Initial Normal Stress (kPa): **1600**

Normal Stiffness (kPa/mm): **1600**

Siltstone Fractal Profile MF5_5 Prediction of Shear Response

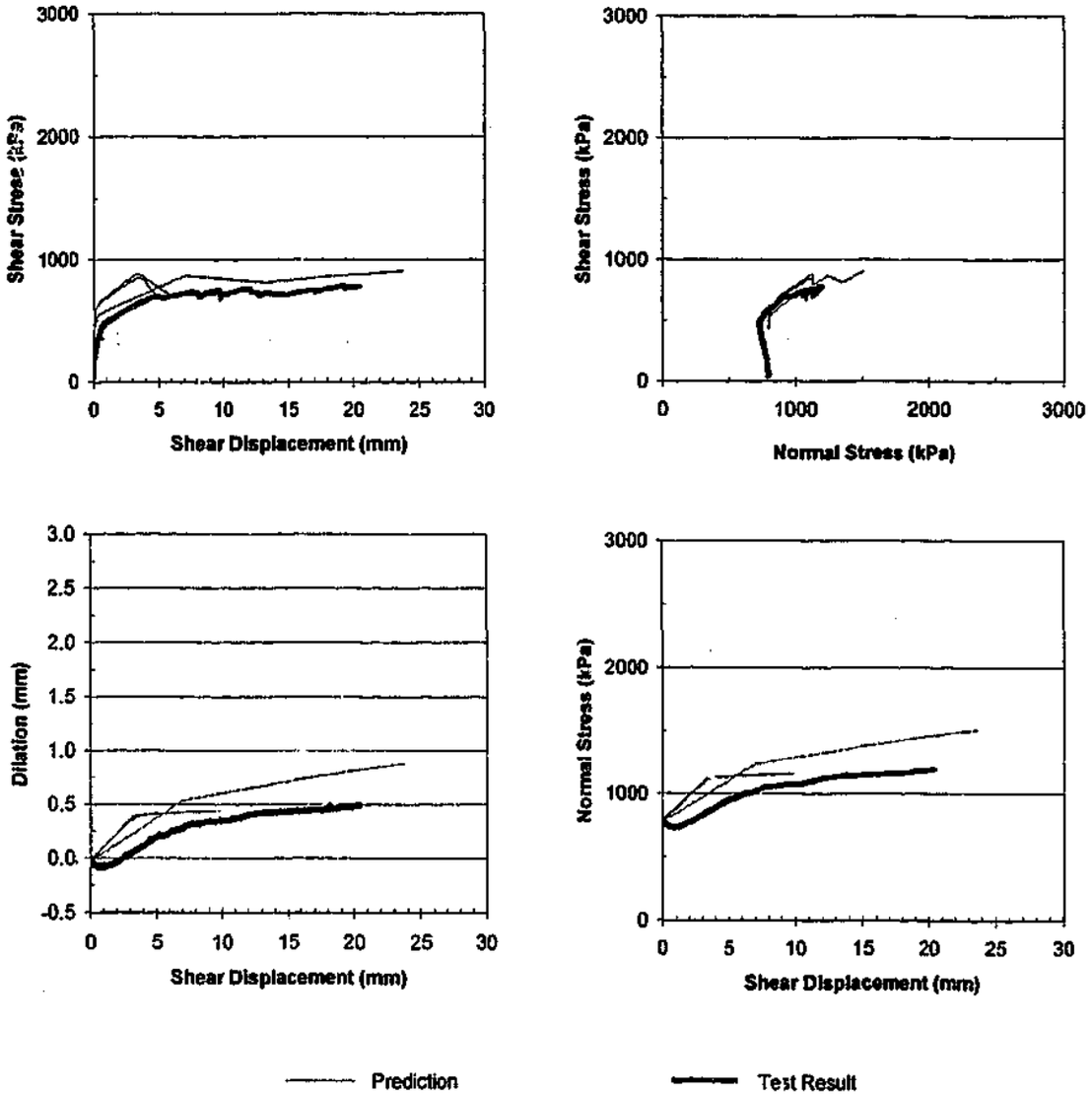

Sample : MF5_5

Failure Stress = UCS

Initial Normal Stress (kPa): 800

Normal Stiffness (kPa/mm): 800

Chord Lengths Used For Predictions : 5mm, 10mm, 24mm

Siltstone Fractal Profile MF10_5 Prediction of Shear Response

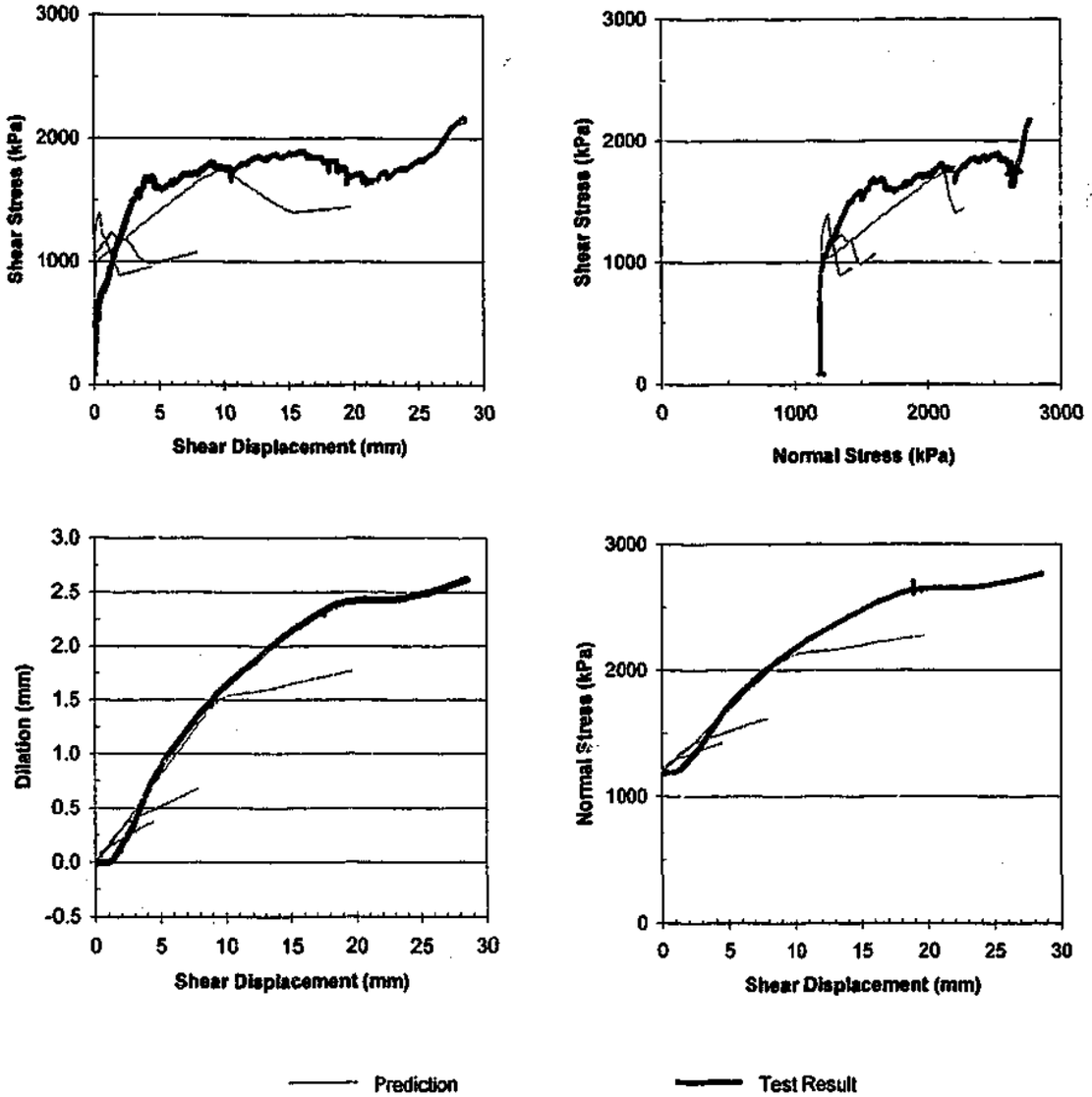

Sample : MF10_5

Failure Stress = UCS

Initial Normal Stress (kPa): **1200**

Normal Stiffness (kPa/mm): **600**

Chord Lengths Used For Predictions : 4.5mm, 8mm, 20mm

Siltstone Fractal Profile MF10a_5 Prediction of Shear Response

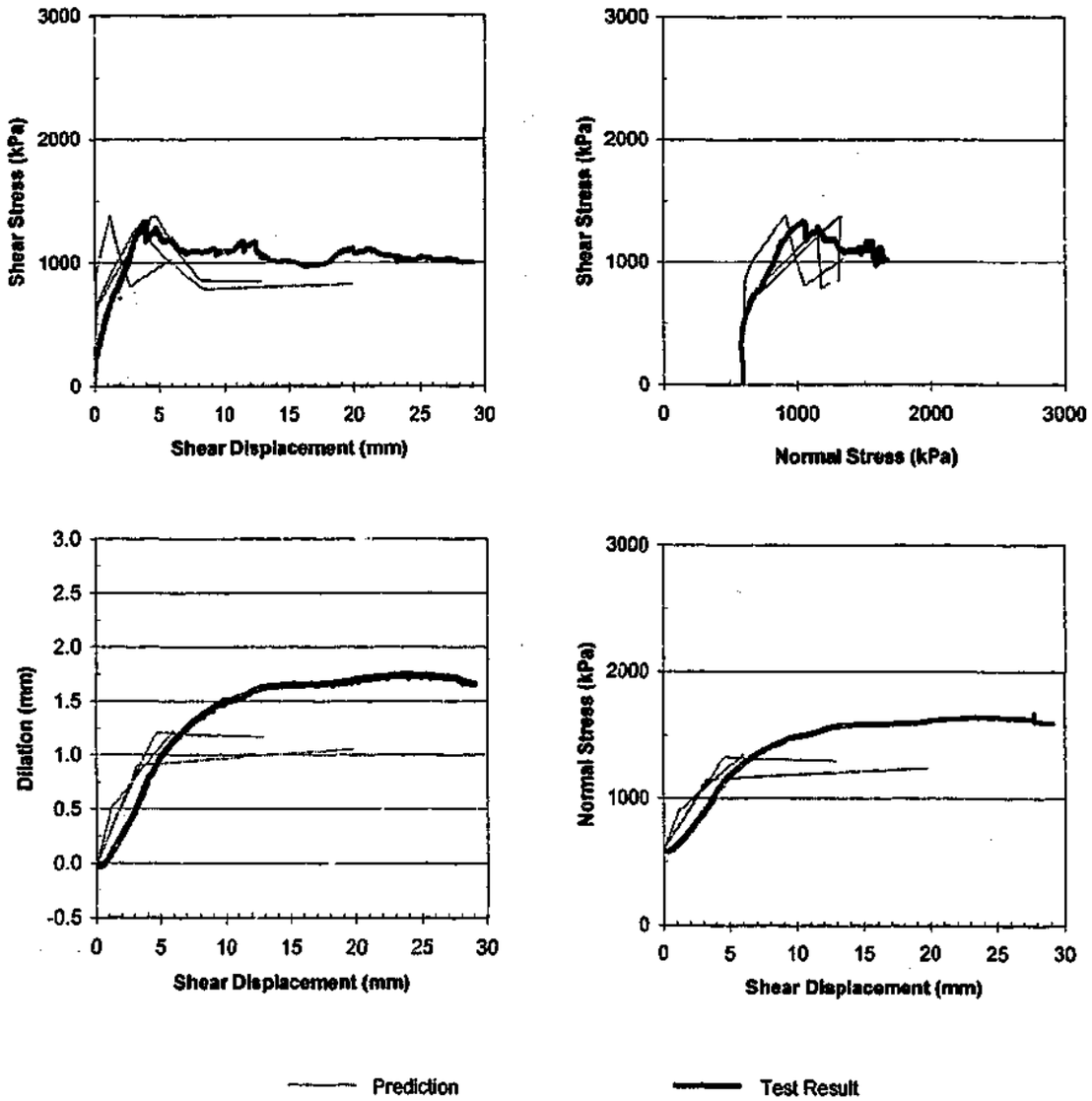

Sample : MF10a_5

Failure Stress = UCS

Initial Normal Stress (kPa): 600

Normal Stiffness (kPa/mm): 600

Chord Lengths Used For Predictions : 6mm, 13mm, 20mm

Siltstone Fractal Profile MF15_5 Prediction of Shear Response

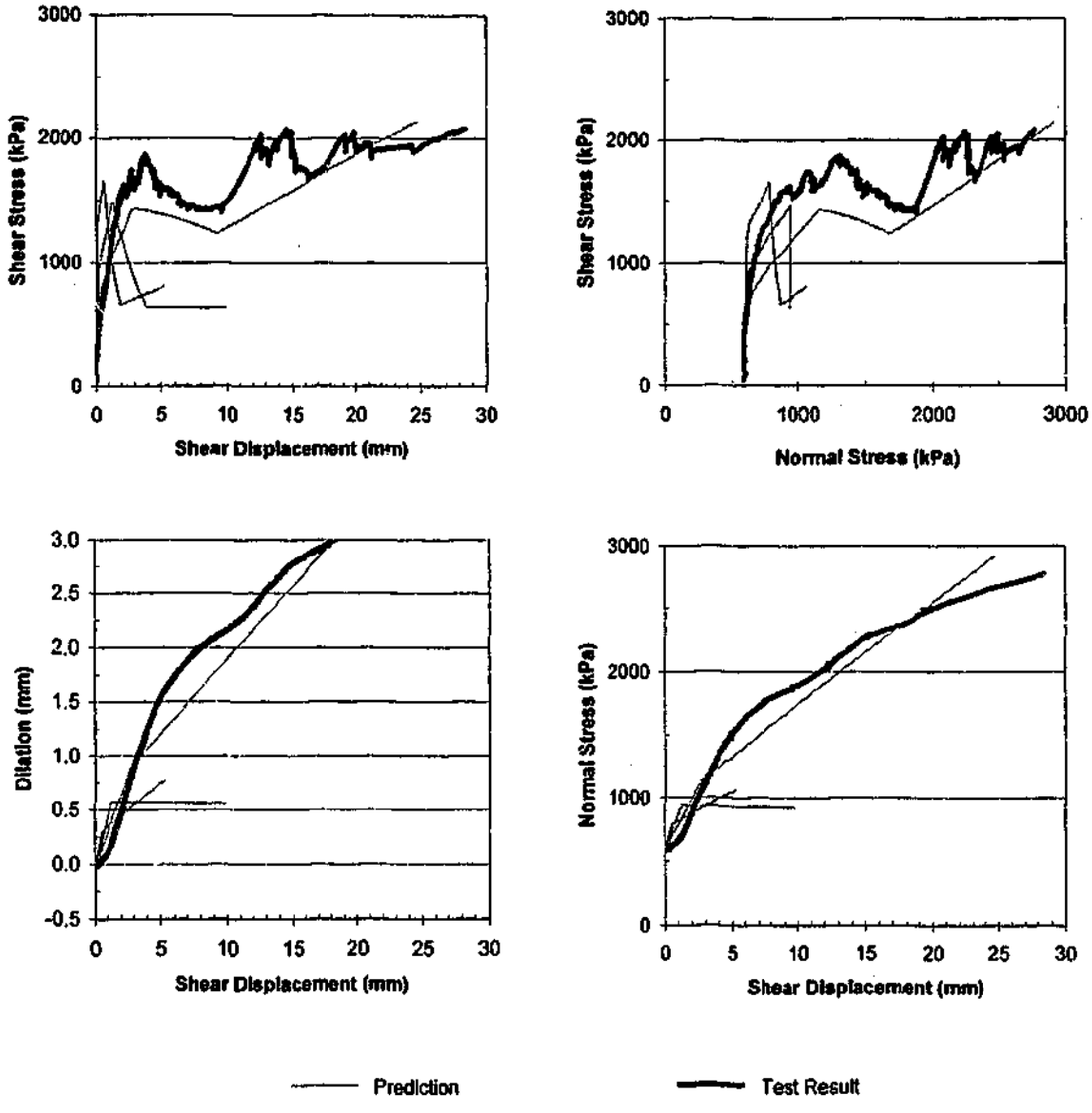

Sample : MF15_5

Failure Stress = UCS

Initial Normal Stress (kPa): 600

Normal Stiffness (kPa/mm): 600

Chord Lengths Used For Predictions : 5.3mm, 10mm, 25mm

Siltstone Split Surface MS_1 Prediction of Shear Response

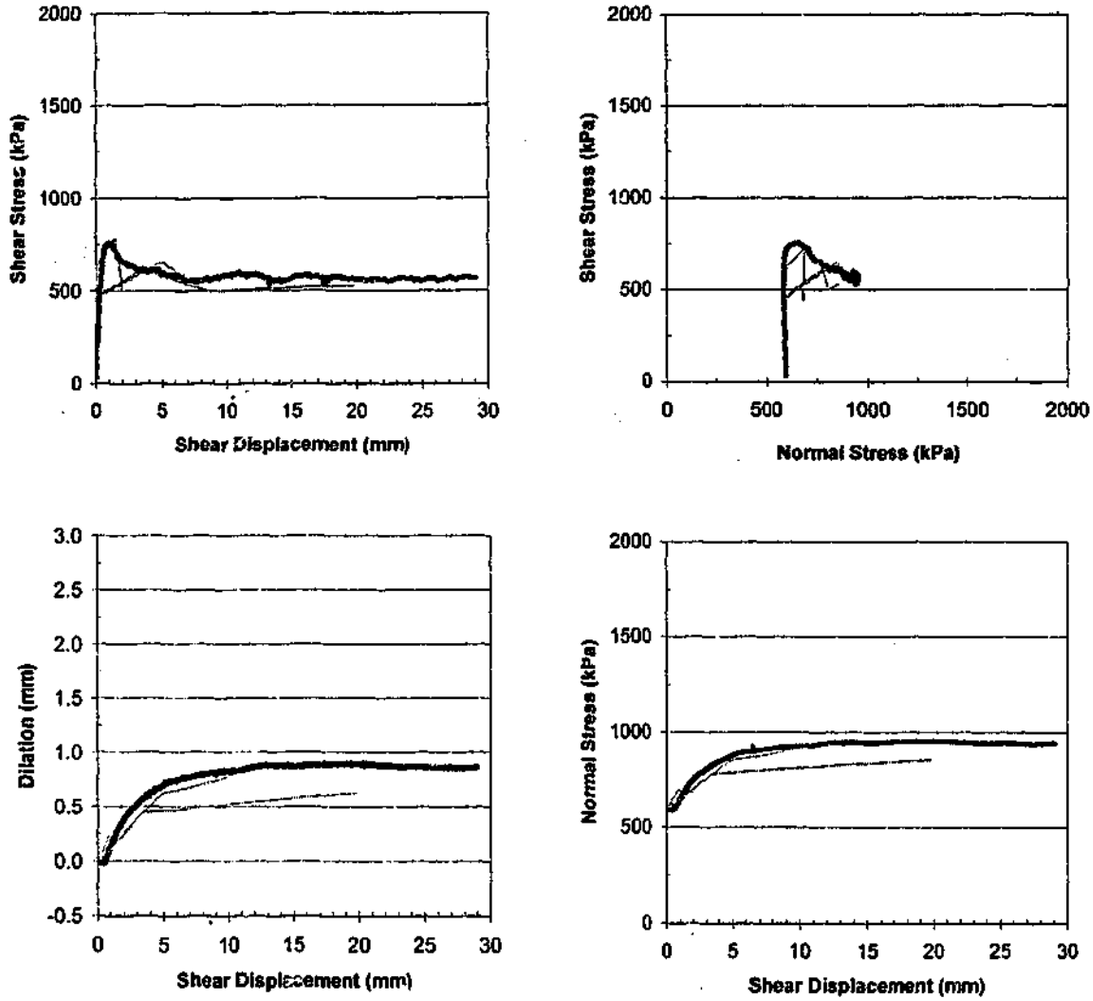

Sample : MS_1

Failure Stress < 2mm chord length = UCS matrix

Failure Stress > 2mm chord length = UCS bedding

Initial Normal Stress (kPa): 600

Normal Stiffness (kPa/mm): 400

Chord Lengths Used For Predictions : 2mm, 11mm, 20mm

Siltstone Split Surface MS_2 Prediction of Shear Response

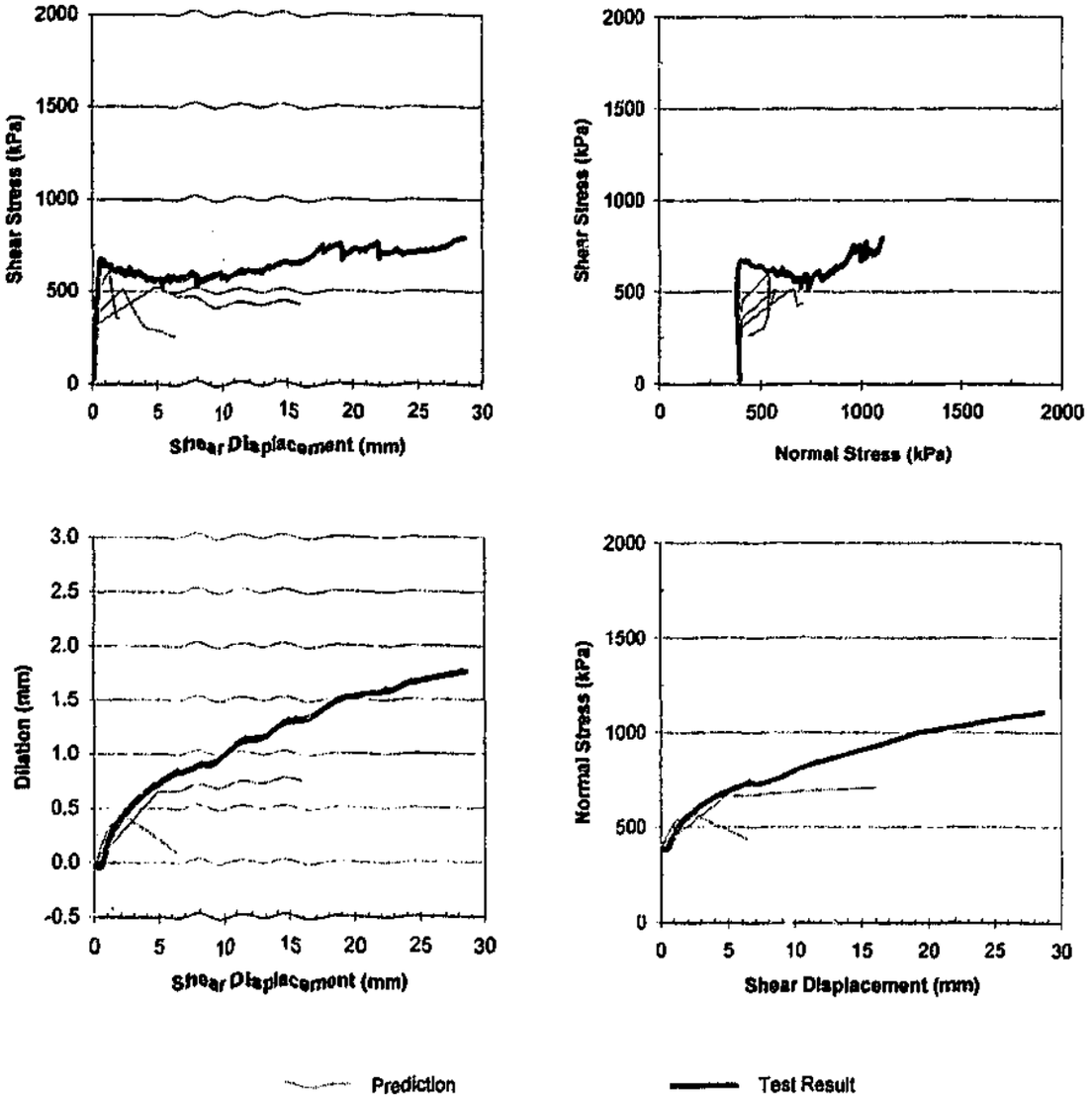

Sample : MS_2

Failure Stress < 2mm chord length = UCS matrix

Failure Stress > 2mm chord length = UCS bedding

Initial Normal Stress (kPa): 400

Normal Stiffness (kPa/mm): 400

Chord Lengths Used For Predictions : 2mm, 6.5mm, 16mm

Siltstone Split Surface MS_3 Prediction of Shear Response

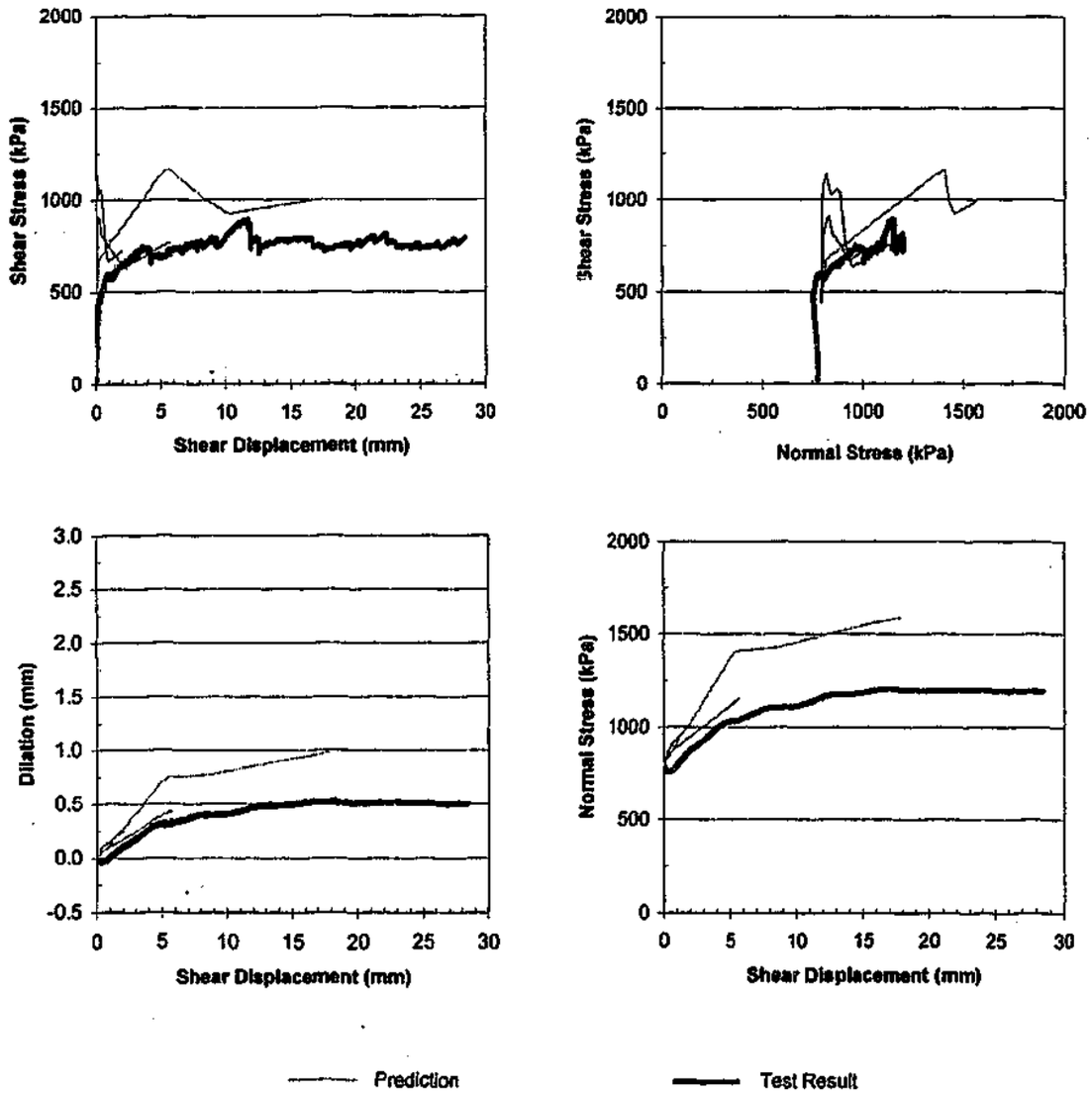

Sample : MS_3

Failure Stress = UCS bedding

Initial Normal Stress (kPa): **800**

Normal Stiffness (kPa/mm): **800**

Chord Lengths Used For Predictions : 2mm, 5.8mm, 18mm

Siltstone Split Surface MS_4 Prediction of Shear Response

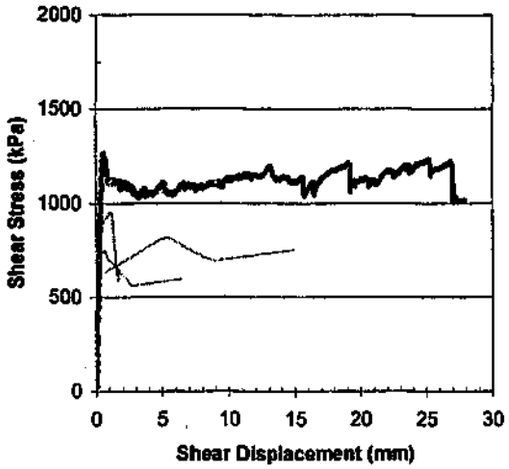

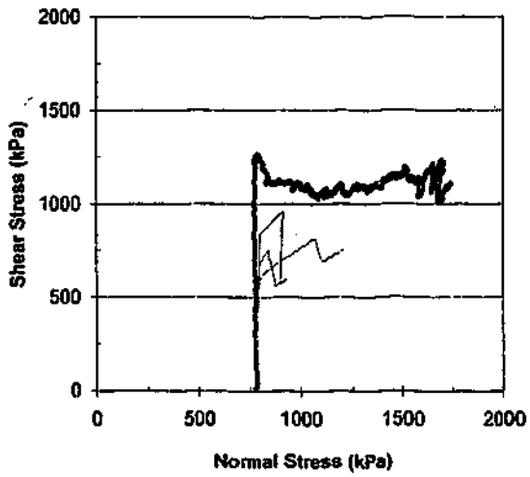

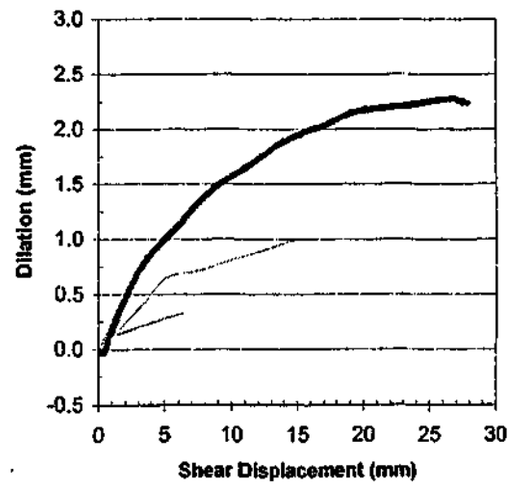

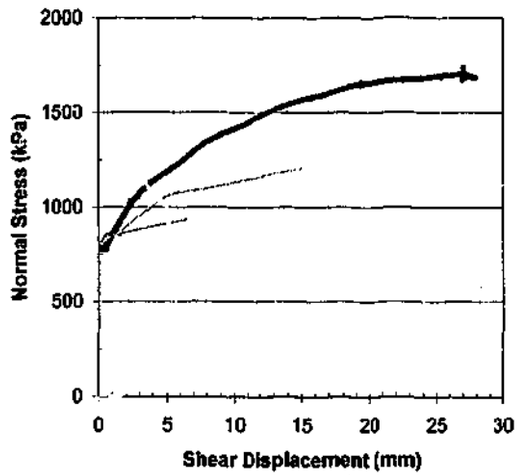

Prediction — Test Result

Sample : MS_4

Failure Stress < 2mm chord length = UCS matrix

Failure Stress > 2mm chord length = UCS bedding

Initial Normal Stress (kPa): 800

Normal Stiffness (kPa/mm): 400

Chord Lengths Used For Predictions : 1.7mm, 6.5mm, 15mm

Siltstone Split Surface MS_5 Prediction of Shear Response

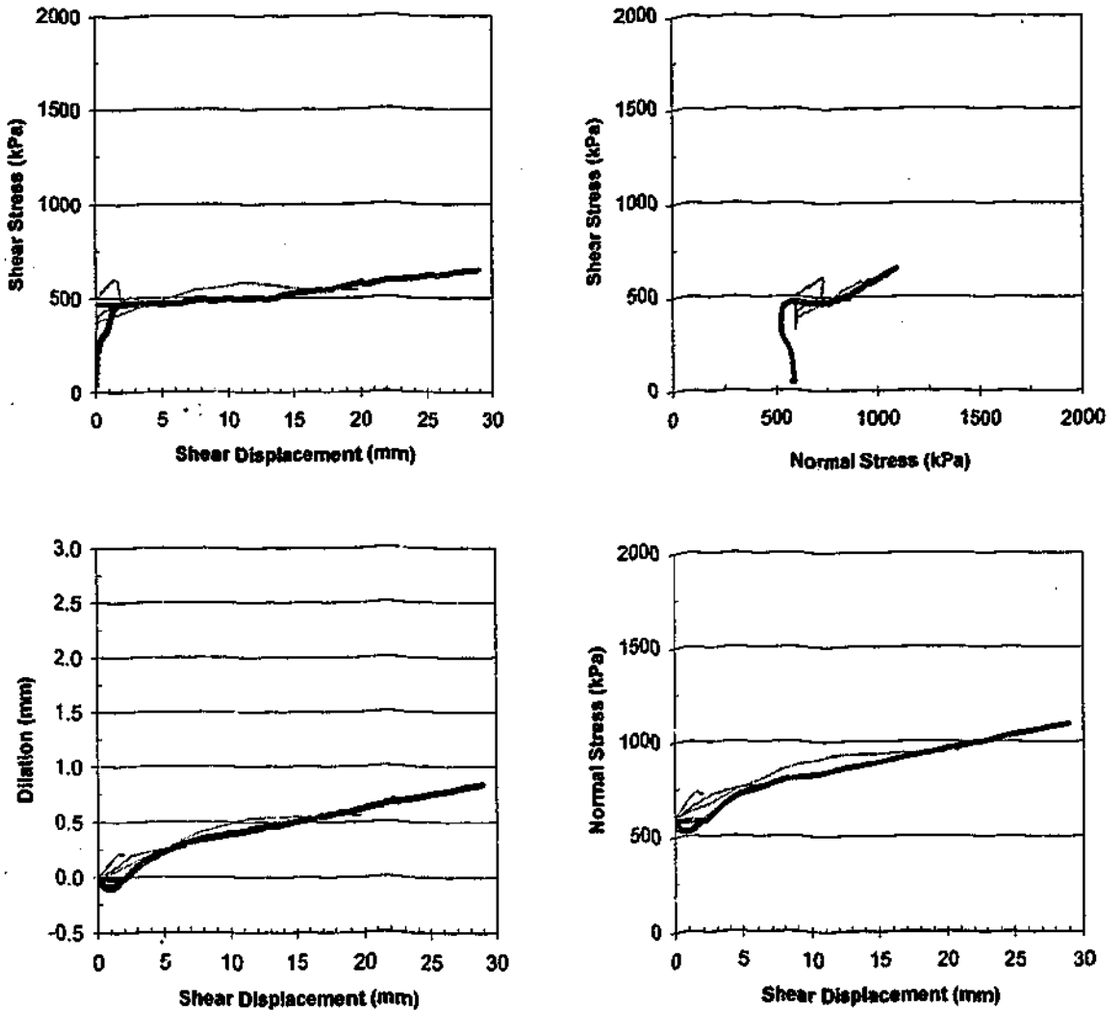

Sample : MS_5

Failure Stress = UCS bedding

Initial Normal Stress (kPa): 600

Normal Stiffness (kPa/mm): 600

Chord Lengths Used For Predictions : 2mm, 9mm, 20mm

Siltstone Split Surface MS_6 Prediction of Shear Response

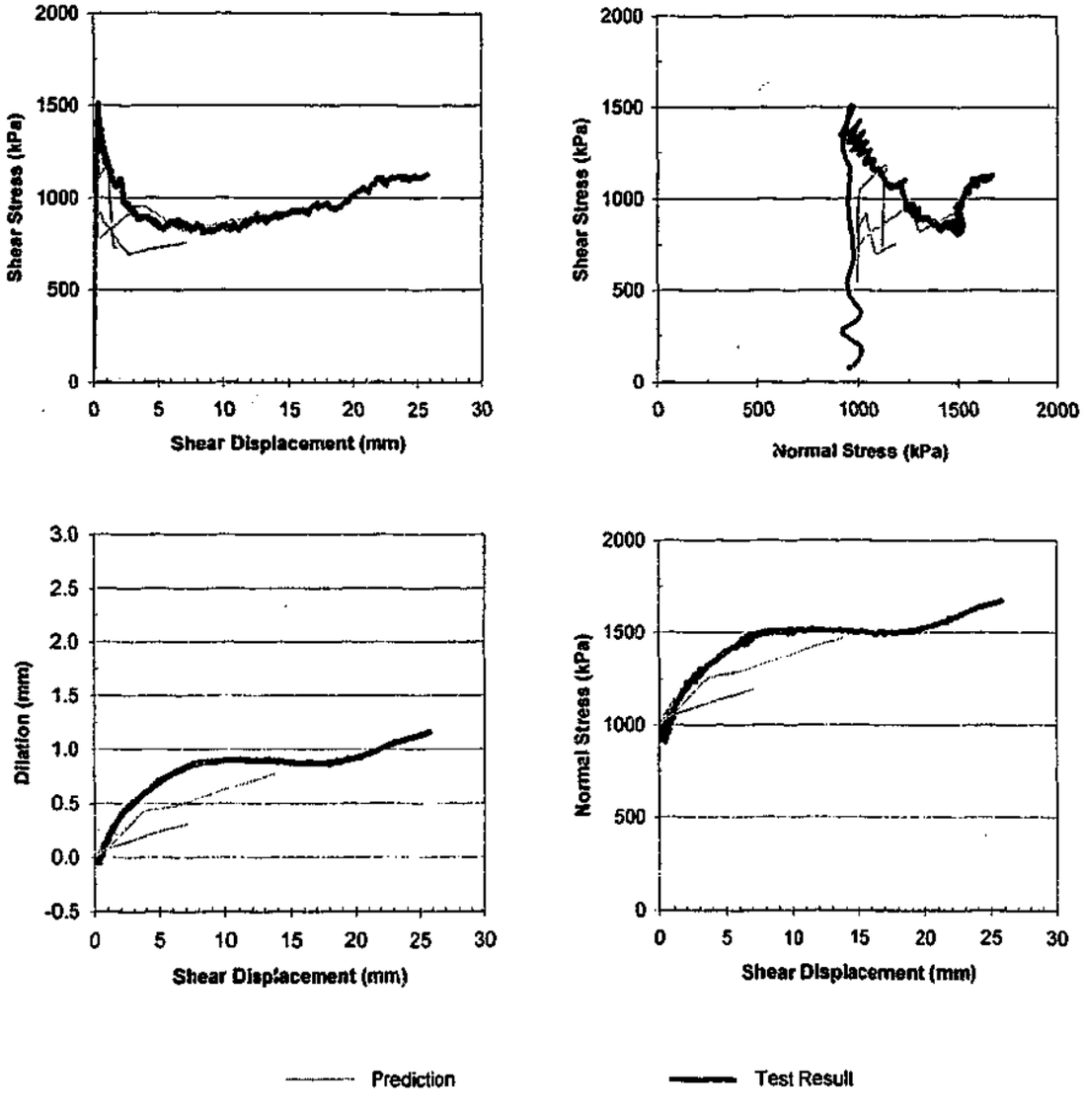

Sample : MS_6

Failure Stress < 2mm chord length = UCS matrix

Failure Stress > 2mm chord length = UCS bedding

Initial Normal Stress (kPa): 1000

Normal Stiffness (kPa/mm): 600

Chord Lengths Used For Predictions : 1.8mm, 7.2mm, 14mm

Siltstone Split Surface MS_7 Prediction of Shear Response

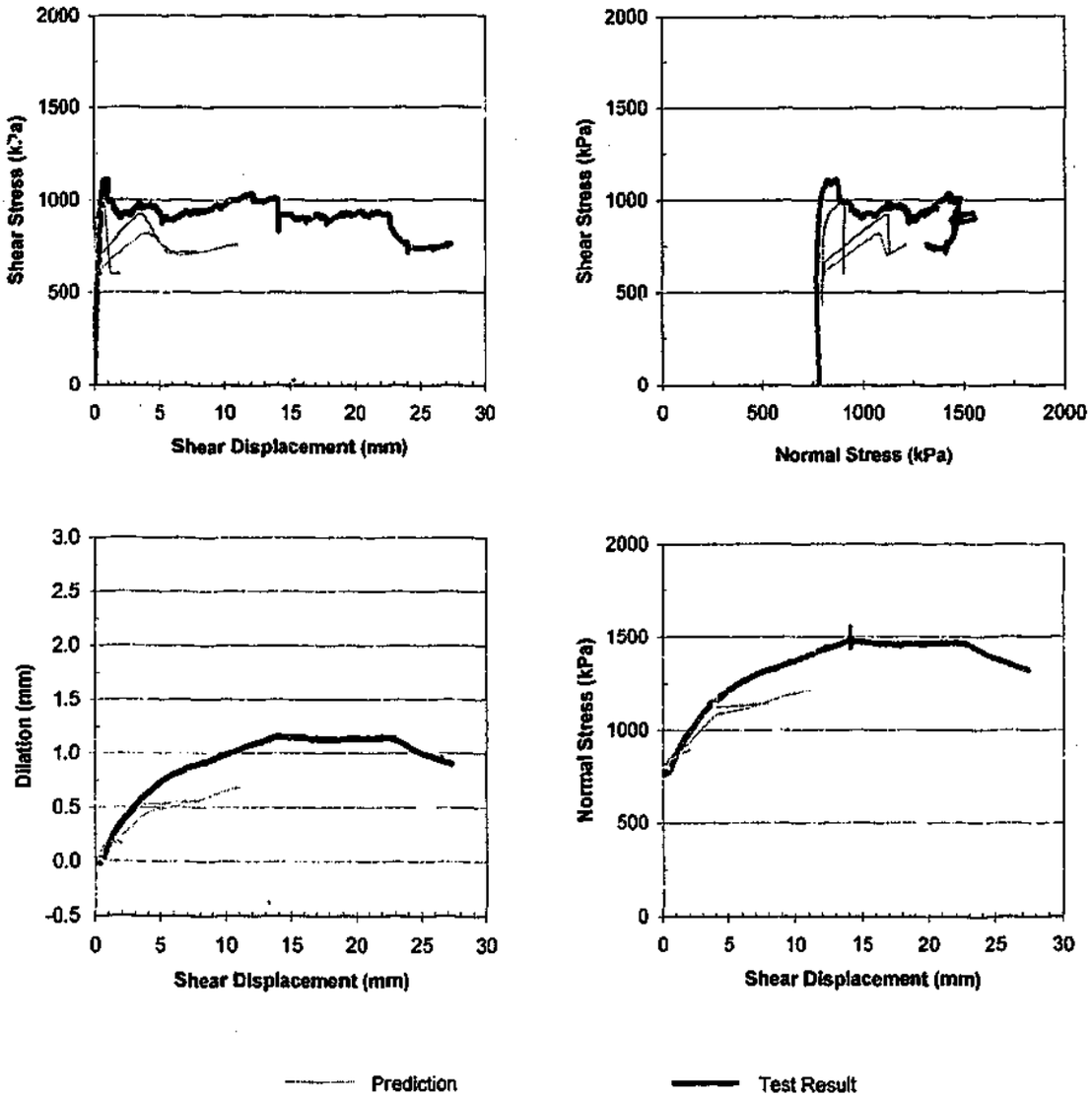

Sample : MS_7

Failure Stress < 2mm chord length = UCS matrix

Failure Stress > 2mm chord length = UCS bedding

Initial Normal Stress (kPa): 800

Normal Stiffness (kPa/mm): 600

Chord Lengths Used For Predictions : 2mm, 8mm, 11mm

Basalt Direct Shear Test Predictions

In this section the predictions produced using the program Rocket are compared with direct shear tests conducted on basalt samples.

The following parameters were used in the predictions:

Parameter	Adopted value
Young's Modulus	62GPa
Poisson's Ratio	0.15
Intact Friction Angle	48°
Residual Friction Angle	34°
Cohesion	20MPa
Joint Normal Stiffness – water-jet surface	7.6MPa/mm
Joint Normal Stiffness – split surface	7.5MPa/mm
Failure Stress	120MPa

Basalt Regular Triangular Profile BR5_16 Prediction of Shear Response

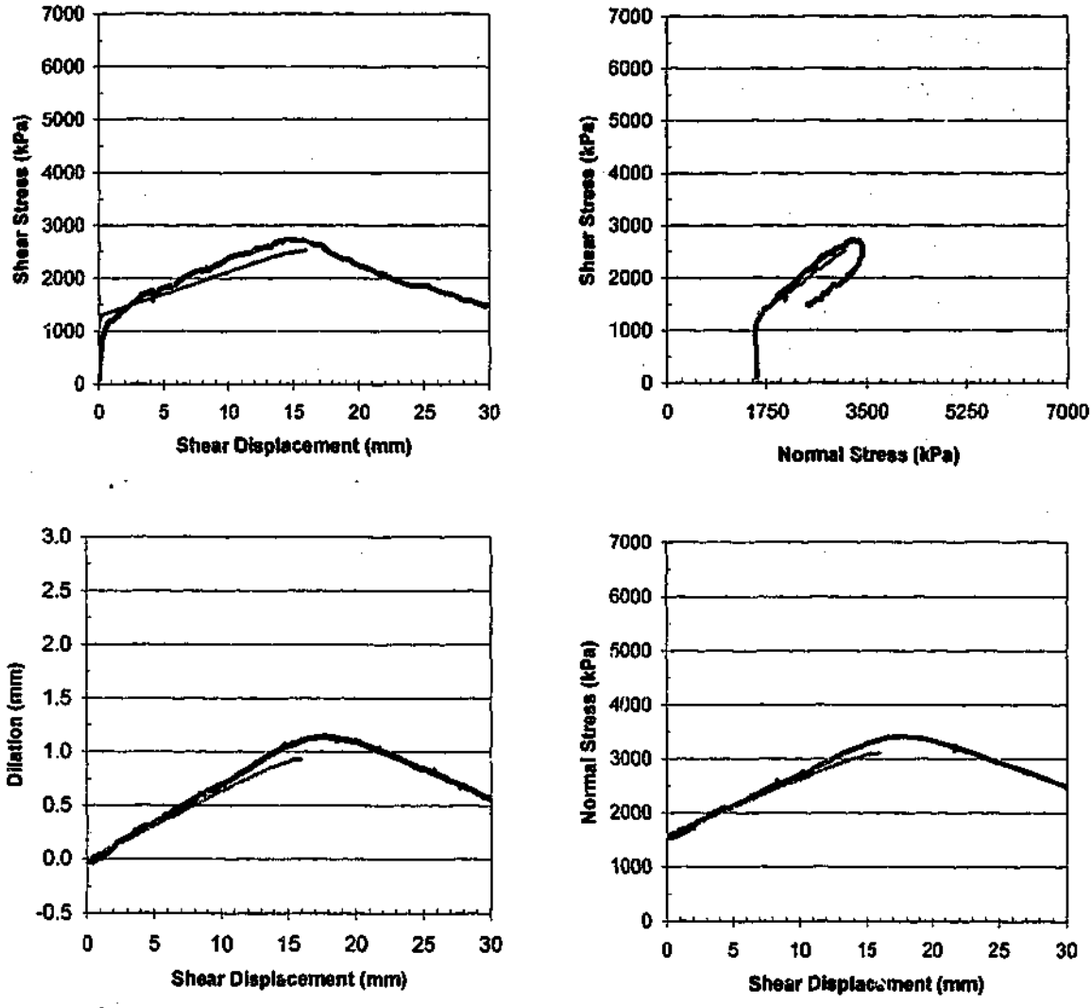

Sample : BR5_16

failure stress =UCS

Initial Normal Stress (kPa): **1600**

Normal Stiffness (kPa/mm): **1600**

Basalt Regular Triangular Profile BR10_16 Prediction of Shear Response

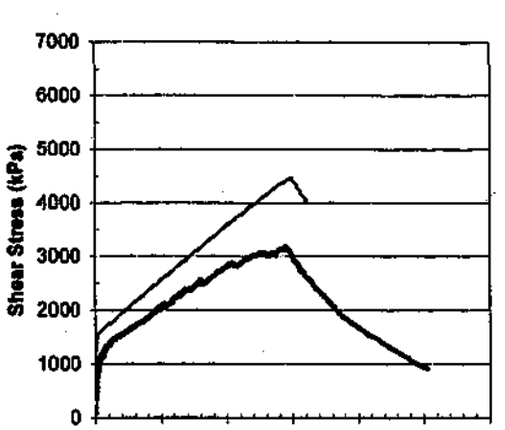

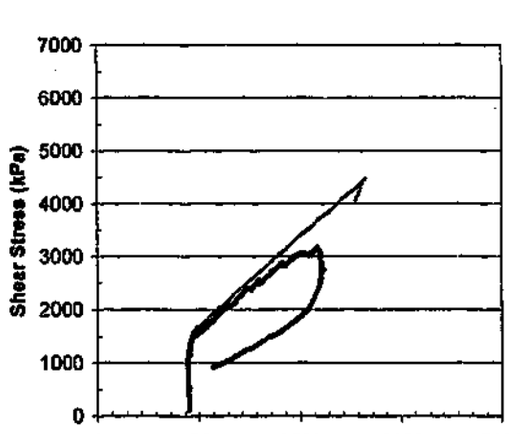

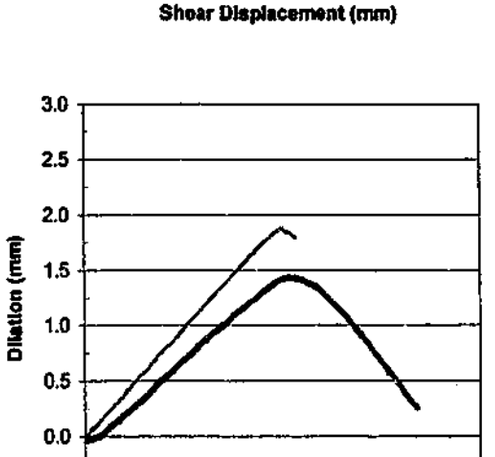

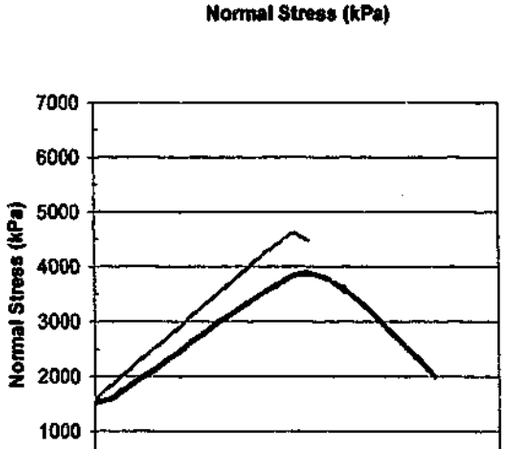

Prediction Test Result

Sample : BR10_16

Failure Stress = UCS

Initial Normal Stress (kPa): **1600**

Normal Stiffness (kPa/mm): **1600**

Basalt Regular Triangular Profile BR15_16 Prediction of Shear Response

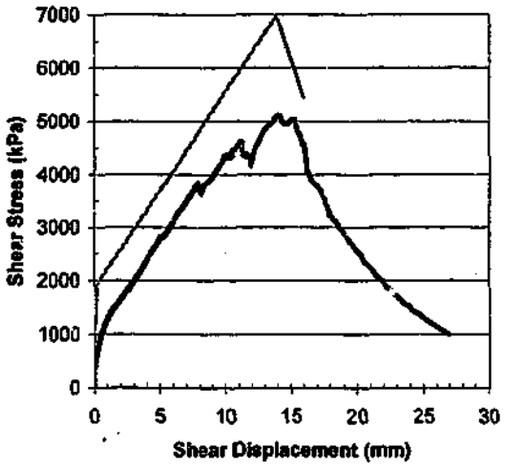

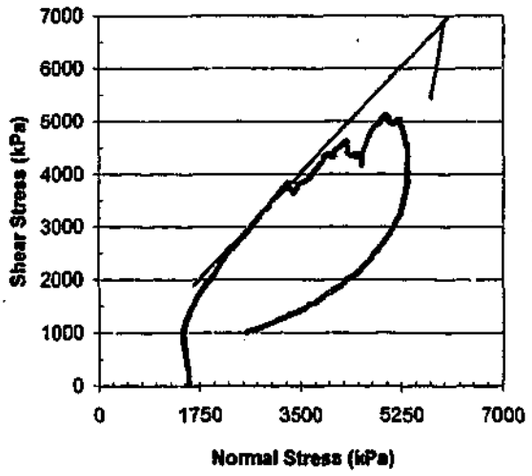

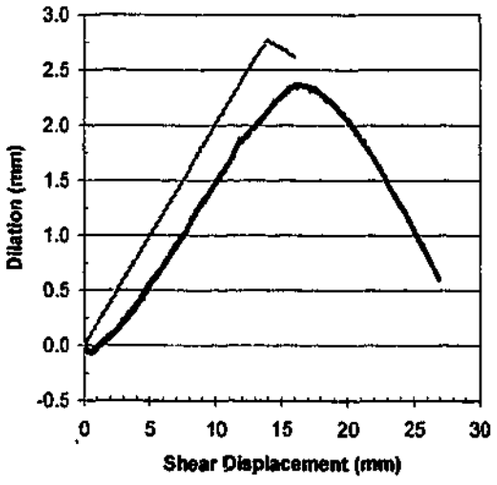

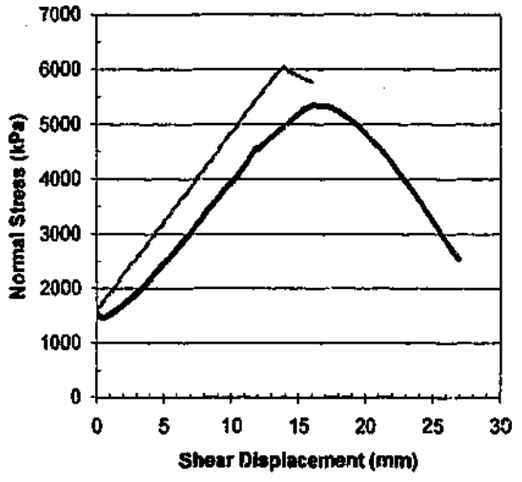

Prediction Test Result

Sample : BR15_16

Failure Stress = UCS

Initial Normal Stress (kPa): 1600

Normal Stiffness (kPa/mm): 1600

Basalt Fractal Profile BFR_10 Prediction of Shear Response

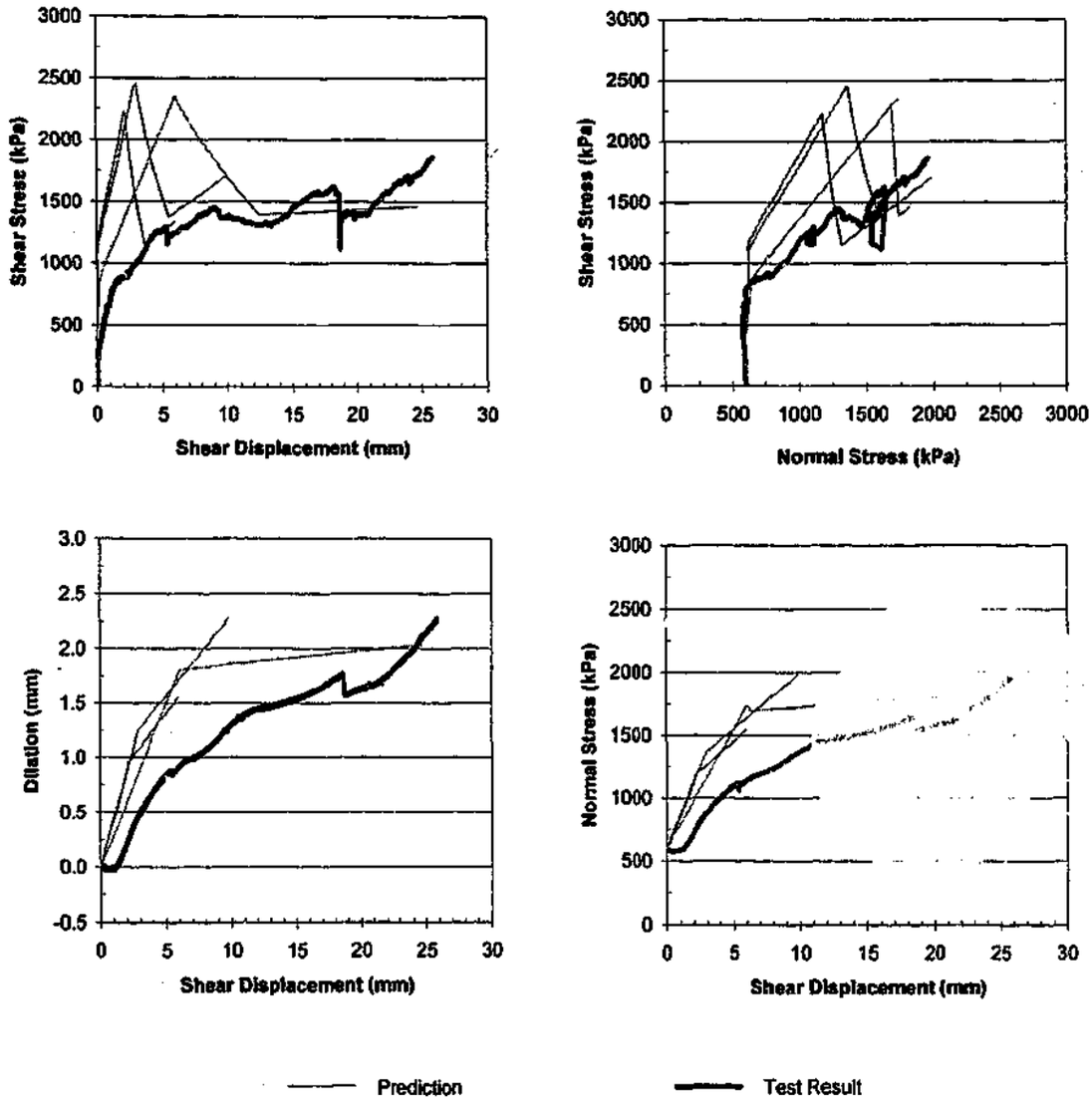

Sample : BFR_10

Failure Stress = UCS

Initial Normal Stress (kPa): 600

Normal Stiffness (kPa/mm): 600

Chord Lengths Used For Predictions : 6mm, 10mm, 25mm

Basalt Fractal Profile BFR_15 Prediction of Shear Response

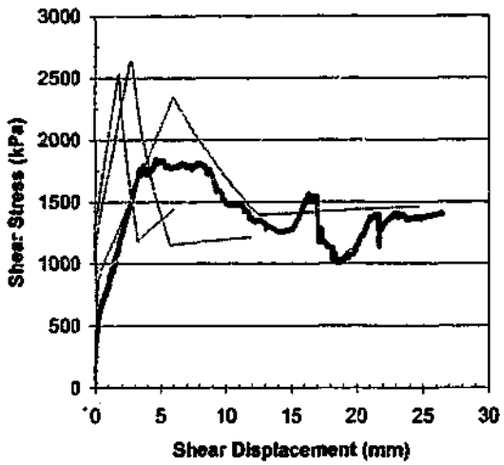

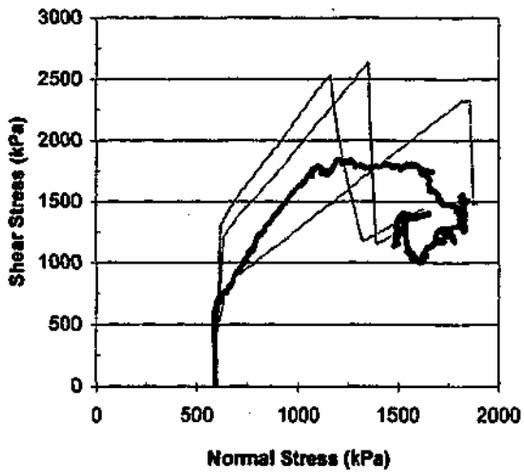

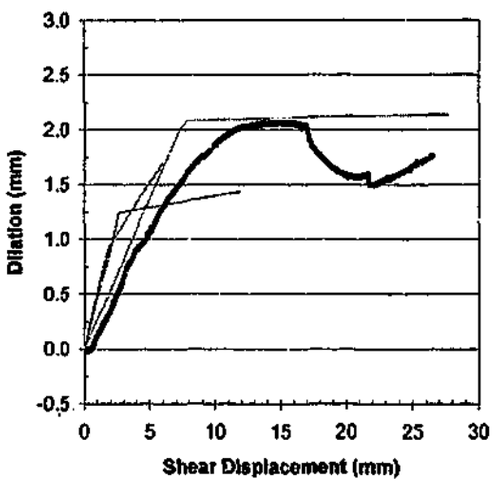

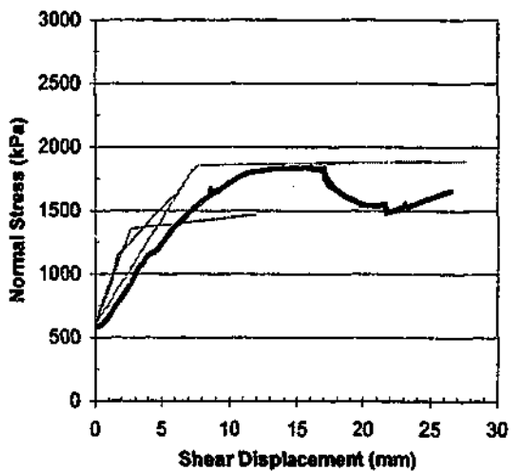

Prediction — Test Result

Sample : BFR_15

Failure Stress = UCS

Initial Normal Stress (kPa): 600

Normal Stiffness (kPa/mm): 600

Chord Lengths Used For Predictions : 6mm, 12mm, 28mm

Basalt Split Surface BS_1 Prediction of Shear Response

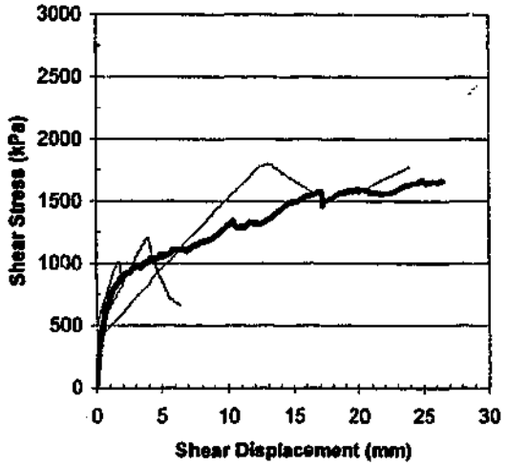

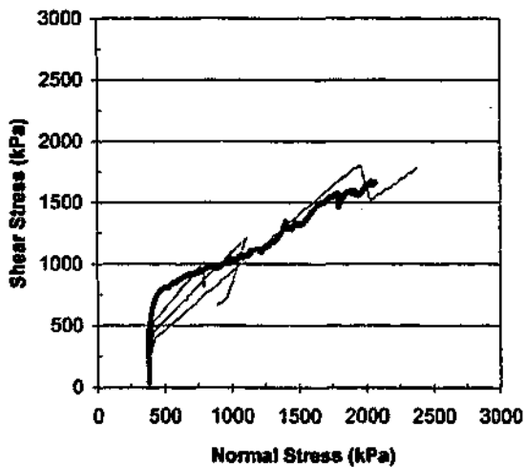

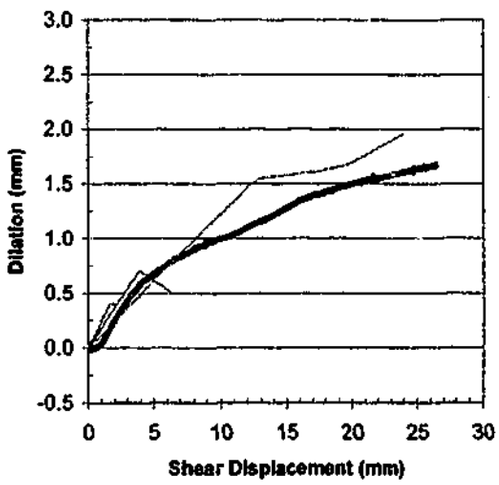

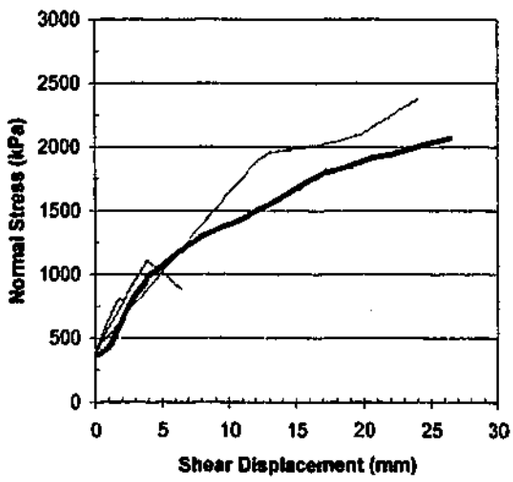

Prediction Test Result

Sample : BS_1

Failure Stress = UCS

Initial Normal Stress (kPa): 400

Normal Stiffness (kPa/mm): 1000

Chord Lengths Used For Predictions : 2mm, 6.5mm, 20mm

Basalt Split Surface BS_2 Prediction of Shear Response

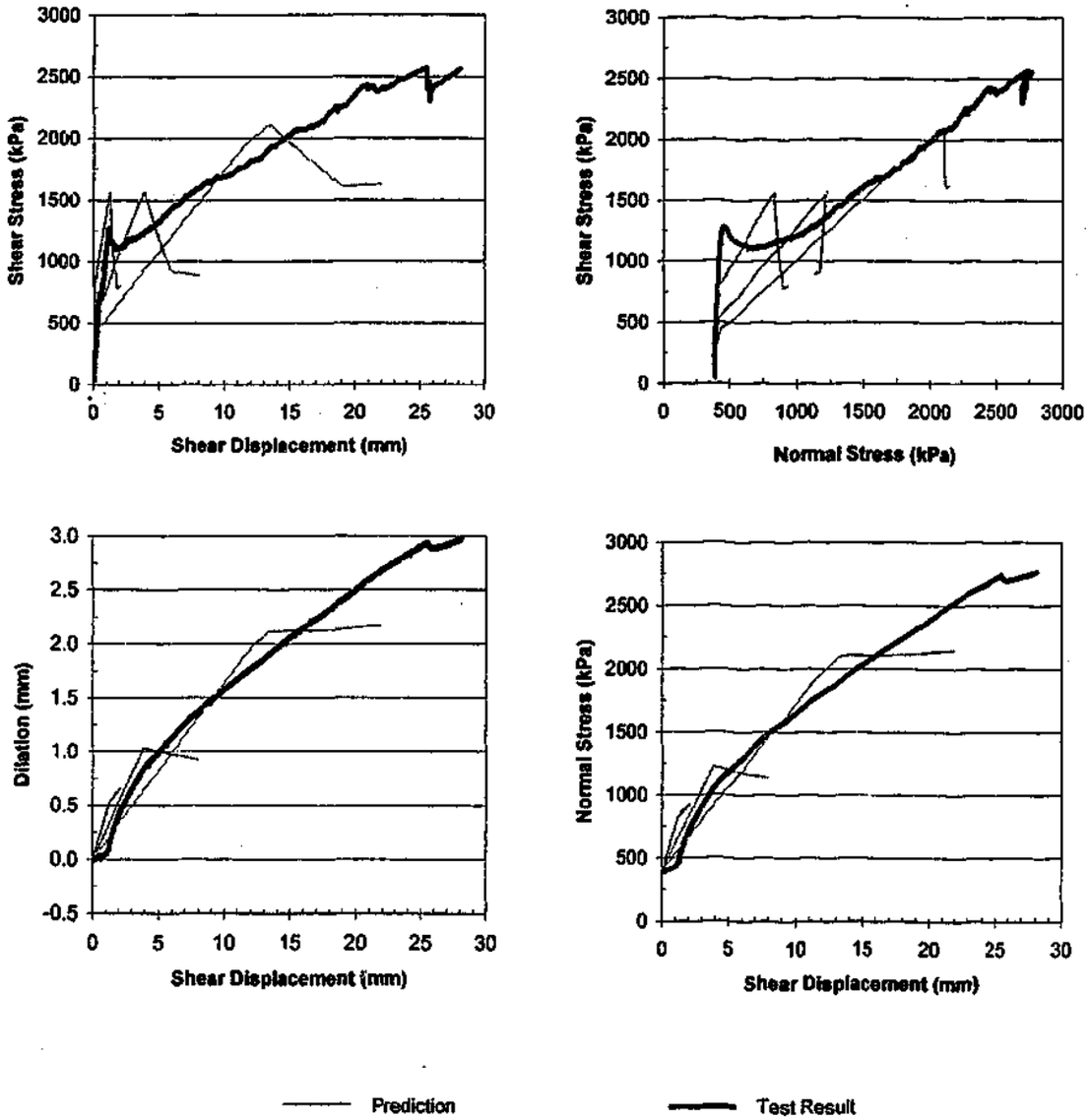

Sample : BS_2

Failure Stress = UCS

Initial Normal Stress (kPa): **400**

Normal Stiffness (kPa/mm): **800**

Chord Lengths Used For Predictions : 2.2mm, 8mm, 22mm

Basalt Split Surface BS_3 Prediction of Shear Response

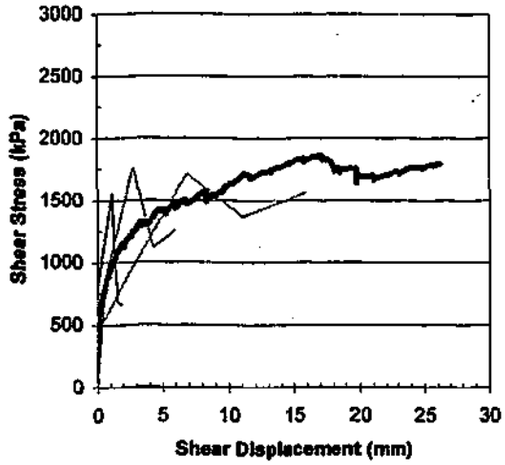

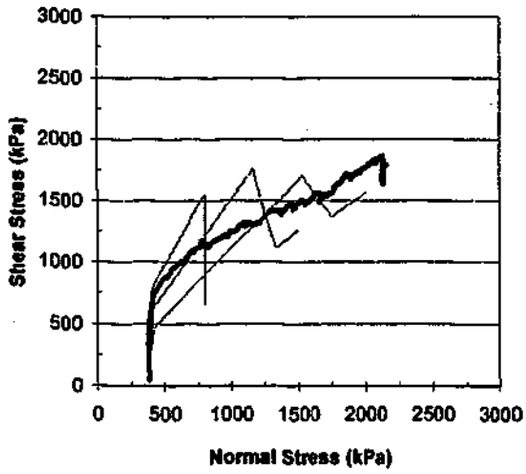

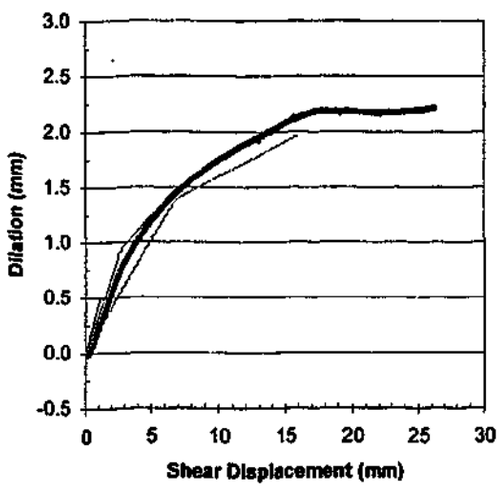

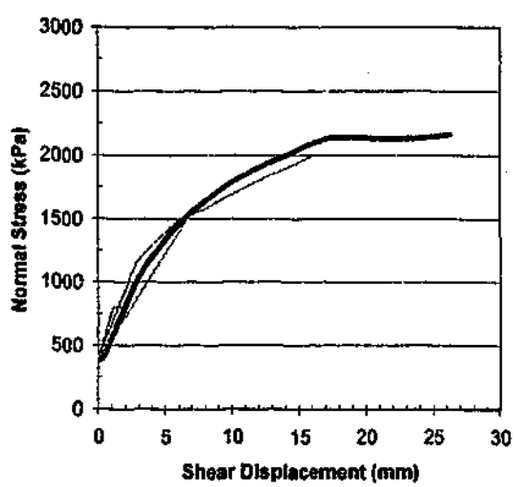

Prediction Test Result

Sample : BS_3

Failure Stress = UCS

Initial Normal Stress (kPa): 400

Normal Stiffness (kPa/mm): 800

Chord Lengths Used For Predictions : 2mm, 6mm, 16mm

Granite Direct Shear Test Predictions

In this section the predictions produced using the program Rocket are compared with direct shear tests conducted on granite samples.

The following parameters were used in the predictions:

Parameter	Adopted value
Young's Modulus	61GPa
Poisson's Ratio	0.15
Intact Friction Angle	50°
Residual Friction Angle	36.5°
Cohesion	35MPa
Joint Normal Stiffness – water-jet surface	7.8MPa/mm
Joint Normal Stiffness – split surface	7.5MPa/mm
Failure Stress	180MPa

Granite Regular Triangular Profile GR10_8 Prediction of Shear Response

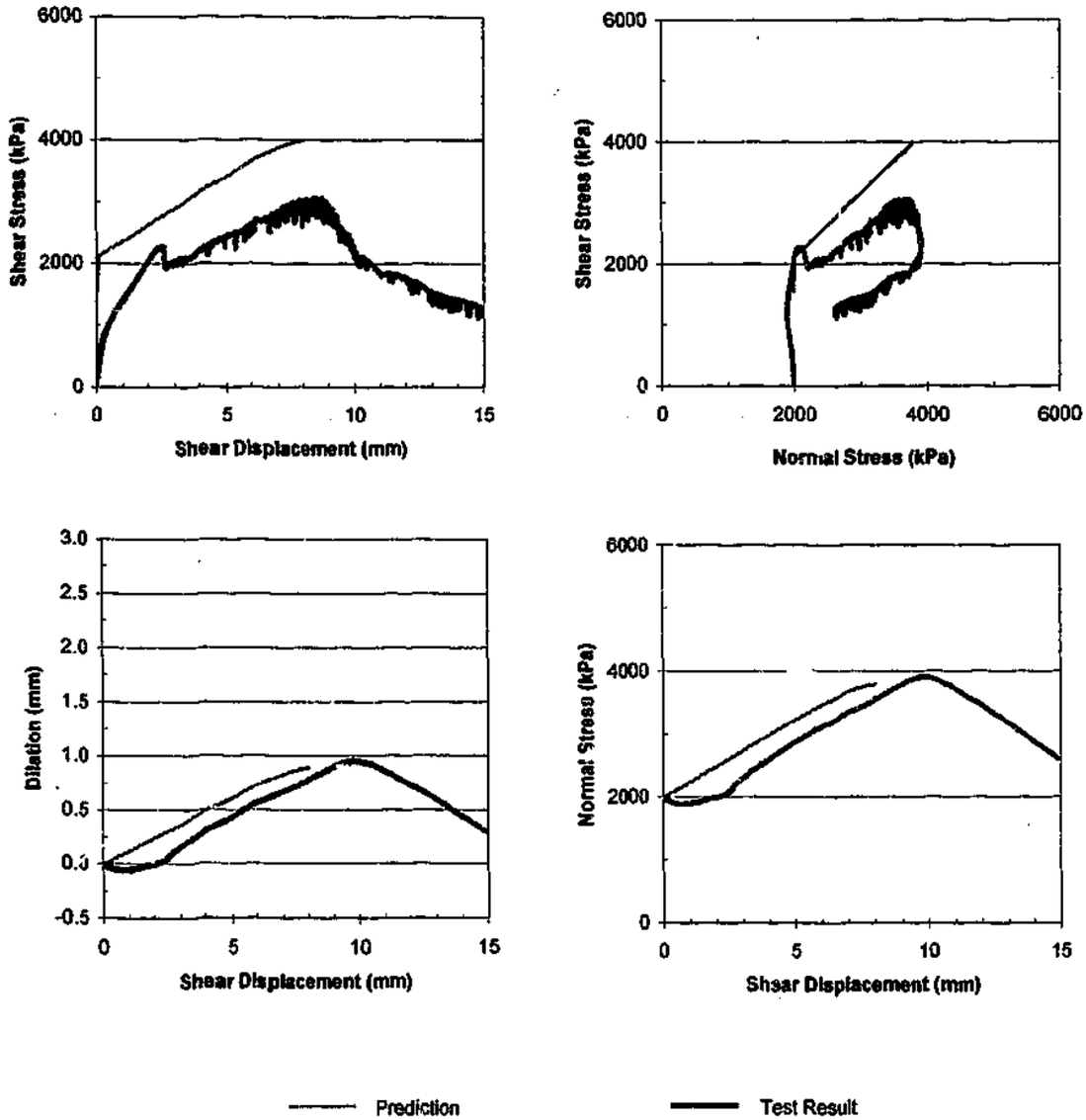

Sample : GR10_8

Failure Stress = UCS

Initial Normal Stress (kPa): **2000**

Normal Stiffness (kPa/mm): **2000**

Granite Regular Triangular Profile GR10a_8 Prediction of Shear Response

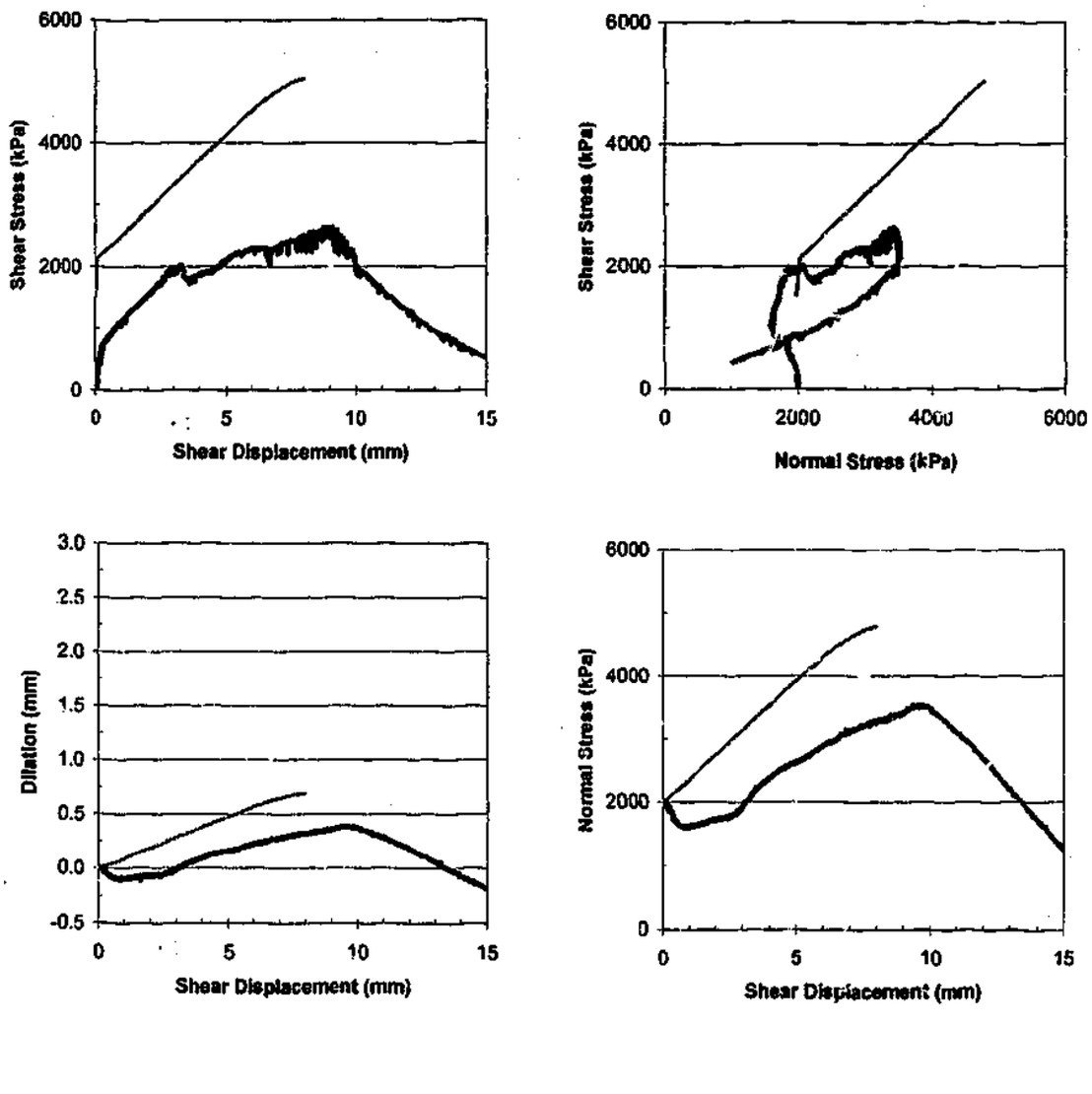

Sample : GR10a_8

Failure Stress = UCS

Initial Normal Stress (kPa): 2000

Normal Stiffness (kPa/mm): 4000

Granite Regular Triangular Profile GR20_8 Prediction of Shear Response

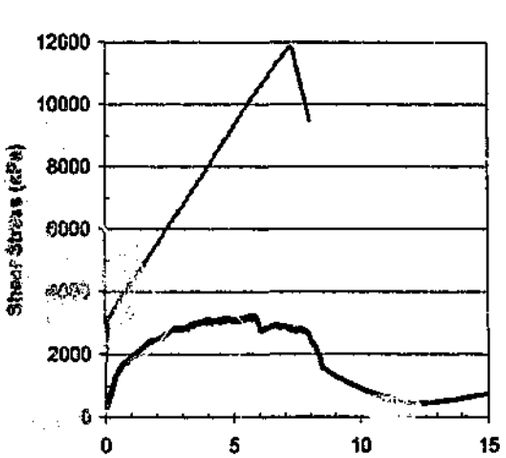

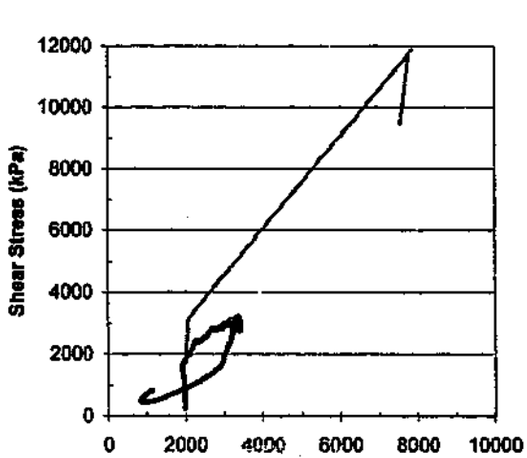

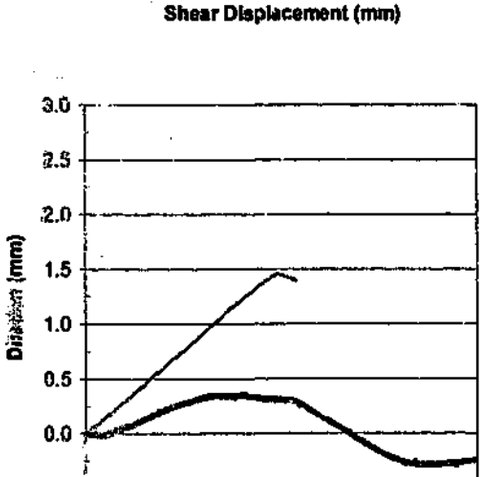

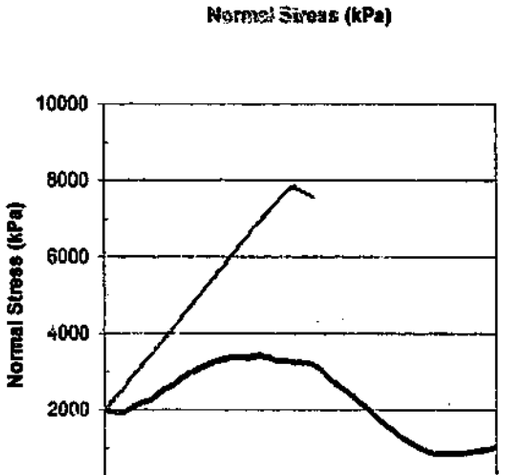

Prediction Test Result

Sample : GR20_8

Failure Stress = UCS

Initial Normal Stress (kPa): **2000**

Normal Stiffness (kPa/mm): **4000**

Granite Split Surface GS_1 Prediction of Shear Response

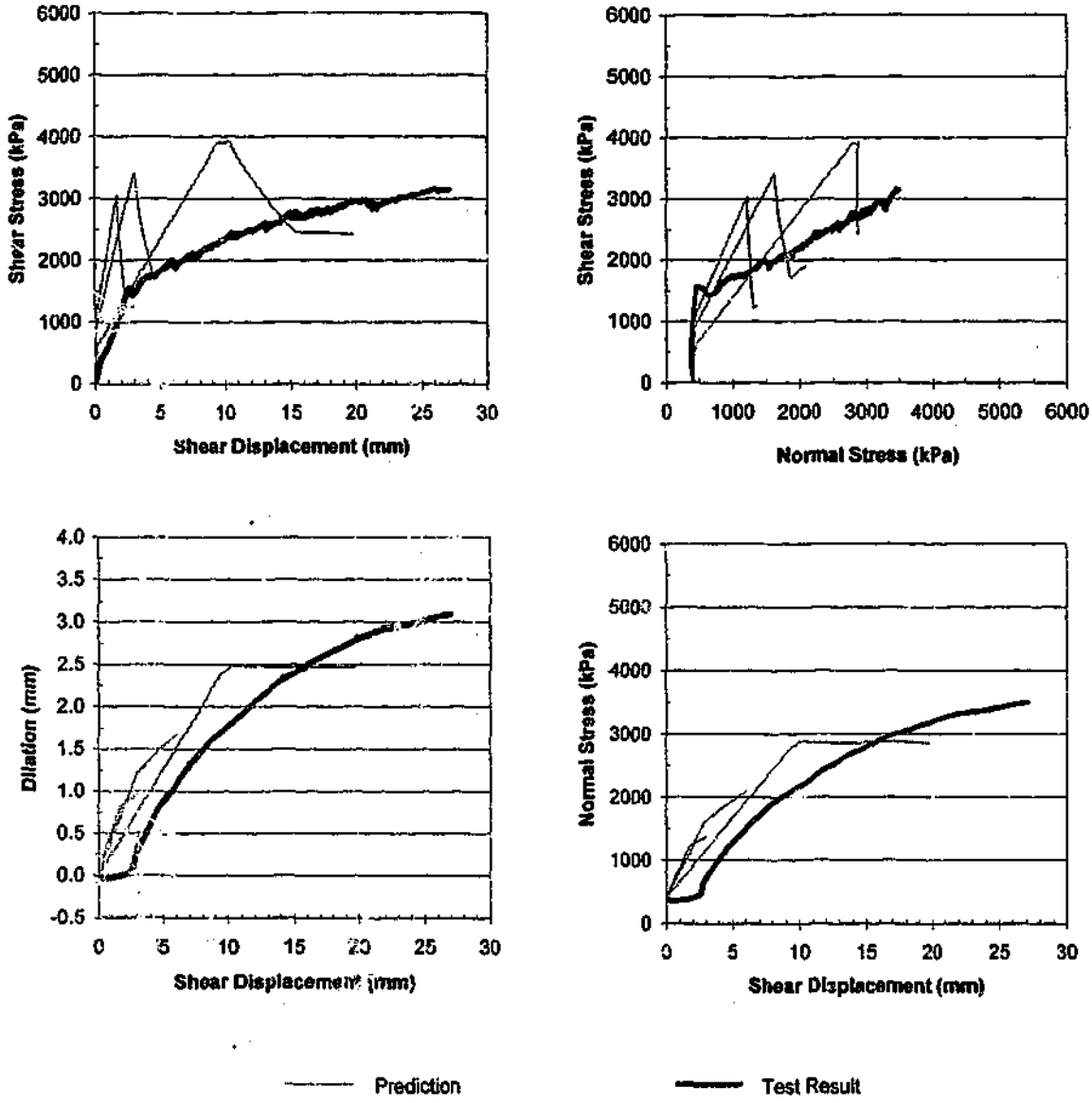

Sample : GS_1

Failure Stress = UCS

Initial Normal Stress (kPa): **400**

Normal Stiffness (kPa/mm): **1000**

Chord Lengths Used For Predictions : 3mm, 6mm, 20mm

Granite Split Surface GS_2 Prediction of Shear Response

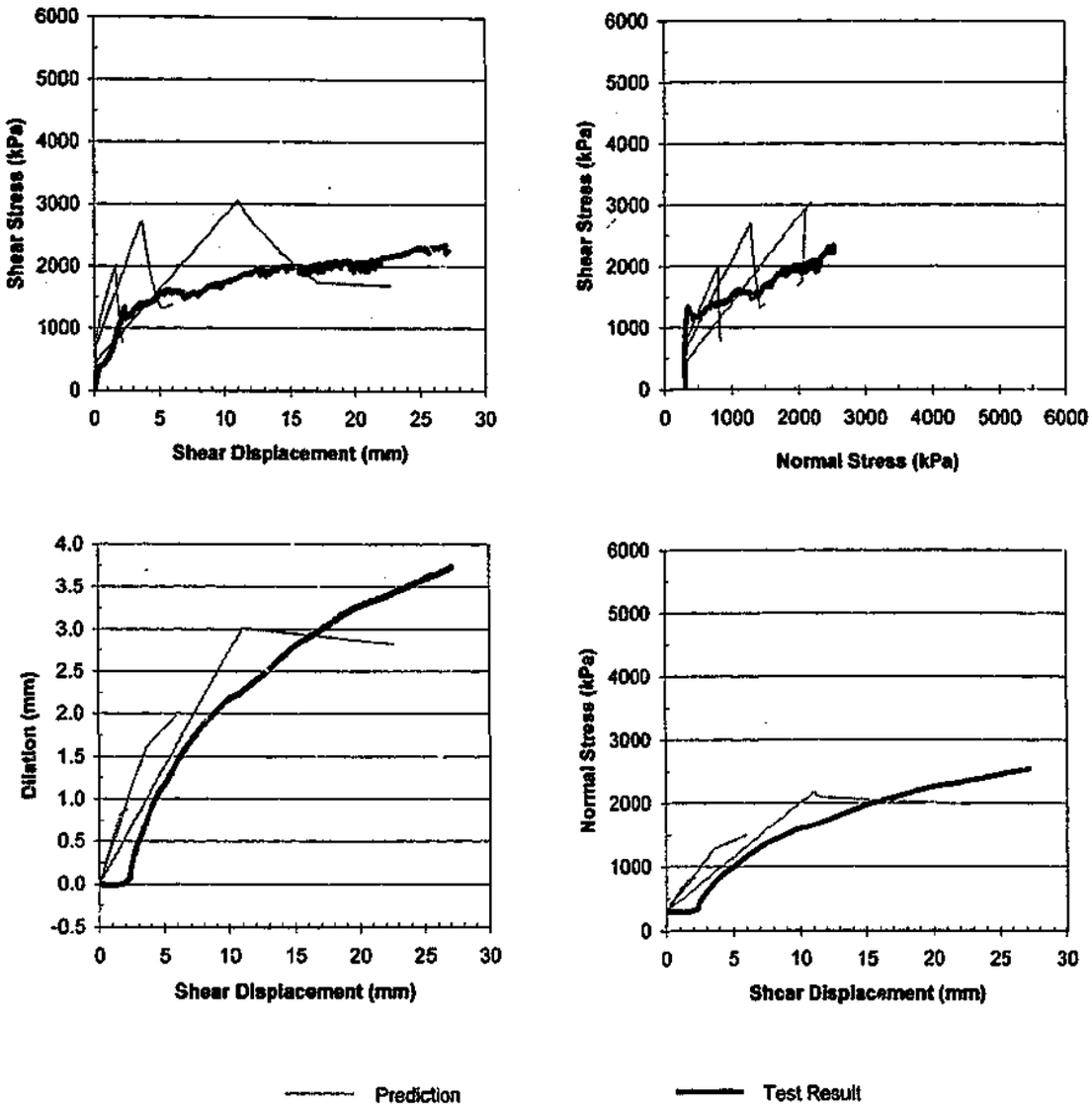

Sample : GS_2

Failure Stress = UCS

Initial Normal Stress (kPa): **300**

Normal Stiffness (kPa/mm): **600**

Chord Lengths Used For Predictions : 2.2mm, 6mm, 23mm

Granite Split Surface GS_3 Prediction of Shear Response

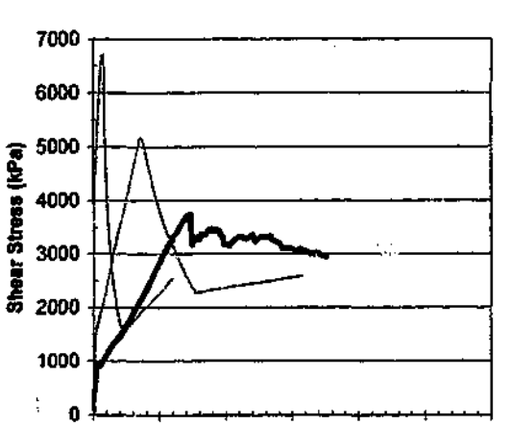

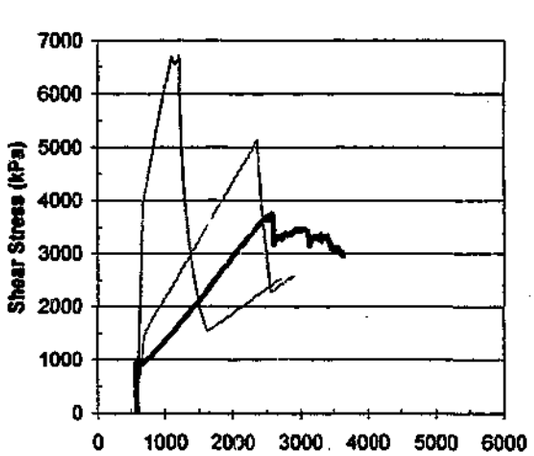

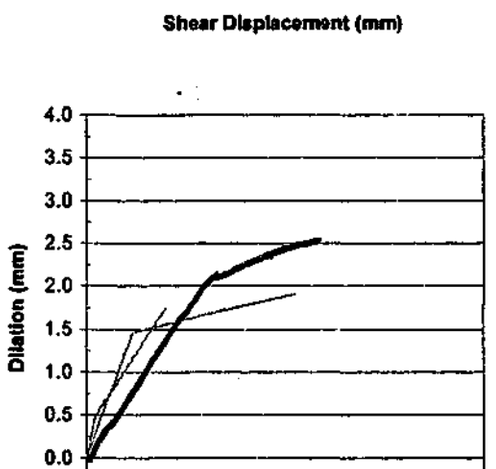

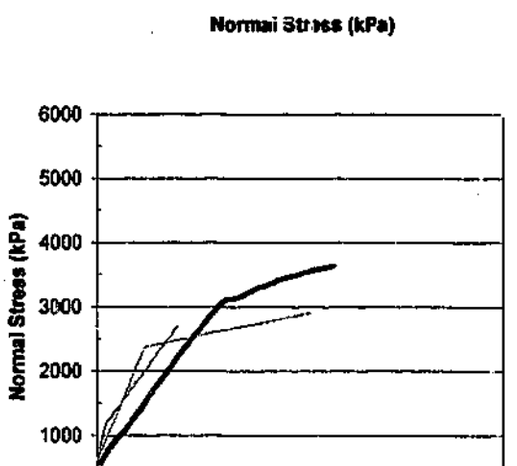

Prediction Test Result

Sample : GS_3

Failure Stress = UCS

Initial Normal Stress (kPa): **600**

Normal Stiffness (kPa/mm): **1200**

Chord Lengths Used For Predictions : 6mm, 16mm

Granite Split Surface GS_4 Prediction of Shear Response

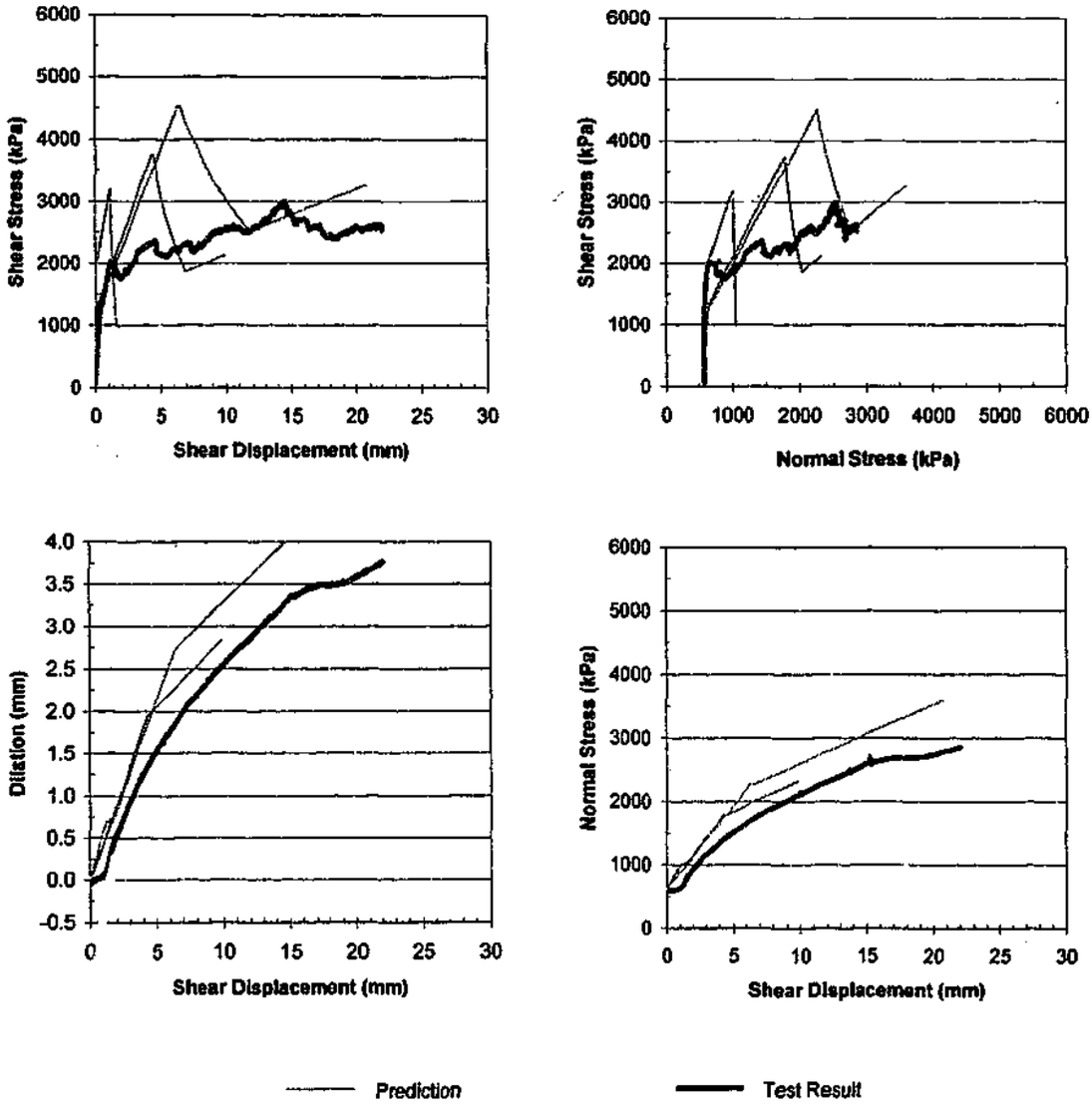

Sample : GS_4

Failure Stress = UCS

Initial Normal Stress (kPa): 600

Normal Stiffness (kPa/mm): 600

Chord Lengths Used For Predictions : 2mm, 10mm, 21mm